STRUCTURE AND FUNCTION OF CHLOROPLASTS - VOLUME II

EDITED BY: Hongbo Gao, Jürgen Soll, Rebecca L. Roston, Yan Lu and Luning Liu

PUBLISHED IN: Frontiers in Plant Science

frontiers Research Topics

ISSN 1664-8714
ISBN 978-2-88966-373-6
DOI 10.3389/978-2-88966-373-6

About Frontiers

Frontiers is more than just an open-access publisher of scholarly articles: it is a pioneering approach to the world of academia, radically improving the way scholarly research is managed. The grand vision of Frontiers is a world where all people have an equal opportunity to seek, share and generate knowledge. Frontiers provides immediate and permanent online open access to all its publications, but this alone is not enough to realize our grand goals.

Frontiers Journal Series

The Frontiers Journal Series is a multi-tier and interdisciplinary set of open-access, online journals, promising a paradigm shift from the current review, selection and dissemination processes in academic publishing. All Frontiers journals are driven by researchers for researchers; therefore, they constitute a service to the scholarly community. At the same time, the Frontiers Journal Series operates on a revolutionary invention, the tiered publishing system, initially addressing specific communities of scholars, and gradually climbing up to broader public understanding, thus serving the interests of the lay society, too.

Dedication to Quality

Each Frontiers article is a landmark of the highest quality, thanks to genuinely collaborative interactions between authors and review editors, who include some of the world's best academicians. Research must be certified by peers before entering a stream of knowledge that may eventually reach the public - and shape society; therefore, Frontiers only applies the most rigorous and unbiased reviews.
Frontiers revolutionizes research publishing by freely delivering the most outstanding research, evaluated with no bias from both the academic and social point of view. By applying the most advanced information technologies, Frontiers is catapulting scholarly publishing into a new generation.

What are Frontiers Research Topics?

Frontiers Research Topics are very popular trademarks of the Frontiers Journals Series: they are collections of at least ten articles, all centered on a particular subject. With their unique mix of varied contributions from Original Research to Review Articles, Frontiers Research Topics unify the most influential researchers, the latest key findings and historical advances in a hot research area! Find out more on how to host your own Frontiers Research Topic or contribute to one as an author by contacting the Frontiers Editorial Office: frontiersin.org/about/contact

STRUCTURE AND FUNCTION OF CHLOROPLASTS - VOLUME II

Topic Editors:
Hongbo Gao, Beijing Forestry University, China
Jürgen Soll, Ludwig Maximilian University of Munich, Germany
Rebecca L. Roston, University of Nebraska-Lincoln, United States
Yan Lu, Western Michigan University, United States
Luning Liu, University of Liverpool, United Kingdom

Dr. Deqiang Duanmu based at Huazhong Agricultural University in China is collaborating with Dr. Gao, Dr. Soll, Dr. Rosten, Dr. Lu and Dr. Liu as an editorial assistant in this Research Topic.

Citation: Gao, H., Soll, J., Roston, R. L., Lu, Y., Liu, L., eds. (2021). Structure and Function of Chloroplasts - Volume II. Lausanne: Frontiers Media SA.
doi: 10.3389/978-2-88966-373-6

Table of Contents

frontiers in Plant Science

EDITORIAL
published: 25 November 2020
doi: 10.3389/fpls.2020.620152

Editorial: Structure and Function of Chloroplasts - Volume II

Yan Lu[1], *Lu-Ning Liu*[2], *Rebecca L. Roston*[3], *Jürgen Soll*[4] *and Hongbo Gao*[5]*

[1] Department of Biological Sciences, Western Michigan University, Kalamazoo, MI, United States, [2] Institute of Systems, Molecular and Integrative Biology, University of Liverpool, Liverpool, United Kingdom, [3] Department of Biochemistry, University of Nebraska-Lincoln, Lincoln, NE, United States, [4] Ludwig Maximilian University of Munich, Munich, Germany, [5] College of Biological Sciences and Biotechnology, Beijing Forestry University, Beijing, China

Keywords: chloroplast, envelope, thylakoid, protein import, photosynthesis

Editorial on the Research Topic

Structure and Function of Chloroplasts - Volume II

As the site of photosynthesis, the chloroplast is responsible for producing all the biomass in plants. It is also a metabolic center for production or modification of many important compounds, such as carbohydrates, purines, pyrimidines, amino acids, fatty acids, precursors of several plant hormones, and many secondary metabolites. The chloroplast also extensively communicates with other parts and organelles of the cell. We were fortunate enough to have submissions from ∼100 talented chloroplast researchers. This topic contains 17 papers of which 11 are original research, 4 are reviews or mini-reviews, and one is a perspective.

As the chloroplast is semi-autonomous, the biogenesis, development, division, and partitioning of chloroplasts rely on nuclear-encoded proteins as well. A nuclear-encoded chloroplast-localized translation elongation factor EF-Tu was found to be essential to chloroplast development in the flowering plant *Arabidopsis thaliana* (Liu S. et al.). This prokaryotic-type translation elongation factor also acts cooperatively with the chloroplast translation initiation factor IF3 to control leaf vascular development.

Although most of the chloroplast proteins are encoded by the nuclear genome, the chloroplast genome still contains >100 genes. Efficient transcription of these chloroplast-encoded genes and subsequent translation of protein-coding transcripts is essential to chloroplast function. Nuclear encoded pentatricopeptide repeat proteins (PPRs) have been repeatedly found to be involved in transcription, transcript stabilization, intron splicing, editing, and translation in the chloroplast. Wang et al. discovered that Pigment-Defective Mutant4 (PDM4), a chloroplast P-type PPR protein, plays a crucial role in the expression of chloroplast genes and the development of chloroplasts in Arabidopsis. PDM4 was also found to participate in the splicing of group II introns and possibly the assembly of the large subunit of chloroplast ribosomes. Another chloroplast P-type PPR protein covered by this special issue is Biogenesis Factor required for ATP synthase 2 (BFA2). This protein is capable of binding to the *atpF-atpA* intergenic region in a sequence-specific manner, thus preventing the degradation of the dicistronic *atpH/F* transcript by exoribonucleases (Zhang et al.). The characterizations of two PPR proteins in this special issue demonstrate the importance of PPR proteins in regulating transcription and RNA metabolism in the chloroplast.

Most chloroplast proteins are imported into the chloroplast and delivered to chloroplast subcompartments via complex machinery. Worn-out and damaged chloroplasts and chloroplast components are turned over efficiently to safeguard chloroplast function. Yang et al. reviewed the molecular mechanisms and regulatory pathways of chloroplast protein import and degradation. Relatively little is known about the targeting machinery of tail-anchored proteins, which have stromal-exposed N-terminal domains and a C-terminal transmembrane domain. By studying membrane-specific targeting of two Arabidopsis chloroplast secretory translocase proteins SECE1

OPEN ACCESS

Edited and reviewed by:
Alistair McCormick, University of Edinburgh, United Kingdom

***Correspondence:**
Hongbo Gao
gaohongbo@bjfu.edu.cn

Specialty section:
This article was submitted to Plant Physiology, a section of the journal Frontiers in Plant Science

Received: *22 October 2020*
Accepted: *30 October 2020*
Published: *25 November 2020*

Citation:
Lu Y, Liu L-N, Roston RL, Soll J and Gao H (2020) Editorial: Structure and Function of Chloroplasts - Volume II. Front. Plant Sci. 11:620152. doi: 10.3389/fpls.2020.620152

and SECE2, which localize to thylakoid membranes and the inner envelope respectively, Anderson et al. discovered that the transmembrane domain and the C-terminal tail of tail-anchored proteins are important for their membrane-specific targeting. Chloroplast stromal chaperone proteins (e.g., HSP90C, HSP70s, and HSP40s) and the GrpE-type nucleotide exchange factors have been proposed to participate in chloroplast protein import, thylakoid integration, assembly and disassembly. Arabidopsis has two nuclear-encoded chloroplast-targeted GrpE proteins: CGE1 and CGE1. Su et al. reported that CGE1 is the main functional homolog among the two and that CGE2 may have a subsidiary or regulatory function.

A chloroplast division site regulator protein, PARC6, was discovered to be critical for chloroplast morphology in pavement and guard cells, and leucoplast morphology in *Arabidopsis* trichome cells (Ishikawa et al.). Analysis of PARC6 fused to a flurorescent protein through confocal microscopysuggested that it forms a ring at the chloroplast division site that changes configuration during chloroplast division. Due to the highly uniform size and shape of leaf epidermal guard cells and the relatively stable number and morphology of chloroplasts in them, leaf epidermal guard cells were recently proposed to be an excellent model system to investigate chloroplast multiplication and partitioning in plants (Fujiwara et al.).

The thylakoid membranes of cyanobacteria and chloroplasts house a series of photosynthetic electron transport complexes. The biogenesis, stabilization, and maintenance of thylakoid membranes require the participation of the inner membrane-associated protein of 30 kDa (IM30), which is also known as the vesicle-inducing protein in plastids 1 (Vipp1). Siebenaller et al. reviewed that the ability of IM30 to form homo-oligomeric protein complexes is crucial to its roles in thylakoid membrane protection and remodeling. In the cyanobacterium *Synechocystis* sp. PCC 6803, thylakoid membranes are reduced in size, function under nitrogen starvation, and are quickly recovered after nitrogen replenishment. Kobayashi et al. reported that the contents of phosphatidylglycerol, an essential phospholipid of photosystem complexes, and glycoglycerolipids, the main constituents of thylakoid membrane lipid bilayers, could be differentially regulated during the recovery from nitrogen starvation. The levels of phosphatidylglycerol recovers quickly after nitrogen is replenished whereas the content of glycoglycerolipids recovers gradually.

Excess light exposure causes oxidative damage to photosynthetic electron transport complexes, especially to the reaction center of photosystem II (PSII). Liu J. et al. reviewed recent advances on reaction center-based approaches for repairing photodamaged PSII and antenna-based approaches for rapid control of PSII light harvesting. Photosynthetic organisms employ these diverse strategies to ensure PSII function under static or fluctuating high light environments. Because of the differences in mobility and environments, land plants are subject to broader high light stress than algae and cyanobacteria. Therefore, land plants developed additional thiol/disulfide-modulating proteins, such as Low Quantum Yield of PSII 1 (LQY1), to repair photodamaged PSII. Wessendorf and Lu found that introducing an Arabidopsis homolog of this protein into the cyanobacterium *Synechocystis* significantly increases the photochemical efficiency of PSII under elevated light conditions. This finding further demonstrated the role of thiol/disulfide-modulating proteins in PSII repair. Photoacclimation of light-dependent reactions involves reversible phosphorylation of thylakoid proteins and redistribution of light-harvesting antenna complexes between PSII and photosystem I (PSI). As a phosphorylation target of state transition kinases 7 and 8, the calcium sensor receptor protein (CAS) was found to play a role in phosphorylation-mediated photoacclimation in Arabidopsis (Cutolo et al.). It was postulated that CAS may modulate photosynthetic function by being phosphorylated in a calcium-dependent manner and/or by influencing the dynamics of chloroplast calcium concentration.

In addition to being a target of calcium signaling, the chloroplast is also an active player in intracellular calcium signaling. Navazio et al. discussed the role of chloroplast calcium signaling under biotic and abiotic stresses and reviewed latest advances in the discovery and characterization of calcium sensors and calcium channels/transporters, especially those that localize to the chloroplast. In the chloroplast, PSI and PSII are major generators of reactive oxygen species (ROS). Although excessive ROS causes oxidative damage, low levels of ROS production triggers retrograde signaling between chloroplasts and the nucleus (Kim), which is beneficial. Beta-carotene and the Executer 1 protein associated with PSII have been proposed to mediate retrograde signaling in the grana core and grana margins, respectively. In addition, the accumulation of ROS-damaged PSII core proteins may trigger a damaged protein response, which induces the expression of protein quality control- and ROS detoxification-related nuclear genes. Furthermore, PSI-driven ROS may inactivate 3′-phosphoadenosine 5′-phosphate (PAP) phosphatase, which leads to PAP accumulation-mediated retrograde signaling. Retrograde signaling also plays vital roles in regulating the expression of nuclear-encoded chloroplast proteins involved in carbohydrate metabolism. For example, the expression of glucose-6-phosphate/phosphate translocator 2 (GPT2) increases rapidly if the growth light is elevated or if starch metabolism is disrupted. The increase of the *GPT2* transcript is preceded by the transcript increases of transcription factors involved in retrograde signaling, including Redox Responsive Transcription Factor 1 (RRTF1) (Weise et al.). Further analyses demonstrated that transcription of the *GPT2* gene requires and the export of triose phosphates from the chloroplast and the expression of RRTF1. In addition to producing sugars and starch, the chloroplast is also a manufacturer for other metabolic important compounds, including purines. The first committing step of de novo purine synthesis is catalyzed by glutamine phosphoribosylpyrophosphate amidotransferases (GPRATs). Cao et al. solved the crystal structure of GPRAT2 and identified the structural differences between *Arabidopsis* GPRAT2 and its bacterial homologs. GPRAT2 was previously identified as the target of a small molecule, DAS34. The inhibition mechanism of DAS34

was characterized at the structural level in this study. This work sheds light on further development of herbicides targeting GPRATs.

Altogether, this volume of the Research Topic provides exiting works in the area of the structure, functions and maintenance of chloroplasts, ranging from the biogenesis and development of chloroplasts to gene transcription, protein synthesis and turnover, metabolism, as well as the dynamics, signaling and regulation of chloroplast functions including photosynthesis. With the efforts of many researchers worldwide, the frontiers of this topic keep evolving at a rapid pace.

AUTHOR CONTRIBUTIONS

All authors listed have made a substantial, direct and intellectual contribution to the work, and approved it for publication.

FUNDING

YL was supported by US National Science Foundation (Grant No. MCB-1244008). LL was supported by the Royal Society University Research Fellowship (Grant No. URF\R\180030), Biotechnology and Biological Sciences Research Council (Grant No. BB/R003890/1). RR was partially supported by the Nebraska Agricultural Experiment Station with funding from the Hatch Multistate Research capacity funding program (Accession No. NC1203) from USDA NIFA. HG was supported by National Nature Science Foundation of China (Grant No. 31570182, 32070696).

ACKNOWLEDGMENTS

We thank all the authors and reviewers that have contributed to this Research Topic.

Conflict of Interest: The authors declare that the research was conducted in the absence of any commercial or financial relationships that could be construed as a potential conflict of interest.

frontiers in Plant Science

ORIGINAL RESEARCH
published: 12 March 2019
doi: 10.3389/fpls.2019.00295

Chloroplast Translation Elongation Factor EF-Tu/SVR11 Is Involved in *var2*-Mediated Leaf Variegation and Leaf Development in *Arabidopsis*

*Siyu Liu†, Lu Zheng†, Jia Jia, Jia Guo, Mengdi Zheng, Jun Zhao, Jingxia Shao, Xiayan Liu, Lijun An, Fei Yu and Yafei Qi**

State Key Laboratory of Crop Stress Biology for Arid Areas and College of Life Sciences, Northwest A&F University, Yangling, China

Chloroplasts are semiautonomous organelles, retaining their own genomes and gene expression apparatuses but controlled by nucleus genome encoded protein factors during evolution. To analyze the genetic regulatory network of FtsH-mediated chloroplast development in *Arabidopsis*, a set of suppressor mutants of *yellow variegated* (*var2*) have been identified. In this research, we reported the identification of another new *var2* suppressor locus, *SUPPRESSOR OF VARIEGATION11* (*SVR11*), which encodes a putative chloroplast-localized prokaryotic type translation elongation factor EF-Tu. *SVR11* is likely essential to chloroplast development and plant survival. *GUS* activity reveals that *SVR11* is abundant in the juvenile leaf tissue, lateral roots, and root tips. Interestingly, we found that *SVR11* and *SVR9* together regulate leaf development, including leaf margin development and cotyledon venation patterns. These findings reinforce the notion that chloroplast translation state triggers retrograde signals regulate not only chloroplast development but also leaf development.

Keywords: EF-Tu, chloroplast development, leaf variegation, retrograde signal, VAR2

OPEN ACCESS

Edited by:
Jürgen Soll, Ludwig Maximilian University of Munich, Germany

Reviewed by:
Zach Adam, Hebrew University of Jerusalem, Israel
Christian Schmitz-Linneweber, Humboldt-Universität zu Berlin, Germany

****Correspondence:***
Yafei Qi
Yafei.Qi@nwsuaf.edu.cn

† These authors have contributed equally to this work

Specialty section:
This article was submitted to Plant Physiology, a section of the journal Frontiers in Plant Science

Received: *10 December 2018*
Accepted: *22 February 2019*
Published: *12 March 2019*

Citation:
Liu S, Zheng L, Jia J, Guo J, Zheng M, Zhao J, Shao J, Liu X, An L, Yu F and Qi Y (2019) Chloroplast Translation Elongation Factor EF-Tu/SVR11 Is Involved in var2-Mediated Leaf Variegation and Leaf Development in Arabidopsis. Front. Plant Sci. 10:295. doi: 10.3389/fpls.2019.00295

INTRODUCTION

Chloroplasts are essential organelles for eukaryotic photosynthetic species, enabling the chemical reactions powered by light energy to reduce CO_2 to carbohydrates. It is believed that chloroplasts evolved from ancient prokaryotic cyanobacteria through endosymbiosis (Martin et al., 2002). This co-evolution process, especially the transfer of most genes of chloroplast progenitors to the host nuclear genomes, have given rise to modern-day chloroplast genomes with only around 120 genes, in contrast to the more than 3,000 genes of the current genome of cyanobacteria, such as *Synechocystis* sp. (Timmis et al., 2004). The physical separation of nuclear and chloroplast genomes raises at least two important implications. First, the remaining genes in chloroplast genomes are expressed with prokaryotic gene expression systems, which are regulated by the nuclear genome and must respond to developmental and environmental conditions (Jarvis and López-Juez, 2013).

Abbreviations: CaMV, Cauliflower Mosaic Virus; EF-Ts, elongation factor thermo stable; EF-Tu, elongation factor thermo unstable; FtsH, filamentous temperature sensitive H; GFP, green fluorescence protein; *SVR*, *SUPPRESSOR OF VARIEGATION;* UTR, untranslated region; *var2*, *yellow variegated2.*

Second, many photosynthetic protein complexes are chimeric in nature, and are composed of subunits encoded by both nuclear and plastid genomes, and intricate regulation at different levels are necessary for the optimal assembly of these complexes. The semi-autonomous nature of the chloroplast thus necessitates a fine coordination between the two genomes (Kleine and Leister, 2016).

Higher plants have evolved multiple strategies to facilitate the expression and coupling of nuclear and chloroplast genomes. At the translation level, chloroplasts utilize a prokaryotic translation system featuring the 70S ribosome (Yamaguchi and Subramanian, 2000; Yamaguchi et al., 2000; Tiller and Bock, 2014). Prokaryotic translation initiates through the binding of 30S ribosomal subunit to the Shine-Dalgarno sequence of mRNA, and the subsequent association of initiator tRNA leads to the formation of pre-initiation complex, and this process is assisted by initiation factors IFs (Laursen et al., 2005). In *Arabidopsis*, chloroplast IF1 and IF2 homologs are encoded by the nuclear genome, and null mutant alleles of *Arabidopsis* IF1 and IF2 are embryonic lethal, indicating they are essential genes for plant viability (Miura et al., 2007; Shen et al., 2013; Nesbit et al., 2015). Further recruitment of the 50S ribosomal subunit to pre-initiation complex forms an active initiation complex (Laursen et al., 2005). The translation process requires elongation factors EF-Tu, EF-G, and EF-Ts to incorporate aminoacyl-tRNAs into 70S ribosomes (Krab and Parmeggiani, 2002). EF-Tu is a prokaryotic elongation factor belonging to the GTP-binding protein family (Krab and Parmeggiani, 2002). During translation elongation, GTP-bound EF-Tu forms a ternary complex with aminoacyl-tRNA to facilitate the transport of cognate aminoacyl-tRNA to the A-site of the 70S ribosome. Next, the innate GTPase activity of EF-Tu hydrolyzes the GTP to GDP, and GDP-bound EF-Tu is released from ribosome and recycled to GTP-bound EF-Tu mediated by EF-Ts for the next round of elongation (Krab and Parmeggiani, 1998). During endosymbiosis, genes coding for many of the chloroplast 70S ribosomal proteins and most translational factors have been transferred to the nuclear genome and are subject to nuclear regulation. Partial loss of chloroplast EF-Tu activities in *Arabidopsis*, maize, and tomato reduced heat tolerance, suggesting chloroplast EF-Tu is involved in the plant response to environmental changes (Ristic et al., 2004; Li et al., 2018).

Chloroplast gene expression is also regulated by post-translational mechanisms including the operation of a vast array of protease systems (Nishimura et al., 2016). An intriguing group of proteolytic enzymes that has attracted attention is the chloroplast FtsH proteases, due to the unique leaf variegation phenotypes of *yellow variegated1* (*var1*) and *yellow variegated2* (*var2*) mutants, defective in thylakoid-localized FtsH proteins AtFtsH5 and AtFtsH2, respectively (Chen et al., 2000; Takechi et al., 2000; Sakamoto et al., 2002). FtsH proteins belong to the AAA (ATPase associated with various cellular activities) ATPase superfamily, which is ubiquitously present in prokaryotes and eukaryotes, as well as in mitochondria and chloroplasts (Janska et al., 2013). Thylakoid FtsH complexes comprise four members of FtsH proteins, FtsH1 and FtsH5 (type A) and FtsH2 and FtsH8 (type B), in which VAR2/AtFtsH2 is one of the most abundant subunits (Yu et al., 2004; Zaltsman et al., 2005; Nishimura et al., 2016). Biochemical analysis suggested that thylakoid FtsHs are required to degrade photo-damaged reaction center protein D1 during Photosystem II repair cycle (Lindahl et al., 2000; Kato et al., 2009; Malnoë et al., 2014). Interestingly, VAR2/AtFtsH2-mediated post-translational regulation is closely related with chloroplast translation. Multiple genetic screens for *var2* suppressors in several laboratories have yielded an increasing number of genetic factors involved in chloroplast transcription, translation and post-translational turnover (Park and Rodermel, 2004; Yu et al., 2008; Adam et al., 2011; reviewed in Liu et al., 2010 and Putarjunan et al., 2013). Recently, we reported a new *var2* suppressor mutant, *svr9-1*, which is defective in a bona fide chloroplast-localized prokaryotic translation initiation factor IF3 (Zheng et al., 2016). In Bacteria, initiation factor IF3, encoded by the essential *infC* gene, binds to the 30S ribosomal subunit to promote dissociation of the 70S ribosome for ribosome recycling and translation initiation (Laursen et al., 2005). Down regulation of *SVR9*, alone or with its homologous gene *SVR9L1*, not only suppresses *var2* leaf variegation phenotype, but also causes leaf developmental abnormalities including serrated leaf margin and altered cotyledon venation patterns (Zheng et al., 2016). The characterization of *var2* suppressor genes thus provides a unique opportunity to uncover additional regulators of chloroplast translation.

Here, we report the identification of a new *var2* suppressor mutant, *svr11-1*. Molecular cloning, complementation and protein localization studies confirmed that *SVR11* encodes a putative prokaryotic translation elongation factor EF-Tu, which is localized in chloroplasts. Interestingly, functional genetic analysis of *SVR11*, *SVR9*, and *SVR9L1* showed that *svr11-1 svr9-1* double mutants display a more serrated leaf margin and altered cotyledon venation patterns compared to those of the wild type, while *svr11-1 svr9-1 svr9-1l-1*/+ mutants have an even more pronounced leaf serration. These data suggest that chloroplast translation elongation factor EF-Tu/SVR11 not only regulate chloroplast development, but also act synergistically with chloroplast translation initiation factor IF3/SVR9 to dictate leaf margin and cotyledon vascular development. Our findings uncover a new translation elongation factor in regulating chloroplast and leaf development in *Arabidopsis*.

MATERIALS AND METHODS

Plant Materials and Growth Conditions

Arabidopsis thaliana plants used in this study are all in the Columbia-0 background. The T-DNA insertion line *CS819179* (*svr11-3*) was obtained from the *Arabidopsis* Biological Resource Center (ABRC); the accurate position of each T-DNA insertion sites were identified by sequencing PCR products that include plant genomic DNA and T-DNA left border sequences. *Arabidopsis* seeds were grown at 22°C under continuous illumination (∼100 μmol $m^{-2}s^{-1}$) on commercial soil mix (Pindstrup, Denmark). All seeds were stratified for 2 days at 4°C before sown on soil or half strength MS medium. For

heat stress at a moderate level, 8-day-old seedlings were treated at 38°C for 90 min, and then moved into 22°C for recovery (Queitsch et al., 2000).

Chlorophyll Fluorescence Imaging

Chlorophyll fluorescence was measured with 2-week-old plants using Open FluorCam FC800-O (Photon Systems Instruments; Czechia). Whole plants were dark adapted for 10 min to oxidize the plastoquinone pool before measurement, and the minimum fluorescence F_O was measured. The maximum fluorescence F_M was determined by a saturating flash of light. The maximum quantum yield of photosystem II (F_V/F_M) is calculated as $F_M - F_O/F_M$. Measurement of F_V/F_M was performed in three independent biological repeats.

RNA Manipulations, Vector Constructions, and Transformations

Total RNAs were extracted using Trizol RNA reagent (Life Technologies, Carlsbad, CA, United States) according to the manufacturer's instructions. For semi-quantitative RT-PCR analysis, first-strand cDNA was synthesized from 1 μg DNase-treated total RNA using a PrimeScript reverse transcription kit (Roche, Switzerland). The gene-specific primers used in this study are listed in **Table 1**. The semi-quantitative RT-PCR was performed in three independent biological repeats.

To complement the *svr11-1* and *049-002* mutants, a full-length At4g20360 (*SVR11*) cDNA was amplified by Primer STAR^{TM} HS DNA polymerase (Takara) using primers 20360F and 20360R. The PCR product was digested with *Bam*HI and cloned into the *Bam*HI site of pBluescript KS+. The sequenced *SVR11* fragment was then transferred into pBI111L-intron plasmid which is modified from pBI111L plasmid (Yu et al., 2004). In brief, the first intron sequence of At5g27700 at its 5′ UTR region were amplified with primers 27700inF (*X*baI) and 27700inR (*Bam*HI), and inserted into the multiple cloning site of pBI111L as a chimeric intron at the 5′ UTR region of insertion genes. The resulting construct was transformed into Agrobacterium by electroporation. *Arabidopsis* transformation was performed as described (Clough and Bent, 1998).

Inverse PCR

Genomic DNA extracted from *049-002* homozygous plants was digested with restriction enzyme *Eco*RI overnight. The DNA fragments were further precipitated with 2.5 volumes of ethanol and 0.1 volumes of 3M sodium acetate (pH 5.2). After dissolving in Milli-Q water, DNA fragments were ligated with T4 DNA Ligase. Inverse PCR were performed with Pfu DNA Polymerase using primers SKC12 and OCS3. One 1.5 kb PCR amplified band was sequenced with the SKC12 primer.

Evolutionary Analysis

Full-length protein sequences of SVR11 homologous proteins from dicots *Arabidopsis thaliana*, monocots *Oryza sativa*, moss *Physcomitrella patens*, green algae *Chlamydomonas reinhardtii*, yeast *Saccharomyces cerevisiae*, and prokaryotic species such as *Synechocystis* and *Escherichia coli* were obtained from NCBI using the BLASTP program. Evolutionary analyses were conducted in MEGA X, and the Neighbor-joining algorithm was used to generate the initial tree (Kumar et al., 2018). The accession numbers of protein sequences were included.

Transient Expression of SVR11-GFP and SVR11-Like-GFP

In order to generate a C-terminal GFP-tagged SVR11, the coding sequences of SVR11 amplified with primers 20360F and 20360 GFPR, SVR11-like with 02930F and 02930 GFPR, were cloned into transient expression vector pTF486. The resulting construct were designated *p35S::SVR11-GFP* and *p35S::SVR11-like-GFP*.

TABLE 1 | Primers used in this study.

Primer name	Primer sequences	Notes
20360 F	5′-CATGGATCCACCCTAGCTTCTCGATTTCTC-3′	*p35S:: intronSVR11*
20360 R	5′-CATGGATCCGAAAGCAAGTAGAGATGCTCAC-3′	
27700 inF	5′-CATCTCGAGACTCTCGCTTTCTTCATCATCTC-3′	*p35S:: intronSVR11*
27700 inR	5′-CATTCTAGAGCTTTGAAAGAGTAAACGAGTCC-3′	
20360 GFPR	5′-CATGGGATCCACCACCACCACCACCTTGAGGATCGTCCCAATAAC-3′	*p35S:: SVR11-GFP*
02930 F	5′-CGCGGATCCATGGCGTCCGTTGTTCTTCG-3′	*p35S:: SVR11-like-GFP*
02930 GFPR	5′-CGCGGATCCGGTCATCACTTTTGATACAAC-3′	
20360 PF	5′-CATTCTAGACTACCCTTTTGCTGTCTTGTAAG-3′	*pSVR11::uidA*
20360 PR	5′-CATGGATCCGAAGATGGAATTGGAGAGCAGAG-3′	
20360 F3	5′-GTTACGATTTGTGACGTGTG-3′	Genotyping
20360 F1	5′-ACCCTAGCTTCTCGATTTCTC-3′	
20360 R1:	5′-GAAAGCAAGTAGAGATGCTCAC-3′	
20360 R2:	5′-CAGCTAAAGCCTCATCAAGAATC-3′	
CM35E	5′-AAGATGCCTCTGCCGACAGT-3′	Sequencing
pCB308R	5′-AACGACAATCTGAGCTCCAC-3′	Genotyping
uidA-R	5′-GTTCAGTTCGTTGTTCACAC-3′	Genotyping
SKC12	5′-TTGACAGTGACGACAAATCG-3′	Inverse PCR
OCS3	5′-TAGAGCTCTTATACTCGAGG-3′	Inverse PCR

Arabidopsis leaf protoplast preparation and transient expression of GFP constructs were performed as described by Yoo et al. (2007). Bright field images and fluorescent signals from GFP and chlorophyll autofluorescence were monitored using a Leica DM5000B fluorescent microscope (Leica, Germany).

Histochemical GUS Staining

Amplified with primers 20360 PF and 20360 PR, a 1,493-bp genomic DNA fragment upstream of the start codon of At4g20360 was cloned into pCB308 (Xiang et al., 1999), to generate *SVR11* promoter-β-glucuronidase (GUS) construct *pSVR11::uidA*. The construct *pSVR11::uidA* was transformed into wild-type *Arabidopsis* plant, and *pSVR11::uidA* lines were screened with BASTA. GUS activities were assayed in the T2 generations (Jefferson et al., 1987). The GUS staining was performed with three independent transgenic lines.

Leaf Silhouettes and Cotyledon Veins Observation

For leaf silhouettes imaging, individual true leaves were covered with water and photographed using Research stereo microscope (SMZ25; Nikon) equipped with a CCD camera (DS-U3; Nikon). Those photos were converted to black and white by Adobe Photoshop 8.0.1 by filled the leaf blades with black, so that it is easier to observe the silhouettes of leaves between different phenotypes. The leaf dissection index was calculated as described ($perimeter^2/4\pi$*leaf area, Bilsborough et al., 2011). For cotyledon veins observation, cotyledons of 10-day-old plants were cut down and decolorized in 70% ethanol, till the cotyledons blade turned colorless without chlorophyll and the veins become clearly visible then the cotyledon samples were photographed by stereo microscope photographing. Cotyledon vein patterns were quantified in three independent biological replicates with tested lines containing at least 100 seedlings each time.

RESULTS

Identification of *049-002* and *svr11-1*

We have performed extensive genetic suppressor screens for mutants that could reverse the *var2* leaf variegation phenotype (reviewed in Liu et al., 2010 and Putarjunan et al., 2013). Here, we report the identification of a new recessive suppressor line, designated as *049-002*, from the activation tagging T-DNA mutant population in the *var2-5* mutant background (Yu et al., 2008). Following our naming sequence, the suppressor gene locus was named as *SUPPRESSOR OF VARIEGATION11* (*SVR11*) and the mutant allele in *049-002* as *svr11-1*. Overall, *049-002* (*var2-5 svr11-1*) did not show the characteristic leaf variegation phenotype of *var2-5*, indicating that *svr11-1* is a robust suppressor of *var2-5* (**Figure 1A**). In addition, the statures of *049-002* and *svr11-1* resembled that of wild type, suggesting overall plant growth was not dramatically altered by the *svr11-1* mutation. Interestingly, both *049-002* and *svr11-1* showed a virescent phenotype, i.e., a gradual yellow to green leaf color gradient along the leaf proximal-distal axis (**Figure 1A**). This virescence phenotype was correlated with a reduction of photosynthetic parameters, as indicated by the F_V/F_M (the maximum quantum yield of photosystem II) of whole plant chlorophyll fluorescence imaging (**Figure 1B**). *svr11-1* could also reverse the leaf variegation of the *var2-4* mutant, a stronger allele of *var2*, indicating that the suppression of *var2* leaf variegation by *svr11-1* does not depend on the nature of *var2* mutation and is not allele specific (**Figures 1C,D**).

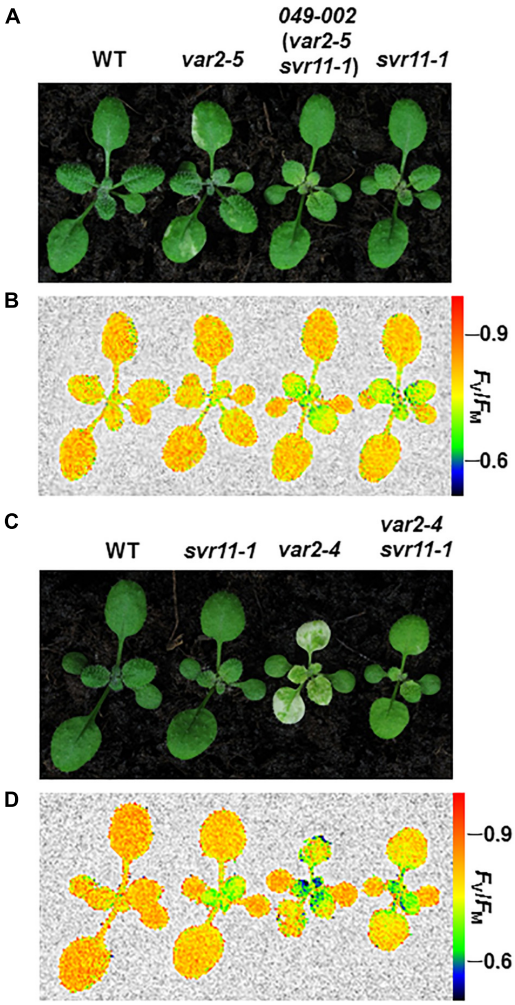

FIGURE 1 | Phenotypes of single and double suppressor mutants. **(A)** Representative 2-week-old seedlings of wild type (WT), *var2-5*, double suppressor mutant *049-002* (*var2-5 svr11-1*), and *svr11-1* plants. **(C)** Representative 2-week-old seedlings of wild type (WT), *svr11-1*, *var2-4*, and the double mutant *var2-4 svr11-1*. **(B,D)** Representative F_V/F_M measurement of the same group of plants used in **(A,C)**, respectively. The false color scale representing for the value of F_V/F_M is at the right of the figure. The measurement of F_V/F_M was repeated three times.

Molecular Cloning of *SVR11*

To clone *SVR11*, we first determined that the *svr11-1* mutant phenotype co-segregated with the resistance to herbicide Basta, suggesting the mutant is tagged by T-DNA insert(s) (data not

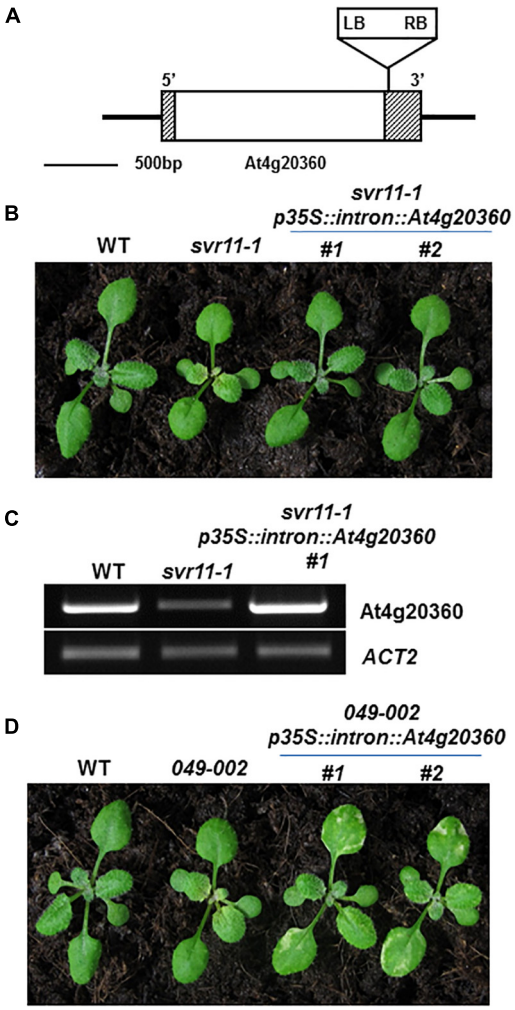

FIGURE 2 | Cloning of *SVR11* and complementation of *svr11-1*. **(A)** A T-DNA insertion was identified in the 3′-UTR of At4g20360 by inverse PCR. The left border (LB) and the right border (RB) were indicated. Gray boxes and the white box represent UTRs and the exon, respectively. **(B)** Representative 2-week-old wild-type, *svr11-1* and *svr11-1 p35S::intron At4g20360* (constitutive expression line of *At4g20360* in *svr11-1* background). **(C)** The accumulation of At4g20360 transcripts was indicated by semi-quantitative RT-PCR. The semi-quantitative RT-PCR was repeated three times. **(D)** Representative 2-week-old wild-type, *049-002* and *049-002 p35S::intron At4g20360* (constitutive expression of *At4g20360* in *049-002* background).

shown). Next, we carried out inverse PCR to identify the T-DNA insertion site and sequencing of inverse PCR products confirmed that the T-DNA was inserted in the 3′ UTR of *At4g20360* (**Figure 2A**). We found that *At4g20360* expression was reduced in *svr11-1*, likely a consequence of T-DNA insertion in 3′ UTR (**Figure 2C**). Complementation analysis was executed to confirm that the virescent phenotype in *svr11-1* and the suppression of *var2* variegation in *049-002* were due to the disruption of *SVR11* expression. To this end, we generated a binary vector in which a full-length *At4g20360* cDNA was driven by the constitutive CaMV 35S promoter. In addition, sequences of the first intron of At5g27700 were placed between the 35S promoter and the cDNA sequences to achieve better expression (Rose et al., 2008). This construct (p35S::intron::At4g20360) was transformed into *svr11-1* and *049-002*, respectively. We recovered multiple independent transgenic lines and confirmed that elevated expression of At4g20360 was able to complement the virescent phenotype of *svr11-1* (**Figure 2B**). Furthermore, ectopic expression of At4g20360 was able to restore the *var2-5* leaf variegation phenotype in *049-002* background (**Figure 2D**). Together, these data indicate that the virescent chloroplast defect in *svr11-1* and the suppression of *var2* leaf variegation in *049-002* were caused by reduced expression of At4g20360, and that *At4g20360* is *SVR11*.

SVR11/At4g20360 Defines a Putative Prokaryotic EF-Tu in Chloroplasts

Homologous sequences of SVR11 from different species were obtained from National Center for Biotechnology Information (NCBI) and their evolutionary relationship was analyzed (**Figure 3A**). SVR11 and SVR11-like proteins from these species were all annotated as prokaryotic translation elongation factor EF-Tu homologs. In prokaryotic organisms such as cyanobacteria and *E. coli*, only one copy of EF-Tu was identified. In contrast, eukaryotic photosynthetic species such as *Arabidopsis*, rice, moss, and green algae contains at least two EF-Tu homologs (**Figure 3A**).

The EF-Tu sequences grouped in the same clade with SVR11 in the phylogenetic tree were all predicted to contain chloroplast transit peptides (**Figure 3A** Clade 2, Emanuelsson et al., 1999). To confirm the sub-cellular localizations of SVR11, a transient expression vector was generated expressing a full-length *SVR11* cDNA fused in-frame at its C-terminus with green fluorescent protein (GFP), under the control of the 35S promoter (*p35S::SVR11-GFP*). This construct, as well as a control vector containing only the GFP (*p35S::GFP*), were introduced into Wild-type *Arabidopsis* leaf protoplasts, respectively, and their expressions were monitored by confocal microscopy. **Figure 3B** shows that GFP signals for *p35S::SVR11-GFP* appeared as distinct foci, which overlapped nicely with chlorophyll auto-fluorescence signals, suggesting co-localizations with chloroplasts. To examine if SVR11-GFP could also be targeted to mitochondria, we transient expressed *p35S::SVR11-GFP* in protoplasts isolated from transgenic lines stably expressing a mitochondrion marker protein tagged with mCherry, ScCOX4-mCherry (Nelson et al., 2007). SVR11-GFP did not overlap with signals of ScCOX4-mCherry, suggesting SVR11-GFP is likely not targeted to mitochondria (**Figure 3C**). These results demonstrate that the SVR11-GFP is targeted into the chloroplast and SVR11 is a nuclear encoded chloroplast protein. SVR11-like was predicted to be a mitochondrial EF-Tu (Nikolovski et al., 2012), or identified in the mitochondrial soluble protein by mass spectrometry (Ito et al., 2006). Interestingly, SVR11-like-GFP aggregate to large or small dots in the cytosol, neither targeted into mitochondria nor to chloroplasts (**Supplementary Figure S1**).

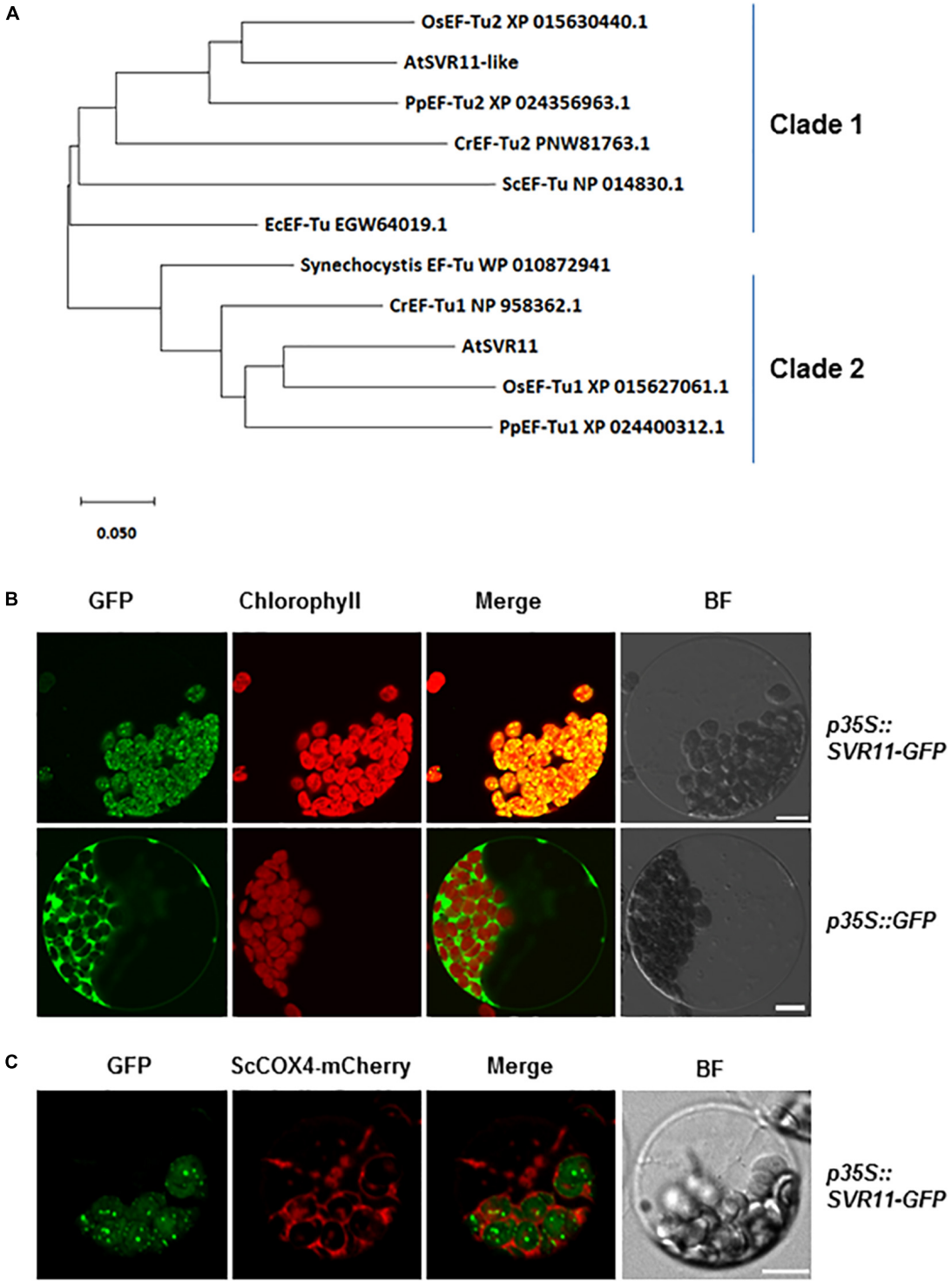

FIGURE 3 | Evolutionary relationships of SVR11 homologs and subcellular localization of SVR11. **(A)** Phylogenetic analysis of the SVR11 protein family. Full-length protein sequences of SVR11 homologous proteins of different species indicated by the accession numbers were obtained from NCBI using BLASTP. The neighbor-joining algorithm was used to generate the initial tree. **(B)** Leaf protoplasts prepared from wild type *Arabidopsis* plants were transformed with the *p35S::SVR11-GFP* fusion construct or the control construct p35S::GFP. Confocal microscopy was used to monitor fluorescence signals from the GFP channel (500–550 nm) and chlorophyll autofluorescence (663–738 nm). Bright field (BF) images served as controls for protoplast integrity. **(C)** Transient expression of *p35S::SVR11-GFP* fusion protein in protoplasts isolated from plants expressing a mitochondrion marker ScCOX4-mCherry (570–620 nm). Representative images of a single protoplast are shown. Bar stands for 10 μm.

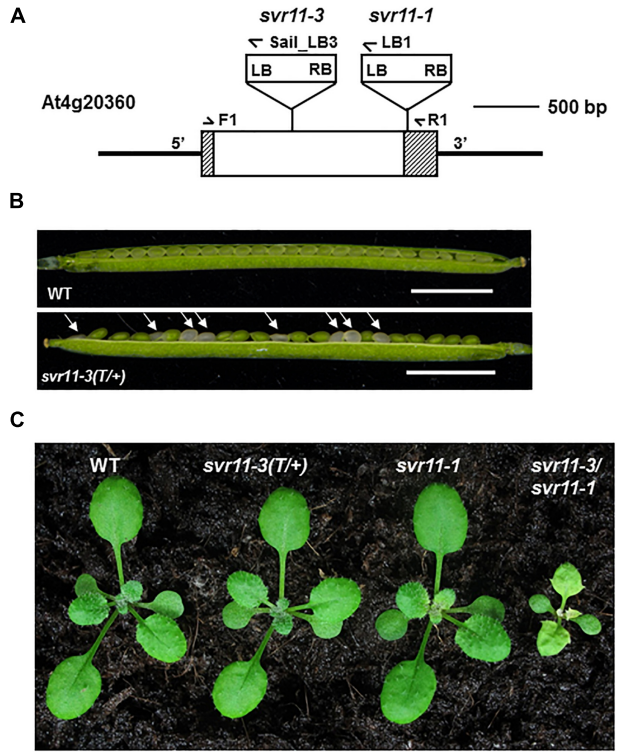

FIGURE 4 | Phenotypic characterization of the *svr11* T-DNA insertion null allele mutant. **(A)** Identification of a null allele of *SVR11*, *svr11-3*. **(B)** Developing seeds within a silique from a heterozygous *svr11-3* mutant and wild-type at the same developing state. Bar stands for 2,500 μm. **(C)** Representative 2-week-old wild-type, *svr11-3(T/+)*, *svr11-1*, *svr11-3/svr11-1* plants.

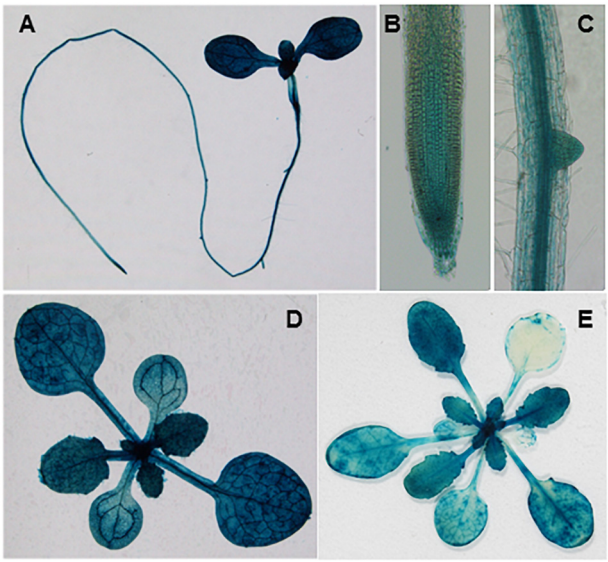

FIGURE 5 | Tissue expression patterns of *SVR11*. GUS staining of transgenic plants expressing the *SVR11* promoter-GUS fusion vector *pSVR11::uidA*. The GUS staining was performed with three independent transgenic lines. Representative whole seedling **(A)**, root tip **(B)**, and lateral root **(C)** of 6-day-old transgenic seedling grown on half-strength Murashige and Skoog (MS) solid medium containing 1% sucrose. Representative leaf tissues above the soil from 2-week-old **(D)** and 3-week-old **(E)** plants.

Moderate Heat Stress Has Little Impact on *var2* Variegations

It was reported that knock-down of chloroplastic EF-Tu in maize, *Arabidopsis*, and tomato mutants reduced heat tolerance (Ristic et al., 2004; Li et al., 2018). We then test if heat stress can affect the variegation phenotype of *var2* mutants. To avoid lethality caused by the severe heat stress at 45°C, a moderate level of heat stress at 38°C for 90 min were used as suggested (Queitsch et al., 2000). Moderate heat stress had little impact either on the variegation phenotype of *var2* and *var2* background suppressor mutants, or on the virescent phenotype of *svr11-1* (**Supplementary Figure S2**).

SVR11 Is Essential to Plant Development

To further examine the roles that SVR11 play in plant development, we sought for loss-of-function alleles of *SVR11*. We obtained a second allele of *svr11*, *CS819179* which contained a T-DNA inserted in the encoding sequence of *SVR11* (**Figure 4A**). No homozygous T-DNA insertion line was identified even backcrossed to wild-type five times, probably due to homozygote is embryo lethal. Terminated ovules were observed in the developing siliques in heterozygous mutants (**Figure 4B**). We renamed *CS819179* as *svr11-3*, and then crossed heterozygous *svr11-3(T/+)* to *svr11-1*. *svr11-1/svr11-3* was obtained by genotyping F1 generation, which is much smaller in size than *svr11-1* and the leaf blade is yellow-colored. We speculated that the phenotypic defect severity was determined by *SVR11* damage degree (**Figure 4C**).

SVR11 Is Abundant in Juvenile Tissues

To characterize the spatial and temporal expression profiles of *SVR11*, we generated a fusion construct in which the β-glucuronidase gene (GUS) gene was controlled by the *SVR11* promoter (1.5-kb region upstream of the *SVR11* start codon). This vector was transformed into wild-type plants and GUS activities of *pSVR11:GUS* transgenic lines were assayed at different growth stages. In brief, in 6-day-old seedlings GUS expression was detected including in the root tip and lateral roots, suggesting that SVR11 activities are necessary for both photosynthetic and non-photosynthetic tissues (**Figures 5A–C**), also in 2-week-old plants and 3-week-old juvenile rosette leaves (**Figures 5D,E**).

Chloroplast EF-Tu and IF3 Regulate Leaf Development

Previously, we have reported a *var2* suppressor locus *SVR9*, encoding a chloroplast translation initiation factor IF3, which mediates *var2* leaf variegation and leaf marginal serration formation (Zheng et al., 2016). Next, we tested genetically

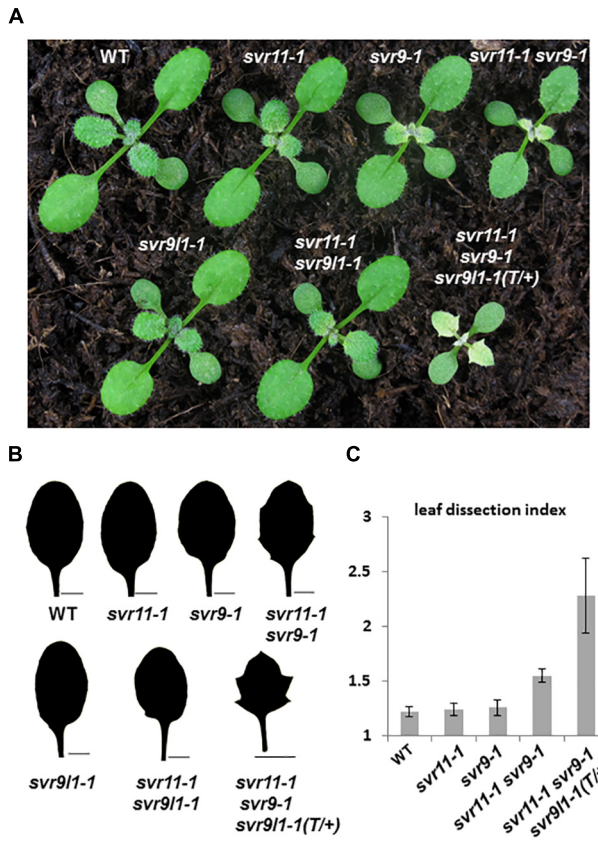

FIGURE 6 | Genetic interaction between *SVR11* and *SVR9*. **(A)** Representative 12-day-old wild-type, *svr11-1*, *svr9-1*, *svr11-1svr9-1*, *svr9l1-1*, *svr11-1 svr9l1-1,* and *svr11-1 svr9-1 svr9l1-1(T/+)*. **(B)** The third leaf silhouettes of 20-day-old plants. Bar for 2,000 μm. **(C)** Quantitative comparisons of leaf shapes in WT, *svr11-1*, *svr9-1*, *svr11-1 svr9-1*, and *svr11-1 svr9-1svr9l1-1(T/+)* shown in **(B)**, based on the leaf dissection index (perimeter^2/4π*leaf area). Fifteen individuals of each genotype were used in the statistical analysis.

the functional relationships between *SVR11* and *SVR9*, as well as *SVR9L1*, a functionally redundant homolog of *SVR9* (**Figure 6**) (Zheng et al., 2016). At the single mutant level, *svr9-1* showed a stronger degree of virescence than that of *svr11-1*, and *svr9l1-1* showed a WT-like phenotype, as reported (**Figure 6A**) (Zheng et al., 2016). Consistent with both EF-Tu and IF3's involvement in translation, *svr11-1 svr9-1* mutants were more virescent (**Figure 6**). The virescent level of *svr11-1*, *svr9-1* and *svr11-1 svr9-1* double mutants were quantified by measurement of F_V/F_M (**Supplementary Figure S3**). Interestingly, *svr11-1 svr9-1*, but not *svr11-1 svr9l1-1*, showed a prominent leaf margin serration phenotype (**Figure 6B**). Furthermore, we obtained mutants that are homozygous for *svr11-1* and *svr9-1* while heterozygous for *svr9l1-1* (*svr11-1 svr9-1 svr9l1-1* T/+). These mutants not only showed strong virescence phenotype, the leaf serration was also the most conspicuous (**Figures 6B,C**). The leaf serrations were further quantified by the leaf dissection index (perimeter^2/4π*leaf area) (Bilsborough et al., 2011) (**Figure 6C**).

We have shown that leaf serration phenotype may be associated with leaf vasculature development (Zheng et al., 2016). We then tested leaf vascular development and examined the cotyledon venation patterns in *svr11-1* and *svr11-1 svr9-1* double mutant. The numbers of closed areoles in mature cotyledons are indicators of leaf vascular development (Sieburth, 1999), and cotyledons from 10-day-old seedlings were observed under a dissecting microscope. Wild type cotyledons with two, three, and four areoles were predominant (Zheng et al., 2016, and also in the research, **Table 2**). In *svr11-1*, although the similar percentage of cotyledons show two, three or four areoles compared to wild type, cotyledons with only one areole were also identified in *svr11-1* (**Table 2**). Noticeably, cotyledons with only one areole or no closed areoles were drastically increased in *svr11-1 svr9-1* (**Figure 7** and **Table 2**). Taken together, these data show that chloroplast translation EF-Tu and IF3 activities act synergistically to regulate leaf margin and cotyledon vascular development.

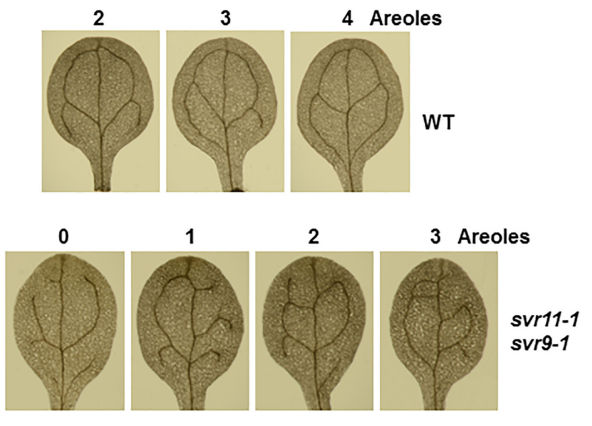

FIGURE 7 | Representative 10-day-old cotyledon vein patterns with different numbers of areoles from wild-type and *svr11-1 svr9-1*.

TABLE 2 | Quantification of cotyledon vein patterns in wild type, *svr11-1* and *svr11-1 svr9-1*.

Genotype	Total	Zero areole	One areole	Two areoles	Three areoles	Four areoles	Five areoles
WT	353	N.A.	N.A.	171 (48.4%)	134 (38.0%)	48 (13.6%)	N.A.
svr11-1	432	N.A.	21 (4.8%)	194 (44.9%)	167 (38.7%)	50 (11.6%)	N.A.
svr11-1 svr9-1	345	56 (16.2%)	147 (42.6%)	105 (30.4%)	32 (9.3%)	5 (1.4%)	N.A.

Cotyledon vein patterns were quantified in three independent biological replicates with each genotype line containing at least 100 seedlings. Numbers were added together from three independent biological replicates. Percentages of different types of areoles are indicated in the parentheses. N.A., not applicable.

DISCUSSION

Chloroplasts are semi-autonomous organelles that derived from ancient cyanobacterium-like organisms through the process of endosymbiosis (Nowack and Weber, 2018). One of the key evidence supporting the endosymbiosis theory is the discovery of prokaryotic gene expression systems in the chloroplast. In this study, we identified *svr11-1* as a genetic suppressor of the *Arabidopsis var2* mutant and confirmed that *SVR11* codes for a chloroplast-localized prokaryotic translation elongation factor EF-Tu. As a prokaryotic elongation factor, GTP-bound EF-Tu facilitates the transport of aminoacyl-tRNA to the A-site of the 70S ribosome during translation elongation (Krab and Parmeggiani, 2002). Consistent with their critical roles in translation, null alleles or higher-order mutants of many translation factors are lethal, suggesting essential roles of these factors for plant survival (Miura et al., 2007; Bryant et al., 2011; Zheng et al., 2016). Interestingly, *svr11-1* mutant is phenotypically reminiscent of *svr9-1*, defective in a chloroplast translation initiation factor IF3 (Zheng et al., 2016). Both mutants show a distinct virescent phenotype with more pronounced reductions of chlorophyll accumulation and photosynthetic capacities at young, dividing tissues, suggesting their activities are required at early process (Lopez-Juez and Pyke, 2005). This is in agreement with the higher expression of these genes in young tissues and higher needs for their activities in those tissues. It is conceivable that a higher demand for translation capacities at younger stage of development is necessary to establish robust phototropic growth. Findings from our group and others have shown that mutations in chloroplast 70S ribosome proteins mostly lead to rather uniform pale green or pale yellow leaf colorations (Bryant et al., 2011; Romani et al., 2012; Tiller et al., 2012; Liu et al., 2013). These findings suggest a possible regulatory way for translation factors and ribosomal proteins during chloroplast and leaf development at early stages.

Thylakoid-localized FtsHs are ATP-dependent zinc metalloproteases participating in the degradation of damaged photosynthetic subunits, especially damaged PSII reaction center D1 subunits during photoinhibition (Nishimura et al., 2016). *Arabidopsis* mutants *var1* and *var2*, defective in thylakoid-localized FtsH proteins VAR1/AtFtsH5 and VAR2/AtFtsH2, respectively, show unique leaf variegation phenotypes, suggesting that these FtsHs may play additional roles in chloroplast development besides D1 degradation (Chen et al., 2000; Takechi et al., 2000). Molecular genetics analyses of *var2* suppressor mutants have also established that the chloroplast development defect, i.e., the leaf variegation phenotype, of *var2* is dependent on functional chloroplast gene expression, especially chloroplast translation, providing further support for additional roles of VAR2/AtFtsH2 in chloroplast development (Miura et al., 2007; Yu et al., 2008; Liu et al., 2010, 2013; Putarjunan et al., 2013). Recently, we reported two *var2* suppressor loci, *SVR10*, coding for a member of circularly permuted GTPase family involved in the processing of plastid ribosomal RNAs, and *SVR9*, a chloroplast translation initiation factor IF3 involved in chloroplast translation (Kim et al., 2012; Qi et al., 2016; Zheng et al., 2016). In this report, building on the *var2* suppressor screening work, we found that a mutation in *SVR11*, encoding a chloroplast translation elongation factor EF-Tu, can suppress *var2* leaf variegated phenotype. The identification of *SVR11* as a *var2* suppression locus on one hand strengthens the functional relationship between VAR2/AtFtsH2 and chloroplast translation, on the other hand, it also provides further indication that VAR2/AtFtsH2 is related to the chloroplast translation process in general, rather than a specific functional link with individual components. Interestingly, through genetic enhancer analysis, we have recently for the first time established an intriguing link between VAR2/AtFtsH2 and cytosolic translation (Wang et al., 2018). In contrary to chloroplast translation, the reduction of cytosolic translation dramatically enhances *var2* leaf variegation, suggesting chloroplast development in *var2* is intimately regulated by cytosolic translation. Based on the suppression by reduced chloroplast translation and the enhancement by reduced cytosolic translation, a model was proposed in which FtsH may serve as an important factor in mediating the balance of cytosolic and chloroplast translation (Wang et al., 2018). Although the molecular mechanism underlying the maintenance of this balance remains unclear in higher plants, nuclear and mitochondrial translation balance has been shown to be vital of protein homeostasis in other model organisms (Topf et al., 2016).

The coordination between the nuclear and the chloroplast genome and gene expression requires fine regulation of bi-directional communications from nucleus to chloroplasts (anterograde) and also from chloroplasts to the nucleus (retrograde) (Jarvis and López-Juez, 2013). Given the importance and complexity, it came as no surprise that multiple regulatory pathways have been uncovered to ensure the coupling of the genomes. Canonical work have used the expressions of nuclear encoded photosynthetic genes, for example *LhcB* or *RbcS*, as marker genes to probe the retrograde regulation of these genes when chloroplast functional states were disturbed, for instance, when treated with photo-bleaching herbicide norflurazon or chloroplast translation inhibitor lincomycin (Nott et al., 2006; Chi et al., 2013; Kleine and Leister, 2016). It has also been long recognized that the retrograde regulation of nuclear gene expression also involves the modulation of leaf development by the functional state of chloroplasts (Pogson et al., 2015). For example, abnormal leaf mesophyll developments were observed in the white leaf sectors of *Arabidopsis immutans* mutant, or in white tissues after norflurazon treatment (Aluru et al., 2009). Despite the accumulating evidence, our understanding of how states of chloroplasts affect leaf development remains limited. We previously reported that the chloroplast translation initiation factor IF3/SVR9 regulates chloroplast development, as well as leaf development, including leaf margin and cotyledon vasculature development (Zheng et al., 2016). In addition, we reported that mutations in *SVR9* affect auxin homeostasis, and leaf margin development in a CUC2-dependent way (Nikovics et al., 2006; Zheng et al., 2016). In this work, we found that *SVR11* also regulate leaf margin and cotyledon venation.

Moreover, *SVR11* and *SVR9* work synergistically to regulate leaf margin development and cotyledon venation patterns. These findings reinforce the notion that chloroplast translation defects can trigger a signaling pathway to regulate leaf development (Zheng et al., 2016). This pathway seems to be activated only by certain types of translation defects caused mainly by the lack of translation factors, as not all chloroplast translation mutant display related phenotypes. Recently, it was shown that VAR2/AtFtsH2 may mediate a singlet oxygen signaling pathway from chloroplasts to the nucleus (Wang et al., 2016). Future research is warranted to address the relationship between these pathways and the components of this signaling pathway from the chloroplast to the nucleus.

AUTHOR CONTRIBUTIONS

YQ and FY conceived and coordinated the study and wrote the manuscript. SL, LZ, JJ, JG, and MZ designed, performed, and analyzed the experiments shown in **Figures 1–7**. JZ, JS, LA, and XL provided technical assistance and contributed to the preparation of the figures. All authors reviewed the results and approved the final version of the manuscript.

FUNDING

This work was supported by National Natural Science Foundation of China Grants 31741010 (to YQ), 31470290 (to LA), and 31770345 (to JS), and by Fundamental Research Funds for the Central Universities Grants 2452018152 (to YQ).

SUPPLEMENTARY MATERIAL

The Supplementary Material for this article can be found online at: https://www.frontiersin.org/articles/10.3389/fpls.2019.00295/full#supplementary-material

FIGURE S1 | Transient expression of *p35S::SVR11-like-GFP* fusion protein in leaf protoplasts of plants expressing the mitochondrion marker ScCOX4-mCherry. Representative images of a single protoplast are shown. Bar stands for 10 μm.

FIGURE S2 | Representative seedlings treated with a moderate level heat stress. Eight-day-old seedlings grown at 22°C were treated at 38°C for 90 min, and then returned into 22°C for recovery. After 6 days recovery, seedlings were photographed.

FIGURE S3 | Representative 2-week-old seedlings and the corresponding F_V/F_M images of wild type, *svr11-1*, *svr9-1*, and the double mutant *svr11-1 svr9-1*. The average value of F_O, F_M, F_V/F_M were calculated from at least 10 individuals from each genotype.

REFERENCES

Adam, Z., Frottin, F., Espagne, C., Meinnel, T., and Giglione, C. (2011). Interplay between N-terminal methionine excision and FtsH protease is essential for normal chloroplast development and function in Arabidopsis. *Plant Cell* 23, 3745–3760. doi: 10.1105/tpc.111.087239

Aluru, M. R., Zola, J., Foudree, A., and Rodermel, S. R. (2009). Chloroplast photooxidation-induced transcriptome reprogramming in Arabidopsis immutans white leaf sectors. *Plant Physiol.* 150, 904–923. doi: 10.1104/pp.109.135780

Bilsborough, G. D., Runions, A., Barkoulas, M., Jenkins, H. W., Hasson, A., Galinha, C., et al. (2011). Model for the regulation of Arabidopsis thaliana leaf margin development. *Proc. Natl. Acad. Sci. U.S.A.* 108, 3424–3429. doi: 10.1073/pnas.1015162108

Bryant, N., Lloyd, J., Sweeney, C., Myouga, F., and Meinke, D. (2011). Identification of nuclear genes encoding chloroplast-localized proteins required for embryo development in Arabidopsis. *Plant Physiol.* 155, 1678–1689. doi: 10.1104/pp.110.168120

Chen, M., Choi, Y., Voytas, D. F., and Rodermel, S. (2000). Mutations in the Arabidopsis VAR2 locus cause leaf variegation due to the loss of a chloroplast FtsH protease. *Plant J.* 22, 303–313. doi: 10.1046/j.1365-313x.2000.00738.x

Chi, W., Sun, X., and Zhang, L. (2013). Intracellular signaling from plastid to nucleus. *Annu. Rev. Plant Biol.* 64, 559–582. doi: 10.1146/annurev-arplant-050312-120147

Clough, S. J., and Bent, A. F. (1998). Floral dip: a simplified method for Agrobacterium-mediated transformation of *Arabidopsis thaliana*. *Plant J.* 16, 735–743. doi: 10.1046/j.1365-313x.1998.00343.x

Emanuelsson, O., Nielsen, H., and von Heijne, G. (1999). ChloroP, a neural network-based method for predicting chloroplast transit peptides and their cleavage sites. *Protein Sci.* 8, 978–984. doi: 10.1110/ps.8.5.978

Ito, J., Heazlewood, J. L., and Millar, A. H. (2006). Analysis of the soluble ATP-binding proteome of plant mitochondria identifies new proteins and nucleotide triphosphate interactions within the matrix. *J. Proteome Res.* 5, 3459–3469. doi: 10.1021/pr060403j

Janska, H., Kwasniak, M., and Szczepanowska, J. (2013). Protein quality control in organelles – AAA/FtsH story. *Biochim. Biophys. Acta* 1833, 381–387. doi: 10.1016/j.bbamcr.2012.03.016

Jarvis, P., and López-Juez, E. (2013). Biogenesis and homeostasis of chloroplasts and other plastids. *Nat. Rev. Mol. Cell Biol.* 14, 787–802. doi: 10.1038/nrm3702

Jefferson, R. A., Kavanagh, T. A., and Bevan, M. W. (1987). GUS fusions: beta-glucuronidase as a sensitive and versatile gene fusion marker in higher plants. *EMBO J.* 6, 3901–3907. doi: 10.1002/j.1460-2075.1987.tb02730.x

Kato, Y., Miura, E., Ido, K., Ifuku, K., and Sakamoto, W. (2009). The variegated mutants lacking chloroplastic FtsHs are defective in D1 degradation and accumulate reactive oxygen species. *Plant Physiol.* 151, 1790–1801. doi: 10.1104/pp.109.146589

Kim, B. H., Malec, P., Waloszek, A., and von Arnim, A. G. (2012). Arabidopsis BPG2: a phytochrome-regulated gene whose protein product binds to plastid ribosomal RNAs. *Planta* 236, 677–690. doi: 10.1007/s00425-012-1638-6

Kleine, T., and Leister, D. (2016). Retrograde signaling: organelles go networking. *Biochim. Biophys. Acta* 1857, 1313–1325. doi: 10.1016/j.bbabio.2016.03.017

Krab, I. M., and Parmeggiani, A. (1998). EF-Tu, a GTPase odyssey. *Biochim. Biophys. Acta* 1443, 1–22. doi: 10.1016/S0167-4781(98)00169-9

Krab, I. M., and Parmeggiani, A. (2002). Mechanisms of EF-Tu, a pioneer GTPase. *Prog. Nucleic Acid Res. Mol. Biol.* 71, 513–551. doi: 10.1016/S0079-6603(02)71050-7

Kumar, S., Stecher, G., Li, M., Knyaz, C., and Tamura, K. (2018). MEGA X: molecular evolutionary genetics analysis across computing platforms. *Mol. Biol. Evol.* 35, 1547–1549. doi: 10.1093/molbev/msy096

Laursen, B. S., Sørensen, H. P., Mortensen, K. K., and Sperling-Petersen, H. U. (2005). Initiation of protein synthesis in bacteria. *Microbiol. Mol. Biol. Rev.* 69, 101–123. doi: 10.1128/MMBR.69.1.101-123.2005

Li, X., Cai, C., Wang, Z., Fan, B., Zhu, C., and Chen, Z. (2018). Plastid translation elongation factor tu is prone to heat-induced aggregation despite its critical role in plant heat tolerance. *Plant Physiol.* 176, 3027–3045. doi: 10.1104/pp.17.01672

Lindahl, M., Spetea, C., Hundal, T., Oppenheim, A. B., Adam, Z., and Andersson, B. (2000). The thylakoid FtsH protease plays a role in the light-induced turnover of the photosystem II D1 protein. *Plant Cell* 12, 419–431. doi: 10.1105/tpc.12.3.419

Liu, X., Rodermel, S. R., and Yu, F. (2010). A var2 leaf variegation suppressor locus, SUPPRESSOR OF VARIEGATION3, encodes a putative chloroplast translation elongation factor that is important for chloroplast development in the cold. *BMC Plant Biol.* 10:287. doi: 10.1186/1471-2229-10-287

Liu, X., Zheng, M., Wang, R., Wang, R., An, L., Rodermel, S. R., et al. (2013). Genetic interactions reveal that specific defects of chloroplast translation are

associated with the suppression of var2-mediated leaf variegation. *J. Integr. Plant Biol.* 55, 979–993. doi: 10.1111/jipb.12078

Lopez-Juez, E., and Pyke, K. A. (2005). Plastids unleashed: their development and their integration in plant development. *Int. J. Dev. Biol.* 49, 557–577. doi: 10.1387/ijdb.051997el

Malnoë, A., Wang, F., Girard-Bascou, J., Wollman, F. A., and de Vitry, C. (2014). Thylakoid FtsH protease contributes to photosystem II and cytochrome b6f remodeling in *Chlamydomonas reinhardtii* under stress conditions. *Plant Cell* 26, 373–390. doi: 10.1105/tpc.113.120113

Martin, W., Rujan, T., Richly, E., Hansen, A., Cornelsen, S., Lins, T., et al. (2002). Evolutionary analysis of Arabidopsis, cyanobacterial, and chloroplast genomes reveals plastid phylogeny and thousands of cyanobacterial genes in the nucleus. *Proc. Natl. Acad. Sci. U.S.A.* 99, 12246–12251. doi: 10.1073/pnas.182432999

Miura, E., Kato, Y., Matsushima, R., Albrecht, V., Laalami, S., and Sakamoto, W. (2007). The balance between protein synthesis and degradation in chloroplasts determines leaf variegation in Arabidopsis yellow variegated mutants. *Plant Cell* 19, 1313–1328. doi: 10.1105/tpc.106.049270

Nelson, B. K., Cai, X., and Nebenführ, A. (2007). A multicolored set of *in vivo* organelle markers for co-localization studies in Arabidopsis and other plants. *Plant J.* 51, 1126–1136. doi: 10.1111/j.1365-313X.2007.03212.x

Nesbit, A. D., Whippo, C., Hangarter, R. P., and Kehoe, D. M. (2015). Translation initiation factor 3 families: what are their roles in regulating cyanobacterial and chloroplast gene expression? *Photosynth. Res.* 126, 147–159. doi: 10.1007/s11120-015-0074-4

Nikolovski, N., Rubtsov, D., Segura, M. P., Miles, G. P., Stevens, T. J., Dunkley, T. P., et al. (2012). Putative glycosyltransferases and other plant Golgi apparatus proteins are revealed by LOPIT proteomics. *Plant Physiol.* 160, 1037–1051. doi: 10.1104/pp.112.204263

Nikovics, K., Blein, T., Peaucelle, A., Ishida, T., Morin, H., Aida, M., et al. (2006). The balance between the MIR164A and CUC2 genes controls leaf margin serration in Arabidopsis. *Plant Cell* 18, 2929–2945. doi: 10.1105/tpc.106.045617

Nishimura, K., Kato, Y., and Sakamoto, W. (2016). Chloroplast proteases: updates on proteolysis within and across suborganellar compartments. *Plant Physiol.* 171, 2280–2293. doi: 10.1104/pp.16.00330

Nott, A., Jung, H. S., Koussevitzky, S., and Chory, J. (2006). Plastid-to-nucleus retrograde signaling. *Annu. Rev. Plant Biol.* 57, 739–759. doi: 10.1146/annurev.arplant.57.032905.105310

Nowack, E. C. M., and Weber, A. P. M. (2018). Genomics-informed insights into endosymbiotic organelle evolution in photosynthetic eukaryotes. *Annu. Rev. Plant Biol.* 69, 51–84. doi: 10.1146/annurev-arplant-042817-040209

Park, S., and Rodermel, S. R. (2004). Mutations in ClpC2/Hsp100 suppress the requirement for FtsH in thylakoid membrane biogenesis. *Proc. Natl. Acad. Sci. U.S.A.* 101, 12765–12770. doi: 10.1073/pnas.0402764101

Pogson, B. J., Ganguly, D., and Albrecht-Borth, V. (2015). Insights into chloroplast biogenesis and development. *Biochim. Biophys. Acta* 1847, 1017–1024. doi: 10.1016/j.bbabio.2015.02.003

Putarjunan, A., Liu, X., Nolan, T., Yu, F., and Rodermel, S. (2013). Understanding chloroplast biogenesis using second-site suppressors of immutans and var2. *Photosynth. Res.* 116, 437–453. doi: 10.1007/s11120-013-9855-9

Qi, Y., Zhao, J., An, R., Zhang, J., Liang, S., Shao, J., et al. (2016). Mutations in circularly permuted GTPase family genes AtNOA1/RIF1/SVR10 and BPG2 suppress var2-mediated leaf variegation in Arabidopsis thaliana. *Photosynth. Res.* 127, 355–367. doi: 10.1007/s11120-015-0195-9

Queitsch, C., Hong, S. W., Vierling, E., and Lindquist, S. (2000). Heat shock protein 101 plays a crucial role in thermotolerance in Arabidopsis. *Plant Cell* 12, 479–492. doi: 10.1105/tpc.12.4.479

Ristic, Z., Wilson, K., Nelsen, C., Momcilovic, I., Kobayashi, S., Meeley, R., et al. (2004). A maize mutant with decreased capacity to accumulate chloroplast protein synthesis elongation factor (EF-Tu) displays reduced tolerance to heat stress. *Plant Sci.* 167, 1367–1374. doi: 10.1016/j.plantsci.2004.07.016

Romani, I., Tadini, L., Rossi, F., Masiero, S., Pribil, M., Jahns, P., et al. (2012). Versatile roles of Arabidopsis plastid ribosomal proteins in plant growth and development. *Plant J.* 72, 922–934. doi: 10.1111/tpj.12000

Rose, A. B., Elfersi, T., Parra, G., and Korf, I. (2008). Promoter-proximal introns in Arabidopsis thaliana are enriched in dispersed signals that elevate gene expression. *Plant Cell* 20, 543–551. doi: 10.1105/tpc.107.057190

Sakamoto, W., Tamura, T., Hanba-Tomita, Y., Murata, M., and Sodmergen. (2002). The VAR1 locus of Arabidopsis encodes a chloroplastic FtsH and is responsible for leaf variegation in the mutant alleles. *Genes Cells* 7, 769–780. doi: 10.1046/j.1365-2443.2002.00558.x

Shen, Y., Li, C., McCarty, D. R., Meeley, R., and Tan, B. C. (2013). Embryo defective12 encodes the plastid initiation factor 3 and is essential for embryogenesis in maize. *Plant J.* 74, 792–804. doi: 10.1111/tpj.12161

Sieburth, L. E. (1999). Auxin is required for leaf vein pattern in Arabidopsis. *Plant Physiol.* 121, 1179–1190. doi: 10.1104/pp.121.4.1179

Takechi, K., Sodmergen, Murata, M., Motoyoshi, F., and Sakamoto, W. (2000). The YELLOW VARIEGATED (VAR2) locus encodes a homologue of FtsH, an ATP-dependent protease in Arabidopsis. *Plant Cell Physiol.* 41, 1334–1346. doi: 10.1093/pcp/pcd067

Tiller, N., and Bock, R. (2014). The translational apparatus of plastids and its role in plant development. *Mol Plant.* 7, 1105–1120. doi: 10.1093/mp/ssu022

Tiller, N., Weingartner, M., Thiele, W., Maximova, E., Schöttler, M. A., and Bock, R. (2012). The plastid-specific ribosomal proteins of Arabidopsis thaliana can be divided into non-essential proteins and genuine ribosomal proteins. *Plant J.* 69, 302–316. doi: 10.1111/j.1365-313X.2011.04791.x

Timmis, J. N., Ayliffe, M. A., Huang, C. Y., and Martin, W. (2004). Endosymbiotic gene transfer: organelle genomes forge eukaryotic chromosomes. *Nat. Rev. Genet.* 5, 123–135. doi: 10.1038/nrg1271

Topf, U., Wrobel, L., and Chacinska, A. (2016). Chatty mitochondria: keeping balance in cellular protein homeostasis. *Trends Cell Biol.* 26, 577–586. doi: 10.1016/j.tcb.2016.03.002

Wang, L., Kim, C., Xu, X., Piskurewicz, U., Dogra, V., Singh, S., et al. (2016). Singlet oxygen- and EXECUTER1-mediated signaling is initiated in grana margins and depends on the protease FtsH2. *Proc. Natl. Acad. Sci. U.S.A.* 113, E3792–E3800. doi: 10.1073/pnas.1603562113

Wang, R., Zhao, J., Jia, M., Xu, N., Liang, S., Shao, J., et al. (2018). Balance between cytosolic and chloroplast translation affects leaf variegation. *Plant Physiol.* 176, 804–818. doi: 10.1104/pp.17.00673

Xiang, C., Han, P., Lutziger, I., Wang, K., and Oliver, D. J. (1999). A mini binary vector series for plant transformation. *Plant Mol. Biol.* 40, 711–717. doi: 10.1023/a:1006201910593

Yamaguchi, K., and Subramanian, A. R. (2000). The plastid ribosomal proteins. Identification of all the proteins in the 50 S subunit of an organelle ribosome (chloroplast). *J. Biol. Chem.* 275, 28466–28482. doi: 10.1074/jbc.M005012200

Yamaguchi, K., von Knoblauch, K., and Subramanian, A. R. (2000). The plastid ribosomal proteins. Identification of all the proteins in the 30 S subunit of an organelle ribosome (chloroplast). *J. Biol. Chem.* 275, 28455–28465. doi: 10.1074/jbc.M004350200

Yoo, S. D., Cho, Y. H., and Sheen, J. (2007). Arabidopsis mesophyll protoplasts: a versatile cell system for transient gene expression analysis. *Nat. Protoc.* 2, 1565–1572. doi: 10.1038/nprot.2007.199

Yu, F., Liu, X., Alsheikh, M., Park, S., and Rodermel, S. (2008). Mutations in SUPPRESSOR OF VARIEGATION1, a factor required for normal chloroplast translation, suppress var2-mediated leaf variegation in Arabidopsis. *Plant Cell* 20, 1786–1804. doi: 10.1105/tpc.107.054965

Yu, F., Park, S., and Rodermel, S. R. (2004). The Arabidopsis FtsH metalloprotease gene family: interchangeability of subunits in chloroplast oligomeric complexes. *Plant J.* 37, 864–876. doi: 10.1111/j.1365-313X.2003.02014.x

Zaltsman, A., Ori, N., and Adam, Z. (2005). Two types of FtsH protease subunits are required for chloroplast biogenesis and Photosystem II repair in Arabidopsis. *Plant Cell* 17, 2782–2790. doi: 10.1105/tpc.105.035071

Zheng, M., Liu, X., Liang, S., Fu, S., Qi, Y., Zhao, J., et al. (2016). Chloroplast translation initiation factors regulate leaf variegation and development. *Plant Physiol.* 172, 1117–1130. doi: 10.1104/pp.15.02040

Conflict of Interest Statement: The authors declare that the research was conducted in the absence of any commercial or financial relationships that could be construed as a potential conflict of interest.

frontiers in Plant Science

ORIGINAL RESEARCH
published: 12 April 2019
doi: 10.3389/fpls.2019.00446

PPR Protein BFA2 Is Essential for the Accumulation of the *atpH/F* Transcript in Chloroplasts

Lin Zhang[1], Wen Zhou[2], Liping Che[1], Jean-David Rochaix[3], Congming Lu[2], Wenjing Li[4] and Lianwei Peng[1]**

[1] Shanghai Key Laboratory of Plant Molecular Sciences, College of Life Sciences, Shanghai Normal University, Shanghai, China, [2] State Key Laboratory of Crop Biology, College of Life Sciences, Shandong Agricultural University, Tai'an, China, [3] Departments of Molecular Biology and Plant Biology, University of Geneva, Geneva, Switzerland, [4] College of Life Sciences, Langfang Normal University, Langfang, China

As a fascinating and complicated nanomotor, chloroplast ATP synthase comprises nine subunits encoded by both the nuclear and plastid genomes. Because of its uneven subunit stoichiometry, biogenesis of ATP synthase and expression of plastid-encoded ATP synthase genes requires assistance by nucleus-encoded factors involved in transcriptional, post-transcriptional, and translational steps. In this study, we report a P-class pentatricopeptide repeat (PPR) protein BFA2 (Biogenesis Factor required for ATP synthase 2) that is essential for accumulation of the dicistronic *atpH/F* transcript in Arabidopsis chloroplasts. A loss-of-function mutation in *BFA2* results in a specific reduction of more than 3/4 of chloroplast ATP synthase, which is likely due to the absence of dicistronic *atpH/F* transcript. BFA2 protein contains 22 putative PPR motifs and exclusively localizes in the chloroplast. Bioinformatics and Electrophoretic Mobility Shift Assays (EMSA) analysis showed that BFA2 binds to the consensus sequence of the *atpF-atpA* intergenic region in a sequence-specific manner. However, translation initiation of the *atpA* was not affected in the *bfa2* mutant. Thus, we propose that the chloroplast PPR protein BFA2 mainly acts as barrier to prevent the *atpH/F* transcript degradation by exoribonucleases by binding to the consensus sequence of the *atpF-atpA* intergenic region.

Keywords: chloroplast ATP synthase, PPR protein, gene expression, photosynthesis, stability

OPEN ACCESS

Edited by:
Hongbo Gao,
Beijing Forestry University, China

Reviewed by:
Peng Wang,
Humboldt University Berlin, Germany
Aigen Fu,
Northwest University, China

****Correspondence:***
Wenjing Li
liwenjing@lfnu.edu.cn
Lianwei Peng
penglianwei@shnu.edu.cn

Specialty section:
This article was submitted to Plant Physiology, a section of the journal Frontiers in Plant Science

Received: *24 February 2019*
Accepted: *25 March 2019*
Published: *12 April 2019*

Citation:
Zhang L, Zhou W, Che L, Rochaix J-D, Lu C, Li W and Peng L (2019) PPR Protein BFA2 Is Essential for the Accumulation of the atpH/F Transcript in Chloroplasts. Front. Plant Sci. 10:446. doi: 10.3389/fpls.2019.00446

INTRODUCTION

Chloroplasts in photosynthetic eukaryotes are thought to have originated from cyanobacteria through endosymbiosis. During evolution, most of the genes from the cyanobacterial ancestor were transferred to the nucleus of the host cell and chloroplasts have only retained about 100 genes (Martin et al., 2002). These plastid genes encode proteins required for transcription and translation as well as the essential components of photosynthetic complexes. To ensure efficient gene expression, chloroplasts require a vast number of nuclear-encoded protein factors facilitating transcription, RNA stabilization, splicing, editing, and translation (Stern et al., 2010; Barkan, 2011). Among these factors, pentatricopeptide repeat (PPR) proteins are highly prominent and involved in

various steps of RNA metabolism and protein translation (Schmitz-Linneweber and Small, 2008). There are hundreds of PPR proteins in land plants most of which function in chloroplast and mitochondrial gene expression (Barkan and Small, 2014). PPR proteins comprise a large class of proteins with tandem arrays of a 35-amino-acid degenerate motif (Small and Peeters, 2000). According to the PPR motif type, PPR proteins can be divided into two major subfamilies, P and PLS. While P-type PPR proteins contain only P (35 amino acids) motifs with one or more tandem arrays, PLS-class PPR proteins have tandem triplet arrays of P, L (35–36 amino acids), and S (31 amino acids) motifs. Extensive studies showed that the P-class PPR proteins are involved in RNA stabilization, cleavage, and splicing as well as in the activation of translation (Barkan and Small, 2014). A few P-class PPR proteins also contain a small-MutS-related (SMR) motif at their C-terminus, which was recently shown to have RNA endonuclease activity *in vitro* (Zhou et al., 2017). The PLS-class PPR proteins usually contain C-terminal E and DYW motifs which are required for RNA editing (Shikanai, 2015).

Chloroplast ATP synthase is a multi-subunit complex located in the thylakoid membranes. It produces ATP from ADP by utilizing the proton motive force generated by photosynthetic electron transport. Chloroplast ATP synthase is composed of the two CF_o and CF_1 modules, and they contain five and four subunits with the stoichiometry $\alpha_3\beta_3\gamma_1\varepsilon_1\delta_1$ and $I_1II_1III_{14}IV_1$, respectively (Hahn et al., 2018), encoded by both the nuclear and chloroplast genomes. Chloroplast-encoded ATP synthase subunits arise from two polycistronic chloroplast transcription units, the large (*atpI/H/F/A*) and the small (*atpB/E*) *atp* operons. Both operons are transcribed by the plastid-encoded RNA polymerase (PEP) and several sigma factors are required (Malik Ghulam et al., 2012).

During the past decade, several nucleus-encoded factors have been shown to be involved in the expression of *atp* genes. For the large *atp* operon, P-class PPR protein PPR10 binds to the intergenic regions of *atpI-atpH* and *psaJ-rpl33* (Pfalz et al., 2009). The binding of PPR10 to the 5′ end of *atpH* not only stabilizes *atpH* transcripts by blocking 5′→3′ exoribonucleases but also alters the structure of the 5′ end of *atpH* to promote activation of translation initiation (Prikryl et al., 2011). The a*tpF* gene contains a single intron which belongs to the group-II intron family. Splicing of the *atpF* intron requires several protein factors such as CRS1, RNC1, WHY1, WTF1, MatK, and AEF1/MPR25 (Till et al., 2001; Watkins et al., 2007; Prikryl et al., 2008; Kroeger et al., 2009; Zoschke et al., 2010; Yap et al., 2015). Besides splicing, PPR protein AEF1/MPR25 is also required for editing *atpF* RNA in Arabidopsis (Yap et al., 2015). In the chloroplast of *Chlamydomonas reinhardtii*, the TDA1 protein is involved in the trapping and translation activation of *atpA* transcripts (Eberhard et al., 2011). In the case of the small *atp* operon, the PPR-SMR protein ATP4/SVR7 as well as the ATP1 protein have been proposed to be involved in the translation of the *atpB/E* mRNA in maize and Arabidopsis (McCormac and Barkan, 1999; Zoschke et al., 2012, 2013).

In this study, we report the characterization of a chloroplast PPR protein called BFA2 (Biogenesis Factors required for ATP synthase 2) that binds to the *atpF-atpA* intergenic region in a sequence-specific manner. Our results demonstrated that binding of BFA2 to the 3′-UTR of *atpH/F* is essential for stabilization of *atpH/F* RNA.

MATERIALS AND METHODS

Plant Material and Growth Conditions

Arabidopsis plants were grown on soil in the greenhouse (80 μmol photons m^{-2} s^{-1}, 16 h photoperiod, 23°C) for 3–4 weeks. The *bfa2-1* mutant was isolated from a collection of pSKI015 insertion Arabidopsis lines using the FluorCam imaging fluorometer (FC 800-C, PSI, Czech Republic) (Zhang et al., 2016). The *bfa2-2* mutant (SAIL_571_H02) was obtained from NASC and its T-DNA insertion site was confirmed by genomic PCR and subsequent sequencing of the PCR products. For complementation analysis, a genomic DNA fragment of the *BFA2* gene (3753 bp) was cloned into the pBI121 binary vector. The resulting construct was transformed into *Agrobacterium tumefaciens* C58C and then introduced into *bfa2-1* and *bfa2-2* plants by floral dip transformation.

RNA Extraction, RNA Blotting, and cRT-PCR Assay

Total RNA was isolated from rosette leaves using TRIzol Reagent (Invitrogen Life Technologies). For RNA blot analyses, a total of 5 μg (for *atpB* and *Actin 7*) or 2.5 μg (for *atpI*, *atpH*, *atpE*, *atpF*, *atpF* intron, and *atpA*) RNA was fractioned by electrophoresis on 1.5% formaldehyde-containing agarose gels and blotted onto nylon membranes (Hybond-N^+, GE Healthcare). The RNA was fixed by UV crosslinking (HL-2000 HybriLinker). Pre-hybridization and hybridization were carried out at 50°C with the DIG Easy Hyb (Roche) buffer. The probes were amplified from DNA and labeled with digoxigenin-11-dUTP according to the manufacturer's instructions. Signals were visualized with chemiluminescence analyzer or X-film.

For circular RT-PCR (cRT-PCR) analysis, total RNA was treated with RNase-free DNase I (Takara) to remove the residual DNA before further analysis. 10 μg of total RNA was self-ligated for 2 h at 25°C with 10 U of T4 RNA ligase (New England Biolabs). After ligation, RNA was extracted and resuspended in 10 μl of DEPC-treated water. Reverse transcription was performed using 20 pmol of primer and 5 μg of self-ligated RNA for 1 h at 42°C with 200 U of M-MLV reverse transcriptase (Thermo). After transcription, 1/20th of cDNA was used in a single PCR amplification reaction and the DNA products were then cloned in the pMD-18T vector for sequencing. The primers used this experiment are listed in **Supplementary Table S2**.

Subcellular Localization of GFP Protein

For subcellular localization of GFP protein, the first 200 amino acids (to ensure the complete targeting information of BFA2, the N-terminal 200 amino acids including the first PPR motif were used) of BFA2 were fused in-frame with GFP in the pBI221 vector. The chloroplast and mitochondrial markers were constructed according to Zhang et al. (2016). The resulting

constructs were transformed into Arabidopsis protoplasts by PEG-mediated transformation and the protoplasts were placed in darkness for 16 h at 23^{o}C. Transient GFP expression was observed using a confocal laser scanning microscope (LSM 510 Meta; Zeiss).

Electrophoretic Mobility Shift Assays

To express the recombinant BFA2-MBP protein, the cDNA sequence encoding amino acids 62–904 of BFA2 was subcloned into the plasmid pMAL-c5x (New England Biolabs). Expression was induced in *E. coli* BL21 strain with 0.3 mM isopropyl β-D-1-thiogalacopyranoside for 20 h at 16^{o}C. Purification of the recombinant protein was performed according to the New England Biolabs protocol. The RNA probe (5′-UAUAGGCAUUAUUUUUUUUUCU-3′, *atpF* sRNA) was chemically synthesized, and its 5′-end was labeled by biotin (Takara Co., Ltd.). For competition assays, a specific probe (nonlabeled *atpF* sRNA) and a nonspecific probe (5′-UUAUGACGAUACUCGGUAGCAUAGAUAUAA-3′; 5′-end of the *ndhA* mRNA) were chemically synthesized.

Recombinant BFA2-MBP was incubated with biotinylated *atpF* sRNA for 30 min at 20^{o}C in the binding buffer (10 mM HEPES, pH 7.5, 20 mM KCl, 2 mM $MgCl_2$, 1 mM DTT, 5% glycerol, 1 μg tRNA). Subsequently, the reactions were resolved on 6% native polyacrylamide gels containing 2.5% glycerol. The signal was detected with the chemiluminescent detection kit (Thermo, 89880). For competition assays, specific probe and nonspecific probes were added in the reaction buffer.

Other Methods

Polyclonal antibody against BFA2 was raised in rabbits using the recombinant BFA2 protein (amino acids 62–300 of BFA2). Chlorophyll fluorescence analysis, thylakoid membrane and stromal protein isolation, BN-PAGE, 2D/SDS-PAGE, and immunoblot analysis were performed as previously described (Li et al., 2019). The $g_H{}^+$ was monitored with the Dual PAM-100 according to previously described methods (Rott et al., 2011; Zhang et al., 2018). Polysome association analyses were performed as previously described (Zhang et al., 2018). The rRNAs were stained by Super GelRed (US Everbright Inc., Suzhou, China) and used as fractionation and loading controls. Chloroplast protein labeling and chase was performed as previously described (Zhang et al., 2016, 2018). Immunoblot signals were detected with a Pro-light HRP Chemiluminescent Kit (TIANGEN) and visualized with a LuminoGraph chemiluminescence analyzer (ATTO). Antibodies against $CF_1\alpha$ (PHY0311), $CF_1\beta$ (PHY0312), $CF_1\gamma$ (PHY0313), $CF_1\varepsilon$ (PHY0314), $CF_1\delta$ (PHY0315), CF_oI (PHY0316), CF_oII (PHY0170S), PsaA (PHY0342), PsaD (PHY0343), D1 (PHY0057), D2 (PHY0060), Cyt *f* (PHY0321), and NdhN (PHY0335) were obtained from PhytoAB (United States).

Accession Numbers

Sequence data from this article can be found in GenBank/EMBL/DDBJ databases under accession number AtBFA2 (AT4G30825, *Arabidopsis thaliana*), GmBFA2 (Glyma.04G155800, *Glycine max*), OsBFA2 (Os09g25550, *Oryza sativa*), ZmBFA2 (XP_008662784, *Zea mays*), NsBFA2 (XP_009792607.1, *Nicotiana sylvestris*), SbBFA2 (SORBIDRAFT_07g007540, *Sorghum bicolor*), PpBFA2-A (Pp3c16_4140, *Physcomitrella patens*), PpBFA2-B (Pp3c5_2530, *Physcomitrella patens*). The aligned sequences of *atpF-atpA* can be found in the chloroplast genomes of *Arabidopsis thaliana* (At; NC_000932), *Glycine max* (Gm; NC_021650), *Nicotiana sylvestris* (Ns; NC_007500.1), *Oryza sativa* (Os; NC_001320), *Zea mays* (Zm; NC_001666). *Physcomitrella patens* (Pp, NC_005087), and *Selaginella moellendorffii* (Sm, nc_013086).

RESULTS

The *bfa2* Mutants Are Defective in Normal Accumulation of the Chloroplast ATP Synthase

While the *bfa2-1* mutant was isolated by screening T-DNA mutant pools (Zhang et al., 2016), *bfa2-2* was obtained from the European Arabidopsis Stock Centre (NASC). Both mutants show high levels of nonphotochemical quenching (NPQ) upon illumination with actinic light (80 μmol photons m^{-2} s^{-1}) (**Figures 1A,B**). During illumination, photosynthetic electron transport induces accumulation of protons in the thylakoid lumen, which persists after illumination for 40 s in the wild-type (WT) plants and triggers the induction of NPQ (**Figure 1C**). Because of the activation of chloroplast ATP synthase in the light, protons accumulated in the thylakoid lumen move out rapidly through the ATP synthase to produce ATP, resulting in the relaxation of NPQ within 2 min of illumination (**Figure 1C**). In contrast, the relaxation of NPQ is less efficient in the *bfa2* mutants and NPQ is maintained at high levels compared with WT (**Figure 1C**). Conductivity of the thylakoids to protons, $g_H{}^+$ (thylakoid conductivity), is usually used to monitor the activity of chloroplast ATP synthase *in vivo* (Cruz et al., 2001). The level of $g_H{}^+$ in *bfa2* is indeed reduced to ∼2/3 of the WT level with an irradiance of 628 μmol photons m^{-2} s^{-1} as actinic light (**Figure 1D**), implying that the high-NPQ phenotype can be ascribed to the low activity of the chloroplast ATP synthase in *bfa2*.

The seedling size of *bfa2* is smaller than that of WT after germination for 25 days on soil (**Figure 1A**). To further characterize the phenotype of *bfa2*, several photosynthetic parameters were measured. Fv/Fm, the ratio between variable and maximum fluorescence, that represents the maximum quantum yield of photosystem II (PSII) was found to be comparable between WT and *bfa2* plants (0.79 ± 0.01 for both genotypes), indicating that the function of PSII is not affected. We also investigated the dependence of ETR (electron transport rate through PSII) and NPQ on irradiance. While the ETR is significantly reduced in *bfa2* at an irradiance above 200 μmol photons m^{-2} s^{-1}, the level of NPQ is higher in *bfa2* than in WT at all light intensities investigated (**Supplementary Figures S1A**,**B**), implying that protons over-accumulate in the thylakoid lumen of *bfa2* and that photosynthetic linear electron transport is inhibited. Analysis of the dependence of 1-qL and the oxidation

of the donor side of PSI on irradiance showed that photosynthetic electron transport is significantly restricted between PSII and PSI in *bfa2* compared to WT plants (**Supplementary Figures S1C,D**). All of these photosynthetic properties in *bfa2* are similar to those of mutants that accumulate low amounts of chloroplast ATP synthase (Zoschke et al., 2012, 2013; Rühle et al., 2014; Fristedt et al., 2015; Grahl et al., 2016; Zhang et al., 2016, 2018).

Immunoblot analysis showed that the levels of the chloroplast ATP synthase subunits in *bfa2* are reduced to ∼25–50% of those of wild-type plants (**Figure 1E**). In contrast, accumulation of PSI (PsaA and PsaD), PSII (D1 and D2), Cytochrome b_6f (Cyt *f*), and NADH dehydrogenase-like (NDH) complex (NdhH and NdhN) in *bfa2* was as in WT (**Figure 1E**). Consistent with these results, blue native-PAGE (BN-PAGE) and subsequent two dimensional (2D) SDS-PAGE analysis showed that formation of the NDH-PSI supercomplex, PSII supercomplexes, PSII dimer, PSI monomer and other chlorophyll-containing complexes was not affected in *bfa2* (**Supplementary Figure S2A**). Although the levels of $CF_1\alpha/\beta/\gamma$ were reduced to about one quarter in *bfa2*, the remaining subunits were assembled into the intact ATP synthase and CF_1 subcomplex (**Supplementary Figure S2B**), which accounts for the ∼2/3 activity of ATP synthase in *bfa2* and for its photoautotrophic growth (**Figures 1A,D**). Taken together, we conclude that accumulation of chloroplast ATP synthase is specifically impaired whereas other thylakoid protein complexes are not affected in *bfa2*. Similar to the *bfa1* and *bfa3* mutants we characterized previously (Zhang et al., 2016, 2018), *bfa2* is also a mutant that accumulates lower amounts of chloroplast ATP synthase.

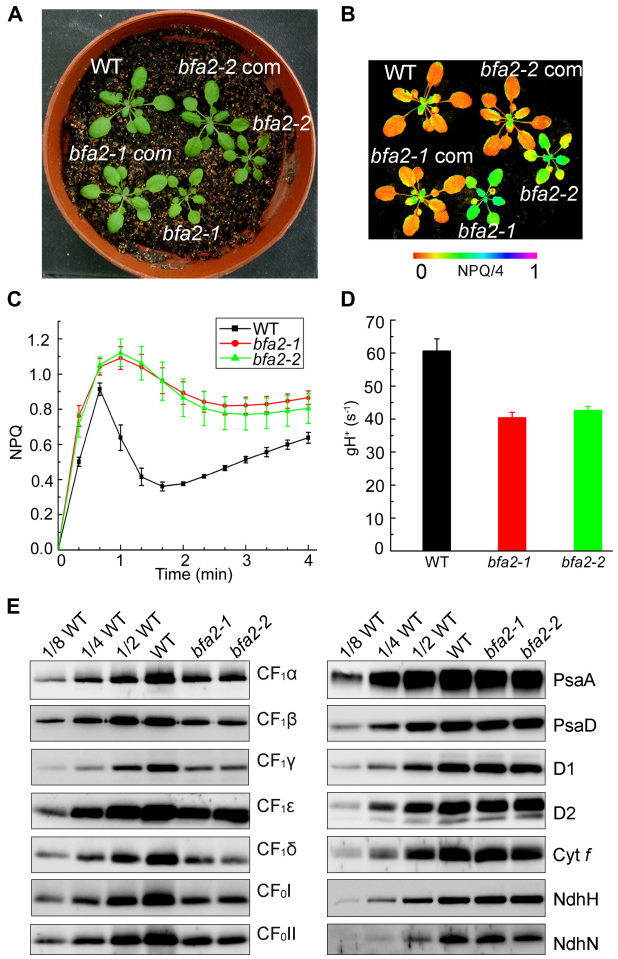

FIGURE 1 | Identification and characterization of the *bfa2* mutants. **(A)** Phenotype of the *bfa2* mutants. *bfa2-1* com and *bfa2-2* com, complemented lines with overexpression of BFA2 in *bfa2-1* and *bfa2-2*, respectively. **(B)** Image of NPQ. The image was captured upon illumination (80 μmol photons m^{-2} s^{-1}) for 2 min. Values for NPQ/4 are indicated at the bottom on a false color scale. **(C)** Time course of NPQ induction. NPQ induction kinetics was measured upon illumination with AL (Actinic light) light (80 μmol photons m^{-2} s^{-1}) for 4 min. Means ± SD (n = 4). **(D)** H^+ conductivity through ATP synthase (g_{H^+}) under an irradiance of 628 μmol photons m^{-2} s^{-1}. Means ± SD (n = 4). **(E)** Immunoblot analysis of the thylakoid membrane proteins in *bfa2* and WT plants. Proteins were loaded on an equal chlorophyll basis and blots were probed with the indicated antibodies.

BFA2 Is a PPR Protein Present in the Chloroplast Stroma

Map-based cloning detected a 17-nucleotide deletion (2130–2146 bp) in the coding region of *AT4G30825* in *bfa2-1*, resulting in a premature stop codon (**Figure 2A**). A T-DNA was inserted in the same gene in the *bfa2-2* mutant. Furthermore, overexpression of *AT4G30825* under the control of the *35S* promoter of cauliflower mosaic virus in the *bfa2-1* and *bfa2-2* mutants fully rescued their phenotype (**Figures 1A,B**). From these results, we conclude that the *AT4G30825* gene corresponds to *BFA2* that is required for full chloroplast ATP synthase activity *in vivo*.

The *BFA2* gene encodes a PPR protein of 904 amino acid residues with unknown function (**Figure 2A**). Sequence analysis revealed that the BFA2 protein belongs to the P subfamily and comprises 22 PPR motifs spanning amino acid residues 139–904 (**Figure 2A** and **Supplementary Figure S3**). The last PPR motif only contains 32 residues and may represent an incomplete PPR motif (**Supplementary Figure S3**). Genes with significant sequence identity (more than 50%) to BFA2 are found in eudicotyledons and monocotyledons (**Supplementary Figure S4**). A blast search also revealed two proteins (PpBFA2-A and PpBFA2-B) in *Physcomitrella patens* (*P. patens*) with low sequence identity to BFA2 (35–38%, **Supplementary Figure S4**). No genes significantly related to BFA2 were found in *Selaginella moellendorffii* and *Chlamydomonas*. This fact implies that BFA2 may have evolved when land plants including bryophytes originated and was probably lost in the lycophytes during evolution.

BFA2 is predicted to have a putative chloroplast transit peptide of 61 amino acids at its N-terminus. To confirm its chloroplast localization, the DNA region coding for the first 200 amino acids of BFA2 was fused in-frame with GFP in the pBI221 vector and the resulting vector was introduced into Arabidopsis protoplasts by transient transformation. Analysis by confocal laser scanning microscopy showed that the BFA2-GFP signal co-localizes with the chloroplast fluorescence, indicating that BFA2 is targeted to

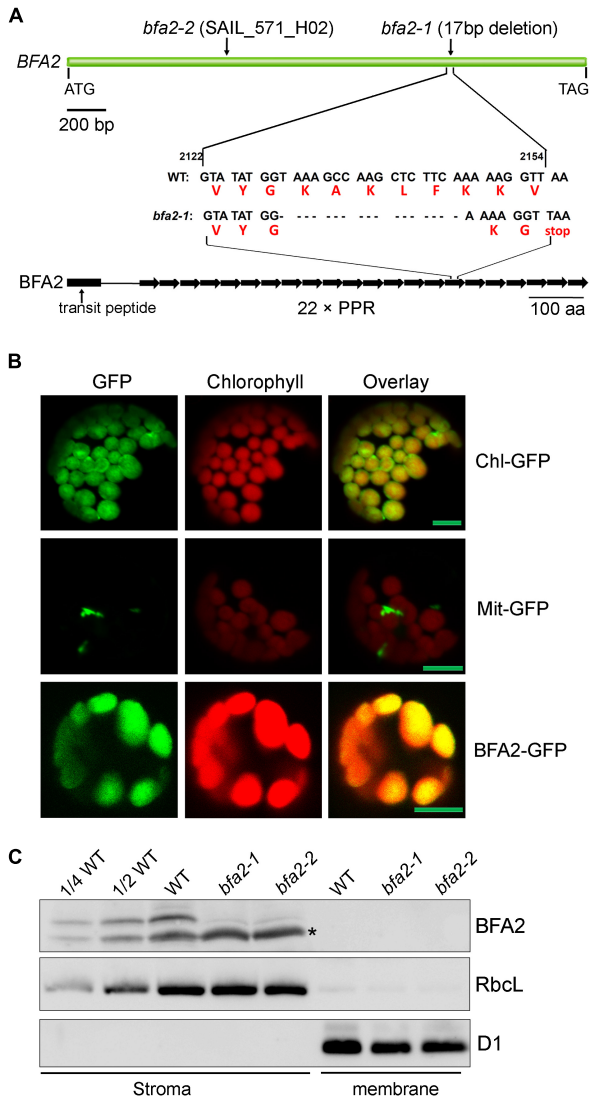

FIGURE 2 | Characterization of the BFA2 protein. **(A)** Schematic representation of *BFA2* gene (Top panel) and BFA2 protein (bottom panel). Positions for nucleotide deletion in *baf2-1* and T-DNA insertion in *bfa2-2* are indicated. Each right arrow represents one PPR domain. The 17-nucleotide deletion results in a premature stop codon at the position of the 16th PPR motif in BFA2. **(B)** Subcellular localization of BFA2 by GFP assay. The first 200 amino acids of BFA2 were fused with GFP (BFA2-GFP) and expressed in Arabidopsis protoplasts. The signal of GFP was visualized using a confocal laser scanning microscope. Chl-GFP and Mit-GFP represent chloroplast and mitochondrial controls, respectively. Bars = 5 μm. **(C)** Immunolocalization of BFA2. Intact chloroplasts isolated from WT and *bfa2* mutants were fractionated into stromal and membrane fractions. Proteins were separated by SDS-PAGE and immunodetected with antibodies against BFA2, RbcL, and D1. The series of WT dilutions is indicated. A major nonspecific band detected in the stromal fractions with BFA2 antibody is indicated by an asterisk. A weak band above the major nonspecific band detected in *bfa2* stroma also appears to be nonspecific.

the chloroplast (**Figure 2B**). To further determine the precise location of BFA2 within chloroplasts, a polyclonal antibody against recombinant BFA2 protein was raised. A signal with a molecular mass of ∼100 kDa (the predicted molecular mass of mature BFA2 is 94 kDa) was detected in the stromal fractions isolated from WT plants, but absent in the stromal fraction from *bfa2* mutants as well as in the thylakoid membranes from WT and *bfa2* plants (**Figure 2C**). These results indicate that BFA2 is localized to the chloroplast stroma.

BFA2 Is Required for Accumulation of the *atpH/F* Transcript

Since the PPR proteins are well known to be involved in organelle gene expression, it is very likely that the expression of one or more chloroplast genes encoding ATP synthase subunits is affected in the *bfa2* mutants. To investigate this possibility, we performed RNA gel blot analysis with probes for the large (*atpI/H/F/A*) and the small (*atpB/E*) *atp* operons (**Figure 3**). For the large *atp* operon, the most striking difference is that the dicistronic *atpH/F* transcript is barely detected in the *bfa2* mutants (Transcript 8; **Figures 3A,D**), indicating that BFA2 is essential for accumulation of this transcript. However, the level of the monocistronic *atpH* transcripts (transcripts 10, 11, and 12) in the *bfa2* mutants is higher than that in WT (**Figure 3A**), excluding the possibility that absence of the *atpH/F* transcripts in *bfa2* is due to deficient cleavage between *atpI* and *atpH*. RNA blot analysis using *atpI*, *atpH*, *atpF* exon, and *atpF* intron probes also detected a ∼3 kb transcript in WT plants that was absent in the *bfa2* mutants (transcript 2, **Figures 3A,D**). Given the detection of this transcript with these four probes and its size, it is likely that this transcript corresponds to the unspliced *atpI/H/F* transcript (transcript 2, **Figure 3D**). The monocistronic unspliced *atpF* transcript was detected with the *atpF* intron probe in the WT plants but was absent in the *bfa2* mutants (transcript 9, **Figure 3A**).

The *atpA* RNA was mainly detected in the polycistronic *atpH/F/A* transcript (transcript 1, **Figure 3A**), which is inconsistent with previous reports (Malik Ghulam et al., 2013). In addition to this main polycistronic mRNA, the *atpA* probe also detected a fuzzy weak band around 1600 nucleotides in WT, but the level of this band was significantly reduced in the *bfa2* mutants (transcript 5, **Figures 3A,D**). As discussed by Malik Ghulam et al. (2013), the monocistronic *atpA* transcript is present in very low amounts *in vivo* and usually possesses truncated 3′ ends whereas most of the 5′ ends of this RNA map at positions -237 (inside the *atpF* mRNA) and −50 (just overlapping with the 3′ end of *atpF*) relative to the *atpA* start codon (**Figure 3D**; Malik Ghulam et al., 2013). Thus, the weak bands detected in our RNA blot (transcript 5 and several bands below transcript 5) correspond most likely to the monocistronic *atpA* transcript with different 5′ ends, overlapping the *atpF* 3′ end, and truncated 3′ ends (**Figure 3D**). Reduction of transcript 5 in the *bfa2* mutants indicates that some type of monocistronic *atpA* transcript is unstable in the absence of BFA2.

In the case of the small *atp* operon *atpB/E*, two major bands can be detected by the *atpB* probe (**Figure 3B**). The monocistronic *atpE* transcript can also be detected by the *atpE* probe (**Figure 3B**). While the upmost band represents the primary dicistronic *atpB/E* transcript with two isoforms (−520

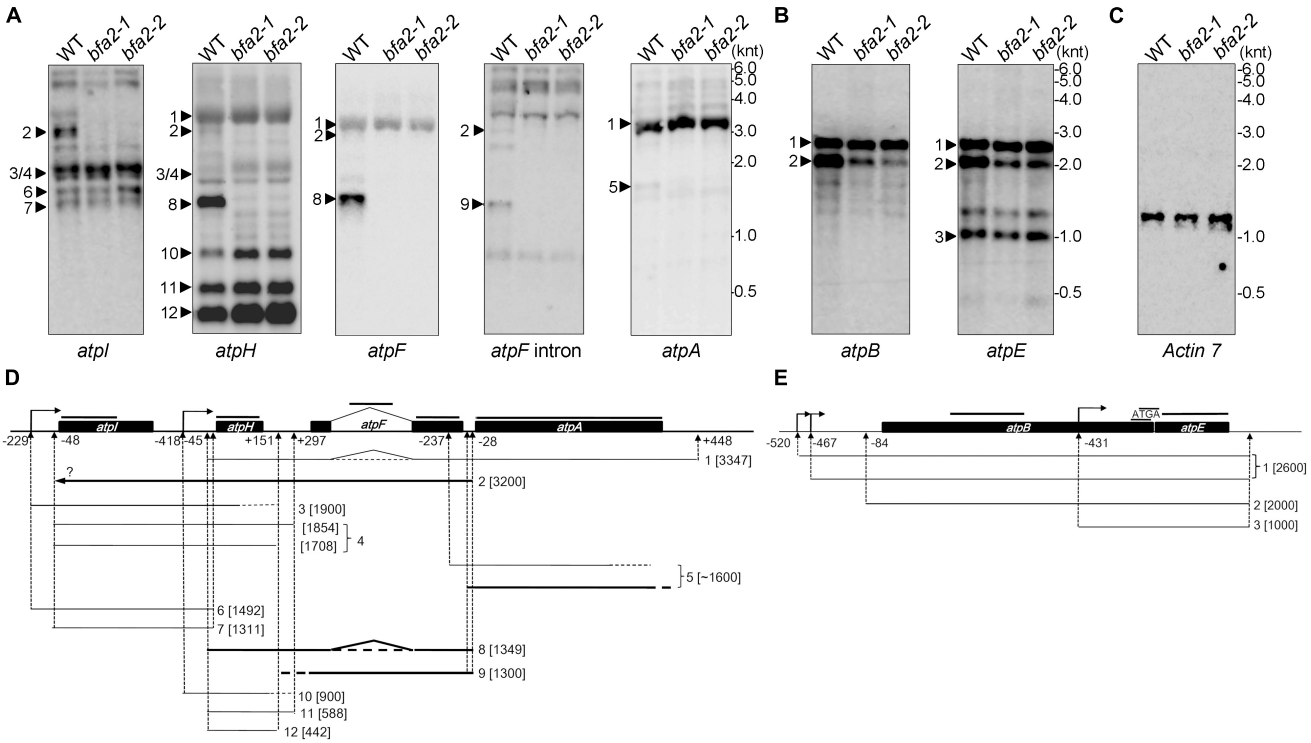

FIGURE 3 | RNA blot analysis of the plastid-encoded ATP synthase genes. **(A–C)** Total RNA isolated from WT and *bfa2* mutants was probed with digoxigenin-labeled probes corresponding to the genes in the large **(A)** and small **(B)** *atp* operons. A blot with the *Actin 7* probe was used as a loading control **(C)**. The positions of RNA markers are shown in kilonucleotides (knt). **(D,E)** Partial transcript map of the *atpI/H/F/A* **(D)** and *atpB/E* **(E)** operons in Arabidopsis. The map was generated based on the transcript size in **(A,B)** as well as on previous reports (Malik Ghulam et al., 2012, 2013). Transcripts absent in *bfa2* are shown as bold black lines. The positions of the probes are indicated above the operons. The numbers refer to the distance upstream of the initiation codon (–) and downstream of the termination codon (+).

and −467), the second band corresponds to the processed dicistronic *atpB/E* transcript ending at -84 (**Figure 3E**, Malik Ghulam et al., 2012). Our results show that the level of the −84 processed *atpB/E* dicistronic mRNA is significantly reduced in the *bfa2* mutants compared with WT plants (**Figures 3B,E**). The level of primary dicistronic *atpB/E* and the monocistronic *atpE* transcripts are identical in the *bfa2* mutants compared with WT plants (**Figure 3E**). Reduction of the processed dicistronic *atpB/E* transcript was also observed in the *bfa1-1* and *cgl160* mutants, in which assembly of the chloroplast ATP synthase CF_1 and CF_o subcomplexes, respectively, is less efficient (Rühle et al., 2014; Zhang et al., 2018). Thus, reduction of processed dicistronic *atpB/E* likely represents a secondary effect due to impairment in the assembly of chloroplast ATP synthase.

Translation Initiation of *atpA* Is Not Affected in the Absence of BFA2

To rule out the possibility that reduction of the chloroplast ATP synthase in *bfa2* is due to defects in the translation of *atp* mRNAs, we performed a polysome association analysis to investigate translation initiation (**Figure 4**). Our results show that the distribution of the *atpH/F/A* mRNAs in *bfa2* was slightly shifted toward lower molecular weight fractions compared with WT (transcript 1, **Figure 4A**). The distribution of other transcripts in the *atpI/H/F/A* operon, such as monomeric *atpH*, was almost identical between *bfa2-1* and WT plants. For the *atpB/E* operon, a clear shift of primary dicistronic *atpB/E* transcript toward lower molecular weight fractions in the *bfa2-1* mutant compared with the wild type was observed (transcript 1, **Figure 4B**). The shift of the primary dicistronic *atpB/E* transcript is also observed in the *bfa1* and *cgl160* mutants and is unlikely to be the cause for the low accumulation of chloroplast ATP synthase in *bfa2* (Zhang et al., 2018).

To investigate whether the alteration of the polysome association with *atpH/F/A* and primary dicistronic *atpB/E* transcripts in *bfa2-1* is responsible for the defect in chloroplast ATP synthase accumulation, *in vivo* protein labeling of the chloroplast proteins with [^{35}S]-Met was performed (**Figure 5**). Cycloheximide, an inhibitor of cytosolic translation, was added to avoid interference with the synthesis of nucleus-encoded proteins. After labeling, thylakoid membranes were isolated and the newly synthesized thylakoid proteins were separated by SDS-PAGE. Radiolabeled thylakoid proteins were detected by autoradiography. The results showed that, as expected, the levels of the newly synthesized PsaA/B, CP47, CP43, D2/pD1, and D1 protein were comparable between WT and *bfa2*

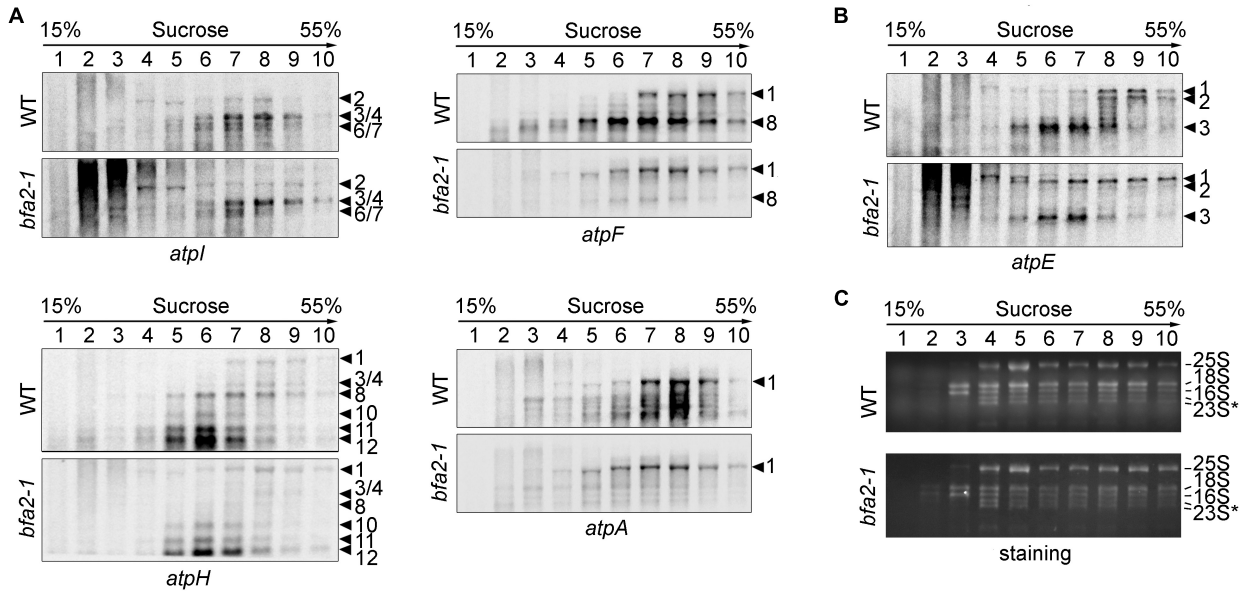

FIGURE 4 | Analysis of polysome association of the plastid transcripts encoding ATP synthase subunits. **(A,B)** Total leaf extracts from wild-type and *bfa2-1* plants were fractionated by centrifugation on 15–55% sucrose density gradients. After centrifugation, the sucrose gradients were divided into 10 fractions of equal volume for RNA isolation. The isolated RNAs were blotted with DIG-labeled DNA probes corresponding to the plastid *atpA*, *atpF*, *atpH*, and *atpI* **(A)** as well as *atpE* **(B)** transcripts. The numbers to the right of the panels correspond to the corresponding transcripts illustrated in **Figures 3D,E**. **(C)** Staining of the rRNA was used as fractionation and loading control. 23S*, two breakdown products of the chloroplast 23S rRNA. The numbers on the right indicate sedimentation coefficients of the major rRNAs.

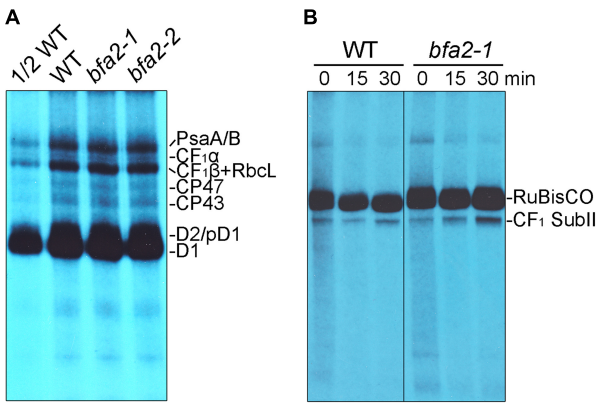

FIGURE 5 | *In vivo* protein labeling analysis of plastid-encoded proteins. **(A)** Pulse labeling of chloroplast thylakoid proteins of WT and *bfa2* mutants. Chloroplast thylakoid proteins were extracted from primary leaves of 12 days old seedlings after labeling with [^{35}S]-Met for 20 min, and separated by SDS-urea-PAGE. The labeled proteins were visualized using autoradiography. **(B)** Pulse-chase labeling of chloroplast stromal protein complexes of WT and *bfa2-1* plants. After pulse labeling for 20 min (indicated as 0 min), the leaves were chased with cold Met for 15 and 30 min. Total soluble protein complexes extracted from the leaves were separated by CN-PAGE and the newly assembled complexes were detected by autoradiography.

mutants (**Figure 5A**), which is consistent with the fact that *bfa2* is specifically defective in accumulation of chloroplast ATP synthase. For the chloroplast ATP synthase $CF_1\alpha$ subunit, a very weak signal was detected below the PsaA/B subunits and its level is identical in both WT and two *bfa2* mutant genotypes (**Figure 5A**). The levels of newly synthesized $CF_1\beta$ subunits of as well as RbcL contamination in thylakoids were also identical in *bfa2* and WT plants after labeling for 20 min (**Figure 5A**).

$CF_1\alpha$ and $CF_1\beta$ are components of the ATP synthase CF_1 subcomplex. To further prove that protein synthesis of $CF_1\alpha$ and $CF_1\beta$ and their subsequent incorporation into functional CF_1 is not affected in *bfa2*, we analyzed the assembly of the CF_1 subcomplex in the chloroplast stroma by pulse-chase labeling. We designated this subcomplex CF_1 SubII in our previous report (**Figure 5B**, Zhang et al., 2018), and it contains subunits of $CF_1\alpha$, $CF_1\beta$, $CF_1\gamma$, $CF_1\varepsilon$, and $CF_1\delta$, but not CF_oI, which is the product of *atpF* (Zhang et al., 2016). Our results show that formation of CF_1 SubII is as efficient in *bfa2-1* as in WT plants after pulse-labeling for 20 min and a subsequent chase for 15 and 30 min (**Figure 5B**). These results are different from those obtained with *bfa1* and *bfa3* (Zhang et al., 2016, 2018), further confirming that synthesis of $CF_1\alpha$ and $CF_1\beta$ is not affected in *bfa2*, although the level of processed dicistronic *atpB/E* was reduced and polysome association with *atpH/F/A* and primary dicistronic *atpB/E* was slightly altered in the *bfa2* mutants (**Figures 3**, **4**).

Taken together, we conclude that absence of the dicistronic *atpH/F* is the primary cause for the decreased accumulation of chloroplast ATP synthase in *bfa2*, and that BFA2 is likely directly required for the accumulation of the RNAs with a 3′-end or 5′-end mapping between *atpF* and *atpA* (**Figures 3A,D**).

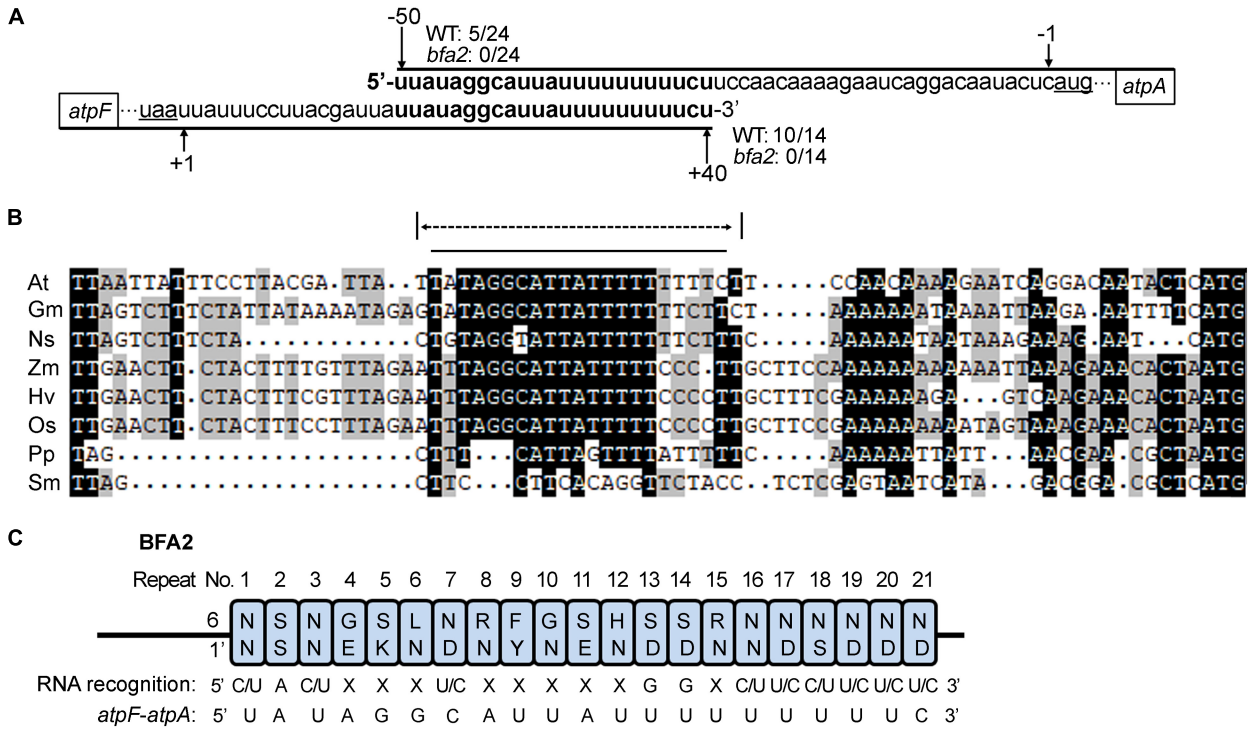

FIGURE 6 | Position of the BFA2-dependent RNA termini. **(A)** Overlapping transcript termini in the *atpF/A* intergenic region. Nucleotide positions relative to the start codon of *atpA* (−50 and −1) and stop codon of *atpF* (+40 and +1) are shown above and below the sequences, respectively. The numbers of 5/24, 0/24, 10/14, and 0/14 represent the ratio of the clones with a 5′ or 3′ end positions from the WT or *bfa2* samples in the cRT-PCR analyses (**Supplementary Figure S5** and **Supplementary Table S1**). **(B)** Alignment of the *atpF/A* intergenic regions (from the stop codon of *atpF* to the start codon of *atpA*). The overlapping transcript termini in the *atpF/A* intergenic regions and the sequence predicted for BFA2 binding are indicated by the dotted and black lines, respectively. Nucleotides U are indicated by T. At, *Arabidopsis thaliana*; Gm, *Glycine max*; Os, *Oryza sativa*; Zm, *Zea mays*; Ns, *Nicotiana sylvestris*; Hv, *Hordeum vulgare*; Pp, *Physcomitrella patens*; Sm, *Selaginella moellendorffii*. **(C)** Prediction of the nucleotide-binding site for BFA2. The residues that determine nucleotide-binding specificity (residues 6 and 1' in **Supplementary Figure S3**) in each PPR motif were extracted according to Barkan et al. (2012). The overlapping sequence in the *atpF/A* intergenic RNA (from the second nucleotide) is shown.

The BFA2 protein belongs to the P class PPR proteins and this class of proteins can act as barrier to prevent the RNA degradation by exoribonucleases (Barkan and Small, 2014). Since PPR10 binds to the 5′ termini of *atpH/F*, we hypothesize that BFA2 binds to the 3′ termini of *atpH/F* as well as to other transcripts overlapping the intergenic region of *atpF-atpA* (**Figure 3D**).

BFA2 Binds to the Consensus Sequence in the *atpF* 3′-UTR and *atpA* 5′-UTR

A small RNA (sRNA) corresponding to the *atpF* 3′ region was detected in barley and rice and this sRNA is predicted to be the footprint of uncharacterized PPR-like proteins (Ruwe and Schmitz-Linneweber, 2012; Zhelyazkova et al., 2012). These facts led us to propose that the sRNA from the *atpF-atpA* intergenic region is the footprint of BFA2 in Arabidopsis. To confirm this hypothesis, we first determined the transcript termini in the *atpF-atpA* intergenic region by circularization RT-PCR (cRT-PCR) (**Supplementary Figure S5**). Consistent with the results reported by Malik Ghulam et al. (2013), our results show that most clones (10 out of 14) had their 3′ end at position +40 from the *atpF* stop codon and 5 out of 24 clones had their 5′ end at position -50 from the *atpA* start codon in WT (**Figure 6A** and **Supplementary Table S1**). However, neither 3′ ends of *atpF* nor 5′ ends of *atpA* were mapped to these two positions in *bfa2* (**Figure 6A** and **Supplementary Table S1**). These results suggest that BFA2 binds to the *atpF-atpA* intergenic region to stabilize the corresponding mRNA *in vivo*. Moreover, the overlapping region comprises 23 residues and is basically consistent with the number of PPR motifs (22 PPR motifs) of the BFA2 protein (**Figure 6A**).

Alignment analysis showed that the overlapping region (except for the first residue) in the *atpF* 3′-UTR and *atpA* 5′-UTR in Arabidopsis is highly conserved in Angiosperms, but not in *Physcomitrella patens* and *Selaginella moellendorffii* (**Figure 6B**), which is in line with the fact that two proteins (PpBFA2-A and PpBFA2-B) in *Physcomitrella patens* (*P. patens*) show low sequence identity with BFA2 (35–38%) and that no BFA2-like protein was found in *S. moellendorffii* (**Supplementary Figure S4**). Although the last 6 residues vary among different plant species, most residues in this region are U and C (**Figure 6B**). Since the first residue

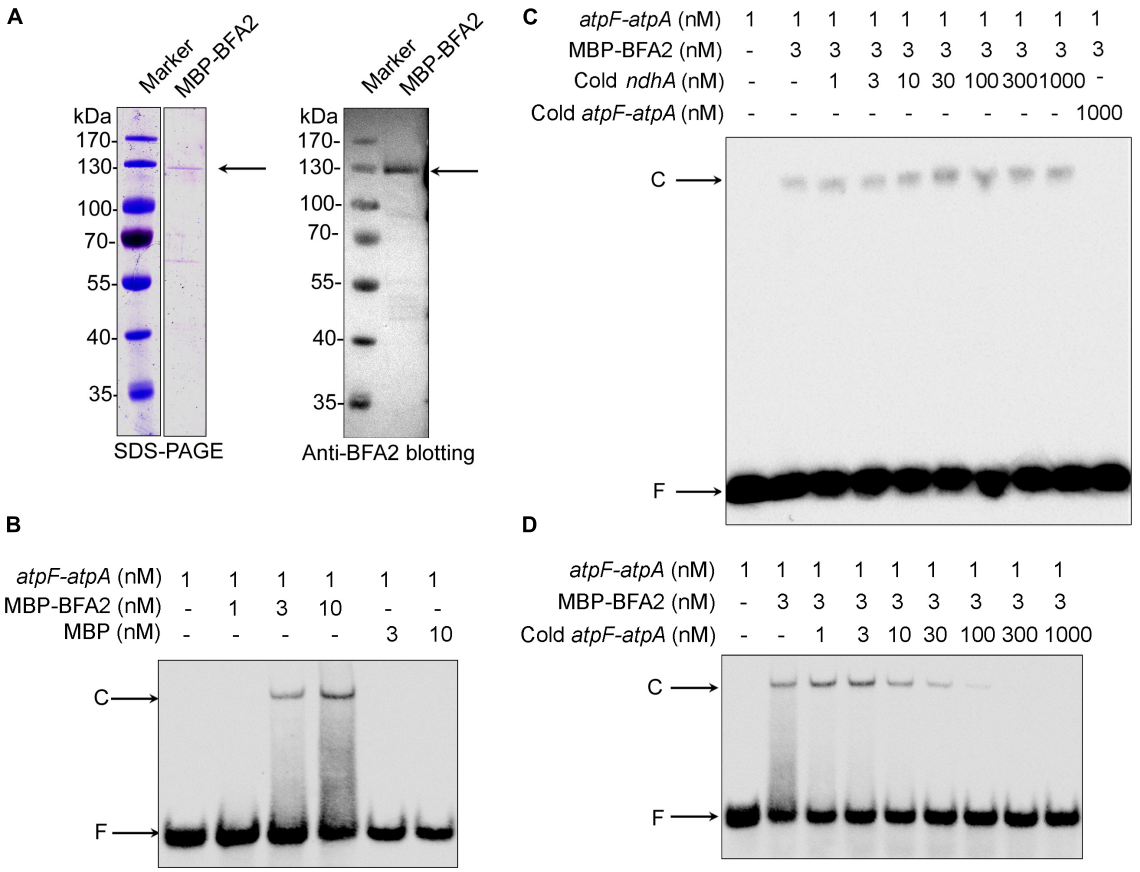

FIGURE 7 | Gel mobility shift assays of the RNA binding activity of BFA2. **(A)** Purified MBP-BFA2 used in the RNA binding assays. The purified recombinant BFA2 was separated by SDS-PAGE and visualized by Coomassie Brilliant Blue (CBB) staining (left) and immunoblotting with anti-BFA2 antibody (right). **(B)** Gel mobility shift assays demonstrating that MBP-BFA2 binds with high affinity to the *atpF* sRNA. The concentrations of labeled sRNA probe, recombinant BFA2, and recombinant MBP are indicated above each lane. C and F indicate the BFA2-RNA complex and free labeled RNA, respectively. **(C,D)** Competition experiments using nonlabeled *ndhA* sRNA **(C)** and nonlabeled *atpF-atpA* sRNA **(D)**. The concentrations of probes and protein are indicated above the gel. In each reaction, 1 μg yeast tRNA was added to lower the background of nonspecific RNA binding.

is not conserved (**Figure 6B**), BFA2 may bind to the 22 conserved residues from the second residue in the sRNA. To confirm our hypothesis, the potential binding sequence of BFA2 was predicted according to the PPR code established previously (Barkan et al., 2012). As shown in **Figure 6C**, the 21 nucleotides predicted to bind by the 21 PPR motifs of BFA2 are (C/U)A(C/U)XXX(U/C)XXXXXGGX(C/U)(U/C)(C/U)(U/C)(U/C)(U/C)(U/C). While X represents any nucleotide that cannot be precisely predicted, the nucleotides in parentheses are optional. Among the 21 nucleotides, 10 of them match with the corresponding residues in the overlapping transcript termini of the *atpF-atpA* intergenic region (**Figure 6C**). For the 5th and 11th PPR motifs, serine (S) was identified at position 6 (**Figure 6C**). It has been suggested that S_6 shows a strong correlation with purines (Barkan et al., 2012), which is consistent with fact that G and A were found in the corresponding position of the *atpF-atpA* intergenic region (**Figure 6C**). These results support our view that BFA2 binds to the overlapping transcript termini in the *atpH-atpA* intergenic region starting from the second residue.

In vitro electrophoretic mobility shift assays (EMSA) were performed. Recombinant mature BFA2 protein fused with the MBP (maltose-binding protein) tag was expressed in *Escherichia coli* (*E. coli*) and purified (**Figure 7A**). The molecular mass of the purified fusion protein is about 130 kDa and is consistent with the predicted molecular mass of BFA2-MBP (136 kDa). The biotinylated RNA corresponding to the overlapping transcript termini in *atpF-atpA* was chemically synthesized and incubated with the BFA2-MBP fusion protein. The BFA2-RNA complex can be detected when the protein molar concentration is three times higher than that of the RNA (**Figure 7B**). There was no shift when the biotinylated RNA was incubated with MBP protein (**Figure 7B**). A set of competition assays were performed to confirm the binding specificity of BFA2. The 5′ end of *ndhA* mRNA has been shown to be the binding site of PGR3 (PROTON GRADIENT REGULATION 3) (Cai et al., 2011). Even addition of 1000-fold amount of cold *ndhA* mRNA did not affect the formation of the BFA2-RNA complex (**Figure 7C**). However, the addition of >30-fold amount of unlabeled *atpF-atpA* RNA significantly

inhibited the binding of BFA2 with the labeled RNA probe (**Figure 7D**). These results clearly demonstrate that BFA2 protein binds to the *atpF-atpA* intergenic region in a sequence-specific manner.

DISCUSSION

The plastid-encoded *atpF* gene encodes the CF_oI subunit of the chloroplast ATP synthase. CF_oI interacts with the *atpG* product CF_oII to form the peripheral stalk holding CF_o and CF_1 together (Rühle and Leister, 2015). In chloroplasts, the *atpF* RNA is solely detected in the polycistronic *atpH/F/A* and dicistronic *atpH/F* transcripts (**Figure 3A**; Malik Ghulam et al., 2013). Analysis of chloroplast small RNAs (sRNAs) in rice and barely reveals two sRNAs mapping at the two ends of dicistronic *atpH/F* mRNA, respectively (Ruwe and Schmitz-Linneweber, 2012; Zhelyazkova et al., 2012). Both of them are predicted to represent footprints of PPR proteins (Zhelyazkova et al., 2012; Malik Ghulam et al., 2013). While the sRNA at the 5′-end of *atpH/F* includes the binding site for PPR10 (Pfalz et al., 2009; Prikryl et al., 2011), the putative PPR protein binding to the 3′-end of the dicistronic *atpH/F* transcript was not yet known. In this study, we provide evidence that P-class PPR protein BFA2 binds to this site.

Our conclusion is mainly supported by the following evidence. (1) The level of the chloroplast ATP synthase is specifically reduced in the absence of BFA2, while accumulation of other thylakoid complexes is not affected (**Figure 1E** and **Supplementary Figure S2**). This is also consistent with the photosynthetic properties detected in *bfa2* (**Figure 1** and **Supplementary Figure S1**). (2) Dicistronic *atpH/F* transcript is absent in *bfa2* and other transcripts with termini in the intergenic region of *atpF-atpA* also appear to be unstable in the absence of BFA2 (**Figure 3**). (3) The BFA2 binding site was predicted to cover the overlapping region between the 3′ end of *atpF* and the 5′ end of *atpA* (**Figure 6**). (4) EMSA analyses showed that BFA2 protein binds to the *atpF-atpA* intergenic region in a sequence-specific manner (**Figure 7**). Sequence alignment analysis showed that BFA2 belongs to the P-class PPR proteins with 22 PPR motifs (**Supplementary Figure S3**). Our results suggest that BFA2 acts analogously to other typical PPR proteins such as PPR10, PGR3, and HCF152, by directly binding to the *atpF-atpA* intergenic region to prevent degradation of BFA2-dependent transcripts by blocking exoribonucleases acting either from the 5′ or 3′ ends (Barkan and Small, 2014). However, because several nucleotides that bind to the PPR motifs in BFA2 can not be precisely predicted (**Figure 6C**), BFA2 may have another binding site(s) in the chloroplast-encoded genes, which need to be investigated in the further analyses.

For some P-class PPR proteins like PPR10, they not only act as site-specific barriers to protect target RNA segments by blocking exoribonuclease intruding from either direction, but also remodel the structure of ribosome-binding sites in the target RNA to enhance translation (Prikryl et al., 2011). Since BFA2 binds to the intergenic regions of *atpF-atpA*, which is just upstream of the start codon of *atpA*, is it possible that binding of BFA2 in this region releases the ribosome binding site of *atpA*? In Arabidopsis, monomeric *atpA* transcript was barely detectable in chloroplasts (Malik Ghulam et al., 2013; **Figure 3**). Thus, *atpA* translation should arise from the polycistronic *atpH/F/A* transcript. Although polysome association with *atpH/F/A* transcript was slightly reduced in the *bfa2* mutant (**Figure 4A**), $CF_1\alpha$ synthesis and subsequent assembly into CF_1 were not affected (**Figure 5**). These facts suggest that binding of BFA2 in the intergenic region of *atpF-atpA* is not required for the translation of *atpA*. However, we cannot fully rule out the possibility that BFA2 is involved in the activation of *atpA* translation since no solid evidence was obtained by more direct approaches like polysome profiling.

Our results demonstrate that absence of dicistronic *atpH/F* transcript is the main cause of the low ATP synthase accumulation phenotype of *bfa2* (**Figures 3–5**). The dicistronic *atpH/F* transcript is barely detectable in *bfa2* (**Figure 3**). This raises the question of how the *atpF* product CF_oI can accumulate to about one-quarter in *bfa2* as compared to WT (**Figure 1**)? One possibility is that *atpF* translation proceeds to a small extent from the polycistronic *atpH/F/A* transcript which accumulates normally in the *bfa2* mutants (**Figure 3**).

Homologs of BFA2 are found in angiosperms, consistent with the highly conserved intergenic regions of *atpF-atpA* among angiosperms (**Figure 6B** and **Supplementary Figure S4**, Zhelyazkova et al., 2012). Moreover, two putative BFA2 homologs were found in *P. patens* although they display low sequence identity with BFA2 from higher plants (**Supplementary Figure S4**). However, although a ∼20 nt sequence in the *atpF-atpA* regions from *P. patens* chloroplasts shows high similarity to the BFA2-binding sequence of higher plants, a 3 nt deletion was found in this sequence (**Figure 6B**). Moreover, this sequence is located just downstream of the stop codon of *atpF* (**Figure 6B**). It is reasonable to assume that translation termination may be affected if the BFA2-like proteins in *P. patens* bind to this region. Thus, detailed analyses are necessary to clarify the function of these two proteins in *P. patens*.

In summary, our genetic approaches have identified a P-class PPR protein BFA2, which is specifically required for the normal accumulation of chloroplast ATP synthase. We have demonstrated that BFA2 binds to the intergenic region of *atpF-atpA* and mainly acts as a site-specific barrier to protect *atpH/F* mRNA by blocking exoribonuclease degradation from the 3′-direction. Thus, stabilization of the *atpH/F* transcript requires two independent PPR proteins, PPR10 and BFA2, to protect the mRNA against exoribonucleases.

SIGNIFICANCE STATEMENT

In this study, we discovered a chloroplast PPR protein BFA2, which protects target mRNAs from degradation by exoribonucleases by binding to the consensus sequence of the *atpF-atpA* intergenic region.

AUTHOR CONTRIBUTIONS

LZ, WL, and LP conceived the study and designed the experiments. LZ, WL, WZ, and LC performed the experiments. LZ and WL produced the figures. LZ, WL, J-DR, and LP wrote the manuscript. LP supervised the whole study. All authors analyzed the data.

FUNDING

This work was supported by the National Science Foundation for Young Scientists of China (31500196 and 31700202), the China Postdoctoral Science Foundation (2017M621511), and the funds from the Shanghai Engineering Research Center of Plant Germplasm Resources (17DZ2252700) and the Science and Technology Commission of Shanghai Municipality (18DZ2260500).

ACKNOWLEDGMENTS

We thank NASC for providing the mutant seeds.

SUPPLEMENTARY MATERIAL

The Supplementary Material for this article can be found online at: https://www.frontiersin.org/articles/10.3389/fpls.2019.00446/full#supplementary-material

REFERENCES

Barkan, A. (2011). Expression of plastid genes: organelle-specific elaborations on a prokaryotic scaffold. *Plant Physiol.* 155, 1520–1532. doi: 10.1104/pp.110.171231

Barkan, A., Rojas, M., Fujii, S., Yap, A., Chong, Y. S., Bond, C. S., et al. (2012). A combinatorial amino acid code for RNA recognition by pentatricopeptide repeat proteins. *PLoS Genet.* 8:e1002910. doi: 10.1371/journal.pgen.1002910

Barkan, A., and Small, I. (2014). Pentatricopeptide repeat proteins in plants. *Annu. Rev. Plant. Biol.* 65, 415–442. doi: 10.1146/annurev-arplant-050213-040159

Cai, W., Okuda, K., Peng, L., and Shikanai, T. (2011). PROTON GRADIENT REGULATION 3 recognizes multiple targets with limited similarity and mediates translation and RNA stabilization in plastids. *Plant J.* 67, 318–327. doi: 10.1111/j.1365-313X.2011.04593.x

Cruz, J. A., Sacksteder, C. A., Kanazawa, A., and Kramer, D. M. (2001). Contribution of electric field ($\Delta\Psi$) to steady-state transthylakoid proton motive force (*pmf*) *in vitro* and *in vivo*. Control of pmf Parsing into $\Delta\psi$ and ΔpH by ionic strength. *Biochemistry* 40, 1226–1237. doi: 10.1021/bi0018741

Eberhard, S., Loiselay, C., Drapier, D., Bujaldon, S., Girard-Bascou, J., Kuras, R., et al. (2011). Dual functions of the nucleus-encoded factor TDA1in trapping and translation activation of *atpA* transcripts in *Chlamydomonas reinhardtii* chloroplasts. *Plant J.* 67, 1055–1066. doi: 10.1111/j.1365-313X.2011.04657.x

Fristedt, R., Martins, N. F., Strenkert, D., Clarke, C. A., Suchoszek, M., Thiele, W., et al. (2015). The thylakoid membrane protein CGL160 supports CF1CFo ATP synthase accumulation in *Arabidopsis thaliana*. *PLoS One* 10:e0121658. doi: 10.1371/journal.pone.0121658

Grahl, S., Reiter, B., Gügel, I. L., Vamvaka, E., Gandini, C., Jahns, P., et al. (2016). The Arabidopsis protein CGLD11 is required for chloroplast ATP synthase accumulation. *Mol. Plant* 9, 885–899. doi: 10.1016/j.molp.2016.03.002

Hahn, A., Vonck, J., Mills, D. J., Meier, T., and Kühlbrandt, W. (2018). Structure, mechanism, and regulation of the chloroplast ATP synthase. *Science* 360:eaat4318. doi: 10.1126/science.aat4318

Kroeger, T. S., Watkins, K. P., Friso, G., van Wijk, K. J., and Barkan, A. (2009). A plant-specific RNA-binding domain revealed through analysis of chloroplast group II intron splicing. *Proc. Natl. Acad. Sci. U.S.A.* 106, 4537–4542. doi: 10.1073/pnas.0812503106

Li, Y., Liu, B., Zhang, J., Kong, F., Zhang, L., Meng, H., et al. (2019). OHP1, OHP2, and HCF244 form a transient functional complex with the photosystem II reaction center. *Plant Physiol.* 179, 195–208. doi: 10.1104/pp.18.01231

Malik Ghulam, M., Courtois, F., Lerbs-Mache, S., and Merendino, L. (2013). Complex processing patterns of mRNAs of the large ATP synthase operon in Arabidopsis chloroplasts. *PLoS One* 8:e78265. doi: 10.1371/journal.pone.0078265

Malik Ghulam, M., Zghidi-Abouzid, O., Lambert, E., Lerbs-Mache, S., and Merendino, L. (2012). Transcriptional organization of the large and the small ATP synthase operons, *atpI/H/F/A* and *atpB/E*, in *Arabidopsis thaliana* chloroplasts. *Plant Mol. Biol.* 79, 259–272. doi: 10.1007/s11103-012-9910-5

Martin, M., Rujan, T., Richly, E., Hansen, A., Cornelsen, S., Lins, T., et al. (2002). Evolutionary analysis of *Arabidopsis*, cyanobacterial, and chloroplast genomes reveals plastid phylogeny and thousands of cyanobacterial genes in the nucleus. *Proc. Natl. Acad. Sci. U.S.A.* 99, 12246–12251. doi: 10.1073/pnas.182432999

McCormac, D. J., and Barkan, A. (1999). A nuclear gene in maize required for the translation of the chloroplast *atpB/E* mRNA. *Plant Cell* 11, 1709–1716. doi: 10.1105/tpc.11.9.1709

Pfalz, J., Bayraktar, O. A., Prikryl, J., and Barkan, A. (2009). Site-specific binding of a PPR protein defines and stabilizes 5′and 3′mRNA termini in chloroplasts. *EMBO J.* 28, 2042–2052. doi: 10.1038/emboj.2009.121

Prikryl, J., Rojas, M., Schuster, G., and Barkan, A. (2011). Mechanism of RNA stabilization and translational activation by a pentatricopeptide repeat protein. *Proc. Natl. Acad. Sci. U.S.A.* 108, 415–420. doi: 10.1073/pnas.1012076108

Prikryl, J., Watkins, K. P., Friso, G., van Wijk, K. J., and Barkan, A. (2008). A member of the Whirly family is a multifunctional RNA- and DNA-binding protein that is essential for chloroplast biogenesis. *Nucleic Acids Res.* 36, 5152–5165. doi: 10.1093/nar/gkn492

Rott, M., Martins, N. F., Thiele, W., Lein, W., Bock, R., Kramer, D. M., et al. (2011). ATP synthase repression in tobacco restricts photosynthetic electron transport, CO2 assimilation, and plant growth by over acidification of the thylakoid lumen. *Plant Cell* 23, 304–321. doi: 10.1105/tpc.110.079111

Rühle, T., and Leister, D. (2015). Assembly of F1F0-ATP synthases. *Biochim. Biophys. Acta* 1847, 849–860. doi: 10.1016/j.bbabio.2015.02.005

Rühle, T., Razeghi, J. A., Vamvaka, E., Viola, S., Gandini, C., Kleine, T., et al. (2014). The Arabidopsis protein CONSERVED ONLY IN THE GREEN LINEAGE160 promotes the assembly of the membranous part of the chloroplast ATP synthase. *Plant Physiol.* 165, 207–226. doi: 10.1104/pp.114.237883

Ruwe, H., and Schmitz-Linneweber, C. (2012). Short non-coding RNA fragments accumulating in chloroplasts: footprints of RNA binding proteins. *Nucleic Acids Res.* 40, 3106–3116. doi: 10.1093/nar/gkr1138

Schmitz-Linneweber, C., and Small, I. (2008). Pentatricopeptide repeat proteins: a socket set for organelle gene expression. *Trends Plant Sci.* 13, 663–670. doi: 10.1016/j.tplants.2008.10.001

Shikanai, T. (2015). RNA editing in plants: machinery and flexibility of site recognition. *Biochim. Biophys. Acta* 1847, 779–785. doi: 10.1016/j.bbabio.2014.12.010

Small, I. D., and Peeters, N. (2000). The PPR motif - a TPR-related motif prevalent in plant organellar proteins. *Trends Biochem. Sci.* 25, 46–47. doi: 10.1016/S0968-0004(99)01520-0

Stern, D. B., Goldschmidt-Clermont, M., and Hanson, M. R. (2010). Chloroplast RNA metabolism. *Annu. Rev. Plant Biol.* 61, 125–155. doi: 10.1146/annurev-arplant-042809-112242

Till, B., Schmitz-Linneweber, C., Williams-Carrier, R., and Barkan, A. (2001). CRS1 is a novel group II intron splicing factor that was derived from a domain of ancient origin. *RNA* 7, 1227–1238. doi: 10.1017/S1355838201010445

Watkins, K. P., Kroeger, T. S., Cooke, A. M., Williams-Carrier, R. E., Friso, G., Belcher, S. E., et al. (2007). A ribonuclease III domain protein functions

in group II intron splicing in maize chloroplasts. *Plant Cell* 19, 2606–2623. doi: 10.1105/tpc.107.053736

Yap, A., Kindgren, P., Colas des Francs-Small, C., Kazama, T., Tanz, S. K., Toriyama, K., et al. (2015). AEF1/MPR25 is implicated in RNA editing of plastid *atpF* and mitochondrial *nad5*, and also promotes *atpF* splicing in Arabidopsis and rice. *Plant J.* 81, 661–669. doi: 10.1111/tpj.12756

Zhang, L., Duan, Z., Zhang, J., and Peng, L. (2016). BIOGENESIS FACTOR REQUIRED FOR ATP SYNTHASE 3 facilitates assembly of the chloroplast ATP synthase complex. *Plant Physiol.* 171, 1291–1306. doi: 10.1104/pp.16.00248

Zhang, L., Pu, H., Duan, Z., Li, Y., Liu, B., Zhang, Q., et al. (2018). Nucleus-encoded protein BFA1 promotes efficient assembly of the chloroplast ATP synthase coupling factor 1. *Plant Cell* 30, 1770–1788. doi: 10.1105/tpc.18.00075

Zhelyazkova, P., Hammani, K., Rojas, M., Voelker, R., Vargas-Suarez, M., Börner, T., et al. (2012). Protein-mediated protection as the predominant mechanism for defining processed mRNA termini in land plant chloroplasts. *Nucleic Acids Res.* 40, 3092–3105. doi: 10.1093/nar/gkr1137

Zhou, W., Lu, Q., Li, Q., Wang, L., Ding, S., Zhang, A., et al. (2017). PPR-SMR protein SOT1 has RNA endonuclease activity. *Proc. Natl. Acad. Sci. U.S.A.* 114, E1554–E1563. doi: 10.1073/pnas.1612460114

Zoschke, R., Kroeger, T., Belcher, S., Schottler, M. A., Barkan, A., and Schmitz-Linneweber, C. (2012). The pentatricopeptide repeat-SMR protein ATP4 promotes translation of the chloroplast *atpB/E* mRNA. *Plant J.* 72, 547–558. doi: 10.1111/j.1365-313X.2012.05081.x

Zoschke, R., Nakamura, M., Liere, K., Sugiura, M., Börner, T., and Schmitz-Linneweber, C. (2010). An organellar maturase associates with multiple group II introns. *Proc. Natl. Acad. Sci. U.S.A.* 107, 3245–3250. doi: 10.1073/pnas.0909400107

Zoschke, R., Qu, Y., Zubo, Y. O., Börner, T., and Schmitz-Linneweber, C. (2013). Mutation of the pentatricopeptide repeat-SMR protein SVR7 impairs accumulation and translation of chloroplast ATP synthase subunits in *Arabidopsis thaliana*. *J. Plant Res.* 126, 403–414. doi: 10.1007/s10265-012-0527-1

Conflict of Interest Statement: The authors declare that the research was conducted in the absence of any commercial or financial relationships that could be construed as a potential conflict of interest.

frontiers in Plant Science

ORIGINAL RESEARCH
published: 27 June 2019
doi: 10.3389/fpls.2019.00827

Transcriptional Regulation of the Glucose-6-Phosphate/Phosphate Translocator 2 Is Related to Carbon Exchange Across the Chloroplast Envelope

*Sean E. Weise[1,2], Tiffany Liu[3], Kevin L. Childs[3], Alyssa L. Preiser[1], Hailey M. Katulski[1], Christopher Perrin-Porzondek[1] and Thomas D. Sharkey[1,2,4]**

[1] MSU-DOE Plant Research Laboratory, Michigan State University, East Lansing, MI, United States, [2] Department of Biochemistry and Molecular Biology, Michigan State University, East Lansing, MI, United States, [3] Department of Plant Biology, Michigan State University, East Lansing, MI, United States, [4] Plant Resilience Institute, Michigan State University, East Lansing, MI, United States

The exchange of reduced carbon across the inner chloroplast envelope has a large impact on photosynthesis and growth. Under steady-state conditions it is thought that glucose 6-phosphate (G6P) does not cross the chloroplast membrane. However, growth at high CO_2, or disruption of starch metabolism can result in the *GPT2* gene for a G6P/P_i translocator to be expressed presumably allowing G6P exchange across the chloroplast envelope. We found that after an increase in light, the transcript for GPT2 transiently increases several 100-fold within 2 h in both the Col-0 and WS ecotypes of *Arabidopsis thaliana*. The increase in transcript for GPT2 is preceded by an increase in transcript for many transcription factors including Redox Responsive Transcription Factor 1 (RRTF1). The increase in *GPT2* transcript after exposure to high light is suppressed in a mutant lacking the RRTF1 transcription factor. The *GPT2* response was also suppressed in a mutant with a T-DNA insert in the gene for the triose-phosphate/P_i translocator (TPT). However, plants lacking TPT still had a robust rise in *RRTF1* transcript in response to high light. From this, we conclude that both RRTF1 (and possibly other transcription factors) and high amounts of cytosolic triose phosphate are required for induction of the expression of *GPT2*. We hypothesize that transient *GPT2* expression and subsequent translation is adaptive, allowing G6P to move into the chloroplast from the cytosol. The imported G6P can be used for starch synthesis or may flow directly into the Calvin-Benson cycle via an alternative pathway (the G6P shunt), which could be important for regulating and stabilizing photosynthetic electron transport and carbon metabolism.

Keywords: glucose 6-phosphate, G6P, GPT2, RRTF1, TPT, GAP, PGA, redox regulation

OPEN ACCESS

Edited by:
Jürgen Soll,
Ludwig Maximilian University of Munich, Germany

Reviewed by:
Hans-Henning Kunz,
Washington State University, United States
Rainer Erich Häusler,
University of Cologne, Germany
Anja Schneider,
Ludwig Maximilian University of Munich, Germany

***Correspondence:**
Thomas D. Sharkey
tsharkey@msu.edu

Specialty section:
This article was submitted to Plant Physiology, a section of the journal Frontiers in Plant Science

Received: *15 March 2019*
Accepted: *07 June 2019*
Published: *27 June 2019*

Citation:
Weise SE, Liu T, Childs KL, Preiser AL, Katulski HM, Perrin-Porzondek C and Sharkey TD (2019) Transcriptional Regulation of the Glucose-6-Phosphate/Phosphate Translocator 2 Is Related to Carbon Exchange Across the Chloroplast Envelope. Front. Plant Sci. 10:827. doi: 10.3389/fpls.2019.00827

INTRODUCTION

Plants live in a stochastic environment with drivers of photosynthesis such as CO_2 availability and light changing rapidly as abiotic factors such as cloud cover or humidity change over the course of minutes and hours. Hexose phosphate transport into plastids has been shown to allow plants achieve higher rates of photosynthesis over the course of several days when irradiance is increased (Dyson et al., 2015). This process of acclimation involves the differential expression (DE) and changes in abundance of hundreds of proteins in the chloroplast (Miller et al., 2017). The glucose-6-phosphate/phosphate translocator 2 (GPT2) in *Arabidopsis* is of particular interest as the expression for this protein increases rapidly, hours as opposed to days, when irradiance is increased (Athanasiou et al., 2010). We wanted to better understand the more rapid changes in gene expression, as opposed to acclimation, that occur when the photosynthetic rate of a plant increases. To this end, we focused on the role of GPT2 in carbon exchange across the chloroplast envelope.

Hexose phosphate transport into plastids was first documented 30 years ago. It was determined that starch synthesis in heterotrophic amyloplasts used imported hexose phosphates rather than triose phosphates (Keeling et al., 1988; Tyson and ap Rees, 1988). In 1995 it was discovered that autotrophic chloroplasts could also transport glucose 6-phosphate (G6P) if they were made heterotrophic by feeding sugars *in vitro* or when sugars accumulate in the cytosol *in vivo* (Quick et al., 1995; Lloyd and Zakhleniuk, 2004). It is now known that the hexose phosphate/phosphate (P_i) translocators are part of a family of sugar phosphate and phosphoenolpyruvate translocators that include triose phosphate/P_i translocators, pentose phosphate/P_i translocators, and phosphoenolpyruvate/P_i translocators (Fischer et al., 1997; Kammerer et al., 1998; Hejazi et al., 2014). The hexose phosphate/P_i translocators (GPTs) work like the triose-phosphate/P_i translocators (TPTs). One molecule of hexose monophosphate is exchanged for one molecule of P_i or another sugar phosphate (Lee et al., 2017). The GPTs are promiscuous and will transport triose phosphates as well as, or better than, G6P, but GPTs will not transport G1P or F6P (Kammerer et al., 1998; Eicks et al., 2002).

The concentration of G6P in the chloplast and cytosol has been measured in the light five times in four species, spinach,potato, bean, and *Arabidopsis* and one species, bean, in the dark. In all cases the G6P concentration was found to be greater in the cytosol than the stroma both day and night (Gerhardt et al., 1987; Sharkey and Vassey, 1989; Schleucher et al., 1999; Weise et al., 2006; Szecowka et al., 2013). This makes it unlikely that expression of a glucose-6-phosphate/P_i translocator results in net G6P export from the chloroplast but rather G6P would be transported from the cytosol to the stroma. Two GPTs have been identified in *Arabidopsis*, *GPT1* At5g54800, and *GPT2* At1g61800 (Niewiadomski et al., 2005). *GPT1* has a low constitutive level of expression in almost all tissue and is necessary for embryo sac development and pollen maturation; *gpt1* mutants are embryo lethal (Niewiadomski et al., 2005). *GPT2* has low, almost undetectable, expression in all tissues but high expression amounts have been seen in leaves when plants are fed or accumulate sugars (Lloyd and Zakhleniuk, 2004; Dyson et al., 2014). Plants in which starch metabolism is compromised have higher expression of *GPT2* and chloroplast membranes are able to transport G6P (Kunz et al., 2010). *GPT2* transcript also increases in leaves in response to an increase in light and plays a role in the photosynthetic acclimation to high light (Athanasiou et al., 2010; Dyson et al., 2015).

Our goal was to better understand the regulation and metabolic role of GPT2 in day time metabolism. We measured transcript amounts using both qPCR and RNA-Seq of *GPT2* and other related genes in both the Columbia-0 and Wassilewskija ecotypes of *Arabidopsis* and a number of mutants under a variety of photosynthetic conditions. From this work, we found that *GPT2* is transcriptionally regulated and requires both triose phosphate export from the chloroplast and the Redox Responsive Transcription Factor 1 (RRTF1) for expression. We hypothesize that GPT2 plays an important role in facilitating starch synthesis in stochastic high light conditions and may be necessary to maintain the redox poise of the cytosol.

MATERIALS AND METHODS

Plant Material and Growing Conditions

Wild-type *Arabidopsis thaliana* ecotype Columbia-0 (Col-0) and Wassilewskija (WS) and the mutants listed in **Table 1** were used. All mutants used have been previously characterized with the exception of *tpt-3* SALK_028503. We found that the T-DNA insert was in the first exon based on the primer sites used to confirm the line was homozygous for the insert. Transcript of the *TPT* gene was checked by qPCR and was below our detection limit (results not shown).

Plants were grown in a fluorescently lit growth chamber under a 12 h photoperiod with a photon flux density (PFD) of 120 μmol m^{-2} s^{-1}. The daytime temperature was 23°C and the nighttime temperature was 20°C. Humidity was held at a minimum of 60% relative humidity. All plants used in this study were grown hydroponically to prevent drought stress and other stresses that might affect expression of genes being studied. The hydroponic setup used also minimized water vapor and CO_2 loss from soil which can confound gas exchange measurements. Seeds were germinated on rockwool plugs which were placed in 1.5 ml microfuge tubes with the lower 1.5 cm tip cut off and watered with half-strength Hoagland's solution (Hoagland and Arnon, 1938). Once roots started to grow through the bottom of the plug, the plants were transferred to a water culture hydroponic system in which plants were suspended over a vigorously aerated half-strength Hoagland's solution contained in a dark tub. For all experiments, except RNA-Seq, data was collected from five biological replicates.

Changing Light and CO_2 Environments

Plants were placed so that their roots were suspended in a 50 ml disposable conical centrifuge tube containing half-strength Hoagland's solution. The tube and plant were then placed in a LI-COR 6800 or 6400 portable gas exchange system (LI-COR Biosciences, Lincoln, NE, United States). Both systems used the

TABLE 1 | *Arabidopsis* mutants used in this study.

Enzyme disrupted	Mutant	Gene locus	Ecotype	Mutant line and references
Glucan water dikinase	*sex1-8*	At1g10760	Col-0	SALK_077211 (Ritte et al., 2006)
Plastid fructose 1,6-bisphosphatase	*hcef1*	At3g54050	Col-0	Livingston et al., 2010
Glucose-6-phosphate/P_i translocator 2	*gpt2-1*	At1g61800	Col-0	GABI_454H06 (Dyson et al., 2014)
Plastid phosphoglucomutase	*pgm1-1*	At5g51820	Col-0	TC75, *pgm1-1* (Egli et al., 2010)
Redox responsive transcription factor 1	*rrtf1-1*	At4g34410	Col-0	Δ*rrtf1* SALK_150614 (Khandelwal et al., 2008)
Triose phosphate/P_i translocator	*tpt-3*	At5g46110	Col-0	SALK_028503 (This study)
Xylose-5-phosphate/P_i translocator	*xpt-2*	At5g17630	Col-3	SAIL_378_C01 (Hilgers et al., 2018)
Plastid phosphoglucomutase	*pgm1*	At5g51820	WS	ACG21 (Kiss et al., 1996)
Plastid starch phosphorylase	*phs1-1*	At3g29320	WS	Zeeman et al., 2004
Triose phosphate/P_i translocator	*tpt-1*	At5g46110	WS	Schneider et al., 2002

small plant chamber lit with a LI-COR 6800-03 or LI-COR 6400-18A light source set to white light. Plants from each ecotype and mutant line were used in both systems to control for any system effect on gene expression. White light was maintained at a PFD of 120 μmol m^{-2} s^{-1} or 500 μmol m^{-2} s^{-1}. Air temperature was held constant at 23°C and humidity was controlled at a dew point of 17 to 18.5°C. The CO_2 concentration in the sample air, C_a, was held at 20, 400, or 1000 ppm. A single leaf was taken from each plant after 0, 15, 30, 60, 120, and 240 min.

Photosynthesis Measurements

For photosynthetic and fluorescence measurements a single leaf was placed in a LI-COR 6800-01A multiphase flash fluorometer gas exchange chamber. For these measurements, leaf temperature was held constant at 23°C and humidity was controlled at a dew point of 17 to 18.5°C. The lighting was 50% red and 50% blue actinic light which was provided by the LEDs in the fluorometer head. All fluorometer settings were left at the factory default. The relative electron transport rate was calculated as ΦPSII × I (light intensity) × α (leaf absorptivity assumed to be 0.85) × β (fraction of quanta absorbed by PSII, assumed to be 0.5). The numbers for α and β are the default parameters provided by LI-COR. Because these were not measured in our leaves the ETR is taken as a relative rather than absolute measurement.

qPCR and Transcript Analysis

RNA was extracted using a Qiagen RNeasy Plant Mini Kit according to the manufacturer's directions. Once RNA was isolated, cDNA was synthesized using 1 μg of total RNA. Invitrogen Super Script II reverse transcriptase (18064, Thermo Fisher Scientific, Waltham, MA, United States) was used according to manufacturer's directions. An Eppendorf Mastercycler ep Realplex qPCR thermocycler with a 96 position silver block with SYBR green PCR master mix (4309155 Applied Biosystems, Carlsbad, CA United States) was used according to the manufacturer's directions. The thermal profile was: 95°C for 10 min; 40 cycles of 95°C for 15 s, and 60°C for 1 min during which fluorescence was measured. This was followed by a melting curve of: 95°C for 15 s, 60°C for 15 s, a ramp from 60 to 95°C over a 20 min period during which time fluorescence was monitored, and 95°C for 15 s. Transcript amounts were normalized using the *ACTIN2* (*ACT2*) or *ISOPENTENYL DIPHOSPHATE ISOMERASE2* (*IDI2*) housekeeping genes. Absolute transcript amounts of these genes were checked during the 4-h time course in altered light or CO_2 environments. This was done to ensure that the experimental treatment did not result in changes in housekeeping gene transcripts. Sequences for primers used are listed in **Supplementary Table S1**. Absolute copy number of transcripts was determined by using a slightly larger cDNA fragment of each target sequence as a standard. These cDNA standards were quantitated and dilutions were used to prepare standard curves.

Statistics

Box plots and statistical differences in *GPT2* expression between WT and mutants were tested by one-way ANOVA followed by Tukey's test using Microcal Origin 8.0 (Origin Lab Corporation, Northampton, MA, United States). Three levels of significance were tested and indicated by + α = 0.1; *α = 0.05; **α = 0.01. Box plots are presented with the box encompassing the middle two quartiles, the mean shown as an open square inside the box, the median as a line inside the box, and the whiskers showing the standard error of the data.

RNA-Seq Sampling and Sequencing

Three Col-0 and WS plants were used for RNA-Seq analysis and treated to a PFD of 500 μmol m^{-2} s^{-1} and sampled as above. All samples had an RNA integrity number of at least 7.0 as determined with a 2100 Bioanalyzer (Agilent Technologies, Santa Clara, CA, United States).

Single-end 50-bp mRNA sequencing was performed at the Michigan State University Research Technology Support Facility Genomics Core[1]. Libraries were prepared using the Illumina TruSeq Stranded mRNA Library Preparation Kit (Illumina, San Diego, CA, United States) following the manufacturer's recommendations. Completed libraries were assessed for quality and quantified using a combination of *Qubit dsDNA* High Sensitivity Assay Kit (Qubit, Carlsbad, CA, United States), Caliper LabChipGX System and a DNA High Sensitivity Assay Kit (Caliper Life Sciences, Waltham, MA, United States), and Kapa Illumina Library Quantification qPCR assays (Illumina, San Diego, CA, United States). Each set of libraries were pooled

[1]https://rtsf.natsci.msu.edu/genomics/

in equimolar quantities and loaded on one lane of an Illumina HiSeq 2500 High Output flow cell (v4) (Illumina, San Diego, CA, United States). Sequencing was carried out in a 1 × 50 bp (SE50) format using HiSeq SBS reagents (v4) (Illumina, San Diego, CA, United States). Base calling was done by Illumina Real-Time Analysis (R-TA) v1.18.64 and output of RTA was demultiplexed and converted to FastQ format with Illumina Bcl2fastq v1.8.4. The average number of sequencing reads was 41.7 ± 11.2 million per sample.

RNA-Seq Data Analysis

RNA-Seq data were subjected to gene DE analysis. Briefly, sequencing adapters and low quality bases were trimmed from sequencing reads using Trimmomatic version 0.32 (Bolger et al., 2014), and cleaned reads were examined using FASTQC software[2] for quality evaluation. Reads were aligned to the reference genome, *A. thaliana* TAIR10 (Berardini et al., 2015), using the STAR (2.3.0e) alignment program (Dobin et al., 2013). The featureCounts function in the Rsubread (version 3) package for R was used to calculate read counts for each gene (Liao et al., 2013), and data were normalized as reads per kilobase of transcript per million mapped reads, (RPKM). We removed data for genes that had no reading higher that 7 RPKM and genes whose expression did not vary by more than two-fold ($\log_2 < 1$). Data represented in heat maps is after 15, 30, 60, 120, or 240 min at a PFD of 500 μmol m^{-2} s^{-1}. For metabolic genes the data is the $\log_2$ of the ratio of the average RPKM value before and after light treatment. Data represented in heat maps of transcription factors is the $\log_2$ of the difference in the average RPKM value plus one before and after light treatment. Data for heat maps of transcription factors was calculated as a difference rather than a ratio because many transcription factors were not expressed or had expression amounts below our detection limit, RPKM = 0, before the light treatment. Heat maps were generated using the online Morpheus software[3]. The raw and processed data were deposited in the Gene Expression Omnibus (Edgar et al., 2002) and are accessible through GEO Series accession number GSEXXXXX[4]. (Raw RNA-Seq data is being submitted to NCBI, and accession numbers will be added during the revision process).

RESULTS

GPT2 Expression Is Related to Daytime Rather Than Nighttime Metabolism

In mutants of *Arabidopsis* that are unable to synthesize starch due to a mutation in the gene encoding the plastid phosphoglucomutase (*pgm1-1*), *GPT2* transcripts amounts were more than two-fold higher than in the wild type WS (**Figure 1A**). A similar result is seen in a mutant lacking the glucan water dikinase 1 (*sex1-8*) (**Figure 1B**). In both the *pgm1-1* and *sex1-8* mutants starch synthesis does not occur in fully mature leaves. Although *sex1-8* mutant leaves have a lot more starch than wild-type, a threshold is reached at some point in the life cycle of the leaf and further accumulation does not occur (Caspar et al., 1991; Trethewey and ap Rees, 1994; Hejazi et al., 2014). However, when the ability to make G6P from starch degradation in the plastid is blocked by eliminating the plastidic starch phosphorylase (*phs1-1*), *GPT2* transcript amounts were unchanged (**Figure 1C**). *GPT2* transcript amounts were also elevated in a mutant lacking plastidic Calvin-Benson cycle enzyme fructose 1,6-bisphosphatase (*hcef1*) (**Figure 1D**). *GPT2* transcript increases when starch synthesis or early steps in the Calvin-Benson cycle are blocked. However, the lack of *GPT2* transcript when, G6P producing, phosphorolytic starch degradation is blocked, suggests a more significant role for GPT2 in daytime metabolism.

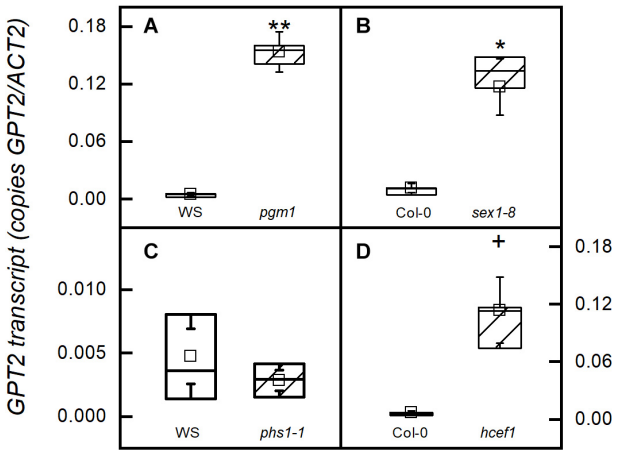

FIGURE 1 | *GPT2* expression in starch related mutants. All samples were taken from plants in growth conditions, PFD 120 μmol m^{-2} s^{-1} and 400 ppm CO_2. Transcripts were measured in **(A)** a starchless mutant (*pgm1-1*), **(B)** a starch excess mutant (*sex1-8*) that cannot degrade starch, **(C)** a starch phosphorylase knock out (*phs1-1*) that cannot carry out phosphorolytic starch degradation, and **(D)** a chloroplastic FBPase mutant (*hcef1*). *α = 0.05; **α = 0.01; + α = 0.1, *n* = 5.

GPT2 Is Expressed When Photosynthesis Is Increased by Light

A switch from a PFD of 120 to 500 μmol m^{-2} s^{-1} increased *GPT2* expression in Col-0, but 500 μmol m^{-2} s^{-1} of light with photosynthesis restricted by 20 ppm CO_2 did not result in increased expression (**Figures 2A,B**). 1000 ppm CO_2 alone did not result in an increase in *GPT2* transcript (**Figure 2C**). Plants were also placed in the gas exchange system at growth conditions of 120 μmol m^{-2} s^{-1} of light and 400 ppm CO_2 to make sure that moving the plants into the gas exchange system for 4 h did not result in an increase in transcript (**Figure 2D**). The same patterns were observed in the WS ecotype (**Supplementary Figure S1**).

The effect of an increased PFD of 500 μmol m^{-2} s^{-1} on photosynthesis was determined by taking *A*-C_i curves before and after the 4-h light treatment. No change was observed in the Col-0 or WS ecotype, indicating that there were no significant non-photochemical processes or photo damage (**Figure 3** and

[2]https://www.bioinformatics.babraham.ac.uk/projects/fastqc/

[3]https://software.broadinstitute.org/morpheus

[4]http://www.ncbi.nlm.nih.gov/geo/query/acc.cgi?acc=GSEXXXXX

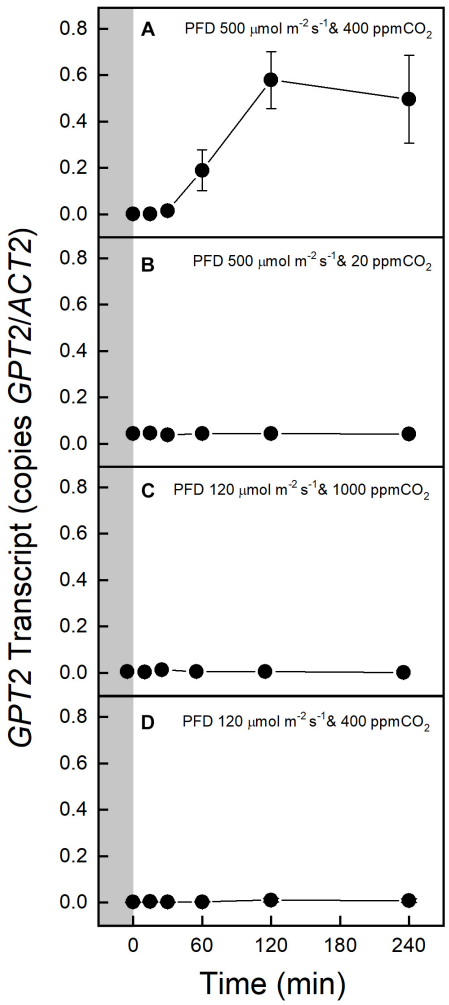

FIGURE 2 | Expression of *GPT2* in Col-0 before and after transfer to an altered light or CO_2 environment. The gray block indicates sampling in growth conditions, PFD 120 μmol m^{-2} s^{-1} and 400 ppm CO_2. Panels **A–D** show responses to various light and CO_2 treatments as indicated on the figure. $n = 5$.

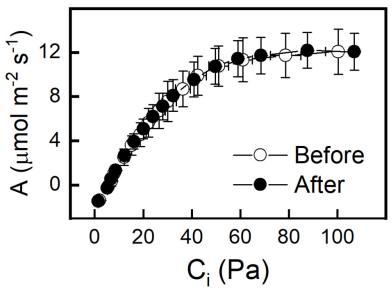

FIGURE 3 | A – C_i curves of Col-0 taken before and after 4 h incubation at a PFD of 500 μmol m^{-2} s^{-1} and C_a of 400 ppm. A – C_i curves were done at a PFD of 500 μmol m^{-2} s^{-1}. $n = 5$.

Supplementary Figure S2). To better understand why increased light but not increased CO_2 resulted in an increase in *GPT2* transcript both photosynthesis and relative electron transport rates (ETR) were measured at a variety of different PFDs and CO_2 concentrations. The relative electron transport rate divided by four was taken as an approximate turnover rate of the Calvin-Benson cycle. This is because four electrons are used per two NADPH needed for RuBP regeneration. Increasing the PFD from 120 to 500 μmol m^{-2} s^{-1} increased the photosynthetic rate by 86% and increased the Calvin-Benson cycle turnover by 122% (**Supplementary Figures S3A,B**). Increasing CO_2 alone caused a 40% increase in assimilation but only a 1.4% increase in Calvin-Benson cycle turnover (**Supplementary Figures 3C,D**). The increase in light resulted in a much larger increase in photosynthesis and Calvin-Benson cycle turnover than did an increase in CO_2.

GPT2 and *XPT* Expression Are Not Affected by Each Other

The XPT may transport pentose phosphates into the chloroplast from the cytosolic oxidative pentose phosphate pathway (cytosolic G6P shunt). *GPT2* transcript was measured in the *xpt-2* mutant. No significant difference was observed between the *xpt-2* mutant and wild type in response to an increased PFD of 500 μmol m^{-2} s^{-1} (**Supplementary Figure S4A**). There was also no difference in *GPT2* expression when the plastidic starch phosphorylase (*phs1-1*) was missing (**Supplementary Figure S4B**). Conversely *XPT* transcript was measured in response to increased light in the *gpt2-1* mutant. There was no transcriptional evidence for XPT compensating for GPT2. Transcript amount of *XPT* was low and unchanged and was also unchanged in the *phs1-1* mutant background (**Supplementary Figures S4C,D**).

Starch Synthesis Is Upregulated While Other Pathways Are Downregulated

An RNA-Seq analysis was performed to examine changes in the entire transcriptome when plants were taken from low to high light. RNA was taken from leaves after they were exposed to high light at ambient CO_2 conditions for 15, 30, 60, 120, and 240 min and the ratio in transcript amount from the zero time point (low light, ambient CO_2) was determined. Genes coding for enzymes in the Calvin-Benson cycle, the chloroplast G6P shunt, starch synthesis, sucrose synthesis, and cytosolic glycolysis were identified. A complete list of the gene loci for biochemical pathways of interest was collated (**Supplementary Appendix S1**). From these lists, only transcripts with an RPKM value greater than 7 and an absolute fold change greater than 2 ($\log_2$ value $> |1|$) at any one time point were examined. The *Arabidopsis* gene loci from **Supplementary Appendix S1** that were identified as being differentially expressed are listed in **Supplementary Table S2**.

Transcripts for every enzyme in the Calvin-Benson cycle and of genes coding for electron transport proteins, identified by Dyson et al. (2015), decreased during the 240 min high light treatment. The transcripts meeting the cutoff stated above for enzymes in the Calvin-Benson cycle are shown in **Figure 4**. There

was a large increase in transcript amounts for most enzymes involved in starch synthesis (**Figure 4**). There was a steep decline in transcripts for the most highly expressed sucrose synthesizing enzymes sucrose-phosphate synthase 4 (SPS4) and sucrose-phosphate phosphatase 2 (SPP2) (**Figure 4**). *GPT2* transcript was much higher in the RNA-Seq experiment as had been seen with qPCR (**Figure 2A**). The transcript amount for the *TPT* decreased by 15 min and was down 65% after 120 min. The same pattern of changes was observed in the WS ecotype (**Supplementary Figure S5**).

Transcript amounts for proteins involved in the cytosolic glycolysis pathway were examined. Most genes in this pathway were not differentially expressed. Two uncharacterized pyruvate kinases, At5g63680, and At3g52990 had increased transcript amounts (data not shown). *Arabidopsis* has three glyceraldehyde phosphate dehydrogenases in the cytosol. The only one

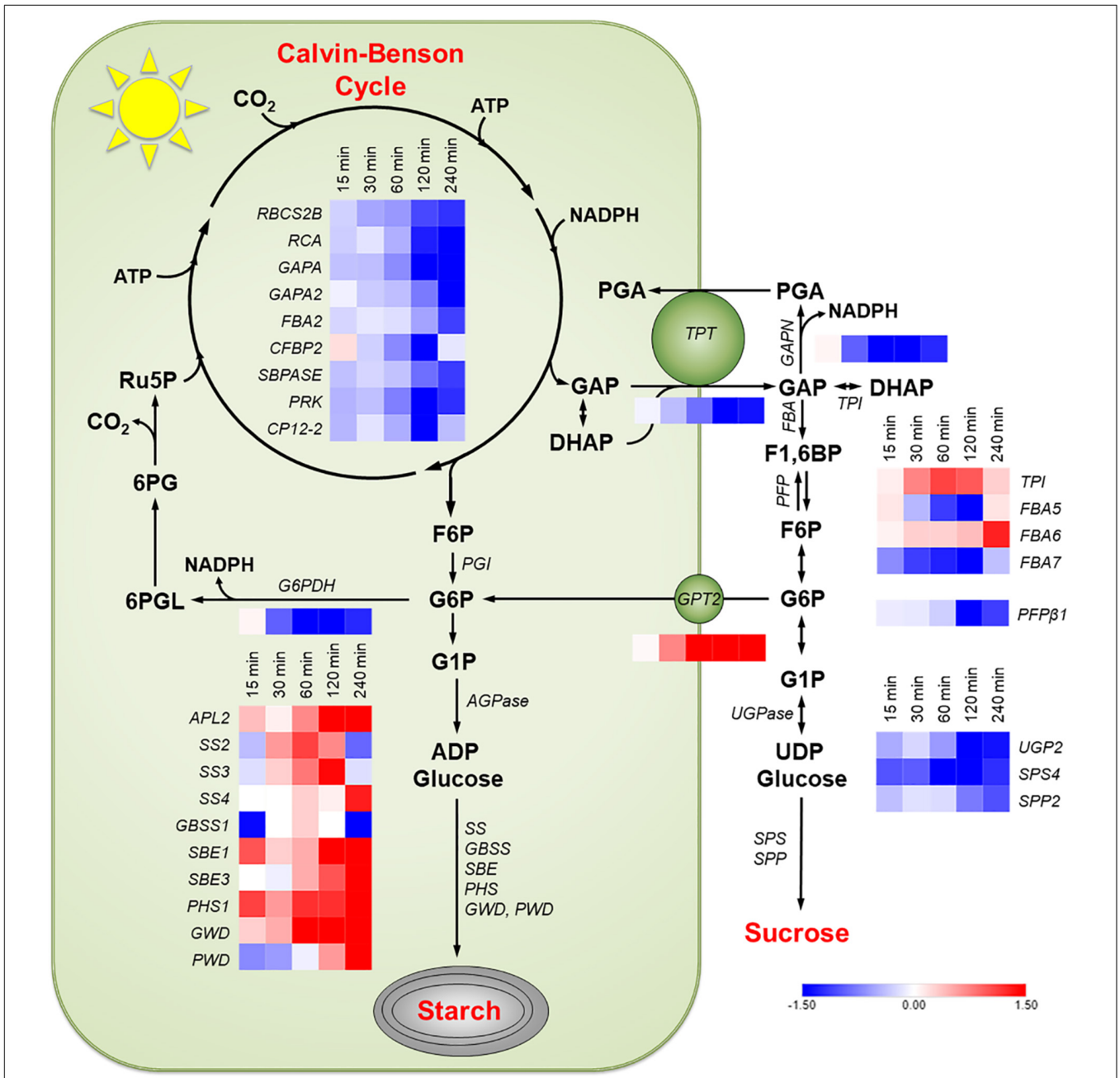

FIGURE 4 | Changes in transcription in Col-0 in response to an increase in PFD from 120 to 500 μmol m^{-2} s^{-1}. Transcripts of the following pathways or genes are shown: Calvin-Benson cycle, starch synthesis, sucrose synthesis, the G6P shunt, the non-phosphorylating GAPDH (*GAPN*) in the cytosol, the glucose-6-phosphate transporter (*GPT2*), and the triose phosphate transporter (*TPT*). Red boxes represent an increase in transcription and blue a decrease. Expression values shown had a $\log_2$ RPKM fold change greater than one and are on an absolute scale of −1.5 to 1.5. $n = 3$.

that was differentially expressed in response to high light was the non-phosphorylating glyceraldehyde-3-phosphate dehydrogenase (GAPN). *GAPN* transcript was down 56% after 120 min (**Figure 4**). This pattern was also observed in the WS ecotype (**Supplementary Figure S5**). G6P shunt (Sharkey and Weise, 2016) transcripts were also examined in Col-0 and WS. Transcript for *glucose-6-phosphate dehydrogenase 1* (*G6PDH*) decreased by 87% (**Figure 3** and **Supplementary Figure S6**). This decrease was validated by qPCR. *G6PDH2* also decreased and *G6PDH3* had a very low and unchanging expression amount (**Figure 5** and **Supplementary Figure S6**).

Transcript amounts for proteins involved in protecting photosynthetic electron transport and PSII repair were examined to determine if light stress was a factor in these experiments. Transcripts of eight genes were differentially expressed according to the cutoff criteria stated above. From this group of eight, seven had decreasing transcript amounts and only one PSII assembly factor *Slr1768* At5g51570 (Nickelsen and Rengstl, 2013), had an approximate 2.7 fold increase after 4 h (data not shown). Because there was no decrease in photosynthesis after 4 h at a PFD of 500 μmol m^{-2} s^{-1} and transcript of only one gene for PSII repair increased, it was concluded that light stress was not a significant factor.

Transcripts for 30% of Transcription Factors Were Differentially Expressed

Transcript amounts were examined from the RNA-Seq data of all genes identified as transcription factors or possible transcription factors by the *Arabidopsis* Gene Regulatory Information Server (AGRIS[5]). From this initial pool of 1823 genes 183 were discarded because their sequences were not detected in this experiment. Four hundred and 84 genes, 30%, were selected that had a change in the RPKM value (ΔRPKM) between zero and either 15, 30, 60, 120, or 240 min time points in either Col-0 or WS that was greater than or equal to seven. This cutoff eliminated as many non-responding transcription factors as possible while still containing 15 of the 19 transcription factors that were identified by Vogel et al. (2014) as being quickly upregulated in response to high light and involved in retrograde, chloroplast to nucleus, signaling. From this pool 227 and 209 transcription factors, 13%, in Col-0 and WS, respectively, were selected that showed increased expression in response to light. Increased expression was defined as transcripts with a RPKM value that increased from the initial time zero value by two or more at any of the sampling time points and did not decrease at any time point by more than the initial RPKM value minus two. These pools contained 11 and 10 of the Vogel et al. (2014) transcription factors in Col-0 and WS, respectively.

Waves of increased expression of transcription factors were observed between the 15 and 240 min sampling time points (**Figure 6** and **Supplementary Figure S5**). Transcription factors that had a maximal transcript abundance at the 30 or 60 min sampling time points were of particular interest because they preceded the maximal abundance of *GPT2* at 120 min (**Figures 2**, **4**). From this list of 19 transcription factors identified by Vogel et al. (2014) the *RRTF1* had the highest transcript abundance at the 30 or 60 min sampling time (**Figure 6** and **Supplementary Figure S7**).

[5]https://agris-knowledgebase.org/

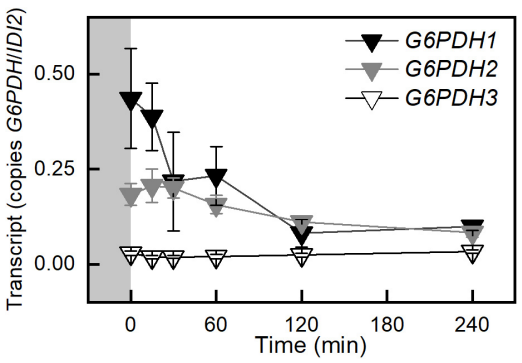

FIGURE 5 | Changes in transcription of the plastid *G6PDHs* in Col-0 in response to an increase in PFD from 120 to 500 μmol m^{-2} s^{-1} C_a 400 ppm. Gray block indicates sampling in growth conditions, PFD 120 μmol m^{-2} s^{-1} and 400 ppm CO_2. $n = 5$.

GPT2 Expression Is Repressed in the *tpt-3* and *rrtf1-1* Mutants

Based on the results of transcript analysis by qPCR or RNA-Seq the expression of *GPT2* or *RRTF1* was examined in various mutant backgrounds. *GPT2* transcript was elevated 34 fold in the *pgm1-1* mutant at time 0 in a PFD of 120 μmol m^{-2} s^{-1} (**Figure 7A**). This was similar in magnitude to the increased *GPT2* expression in the *pgm1-1* mutant observed in **Figure 1**. This 34 fold increase in *GPT2* was dwarfed by the 1,321 fold increase observed after 4 h at a PFD of 500 μmol m^{-2} s^{-1} and thus cannot be seen in the figure (**Figure 7A**). In Col-0 or WS after 240 min the expression of *GPT2* was attenuated. This attenuation did not occur in *pgm1-1* mutant plants with transcript amounts of 120% higher than WT (**Figure 7A**). In plants missing the TPT, the increase in expression of *GPT2* in response to high light was reduced by 74% (**Figure 7A**). This was also observed in a *tpt-1* mutant line in the WS background (**Supplementary Figure S8A**). *GPT2* expression was reduced in *rrtf1-1* mutant plants (**Figure 7A**). To determine if triose phosphates in the cytosol controlled the expression of *RRTF1*, *RRFT1* expression was measured in *tpt-3* mutant plants. *RRTF1* transcript increased in response to high light in the *tpt-3* mutant to the same degree as WT in with the Col-0 and WS backgrounds (**Figure 7B** and **Supplementary Figure S8B**). The pattern of *RRTF1* expression was the same as was observed in the RNA-Seq data.

DISCUSSION

Expression of GPT2 Requires Triose Phosphate Export and RRTF1

Expression of both *TPT* and *RRTF1* are necessary for the increased expression of *GPT2*. If either one of these is missing

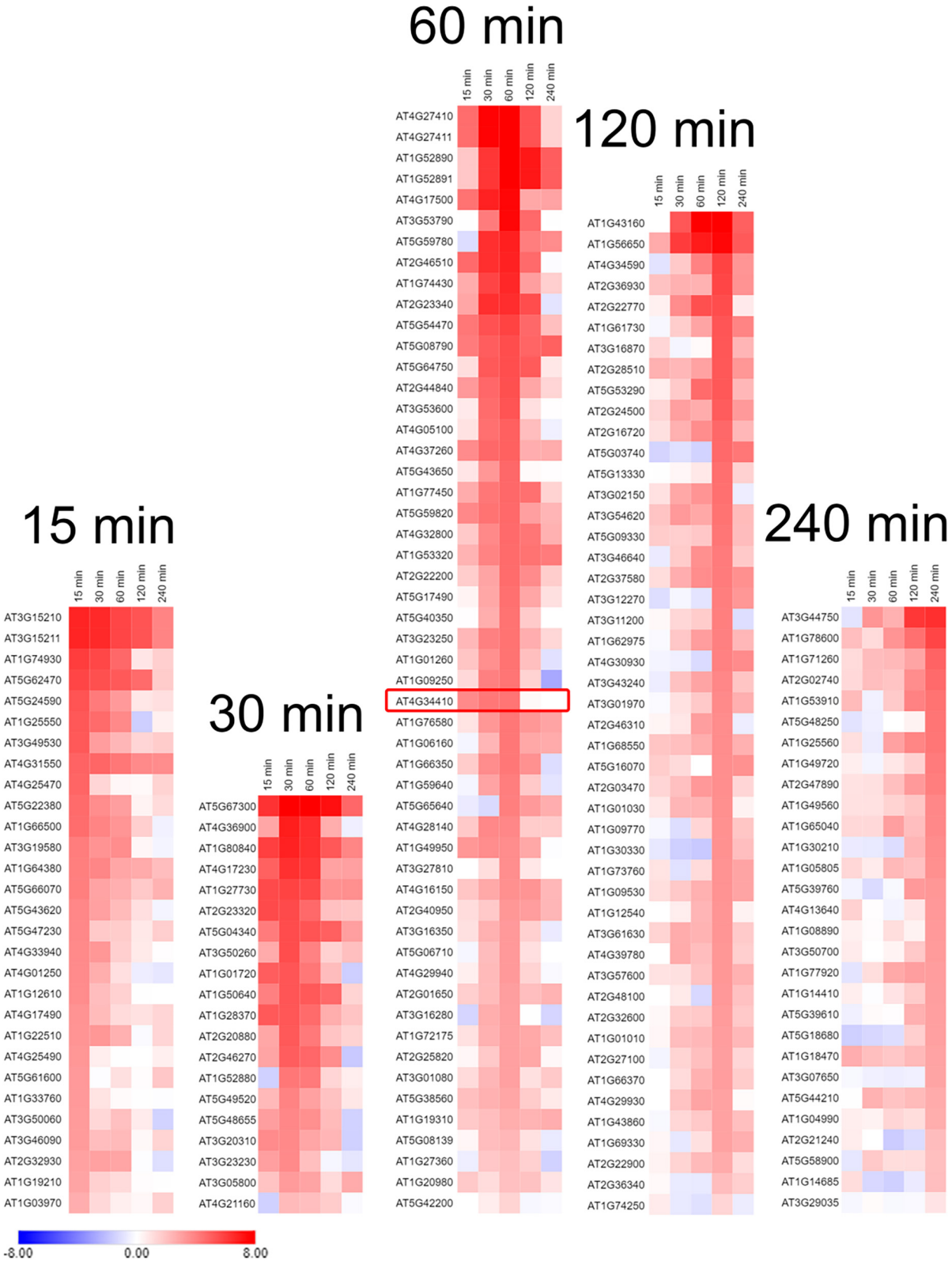

FIGURE 6 | Transcription factors in Col-0 whose expression was increased in response to an increase in PFD from 120 to 500 μmol m^{-2} s^{-1}. Transcription factors are grouped according to the time they had the highest transcript abundance after transfer to high light. The red box is around the *RRTF1* transcription factor. Expression values used for heat map generation are the $\log_2$ ΔRPKM + 1 and are on an absolute scale of –8 to 8. n = 3.

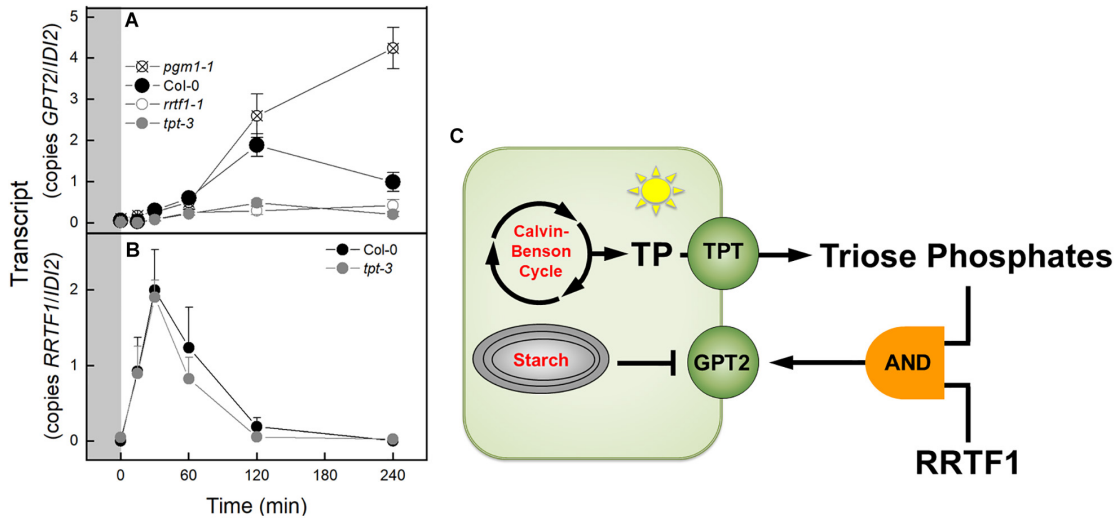

FIGURE 7 | Expression of *GPT2* and *RRTF1* in response to an increase in PFD from 120 to 500 μmol m^{-2} s^{-1} C_a 400 ppm in Col-0 and mutants and model of transcriptional regulation of *GPT2*. **(A)** qPCR data of expression of *GPT2* in Col-0 and *pgm1-1*, *rrtf1-1*, and *tpt-3* mutants. $n = 5$ **(B)** qPCR data of expression of *RRTF1* in Col-0 and *tpt-3* mutant. $n = 5$ **(C)** Model of transcriptional regulation of *GPT2* expression. Triose phosphates in the cytosol and *RRTF1* are both required for expression of *GPT2* (shown as an "AND" logic gate) while starch synthesis represses *GPT2* expression.

transcript of *GPT2* does not increase in response to an increase in light. The lack of *GPT2* transcript response to an increase in light in a *tpt* mutant has been seen before (Kunz et al., 2010; Heinrichs et al., 2012). This is presumably due to low triose phosphate concentration in the cytosol. The triose phosphates themselves could act as a signal (Häusler et al., 2014). Another possibility is that the sucrose generated from the triose phosphates is acting as a signal. In similar light jump experiments to ours, Schmitz et al. (2014) measured sucrose amounts in Col-0 and the *adg1-1* starchless mutant of *Arabidopsis* for 8.3 h after being transferred from a PFD of 30 to 300 μmol m^{-2} s^{-1}. The pattern of sucrose accumulation in the leaves mirrors the pattern of *GPT2* transcript seen in WT and the *pgm1-1* mutant. Sucrose would present a more stable signal than rapidly fluctuating triose phosphate amounts and signaling by sucrose via invertases and hexokinase is well documented (Li and Sheen, 2016).

A third possibility is that a change in export of triose phosphates could cause change in the redox status of the cytosol. Glyceraldehyde 3-phosphate (GAP) could be converted to phosphoglycerate (PGA) by the non-phosphorylating glyceraldehyde-3-phosphate dehydrogenase (GAPN) resulting in the production of NADPH in the cytosol (Habenicht, 1997). The PGA could then be reimported to the chloroplast via the TPT or further metabolized and imported as PEP, or pyruvate. This could result in a change in the redox poise of the cytosol that is concomitant with a change in triose phosphate export. This change in redox could be the signal that activates *RRTF1* (Vogel et al., 2014). However, based on our results, *RRTF1* is induced independently of triose phosphate concentration in the cytosol. The increase in *RRTF1* transcript in the *tpt-3* mutant (**Figure 7B**) was not seen by Vogel et al. (2014). After carefully scrutinizing the methods of the Vogel et al. (2014) study the reason for this difference is unclear.

There are likely other transcription factors that influence GPT2 expression. Our RNA-Seq results revealed over 70 transcription factors with a similar transcript profile to *RRTF1* (**Figure 6**). Further the regulation of *GPT2* transcript by RRTF1 may be indirect. However, RRTF1 was of particular interest because of its identification by Vogel et al. (2014) as early acting – minutes as opposed to days – in response to increased light and to be involved in retrograde, chloroplast to nucleus, signaling. *RRTF1* had the highest expression of the 19 transcription factors identified by Vogel in the 30–60 min window preceding the rise in *GPT2* expression. To determine if the interaction between *GPT2* and RRTF1 is direct, experiments could be done in which the promoter of GPT2 is tested for interaction with RRTF1 protein using a yeast one-hybrid system or a plant cell GUS-dependent assay (Berger et al., 2007). Based on our results with both *tpt-3* and *rrtf1-1* mutants we conclude that at least both TPT and RRTF1 are required for expression of *GPT2*, the two acting as inputs to a logic "AND" gate (**Figure 7C**).

When starch metabolism is blocked, *GPT2* transcript continues to increase in response to increased light but in WT, *GPT2* transcript amount declines after 4 h (**Figure 7A**). This attenuation could be caused by a reduction of triose phosphate entry into the cytosol. It could also be caused by an increase in triose phosphate conversion to hexose phosphate and re-import into the chloroplast and starch synthesis. This possibility is consistent with the increase in TPI and FBP aldolase (FBA6) expression (**Figure 4**). Transcript amounts for enzymes in starch synthesis increased after 15 min of higher light and an increase in protein and activity would be possible after 2- 4 h (**Figure 4** and **Supplementary Figure S5**), when a drop in *GPT2* transcript is observed (**Figure 2A** and **Supplementary Figure S1A**).

GPT2 could play an important role in controlling the source-sink balance of triose phosphates in the cytosol. When there

is a rapid increase in the photosynthetic rate, caused by light, transcripts of genes related to sugar phosphate anabolism might be expected to increase. However, there is a large decline in transcripts of genes in the Calvin-Benson cycle and of the triose phosphate transporter. This leads to the hypothesis that unregulated triose phosphate production and export are a problem for the plant. *GPT2* expression could lead to more GPT2 protein in the chloroplast envelope. This may result in a larger plastid sink for hexose phosphate and in turn a greater proportion of triose phosphates being converted to hexose phosphates and used in starch synthesis. This would decrease the amount of GAP that could be acted upon by GAPN (**Figure 4**, Pathway) and prevent an over reduction of the cytosol.

Starch and sucrose are the two largest end products of photosynthesis (McClain and Sharkey, 2019). When photosynthesis increases, an increase in transcript amounts for enzymes in both starch and sucrose synthesis could be expected. However, a reduction in expression of three critical genes involved in sucrose synthesis was observed (**Figure 4** and **Supplementary Figure S5**). In the process of acclimation, days as opposed to hours, an increase in enzymes related to sucrose synthesis has been observed in response to increased light (Miller et al., 2017). In the short term, there is generally a stronger increase of transcripts for processes leading from triose phosphates to hexose phosphate with triose phosphate isomerase standing out, having over a twofold increase in transcript amounts 60 min after being transferred to high light. Changes in expression related to G6P metabolism and transport may serve two functions. It may increase starch synthesis by bypassing the plastidic PGI, or it may provide an additional sink for triose phosphates so that GAP is not converted to PGA by GAPN, disturbing the redox poise of the cytosol.

Decreasing Transcript for G6PDH1 May Limit Carbon Entry Into the G6P Shunt

The import of G6P via GPT2 could be problematic because it could also be acted on by glucose-6-phosphate dehydrogenase (G6PDH) in the chloroplast (Preiser et al., 2019). G6PDH is generally considered to be deactivated in the light when the chloroplast stroma is reduced. During the day, when the stroma is reduced, the K_m of G6PDH increases, but some residual activity remains (Scheibe et al., 1989; Hauschild and von Schaewen, 2003; Preiser et al., 2019). It has been shown that this inhibition of activity can be reversed in bacteria by low mM concentrations of G6P (Cossar et al., 1984). This would result in the G6P entering the G6P shunt leading to a futile cycle consuming ATP and releasing CO_2 (Sharkey and Weise, 2016; Preiser et al., 2019). Under certain circumstances this shunt may be adaptive allowing the generation of pentose phosphates to restart the Calvin-Benson cycle when triose phosphates are depleted. It could also mitigate a high ATP/NADPH ratio under conditions of high cyclic electron transport (Sharkey and Weise, 2016). *Arabidopsis* has three G6PDH enzymes in the chloroplast, G6PDH1, 2, and 3 (Wakao and Benning, 2005). Transcript for G6PDH1 (**Figure 5** and **Supplementary Figure S6**), and to a lesser extent G6PDH2, rapidly decrease after the light is increased. It has been proposed that these two contribute the majority of activity for the chloroplast G6PDHs (Wakao and Benning, 2005). One interpretation of the data is that expression of *GPT2* in response to increased light leads to an increase in G6P concentration in the stroma and the reduction in expression of *G6PDH1* and *2* lead to reduced G6PDH activity, limiting the flow of carbon into the G6P shunt.

GPT2 Expression May Reflect Daytime Metabolic Needs Rather Than Nighttime

Mutants of *Arabidopsis* that are unable to make starch due to a mutation in the plastidic *PGM* have elevated transcript for *GPT2* (**Figure 1**). The effect of mutations in genes required for starch synthesis on *GPT2* expression has been seen before in mutants in *PGI1*, *PGM1*, and *AGPase* (Bläsing et al., 2005; Kunz et al., 2010). A mutant with a T-DNA insert in the gene for the glucan water dikinase enzyme, the *sex1-81* mutant, can make starch but cannot use it (Ritte et al., 2002). An increase in *GPT2* transcript is also seen in this mutant. The starch phosphorylase, *phs1-1*, mutant does not have elevated *GPT2* transcript (**Figure 1**). Because of this the increase in *GPT2* transcript in mutants unable to make or mobilize starch is probably not caused by a depletion of hexose phosphates at night. Additionally, it has been shown that *GPT2* transcript in starchless mutants is repressed in the dark (Kunz et al., 2010).

The increase in *GPT2* transcript in the starchless or starch excess mutants could be the result of increased triose phosphates in the cytosol that are not being partitioned into starch. It has been suggested that in starchless mutants, GPT2 may serve to export G6P from the chloroplast (Kunz et al., 2010). In a wild type plant, export of G6P would be unlikely due to the large concentration gradient of G6P measured between the cytosol and chloroplast (Gerhardt et al., 1987; Weise et al., 2006; Szecowka et al., 2013). The concentration difference of G6P between the chloroplast and cytosol in starchless mutant or starch excess mutants is unknown. GPT2 can transport triose phosphates as well as or better than hexose phosphates (Kammerer et al., 1998; Eicks et al., 2002) leaving open the possibility that GPT2 simply serves as an additional export mechanism for triose phosphates in the starchless background.

GPT2 Expression Allows a Bypass of Calvin-Benson Cycle FBPase

When the Calvin-Benson cycle enzyme fructose-1,6-bisphosphatase (FBPase) is missing, *GPT2* transcript amounts are increased (**Figure 1**). The cytosolic FBPase could be used, bypassing the stromal FBPase when GPT2 is present. This comes at a cost of growth and increased cyclic electron transport (Livingston et al., 2010). The chloroplast PGI favors the reaction from F6P to G6P (Preiser et al., 2018). Therefore, *GPT2* expression could result in the chloroplastic G6P concentration being higher than normal. This G6P could be acted on by G6PDH and enter the G6P shunt, detailed above. Any increase in the G6P shunt would result in the need for extra ATP which could be provided by cyclic electron transport. A similar scenario has been seen in *Arabidopsis* plants in which the plastidic triose

phosphate isomerase is inhibited by high concentrations of 2-phosphoglycolate. These plants also have elevated expression of *GPT2* and have higher cyclic electron transport (Li et al., 2019). Plants lacking the stromal FBP aldolase have higher cyclic electron flow consistent with this hypothesis (Gotoh et al., 2010) although it is not known if they have increased expression of *GPT2*. In another study using a chloroplast FBPase mutant, elevated *GPT2* transcript was seen but only in the roots (Soto-Suárez et al., 2016). The reasons for the spatial difference in *GPT2* expression observed between our study and that one are unclear. Another possible explanation for the survival of the *hcef1* mutant is a novel redox insensitive plastid FBPase that was found in strawberry but appears to have an ortholog in *Arabidopsis* (Serrato et al., 2009). This use of an alternative FBPase does not explain the increased *GPT2* transcript and high cyclic ETR seen in the *hcef1* mutant.

Another possible pathway for carbon exit and reentry into the chloroplast is the oxidative pentose phosphate pathway in the cytosol. It has been shown that the cytosolic G6PDH in potato is sensitive to the sugar status of the cell and is transcriptionally regulated (Hauschild and von Schaewen, 2003). Using this pathway, carbon could reenter the chloroplast though the xylulose-5-phosphate transporter (XPT). If this pathway is used there is no evidence for transcriptional regulation of it. The transcript amount for XPT was unchanged in the wild type, *gpt2-1* or *phs1-1* mutants (**Supplementary Figure S4**). Further, no change in transcript was seen in the RNA-Seq data for XPT or any enzyme, including the three G6PDHs in the cytosolic pentose phosphate pathway (data not shown).

Only an Increase in Calvin-Benson Cycle Activity Caused *GPT2* Transcript to Increase

Increasing CO_2 has been shown to increase the expression of a homologous gene to *GPT2* in soybean in a Free Atmosphere CO_2 Enrichment (FACE) experiment (Leakey et al., 2009). In our experiment, CO_2 was increased under a PFD of 120 μmol m^{-2} s^{-1} rather than the higher PFD of the FACE site field conditions. No change in *GPT2* expression was observed (**Figure 2C** and **Supplementary Figure S1C**). Under these conditions the assimilation rate and electron transport rate increased only modestly (**Supplementary Figure S3**). This most likely did not result in a large change in cytosolic triose phosphate or sucrose concentration or redox status that appears likely to be the drivers of *GPT2* expression.

CONCLUSION

Glucose-6-phosphate/phosphate translocator 2 is at the confluence of metabolic adjustment to sudden increases in carbon assimilation. While normally not expressed, *GPT2* transcript rapidly increases when the rate of photosynthesis increases. The time course of RNA-Seq results after an increase in photosynthesis provides valuable insights into the metabolic tradeoffs plants make. When photosynthesis increases, GPT2 may act as a safety-valve, shunting sugar phosphates away from the NADPH-producing non-phosphorylating GAPDH. At the same time GPT2 can also shunt extra carbon toward starch synthesis, bypassing the regulatory stromal PGI. Connecting the cytosolic and stromal G6P pools comes at a cost. The increase in G6P in the chloroplast may activate the stromal G6PDH leading to loss of ATP and loss of carbon, when 6-phosphogluconate dehydrogenase in the G6P shunt releases CO_2. However, the reduction in expression of genes related to sucrose synthesis is puzzling.

DATA AVAILABILITY

The datasets generated for this study can be found in Gene Expression Omnibus. The raw and processed data were deposited in the Gene Expression Omnibus (Edgar et al., 2002) and are accessible through the GEO Series accession number GSE132626 (http://www.ncbi.nlm.nih.gov/geo/query/acc.cgi?acc=GSE132626) (Raw RNA-Seq data is being submitted to the NCBI, and accession numbers will be added during the revision process).

AUTHOR CONTRIBUTIONS

SW and TS designed the experiments. SW carried out the bulk of the research. KC and TL carried out the RNA-Seq and the initial analysis of RNA-Seq data. AP, HK, and CP-P worked out some of the qPCRs and analyzed the results. SW wrote the manuscript. TS edited the manuscript.

FUNDING

This work was supported by the United States Department of Energy Grant DE-FG02-91ER2002 and partially supported by Michigan AgBioResearch to TS. AP was partially supported by a fellowship from Michigan State University under the Training Program in Plant Biotechnology for Health and Sustainability (T32-GM110523).

ACKNOWLEDGMENTS

We thank Dr. Ching Man (Jennifer) Wai for many thoughtful discussions about hexose phosphate transport and RNA-Seq data, Dr. David Kramer for many thoughtful insights and discussion, and Dr. Mio Sato-Cruz for help with hcef1, and the two reviewers for pointing out the potential for sucrose signaling in *GPT2* expression.

SUPPLEMENTARY MATERIAL

The Supplementary Material for this article can be found online at: https://www.frontiersin.org/articles/10.3389/fpls.2019.00827/full#supplementary-material

REFERENCES

Athanasiou, K., Dyson, B. C., Webster, R. E., and Johnson, G. N. (2010). Dynamic acclimation of photosynthesis increases plant fitness in changing environments. *Plant Physiol.* 152, 366–373. doi: 10.1104/pp.109.149351

Berardini, T. Z., Reiser, L., Li, D. H., Mezheritsky, Y., Muller, R., Strait, E., et al. (2015). The *Arabidopsis* information resource: making and mining the "gold standard" annotated reference plant genome. *Genesis* 53, 474–485. doi: 10.1002/dvg.22877

Berger, B., Stracke, R., Yatusevich, R., Weisshaar, B., Flügge, U.-I., and Gigolashvili, T. (2007). A simplified method for the analysis of transcription factor–promoter interactions that allows high-throughput data generation. *Plant J.* 50, 911–916. doi: 10.1111/j.1365-313X.2007.03088.x

Bläsing, O. E., Gibon, Y., Günther, M., Höhne, M., Morcuende, R., Osuna, D., et al. (2005). Sugars and circadian regulation make major contributions to the global regulation of diurnal gene expression in *Arabidopsis*. *Plant Cell* 17, 3257–3281. doi: 10.1105/tpc.105.035261

Bolger, A. M., Lohse, M., and Usadel, B. (2014). Trimmomatic: a flexible trimmer for Illumina sequence data. *Bioinformatics.* 30, 2114–2120. doi: 10.1093/bioinformatics/btu170

Caspar, T., Lin, T. P., Kakefuda, G., Benbow, L., Preiss, J., and Somerville, C. (1991). Mutants of *Arabidopsis* with altered regulation of starch degradation. *Plant Physiol.* 95, 1181–1188. doi: 10.1104/pp.95.4.1181

Cossar, J. D., Rowell, P., and Stewart, W. D. P. (1984). Thioredoxin as a modulator of glucose-6-phosphate dehydrogenase in a N2-fixing cyanobacterium. *Microbiology.* 130, 991–998. doi: 10.1099/00221287-130-4-991

Dobin, A., Davis, C. A., Schlesinger, F., Drenkow, J., Zaleski, C., Jha, S., et al. (2013). STAR: ultrafast universal RNA-seq aligner. *Bioinformatics.* 29, 15–21. doi: 10.1093/bioinformatics/bts635

Dyson, B. C., Allwood, J. W., Feil, R., Xu, Y., Miller, M., Bowsher, C. G., et al. (2015). Acclimation of metabolism to light in *Arabidopsis thaliana*: the glucose 6-phosphate/phosphate translocator GPT2 directs metabolic acclimation. *Plant Cell Environ.* 38, 1404–1417. doi: 10.1111/pce.12495

Dyson, B. C., Webster, R. E., and Johnson, G. N. (2014). GPT2: a glucose 6-phosphate/phosphate translocator with a novel role in the regulation of sugar signalling during seedling development. *Ann. Bot.* 113, 643–652. doi: 10.1093/aob/mct298

Edgar, R., Domrachev, M., and Lash, A. E. (2002). Gene Expression Omnibus: NCBI gene expression and hybridization array data repository. *Nucleic Acids Res.* 30, 207–210. doi: 10.1093/nar/30.1.207

Egli, B., Kolling, K., Kohler, C., Zeeman, S. C., and Streb, S. (2010). Loss of cytosolic phosphoglucomutase compromises gametophyte development in *Arabidopsis*. *Plant Physiol.* 154, 1659–1671. doi: 10.1104/pp.110.165027

Eicks, M., Maurino, V., Knappe, S., Flügge, U. I., and Fischer, K. (2002). The plastidic pentose phosphate translocator represents a link between the cytosolic and the plastidic pentose phosphate pathways in plants. *Plant Physiol.* 128, 512–522. doi: 10.1104/pp.128.2.512

Fischer, K., Kammerer, B., Gutensohn, M., Arbinger, B., Weber, A., Häusler, R. E., et al. (1997). A new class of plastidic phosphate translocators: a putative link between primary and secondary metabolism by the phosphoenolpyruvate/phosphate antiporter. *Plant Cell* 9, 453–462. doi: 10.1105/tpc.9.3.453

Gerhardt, R., Stitt, M., and Heldt, H. W. (1987). Subcellular metabolite levels in spinach leaves. Regulation of sucrose synthesis during diurnal alterations in photosynthetic partitioning. *Plant Physiol* 83, 399–407. doi: 10.1104/pp.83.2.399

Gotoh, E., Matsumoto, M., Ogawa, K., Kobayashi, Y., and Tsuyama, M. (2010). A qualitative analysis of the regulation of cyclic electron flow around photosystem I from the post-illumination chlorophyll fluorescence transient in *Arabidopsis*: a new platform for the in vivo investigation of the chloroplast redox state. *Photosynthesis Res.* 103, 111–123. doi: 10.1007/s11120-009-9525-0

Habenicht, A. (1997). The non-phosphorylating glyceraldehyde-3-phosphate dehydrogenase: biochemistry, structure, occurrence and evolution. *Biol. Chem.* 378, 1413–1419. doi: 10.1515/bchm.1997.378.12.1413

Hauschild, R., and von Schaewen, A. (2003). Differential regulation of glucose-6-phosphate dehydrogenase isoenzyme activities in potato. *Plant Physiol.* 133, 47–62. doi: 10.1104/pp.103.025676

Häusler, R. E., Heinrichs, L., Schmitz, J., and Flügge, U. I. (2014). How sugars might coordinate chloroplast and nuclear gene expression during acclimation to high light intensities. *Mol. Plant.* 7, 1121–1137. doi: 10.1093/mp/ssu064

Heinrichs, L., Schmitz, J., Flügge, U.-I., and Häusler, R. E. (2012). The mysterious rescue of adg1-1/tpt-2 - an *Arabidopsis thaliana* double mutant impaired in acclimation to high light – by exogenously supplied sugars. *Front. Plant Sci.* 3:265. doi: 10.3389/fpls.2012.00265

Hejazi, M., Mahlow, S., and Fettke, J. (2014). The glucan phosphorylation mediated by α-glucan, water dikinase (GWD) is also essential in the light phase for a functional transitory starch turn-over. *Plant Signal. Behav.* 9:e28892. doi: 10.4161/psb.28892

Hilgers, E. J. A., Schöttler, M. A., Mettler-Altmann, T., Krueger, S., Dörmann, P., Eicks, M., et al. (2018). The combined loss of triose phosphate and xylulose 5-phosphate/phosphate translocators leads to severe growth retardation and impaired photosynthesis in *Arabidopsis thaliana* tpt/xpt double mutants. *Front. Plant Sci.* 9:1331. doi: 10.3389/fpls.2018.01331

Hoagland, D. R., and Arnon, D. I. (1938). The water culture method for growing plants without soil. *UC Agric. Exp. Sta. Circular* 347, 1–39.

Kammerer, B., Fischer, K., Hilpert, B., Schubert, S., Gutensohn, M., Weber, A., et al. (1998). Molecular characterization of a carbon transporter in plastids from heterotrophic tissues: the glucose 6-phosphate/phosphate antiporter. *Plant Cell* 10, 105–117. doi: 10.1105/tpc.10.1.105

Keeling, P. L., Wood, J. R., Tyson, R. H., and Bridges, I. G. (1988). Starch biosynthesis in developing wheat-grain: evidence against the direct involvement of triose phosphates in the metabolic pathway. *Plant Physiol.* 87, 311–319. doi: 10.1104/pp.87.2.311

Khandelwal, A., Elvitigala, T., Ghosh, B., and Quatrano, R. S. (2008). *Arabidopsis* transcriptome reveals control circuits regulating redox homeostasis and the role of an AP2 transcription factor. *Plant Physiol.* 148, 2050–2058. doi: 10.1104/pp.108.128488

Kiss, J. Z., Wright, J. B., and Caspar, T. (1996). Gravitropism in roots of intermediate-starch mutants of *Arabidopsis*. *Physiol. Plant.* 97, 237–244. doi: 10.1034/j.1399-3054.1996.970205.x

Kunz, H. H., Häusler, R. E., Fettke, J., Herbst, K., Niewiadomski, P., Gierth, M., et al. (2010). The role of plastidial glucose-6-phosphate/phosphate translocators in vegetative tissues of *Arabidopsis thaliana* mutants impaired in starch biosynthesis. *Plant Biol.* 12, 115–128. doi: 10.1111/j.1438-8677.2010.00349.x

Leakey, A. D. B., Xu, F., Gillespie, K. M., McGrath, J. M., Ainsworth, E. A., and Ort, D. R. (2009). Genomic basis for stimulated respiration by plants growing under elevated carbon dioxide. *Proc. Natl Acad. Sci. U.S.A.* 106, 3597–3602. doi: 10.1073/pnas.0810955106

Lee, Y., Nishizawa, T., Takemoto, M., Kumazaki, K., Yamashita, K., Hirata, K., et al. (2017). Structure of the triose-phosphate/phosphate translocator reveals the basis of substrate specificity. *Nature Plants.* 3, 825–832. doi: 10.1038/s41477-017-0022-8

Li, J., Weraduwage, S. M., Peiser, A. L., Tietz, S., Weise, S. E., Strand, D. D., et al. (2019). A cytosolic bypass and G6P shunt in plants lacking peroxisomal hydroxypyruvate reductase. *Plant Physiol.* 180, 783–792. doi: 10.1104/pp.19.00256

Li, L., and Sheen, J. (2016). Dynamic and diverse sugar signaling. *Curr. Opin. Plant Biol.* 33, 116–125. doi: 10.1016/j.pbi.2016.06.018

Liao, Y., Smyth, G. K., and Shi, W. (2013). The Subread aligner: fast, accurate and scalable read mapping by seed-and-vote. *Nucleic Acids Res.* 41:e108. doi: 10.1093/nar/gkt214

Livingston, A. K., Cruz, J. A., Kohzuma, K., Dhingra, A., and Kramer, D. M. (2010). An *Arabidopsis* mutant with high cyclic electron flow around Photosystem I (*hcef*) involving the NADPH dehydrogenase complex. *Plant Cell* 22, 221–233. doi: 10.1105/tpc.109.071084

Lloyd, J. C., and Zakhleniuk, O. V. (2004). Responses of primary and secondary metabolism to sugar accumulation revealed by microarray expression analysis of the *Arabidopsis* mutant, pho3. *J. Exp. Bot.* 55, 1221–1230. doi: 10.1093/jxb/erh143

McClain, A. M., and Sharkey, T. D. (2019). Triose phosphate utilization and beyond: from photosynthesis to end product synthesis. *J. Exp. Bot.* 70, 1755–1766. doi: 10.1093/jxb/erz058

Miller, M. A. E., O'Cualain, R., Selley, J., Knight, D., Karim, M. F., Hubbard, S. J., et al. (2017). Dynamic acclimation to high light in *Arabidopsis thaliana*

involves widespread reengineering of the leaf proteome. *Front. Plant Sci.* 8:1239. doi: 10.3389/fpls.2017.01239

Nickelsen, J., and Rengstl, B. (2013). Photosystem II assembly: from cyanobacteria to plants. *Annu. Rev. Plant Biol.* 64, 609–635. doi: 10.1146/annurev-arplant-050312-120124

Niewiadomski, P., Knappe, S., Geimer, S., Fischer, K., Schulz, B., Unte, U. S., et al. (2005). The *Arabidopsis* plastidic glucose 6-phosphate/phosphate translocator GPT1 is essential for pollen maturation and embryo sac development. *Plant Cell* 17, 760–775. doi: 10.1105/tpc.104.029124

Preiser, A. L., Banerjee, A., Fisher, N., and Sharkey, T. D. (2018). Supply and consumption of glucose 6-phosphate in the chloroplast stroma. *bioRxiv* 442434. doi: 10.1101/442434

Preiser, A. L., Fisher, N., Banerjee, A., and Sharkey, T. D. (2019). Plastidic glucose-6-phosphate dehydrogenase is regulated to maintain activity in the light. *Biochem. J.* 476, 1539–1551. doi: 10.1042/bcj20190234

Quick, W. P., Scheibe, R., and Neuhaus, H. E. (1995). Induction of hexose-phosphate translocator activity in spinach chloroplasts. *Plant Physiol.* 109, 113–121. doi: 10.1104/pp.109.1.113

Ritte, G., Heydenreich, M., Mahlow, S., Haebel, S., Kotting, O., and Steup, M. (2006). Phosphorylation of C6- and C3-positions of glucosyl residues in starch is catalysed by distinct dikinases. *FEBS Lett.* 580, 4872–4876. doi: 10.1016/j.febslet.2006.07.085

Ritte, G., Lloyd, J. R., Eckermann, N., Rottmann, A., Kossmann, J., and Steup, M. (2002). The starch-related R1 protein is an α-glucan, water dikinase. *Proc. Natl Acad. Sci. U.S.A.* 99, 7166–7171. doi: 10.1073/pnas.062053099

Scheibe, R., Geissler, A., and Fickenscher, K. (1989). Chloroplast glucose-6-phosphate dehydrogenase: Km shift upon light modulation and reduction. *Arch. Biochem. Biophys.* 274, 290–297. doi: 10.1016/0003-9861(89)90441-4

Schleucher, J., Vanderveer, P., Markley, J. L., and Sharkey, T. D. (1999). Intramolecular deuterium distributions reveal disequilibrium of chloroplast phosphoglucose isomerase. *Plant Cell Environ.* 22, 525–533. doi: 10.1046/j.1365-3040.1999.00440.x

Schmitz, J., Heinrichs, L., Scossa, F., Fernie, A. R., Oelze, M.-L., Dietz, K.-J., et al. (2014). The essential role of sugar metabolism in the acclimation response of *Arabidopsis thaliana* to high light intensities. *J. Exp. Bot.* 65, 1619–1636. doi: 10.1093/jxb/eru027

Schneider, A., Hausler, R. E., Kolukisaoglu, U., Kunze, R., van der Graaff, E., Schwacke, R., et al. (2002). An *Arabidopsis thaliana* knock-out mutant of the chloroplast triose phosphate/phosphate translocator is severely compromised only when starch synthesis, but not starch mobilisation is abolished. *Plant J.* 32, 685–699. doi: 10.1046/j.1365-313X.2002.01460.x

Serrato, A. J., Yubero-Serrano, E. M., Sandalio, L. M., Munoz-Blanco, J., Chueca, A., Caballero, J. L., et al. (2009). cpFBPaseII, a novel redox-independent chloroplastic isoform of fructose-1,6-bisphosphatase. *Plant Cell Environ.* 32, 811–827. doi: 10.1111/j.1365-3040.2009.01960.x

Sharkey, T. D., and Vassey, T. L. (1989). Low oxygen inhibition of photosynthesis Is caused by inhibition of starch synthesis. *Plant Physiol.* 90, 385–387. doi: 10.1104/pp.90.2.385

Sharkey, T. D., and Weise, S. E. (2016). The glucose 6-phosphate shunt around the Calvin-Benson cycle. *J. Exp. Bot.* 67, 4067–4077. doi: 10.1093/jxb/erv484

Soto-Suárez, M., Serrato, A. J., Rojas-González, J. A., Bautista, R., and Sahrawy, M. (2016). Transcriptomic and proteomic approach to identify differentially expressed genes and proteins in *Arabidopsis thaliana* mutants lacking chloroplastic 1 and cytosolic FBPases reveals several levels of metabolic regulation. *BMC Plant Biol.* 16:258. doi: 10.1186/s12870-016-0945-7

Szecowka, M., Heise, R., Tohge, T., Nunes-Nesi, A., Vosloh, D., Huege, J., et al. (2013). Metabolic fluxes in an illuminated *Arabidopsis* rosette. *Plant Cell.* 25, 694–714. doi: 10.1105/tpc.112.106989

Trethewey, R. N., and ap Rees, T. (1994). The role of the hexose transporter in the chloroplasts of *Arabidopsis thaliana* L. *Planta* 195, 168–174. doi: 10.1007/bf00199675

Tyson, R. H., and ap Rees, T. (1988). Starch synthesis by isolated amyloplasts from wheat endosperm. *Planta* 175, 33–38. doi: 10.1007/bf00402879

Vogel, M. O., Moore, M., Konig, K., Pecher, P., Alsharafa, K., Lee, J., et al. (2014). Fast retrograde signaling in response to high light involves metabolite export, MITOGEN-ACTIVATED PROTEIN KINASE6, and AP2/ERF transcription factors in *Arabidopsis*. *Plant Cell* 26, 1151–1165. doi: 10.1105/tpc.113.121061

Wakao, S., and Benning, C. (2005). Genome-wide analysis of glucose-6-phosphate dehydrogenases in *Arabidopsis*. *Plant J.* 41, 243–256. doi: 10.1111/j.1365-313X.2004.02293.x

Weise, S. E., Schrader, S. M., Kleinbeck, K. R., and Sharkey, T. D. (2006). Carbon balance and circadian regulation of hydrolytic and phosphorolytic breakdown of transitory starch. *Plant Physiol.* 141, 879–886. doi: 10.1104/pp.106.081174

Zeeman, S. C., Thorneycroft, D., Schupp, N., Chapple, A., Weck, M., Dunstan, H., et al. (2004). Plastidial α-glucan phosphorylase is not required for starch degradation in *Arabidopsis* leaves but has a role in the tolerance of abiotic stress. *Plant Physiol.* 135, 849–858. doi: 10.1104/pp.103.032631

Conflict of Interest Statement: The authors declare that the research was conducted in the absence of any commercial or financial relationships that could be construed as a potential conflict of interest.

frontiers in Plant Science

MINI REVIEW
published: 25 July 2019
doi: 10.3389/fpls.2019.00958

Targeted Control of Chloroplast Quality to Improve Plant Acclimation: From Protein Import to Degradation

Xiaolong Yang†, Yangyang Li†, Mingfang Qi, Yufeng Liu and Tianlai Li**

Key Laboratory of Protected Horticulture of Ministry of Education, National & Local Joint Engineering Research Center of Northern Horticultural Facilities Design & Application Technology (Liaoning), Horticulture Department, Shenyang Agricultural University, Shenyang, China

The chloroplast is an important energy-producing organelle acting as an environmental sensor for the plant cell. The normal turnover of the entire damaged chloroplast and its specific components is required for efficient photosynthesis and other metabolic reactions under stress conditions. Nuclear-encoded proteins must be imported into the chloroplast through different membrane transport complexes, and the orderly protein import plays an important role in plant adaptive regulation. Under adverse environmental conditions, the damaged chloroplast or its specific components need to be degraded efficiently to ensure normal cell function. In this review, we discuss the molecular mechanism of protein import and degradation in the chloroplast. Specifically, quality control of chloroplast from protein import to degradation and associated regulatory pathways are discussed to better understand how plants adapt to environmental stress by fine-tuning chloroplast homeostasis, which will benefit breeding approaches to improve crop yield.

Keywords: chloroplast protein import, selective autophagy, ubiquitin-26s proteasome system, chloroplast retrograde signaling, environmental stress, chloroplast homeostasis

OPEN ACCESS

Edited by:
Hongbo Gao,
Beijing Forestry University, China

Reviewed by:
Saijaliisa Kangasjärvi,
University of Turku, Finland
Ute Vothknecht,
University of Bonn, Germany

****Correspondence:***
Yufeng Liu
yufengliu@syau.edu.cn
Tianlai Li
ltl@syau.edu.cn

†These authors have contributed equally to this work

Specialty section:
This article was submitted to Plant Physiology, a section of the journal Frontiers in Plant Science

Received: *16 February 2019*
Accepted: *09 July 2019*
Published: *25 July 2019*

Citation:
Yang X, Li Y, Qi M, Liu Y and Li T (2019) Targeted Control of Chloroplast Quality to Improve Plant Acclimation: From Protein Import to Degradation. Front. Plant Sci. 10:958. doi: 10.3389/fpls.2019.00958

INTRODUCTION

As sessile organisms, the ability to quickly sense and adapt to their surroundings is essential for plant survival. Understanding stress signaling and response will enable us to improve stress resistance in crops, which are critical to agricultural productivity and sustainability in changing environments. The stress-generated signals in organelles can regulate stress-responsive gene expression and cellular activities to maintain cellular homeostasis (Zhu, 2016). Many previous studies have focused on photoinhibition and photoprotection mechanisms of plants growing in fluctuating environments; however, the turnover of chloroplast proteins is also essential for maintaining efficient photosynthesis and metabolism. A comprehensive understanding of how chloroplast maintains homeostasis will provide detailed insights for plant resistance and crop improvement. In this mini-review, we first introduce the most important recent publications which revealed the molecular mechanism of chloroplast protein import and then review chloroplast protein degradation processes including proteolysis, the ubiquitin-proteasome system (UPS), the newly confirmed autophagy process, and other related pathways (Ling and Jarvis, 2016; Izumi et al., 2017; Chen et al., 2018; Ganesan et al., 2018; Kikuchi et al., 2018). Finally, we discuss biological processes related to chloroplast quality control, in order to enhance plants' adaptability to the fluctuating environments.

THE MAINTENANCE OF CHLOROPLAST HOMEOSTASIS INVOLVES PROTEIN IMPORT AND DEGRADATION

The chloroplast is a complex organelle that contains three membrane systems – the outer envelope, the inner envelope, and the thylakoid membrane; as well as three major sub-compartments – the intermembrane space between the outer and inner envelope, the stroma, and the thylakoid lumen (Nakai, 2018). Chloroplast division is accomplished by the constriction of plastid division machinery, which is essential for maintaining an optimal plastid number in plant cells (Gao et al., 2013; Wang et al., 2017a,b). The chloroplast genome encodes less than 100 proteins and most proteins (about 95%) in the chloroplast are encoded by nuclear genes. Nuclear gene-encoded proteins must be translocated to the chloroplast for its biogenesis and functional maintenance.

Abiotic stresses such as strong light, CO_2 limitation, or extreme temperatures can induce the photoinhibition of PSII and PSI and impose continuous oxidative damage to the chloroplast during energy production, which further inhibit photosynthesis efficiency and plant growth (Dietz et al., 2016; Malnoë, 2018). Proteins in the photosynthetic electron transport chain are vulnerable targets of oxidative damage. All photodamage and photoprotection responses involve the rapid turnover of specific photosynthetic proteins (Li et al., 2018). Recent protein turnover studies found that PetD (a subunit of the cytochrome b6f complex), PIFI (an auxiliary subunit associated with the NDH complex), NAD(P)H dehydrogenase subunit K (NDHK), zeaxanthin epoxidase (ZEP), and proton gradient regulation-like 1 (PGRL1) have rapid import and degradation rates (Li et al., 2017). Together with the discovery of photodamage-induced chlorophagy, these results indicate that the photosynthetic electron transport chain is essential for chloroplast quality.

Many biological processes need to be strict yet flexibly controlled in the chloroplast because the functional proteins are encoded by two separated organelles – the nucleus and the chloroplast. Light signals, developmental stage, hormones, metabolites, and environmental changes all can lead to transcriptional reprogramming in the chloroplast (Wang et al., 2017a,b). Communication between chloroplast and the nucleus under stress conditions is closely connected to chloroplast protein import and degradation. Many biological processes in chloroplast are regulated by nuclear factors (anterograde signals), while the transcription of some nuclear genes is sensitive to signals from the developing chloroplast (retrograde signals).

THE ENTRANCE OF CHLOROPLAST PROTEIN IMPORT IS PRECISELY CONTROLLED

Proteins are imported into the chloroplast through four major steps: (1) specific sorting of a precursor protein in the cytoplasm; (2) recognition by the receptor at the outer membrane of the chloroplast; (3) consecutive translocation across both membranes; and (4) accurate processing and sorting after the protein is imported (Lee et al., 2017). Precursor proteins interact with many cytoplasmic molecular chaperones to form guidance complexes; transmembrane transport is launched once these complexes are recruited by the import receptor at the chloroplast envelope (Nakai, 2018). Precursor proteins usually contain a chloroplast transit peptide (cTP) – a cleavable N terminal signaling sequence that guides the preproteins target to chloroplast. cTPs can be removed by a stromal processing peptidase (SPP), while the thylakoid-transfer signal (TTs) is cleaved by thylakoid processing peptidase (TPP). Each transit peptide usually contains motifs that can interact with different translocon components; thus, cTP determines plastid types, precursor protein selectivity, and import pathways in different developmental stages and environmental conditions (Li and Teng, 2013). A site-specific crosslinking approach to map the topological structure of transit peptides revealed that the signal peptides were sequentially recognized by the translocon on the outer (Toc) and inner (Tic) envelope supercomplexes during protein import (Richardson et al., 2018).

The Toc-Tic supercomplex is generally considered to be the gateway for most chloroplast proteins (**Figure 1**; Chen and Li, 2017). The Toc complex dominates the initial recognition and translocation of preproteins at the outer membrane. Toc core proteins include the membrane channel protein Toc75, and two GTPase receptors, Toc34 and Toc159. The cTP of a precursor protein can be specifically recognized by Toc34 and Toc159 before the precursor protein is transported by the channel protein Toc75. The polypeptide transport-associated (POTRA) domains of Toc75 can directly interact with cTP to facilitate import (Chang et al., 2017; O'Neil et al., 2017). Moreover, Toc64 functions as an essential transport component with dual function. Toc64 can recognize Hsp90 and deliver precursor proteins *via* a cytosolic exposed domain that contains three tetratrico-peptide repeat motifs, and also functions as a major component of a complex facing the intermembrane space (Qbadou et al., 2007; Tillmann et al., 2015). As a molecular chaperone in the chloroplast intermembrane space, Tic22 can interact with the precursor protein to ensure correct targeting during its transport from the Toc complex to the Tic complex (Rudolf et al., 2013). Research on components of the Tic complex is controversial; the classical model of the Tic complex generally assumes that Tic40 can directly interact with Tic110 and the stroma molecule chaperone to assist transmembrane transport (Flores-Pérez and Jarvis, 2013; Bédard et al., 2017). However, this model was called into question by Nakai and associates, who proposed the Tic20/Tic56/Tic100/Tic214 complex as the main import route of chloroplast inner membrane transport (Kikuchi et al., 2013). Recently, a 2-MD heteromeric AAA-ATPase complex was identified as the import motor pulling preproteins across the inner envelope (Kikuchi et al., 2018). Chen et al. (2018) identified a new Tic component, Tic236, which is anchored to the inner membrane and binds directly to the outer-membrane channel Toc75. This long and stable protein bridge between Tic and Toc complex is necessary for protein translocation into the chloroplast. A recent study found that the functional pore size of the Toc-Tic complexes is greater than 25.6 Å and

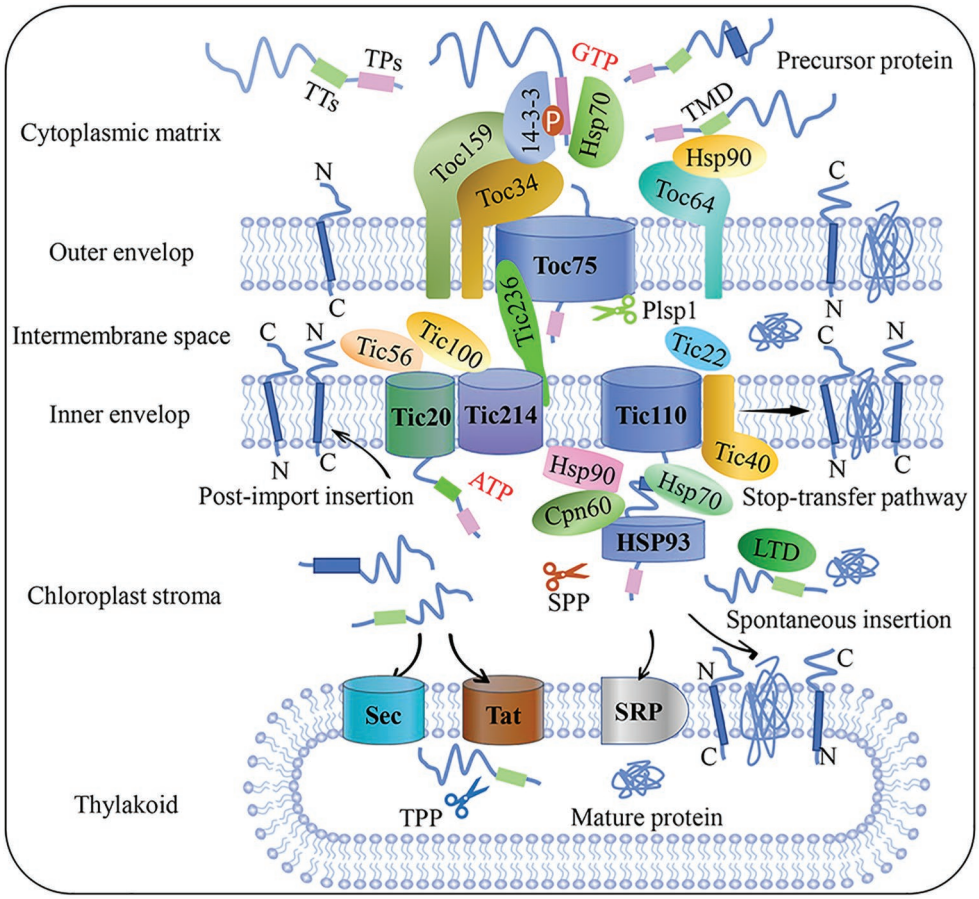

FIGURE 1 | Flow chart of plant chloroplast protein import. Precursor protein entered the intermembrane space through the Toc complex after recognition by the guidance complex. With the aid of molecular chaperones and stroma processing peptidase, precursor protein is then translocated into the chloroplast stroma through the Tic complex. Preproteins target the inner membrane through post-import insertion and stop-transfer pathways. Preproteins can also be inserted into the thylakoid membrane through SRP or spontaneous insertion and translocation across the thylakoid membrane through the Sec and Tat complex, respectively. Plsp1: plastid type I signal peptidase 1; Sec: secretion; SPP: stromal processing peptidase; SRP: signal recognition particle; Tat: twin-arginine translocation; Tic: translocon at the inner envelope membrane of chloroplasts; TMD: transmembrane domain; Toc: translocon at the outer envelope membrane of chloroplasts; TPs: transit peptide sequence; TTs: thylakoid targeting sequence.

the pores have a strong unfoldase activity, providing flexibility and expandability to accommodate and import folded proteins into the chloroplast. This unique character is essential for controlling chloroplast protein import (Ganesan et al., 2018).

The chloroplast protein import apparatus must be dynamically and precisely regulated to control translocation efficiency and the abundance of new protein sets. Reversible phosphorylation is emerging as an important regulatory mechanism during cytosolic sorting and targeting of chloroplast preproteins prior to translocation. Recent studies reported that kinase of the outer chloroplast membrane 1 (KOC1) can phosphorylate the A-domain of the import receptor Toc159 *in vitro* and accelerate precursor protein import (Zufferey et al., 2017). Furthermore, a relationship between the degradation of chloroplast outer envelope proteins and the UPS has come to light in recent years. This proteolytic system is referred to as chloroplast-associated protein degradation, or CHLORAD, which involves SP1 (suppressor of ppi1 locus 1 E3 ligase), SP2 (an Omp85-type b-barrel channel of the OEM), and CDC48 – a cytosolic AAA+ (ATPase associated with diverse cellular activities) chaperone, is vital for organelle functions and plant development (Ling and Jarvis, 2015; Ling et al., 2019). In addition, photosynthetic electron transport in the chloroplast is a dynamic process of oxidation and reduction, so the fluctuating redox state can affect either the activity of the Tic channel or the binding capacity of both the Toc and Tic translocation apparatuses at different stages of import, especially under adverse conditions. Though Toc-Tic supercomplexes is the general import pathway, the recognition can be lack specificity as seen in dual-targeted proteins transport process, in addition, other alternative protein import pathways were found, such as the transit peptide-independent import pathway and protein deliver from the ER/Golgi apparatus to the chloroplasts. More detailed overviews on chloroplast protein import and related regulatory pathways can be found in several recent reviews (Li and Chiu, 2010; Lee et al., 2017).

INTERNAL DEGRADATION OF DAMAGED CHLOROPLAST COMPONENTS *VIA* PROTEOLYSIS

More than 20 proteolytic enzymes have been found to hydrolyze chloroplast proteins, including the caseinolytic protease (Clp), degradation of periplasmic (Deg) protease, filamentation temperature-sensitive H (FtsH), organellar oligopeptidase (OOP), presequence peptidases (PreP), and chloroplast nucleoid DNA-binding protein 41 (Cnd41) (Nishimura et al., 2017). The proteolytic machinery is widely involved in the import of newly synthesized chloroplast proteins and degradation of damaged components. Upon import into the chloroplast, cTPs of the preproteins are cleaved off by stromal processing peptidase (SPP) and the cleaved cTP fragments are then degraded by PreP and OOP (Nishimura et al., 2017). The proteolytic subunit 3 of Clp protease could degrade damaged chloroplast proteins and recycle amino acids in dark-treated *Camellia sinensis* leaves (Chen et al., 2017). The downregulation of genes encoding Clp subunits can affect chloroplast development and cause abnormal plant or embryo development (Kim et al., 2015; Nishimura and van Wijk, 2015). Deg and FtsH proteases are crucial for the photodamage repair cycle by accelerating the turnover of photosystem II reaction center protein D1 and cytochrome *b6f* complex, which plays a key role in regulating photosynthesis and photoprotection (Malnoë et al., 2014; Kato et al., 2018; Knopf and Adam, 2018).

MULTIPLE EXTRAPLASTIDIC DEGRADATION PROCESSES OF THE WHOLE CHLOROPLAST AND ITS SPECIFIC COMPONENTS

Ubiquitin is an essential signaling molecule for the selective degradation of proteins, which depends on the UPS (Hua and Vierstra, 2016). UPS can specifically identify and degrade protein substrates through E3 ligase. Proteomic analysis revealed that the 26S proteasome subunits RPT2a/b and RPT5a interact directly with the transit peptides of three chloroplast proteins in the cytosol, and are essential for the degradation of unimported chloroplast protein precursors (Sako et al., 2014). Under certain conditions, the *Arabidopsis ferrochelatase 2* (*fc2*) mutant accumulates excessive amounts of protoporphyrin IX and $^1O_2$ in the chloroplast. Thereby, damaged chloroplasts are tagged with ubiquitin for selective degradation, which is accelerated by plant U-box (PUB4) E3 ligase (Woodson et al., 2015). The SP1 E3 ligase mediates the degradation of specific components of the Toc complex *via* 26s proteasomes under moderate stress conditions, while under severe stress, the PUB4 E3 ligase mediates the ubiquitination of chloroplast membrane proteins and subsequent degradation of the entire damaged chloroplast (Ling and Jarvis, 2016).

Autophagy is a ubiquitous macromolecular degradation process in eukaryotic cells mediated by proteins encoded by autophagy-related genes (ATGs) (Marshall and Vierstra, 2018). RuBisCO-containing bodies (RCBs), ATG8-interacting protein 1 positive bodies (ATI1-PS), and small starch-like granule bodies (SSLGs) are responsible for the selective autophagy of chloroplast components and the entire damaged chloroplasts (**Figure 2**; Otegui, 2017; Izumi and Nakamura, 2018). The formation and transport of RCBs depend on the cellular carbon status and can be inhibited by light or sugar addition in the substrate, indicating that RCBs can recycle energy and carbon from stroma proteins and especially the small subunits of RuBisCO in energy-constrained conditions (Ishida et al., 2014). Carbon starvation-induced ATI1 expression can cause selective autophagy of specific plastid proteins, which are eventually transferred to the vacuole for degradation (Michaeli et al., 2014). In addition, Izumi et al. (2017) reported that photooxidative damage-induced chlorophagy can transport the entire chloroplast to the vacuole for degradation. Further studies revealed that the induction of chlorophagy can be mediated by chloroplast swelling due to high light-induced envelope damage and executed *via* tonoplast-mediated sequestering (Nakamura et al., 2018). This entire-organelle-type chloroplast autophagy is different from piecemeal chlorophagy, which involves the removal of small membrane vesicles from the organelle (Otegui, 2017).

Other extraplastidic degradation pathways through senescence-associated vacuoles (SAVs) and chloroplast vesiculation-containing vesicles (CCVs) have also been discovered (Otegui et al., 2005; Wang and Blumwald, 2014). SAVs have higher proteolytic activity and acidity than the central vacuole. SAVs accumulate in senescing leaves and are involved in the degradation of soluble photosynthetic proteins in the chloroplast stroma (Otegui et al., 2005; Martínez et al., 2008). Unlike autophagy, SAVs can degrade chloroplast components, while how SAVs are formed and how the chloroplast components are translocated to SAVs remain unknown (Carrión et al., 2013). A recent study has illustrated that SAVs have strong cysteine protease activity and the most widely used senescence-associated protein SAG12 may participate in RuBisCO breakdown during leaf senescence (James et al., 2018). Chloroplast degradation through CCVs is independent of autophagy and SAVs. After proteins are transported to the chloroplast, chloroplast vesiculation (CV) destabilizes the chloroplast and induces the formation of CCVs during senescence or under abiotic stress conditions, further delivering chloroplast proteins to the vacuole for proteolysis (Wang and Blumwald, 2014). Recently, researchers found that CV-related gene expression was induced by the NAC (NAM, ATAF1/2, and CUC2) transcription factor RD26, which directly regulates the degradation of chloroplast proteins during senescence (Kamranfar et al., 2018). Under water-limited conditions, the expression of *OsCV* increased in wild-type plants, whereas *OsCV*-silenced plants exhibited an improved carbon and nitrogen fixation efficiency and environmental acclimation (Sade et al., 2017).

RETROGRADE SIGNALING AND TRANSCRIPTIONAL CONTROL OF CHLOROPLAST COMPOSITION

Chloroplast protein import especially through the Toc-Tic supercomplexes and multiple degradation machineries function

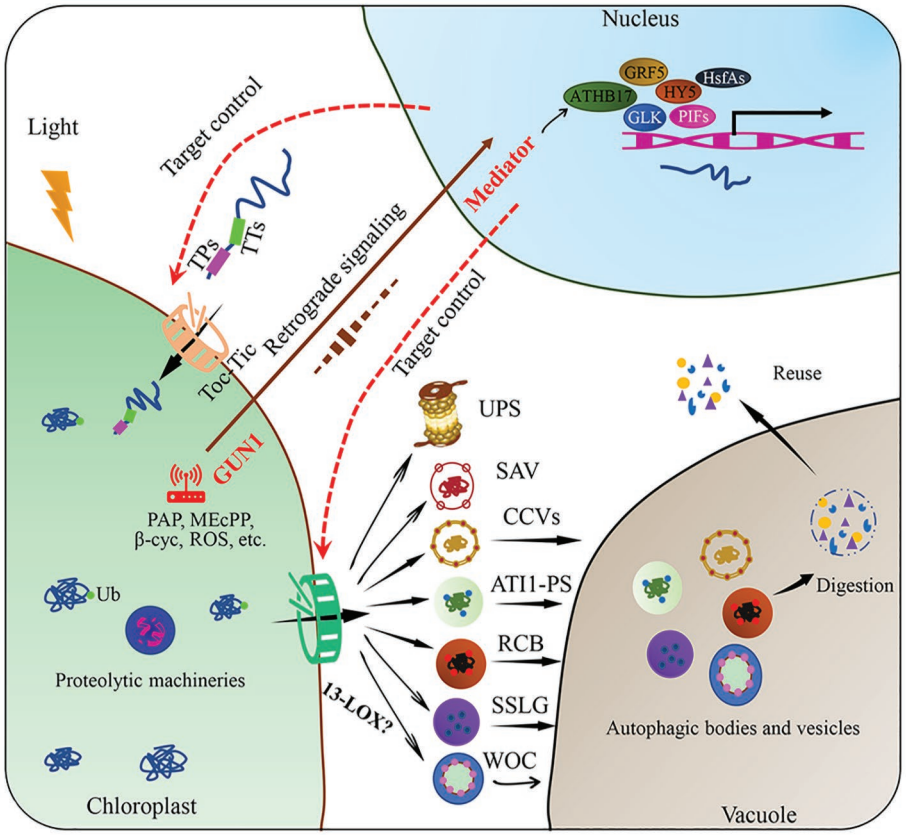

FIGURE 2 | Targeted control of plant chloroplast quality. Chloroplast proteins encoded in the nucleus are transported across the chloroplast envelope through Toc-Tic complexes. Chloroplast protein degradation through various pathways, including chloroplast protein hydrolysis and the SAVs, CCVs, ATI1-PS, RCB, SSLG, or WOC, these degraded substances can be reused within the cell after degradation. Chloroplast retrograde signaling is involved in the regulation of chloroplast proteome remodeling under fluctuating environmental conditions. Plastid metabolism includes phosphonucleotide 3′-phosphoadenosine 5′-phosphate (PAP), methyl erythritol (MEcPP), beta cyclocitral (beta cyc), fatty acids (FAs), and ROS. After environmental stimuli are perceived by the chloroplast, some transcription factors, such as PIFs, GLK, HY5, GRF5, HsfAs, and ATHB17, are involved. Chloroplast protein import and export are the potential targets of chloroplast quality control. Ub: ubiquitin; RCBs: RuBisCO-containing bodies; ATI1-PS: ATG8-interacting protein 1 positive bodies; SSLGs: small starch-like granule bodies; SAVs: senescence-associated vacuoles; CCVs: chloroplast vesiculation-containing vesicles; PIFs: phytochrome interaction factors; HY5: elongated hypocotyl 5; GLK: golden 2-like, ATHB17: *Arabidopsis thaliana* homeobox17, GRF5: growth retardation factor 5; HsfAs: heat stress transcription factors.

as key control targets of chloroplast quality. Chloroplast protein import is highly dependent on developmental stages and environmental factors. The operating efficiency of the import channel is regulated by redox state, phosphorylation, ubiquitylation, and molecular chaperones in the cytoplasm and stroma (Woodson, 2016). Autophagy and vesicles are the final steps in the degradation of chloroplast and its constituents, while the initial steps remain unclear. A previous study showed that 13-lipoxygenase (13-LOX), which targets the chloroplast, induces programmed chloroplast injury. Once imported into the chloroplast, 13-LOX generates holes in the chloroplast envelope by oxidizing unsaturated fatty acids in the chloroplast membrane, allowing the delivery of stroma proteins across the chloroplast envelope (Springer et al., 2016).

Chloroplast retrograde signaling, which triggers a precise spatial transcriptional regulation trade-off between protein import and degradation, could be an important strategy to control chloroplast quality. As the main communication language between the chloroplast and nucleus, operational chloroplast retrograde signals can regulate energy allocation between stress acclimation and growth by coordinating transcriptional reprogramming to control chloroplast quality (Watson et al., 2018). The most studied chloroplast retrograde signals include methyl erythritol (MEcPP), phosphonucleotide 3′-phosphoadenosine 5′-phosphate (PAP), beta cyclocitral (beta cyc), fatty acids (FAs), and ROS (Chi et al., 2015; Benn et al., 2016; Dietz et al., 2016; Page et al., 2017). These stress-triggered chloroplast retrograde signals must be integrated with the cytosolic stress signaling network, transduced to the nucleus and connected to transcriptional regulators. For example, genomes uncoupled 1 (GUN1) may act as a central hub in the chloroplast by integrating different retrograde signals; whereas the mediator of transcriptional co-activator complex may function as a regulatory hub in the nucleus by integrating complex stress signaling networks to control the transcriptional remodeling required for stress acclimation (Crawford et al., 2017; Hernández-Verdeja and Strand, 2018).

Epigenetic modification and transcriptional regulatory factors may be activated to maintain the stability of the chloroplast proteome after sensing special environmental stimuli. Redox metabolism through key intermediates in the chloroplast is closely linked to numerous epigenetic markers and stress responses (Locato et al., 2018). DNA methylation in the promoter region of *OsAK1* caused albinism in young leaves and abnormal chloroplast development in rice (Wei et al., 2017). DNA methylation and histone acetylation that regulate photosynthesis and development are conserved in *Arabidopsis thaliana* and *Populus trichocarpa* (Valledor et al., 2015). Chloroplast signals participate in epigenetic controlling the MUTS HOMOLOG1 (MSH1) protein targeted to both the mitochondria and chloroplasts, fulfilling essential functions in control of plant development (Virdi et al., 2016). Transcription factors specifically regulate chloroplast development, and expression of the photosynthesis-related genes is induced by photoreceptor-mediated light signal related transcription factors, such as the phytochrome interaction factors (PIFs) and elongated hypocotyl 5 (HY5) (Kharshiing and Sinha, 2016; Wang et al., 2017a,b). In addition, golden 2-like (GLK), *Arabidopsis thaliana* homeobox 17 (ATHB17), growth regulation factor 5 (GRF5), and heat stress transcription factors (HsfAs) can integrate different developmental, hormonal, or environmental signals to control photosynthetic gene expression and chloroplast development (Vercruyssen et al., 2015; Leister and Kleine, 2016; Zhao et al., 2017). Further studies are required to better understand the molecular mechanism of chloroplast signals and transcription factors in the regulation of chloroplast protein import or degradation. How photosynthesis and metabolism control chloroplast quality under abiotic stress should also be investigated.

CONCLUSIONS AND PERSPECTIVES

Environmental stress induced oxidative damage to the chloroplast and its components significantly decrease photosynthetic efficiency and crop yield. The rapid turnover of the entire chloroplast and its specific components is crucial for maintaining photosynthesis and metabolism but the relationship between photoinhibition and chloroplast quality under stress conditions require further clarification (Li et al., 2017; Tamburino et al., 2017). We propose that the targeted control of chloroplast quality through regulating the channels by which proteins are imported and exported across the membranes can be used to improve plant acclimation to changing environments (**Figure 2**). The advanced and widely used genome editing technology can be utilized to control chloroplast quality through precise genetic modification of import and export channels and related transcriptional regulatory pathways, and we believe it is an important future research direction especially in the field of plant stress biology. However, the potential effects of targeted control of chloroplast homeostasis on the adaptability to fluctuating environments of plants and improved production in major crops require further evaluation.

AUTHOR CONTRIBUTIONS

XY, YLiu, and TL are responsible for the general overview of the opinions stated in the manuscript. XY and YLi wrote and modified the manuscript. MQ reviewed and modified the manuscript. All authors reviewed and approved the final version of the submitted manuscript.

FUNDING

This work was supported by the National Key Research and Development Program of China (2018YFD1000800), the National Natural Science Foundation of China (Grant No. 31772356), the China Agriculture Research System (Grant No. CARS-23-1), and the Program for Liaoning Innovative Research Team in University (LZ2015025).

REFERENCES

Bédard, J., Trösch, R., Wu, F., Ling, Q., Flores-Pérez, Ú., Töpel, M., et al. (2017). Suppressors of the chloroplast protein import mutant tic40 reveal a genetic link between protein import and thylakoid biogenesis. *Plant Cell* 29, 1726–1747. doi: 10.1105/tpc.16.00962

Benn, G., Bjornson, M., Ke, H., De Souza, A., Balmond, E. I., Shaw, J. T., et al. (2016). Plastidial metabolite MEcPP induces a transcriptionally centered stress-response hub via the transcription factor CAMTA3. *Proc. Natl. Acad. Sci. USA* 113, 8855–8860. doi: 10.1073/pnas.1602582113

Carrión, C. A., Costa, M. L., Martínez, D. E., Mohr, C., Humbeck, K., and Guiamet, J. J. (2013). *In vivo* inhibition of cysteine proteases provides evidence for the involvement of 'senescence-associated vacuoles' in chloroplast protein degradation during dark-induced senescence of tobacco leaves. *J. Exp. Bot.* 64, 4967–4980. doi: 10.1093/jxb/ert285

Chang, J. S., Chen, L. J., Yeh, Y. H., Hsiao, C. D., and Li, H. M. (2017). Chloroplast preproteins bind to the dimer interface of the toc159 receptor during import. *Plant Physiol.* 173, 2148–2162. doi: 10.1104/pp.16.01952

Chen, Y. L., Chen, L. J., Chu, C. C., Huang, P. K., Wen, J. R., and Li, H. M. (2018). TIC236 links the outer and inner membrane translocons of the chloroplast. *Nature* 564, 125–129. doi: 10.1038/s41586-018-0713-y

Chen, Y., Fu, X., Mei, X., Zhou, Y., Cheng, S., Zeng, L., et al. (2017). Proteolysis of chloroplast proteins is responsible for accumulation of free amino acids in dark-treated tea (*Camellia sinensis*) leaves. *J. Proteome* 157, 10–17. doi: 10.1016/j.jprot.2017.01.017

Chen, L. J., and Li, H. M. (2017). Stable megadalton TOC-TIC supercomplexes as major mediators of protein import into chloroplasts. *Plant J.* 92, 178–188. doi: 10.1111/tpj.13643

Chi, W., Feng, P., Ma, J., and Zhang, L. (2015). Metabolites and chloroplast retrograde signaling. *Curr. Opin. Plant Biol.* 25, 32–38. doi: 10.1016/j.pbi.2015.04.006

Crawford, T., Lehotai, N., and Strand, Å. (2017). The role of retrograde signals during plant stress responses. *J. Exp. Bot.* 69, 2783–2795. doi: 10.1093/jxb/erx481

Dietz, K. J., Turkan, I., and Krieger-Liszkay, A. (2016). Redox-and reactive oxygen species-dependent signaling into and out of the photosynthesizing chloroplast. *Plant Physiol.* 171, 1541–1550. doi: 10.1104/pp.16.00375

Flores-Pérez, Ú., and Jarvis, P. (2013). Molecular chaperone involvement in chloroplast protein import. *BBA-Mol. Cell. Res.* 1833, 332–340. doi: 10.1016/j.bbamcr.2012.03.019

Ganesan, I., Shi, L. X., and Theg, S. M. (2018). Evaluating the functional pore size of chloroplast TOC and TIC protein translocons: import of folded proteins. *Plant Cell* 30, 2161–2173. doi: 10.1105/tpc.18.00427

Gao, Y., Liu, H., An, C., Shi, Y., Liu, X., Yuan, W., et al. (2013). *Arabidopsis* FRS4/CPD25 and FHY3/CPD45 work cooperatively to promote the expression of the chloroplast division gene ARC5 and chloroplast division. *Plant J.* 75, 795–807. doi: 10.1111/tpj.12240

Hernández-Verdeja, T., and Strand, Å. (2018). Retrograde signals navigate the path to chloroplast development. *Plant Physiol.* 176, 967–976. doi: 10.1104/pp.17.01299

Hua, Z., and Vierstra, R. D. (2016). Ubiquitin goes green. *Trends Cell Biol.* 26, 3–5. doi: 10.1016/j.tcb.2015.12.001

Ishida, H., Izumi, M., Wada, S., and Makino, A. (2014). Roles of autophagy in chloroplast recycling. *BBA-Bioenergetics* 1837, 512–521. doi: 10.1016/j.bbabio.2013.11.009

Izumi, M., Ishida, H., Nakamura, S., and Hidema, J. (2017). Entire photodamaged chloroplasts are transported to the central vacuole by autophagy. *Plant Cell* 29, 377–394. doi: 10.1105/tpc.16.00637

Izumi, M., and Nakamura, S. (2018). Chloroplast protein turnover: the influence of extraplastidic processes, including autophagy. *Int. J. Mol. Sci.* 19:828. doi: 10.3390/ijms19030828

James, M., Poret, M., Masclaux-Daubresse, C., Marmagne, A., Coquet, L., Jouenne, T., et al. (2018). SAG12, a major cysteine protease involved in nitrogen mobilization during senescence for seed production in *Arabidopsis thaliana*. *Plant Cell Physiol.* 59, 2052–2063. doi: 10.1093/pcp/pcy125

Kamranfar, I., Xue, G. P., Tohge, T., Sedaghatmehr, M., Fernie, A. R., Balazadeh, S., et al. (2018). Transcription factor RD26 is a key regulator of metabolic reprogramming during dark-induced senescence. *New Phytol.* 4, 1543–1557. doi: 10.1111/nph.15127

Kato, Y., Hyodo, K., and Sakamoto, W. (2018). The photosystem II repair cycle requires FtsH turnover through the EngA GTPase. *Plant Physiol.* 178, 596–611. doi: 10.1104/pp.18.00652

Kharshiing, E., and Sinha, S. P. (2016). Deficiency in phytochrome A alters photosynthetic activity, leaf starch metabolism and shoot biomass production in tomato. *J. Photochem. Photobiol. B* 165, 157–162. doi: 10.1016/j.jphotobiol.2016.10.026

Kikuchi, S., Asakura, Y., Imai, M., Nakahira, Y., Kotani, Y., Hashiguchi, Y., et al. (2018). A Ycf2-FtsHi heteromeric AAA-ATPase complex is required for chloroplast protein import. *Plant Cell* 30, 2677–2703. doi: 10.1105/tpc.18.00357

Kikuchi, S., Bédard, J., Hirano, M., Hirabayashi, Y., Oishi, M., Imai, M., et al. (2013). Uncovering the protein translocon at the chloroplast inner envelope membrane. *Science* 339, 571–574. doi: 10.1126/science.1229262

Kim, J., Kimber, M. S., Nishimura, K., Friso, G., Schultz, L., Ponnala, L., et al. (2015). Structures, functions, and interactions of ClpT1 and ClpT2 in the Clp protease system of *Arabidopsis* chloroplasts. *Plant Cell* 27, 1477–1496. doi: 10.1105/tpc.15.00106

Knopf, R. R., and Adam, Z. (2018). Lumenal exposed regions of the D1 protein of PSII are long enough to be degraded by the chloroplast Deg1 protease. *Sci. Rep.* 1:5230. doi: 10.1038/s41598-018-23578-x

Lee, D. W., Lee, J., and Hwang, I. (2017). Sorting of nuclear-encoded chloroplast membrane proteins. *Curr. Opin. Plant Biol.* 40, 1–7. doi: 10.1016/j.pbi.2017.06.011

Leister, D., and Kleine, T. (2016). Definition of a core module for the nuclear retrograde response to altered organellar gene expression identifies GLK overexpressors as gun mutants. *Physiol. Plant.* 157, 297–309. doi: 10.1111/ppl.12431

Li, L., Aro, E. M., and Millar, A. H. (2018). Mechanisms of photodamage and protein turnover in photoinhibition. *Trends Plant Sci.* 23, 667–676. doi: 10.1016/j.tplants.2018.05.004

Li, H. M., and Chiu, C. C. (2010). Protein transport into chloroplasts. *Annu. Rev. Plant Biol.* 61, 157–180. doi: 10.1146/annurev-arplant-042809-112222

Li, L., Nelson, C. J., Trösch, J., Castleden, I., Huang, S., and Millar, A. H. (2017). Protein degradation rate in *Arabidopsis thaliana* leaf growth and development. *Plant Cell* 29, 207–228. doi: 10.1105/tpc.16.00768

Li, H. M., and Teng, Y. S. (2013). Transit peptide design and plastid import regulation. *Trends Plant Sci.* 18, 360–366. doi: 10.1016/j.tplants.2013.04.003

Ling, Q., Broad, W., Trösch, R., Töpel, M., Sert, T. D., Lymperopoulos, P., et al. (2019). Ubiquitin-dependent chloroplast-associated protein degradation in plants. *Science* 363:eaav4467. doi: 10.1126/science.aav4467

Ling, Q., and Jarvis, P. (2015). Regulation of chloroplast protein import by the ubiquitin E3 ligase SP1 is important for stress tolerance in plants. *Curr. Biol.* 25, 2527–2534. doi: 10.1016/j.cub.2015.08.015

Ling, Q., and Jarvis, P. (2016). Plant signaling: ubiquitin pulls the trigger on chloroplast degradation. *Curr. Biol.* 26, R38–R40. doi: 10.1016/j.cub.2015.11.022

Locato, V., Cimini, S., and De Gara, L. (2018). ROS and redox balance as multifaceted players of cross-tolerance: epigenetic and retrograde control of gene expression. *J. Exp. Bot.* 69, 3373–3391. doi: 10.1093/jxb/ery168

Malnoë, A. (2018). Photoinhibition or photoprotection of photosynthesis? Update on the (newly termed) sustained quenching component qH. *Environ. Exp. Bot.* 154, 123–133. doi: 10.1016/j.envexpbot.2018.05.005

Malnoë, A., Wang, F., Girard-Bascou, J., Wollman, F. A., and de Vitry, C. (2014). Thylakoid FtsH protease contributes to photosystem II and cytochrome b6f remodeling in *Chlamydomonas reinhardtii* under stress conditions. *Plant Cell* 1, 373–390. doi: 10.1105/tpc.113.120113

Marshall, R. S., and Vierstra, R. D. (2018). Autophagy: the master of bulk and selective recycling. *Annu. Rev. Plant Biol.* 69, 173–208. doi: 10.1146/annurev-arplant-042817-040606

Martínez, D. E., Costa, M. L., Gomez, F. M., Otegui, M. S., and Guiamet, J. J. (2008). Senescence-associated vacuoles' are involved in the degradation of chloroplast proteins in tobacco leaves. *Plant J.* 2, 196–206. doi: 10.1111/j.1365-313X.2008.03585.x

Michaeli, S., Honig, A., Levanony, H., Peled-Zehavi, H., and Galili, G. (2014). *Arabidopsis* ATG8-INTERACTING PROTEIN1 is involved in autophagy-dependent vesicular trafficking of plastid proteins to the vacuole. *Plant Cell* 26, 4084–4101. doi: 10.1105/tpc.114.129999

Nakai, M. (2018). New perspectives on chloroplast protein import. *Plant Cell Physiol.* 59, 1111–1119. doi: 10.1093/pcp/pcy083

Nakamura, S., Hidema, J., Sakamoto, W., Ishida, H., and Izumi, M. (2018). Selective elimination of membrane-damaged chloroplasts via microautophagy. *Plant Physiol.* 177, 1007–1026. doi: 10.1104/pp.18.00444

Nishimura, K., Kato, Y., and Sakamoto, W. (2017). Essentials of proteolytic machineries in chloroplasts. *Mol. Plant* 10, 4–19. doi: 10.1016/j.molp.2016.08.005

Nishimura, K., and van Wijk, K. J. (2015). Organization, function and substrates of the essential Clp protease system in plastids. *BBA-Bioenergetics* 1847, 915–930. doi: 10.1016/j.bbabio.2014.11.012

O'Neil, P. K., Richardson, L. G., Paila, Y. D., Piszczek, G., Chakravarthy, S., Noinaj, N., et al. (2017). The POTRA domains of Toc75 exhibit chaperone-like function to facilitate import into chloroplasts. *Proc. Natl. Acad. Sci. USA* 114, E4868–E4876. doi: 10.1073/pnas.1621179114

Otegui, M. S. (2017). Vacuolar degradation of chloroplast components: autophagy and beyond. *J. Exp. Bot.* 69, 741–750. doi: 10.1093/jxb/erx234

Otegui, M. S., Noh, Y. S., Martínez, D. E., Vila Petroff, M. G., Andrew Staehelin, L., Amasino, R. M., et al. (2005). Senescence-associated vacuoles with intense proteolytic activity develop in leaves of *Arabidopsis* and soybean. *Plant J.* 41, 831–844. doi: 10.1111/j.1365-313X.2005.02346.x

Page, M. T., McCormac, A. C., Smith, A. G., and Terry, M. J. (2017). Singlet oxygen initiates a plastid signal controlling photosynthetic gene expression. *New Phytol.* 213, 1168–1180. doi: 10.1111/nph.14223

Qbadou, S., Becker, T., Bionda, T., Reger, K., Ruprecht, M., Soll, J., et al. (2007). Toc64-a preprotein-receptor at the outer membrane with bipartide function. *J. Mol. Biol.* 367, 1330–1346. doi: 10.1016/j.jmb.2007.01.047

Richardson, L. G., Small, E. L., Inoue, H., and Schnell, D. J. (2018). Molecular topology of the transit peptide during chloroplast protein import. *Plant Cell* 30, 1789–1806. doi: 10.1105/tpc.18.00172

Rudolf, M., Machettira, A. B., Groß, L. E., Weber, K. L., Bolte, K., Bionda, T., et al. (2013). *In vivo* function of Tic22, a protein import component of the intermembrane space of chloroplasts. *Mol. Plant* 6, 817–829. doi: 10.1093/mp/sss114

Sade, N., Umnajkitikorn, K., Rubio Wilhelmi, M. D. M., Wright, M., Wang, S., and Blumwald, E. (2017). Delaying chloroplast turnover increases water-deficit stress tolerance through the enhancement of nitrogen assimilation in rice. *J. Exp. Bot.* 69, 867–878. doi: 10.1093/jxb/erx247

Sako, K., Yanagawa, Y., Kanai, T., Sato, T., Seki, M., Fujiwara, M., et al. (2014). Proteomic analysis of the 26S proteasome reveals its direct interaction with transit peptides of plastid protein precursors for their degradation. *J. Proteome Res.* 13, 3223–3230. doi: 10.1021/pr401245g

Springer, A., Kang, C., Rustgi, S., Von Wettstein, D., Reinbothe, C., Pollmann, S., et al. (2016). Programmed chloroplast destruction during leaf senescence involves 13-lipoxygenase (13-LOX). *Proc. Natl. Acad. Sci. USA* 113, 3383–3388. doi: 10.1073/pnas.1525747113

Tamburino, R., Vitale, M., Ruggiero, A., Sassi, M., Sannino, L., Arena, S., et al. (2017). Chloroplast proteome response to drought stress and recovery in tomato (*Solanum lycopersicum* L.). *BMC Plant Biol.* 17:40. doi: 10.1186/s12870-017-0971-0

Tillmann, B., Röth, S., Bublak, D., Sommer, M., Stelzer, E. H., Scharf, K. D., et al. (2015). Hsp90 is involved in the regulation of cytosolic precursor protein abundance in tomato. *Mol. Plant* 8, 228–241. doi: 10.1016/j.molp.2014.10.005

Valledor, L., Pascual, J., Meijón, M., Escandón, M., and Cañal, M. J. (2015). Conserved epigenetic mechanisms could play a key role in regulation of photosynthesis and development-related genes during needle development of *Pinus radiata*. *PLoS One* 10:e0126405. doi: 10.1371/journal.pone.0126405

Vercruyssen, L., Tognetti, V. B., Gonzalez, N., Van Dingenen, J., De Milde, L., Bielach, A., et al. (2015). Growth regulating factor 5 stimulates *Arabidopsis* chloroplast division, photosynthesis, and leaf longevity. *Plant Physiol.* 167, 817–832. doi: 10.1104/pp.114.256180

Virdi, K. S., Wamboldt, Y., Kundariya, H., Laurie, J. D., Keren, I., Kumar, K. S., et al. (2016). MSH1 is a plant organellar DNA binding and thylakoid protein under precise spatial regulation to alter development. *Mol. Plant* 9, 245–260. doi: 10.1016/j.molp.2015.10.011

Wang, S., and Blumwald, E. (2014). Stress-induced chloroplast degradation in *Arabidopsis* is regulated via a process independent of autophagy and senescence-associated vacuoles. *Plant Cell* 26, 4875–4888. doi: 10.1105/tpc.114.133116

Wang, P., Hendron, R. W., and Kelly, S. (2017a). Transcriptional control of photosynthetic capacity: conservation and divergence from *Arabidopsis* to rice. *New Phytol.* 216, 32–45. doi: 10.1111/nph.14682

Wang, W., Li, J., Sun, Q., Yu, X., Zhang, W., Jia, N., et al. (2017b). Structural insights into the coordination of plastid division by the ARC6-PDV2 complex. *Nat Plants* 3:17011. doi: 10.1038/nplants.2017.11

Watson, S. J., Sowden, R. G., and Jarvis, P. (2018). Abiotic stress-induced chloroplast proteome remodelling: a mechanistic overview. *J. Exp. Bot.* 11, 2773–2781. doi: 10.1093/jxb/ery053

Wei, X., Song, X., Wei, L., Tang, S., Sun, J., Hu, P., et al. (2017). An epiallele of rice AK1 affects photosynthetic capacity. *J. Integr. Plant Biol.* 59, 158–163. doi: 10.1111/jipb.12518

Woodson, J. D. (2016). Chloroplast quality control–balancing energy production and stress. *New Phytol.* 212, 36–41. doi: 10.1111/nph.14134

Woodson, J. D., Joens, M. S., Sinson, A. B., Gilkerson, J., Salomé, P. A., Weigel, D., et al. (2015). Ubiquitin facilitates a quality-control pathway that removes damaged chloroplasts. *Science* 350, 450–454. doi: 10.1126/science.aac7444

Zhao, P., Cui, R., Xu, P., Wu, J., Mao, J. L., Chen, Y., et al. (2017). ATHB17 enhances stress tolerance by coordinating photosynthesis associated nuclear gene and ATSIG5 expression in response to abiotic stress. *Sci. Rep.* 7:45492. doi: 10.1038/s41598-017-16948-4

Zhu, J. K. (2016). Abiotic stress signaling and responses in plants. *Cell* 167, 313–324. doi: 10.1016/j.cell.2016.08.029

Zufferey, M., Montandon, C., Douet, V., Demarsy, E., Agne, B., Baginsky, S., et al. (2017). The novel chloroplast outer membrane kinase KOC1 is a required component of the plastid protein import machinery. *J. Biol. Chem.* 292, 6952–6964. doi: 10.1074/jbc.M117.776468

Conflict of Interest Statement: The authors declare that the research was conducted in the absence of any commercial or financial relationships that could be construed as a potential conflict of interest.

frontiers in Plant Science

ORIGINAL RESEARCH
published: 30 July 2019
doi: 10.3389/fpls.2019.00974

The High Light Response in Arabidopsis Requires the Calcium Sensor Protein CAS, a Target of STN7- and STN8-Mediated Phosphorylation

*Edoardo Cutolo[1†], Nargis Parvin[2], Henning Ruge[3], Niloufar Pirayesh[1], Valentin Roustan[4], Wolfram Weckwerth[4], Markus Teige[4], Michele Grieco[5], Veronique Larosa[6] and Ute C. Vothknecht[1]**

[1] Plant Cell Biology, Institut für Zelluläre und Molekulare Botanik, University of Bonn, Bonn, Germany, [2] Department of Plant Nutrition, Institut für Nutzpflanzenwissenschaften und Ressourcenschutz, University of Bonn, Bonn, Germany, [3] Department of Biology I, Ludwig Maximilian University of Munich, Munich, Germany, [4] Department of Molecular Systems Biology, University of Vienna, Vienna, Austria, [5] Leibniz Institute of Plant Genetics and Crop Plant Research (IPK), Gatersleben, Germany, [6] Laboratory of Genetics and Physiology of Microalgae, InBios, University of Liège, Liège, Belgium

Reversible phosphorylation of thylakoid proteins contributes to photoacclimation responses in photosynthetic organisms, enabling the fine-tuning of light harvesting under changing light conditions and promoting the onset of photoprotective processes. However, the precise functional role of many of the described phosphorylation events on thylakoid proteins remains elusive. The calcium sensor receptor protein (CAS) has previously been indicated as one of the targets of the state transition kinase 8 (STN8). Here we show that in *Arabidopsis thaliana*, CAS is also phosphorylated by the state transition kinase 7 (STN7), as well as by another, so-far unknown, Ca^{2+}-dependent kinase. Phosphoproteomics analysis and *in vitro* phosphorylation assays on CAS variants identified the phylogenetically conserved residues Thr-376, Ser-378, and Thr-380 as the major phosphorylation sites of the STN kinases. Spectroscopic analyses of chlorophyll fluorescence emission at 77K further showed that, while the *cas* mutant is not affected in state transition, it displays a persistent strong excitation of PSI under high light exposure, similar to the phenotype previously observed in other mutants defective in photoacclimation mechanisms. Together with the observation of a strong concomitant phosphorylation of light harvesting complex II (LHCII) and photosynthetic core proteins under high irradiance in the *cas* mutant this suggests a role for CAS in the STN7/STN8/TAP38 network of phosphorylation-mediated photoacclimation processes in Arabidopsis.

Keywords: calcium sensor protein, CAS, state transition, STN7, STN8, phosphorylation, chloroplast, photoacclimation

Abbreviations: CAS, calcium sensor protein; CEF, Cyclic Electron Flow; GL, growth light; LHCII, light harvesting complex II (LHCII); PGR5, proton gradient regulation 5; saGFP, self-assembly green fluorescent protein; SSU, small subunit of the Ribulose-1,5-bisphosphate carboxylase/oxygenase; STN, state transition kinase; TAP38, thylakoid-associated phosphatase 38.

OPEN ACCESS

Edited by:
Yan Lu,
Western Michigan University,
United States

Reviewed by:
Jean-David Rochaix,
Université de Genève, Switzerland
Cornelia Spetea,
University of Gothenburg, Sweden
Rikard Fristedt,
Vrije Universiteit Amsterdam,
Netherlands

***Correspondence:**
Ute C. Vothknecht
vothknecht@uni-bonn.de

†Present address:
Edoardo Cutolo,
Laboratory of Photosynthesis and Bioenergy, Department of Biotechnology, University of Verona, Verona, Italy

Specialty section:
This article was submitted to Plant Physiology, a section of the journal Frontiers in Plant Science

Received: *09 April 2019*
Accepted: *11 July 2019*
Published: *30 July 2019*

Citation:
Cutolo E, Parvin N, Ruge H, Pirayesh N, Roustan V, Weckwerth W, Teige M, Grieco M, Larosa V and Vothknecht UC (2019) The High Light Response in Arabidopsis Requires the Calcium Sensor Protein CAS, a Target of STN7- and STN8-Mediated Phosphorylation. Front. Plant Sci. 10:974. doi: 10.3389/fpls.2019.00974

INTRODUCTION

In their daily life, plants experience drastic fluctuations of the light environment that could significantly impact their photosynthetic activity. Accordingly, rapid and dynamic adjustment mechanisms and multi-layered control strategies have evolved in phototrophic organisms to ensure proper functionality of the photosynthetic apparatus, especially under limiting or stressing light conditions (Rochaix, 2011). Efficient, light-dependent photosynthetic ATP and NADPH production relies in the first place on the balanced excitation of the two photosystems (PSI and PSII), and on the unimpaired electron flow through the electron transport chain (ETC). Operational resilience of the photosynthetic machinery is achieved through a series of built-in mechanisms that enable a fast acclimation to the changing environment and ensure protection of sensitive photosynthetic core components from damage caused by excessive light (Tikkanen et al., 2010; Pesaresi et al., 2011; Rochaix, 2011; Larosa et al., 2018).

Under limiting light conditions, excitation energy can be balanced between the two photosystems via the so-called phenomenon of state transitions (Bonaventura and Myers, 1969; Murata, 1969). This highly conserved adaptive mechanism (Ruban and Johnson, 2009; Papageorgiou and Govindjee, 2011; Kodru et al., 2015) is mediated by reversible protein phosphorylation and represents an important short-term acclimation mechanism enabling photosynthetic organisms to actively respond to rapid changes in light conditions (Rochaix, 2014). The canonical model of state transitions proposes that a mobile fraction of the light-harvesting complex II (LHCII) antenna is dynamically relocated between PSI and PSII in response to the prevailing light condition. This mechanism transiently modifies the size of the relative antenna cross section of the two photosystems and alters their light harvesting capability, thus promoting optimal photon use and preventing redox imbalances along the electron transfer chain. Reversible phosphorylation of LHCII depends on the antagonistic activities of the thylakoid-localized state transition kinase 7 (STN7) and the thylakoid-associated phosphatase 38 (PPH1/TAP38) (Pesaresi et al., 2010; Pribil et al., 2010; Shapiguzov et al., 2010). While STN7 is activated through sensing of over-reduction of the plastoquinone pool (Vener et al., 1997), PPH1/TAP38 is believed to be constitutively active (Silverstein et al., 1993; Pribil et al., 2010). In this model, STN7 and TAP38 thus regulate the excitation balance between PSI and PSII by phosphorylating/de-phosphorylating mobile LHCII trimers and causing their preferential association with PSI or PSII, which are enriched in different regions of the thylakoid membrane system (Tikkanen et al., 2006; Minagawa, 2011; Tikkanen and Aro, 2012). This model has been nevertheless partially challenged recently by findings that indicate that LHCII is found phosphorylated independently from its localization within the thylakoid membrane structure (Mekala et al., 2015). More research is required to truly understand the intricate network of protein phosphorylation, lateral complex migration and protein interactions that enable the optimization of photosynthetic energy fluxes.

A close paralog of STN7, the state transition kinase 8 (STN8), is mainly responsible for the phosphorylation of a set of PSII core components, including the D1, D2, and CP43 proteins, especially under high irradiance (Bonardi et al., 2005; Vainonen et al., 2005). For this reason, the role of STN8 has been connected with the repair cycle of photodamaged PSII reaction centers, where it appears to regulate the displacement of damaged D1 proteins (Fristedt et al., 2009). However, phosphorylation of PSII core proteins and thus STN8 are also part of the broader array of phosphorylation-dependent photoacclimation mechanisms (Mekala et al., 2015).

Aside from LHCII and the PSII core components, additional phosphoproteins populate the thylakoid membrane system, but for many of these entities neither the corresponding kinase nor the precise function behind their phosphorylation is clear. The calcium sensing receptor (CAS; At5g23060) is a thylakoid-localized phosphoprotein of unknown function. It has a proposed role in mediating stromal and cytoplasmic Ca^{2+} signals in connection with stomatal movement and immunity-related gene expression in Arabidopsis (Nomura et al., 2008; Weinl et al., 2008; Nomura et al., 2012). Phosphorylation of CAS has been described both as a Ca^{2+}-dependent (Stael et al., 2012) as well as a high light-induced, STN8-dependent event (Vainonen et al., 2008), but the functional consequences of this reversible modification remain elusive. *In silico* topology predictions suggest that CAS possesses a single transmembrane domain that splits the protein in two halves of about equal size. Apart from the chloroplast targeting sequence, the N-terminal domain does not possess any identifiable functional characteristics but was described to be able to bind Ca^{2+} *in vitro* with low affinity and high capacity (Han et al., 2003; Wang et al., 2016). The C-terminal domain contains a so-called "non-catalytic rhodanese homology domain" as well as all of the described phosphorylation sites.

In the present work, we investigated the phosphorylation profile of CAS by dissecting the potential contribution of different phosphorylation sites and the involvement of the major thylakoid-localized kinases STN7 and STN8 in its reversible modification. Bioinformatics and phosphoproteomics analyses identified several evolutionary conserved phosphorylation sites and *in vitro* kinase assays provided further evidence of multiple phosphorylation events affecting CAS. Characterization of *cas* mutant plants by analysis of chlorophyll fluorescence emission at 77K revealed similarities to the photosynthetic mutants *tap38/pph1* and *pgr5* (Mekala et al., 2015). Altogether, our results suggest a role of CAS in the STN7/STN8/TAP38-dependent photoacclimation network.

MATERIALS AND METHODS

Plant Material and Growth Conditions

Unless otherwise stated *Arabidopsis thaliana* wild type (ecotype Col-0) and previously described mutant lines *cas-1* (SALK_070416; Nomura et al., 2008; Weinl et al., 2008), *stn7* (SALK_073254; Bellafiore et al., 2005), *stn8* (SALK_060869; Vainonen et al., 2005), and *stn7/8* double mutant (Fristedt et al., 2009) were grown on soil in a growth chamber

(equipped with Philips TLD 18W of alternating 830/840 light color temperature) under a 16 h/8 h day/night regime with 100 μmol photons m^{-2} s^{-1}.

Isolation of Protein Extracts From Chloroplast Subfractions

Intact chloroplasts were purified from 4 weeks old Arabidopsis plants as previously described (Seigneurin-Berny et al., 2008) starting from leaf material that was harvested at the end of the dark period or after 4 h in growth light (GL). Intact chloroplast pellets were frozen in liquid nitrogen and stored at −80°C if not used immediately. Thylakoid membrane and stromal protein fractions were obtained as previously described (Rocha et al., 2014) by disrupting intact chloroplasts in lysis buffer (20 mM Tricine/HCl, pH 7.6, 10% (v/v) glycerol and 1 mM DTT) supplemented with protease inhibitors (complete™, EDTA-free; Roche, Mannheim, Germany) and, depending on the type of experiment, with phosphatase inhibitors (PhosphoStop; Roche, Mannheim, Germany). After incubation on ice for 15 min, membranes and soluble components were separated by centrifugation at 20,000 *g* for 10 min and the thylakoid fraction was washed several times with lysis buffer. All procedures were carried out at 4°C.

Protein concentration of protein extracts was determined by using the Coomassie Bradford protein assay kit (Life Technologies, Darmstadt, Germany) according to the manufacturer's instructions. Chlorophyll concentration was determined as previously described (Arnon, 1949). Purity of the fractions was confirmed by SDS-PAGE and Western Blot analysis using antibodies against transketolase (α-TKL), fructose 1,6-bisphosphatase (α-FBP), 33 kDa subunit of the oxygen evolving system (α-OE33) and ATP-Synthase (α-ATPase).

Cloning and Purification of Recombinant CAS Constructs

The CAS-C construct, ranging from AA 216 to 387 of the CAS protein (At5g23060), was the same as used in Stael et al. (2012). All non-phosphorylatable CAS-C variants (CAS-C_{T376V}, CAS-C_{S378A}, CAS-C_{T380V}) were obtained via QuickChange site directed mutagenesis (Zheng et al., 2004) on the original CAS-C construct (for a list of primers see **Supplementary Table S1**). PCR reaction products were treated with *DpnI* enzyme to digest parental vector DNA and transformed in *E. coli* DH5α cells for plasmid amplification.

The CAS-N fragment was cloned in-frame with an N-terminal intein tag into the pTWIN1 vector (New England Biolabs). To this end, the sequence corresponding to amino acidic positions 34–147 of CAS was obtained by PCR from *Arabidopsis thaliana* cDNA using primers containing the restriction sites for *Nco*I and *Pst*I (**Supplementary Table S1**).

Recombinant CAS-C and CAS-N fragments, including the non-phosphorylatable CAS-C variants, were expressed in *E. coli* strain ER2566 cells and purified under native conditions using the IMPACT™-TWIN system (New England Biolabs, Frankfurt, Germany) following the manufacturer's instructions. Protein concentration of purified recombinant proteins was determined by using the Coomassie Bradford protein assay kit.

For expression of CAS-YFP and CAS_{34-387}-YFP in tobacco mesophyll cells, the full-length CAS coding sequence and a truncated variant lacking the first 33 amino acids corresponding to the predicted transit peptide were cloned N-terminally to the YFP sequence into the plant expression vector pBIN19 (Datla et al., 1992). For self-assembly green fluorescent protein (saGFP) analysis (Cabantous et al., 2005), the full-length coding sequences of CAS and the small subunit of RUBISCO were cloned into the pBIN19-saGFP$_{1-10}$ and pBIN19-saGFP$_{11}$ vectors as described in Ruge et al. (2016).

A list of all construct used in this study is provided in **Supplementary Table S2**.

In vitro Phosphorylation Assays

In vitro phosphorylation of recombinant CAS-C fragments were conducted as previously described (Stael et al., 2012) using ∼200 ng of CAS-C substrates and catalytic amounts (equivalent to ∼2 μg of chlorophyll) of thylakoid membranes. All assays were carried out for 10 min (unless stated otherwise) at room temperature (22°C) in a total volume of 25 μl in kinase buffer containing 20 mM Tricine/HCl, pH 7.6, 10 mM $MgCl_2$, 10% (v/v) glycerol, 1 mM DTT, 5 μM ATP and 70–180 kBq of [γ^{32}-P]ATP (PerkinElmer, Waltham, MA, United States). Depending on the experiment, assays were conducted at ambient light or in dark and supplemented with 1 μM $CaCl_2$ or 2 mM EGTA. Reactions were stopped by the addition of SDS solubilization buffer (Laemmli, 1970) and boiling for 2 min at 96°C. Reaction products were separated via SDS-PAGE, followed by Coomassie staining and drying of the gel. Phosphorylation signals were revealed by exposing dried gels to X-ray films (Carestream® Kodak® X-Omat LS film, Rochester, NY, United States) followed by film processing and development (AGFA G153 developer, Fix AG fixer, Mortsel, Belgium).

Immunoblot Analysis

Custom polyclonal primary antibodies were generated in rabbit against purified CAS-C and CAS-N fragments (Davids Biotechnologies, Regensburg, Germany). The α-OE33 antiserum was a kind gift from Prof. J. Soll (LMU Munich). The α-pThr antibody was purchased from Cell Signaling (Danvers, MA, United States) and used as previously described (Mekala et al., 2015). Proteins were separated on 10% SDS-PAGE gels and visualized by western blotting using an anti-rabbit secondary antibody coupled to horseradish peroxidase (Sigma-Aldrich, St. Louis, MO, United States), an enhanced chemiluminescence kit (SERVALight EOS, SERVA, Heidelberg, Germany) and the Chemidoc Imaging System (BioRad).

For immune detection-based topology analysis of CAS, a protease treatment of isolated thylakoids was performed prior to SDS-PAGE separation. Isolated thylakoid membranes were resuspended in 0.1 M sucrose, 10 mM HEPES-NaOH, pH 8.0 at 0.5 mg chlorophyll/ml. Depending on the sample, the detergent Triton X-100 was included to a concentration of 1% before the addition of the protease. Untreated and detergent-treated thylakoid samples were incubated with thermolysin

(Sigma-Aldrich, St. Louis, MO, United States) in a concentration of 100 μg/ml with 1 mM $CaCl_2$ for 20 min on ice. The digestion reaction was stopped by addition of 20 mM EDTA and 4× SDS-sample buffer followed by boiling for 2 min at 96°C. The samples were analyzed by SDS-PAGE and western blot using antibodies against CAS-C, CAS-N, and OE33.

Confocal Laser Scanning Fluorescence Microscopy

Agrobacterium-mediated transient transformation of tobacco leaf cells was performed as previously described (Voinnet et al., 2003). Infiltrated leaves with transiently expressed and co-expressed proteins of interest were harvested after 48 h and used for protoplast isolation (Koop et al., 1996). The subcellular localization of protein was analyzed with a Leica TCS SP5 confocal laser scanning microscope (Leica Microsystems, Germany) using excitation with the 488 nm line of an argon laser for GFP, YFP and chlorophyll. Emission spectra were recorded from 496 to 523 nm (GFP, YFP) and 680 to 713 nm (chlorophyll). Images were taken with a HCX PL APO CS 100.0 × 1.46 OIL objective and image processing was performed using the Leica Application Suite for Advanced Fluorescence (LAS AF) software.

Analysis of Chlorophyll Fluorescence Emission at 77K

Chlorophyll fluorescence emission spectra were recorded at 77K from frozen thylakoids. Thylakoid membranes were extracted as previously described (Tikkanen et al., 2006) from leaves of 3 weeks old Arabidopsis plants after the following light treatments: end of night (dark, D), 2 h of GL (100 μmol photons m^{-2} s^{-1}, alternating Osram Luminux 35W/840 and Philips TLD 18W/860; GL) and subsequent 2 h of high light (1000 μmol photons m^{-2} s^{-1}, LED of 3000 K; HL). Briefly, leaves were flash frozen in liquid nitrogen and grinded into powder in a homogenization buffer containing 50 mM Hepes/KOH, pH 7.5, 330 mM sorbitol, 2 mM EDTA, 1 mM $MgCl_2$, 5 mM ascorbate, 0.05% (w/v) BSA and 10 mM of the phosphatase inhibitor NaF. All steps were performed at 4°C and under dim green light. The material was subsequently filtered through Miracloth and pelleted by centrifugation at 2500 *g* for 4 min at 4°C, followed by a second wash step in homogenization buffer. For measurements, thylakoids were diluted to a chlorophyll concentration of 1 μg ml^{-1} concentration.

Chlorophyll fluorescence emission spectra were measured from frozen thylakoids by exciting the samples at 480 nm and recording the emission spectrum between 650 and 800 nm using an Ocean Optics QE Pro Spectrometer. Three biological and technical replicates for each genotype and treatment were measured. Ratio values of chlorophyll fluorescence emission peaks of PSI over PSII were calculated by manual normalization of the traces to the PSII peak value at 685 nm.

LC-MS/MS Analysis of Phosphopeptides From Thylakoid Membranes

Intact chloroplasts were isolated as described above from wild type and *stn8* mutant plants after 4 h of GL exposure. Preparation of surface-exposed peptides from thylakoid membranes via trypsin digestion was performed as previously described (Vener and Strålfors, 2005; Rokka et al., 2011). Samples were flash frozen in liquid nitrogen, thawed, and the digestion products were centrifuged for 20 min at 14,000 *g*. Enrichment of released phosphopeptides was performed using 5 mg of TiO_2 (Glygen Corp.) as described previously (Bodenmiller et al., 2007; Chen et al., 2010). Subsequently, peptides were lyophilized to dryness in a vacuum concentrator.

Phosphopeptide analysis of the lyophilized samples was performed as described in Roustan et al. (2017). MaxQuant 1.5[1] and the Andromeda search algorithm were used against the TAIR-10 database to perform peptide identification, phosphorylation site mapping and phosphopeptide quantification (Cox and Mann, 2008; Cox et al., 2011). The following stringency criteria were applied in the analysis: three missed cleavages were allowed and methionine oxidation and protein N-terminal acetylation were endorsed as dynamic modifications. Additionally, phosphorylation of serine, threonine and tyrosine residues was permitted to occur as dynamic modifications. Mass tolerance was set to 5 ppm for parental ions and 0.5 Da for the MS/MS fragment. For both peptide and protein levels, false discovery rate was set to 1%. Quantification was done at the peptide level. Perseus 1.5 software was used for further filtering and data processing (Tyanova et al., 2016). Phosphopeptides were accounted for quantification if they could have been quantified in at least 70% of the biological samples. Additionally, only phosphopeptides that passed the class I criteria (phosphosite probability > 75% and score difference >5) were included in the final dataset (Olsen et al., 2006).

Bioinformatics Analysis

Orthologs of CAS in various organisms were identified by blastp or tblastn searches at NCBI. Alignments were performed using Clustal X 2.0 (Thompson et al., 1997). For dicots, monocots, gymnosperms and green algae consensus sequences were defined based on the full alignments shown in **Supplementary Data S1–S4**. Some hand-alignment was performed to give what we consider the best fit.

Accession Numbers

Accession numbers for all sequence data can be found in **Supplementary Table S3**.

RESULTS

Phylogenetic Conservation of CAS Phosphorylation Sites

The state transition kinases STN7 and STN8 are the best-described protein kinases in the thylakoid membrane (Bellafiore et al., 2005; Bonardi et al., 2005; Vainonen et al., 2005; Pesaresi et al., 2011) and the CAS protein was initially described as a potential target of STN8 (Vainonen et al., 2008). At the same time, *in vitro* phosphorylation studies have shown Ca^{2+}-dependent

[1] http://www.maxquant.org

phosphorylation of CAS (Stael et al., 2012), indicating that this protein might be a shared target of multiple kinases.

Vainonen and co-workers suggested Thr-380 as the site of STN8 phosphorylation (**Figure 1A**). However, further experimental studies (mostly in the form of large-scale phosphoproteomics analyses; **Table 1**) have indicated multiple phosphorylated Thr and Ser residues (Heazlewood et al., 2008; Durek et al., 2010), the majority of which are located close to the C-proximal end of CAS. For seven positions, the phosphoresidue was identified unequivocally (**Figure 1A**, asterisks; **Table 1**), while in all other cases the precise position of the modification within an identified phosphopeptide was not assigned (**Figure 1A**, hash).

We performed a comparative analysis of CAS orthologs to investigate the phylogenetic conservation of the phosphosites described for Arabidopsis. Proteins with significant sequence similarity to CAS can be found in all organisms of the *Viridiplantae* clade for which complete genomes or substantial genomic data are available (**Supplementary Table S4**). For groups such as dicots, monocots, gymnosperms and green algae, where multiple sequences are available, consensus sequences were obtained using Clustal X on which the data in **Figure 1B** are based. For ferns, only a single complete sequence was available from *Pteris vittata* (Pvi) and in case of the bryophytes, the sequences from *Physcomitrella patens* (Ppa) and *Marchantia polymorpha* (Mpo) deviated in their C-terminus so much that a consensus could not be made. *Medicago truncatula* (Mtr) and *Gossypium hirsutum* (Ghi; dicots), *Oryza sativa* (Osa), *Zea mays* (Zma), *Triticum aestivum* (Tae) and *Brachypodium distachyon* (Bdi; monocots), *Selaginella moellendorffii* (Smo; early diverging lineage of vascular plant) as well as *Chlamydomonas reinhardtii* (Cre; green algae) are listed individually because phospo-peptide

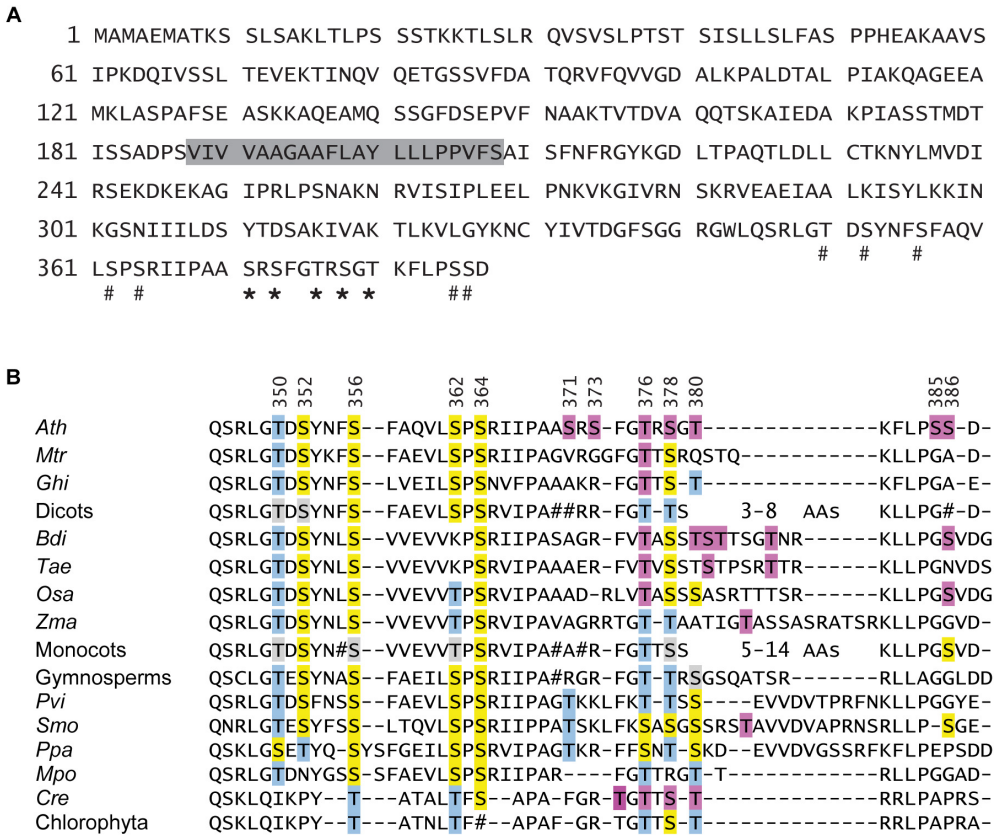

FIGURE 1 | CAS domain structure and phylogenetic conservation of phosphorylation sites. **(A)** Amino acid sequence of the CAS (At5g23060) protein of *A. thaliana*. The predicted transit sequence and the transmembrane domain are marked by a solid line and a gray box, respectively. Thr and Ser residues that were unambiguously identified by phospho-proteomic studies are marked by an asterisk, while sites that are part of a phosphopeptide (tentative sites) are marked by a hash. **(B)** Sequence alignment of the CAS C-terminal domain from organisms throughout the *Viridiplantae* clade. For dicots, monocots, gymnosperms and green algae, a consensus sequence was created based on alignments shown in **Supplementary Data S1–S4**. Those organisms, for which phosphoproteomics data on CAS are available, are listed separately. Residues for which phosphorylation was shown unambiguously are indicated by a purple box. For Arabidopsis, five more Ser and Thr residues are present in phosphopeptides for which the exact phosphoresidue was not determined. These and all Ser and Thr residues that can be aligned to potential pSer or pThr from Arabidopsis CAS are marked in yellow or blue, respectively. Positions where a majority but not all sequences from a consensus have a Ser or Thr are marked in light gray. Positions where no clear conservation (<70%) was observed in a consensus are marked by #. In many sequences from the mono- and dicots, a stretch of variable length is found toward the C-proximal end. In all cases this part contains at least one Ser or Thr residue. *Ath, A. thaliana; Mtr, M. truncatula; Ghi, G. hirsutum; Bdi, B. distachyon; Tae, T. aestivum; Osa, O. sativa; Zma, Z. mays; Pvi, P. vittata; Smo, S. moellendorffii; Ppa, P. patens; Mpo, M. polymorpha; Cre, C. reinhardtii.*

TABLE 1 | Phosphopeptides identified for CAS proteins from various organisms.

Species	Phosphosite	Corresponding site in *A. thaliana*	Phosphosite(s) or phosphopeptide	References
A. thaliana	Thr-350; Ser-352; Ser-362; Ser-364		LGTDSYNFSFAQVLSPSR	a, b
	Ser-371		IIPAA**pS**R**pS**FGTR IIPAA**pS**R**pS**FG**pT**R	g, h
	Ser-373		IIPAA**pS**R**pS**FGTR IIPAA**pS**R**pS**FG**pT**R IIPAASR**pS**FG**pT**R **pS**FGTRSGTKFLPSSD **pS**FGTR**pS**GTKFLPSSD **pS**FGTRSG**pT**KFLPSSD	a–c, f–h
	Thr-376		IIPAASR**pS**FG**pT**R IIPAA**pS**R**pS**FG**pT**R SFG**pT**RSGTKFLPSSD SFG**pT**RSG**pT**KLPSSD	b, f, h this work
	Ser-378		SFGTR**pS**G**pT**K **pS**GTKFLPSSD **pS**FGTR**pS**GTKFLPSSD	a–f, h this work
	Thr-380		SFGTRSG**pT**KFLPSSD **pS**FGTRSG**pT**KFLPSSD SFG**pT**RSG**pT**KLPSSD SG**pT**KFLPSSD SFGTR**pS**G**pT**K	c, f–i this work
	Ser-385; Ser-386		SGTKFLPSSD	b
M. truncatula	**Thr-378**	**Thr-376**	GGFG**pT**TSR	J
G. hirsutum	**Thr-390**	**Thr-376**	FG**pT**TSTK	k
B. distachyon	**Thr-369**	**Thr-376**	FV**pT**ASS**pT**pSTTSGTNR FV**pT**ASSTS**pT**TSG**pT**NR	m, n
	Thr-373	**Thr-380**	FV**pT**ASS**pTpS**TTSGTNR	m
	Ser-374	-/-	FV**pT**ASS**pTpS**TTSGTNR	m
	Thr-375	-/-	FV**pT**ASSTS**pT**TSG**pT**NR	n
	Thr-379	-/-	FV**pT**ASSTS**pT**TSG**pT**NR	n
	Ser-387	**Ser-386**	KLLPG**pS**VDG	m, n
T. aestivum	**Thr-368**	**Thr-376**	FV**pT**VSSTSTPSR**pT**SR	l
	Ser-373	-/-	FV**pT**VSST**pS**TPSRTTR	l
	Thr-378	-/-	FV**pT**VSSTSTPSR**pT**SR	l
O. sativa	**Ser-384**	**Ser-386**	KLLPG**pS**VDG	m
	Thr-366	**Thr-376**	LV**pT**ASSSASR	n
Z. mays	**Thr-377**	-/-	IG**pT**ASSASR	p, q
C. reinhardtii	**Thr-365**	-/-	GR**pT**G**pT**TSTR	r
	Thr-367	**Thr-376**	GR**pT**G**pT**TSTR TG**pT**TS**pT**RRLPAPR	r
	Ser-369	**Ser-378**	TG**pT**TS**pT**RRLPAPR	r
	Thr-370	**Thr-380**	TGTT**pSpT**RRLPAPR	r

Unambiguously identified phosphoresidues are indicated in bold. Accession numbers can be found in ***Supplementary Table S3****. (a) Reiland et al. (2009), (b) Reiland et al. (2011), (c) Nguyen et al. (2012), (d) Hoehenwarter et al. (2013), (e) Wang et al. (2013), (f) Yang et al. (2013), (g) Lin et al. (2015), (h) Roitinger et al. (2015), (i) Bhaskara et al. (2017); (j) Rose et al. (2012); (k) Fan et al. (2014); (l) Lv et al. (2014a), (m) Lv et al. (2014b), (n) Lv et al. (2014c); (o) Whiteman et al. (2008); (p) Bonhomme et al. (2012), (q) Fristedt et al. (2012), (r) Wang et al. (2014).*

data on CAS from these organisms are available (**Table 1**). Of note, no CAS orthologs were identified in cyanobacteria, red algae or glaucophyta.

The evolutionary conservation of all 12 Ser and Thr residues found within the C-proximal end of the Arabidopsis CAS protein is represented in **Figure 1B**. Residues for which phosphorylation was shown unambiguously independent of the organism are indicated by a purple box. For Arabidopsis, five more Ser and Thr residues are part of phosphopeptides for which the exact phosphoresidue position was not determined. These and all Ser and Thr residues that can be aligned to proven and potential pSer or pThr from Arabidopsis CAS (see also **Table 1**) are marked in yellow or blue, respectively, in **Figure 1B**. Up to Ser-371 in the Arabidopsis sequence, all CAS sequences show a quite

high degree of similarity. Unfortunately, from there onwards the sequence of CAS proteins becomes much less conserved and only the very proximal end of about 7 amino acids can be reasonably well aligned. In between, the sequences vary between one threonine in *P. patens* up to 14 amino acids in certain monocots. The best fit that we could create for this region suggests a strong evolutionary conservation of Thr-376 and this site can be aligned with good confidence to phosphoresidues identified in *C. reinhardtii*, *O. sativa*, *B. distachyon*, *G. hirsutum,* and *M. truncatula* (**Figure 1B** and **Table 1**). A somewhat similar level of conservation can be observed for Thr-378, which is represented by a Ser or Thr residue in the vast majority of sequences. Instead, Thr-380 shows a lower degree of conservation but seems to be represented by a Ser or Thr residues in many sequences. Also, in the highly variable and therefore difficult to align C-terminal part of most monocot and dicot sequences, at least two Ser or Thr residues can be found that could functionally substitute Thr-380 of Arabidopsis. Indeed, phosphorylated Thr or Ser residues within this variable region were detected in organisms as divergent as *B. distachyon*, *Z. mays, S. moellendoerffii,* and *C. reinhardtii* (**Table 1**). Together, these data indicate a strong evolutionary conservation of some CAS phosphorylation sites that goes back to the origin of the plant cell. Other potential phosphorylation sites show different degrees of phylogenetic conservation. Notably, Ser-371 and Ser-373, which were unambiguously shown as phosphorylated in Arabidopsis (**Table 1**), are not conserved at all, indicating that there might exist a certain level of organism-specific phosphorylation pattern(s) of CAS.

CAS Is a Target of Both State Transition Kinases

When a phosphoproteomics analysis was performed on growth light (GL; 100 μmol photons m^{-2} s^{-1}) acclimated Arabidopsis wild type and *stn8* mutant plants, we found three of the previously described phosphorylation sites, namely Thr-376, Ser-378, and Thr-380 (**Supplementary Table S4** and **Supplementary Data S5**). Phosphorylated versions of all three residues were detectable in wild type and the *stn8* mutant, albeit at lower abundance, indicating that they are target sites of STN8 but can still be phosphorylated in its absence. This is in agreement with Thr-380 having previously been found phosphorylated in the *stn7* and *stn8* single mutants but not in the *stn7/8* double mutant (Ingelsson and Vener, 2012). In our analysis, proteins that are not targets of STN8 (Reiland et al., 2011) showed no difference in phosphorylation (**Supplementary Table S4**), supporting that the reduced levels of CAS phosphorylation are indeed due to the lack of STN8.

We next performed *in vitro* phosphorylation assays using a 171 amino acid long recombinant fragment of CAS (CAS-C) that contains all phosphoresidues determined by different phosphoproteomics studies (AAs 216-387). We generated three non-phosphorylatable variants of the CAS-C fragment by replacing threonine (at Thr-376 and Thr-380) and serine (at Ser-378) residues with valine and alanine, respectively. *In vitro* phosphorylation assays were conducted using thylakoid membranes from GL-adapted wild type plants in the presence of 1 μM Ca^{2+} (unless stated otherwise) to promote full activation of all potentially involved kinases. In agreement with the phosphoproteomics results, all three variants showed a reduction in phosphorylation compared to the wild type construct (**Figure 2A** and **Supplementary Figure S1**). The reduction for CAS-C_{S378A} was only minor, while the strongest reduction was observed for CAS-C_{T376V}. This observation is in contrast with the notion that Thr-380 is the major phosphorylation site of CAS (Vainonen et al., 2008). However, the phosphopeptide detected in that study only started with Arg-377 and thus did not include Thr-376.

Since the phosphoproteomics analysis indicated that CAS is still phosphorylated in the absence of STN8, the *in vitro* phosphorylation of CAS-C was investigated by comparing thylakoid membranes derived from Arabidopsis wild type, *stn7*, *stn8,* and *stn7/8* mutants (**Figure 2B** and **Supplementary Figure S1**). As expected, endogenous LHCII, which is the major target of STN7 (Bonardi et al., 2005), is strongly phosphorylated in the wild type and the *stn8* mutant, while very little phosphorylation is evident in the *stn7* and *stn7/8* mutants. By contrast, phosphorylation of recombinant CAS-C was observed in both single mutants, but was mostly abolished in the *stn7/8* mutant. Similar to endogenous LHCII protein, phosphorylation of CAS-C also appears slightly enhanced in the *stn8* mutant. An increased STN7 activity on LHCII in the absence of STN8 can be observed in similar studies (Bonardi et al., 2005; Tikkanen et al., 2010) and could be due to a compensatory mechanism affecting all targets of STN7, especially if they are shared with STN8. Thus, in line with the phosphoproteomics data, these results show that CAS is not an exclusive target of STN8 but can also be phosphorylated by STN7. When the three phosphosite variants of CAS-C were incubated with thylakoids originating from GL-acclimated *stn7* and *stn8* plants, a similar pattern of phosphorylation reduction as in the wild type was observed for both mutants, suggesting that the two STN kinases do not target different phosphorylation sites of CAS (**Figure 2C** and **Supplementary Figure S1**).

CAS C-Terminal Phosphorylation Sites Are Exposed to the Stroma

Phosphorylation of CAS-C by STN7 and STN8 requires the accessibility of the CAS C-terminus to the active site of these kinases. In the initial paper describing CAS, and in accordance with *in silico* topology predictions, a single transmembrane-spanning domain was suggested that splits the protein into two nearly equal parts (**Figure 1A**, gray boxing). When the thylakoid localization of CAS and its phosphorylation by STN8 were described (Vainonen et al., 2008), it was concluded that the C-terminal domain has to be exposed to the stroma. However, while stromal exposure of the N-terminus could be confirmed by western blot analysis using an antibody directed against the N-terminus of CAS (Nomura et al., 2008), the localization of the C-terminus was never proven experimentally.

We thus analyzed the topology of CAS with two different experimental approaches. After confirming the correct

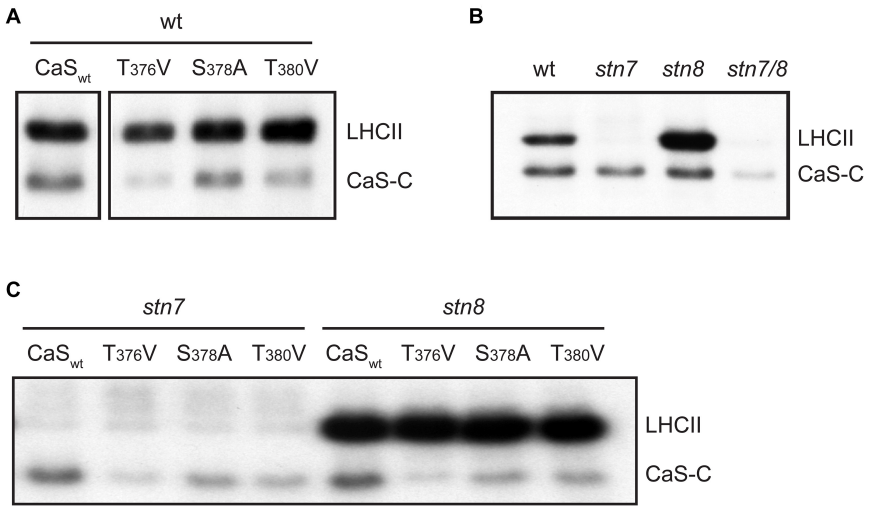

FIGURE 2 | *In vitro* phosphorylation of a recombinant CAS fragment (CAS-C) by thylakoid extracts from wild type, *stn7*, *stn8,* and *stn7/8* plants. **(A)** CAS-C (CaS_{wt}) and variants with altered Ser and Thr residues were phosphorylated using thylakoid extracts from wild type in the presence of Ca^{2+}. Phosphorylation of endogenous LHCII is also visible. **(B)** Phosphorylation assays with the CAS-C fragment were performed in the presence of Ca^{2+} using thylakoid extracts from wild type (wt), *stn7*, *stn8,* and *stn7/8* double mutant plants. **(C)** CAS-C (CaS_{wt}) and variants with altered Ser and Thr residues were phosphorylated in the presence of Ca^{2+} using thylakoid extracts from *stn7* and *stn8* mutant plants. All panels show representative results of experiments performed several times. Corresponding Coomassie stained gels for all panels are shown in **Supplementary Figure S2**.

chloroplast targeting of a CAS-YFP fusion construct in the pBIN19-based vector system (Mehlmer et al., 2012) by transient expression in *N. benthamiana* leaves (**Figure 3A**), we employed a pBIN19-based self-assembling GFP (saGFP) system, which had been previously used to study the topology of membrane proteins (Cabantous et al., 2005; Machettira et al., 2011). We fused CAS or the small subunit of the Ribulose-1,5-bisphosphate carboxylase/oxygenase (SSU) to either the 11th beta sheet (CAS-saGFP$_{11}$; SSU-saGFP$_{11}$) or the first 10 beta-sheets (CAS-saGFP$_{1-10}$; SSU-saGFP$_{1-10}$) of GFP. Assembly of a functional GFP occurs when both parts are present in the same cellular compartment. Co-infection of CAS-saGFP$_{1-10}$ with CAS-saGFP$_{11}$ and SSU-saGFP$_{1-10}$ with SSU-saGFP$_{11}$ resulted in GFP fluorescence clearly overlapping with the chlorophyll fluorescence, indicating that both proteins are correctly targeted into the chloroplast (**Figure 3B**). The same result was achieved when CAS-saGFP$_{1-10}$ was co-infected with SSU-saGFP$_{11}$. Since SSU is a soluble stromal protein, these results strongly support an extrusion of the C-terminal domain of CAS into the stroma.

We furthermore generated polyclonal antibodies against the N-terminal (AA 34–147; α-CAS-N) and the C-terminal domain (AA 216–387; α-CAS-C) of CAS. Both antibodies were able to recognize their recombinant antigen and did not show any cross-reactivity with the other domain (**Supplementary Figure S3**). They both recognize a protein of about 38 kDa in chloroplast extracts and this reaction was absent in the *cas* mutant line (**Figure 3C** and **Supplementary Figure S4**). When tested on different protein fractions, i.e., total chloroplasts, thylakoid membranes, and stromal/soluble proteins, CAS was only detected in chloroplast extracts and the thylakoid membrane fraction (**Figure 3C**), corroborating its predicted localization. We then treated isolated thylakoid membranes with thermolysin to remove those parts of thylakoid membrane proteins that extrude into the stroma. Probing of untreated and treated samples with an antibody against the thylakoid lumen protein OE33 revealed no loss of reactivity after thermolysin digestion, indicating that the thylakoid membrane remained intact throughout the treatment (**Figure 3D**, α-OE33). Thermolysin-mediated degradation of OE33 could only be achieved when a detergent was added to the thylakoid membranes along with the protease. By contrast, no signal was detected in thermolysin-treated thylakoids when probed with antisera against either α-CAS-C or α-CAS-N (**Figure 3D**). These results corroborated the orientation of both termini toward the stromal side of the thylakoid membrane thereby giving the C-terminal phosphorylation sites access to the active domains of STN7 and STN8 (**Figure 3E**).

CAS Is Required for Acclimation to High Light

The work of Vainonen and coworkers suggested a light-dependent regulation behind the *in vivo* phosphorylation of CAS (Vainonen et al., 2008). In line with their suggestion, a clear difference in the *in vitro* phosphorylation intensity of recombinant CAS-C was evident in this work when GL-adapted thylakoid membranes from wild type plants were compared with dark-harvested ones (**Figure 4A** and **Supplementary Figures S4, S5**). A similar difference could be observed in the phosphorylation of the endogenous LHCII, reflecting the light-dependent activation of STN7 (Bellafiore et al., 2005). As expected, no LHCII phosphorylation was observed in the *stn7* mutant, while its phosphorylation was slightly enhanced in the *stn8* mutant. For CAS-C, an impact of the light treatments on its phosphorylation was evident in case of the *stn8* mutant but not

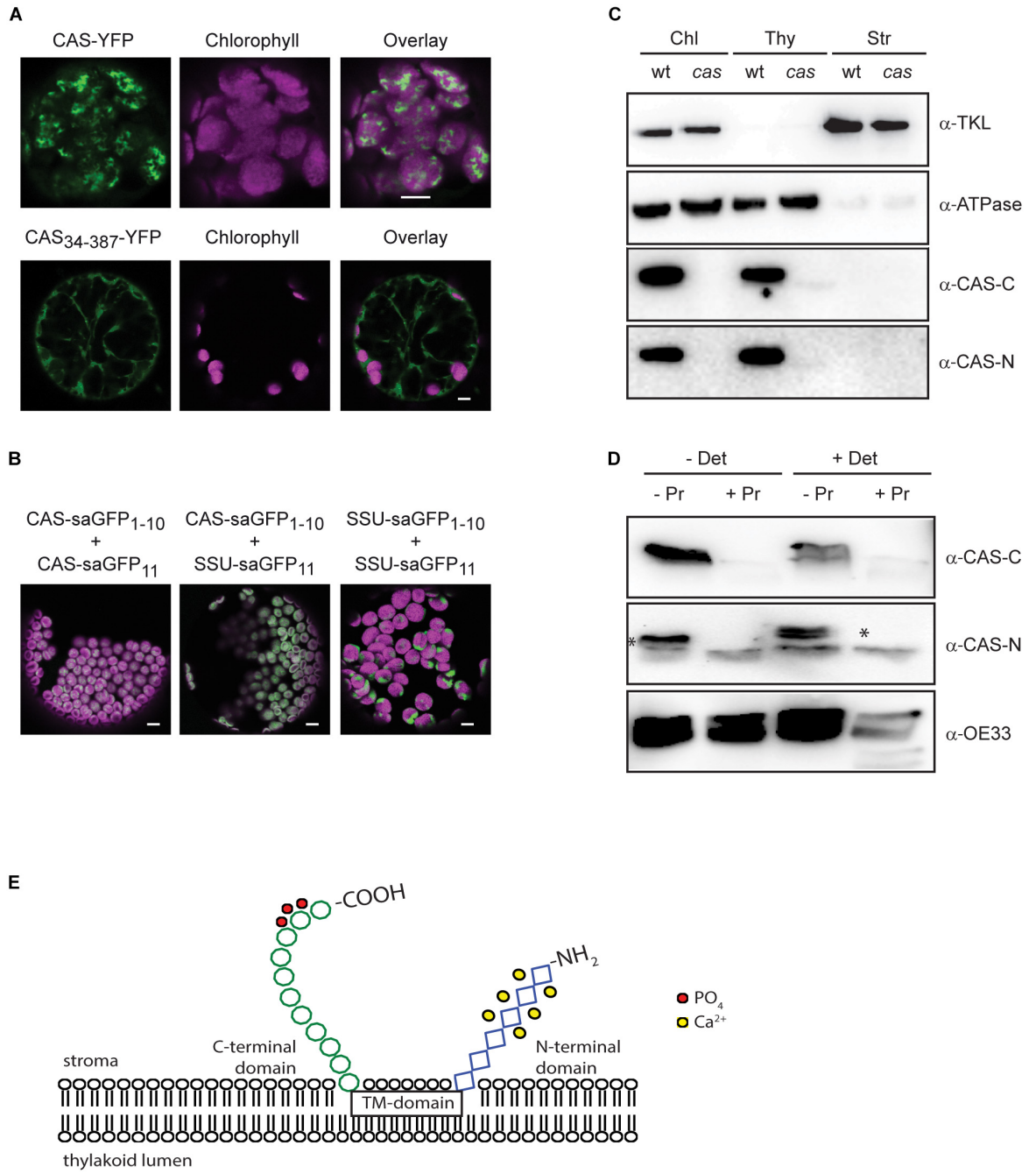

FIGURE 3 | Topology analysis of CAS. **(A)** Expression of CAS-YFP in tobacco protoplasts shows a clear overlap of the YFP and chlorophyll fluorescence signal confirming the correct targeting of CAS-YFP into the chloroplast. Removal of the predicted transit peptide (CAS_{34-387}-YFP) resulted in a cytosolic localization (white bars indicate 5 μm). **(B)** Fluorescence analyses of tobacco leaf cell protoplasts co-transformed with the self-assembly GFP pairs CAS-saGFP$_{1-10}$/CAS-saGFP$_{11}$, CAS-saGFP$_{1-10}$/RUBISCO-saGFP$_{11}$, and RUBISCO-saGFP$_{1-10}$/Rubisco-saGFP$_{11}$ confirm that the C-terminus of CAS is exposed to the stromal side of the thylakoid membrane (white bars indicate 5 μm). **(C)** Isolated chloroplasts from wild type (wt) and *cas* mutant plants were separated into thylakoid membranes and stroma and all fractions were probed with antibodies directed against the two CAS domains (α-CAS-C; α-CAS-N), beta-subunit of the chloroplast ATP-synthase (α-ATPase) and transketolase (α-TKL). A corresponding Coomassie-stained gel is shown in **Supplementary Figure S3**. **(D)** Isolated thylakoid membranes from wild type plants were treated with the protease thermolysin (+/− Pr) in the absence or presence of detergent (+/− Det). All fractions were probed with antibodies against the C- and N-terminal domain of CAS (α-CAS-C, α-CAS-N) as depicted in **Figure 1A**. The asterisk indicates the specific reaction of the α-CAS-N antibody with CAS. An antibody against the oxygen-evolving system protein 33 (α-OE33) was used as a control to assess the integrity of the thylakoid membrane during the treatment. **(E)** Topology model of CAS showing the exposure of conserved phosphorylation sites (red circles) onto the stromal surface of the thylakoids. Ca^{2+}-binding to the stromal exposed N-terminal domain is indicated by yellow circles.

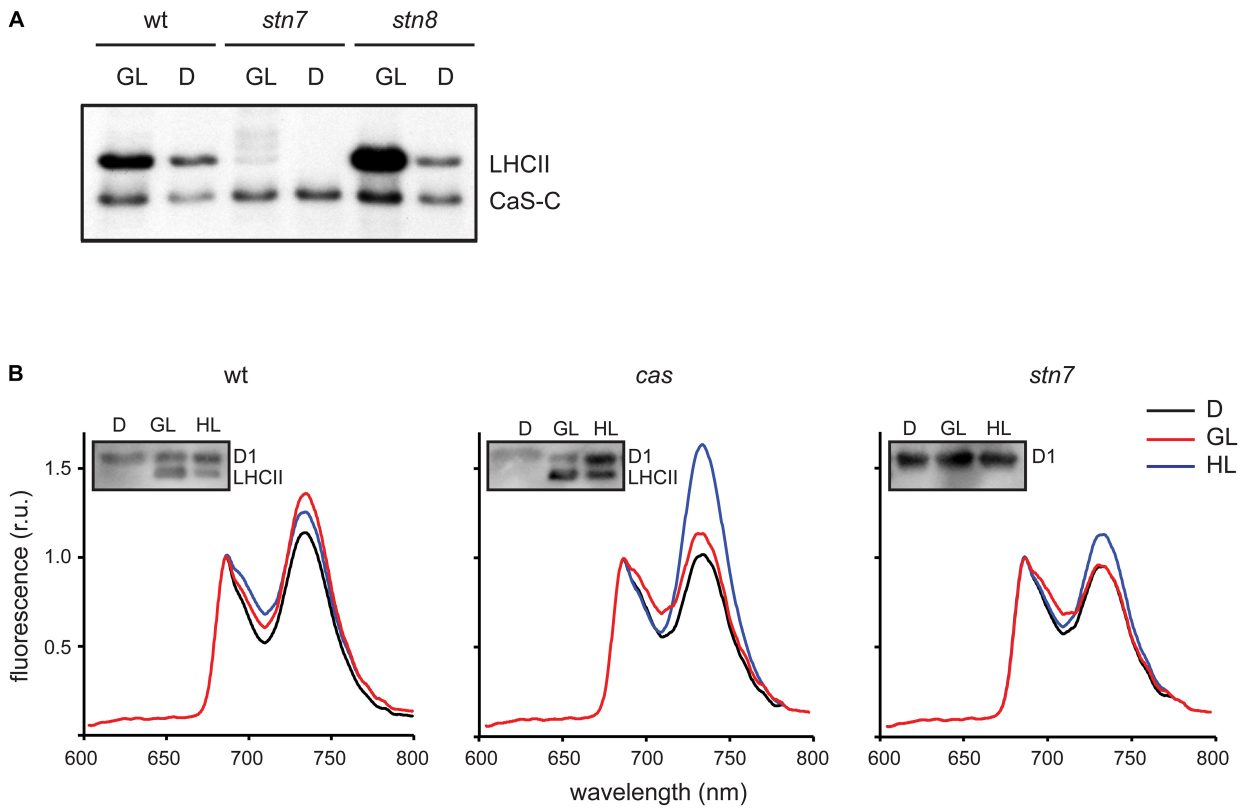

FIGURE 4 | CAS phosphorylation and 77K chlorophyll fluorescence emission spectra of thylakoid membranes harvested under different light conditions. **(A)** *In vitro* phosphorylation assays were performed with the CAS-C fragment using thylakoid extracts from wild type (wt), *stn7, and stn/8* mutant plants harvested in the dark (D) or the growth light (GL) period. **(B)** Chlorophyll fluorescence emission spectra were recorded at 77K using thylakoid membranes isolated from wild type (wt), *cas,* and *stn7* mutant plants harvested in the dark (D), after 2 h of GL (100 μmol photons m^{-2} s^{-1}, GL) and 2 h of high light (1000 μmol photons m^{-2} s^{-1}, HL). Samples from the same thylakoids were probed with an α-pThr antibody to assess the phosphorylation status of the LHCII complex and the D1 protein (inlays).

in *stn7*, indicating that the light-dependent difference observed in the wild type is mediated by the activity of STN7.

The role of STN7 is strongly associated with the regulation of energy distribution between PSI and PSII. In this work, when chlorophyll fluorescence emission spectra at 77K were measured from isolated thylakoid membranes of wild type plants, they showed a typical increase in the PSI peak at 733 nm upon shift from darkness (state 1) to GL (state 2), as visible from both a representative graph (**Figure 4B**) and the averaged peak values of three biological replicates (**Table 2**). As described previously (Tikkanen et al., 2010; Mekala et al., 2015), a slight reduction of the PSI peak occurred after a subsequent 2 h of high light (1000 μmol photons m^{-2} s^{-1}) treatment (**Figure 4B** and **Table 2**; wt), reflecting the disassociation of the mobile LHCII antenna from PSI. The *cas* mutant also showed an increase in the PSI peak upon transition into GL, indicating no major impairment in performing light-induced state 1- state 2 transition. The *stn7* mutant behaved according to what has been described before, showing an inability to perform phosphorylation-mediated state transition, as visible by an equal PSI peak height in dark and GL conditions (**Figure 4B** and **Table 2**; *stn7*). However, *cas* plants did not resemble the *stn7* mutant but showed a slight increase in the PSI peak height between dark and GL and, remarkably, a sustained increase of the PSI peak upon subsequent transfer to high light (**Figure 4B** and **Table 2**; *cas*), suggesting a persistent strong excitation of PSI under this condition. A similar phenotype had been observed for the *tap38/pph1* and the *pgr5* mutants (Mekala et al., 2015), the former not being able to properly dephosphorylate LHCII under high irradiance, while the latter is impaired in the cyclic electron transport around PSI. When the *in vivo* phosphorylation status of thylakoid proteins was tested following the same light treatments using a pThr-specific antibody, the wild type showed a characteristic increase in the phosphorylation of PSII core protein D1 and decreased LHCII phosphorylation under high light, while the *cas* mutant showed a strong concomitant phosphorylation of both LHCII and PSII core (**Figure 4B**, inlays; **Supplementary Figure S5**).

Ca^{2+}-Dependent Phosphorylation of CAS Does Not Involve the STN Kinases

The data shown above suggest a connection between CAS phosphorylation by the thylakoid kinases STN7 and STN8 and photoacclimation, with Thr-376, Thr-380, and Ser-378 as their main and shared targets. However, CAS was also suggested as the target of Ca^{2+}-dependent

phosphorylation (Stael et al., 2012) via experiments in which whole chloroplast and stroma-enriched fractions were used instead of thylakoid membranes.

We thus analyzed the ability of both stroma and isolated thylakoid membranes to phosphorylate CAS-C (**Figure 5** and **Supplementary Figures S1, S2**) either in the presence or absence of Ca^{2+} (1 μM $CaCl_2$ or 2 mM EGTA, respectively). In case of wild type thylakoids, only minor differences in the phosphorylation of CAS-C could be observed under either condition (**Figure 5A**, wt). The residual phosphorylation that could be observed with thylakoids devoid of both STN kinases was completely abolished in the absence of Ca^{2+} (**Figure 5A**, *stn7/8*). This observation supports the notion that CAS is the target of a Ca^{2+}-regulated phosphorylation event, which does not involve STN7 or STN8. When stromal extracts from wild type plants were used in the phosphorylation assay, the Ca^{2+} requirement became much more evident with very little phosphorylation seen in the presence of EGTA (**Figure 5B**), indicating the presence of a Ca^{2+}-dependent kinase in the stroma that targets the stromal exposed C-terminal domain of CAS. The residual Ca^{2+}-dependent phosphorylation of CAS in the thylakoid fraction could be due to some minor amounts of this stromal kinase remaining even after washing of the thylakoids. This is supported by the faint band visible for TKL and Fructose 1,6-bisphosphatase in the thylakoid fraction (**Figure 3C** and **Supplementary Figure S6**). While this needs to be analyzed in much more detail, there is a clear indication that CAS is a target of kinases other than STN7 and STN8, which is also in accordance with the identification of additional phosphorylation sites that are not targeted by these two kinases.

TABLE 2 | Ratio values of chlorophyll fluorescence emission peaks of PSI (at 733 nm) over PSII measured at 77K with thylakoids from wild type (wt), cas, and stn7 mutant lines.

Genotype	Treatment	PSI/PSII peak ratio
Wt	D	1.09 ± 0.03
	GL	1.29 ± 0.05
	HL	1.2 ± 0.05
cas	D	1 ± 0.16
	GL	1.1 ± 0.08
	HL	1.58 ± 0.09
stn7	D	1 ± 0.1
	GL	1 ± 0.02
	HL	1.08 ± 0.05

Thylakoids were isolated during the dark period (D) after 2 h of growth light (GL) or subsequent 2 h of high light (HL). Data are means of three biological replicates ± SD.

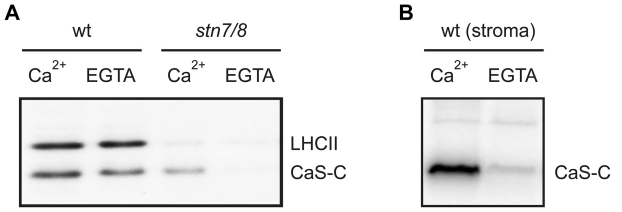

FIGURE 5 | Calcium-dependent phosphorylation of CAS by a stromal kinase. *In vitro* phosphorylation assays with the CAS-C fragment were performed using thylakoid extracts from wild type (wt) and *stn7/8* mutant plants **(A)** or stromal extracts from wild type **(B)** in the presence of either Ca^{2+} or EGTA. All panels show representative results of experiments performed several times. Corresponding Coomassie stained gels for all panels are shown in **Supplementary Figure S2**.

DISCUSSION

Understanding the role of chloroplast protein phosphorylation has been hampered by the fact that only few chloroplast kinases have been identified and that plants devoid of the two so far best described kinases, STN7 and STN8, only show surprisingly mild phenotypes. Moreover, the presence of multiple, evolutionary conserved phosphoresidues is a recurring feature of thylakoid phosphoproteins (Grieco et al., 2016), indicating the existence of complex phosphorylation networks involving differential regulation by multiple kinases in relation to specific environmental cues.

Vainonen et al. (2008) pinpointed Thr-380 of CAS as the target of high light-dependent phosphorylation by the STN8 kinase. In the present work, we could confirm the phosphorylation of CAS by STN8 but could also demonstrate the involvement of STN7 and at least one other, so far unknown Ca^{2+}-dependent kinase. The orientation of the CAS C-terminus, which contains all known phosphorylation sites, is consistent with the predicted localization of the catalytic domains of STN7 and STN8 that are also exposed to the stroma (Wunder et al., 2013). Any additional kinase acting on CAS would also need to either have its catalytic domain exposed to the stromal surface of the thylakoids or be a stromal protein. Indeed, Ca^{2+}-dependent phosphorylation of CAS is much more prevalent when stroma (**Figure 2E**) or total chloroplast extracts (Stael et al., 2012) are used in the phosphorylation assay instead of isolated thylakoid membranes (**Figure 2D**), suggesting that the Ca^{2+}-dependent activity observed with the thylakoid membrane fractions is due to the residual activity of a stromal kinase. Phosphoproteomic analysis of *stn8* mutant plants revealed a substantial decrease in the relative phosphorylation levels not only of Thr-380 but also Thr-376 and Ser-378 (**Supplementary Table S4**). *In vitro*, phosphorylation of CAS by either STN7 or STN8 is strongly reduced in the absence of Thr-376 or Thr-380 and to a lesser extent also of Ser-378 (**Figures 2A,C**). The effect is most pronounced in the absence of Thr-376, which is also the most conserved of those residues for which phosphorylation has been shown unequivocally in Arabidopsis (**Figure 1B**). Amino acid sequence alignments suggest that the corresponding position was also identified as a phosphoresidue in the green alga *C. reinhardtii,* the monocot *Z. mays* and several dicots (**Figure 1B** and **Table 1**). The phosphopeptide identified by Vainonen et al. (2008) study started with Arg-377, which could explain why they did not identify pThr-376. Of note, residue Thr-376 of Arabidopsis, as well as many of the corresponding Thr sites in CAS orthologs included in our phylogenetic analysis (**Figure 1B**

and **Supplementary Data S2–S5**), are preceded at position -1 by a Gly residue. This configuration matches a minimal phosphorylation consensus motif identified by Schönberg et al. (2017) for newly described targets of STN7. Thr-380 and Ser-378 are also highly conserved and the phosphorylation of a corresponding residue was shown for the green alga *C. reinhardtii,* the lycophyte *S. moellendorffii*, the monocot *Z. mays* and two dicots in case of Thr-380 and in *C. reinhardtii* for Ser-378 (**Figure 1B** and **Table 1**). These data indicate that phosphorylation of these three residues is evolutionarily conserved from green algae onwards. For all other potential phosphoresidues the data are much less robust and the corresponding residues display very little conservation.

All proposed phosphoresidues, including Thr-376, Ser-378, and Thr-380, fall within a very confined region found at the very C-proximal end of CAS (**Figure 1A**). It is thus conceivable that this short amino acidic sequence constitutes a hub for the integration of multiple signals in the form of differential phosphorylation events. Phosphorylation could either occur simultaneously on several residues or on individual sites following the activation of distinct protein kinases in response to cues of very diverse origin, such as light signals in the case of the STN kinases, or local increases in Ca^{2+} concentration with respect to the still uncharacterized Ca^{2+}-dependent kinase. The reaching of a certain phosphorylation threshold might be required to fully promote the functional effects of the modification. Alternatively, it could be envisioned that combinatorial, stimulus-dependent phosphorylation events on CAS lead to various, phosphocode-dependent outcomes impacting both developmental as well as stress-related functions of CAS.

Ca^{2+} is best described for its role as second messenger that transduces abiotic and biotic stress signals into a cellular response. However, chloroplasts also display a well-described light-off Ca^{2+} transient and it has been shown that the *cas* mutant is impaired in chloroplast Ca^{2+} responses to elicitors, heat and the light–dark transition (Nomura et al., 2012; Lenzoni and Knight, 2018). Consequently, a potential role of CAS in regulating photosynthetic function could be envisioned by either influencing chloroplast Ca^{2+} dynamics and/or by being differentially phosphorylated in a Ca^{2+}-dependent fashion.

In only few of the phosphoproteomic studies listed in **Table 1**, the light conditions upon harvesting of the samples are described. However, if not otherwise stated, harvesting of the samples during the light period is likely. Thus, in agreement with the results from Vainonen et al. (2008) and because it has been detected as a phosphoprotein in most if not all phosphoproteomics studies of plant proteins, it is likely that CAS is constitutively phosphorylated during daytime. Yet, its overall phosphorylation status and specific phosphorylation profile might subtly change in response to specific environmental cues that promote the activation of different kinases or the opposing phosphatases. It could be envisioned that at early and late day times, characterized by a low light environment, CAS is primarily targeted by the STN7 kinase, leading to a low level of steady-state phosphorylation, which might be required to achieve an optimal excitation balance between PSI and PSII. At midday, when peak irradiance is reached, the STN8 kinase could become more relevant and increase the overall CAS phosphorylation (Vainonen et al., 2008). This situation would place CAS as another shared target of the STN kinases (Bonardi et al., 2005) and their cooperative, differential, or even spatially segregated activity on CAS would dictate the functional outcome(s) of its modifications. The similarity of the *cas* mutant to *tap38* with regard to the 77K chlorophyll fluorescence emission spectra profiles suggests that CAS might be required to promote acclimation responses to excess light, which include the reversal of LHCII phosphorylation (Rintamaki et al., 1997). A phosphorylated form of CAS under the control of STN8 might in fact physically interact or indirectly influence the activity of the TAP38 phosphatase. Alternatively, phosphorylation of CAS by STN8 under high irradiance might negatively regulate the activity of the STN7 kinase, leading to attenuated LHCII phosphorylation and to the physical dissociation of the mobile antenna fraction from PSI reaction centers. In the *cas* mutant such inhibitory effect would be absent and a fully active STN7 would result in PSI being "locked" in state 2 under high light. This situation could explain the impaired PSI de-excitation kinetics observed in the *cas* mutant following excess light treatment. Considering the additional resemblance of the 77K chlorophyll fluorescence emission spectra of *cas* with that of *pgr5*, an involvement of Arabidopsis CAS in the modulation of the Cyclic Electron Flow (CEF) could also be envisioned. CEF is recognized as a safety valve to minimize photo-oxidative damage (Pinnola and Bassi, 2018) and in the green alga *Chlamydomonas reinhardtii* CAS was shown to affect CEF under anoxia (Petroutsos et al., 2011). Finally, the phosphorylation status of CAS could be further altered by a so far unknown Ca^{2+}-dependent kinase, whose activation might follow the physiological increases in stromal free Ca^{2+} levels regularly observed after the light-dark transition and in response to specific stress conditions (Sai and Johnson, 2002; Sello et al., 2016). It will thus be important in the future to properly assess how the overall phosphorylation status and the phosphorylation patterns of CAS are shaped at different daytimes and under different light and/or stress conditions. On the other hand, a more detailed assessment of the basal Ca^{2+} resting levels and stress induced Ca^{2+} transients in the stroma and thylakoid lumen of the *cas* mutant plants might also provide further suggestions for the role of CAS in shaping the plastidal Ca^{2+} landscape.

DATA AVAILABILITY

All datasets for this study are included in the manuscript and/or the **Supplementary Files**.

AUTHOR CONTRIBUTIONS

EC, NP, and UV designed the experiments. UV conceived the project and supervised the experiments. EC performed most of the experiments. HR provided assistance in the bioinformatics and bioimaging analysis. NiP performed some of

the Western blot analysis. VR performed the phosphoproteomics analysis. WW and MT supervised the phosphoproteomics analysis and were involved in the analysis of the data. VL performed the spectroscopic analysis together with EC and analyzed the data together with MG. UV and EC wrote the manuscript with contributions of all other authors.

FUNDING

This work was supported by grants from the EU to EC and VR (GA ITN 2013-607607; CALIPSO), from the DAAD to NP (A/09/74590), from the Deutsche Forschungsgemeinschaft to UV (VO656/5-1) and by the Austrian Science Fund to MT (project P28491). VL acknowledges FNRS for her financial support (Post Doctoral Grant No.1B21813F and EOS Program Grant No. O018218F) and the laboratory of genetics and physiology of microalgae of University of Liège for the infrastructure.

ACKNOWLEDGMENTS

We gratefully thank Dr. Eva-Mari Aro (University of Turku) for providing the *stn7/8* double mutant lines and Dr. Jürgen Soll (LMU Munich) for the OE33 antibody. We further thank Dr. Fatima Chigri for helpful discussions.

SUPPLEMENTARY MATERIAL

The Supplementary Material for this article can be found online at: https://www.frontiersin.org/articles/10.3389/fpls.2019.00974/full#supplementary-material

REFERENCES

Arnon, D. I. (1949). Copper enzymes in isolated chloroplasts. polyphenoloxidase in *Beta vulgaris*. *Plant Physiol.* 24, 1–15. doi: 10.1104/pp.24.1.1

Bellafiore, S., Barneche, F., Peltier, G., and Rochaix, J. D. (2005). State transitions and light adaptation require chloroplast thylakoid protein kinase STN7. *Nature* 433, 892–895. doi: 10.1038/nature03286

Bhaskara, G. B., Wen, T. N., Nguyen, T. T., and Verslues, P. E. (2017). Protein phosphatase 2Cs and microtubule-associated stress protein 1 control microtubule stability, plant growth, and drought response. *Plant Cell* 29, 169–191. doi: 10.1105/tpc.16.00847

Bodenmiller, B., Mueller, L. N., Mueller, M., Domon, B., and Aebersold, R. (2007). Reproducible isolation of distinct, overlapping segments of the phosphoproteome. *Nat. Methods* 4, 231–237. doi: 10.1038/nmeth1005

Bonardi, V., Pesaresi, P., Becker, T., Schleiff, E., Wagner, R., and Pfannschmidt, T. (2005). Photosystem II core phosphorylation and photosynthetic acclimation require two different protein kinases. *Nature* 437, 1179–1182. doi: 10.1038/nature04016

Bonaventura, C., and Myers, J. (1969). Fluorescence and oxygen evolution from *Chlorella pyrenoidosa*. *Biochim. Biophys. Acta* 189, 366–383. doi: 10.1016/0005-2728(69)90168-6

Bonhomme, L., Valot, B., Tardieu, F., and Zivy, M. (2012). Phosphoproteome dynamics upon changes in plant water status reveal early events associated with rapid growth adjustment in maize leaves. *Mol. Cell. Proteomics* 11, 957–972. doi: 10.1074/mcp.m111.015867

Cabantous, S., Terwilliger, T. C., and Waldo, G. S. (2005). Protein tagging and detection with engineered self-assembling fragments of green fluorescent protein. *Nat. Biotechnol.* 23, 102–107. doi: 10.1038/nbt1044

Chen, Y., Hoehenwarter, W., and Weckwerth, W. (2010). Comparative analysis of phytohormone-responsive phosphoproteins in *Arabidopsis thaliana* using TiO2-phosphopeptide enrichment and mass accuracy precursor alignment. *Plant J.* 63, 1–17. doi: 10.1111/j.1365-313X.2010.04218.x

Cox, J., and Mann, M. (2008). MaxQuant enables high peptide identification rates, individualized p.p.b.-range mass accuracies and proteome-wide protein quantification. *Nat. Biotechnol.* 26, 1367–1372. doi: 10.1038/nbt.1511

Cox, J., Neuhauser, N., Michalski, A., Scheltema, R. A., Olsen, J. V., and Mann, M. (2011). Andromeda, a peptide search engine integrated into the MaxQuant environment. *J. Proteome Res.* 10, 1794–1805. doi: 10.1021/pr101065j

Datla, R. S., Hammerlindl, J. K., Panchuk, B., Pelcher, L. E., and Keller, W. (1992). Modified binary plant transformation vectors with the wild-type gene encoding NPTII. *Gene* 122, 383–384. doi: 10.1016/0378-1119(92)90232-e

Durek, P., Schmidt, R., Heazlewood, J. L., Jones, A., MacLean, D., Nagel, A., et al. (2010). PhosPhAt, the *Arabidopsis thaliana* phosphorylation site database. An update. *Nucleic Acids Res.* 38, D828–D834. doi: 10.1093/nar/gkp810

Fan, S., Meng, Y., Song, M., Pang, C., Wei, H., Liu, J., et al. (2014). Quantitative phosphoproteomics analysis of nitric oxide-responsive phosphoproteins in cotton leaf. *PLoS One* 9:e94261. doi: 10.1371/journal.pone.0094261

Fristedt, R., Wasilewska, W., Romanowska, E., and Vener, A. V. (2012). Differential phosphorylation of thylakoid proteins in mesophyll and bundle sheath chloroplasts from maize plants grown under low or high light. *Proteomics* 12, 2852–2861. doi: 10.1002/pmic.201200196

Fristedt, R., Willig, A., Granath, P., Crevecoeur, M., Rochaix, J. D., and Vener, A. V. (2009). Phosphorylation of photosystem II controls functional macroscopic folding of photosynthetic membranes in *Arabidopsis*. *Plant Cell* 21, 3950–3964. doi: 10.1105/tpc.109.069435

Grieco, M., Jain, A., Ebersberger, I., and Teige, M. (2016). An evolutionary view on thylakoid protein phosphorylation uncovers novel phosphorylation hotspots with potential functional implications. *J. Exp. Bot.* 67, 3883–3896. doi: 10.1093/jxb/erw164

Han, S., Tang, R., Anderson, L. K., Woerner, T. E., and Pei, Z. M. (2003). A cell surface receptor mediates extracellular Ca(2+) sensing in guard cells. *Nature* 425, 196–200. doi: 10.1038/nature01932

Heazlewood, J. L., Durek, P., Hummel, J., Selbig, J., Weckwerth, W., and Walther, D. (2008). PhosPhAt, a database of phosphorylation sites in *Arabidopsis thaliana* and a plant-specific phosphorylation site predictor. *Nucleic Acids Res.* 36, D1015–D1021.

Hoehenwarter, W., Thomas, M., Nukarinen, E., Egelhofer, V., Rohrig, H., and Weckwerth, W. (2013). Identification of novel in vivo MAP kinase substrates in *Arabidopsis thaliana* through use of tandem metal oxide affinity chromatography. *Mol. Cell. Proteomics* 12, 369–380. doi: 10.1074/mcp.M112.020560

Ingelsson, B., and Vener, A. V. (2012). Phosphoproteomics of *Arabidopsis* chloroplasts reveals involvement of the STN7 kinase in phosphorylation of nucleoid protein pTAC16. *FEBS Lett.* 586, 1265–1271. doi: 10.1016/j.febslet.2012.03.061

Kodru, S., Malavath, T., Devadasu, E., Nellaepalli, S., Stirbet, A., and Subramanyam, R. (2015). The slow S to M rise of chlorophyll a fluorescence reflects transition from state 2 to state 1 in the green alga *Chlamydomonas reinhardtii*. *Photosynth. Res.* 125, 219–231. doi: 10.1007/s11120-015-0084-2

Koop, H. U., Steinmuller, K., Wagner, H., Rossler, C., Eibl, C., and Sacher, L. (1996). Integration of foreign sequences into the tobacco plastome via polyethylene glycol-mediated protoplast transformation. *Planta* 199, 193–201.

Laemmli, U. K. (1970). Cleavage of structural proteins during the assembly of the head of bacteriophage T4. *Nature* 227, 680–685. doi: 10.1038/227680a0

Larosa, V., Meneghesso, A., La Rocca, N., Steinbeck, J., Hippler, M., and Szabo, I. (2018). Mitochondria affect photosynthetic electron transport and photosensitivity in a green Alga. *Plant Physiol.* 176, 2305–2314. doi: 10.1104/pp.17.01249

Lenzoni, G., and Knight, M. R. (2018). Increases in absolute temperature stimulate free calcium concentration elevations in the chloroplast. *Plant Cell Physiol.* 60, 538–554. doi: 10.1093/pcp/pcy227

Lin, L. L., Hsu, C. L., Hu, C. W., Ko, S. Y., Hsieh, H. L., and Huang, H. C. (2015). Integrating phosphoproteomics and bioinformatics to study brassinosteroid-regulated phosphorylation dynamics in *Arabidopsis*. *BMC Genomics* 16:533. doi: 10.1186/s12864-015-1753-4

Lv, D. W., Ge, P., Zhang, M., Cheng, Z. W., Li, X. H., and Yan, Y. M. (2014a). Integrative network analysis of the signaling cascades in seedling leaves of bread wheat by large-scale phosphoproteomic profiling. *J. Proteome Res.* 13, 2381–2395. doi: 10.1021/pr401184v

Lv, D. W., Li, X., Zhang, M., Gu, A. Q., Zhen, S. M., and Wang, C. (2014b). Large-scale phosphoproteome analysis in seedling leaves of *Brachypodium distachyon* L. *BMC Genomics* 15:375. doi: 10.1186/1471-2164-15-375

Lv, D. W., Subburaj, S., Cao, M., Yan, X., Li, X., Appels, R., et al. (2014c). Proteome and phosphoproteome characterization reveals new response and defense mechanisms of *Brachypodium distachyon* leaves under salt stress. *Mol. Cell. Proteomics* 13, 632–652. doi: 10.1074/mcp.M113.030171

Machettira, A. B., Gross, L. E., Sommer, M. S., Weis, B. L., Englich, G., and Tripp, J. (2011). The localization of Tic20 proteins in *Arabidopsis thaliana* is not restricted to the inner envelope membrane of chloroplasts. *Plant Mol. Biol.* 77, 381–390. doi: 10.1007/s11103-011-9818-5

Mehlmer, N., Parvin, N., Hurst, C. H., Knight, M. R., Teige, M., and Vothknecht, U. C. (2012). A toolset of aequorin expression vectors for in planta studies of subcellular calcium concentrations in *Arabidopsis thaliana*. *J. Exp. Bot.* 63, 1751–1761. doi: 10.1093/jxb/err406

Mekala, N. R., Suorsa, M., Rantala, M., Aro, E. M., and Tikkanen, M. (2015). Plants actively avoid state transitions upon changes in light intensity, role of light-harvesting complex II protein dephosphorylation in high light. *Plant Physiol.* 168, 721–734. doi: 10.1104/pp.15.00488

Minagawa, J. (2011). State transitions–the molecular remodeling of photosynthetic supercomplexes that controls energy flow in the chloroplast. *Biochim. Biophys. Acta* 1807, 897–905. doi: 10.1016/j.bbabio.2010.11.005

Murata, N. (1969). Control of excitation transfer in photosynthesis. I. Light-induced change of chlorophyll a fluorescence in *Porphyridium cruentum*. *Biochim. Biophys. Acta* 172, 242–251. doi: 10.1016/0005-2728(69)90067-x

Nguyen, T. H., Brechenmacher, L., Aldrich, J. T., Clauss, T. R., Gritsenko, M. A., Hixson, K. K., et al. (2012). Quantitative phosphoproteomic analysis of soybean root hairs inoculated with Bradyrhizobium japonicum. *Mol. Cell. Proteomics* 11, 1140–1155. doi: 10.1074/mcp.M112.018028

Nomura, H., Komori, T., Kobori, M., Nakahira, Y., and Shiina, T. (2008). Evidence for chloroplast control of external Ca2+-induced cytosolic Ca2+ transients and stomatal closure. *Plant J.* 53, 988–998. doi: 10.1111/j.1365-313x.2007.03390.x

Nomura, H., Komori, T., Uemura, S., Kanda, Y., Shimotani, K., Nakai, K., et al. (2012). Chloroplast-mediated activation of plant immune signalling in *Arabidopsis*. *Nat. Commun.* 3:926. doi: 10.1038/ncomms1926

Olsen, J. V., Blagoev, B., Gnad, F., Macek, B., Kumar, C., Mortensen, P., et al. (2006). Global, in vivo, and site-specific phosphorylation dynamics in signaling networks. *Cell* 127, 635–648. doi: 10.1016/j.cell.2006.09.026

Papageorgiou, G. C., and Govindjee. (2011). Photosystem II fluorescence, Slow changes - Scaling from the past. *J. Photochem. Photobiol. B* 104, 258–270. doi: 10.1016/j.jphotobiol.2011.03.008

Pesaresi, P., Hertle, A., Pribil, M., Schneider, A., Kleine, T., and Leister, D. (2010). Optimizing photosynthesis under fluctuating light, the role of the *Arabidopsis* STN7 kinase. *Plant Signal. Behav.* 5, 21–25. doi: 10.4161/psb.5.1.10198

Pesaresi, P., Pribil, M., Wunder, T., and Leister, D. (2011). Dynamics of reversible protein phosphorylation in thylakoids of flowering plants, the roles of STN7, STN8 and TAP38. *Biochim. Biophys. Acta* 1807, 887–896. doi: 10.1016/j.bbabio.2010.08.002

Petroutsos, D., Busch, A., Janssen, I., Trompelt, K., Bergner, S. V., Weinl, S., et al. (2011). The chloroplast calcium sensor CAS is required for photoacclimation in *Chlamydomonas reinhardtii*. *Plant Cell* 23, 2950–2963. doi: 10.1105/tpc.111.087973

Pinnola, A., and Bassi, R. (2018). Molecular mechanisms involved in plant photoprotection. *Biochem. Soc. Trans.* 46, 467–482. doi: 10.1042/BST20170307

Pribil, M., Pesaresi, P., Hertle, A., Barbato, R., and Leister, D. (2010). Role of plastid protein phosphatase TAP38 in LHCII dephosphorylation and thylakoid electron flow. *PLoS Biol.* 8:e1000288. doi: 10.1371/journal.pbio.1000288

Reiland, S., Finazzi, G., Endler, A., Willig, A., Baerenfaller, K., Grossmann, J., et al. (2011). Comparative phosphoproteome profiling reveals a function of the STN8 kinase in fine-tuning of cyclic electron flow (CEF). *Proc. Natl. Acad. Sci. U.S.A.* 108, 12955–12960. doi: 10.1073/pnas.1104734108

Reiland, S., Messerli, G., Baerenfaller, K., Gerrits, B., Endler, A., and Grossmann, J. (2009). Large-scale *Arabidopsis* phosphoproteome profiling reveals novel chloroplast kinase substrates and phosphorylation networks. *Plant Physiol.* 150, 889–903. doi: 10.1104/pp.109.138677

Rintamaki, E., Salonen, M., Suoranta, U. M., Carlberg, I., Andersson, B., and Aro, E. M. (1997). Phosphorylation of light-harvesting complex II and photosystem II core proteins shows different irradiance-dependent regulation in vivo. Application of phosphothreonine antibodies to analysis of thylakoid phosphoproteins. *J. Biol. Chem.* 272, 30476–30482. doi: 10.1074/jbc.272.48.30476

Rocha, A. G., Mehlmer, N., Stael, S., Mair, A., Parvin, N., and Chigri, F. (2014). Phosphorylation of *Arabidopsis* transketolase at Ser(428) provides a potential paradigm for the metabolic control of chloroplast carbon metabolism. *Biochem. J.* 458, 313–322. doi: 10.1042/bj20130631

Rochaix, J. D. (2011). Regulation of photosynthetic electron transport. *Biochim. Biophys. Acta* 1807, 375–383. doi: 10.1016/j.bbabio.2010.11.010

Rochaix, J. D. (2014). Regulation and dynamics of the light-harvesting system. *Annu. Rev. Plant Biol.* 65, 287–309. doi: 10.1146/annurev-arplant-050213-040226

Roitinger, E., Hofer, M., Kocher, T., Pichler, P., Novatchkova, M., and Yang, J. (2015). Quantitative phosphoproteomics of the ataxia telangiectasia-mutated (ATM) and ataxia telangiectasia-mutated and rad3-related (ATR) dependent DNA damage response in *Arabidopsis thaliana*. *Mol. Cell. Proteomics* 14, 556–571. doi: 10.1074/mcp.M114.040352

Rokka, A., Aro, E. M., and Vener, A. V. (2011). Thylakoid phosphoproteins: identification of phosphorylation sites. *Methods Mol. Biol.* 684, 171–186. doi: 10.1007/978-1-60761-925-3_15

Rose, C. M., Venkateshwaran, M., Volkening, J. D., Grimsrud, P. A., Maeda, J., Bailey, D. J., et al. (2012). Rapid phosphoproteomic and transcriptomic changes in the rhizobia-legume symbiosis. *Mol. Cell. Proteomics* 11, 724–744. doi: 10.1074/mcp.M112.019208

Roustan, V., Bakhtiari, S., Roustan, P.-J., and Weckwerth, W. (2017). Quantitative in vivo phosphoproteomics reveals reversible signaling processes during nitrogen starvation and recovery in the biofuel model organism *Chlamydomonas reinhardtii*. *Biotech. Biofuels* 10:280. doi: 10.1186/s13068-017-0949-z

Ruban, A. V., and Johnson, M. P. (2009). Dynamics of higher plant photosystem cross-section associated with state transitions. *Photosynth. Res.* 99, 173–183. doi: 10.1007/s11120-008-9387-x

Ruge, H., Flosdorff, S., Ebersberger, I., Chigri, F., and Vothknecht, U. C. (2016). The calmodulin-like proteins AtCML4 and AtCML5 are single-pass membrane proteins targeted to the endomembrane system by an N-terminal signal anchor sequence. *J. Exp. Bot.* 67, 3985–3996. doi: 10.1093/jxb/erw101

Sai, J., and Johnson, C. H. (2002). Dark-stimulated calcium ion fluxes in the chloroplast stroma and cytosol. *Plant Cell.* 14, 1279–1291. doi: 10.1105/tpc.000653

Schönberg, A., Rodiger, A., Mehwald, W., Galonska, J., Christ, G., Helm, S., et al. (2017). Identification of STN7/STN8 kinase targets reveals connections between electron transport, metabolism and gene expression. *Plant J.* 90, 1176–1186. doi: 10.1111/tpj.13536

Seigneurin-Berny, D., Salvi, D., Dorne, A. J., Joyard, J., and Rolland, N. (2008). Percoll-purified and photosynthetically active chloroplasts from *Arabidopsis thaliana* leaves. *Plant Physiol. Biochem.* 46, 951–955. doi: 10.1016/j.plaphy.2008.06.009

Sello, S., Perotto, J., Carraretto, L., Szabo, I., Vothknecht, U. C., and Navazio, L. (2016). Dissecting stimulus-specific Ca2+ signals in amyloplasts and chloroplasts of *Arabidopsis thaliana* cell suspension cultures. *J. Exp. Bot.* 67, 3965–3974. doi: 10.1093/jxb/erw038

Shapiguzov, A., Ingelsson, B., Samol, I., Andres, C., Kessler, F., and Rochaix, J. D. (2010). The PPH1 phosphatase is specifically involved in LHCII

dephosphorylation and state transitions in *Arabidopsis*. *Proc. Natl. Acad. Sci. U.S.A.* 107, 4782–4787. doi: 10.1073/pnas.0913810107

Silverstein, T., Cheng, L., and Allen, J. F. (1993). Chloroplast thylakoid protein phosphatase reactions are redox-independent and kinetically heterogeneous. *FEBS Lett.* 334, 101–105. doi: 10.1016/0014-5793(93)81690-2

Stael, S., Rocha, A. G., Wimberger, T., Anrather, D., Vothknecht, U. C., and Teige, M. (2012). Cross-talk between calcium signalling and protein phosphorylation at the thylakoid. *J. Exp. Bot.* 63, 1725–1733. doi: 10.1093/jxb/err403

Thompson, J. D., Gibson, T. J., Plewniak, F., Jeanmougin, F., and Higgins, D. G. (1997). The CLUSTAL_X windows interface, flexible strategies for multiple sequence alignment aided by quality analysis tools. *Nucleic Acids Res.* 25, 4876–4882. doi: 10.1093/nar/25.24.4876

Tikkanen, M., and Aro, E. M. (2012). Thylakoid protein phosphorylation in dynamic regulation of photosystem II in higher plants. *Biochim. Biophys. Acta* 1817, 232–238. doi: 10.1016/j.bbabio.2011.05.005

Tikkanen, M., Grieco, M., Kangasjarvi, S., and Aro, E. M. (2010). Thylakoid protein phosphorylation in higher plant chloroplasts optimizes electron transfer under fluctuating light. *Plant Physiol.* 152, 723–735. doi: 10.1104/pp.109.150250

Tikkanen, M., Piippo, M., Suorsa, M., Sirpio, S., Mulo, P., Vainonen, J., et al. (2006). State transitions revisited-a buffering system for dynamic low light acclimation of *Arabidopsis*. *Plant Mol. Biol.* 62, 779–793. doi: 10.1007/s11103-006-9044-8

Tyanova, S., Temu, T., Sinitcyn, P., Carlson, A., Hein, M. Y., and Geiger, T. (2016). The perseus computational platform for comprehensive analysis of (prote)omics data. *Nat. Methods* 13, 731–740. doi: 10.1038/nmeth.3901

Vainonen, J. P., Hansson, M., and Vener, A. V. (2005). STN8 protein kinase in *Arabidopsis thaliana* is specific in phosphorylation of photosystem II core proteins. *J. Biol. Chem.* 280, 33679–33686. doi: 10.1074/jbc.m505729200

Vainonen, J. P., Sakuragi, Y., Stael, S., Tikkanen, M., Allahverdiyeva, Y., Paakkarinen, V., et al. (2008). Light regulation of CaS, a novel phosphoprotein in the thylakoid membrane of *Arabidopsis thaliana*. *FEBS J.* 275, 1767–1777. doi: 10.1111/j.1742-4658.2008.06335.x

Vener, A. V., and Strålfors, P. (2005). Vectorial proteomics. *IUBMB Life* 57, 433–440. doi: 10.1080/15216540500138360

Vener, A. V., van Kan, P. J., Rich, P. R., Ohad, I., and Andersson, B. (1997). Plastoquinol at the quinol oxidation site of reduced cytochrome bf mediates signal transduction between light and protein phosphorylation: thylakoid protein kinase deactivation by a single-turnover flash. *Proc. Natl. Acad. Sci. U.S.A.* 94, 1585–1590. doi: 10.1073/pnas.94.4.1585

Voinnet, O., Rivas, S., Mestre, P., and Baulcombe, D. (2003). An enhanced transient expression system in plants based on suppression of gene silencing by the p19 protein of tomato bushy stunt virus. *Plant J.* 33, 949–956. doi: 10.1046/j.1365-313x.2003.01676.x

Wang, H., Gau, B., Slade, W. O., Juergens, M., Li, P., and Hicks, L. M. (2014). The global phosphoproteome of *Chlamydomonas reinhardtii* reveals complex organellar phosphorylation in the flagella and thylakoid membrane. *Mol. Cell. Proteomics* 13, 2337–2353. doi: 10.1074/mcp.M114.038281

Wang, L., Yamano, T., Takane, S., Niikawa, Y., Toyokawa, C., Ozawa, S.-I., et al. (2016). Chloroplast-mediated regulation of CO2-concentrating mechanism by Ca2+-binding protein CAS in the green alga *Chlamydomonas reinhardtii*. *Proc. Natl. Acad. Sci. U.S.A.* 113, 12586–12591. doi: 10.1073/pnas.1606519113

Wang, X., Bian, Y. Y., Cheng, K., Gu, L. F., Ye, M. L., and Zou, H. F. (2013). A large-scale protein phosphorylation analysis reveals novel phosphorylation motifs and phosphoregulatory networks in *Arabidopsis*. *J Proteomics* 78, 486–498. doi: 10.1016/j.jprot.2012.10.018

Weinl, S., Held, K., Schlucking, K., Steinhorst, L., Kuhlgert, S., and Hippler, M. (2008). A plastid protein crucial for Ca2+-regulated stomatal responses. *New Phytol.* 179, 675–686. doi: 10.1111/j.1469-8137.2008.02492.x

Whiteman, S. A., Nuhse, T. S., Ashford, D. A., Sanders, D., and Maathuis, F. J. (2008). A proteomic and phosphoproteomic analysis of *Oryza sativa* plasma membrane and vacuolar membrane. *Plant J.* 56, 146–156. doi: 10.1111/j.1365-313X.2008.03578.x

Wunder, T., Xu, W., Liu, Q., Wanner, G., Leister, D., and Pribil, M. (2013). The major thylakoid protein kinases STN7 and STN8 revisited, effects of altered STN8 levels and regulatory specificities of the STN kinases. *Front. Plant Sci.* 4:417. doi: 10.3389/fpls.2013.00417

Yang, Z., Guo, G., Zhang, M., Liu, C. Y., Hu, Q., Lam, H., et al. (2013). Stable isotope metabolic labeling-based quantitative phosphoproteomic analysis of *Arabidopsis* mutants reveals ethylene-regulated time-dependent phosphoproteins and putative substrates of constitutive triple response 1 kinase. *Mol. Cell. Proteomics* 12, 3559–3582. doi: 10.1074/mcp.M113.031633

Zheng, L., Baumann, U., and Reymond, J. L. (2004). An efficient one-step site-directed and site-saturation mutagenesis protocol. *Nucleic Acids Res.* 32:e115. doi: 10.1093/nar/gnh110

Conflict of Interest Statement: The authors declare that the research was conducted in the absence of any commercial or financial relationships that could be construed as a potential conflict of interest.

frontiers in Plant Science

REVIEW
published: 31 July 2019
doi: 10.3389/fpls.2019.00975

A New Light on Photosystem II Maintenance in Oxygenic Photosynthesis

Jun Liu[1,2], Yan Lu[3], Wei Hua[1]* and Robert L. Last[2,4]*

[1]Department of Functional Genomics and Molecular Biology, Key Laboratory of Biology and Genetic Improvement of Oil Crops, Ministry of Agriculture and Rural Affairs, Oil Crops Research Institute of the Chinese Academy of Agricultural Sciences, Wuhan, China, [2]Department of Biochemistry and Molecular Biology, Michigan State University, East Lansing, MI, United States, [3]Department of Biological Sciences, Western Michigan University, Kalamazoo, MI, United States, [4]Department of Plant Biology, Michigan State University, East Lansing, MI, United States

Life on earth is sustained by oxygenic photosynthesis, a process that converts solar energy, carbon dioxide, and water into chemical energy and biomass. Sunlight is essential for growth and productivity of photosynthetic organisms. However, exposure to an excessive amount of light adversely affects fitness due to photooxidative damage to the photosynthetic machinery, primarily to the reaction center of the oxygen-evolving photosystem II (PSII). Photosynthetic organisms have evolved diverse photoprotective and adaptive strategies to avoid, alleviate, and repair PSII damage caused by high-irradiance or fluctuating light. Rapid and harmless dissipation of excess absorbed light within antenna as heat, which is measured by chlorophyll fluorescence as non-photochemical quenching (NPQ), constitutes one of the most efficient protective strategies. In parallel, an elaborate repair system represents another efficient strategy to maintain PSII reaction centers in active states. This article reviews both the reaction center-based strategy for robust repair of photodamaged PSII and the antenna-based strategy for swift control of PSII light-harvesting (NPQ). We discuss evolutionarily and mechanistically diverse strategies used by photosynthetic organisms to maintain PSII function for growth and productivity under static high-irradiance light or fluctuating light environments. Knowledge of mechanisms underlying PSII maintenance would facilitate bioengineering photosynthesis to enhance agricultural productivity and sustainability to feed a growing world population amidst climate change.

Keywords: photosystem II, photosynthesis, non-photochemical quenching, repair, fluctuating light

OPEN ACCESS

Edited by:
Cornelia Spetea, University of Gothenburg, Sweden

Reviewed by:
Yoshitaka Nishiyama, Saitama University, Japan
Peter J. Gollan, University of Turku, Finland

****Correspondence:***
Jun Liu
liujunocr@caas.cn
Wei Hua
huawei@oilcrops.cn

Specialty section:
This article was submitted to Plant Physiology, a section of the journal Frontiers in Plant Science

Received: *19 April 2019*
Accepted: *11 July 2019*
Published: *31 July 2019*

Citation:
Liu J, Lu Y, Hua W and Last RL (2019) A New Light on Photosystem II Maintenance in Oxygenic Photosynthesis. Front. Plant Sci. 10:975. doi: 10.3389/fpls.2019.00975

INTRODUCTION

Cyanobacteria, algae, and plants convert sunlight into chemical energy through photosynthesis to provide oxygen and food building blocks that are essential for most life forms on earth. Photosynthesis starts with capture of light by light-harvesting antenna, which drives photosynthetic electron flow through photosynthetic machinery comprising several large protein complexes embedded in the thylakoid membranes of prokaryotic cyanobacteria and eukaryotic chloroplasts. Oxygen-evolving photosystem II (PSII) is a highly conserved multi-subunit pigment-containing membrane complex

that functions as a light-driven water:plastoquinone oxidoreductase during photosynthetic electron transport (reviewed in Kern and Renger, 2007; Koochak et al., 2019). The electrons extracted from water are converted and stored into organic molecules. Counter-intuitively, PSII is extremely vulnerable to light irradiance, which causes photodamage to PSII reaction centers (reviewed in Townsend et al., 2018; Leister, 2019). The damage is exacerbated if light energy exceeds what can be utilized for carbon fixation, particularly when photosynthetic organisms are subjected to environmental stresses, such as high light, extreme temperature, drought and nutrient depletion, or combined stresses (Ghotbi-Ravandi et al., 2014; reviewed in Murata et al., 2007; Sainz et al., 2010; Salomon et al., 2013; Strzepek et al., 2019; Wilson and Ruban, 2019). The excess light energy also leads to massive generation of reactive oxygen species (ROS) photoproducts, which damage PSII or suppress the repair of damaged PSII (Mishra and Ghanotakis, 1994; Miyao et al., 1995; Okada et al., 1996; Nishiyama et al., 2001; Kale et al., 2017; reviewed in Pinnola and Bassi, 2018). Paradoxically, ROS also act as critical signal molecules to mediate photoacclimation response (Alboresi et al., 2011; reviewed in Wagner et al., 2004; Dogra et al., 2018).

Photoinhibition occurs when PSII suffers from excess light-induced damage or PSII photochemistry is downregulated, resulting in decreased photosynthetic performance and reduced growth and productivity (Kapri-Pardes et al., 2007; Chen et al., 2019; reviewed in Takahashi and Badger, 2011; Wittenberg et al., 2014; Ting and Owens, 2016; Li et al., 2018). Photosynthetic organisms evolved a suite of photoprotective and adaptive mechanisms to prevent or recover from the deleterious effects of photoinhibitory light. These include fast regulatory mechanisms, for instance, movement of chloroplasts away from high-light intensity, reduction of antenna size, induction of alternative electron transport pathways, and slow regulatory mechanisms, such as operation of both enzymatic and non-enzymatic ROS scavenging systems, and triggering systemic acquired acclimation (reviewed in Jarillo et al., 2001; Frigerio et al., 2007; Okegawa et al., 2010; Erickson et al., 2015). Non-photochemical quenching (NPQ) represents one of the fast regulatory mechanisms that is immediately activated and rapidly inducible upon excess solar energy. It protects against excess absorbed sunlight within the PSII antenna by converting photons into dissipative heat (Niyogi et al., 1998; reviewed in Wobbe et al., 2016). In addition, certain organism-specific protein factors evolved to maintain maximal PSII activity under photoinhibitory light conditions (Chen et al., 2018). The land plant-specific thylakoid membrane proteins MPH1 (MAINTENANCE OF PSII UNDER HIGH LIGHT 1) and HHL1 (HYPERSENSITIVE TO HIGH LIGHT 1) evolved to protect PSII against high-light illumination following the transition from aquatic habitats to terrestrial environments (Jin et al., 2014; Liu and Last, 2015a,b). Despite these multi-faceted photoprotective mechanisms, light-induced damage to PSII still occurs. Photosynthetic organisms employ an efficient repair system to replace damaged subunits within PSII reaction centers and restore PSII function (reviewed in Li et al., 2018). A suite of auxiliary proteins, including kinases, phosphatase(s), proteases, and repair/assembly factors have been documented to promote the repair of damaged PSII core subunits (reviewed in Nickelsen and Rengstl, 2013; Järvi et al., 2015). These auxiliary proteins could also cooperate with each other to facilitate the repair process. For instance, *Arabidopsis thaliana* (a flowering plant model species) LQY1 (LOW QUANTUM YIELD OF PHOTOSYSTEM II 1) protein—interacting with HHL1—regulates repair of damaged core complexes to sustain high PSII efficiency upon exposure to excessive light (Lu, 2011; Lu et al., 2011; Jin et al., 2014). Another example is the recent finding that OHP1 (ONE-HELIX PROTEIN1), OHP2, and HCF244 (HIGH CHLOROPHYLL FLUORESCENCE244) form a transient functional heterotrimeric complex assisting in assembly and/or repair of PSII (Hey and Grimm, 2018; Myouga et al., 2018; Li et al., 2019). These repair and NPQ systems may become especially important and could operate in parallel or synergistically to maintain optimal PSII efficiency under fluctuating light environments because photosynthetic organisms live in—and adapt to—their natural growth conditions where light fluctuates rapidly and unpredictably. This review focuses on antenna- and reaction center-based strategies that coexist in oxygenic organisms to minimize the production of the photosynthetic byproducts ROS, thereby safeguarding PSII under changes in light conditions.

PREVENTION: REGULATION OF LIGHT CAPTURE AS A PHOTOPROTECTIVE MECHANISM ACROSS PHOTOSYNTHETIC ORGANISMS

Non-photochemical Quenching Regulation of Light-Harvesting Efficiency

Photosynthesis is initiated by the capture and trapping of solar energy by light-harvesting systems in thylakoid membranes of cyanobacteria or chloroplasts. However, absorbed light that exceeds what can be used by photosynthesis causes light-induced damage, primarily to PSII. Therefore, maintenance of optimal photosynthetic performance requires efficient regulation of light harvesting for photoprotection. NPQ safely dissipates excess light energy within the PSII antenna system and is found ubiquitously across oxygenic photosynthetic organisms (reviewed in Niyogi and Truong, 2013).

NPQ responds rapidly and prevents ROS formation during photosynthesis (**Figure 1**). It is a protective strategy for photosynthetic machinery to acclimatize to excess light conditions. NPQ consists of a variety of processes, such as redistribution of antenna between PSII and PSI to balance electron transport (qT type of NPQ, or state transition) (Bellafiore et al., 2005; reviewed in Erickson et al., 2015), deepoxidation of violaxanthin into zeaxanthin in the xanthophyll cycle and global structural reorganization of PSII-LHCII complexes (Niyogi et al., 1998; Ruban et al., 2007; Park et al., 2019). The most prominent and fastest component is zeaxanthin-facilitated energy-dependent quenching (qE type quenching or feedback de-excitation) (Li et al., 2000; Tian et al., 2019). Because it operates on a time scale of seconds to minutes, rapid and reversible qE is often referred to as flexible thermal dissipation (Demmig-Adams et al., 2006;

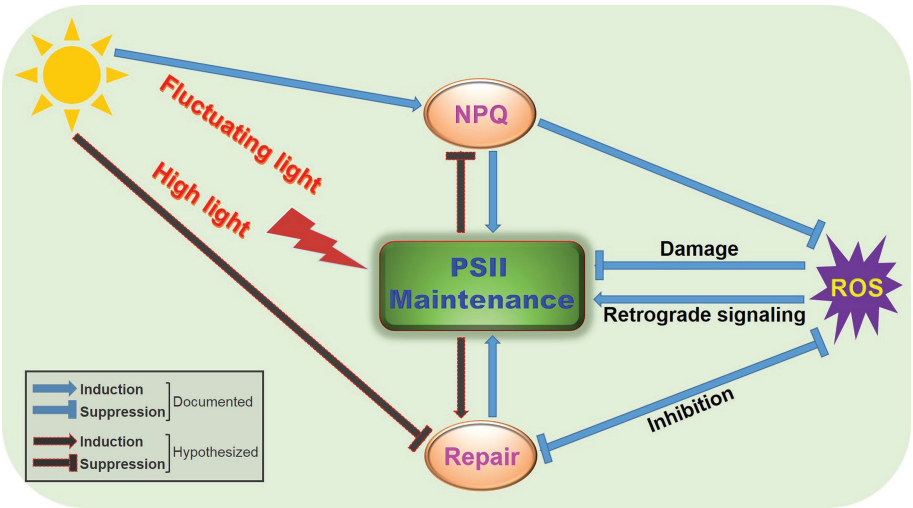

FIGURE 1 | A proposed simplified model illustrating regulation of PSII function by NPQ and repair under fluctuating light environments or high-light irradiance. Fluctuating light or high light can cause damage to PSII and downregulation of PSII photochemistry, with concomitant generation of ROS. To maintain normal PSII function, photosynthetic organisms deploy the antenna-based strategy, NPQ, and the reaction center-based strategy, PSII repair, to efficiently regulate light utilization and energy transfer. ROS act on PSII through damage, inhibition of repair, or retrograde signaling, whose production can be decreased by NPQ or repair. These intricate interplays between NPQ and repair can optimize PSII performance and facilitate acclimation of photosynthetic groups to fluctuating light environments or high-light irradiance.

reviewed in Niyogi and Truong, 2013). qE formation is strictly dependent on a high ΔpH and the PsbS protein but also requires zeaxanthin synthesis (Niyogi et al., 1998; Avenson et al., 2008; Holzwarth et al., 2009). Another NPQ component (qZ type quenching), which is distinguished from qE, is formed within 10–30 min (Nilkens et al., 2010). The formation of qZ is strictly dependent on zeaxanthin but independent of PsbS (Dall'Osto, 2005). The relaxation of qZ depends on zeaxanthin epoxidation and is linked to the kinetics of the zeaxanthin pool. Photoinhibitory quenching is a zeaxanthin-mediated, but not rapidly reversible NPQ component (qI-type quenching or inflexible/sustained thermal dissipation) (Demmig-Adams et al., 2006; reviewed in Pinnola and Bassi, 2018). The relative contribution of each process to the overall NPQ capacity depends on individual photosynthetic organisms and the changing environmental conditions.

Because photosynthetic organisms live in a broad range of habitats, the intensity and spectra of light experienced by different photosynthetic organisms vary extensively. This is particularly true for aquatic organisms, which are subjected to rapidly changing environmental factors, such as abrupt wave movements or phytoplankton migrations. Therefore, it is not surprising that aquatic photosynthetic organisms display distinct photoprotective strategies. For example, the green alga *Chlamydomonas reinhardtii* (a unicellular model species) and diatom *Phaeodactylum tricornutum* both need the LHCSR (LHC STRESS-RELATED PROTEIN) family protein for NPQ formation. Synthesis of the *Chlamydomonas* LHCSR protein is dramatically induced by high light, and it is responsible for the majority of flexible NPQ (Peers et al., 2009; Girolomoni et al., 2019). Notably, the induction of LHCSR expression under high light intensities is found to be controlled by the blue-light photoreceptor phototropin. This suggests that sensing, dissipation, and utilization of light is a concerted process (Petroutsos et al., 2016). Likewise, the LHCSR family protein LHCX1 in *Phaeodactylum* determines NPQ's high capacity, which correlates with its strong ability to cope with various light stresses (Bailleul et al., 2010; Gundermann et al., 2019). However, the expression and accumulation of LHCX1 is not further induced by excess light energy like it is with *Chlamydomonas* LHCSR (Petroutsos et al., 2016). This demonstrates that *Phaeodactylum* has constitutive and highly efficient photoprotection. These differences in photoprotective capacity between the two aquatic groups reflect their unique ecological adaptations to the sudden, strong changes in underwater light environments.

NPQ mechanisms in terrestrial plants are diverse and elaborate, as reflected by the remarkable diversity of plant species that are distributed in different geographic locations with potentially differential ecological effects. The PsbS (PHOTOSYSTEM II SUBUNIT S) protein in higher plants plays a similar role to the algal type LHCSR. It senses the pH of the chloroplast thylakoid lumen when there is excess light and induces flexible NPQ (Niyogi et al., 1998; Li et al., 2004; Liguori et al., 2019). Short-lived, fast-growing plants such as annual crops have lower qE capacity than long-lived, slow-growing species such as tropical evergreens (Demmig-Adams et al., 2006). It is possible that slow-growing species utilize a smaller proportion of solar energy for photosynthesis, thus having lower intrinsic photosynthetic capacities. In contrast, in overwintering evergreen plants, qI is the predominant NPQ component and it operates independent of PsbS and trans-thylakoid pH, which evolved to cope with combined environmental stresses. The component responsible for qI is correlated initially with sustained D1 protein phosphorylation

and xanthophyll cycle arrest and subsequently with newly synthesized zeaxanthin and lutein (Demmig-Adams et al., 2006). This sustained NPQ has critical ecophysiological significance of conferring unique and highly efficient photoprotection in repeated unfavorable seasons over the lifetime of evergreens. It enables these species to downregulate photosynthetic efficiency while continuously harvesting light that does not need to be immediately rechanneled for photosynthesis and growth (reviewed in Demmig-Adams and Adams, 2006). To distinguish the slowly reversible, photoprotective NPQ from qI, this sustained NPQ is termed as qH, which recently has been unveiled to occur in the peripheral antenna of PSII at thylakoid membranes (reviewed in Malnoë, 2018; Malnoë et al., 2018). Genetic screening in *Arabidopsis* discovered that the molecular player of qH is the plastid lipocalin, LCNP (Brooks et al., 2013; Malnoë et al., 2018). Intriguingly, LCNP is a soluble protein localized in the thylakoid lumen, whose expression is induced by stresses such as drought or high light (Levesque-Tremblay et al., 2009). These data suggest that the localization of LCNP to thylakoid membranes likely depends on changes in environments (reviewed in Malnoë, 2018). The importance of sustained quenching is to maintain the normal function of thylakoids by allowing photoprotective NPQ in LHCII under stressful conditions (Lacour et al., 2018; Malnoë et al., 2018).

Coevolution of Flexible Non-photochemical Quenching and Antenna in Photosynthetic Lineages

The wide distribution of NPQ across photosynthetic prokaryotes and eukaryotes highlights its crucial role in PSII photoprotection. Notably, different NPQ systems have evolved in these diverse photosynthetic organisms. Flexible NPQ (qE), the major and also best-studied component of photoprotective excess energy dissipation, constitutes three systems, which are classified based on their associations with the diversification of the light-harvesting equipment in photosynthetic organisms: the OCP (ORANGE CAROTENOID PROTEIN)-dependent system in cyanobacteria, the LHCSR-dependent system in algae and mosses, and the PsbS-dependent system in mosses and vascular plants (Li et al., 2000; Gerotto et al., 2012; Kosuge et al., 2018; Girolomoni et al., 2019; reviewed in Wilson et al., 2006; Rochaix and Bassi, 2019). Therefore, distinct NPQ regulatory mechanisms have evolved to adjust to differential demands of light energy absorption and utilization, allowing ecological adaptations to specific environments. Intriguingly, these diverse types of NPQ are relevant to the diversified antenna systems during evolution of oxygenic photosynthesis. Cyanobacteria deploy thylakoid membrane-bound phycobilisomes as their light-harvesting antenna (reviewed in Kirilovsky and Kerfeld, 2016) and a special carotenoid molecule within OCP to absorb blue-green light and quench excessive excitation energy from phycobilisomes (Wilson et al., 2006; Mezzetti et al., 2019). Cyanobacterial OCP is both the sensor and site of flexible NPQ (Sedoud et al., 2014; Slonimskiy et al., 2019). Algae and plants utilize transmembrane three-helix LHC antennas, which further diversified into algae- and moss-specific LHCSR proteins. Unlike LHC antennas, LHCSR proteins do not absorb light energy but rather act as quenchers by sensing pH across thylakoid membranes and triggering excess light energy dissipation (Bonente et al., 2011; Pinnola et al., 2013; Tian et al., 2019). In an independent evolutionary innovation from the LHC superfamily, the four-helix protein PsbS in vascular plants functions specifically as a thylakoid membrane pH sensor to trigger and accelerate the formation of NPQ within the LHC antenna (Li et al., 2000; reviewed in Niyogi and Truong, 2013). In contrast to LHCSR (Bonente et al., 2011; Liguori et al., 2019), PsbS neither binds pigments nor quenches excess excitation energy (Bonente et al., 2008; Ruban et al., 2009; Wilk et al., 2013). Therefore, the sensor (PsbS) and the site (LHC) of NPQ are separated in higher plants, which allow high plasticity and flexibility in efficient NPQ induction and recovery.

It should be mentioned that algae also contains PsbS but only accumulates transiently during high light stress, contrasting with LHCSR that accumulates over a much longer period. PsbS shows the ability to increase NPQ but no clear photoprotection activity (Tibiletti et al., 2016). PsbS is unable to compensate for the function of LHCSR in the *lhcsr* mutant (Correa-Galvis et al., 2016). LHCSR alone can explain almost all fast induced NPQ in high light acclimated *Chlamydomonas* cells (Peers et al., 2009). Moss represents a transitional state between algae and vascular plants and has both PSBS and LHCSR. PSBS- and LHCSR-dependent NPQ operate independently and additively (Alboresi et al., 2010; Gerotto et al., 2012). An increased need for flexible NPQ might explain why both LHCSR- and PSBS-dependent NPQ systems are present in early land plants like mosses (Gerotto et al., 2011).

Exploiting Natural Non-photochemical Quenching Variation to Optimize Photoprotection and Photochemical Efficiency

Natural variation in NPQ capacity is commonly observed in oxygenic photosynthetic organisms, from cyanobacteria to flowering plants, and even between different populations or accessions of the same species grown in the same conditions (Demmig-Adams, 1998; Demmig-Adams et al., 2006; Wang et al., 2017; Hamdani et al., 2019). For instance, different *Arabidopsis thaliana* ecotypes exhibit diverse maximum levels of NPQ: Col-0 and Ws possess lower NPQ compared to Ll-1, Sf-2 (Jung and Niyogi, 2009). The variations in NPQ are not attributable to differences in PsbS or carotenoids required for NPQ formation but to previously unknown polygenic nuclear traits (Jung and Niyogi, 2009). Identification of these genes and understanding the physiological mechanisms responsible for the high NPQ phenotypes should provide a more complete picture of various NPQ systems and potentially lead to approaches for engineering or breeding plants with enhanced photoprotection capability against adverse environmental conditions while maintaining optimal photosynthetic efficiency.

OPERATION OF EFFICIENT PHOTOSYSTEM II REPAIR CYCLE ALLOWS HIGH PHOTOSYNTHETIC CAPACITY

Susceptibility to light-induced photodamage and/or photoinhibition, which can be measured as an increase in NPQ component qI, is an intrinsic and unavoidable feature of all PSII reaction centers—from cyanobacteria to flowering plants. The main site of photodamage in PSII is the reaction center D1 subunit, which constantly undergoes rapid turnover (degradation and synthesis) (Aro et al., 1993; Reviewed in Järvi et al., 2015). Although cyanobacteria, algae, and plants have repair mechanisms that differ in detail, they share a central feature: the replacement of the photodamaged D1 subunit with a newly synthesized copy (Armbruster et al., 2010; Kato et al., 2012; reviewed in Nixon et al., 2005; Komenda et al., 2012; Lu, 2016). The PSII repair cycle involves disassembly, targeted reaction-center protein proteolysis, replacement of damaged core proteins, and reassembly of new functional PSII supercomplexes (Haußühl et al., 2001; Kato et al., 2018; reviewed in Nickelsen and Rengstl, 2013). In addition, individual steps in the PSII repair cycle are vulnerable to environmental changes (reviewed in Nath et al., 2013), further necessitating an efficient and timely operation of the repair machinery (**Figure 1**).

Cyanobacteria and chloroplasts employ distinct PSII repair mechanisms, which may be relevant to evolutionarily distinct thylakoid structures. The photosynthetic membrane systems in oxygenic photosynthetic organisms have evolved into discrete morphological architectures, despite their common ancestry—eukaryotic chloroplasts evolved from cyanobacteria *via* an ancient endosymbiotic event (reviewed in Ku et al., 2015; Bock, 2017). In plant chloroplasts, photosynthetic membranes are differentiated into a network of extensively stacked grana thylakoids and unstacked stromal lamellae. Grana thylakoids are enriched in functional PSII supercomplexes, while the interconnecting stromal lamellae are enriched in PSI and ATP synthase complexes, with cytochrome b_6f complex evenly distributed between the two (Dekker and Boekema, 2005; Daum et al., 2010). In contrast, cyanobacterial thylakoid membranes are not differentiated in grana and stromal lamellae; therefore, their photosynthetic apparatus are not laterally separated (Liberton et al., 2013; Rast et al., 2019).

In higher plants, the individual repair steps take place in discrete subcompartments and occur in a well-defined order (reviewed in Kosuge et al., 2018). Kinases, phosphatases, proteases, ribosomes, and repair/assembly factors are spatially segregated to ensure an operation with minimal interference (Puthiyaveetil et al., 2014; Koochak et al., 2019). Phosphorylation remodels the thylakoid structure to facilitate monomerization of photodamaged PSII supercomplexes in the grana core. These damaged monomeric PSII complexes are then trafficked to granal margins, where dephosphorylation and disassembly likely occur. This allows damaged D1 to be degraded successively by FtSH and Deg proteases (Haußühl et al., 2001; Kato et al., 2012; Krynická et al., 2015; reviewed in Silva et al., 2003; Sun et al., 2007; Tikkanen et al., 2008; Li et al., 2018). The site of *de novo* D1 protein synthesis is located in unstacked stroma lamellae, whereas reformation of active PSII supercomplexes takes place in the highly stacked grana core (Okada et al., 1996; Danielsson et al., 2006).

The green alga *Chlamydomonas* has a thylakoid membrane organization similar to that in higher plants, though with less stacking of thylakoid membranes in its single cup-shaped chloroplast (Wei et al., 2014). Consistent with the less stacking of thylakoids, experimental evidence indicates that individual PSII repair steps in *Chlamydomonas* are not restricted to thylakoid subdomains but rather are dispersed all over in the thylakoids (Uniacke and Zerges, 2007).

PSII repair in cyanobacteria seems to be restricted to specific sites in the thylakoid membranes named repair zones (Silva et al., 2003; Klinkert et al., 2004). Some other studies demonstrated that these repair zones could also be located in the plasma membrane where repair zones converge with PSII biogenesis centers at PDM (PRATA-DEFINED MEMBRANES) subcompartments to allow damaged D1 to be promptly replaced (Schottkowski et al., 2009; Stengel et al., 2012). Another special feature in cyanobacteria is that the conserved phosphorylatable threonine residues in PSII reaction center proteins are not phosphorylated during PSII repair (Calzadilla et al., 2019; reviewed in Komenda et al., 2012). This suggests that phosphorylation- and dephosphorylation-facilitated PSII repair may be a specific step evolved in photosynthetic eukaryotes.

APPROPRIATE PHOTOSYSTEM II MAINTENANCE ENSURES OPTIMAL PHOTOSYNTHETIC PERFORMANCE UNDER NATURAL FLUCTUATING LIGHT ENVIRONMENTS

Photosynthetic organisms experience abrupt and strong changes in light irradiance from seconds to seasons in their aquatic or terrestrial habitats. A multitude of protective and regulatory mechanisms evolved to facilitate their adaptation to such environmental fluctuations. NPQ appears to be a ubiquitous and major light acclimation mechanism that contributes to fitness under varying environments. LHCSR deficiency caused an increased death rate in *Chlamydomonas* following a shift from low to high light, suggesting that LHCSR-induced NPQ is required for optimal survival under variable light conditions (Peers et al., 2009; Kosuge et al., 2018; Girolomoni et al., 2019; Tian et al., 2019). In *Phaeodactylum*, a decreased LHCX1 level led to reduced fitness under stressful light, and even non-stressful light conditions, suggesting that LHCX-dependent NPQ endows diatoms with maximal survival capacity under a wide range of light environments (Bailleul et al., 2010; Gundermann et al., 2019; Park et al., 2019). In *Arabidopsis* plants, NPQ plays a crucial role in rapidly adjusting PSII to artificial fluctuating light (Armbruster et al., 2014, 2016; Duan et al., 2016; Herdean et al., 2016). In field conditions with natural fluctuating light, the NPQ-defective mutants *npq1* and *npq4* exhibited lower PSII activity and produced fewer seeds than the wild type, although they had no visible vegetative growth defects (reviewed in Külheim et al., 2002; Frenkel et al., 2007;

Wobbe et al., 2016). Compared to what we know of NPQ in algae and plants, little is known about the importance of OCP-dependent NPQ in cyanobacteria under fluctuating light.

So far, there is no published experimental evidence addressing whether PSII deficiency affects cyanobacteria or *Chlamydomonas* growth under variable light conditions, but several studies in *Arabidopsis* identified protein factors required to safeguard PSII under rapidly changing light conditions. TLP18.3 (THYLAKOID LUMEN PROTEIN 18.3) protein is reported to have a crucial role in adjusting *Arabidopsis* photosynthesis to fluctuating light (Sirpio et al., 2007; Jarvi et al., 2016). The *tlp18.3* mutants did not show visible phenotype under standard growth conditions. However, they exhibited retarded growth under fluctuating light and were highly susceptible to high-light stress. More importantly, the phenotypic defects of the *tlp18.3* mutants were found to be associated with inefficient operation of the PSII repair cycle (Sirpio et al., 2007). Two recent studies uncovered that the loss of *Arabidopsis* PSB27 (PHOTOSYSTEM II SUBUNIT 27) and MET1 (MESOPHYLL-ENRICHED THYLAKOID PROTEIN 1) caused stunted phenotypes when exposed to fluctuating light intensities (Bhuiyan et al., 2015; Hou et al., 2015). These loss-of-function mutations did not affect growth and development under normal light conditions. The reduced vegetative growth in the *psb27* mutant under fluctuating light was attributed to decreased PSII efficiency; this, however, was independent to the PSII supercomplex formation (Hou et al., 2015). The growth retardation in *met1* was due to a defect in the regeneration of active PSII supercomplexes that correlated with the reduced PSII activity (Bhuiyan et al., 2015). Other PSII repair-impaired mutants, including the newly characterized *mph2* and *curt1*, displayed growth retardation under fluctuating light (Liu and Last, 2017; Pribil et al., 2018). The association of decreased growth with impairments in PSII repair suggests that proper maintenance of PSII photochemical efficiency represents an important strategy to ensure plant fitness under adverse light conditions. Exploring the mechanisms of PSII repair in algae and cyanobacteria under fluctuating light may offer further insight into the evolution of photosynthesis. Moreover, exploiting PSII repair mechanisms could be promising targets for bioengineering photosynthesis to increase photosynthetic capacity and productivity under controlled photoinhibitory light and natural fluctuating light environments.

OPTIMIZING NON-PHOTOCHEMICAL QUENCHING TO ENHANCE PHOTOSYNTHETIC CAPACITY AND GROWTH IN FIELD CONDITIONS

Deeper understanding of NPQ mechanisms should inform strategies to optimize the balance between photoprotection and photosynthetic productivity. Optimization of photoprotection to improve photosynthetic performance is an emerging strategy in agriculture. It is generally accepted that the solar energy conversion efficiency for crop plants is much lower than the theoretical maximum yield (~12%) (reviewed in Walker, 2009; Blankenship et al., 2011). One major cause for the low efficiency is that upper leaves of a canopy absorb more sunlight than can be used for photochemistry, while photosynthesis of lower leaves is limited by shading (reviewed in Long et al., 2015). Altering the pigment content and leaf arrangement in the canopy may improve crop yield. A smart canopy with even light absorption would have light green vertical leaves at the top of the canopy and dark green horizontal leaves at the bottom (reviewed in Ort et al., 2015). Therefore, an optimized canopy may achieve higher crop yield.

Another major reason for the lower than the expected maximal photosynthetic efficiency in crops (and other plants) is that NPQ relaxation lags behind fluctuations in sunlight during sudden transitions from high to low light. This happens when passing clouds or movement of neighboring leaves/plant species shade sunlit leaves. The slow NPQ response could cost up to 30% of carbon gain (Zhu et al., 2004, reviewed in Zhu et al., 2008), suggesting that accelerating NPQ relaxation would be a strategy for increasing photosynthetic productivity. For example, speeding up the response to natural shading events by enhancing the recovery from photoprotective NPQ in *Nicotiana tabaccum* markedly increased photosynthetic capacity and bulked up leaves, stems, and roots, which contributed to a 15% gain in plant biomass production in field conditions (Kromdijk et al., 2016). Much more rapid NPQ induction in bright light and much faster NPQ relaxation following a drop in light intensity enable plants to track fluctuations in sunlight more closely, contributing to more efficient light energy utilization and carbon fixation. This proof-of-concept field trial opens the door to enhancing photosynthetic performance and productivity in agricultural and natural ecosystems.

CONCLUDING REMARKS AND FUTURE PERSPECTIVES

In oxygenic photosynthesis, it is important to (1) safely handle excess absorbed light energy that would otherwise cause massive ROS production and damage the photosynthetic machinery and (2) efficiently convert solar energy into chemical bond energy. Tight regulation of these two aspects may contribute to an increase in productivity in agriculture and natural ecosystems. Understanding the elaborate NPQ mechanisms and the robust PSII repair systems may help identify targets to optimize photosynthetic efficiency. This would facilitate translational work toward exploring yield potential to sustainably meet the global rising demands for food, fuel, and fiber in the future climate change. Prior to accomplishing these grand goals, multiple outstanding questions await to be addressed:

1. Do antenna-based photoprotection and reaction center-based repair operate in concert or in parallel to regulate PSII efficiency and photosynthetic capacity under photoinhibitory light and other environmental stresses? How does evolution of NPQ in the oxygenic organisms contribute to that of repair and vice versa?
2. How do ROS regulate PSII activity under fluctuating light environments or field conditions?
3. Are the molecular mechanisms of PSII repair under changing light different or similar to those under high-light irradiance? Can photosynthetic species discern PSII damage caused by

these two types of light conditions and initiate distinct repair strategies?

AUTHOR CONTRIBUTIONS

JL and RL conceived the project. JL, YL, WH, and RL wrote and edited the manuscript.

FUNDING

The National Key Basic Research Program of China (2015CB150200), National Natural Science Foundation of China (31800196) and Fundamental Research Funds for Central Non-profit Scientific Institution (1610172019006) supported this work. YL and RL acknowledge funding from the US National Science Foundation (MCB-1244008).

REFERENCES

Alboresi, A., Dall'Osto, L., Aprile, A., Carillo, P., Roncaglia, E., Cattivelli, L., et al. (2011). Reactive oxygen species and transcript analysis upon excess light treatment in wild-type *Arabidopsis thaliana* vs a photosensitive mutant lacking zeaxanthin and lutein. *BMC Plant Biol.* 11:62. doi: 10.1186/1471-2229-11-62

Alboresi, A., Gerotto, C., Giacometti, G. M., Bassi, R., and Morosinotto, T. (2010). *Physcomitrella patens* mutants affected on heat dissipation clarify the evolution of photoprotection mechanisms upon land colonization. *Proc. Natl. Acad. Sci. USA* 107, 11128–11233. doi: 10.1073/pnas.1002873107

Armbruster, U., Carrillo, L. R., Venema, K., Pavlovic, L., Schmidtmann, E., Kornfeld, A., et al. (2014). Ion antiport accelerates photosynthetic acclimation in fluctuating light environments. *Nat. Commun.* 5:5439. doi: 10.1038/ncomms6439

Armbruster, U., Leonelli, L., Correa Galvis, V., Strand, D., Quinn, E. H., Jonikas, M. C., et al. (2016). Regulation and levels of the thylakoid K+/H+ antiporter KEA3 shape the dynamic response of photosynthesis in fluctuating light. *Plant Cell Physiol.* 57, 1557–1567. doi: 10.1093/pcp/pcw085

Armbruster, U., Zühlke, J., Rengstl, B., Kreller, R., Makarenko, E., Rühle, T., et al. (2010). The *Arabidopsis* thylakoid protein PAM68 is required for efficient D1 biogenesis and photosystem II assembly. *Plant Cell* 22, 3439–3460. doi: 10.1105/tpc.110.077453

Aro, E. M., Virgin, I., and Andersson, B. (1993). Photoinhibition of photosystem II. Inactivation, protein damage and turnover. *Biochim. Biophys. Acta Bioenerg.* 1143, 113–134. doi: 10.1016/0005-2728(93)90134-2

Avenson, T. J., Tae, K. A., Zigmantas, D., Niyogi, K. K., Li, Z., Ballottari, M., et al. (2008). Zeaxanthin radical cation formation in minor light-harvesting complexes of higher plant antenna. *J. Biol. Chem.* 283, 3550–3558. doi: 10.1074/jbc.M705645200

Bailleul, B., Rogato, A., de Martino, A., Coesel, S., Cardol, P., Bowler, C., et al. (2010). An atypical member of the light-harvesting complex stress-related protein family modulates diatom responses to light. *Proc. Natl. Acad. Sci. USA* 107, 18214–18219. doi: 10.1073/pnas.1007703107

Bellafiore, S., Barneche, F., Peltier, G., and Rochaix, J. D. (2005). State transitions and light adaptation require chloroplast thylakoid protein kinase STN7. *Nature* 433, 892–895. doi: 10.1038/nature03286

Bhuiyan, N. H., Friso, G., Poliakov, A., Ponnala, L., and van Wijk, K. J. (2015). MET1 Is a thylakoid-associated TPR protein involved in photosystem II supercomplex formation and repair in *Arabidopsis*. *Plant Cell* 27, 262–285. doi: 10.1105/tpc.114.132787

Blankenship, R. E., Tiede, D. M., Barber, J., Brudvig, G. W., Fleming, G., Ghirardi, M., et al. (2011). Comparing photosynthetic and photovoltaic efficiencies and recognizing the potential for improvement. *Science* 332, 805–809. doi: 10.1126/science.1200165

Bock, R. (2017). Witnessing genome evolution: experimental reconstruction of endosymbiotic and horizontal gene transfer. *Annu. Rev. Genet.* 51, 1–22. doi: 10.1146/annurev-genet-120215-035329

Bonente, G., Ballottari, M., Truong, T. B., Morosinotto, T., Ahn, T. K., Fleming, G. R., et al. (2011). Analysis of LhcSR3, a protein essential for feedback de-excitation in the green alga *Chlamydomonas reinhardtii*. *PLoS Biol.* 9:e1000577. doi: 10.1371/journal.pbio.1000577

Bonente, G., Howes, B. D., Caffarri, S., Smulevich, G., and Bassi, R. (2008). Interactions between the photosystem II subunit PsbS and xanthophylls studied *in vivo* and *in vitro*. *J. Biol. Chem.* 283, 8434–8445. doi: 10.1074/jbc.M708291200

Brooks, M. D., Sylak-Glassman, E. J., Fleming, G. R., and Niyogi, K. K. (2013). A thioredoxin-like/-propeller protein maintains the efficiency of light harvesting in *Arabidopsis*. *Proc. Natl. Acad. Sci. USA* 110, 2733–2740. doi: 10.1073/pnas.1305443110

Calzadilla, P. I., Zhan, J., Sétif, P., Lemaire, C., Solymosi, D., Battchikova, N., et al. (2019). The cytochrome b_6f complex is not involved in cyanobacterial state transitions. *Plant Cell* 31, 911–931. doi: 10.1105/tpc.18.00916

Chen, Y.-E., Su, Y.-Q., Mao, H.-T., Wu, N., Zhu, F., Yuan, M., et al. (2018). Terrestrial plants evolve highly assembled photosystem complexes in adaptation to light shifts. *Front. Plant Sci.* 9:1811. doi: 10.3389/fpls.2018.01811

Chen, Y.-E., Yuan, S., Lezhneva, L., Meurer, J., Schwenkert, S., Mamedov, F., et al. (2019). The low molecular mass photosystem II protein PsbTn is important for light acclimation. *Plant Physiol.* 79, 1739–1753. doi: 10.1104/pp.18.01251

Correa-Galvis, V., Redekop, P., Guan, K., Griess, A., Truong, T. B., Wakao, S., et al. (2016). Photosystem II subunit PsbS is involved in the induction of LHCSR protein-dependent energy dissipation in *Chlamydomonas reinhardtii*. *J. Biol. Chem.* 291, 17478–17487. doi: 10.1074/jbc.M116.737312

Dall'Osto, L. (2005). A mechanism of nonphotochemical energy dissipation, independent from PsbS, revealed by a conformational change in the antenna protein CP26. *Plant Cell* 17, 1217–1232. doi: 10.1105/tpc.104.030601

Danielsson, R., Suorsa, M., Paakkarinen, V., Albertsson, P. Å., Styring, S., Aro, E. M., et al. (2006). Dimeric and monomeric organization of photosystem II: distribution of five distinct complexes in the different domains of the thylakoid membrane. *J. Biol. Chem.* 281, 14241–14249. doi: 10.1074/jbc.M600634200

Daum, B., Nicastro, D., Austin, J., McIntosh, J. R., and Kühlbrandt, W. (2010). Arrangement of photosystem II and ATP synthase in chloroplast membranes of spinach and pea. *Plant Cell* 22, 1299–1312. doi: 10.1105/tpc.109.071431

Dekker, J. P., and Boekema, E. J. (2005). Supramolecular organization of thylakoid membrane proteins in green plants. *Biochim. Biophys. Acta Bioenerg.* 1706, 12–39. doi: 10.1016/j.bbabio.2004.09.009

Demmig-Adams, B. (1998). Survey of thermal energy dissipation and pigment composition in sun and shade leaves. *Plant Cell Physiol.* 39, 474–482. doi: 10.1093/oxfordjournals.pcp.a029394

Demmig-Adams, B., and Adams, W. W. (2006). Photoprotection in an ecological context: the remarkable complexity of thermal energy dissipation. *New Phytol.* 172, 11–21. doi: 10.1111/j.1469-8137.2006.01835.x

Demmig-Adams, B., Ebbert, V., Mellman, D. L., Mueh, K. E., Schaffer, L., Funk, C., et al. (2006). Modulation of PsbS and flexible vs sustained energy dissipation by light environment in different species. *Physiol. Plant.* 127, 670–680. doi: 10.1111/j.1399-3054.2006.00698.x

Dogra, V., Rochaix, J. D., and Kim, C. (2018). Singlet oxygen-triggered chloroplast-to-nucleus retrograde signalling pathways: an emerging perspective. *Plant Cell Environ.* 41, 1727–1738. doi: 10.1111/pce.13332

Duan, Z., Kong, F., Zhang, L., Li, W., Zhang, J., and Peng, L. (2016). A bestrophin-like protein modulates the proton motive force across the thylakoid membrane in *Arabidopsis*. *J. Integr. Plant Biol.* 58, 848–858. doi: 10.1111/jipb.12475

Erickson, E., Wakao, S., and Niyogi, K. K. (2015). Light stress and photoprotection in *Chlamydomonas reinhardtii*. *Plant J.* 82, 449–465. doi: 10.1111/tpj.12825

Frenkel, M., Bellafiore, S., Rochaix, J. D., and Jansson, S. (2007). Hierarchy amongst photosynthetic acclimation responses for plant fitness. *Physiol. Plant.* 129, 455–459. doi: 10.1111/j.1399-3054.2006.00831.x

Frigerio, S., Campoli, C., Zorzan, S., Fantoni, L. I., Crosatti, C., Drepper, F., et al. (2007). Photosynthetic antenna size in higher plants is controlled by

the plastoquinone redox state at the post-transcriptional rather than transcriptional level. *J. Biol. Chem.* 282, 29457–29469. doi: 10.1074/jbc.M705132200

Gerotto, C., Alboresi, A., Giacometti, G. M., Bassi, R., and Morosinotto, T. (2011). Role of PSBS and LHCSR in *Physcomitrella patens* acclimation to high light and low temperature. *Plant Cell Environ.* 34, 922–932. doi: 10.1111/j.1365-3040.2011.02294.x

Gerotto, C., Alboresi, A., Giacometti, G. M., Bassi, R., and Morosinotto, T. (2012). Coexistence of plant and algal energy dissipation mechanisms in the moss *Physcomitrella patens*. *New Phytol.* 196, 763–773. doi: 10.1111/j.1469-8137.2012.04345.x

Ghotbi-Ravandi, A. A., Shahbazi, M., Shariati, M., and Mulo, P. (2014). Effects of mild and severe drought stress on photosynthetic efficiency in tolerant and susceptible barley (*Hordeum vulgare* L.) genotypes. *J. Agron. Crop Sci.* 200, 403–415. doi: 10.1111/jac.12062

Girolomoni, L., Cazzaniga, S., Pinnola, A., Perozeni, F., Ballottari, M., and Bassi, R. (2019). LHCSR3 is a nonphotochemical quencher of both photosystems in *Chlamydomonas reinhardtii*. *Proc. Natl. Acad. Sci. USA* 116, 4212–4217. doi: 10.1073/pnas.1809812116

Gundermann, K., Wagner, V., Mittag, M., and Büchel, C. (2019). Fucoxanthin-chlorophyll protein complexes of the centric diatom *Cyclotella meneghiniana* differ in Lhcx1 and Lhcx6 content. *Plant Physiol.* 179, 1779–1795. doi: 10.1104/pp.18.01363

Hamdani, S., Khan, N., Perveen, S., Qu, M., Jiang, J., Govindjee et al. (2019). Changes in the photosynthesis properties and photoprotection capacity in rice (*Oryza sativa*) grown under red, blue, or white light. *Photosynth. Res.* 139, 107–121. doi: 10.1007/s11120-018-0589-6

Haußühl, K., Andersson, B., and Adamska, I. (2001). A chloroplast DegP2 protease performs the primary cleavage of the photodamaged D1 protein in plant photosystem II. *EMBO J.* 20, 713–722. doi: 10.1093/emboj/20.4.713

Herdean, A., Teardo, E., Nilsson, A. K., Pfeil, B. E., Johansson, O. N., Unnep, R., et al. (2016). A voltage-dependent chloride channel fine-tunes photosynthesis in plants. *Nat. Commun.* 7:11654. doi: 10.1038/ncomms11654

Hey, D., and Grimm, B. (2018). One-helix protein 2 (OHP2) is required for the stability of OHP1 and assembly factor HCF244 and is functionally linked to PSII biogenesis. *Plant Physiol.* 177, 1453–1472. doi: 10.1104/pp.18.00540

Holzwarth, A. R., Miloslavina, Y., Nilkens, M., and Jahns, P. (2009). Identification of two quenching sites active in the regulation of photosynthetic light-harvesting studied by time-resolved fluorescence. *Chem. Phys. Lett.* 483, 262–267. doi: 10.1016/j.cplett.2009.10.085

Hou, X., Fu, A., Garcia, V. J., Buchanan, B. B., and Luan, S. (2015). PSB27: a thylakoid protein enabling *Arabidopsis* to adapt to changing light intensity. *Proc. Natl. Acad. Sci. USA* 112, 1613–1618. doi: 10.1073/pnas.1424040112

Jarillo, J. A., Gabrys, H., Capel, J., Alonso, J. M., Ecker, J. R., and Cashmore, A. R. (2001). Phototropin-related NPL1 controls chloroplast relocation induced by blue light. *Nature* 410, 952–954. doi: 10.1038/35073622

Jarvi, S., Isojarvi, J., Kangasjarvi, S., Salojarvi, J., Mamedov, F., Suorsa, M., et al. (2016). Photosystem II repair and plant immunity: lessons learned from *Arabidopsis* mutant lacking the THYLAKOID LUMEN PROTEIN 18.3. *Front. Plant Sci.* 7:405. doi: 10.3389/fpls.2016.00405

Järvi, S., Suorsa, M., and Aro, E. M. (2015). Photosystem II repair in plant chloroplasts–regulation, assisting proteins and shared components with photosystem II biogenesis. *Biochim. Biophys. Acta Bioenerg.* 1847, 900–909. doi: 10.1016/j.bbabio.2015.01.006

Jin, H. L., Liu, B., Luo, L. J., Feng, D. R., Wang, P., Liu, J., et al. (2014). Hypersensitive to high LIGHT1 interacts with low quantum yield of photosystem II1 and functions in protection of photosystem II from photodamage in *Arabidopsis*. *Plant Cell* 26, 1213–1229. doi: 10.1105/tpc.113.122424

Jung, H., and Niyogi, K. K. (2009). Quantitative genetic analysis of thermal dissipation in *Arabidopsis*. *Plant Physiol.* 150, 977–986. doi: 10.1104/pp.109.137828

Kale, R., Hebert, A. E., Frankel, L. K., Sallans, L., Bricker, T. M., and Pospíšil, P. (2017). Amino acid oxidation of the D1 and D2 proteins by oxygen radicals during photoinhibition of photosystem II. *Proc. Natl. Acad. Sci. USA* 114, 2988–2993. doi: 10.1073/pnas.1618922114

Kapri-Pardes, E., Naveh, L., and Adam, Z. (2007). The thylakoid lumen protease Deg1 is involved in the repair of photosystem II from photoinhibition in *Arabidopsis*. *Plant Cell* 19, 1039–1047. doi: 10.1105/tpc.106.046573

Kato, Y., Hyodo, K., and Sakamoto, W. (2018). The photosystem II repair cycle requires FtsH turnover through the EngA GTPase. *Plant Physiol.* 178, 596–611. doi: 10.1104/pp.18.00652

Kato, Y., Sun, X., Zhang, L., and Sakamoto, W. (2012). Cooperative D1 degradation in the photosystem II repair mediated by chloroplastic proteases in *Arabidopsis*. *Plant Physiol.* 159, 1428–1439. doi: 10.1104/pp.112.199042

Kern, J., and Renger, G. (2007). Photosystem II: structure and mechanism of the water: plastoquinone oxidoreductase. *Photosynth. Res.* 94, 183–202. doi: 10.1007/s11120-007-9201-1

Kirilovsky, D., and Kerfeld, C. A. (2016). Cyanobacterial photoprotection by the orange carotenoid protein. *Nat. Plants* 2, 1–7. doi: 10.1038/nplants.2016.180

Klinkert, B., Ossenbühl, F., Sikorski, M., Berry, S., Eichacker, L., and Nickelsen, J. (2004). PratA, a periplasmic tetratricopeptide repeat protein involved in biogenesis of photosystem II in *Synechocystis* sp. PCC 6803. *J. Biol. Chem.* 279, 44639–44644. doi: 10.1074/jbc.M405393200

Komenda, J., Sobotka, R., and Nixon, P. J. (2012). Assembling and maintaining the photosystem II complex in chloroplasts and cyanobacteria. *Curr. Opin. Plant Biol.* 15, 245–251. doi: 10.1016/j.pbi.2012.01.017

Koochak, H., Puthiyaveetil, S., Mullendore, D. L., Li, M., and Kirchhoff, H. (2019). The structural and functional domains of plant thylakoid membranes. *Plant J.* 97, 412–429. doi: 10.1111/tpj.14127

Kosuge, K., Tokutsu, R., Kim, E., Akimoto, S., Yokono, M., Ueno, Y., et al. (2018). LHCSR1-dependent fluorescence quenching is mediated by excitation energy transfer from LHCII to photosystem I in *Chlamydomonas reinhardtii*. *Proc. Natl. Acad. Sci. USA* 115, 3722–3727. doi: 10.1073/pnas.1720574115

Kromdijk, J., Głowacka, K., Leonelli, L., Gabilly, S., Iwai, M., Niyogi, K., et al. (2016). Improving photosynthesis and crop productivity by accelerating recovery from photoprotection. *Science* 354, 857–861. doi: 10.1126/science.aai8878

Krynická, V., Shao, S., Nixon, P. J., and Komenda, J. (2015). Accessibility controls selective degradation of photosystem II subunits by FtsH protease. *Nat. Plants* 1:15168. doi: 10.1038/nplants.2015.168

Ku, C., Nelson-Sathi, S., Roettger, M., Sousa, F. L., Lockhart, P. J., Bryant, D., et al. (2015). Endosymbiotic origin and differential loss of eukaryotic genes. *Nature* 524, 427–432. doi: 10.1038/nature14963

Külheim, C., Agren, J., and Jansson, S. (2002). Rapid regulation of light harvesting and plant fitness in the field. *Science* 297, 91–93. doi: 10.1126/science.1072359

Lacour, T., Larivière, J., Ferland, J., Bruyant, F., Lavaud, J., and Babin, M. (2018). The role of sustained photoprotective non-photochemical quenching in low temperature and high light acclimation in the bloom-forming arctic diatom *Thalassiosira gravida*. *Front. Mar. Sci.* 5:354. doi: 10.3389/fmars.2018.00354

Leister, D. (2019). Genetic engineering, synthetic biology and the light reactions of photosynthesis. *Plant Physiol.* 179, 778–793. doi: 10.1104/pp.18.00360

Levesque-Tremblay, G., Havaux, M., and Ouellet, F. (2009). The chloroplastic lipocalin AtCHL prevents lipid peroxidation and protects *Arabidopsis* against oxidative stress. *Plant J.* 60, 691–702. doi: 10.1111/j.1365-313X.2009.03991.x

Li, L., Aro, E. M., and Millar, A. H. (2018). Mechanisms of photodamage and protein turnover in photoinhibition. *Trends Plant Sci.* 23, 667–676. doi: 10.1016/j.tplants.2018.05.004

Li, X. P., Bjorkman, O., Shih, C., Grossman, A. R., Rosenquist, M., Jansson, S., et al. (2000). A pigment-binding protein essential for regulation of photosynthetic light harvesting. *Nature* 403, 391–395. doi: 10.1038/35000131

Li, X. P., Gilmore, A. M., Caffarri, S., Bassi, R., Golan, T., Kramer, D., et al. (2004). Regulation of photosynthetic light harvesting involves intrathylakoid lumen pH sensing by the PsbS protein. *J. Biol. Chem.* 279, 22866–22874. doi: 10.1074/jbc.M402461200

Li, Y., Liu, B., Zhang, J., Kong, F., Zhang, L., Meng, H., et al. (2019). OHP1, OHP2, and HCF244 form a transient functional complex with the photosystem II reaction center. *Plant Physiol.* 179, 195–208. doi: 10.1104/pp.18.01231

Liberton, M., Page, L. E., O'Dell, W. B., O'Neill, H., Mamontov, E., Urban, V. S., et al. (2013). Organization and flexibility of cyanobacterial thylakoid membranes examined by neutron scattering. *J. Biol. Chem.* 288, 3632–3640. doi: 10.1074/jbc.M112.416933

Liguori, N., Campos, S. R. R., Baptista, A. M., and Croce, R. (2019). Molecular anatomy of plant photoprotective switches: the sensitivity of PsbS to the environment, residue by residue. *J. Phys. Chem. Lett.* 10, 1737–1742. doi: 10.1021/acs.jpclett.9b00437

Liu, J., and Last, R. L. (2015a). A land plant-specific thylakoid membrane protein contributes to photosystem II maintenance in *Arabidopsis thaliana*. *Plant J.* 82, 731–743. doi: 10.1111/tpj.12845

Liu, J., and Last, R. L. (2015b). MPH1 is a thylakoid membrane protein involved in protecting photosystem II from photodamage in land plants. *Plant Signal. Behav.* 10:e1076602. doi: 10.1080/15592324.2015.1076602

Liu, J., and Last, R. L. (2017). A chloroplast thylakoid lumen protein is required for proper photosynthetic acclimation of plants under fluctuating light environments. *Proc. Natl. Acad. Sci. USA* 114, E8110–E8117. doi: 10.1073/pnas.1712206114

Long, S. P., Marshall-Colon, A., and Zhu, X. G. (2015). Meeting the global food demand of the future by engineering crop photosynthesis and yield potential. *Cell* 161, 56–66. doi: 10.1016/j.cell.2015.03.019

Lu, Y. (2011). The occurrence of a thylakoid-localized small zinc finger protein in land plants. *Plant Signal. Behav.* 6, 1881–1885. doi: 10.4161/psb.6.12.18022

Lu, Y. (2016). Identification and roles of photosystem II assembly, stability, and repair factors in *Arabidopsis*. *Front. Plant Sci.* 7:168. doi: 10.3389/fpls.2016.00168

Lu, Y., Hall, D. A., and Last, R. L. (2011). A small Zinc finger thylakoid protein plays a role in maintenance of photosystem II in *Arabidopsis thaliana*. *Plant Cell* 23, 1861–1875. doi: 10.1105/tpc.111.085456

Malnoë, A. (2018). Photoinhibition or photoprotection of photosynthesis? Update on the (newly termed) sustained quenching component qH. *Environ. Exp. Bot.* 154, 123–133. doi: 10.1016/j.envexpbot.2018.05.005

Malnoë, A., Schultink, A., Shahrasbi, S., Rumeau, D., Havaux, M., and Niyogi, K. K. (2018). The plastid lipocalin LCNP is required for sustained photoprotective energy dissipation in *Arabidopsis*. *Plant Cell* 30, 196–208. doi: 10.1105/tpc.17.00536

Mezzetti, A., Alexandre, M., Thurotte, A., Wilson, A., Gwizdala, M., and Kirilovsky, D. (2019). Two-step structural changes in orange carotenoid protein photoactivation revealed by time-resolved Fourier transform infrared spectroscopy. *J. Phys. Chem. B* 123, 3259–3266. doi: 10.1021/acs.jpcb.9b01242

Mishra, N. P., and Ghanotakis, D. F. (1994). Exposure of a photosystem II complex to chemically generated singlet oxygen results in D1 fragments similar to the ones observed during aerobic photoinhibition. *Biochim. Biophys. Acta Bioenerg.* 1187, 296–300. doi: 10.1016/0005-2728(94)90003-5

Miyao, M., Ikeuchi, M., Yamamoto, N., and Ono, T. A. (1995). Specific degradation of the D1 protein of photosystem II by treatment with hydrogen peroxide in darkness: implications for the mechanism of degradation of the D1 protein under illumination. *Biochemistry* 34, 10019–10026. doi: 10.1021/bi00031a025

Murata, N., Takahashi, S., Nishiyama, Y., and Allakhverdiev, S. I. (2007). Photoinhibition of photosystem II under environmental stress. *Biochim. Biophys. Acta Bioenerg.* 1767, 414–421. doi: 10.1016/j.bbabio.2006.11.019

Myouga, F., Takahashi, K., Tanaka, R., Nagata, N., Kiss, A. Z., Funk, C., et al. (2018). Stable accumulation of photosystem II requires ONE-HELIX PROTEIN1 (OHP1) of the light harvesting-like family. *Plant Physiol.* 176, 2277–2291. doi: 10.1104/pp.17.01782

Nath, K., Jajoo, A., Poudyal, R. S., Timilsina, R., Park, Y. S., Aro, E. M., et al. (2013). Towards a critical understanding of the photosystem II repair mechanism and its regulation during stress conditions. *FEBS Lett.* 587, 3372–3381. doi: 10.1016/j.febslet.2013.09.015

Nickelsen, J., and Rengstl, B. (2013). Photosystem II assembly: from cyanobacteria to plants. *Annu. Rev. Plant Biol.* 64, 609–635. doi: 10.1146/annurev-arplant-050312-120124

Nilkens, M., Kress, E., Lambrev, P., Miloslavina, Y., Müller, M., Holzwarth, A. R., et al. (2010). Identification of a slowly inducible zeaxanthin-dependent component of non-photochemical quenching of chlorophyll fluorescence generated under steady-state conditions in *Arabidopsis*. *Biochim. Biophys. Acta Bioenerg.* 1794, 466–475. doi: 10.1016/j.bbabio.2010.01.001

Nishiyama, Y., Yamamoto, H., Allakhverdiev, S. I., Inaba, M., Yokota, A., and Murata, N. (2001). Oxidative stress inhibits the repair of photodamage to the photosynthetic machinery. *EMBO J.* 20, 5587–5594. doi: 10.1093/emboj/20.20.5587

Nixon, P. J., Barker, M., Boehm, M., De Vries, R., and Komenda, J. (2005). FtsH-mediated repair of the photosystem II complex in response to light stress. *J. Exp. Bot.* 56, 357–363. doi: 10.1093/jxb/eri021

Niyogi, K. K., Grossman, A. R., and Bjorkman, O. (1998). *Arabidopsis* mutants define a central role for the xanthophyll cycle in the regulation of photosynthetic energy conversion. *Plant Cell* 10, 1121–1134. doi: 10.1105/tpc.10.7.1121

Niyogi, K. K., and Truong, T. B. (2013). Evolution of flexible non-photochemical quenching mechanisms that regulate light harvesting in oxygenic photosynthesis. *Curr. Opin. Plant Biol.* 16, 307–314. doi: 10.1016/j.pbi.2013.03.011

Okada, K., Ikeuchi, M., Yamamoto, N., Ono, T. A., and Miyao, M. (1996). Selective and specific cleavage of the D1 and D2 proteins of photosystem II by exposure to singlet oxygen: factors responsible for the susceptibility to cleavage of the proteins. *Biochim. Biophys. Acta Bioenerg.* 1274, 73–79. doi: 10.1016/0005-2728(96)00015-1

Okegawa, Y., Kobayashi, Y., and Shikanai, T. (2010). Physiological links among alternative electron transport pathways that reduce and oxidize plastoquinone in *Arabidopsis*. *Plant J.* 63, 458–468. doi: 10.1111/j.1365-313X.2010.04252.x

Ort, D. R., Merchant, S. S., Alric, J., Barkan, A., Blankenship, R. E., Bock, R., et al. (2015). Redesigning photosynthesis to sustainably meet global food and bioenergy demand. *Proc. Natl. Acad. Sci. USA* 112, 8529–8536. doi: 10.1073/pnas.1424031112

Park, S., Steen, C. J., Lyska, D., Fischer, A. L., Endelman, B., Iwai, M., et al. (2019). Chlorophyll–carotenoid excitation energy transfer and charge transfer in *Nannochloropsis oceanica* for the regulation of photosynthesis. *Proc. Natl. Acad. Sci. USA* 116, 3385–3390. doi: 10.1073/pnas.1819011116

Peers, G., Truong, T. B., Ostendorf, E., Busch, A., Elrad, D., Grossman, A. R., et al. (2009). An ancient light-harvesting protein is critical for the regulation of algal photosynthesis. *Nature* 462, 518–521. doi: 10.1038/nature08587

Petroutsos, D., Tokutsu, R., Maruyama, S., Flori, S., Greiner, A., Magneschi, L., et al. (2016). A blue-light photoreceptor mediates the feedback regulation of photosynthesis. *Nature* 537, 563–566. doi: 10.1038/nature19358

Pinnola, A., and Bassi, R. (2018). Molecular mechanisms involved in plant photoprotection. *Biochem. Soc. Trans.* 46, 467–482. doi: 10.1042/BST20170307

Pinnola, A., Dall'Osto, L., Gerotto, C., Morosinotto, T., Bassi, R., and Alboresi, A. (2013). Zeaxanthin binds to light-harvesting complex stress-related protein to enhance nonphotochemical quenching in *Physcomitrella patens*. *Plant Cell* 25, 3519–3534. doi: 10.1105/tpc.113.114538

Pribil, M., Sandoval-Ibáñez, O., Xu, W., Sharma, A., Labs, M., Liu, Q., et al. (2018). Fine-tuning of photosynthesis requires curvature thylakoid1-mediated thylakoid plasticity. *Plant Physiol.* 176, 2351–2364. doi: 10.1104/pp.17.00863

Puthiyaveetil, S., Tsabari, O., Lowry, T., Lenhert, S., Lewis, R. R., Reich, Z., et al. (2014). Compartmentalization of the protein repair machinery in photosynthetic membranes. *Proc. Natl. Acad. Sci. USA* 111, 15839–15844. doi: 10.1073/pnas.1413739111

Rast, A., Schaffer, M., Albert, S., Wan, W., Pfeffer, S., Beck, F., et al. (2019). Biogenic regions of cyanobacterial thylakoids form contact sites with the plasma membrane. *Nat. Plants* 5, 436–446. doi: 10.1038/s41477-019-0399-7

Rochaix, J.-D., and Bassi, R. (2019). LHC-like proteins involved in stress responses and biogenesis/repair of the photosynthetic apparatus. *Biochem. J.* 476, 581–593. doi: 10.1042/BCJ20180718

Ruban, A. V., Berera, R., Ilioaia, C., van Stokkum, I. H. M., Kennis, J. T. M., Pascal, A. A., et al. (2007). Identification of a mechanism of photoprotective energy dissipation in higher plants. *Nature* 450, 575–578. doi: 10.1038/nature06262

Ruban, A. V., Johnson, M. P., Horton, P., Zia, A., and Perez-Bueno, M. L. (2009). The zeaxanthin-independent and zeaxanthin-dependent qE components of nonphotochemical quenching involve common conformational changes within the photosystem II antenna in *Arabidopsis*. *Plant Physiol.* 149, 1061–1075. doi: 10.1104/pp.108.129957

Sainz, M., Díaz, P., Monza, J., and Borsani, O. (2010). Heat stress results in loss of chloroplast Cu/Zn superoxide dismutase and increased damage to photosystem II in combined drought-heat stressed *Lotus japonicus*. *Physiol. Plant.* 140, 46–56. doi: 10.1111/j.1399-3054.2010.01383.x

Salomon, E., Bar-Eyal, L., Sharon, S., and Keren, N. (2013). Balancing photosynthetic electron flow is critical for cyanobacterial acclimation to nitrogen limitation. *Biochim. Biophys. Acta Bioenerg.* 1827, 340–347. doi: 10.1016/j.bbabio.2012.11.010

Schottkowski, M., Gkalympoudis, S., Tzekova, N., Stelljes, C., Schünemann, D., Ankele, E., et al. (2009). Interaction of the periplasmic pratA factor and the PsbA (D1) protein during biogenesis of photosystem II in *synechocystis* sp. PCC 6803. *J. Biol. Chem.* 284, 1813–1819. doi: 10.1074/jbc.M806116200

Sedoud, A., Lopez-Igual, R., Rehman, A. U., Wilson, A., Perreau, F., Boulay, C., et al. (2014). The cyanobacterial photoactive orange carotenoid protein is an excellent singlet oxygen quencher. *Plant Cell* 26, 1781–1791. doi: 10.1105/tpc.114.123802

Silva, P., Thompson, E., Bailey, S., Kruse, O., Mullineaux, C. W., Robinson, C., et al. (2003). FtsH is involved in the early stages of repair of photosystem II in *Synechocystis* sp. PCC 6803. *Plant Cell* 15, 2152–2164. doi: 10.1105/tpc.012609

Sirpio, S., Allahverdiyeva, Y., Suorsa, M., Paakkarinen, V., Vainonen, J., Battchikova, N., et al. (2007). TLP18.3, a novel thylakoid lumen protein regulating photosystem II repair cycle. *Biochem. J.* 406, 415–425. doi: 10.1042/BJ20070460

Slonimskiy, Y. B., Muzzopappa, F., Maksimov, E. G., Wilson, A., Friedrich, T., Kirilovsky, D., et al. (2019). Light-controlled carotenoid transfer between water-soluble proteins related to cyanobacterial photoprotection. *FEBS J.* 286, 1908–1924. doi: 10.1111/febs.14803

Stengel, A., Gügel, I. L., Hilger, D., Rengstl, B., Jung, H., and Nickelsen, J. (2012). Initial steps of photosystem II *de novo* assembly and preloading with manganese take place in biogenesis centers in *Synechocystis*. *Plant Cell* 24, 660–675. doi: 10.1105/tpc.111.093914

Strzepek, R. F., Boyd, P. W., and Sunda, W. G. (2019). Photosynthetic adaptation to low iron, light, and temperature in Southern Ocean phytoplankton. *Proc. Natl. Acad. Sci. USA* 116, 4388–4393. doi: 10.1073/pnas.1810886116

Sun, X., Peng, L., Guo, J., Chi, W., Ma, J., Lu, C., et al. (2007). Formation of DEG5 and DEG8 complexes and their involvement in the degradation of photodamaged photosystem II reaction center D1 protein in *Arabidopsis*. *Plant Cell* 19, 1347–1361. doi: 10.1105/tpc.106.049510

Takahashi, S., and Badger, M. R. (2011). Photoprotection in plants: a new light on photosystem II damage. *Trends Plant Sci.* 16, 53–60. doi: 10.1016/j.tplants.2010.10.001

Tian, L., Nawrocki, W. J., Liu, X., Polukhina, I., van Stokkum, I. H. M., and Croce, R. (2019). pH dependence, kinetics and light-harvesting regulation of nonphotochemical quenching in *Chlamydomonas*. *Proc. Natl. Acad. Sci. USA* 116, 8320–8325. doi: 10.1073/pnas.1817796116

Tibiletti, T., Auroy, P., Peltier, G., and Caffarri, S. (2016). *Chlamydomonas reinhardtii* PsbS protein is functional and accumulates rapidly and transiently under high light. *Plant Physiol.* 171, 2717–2730. doi: 10.1104/pp.16.00572

Tikkanen, M., Nurmi, M., Kangasjärvi, S., and Aro, E.-M. (2008). Core protein phosphorylation facilitates the repair of photodamaged photosystem II at high light. *Biochim. Biophys. Acta Bioenerg.* 1777, 1432–1437. doi: 10.1016/j.bbabio.2008.08.004

Ting, C. S., and Owens, T. G. (2016). The effects of excess irradiance on photosynthesis in the marine diatom *Phaeodactylum tricornutum*. *Plant Physiol.* 106, 763–770. doi: 10.1104/pp.106.2.763

Townsend, A. J., Ware, M. A., and Ruban, A. V. (2018). Dynamic interplay between photodamage and photoprotection in photosystem II. *Plant Cell Environ.* 41, 1098–1112. doi: 10.1111/pce.13107

Uniacke, J., and Zerges, W. (2007). Photosystem II assembly and repair are differentially localized in *Chlamydomonas*. *Plant Cell* 19, 3640–3654. doi: 10.1105/tpc.107.054882

Wagner, D., Przybyla, D., Op Den Camp, R., Kim, C., Landgraf, F., Keun, P. L., et al. (2004). The genetic basis of singlet oxygen-induced stress response of *Arabidopsis thaliana*. *Science* 306, 1183–1185. doi: 10.1126/science.1103178

Walker, D. A. (2009). Biofuels, facts, fantasy, and feasibility. *J. Appl. Phycol.* 21, 509–517. doi: 10.1007/s10811-009-9446-5

Wang, Q., Zhao, H., Jiang, J., Xu, J., Xie, W., Fu, X., et al. (2017). Genetic architecture of natural variation in rice nonphotochemical quenching capacity revealed by genome-wide association study. *Front. Plant Sci.* 13:1773. doi: 10.3389/fpls.2017.01773

Wei, L., Derrien, B., Gautier, A., Houille-Vernes, L., Boulouis, A., Saint-Marcoux, D., et al. (2014). Nitric oxide-triggered remodeling of chloroplast bioenergetics and thylakoid proteins upon nitrogen starvation in *Chlamydomonas reinhardtii*. *Plant Cell* 179, 718–731. doi: 10.1105/tpc.113.120121

Wilk, L., Grunwald, M., Liao, P.-N., Walla, P. J., and Kuhlbrandt, W. (2013). Direct interaction of the major light-harvesting complex II and PsbS in nonphotochemical quenching. *Proc. Natl. Acad. Sci. USA* 110, 5452–5456. doi: 10.1073/pnas.1205561110

Wilson, A., Ajlani, G., Verbavatz, J.-M., Vass, I., Kerfeld, C. A., and Kirilovsky, D. (2006). A soluble carotenoid protein involved in phycobilisome-related energy dissipation in cyanobacteria. *Plant Cell* 18, 992–1007. doi: 10.1105/tpc.105.040121

Wilson, S., and Ruban, A. V. (2019). Quantitative assessment of the high-light tolerance in plants with an impaired photosystem II donor side. *Biochem. J.* 476, 1377–1386. doi: 10.1042/BCJ20190208

Wittenberg, G., Levitan, A., Klein, T., Dangoor, I., Keren, N., and Danon, A. (2014). Knockdown of the *Arabidopsis thaliana* chloroplast protein disulfide isomerase 6 results in reduced levels of photoinhibition and increased D1 synthesis in high light. *Plant J.* 78, 1003–1013. doi: 10.1111/tpj.12525

Wobbe, L., Bassi, R., and Kruse, O. (2016). Multi-level light capture control in plants and green algae. *Trends Plant Sci.* 21, 55–68. doi: 10.1016/j.tplants.2015.10.004

Zhu, X. G., Long, S. P., and Ort, D. R. (2008). What is the maximum efficiency with which photosynthesis can convert solar energy into biomass? *Curr. Opin. Biotechnol.* 19, 153–159. doi: 10.1016/j.copbio.2008.02.004

Zhu, X., Ort, D. R., Whitmarsh, J., and Long, S. P. (2004). The slow reversibility of photosystem II thermal energy dissipation on transfer from high to low light may cause large losses in carbon gain by crop canopies: a theoretical analysis. *J. Exp. Bot.* 55, 1167–1175. doi: 10.1093/jxb/erh141

Conflict of Interest Statement: The authors declare that the research was conducted in the absence of any commercial or financial relationships that could be construed as a potential conflict of interest.

frontiers in Plant Science

ORIGINAL RESEARCH
published: 16 October 2019
doi: 10.3389/fpls.2019.01284

Introducing an *Arabidopsis thaliana* Thylakoid Thiol/Disulfide-Modulating Protein Into *Synechocystis* Increases the Efficiency of Photosystem II Photochemistry

Ryan L. Wessendorf† *and Yan Lu**

Department of Biological Sciences, Western Michigan University, Kalamazoo, MI, United States

OPEN ACCESS

Edited by:
Benoit Schoefs, Le Mans Université, France

Reviewed by:
Imre Vass, Hungarian Academy of Sciences, Hungary
Rikard Fristedt, Vrije Universiteit Amsterdam, Netherlands

***Correspondence:**
Yan Lu
yan.1.lu@wmich.edu

†Present address:
Ryan L. Wessendorf
Program in Plant Biology, School of Biological Sciences, Washington State University, Pullman, WA, United States

Specialty section:
This article was submitted to Plant Physiology, a section of the journal Frontiers in Plant Science

Received: *16 June 2019*
Accepted: *13 September 2019*
Published: *16 October 2019*

Citation:
Wessendorf RL and Lu Y (2019) Introducing an Arabidopsis thaliana Thylakoid Thiol/Disulfide-Modulating Protein Into Synechocystis Increases the Efficiency of Photosystem II Photochemistry. Front. Plant Sci. 10:1284. doi: 10.3389/fpls.2019.01284

Photosynthetic species are subjected to a variety of environmental stresses, including suboptimal irradiance. In oxygenic photosynthetic organisms, a major effect of high light exposure is damage to the Photosystem II (PSII) reaction-center protein D1. This process even happens under low or moderate light. To cope with photodamage to D1, photosynthetic organisms evolved an intricate PSII repair and reassembly cycle, which requires the participation of different auxiliary proteins, including thiol/disulfide-modulating proteins. Most of these auxiliary proteins exist ubiquitously in oxygenic photosynthetic organisms. Due to differences in mobility and environmental conditions, land plants are subject to more extensive high light stress than algae and cyanobacteria. Therefore, land plants evolved additional thiol/disulfide-modulating proteins, such as Low Quantum Yield of PSII 1 (LQY1), to aid in the repair and reassembly cycle of PSII. In this study, we introduced an *Arabidopsis thaliana* homolog of LQY1 (AtLQY1) into the cyanobacterium *Synechocystis* sp. PCC6803 and performed a series of biochemical and physiological assays on AtLQY1-expressing *Synechocystis*. At a moderate growth light intensity (50 μmol photons m^{-2} s^{-1}), AtLQY1-expressing *Synechocystis* was found to have significantly higher F_v/F_m, and lower nonphotochemical quenching and reactive oxygen species levels than the empty-vector control, which is opposite from the loss-of-function *Atlqy1* mutant phenotype. Light response curve analysis of PSII operating efficiency and electron transport rate showed that AtLQY1-expressing *Synechocystis* also outperform the empty-vector control under higher light intensities. The increases in F_v/F_m, PSII operating efficiency, and PSII electron transport rate in AtLQY1-expressing *Synechocystis* under such growth conditions most likely come from an increased amount of PSII, because the level of D1 protein was found to be higher in AtLQY1-expressing *Synechocystis*. These results suggest that introducing AtLQY1 is beneficial to *Synechocystis*.

Keywords: photosynthesis, Photosystem II, thylakoid thiol/disulfide-modulating protein, PSII photochemical efficiency, *Arabidopsis thaliana*, *Synechocystis*

INTRODUCTION

Photosynthesis provides chemical energy for nearly all life forms on earth. In oxygenic photosynthesis, which occurs in cyanobacteria, algae, and land plants, photosynthetic electron transport and ATP synthesis requires Photosystem II (PSII), cytochrome b_6f, Photosystem I (PSI), ATP synthase, as well as mobile electron carriers such as plastoquinone and plastocyanin (Allen et al., 2011; Nickelsen and Rengstl, 2013). During the evolution from cyanobacteria to land plants, core components of the photosynthetic apparatus have been conserved (Allen et al., 2011; Nickelsen and Rengstl, 2013). For example, the core subunits of PSII in cyanobacteria, algae, and land plants are similar except for the composition of light harvesting complexes (LHCs) and oxygenic evolving complexes (OECs) (Hankamer et al., 2001; Allen et al., 2011; Nickelsen and Rengstl, 2013). The LHCs of cyanobacterial and red algal PSII supercomplexes are termed phycobilisomes and consist of three types of phycobiliproteins: allophycocyanin (APC), phycocyanin (PC), and phycoerythrin (PE) (Stadnichuk et al., 2015). These phycobiliproteins contain one or multiple cysteine residues. Phycobilisome chromophores allophycocyanobilin (APCB), phycocyanobilin (PCB), and phycoerythrobilin (PEB) are covalently attached to APC, PC, and PE subunits, respectively, via thioether bonds to conserved cysteine residues (Zhao et al., 2006). The LHCs of PSII (i.e., LHCII) in land plants consist of trimeric antenna proteins LHCB1 (LHCB stands for PSII light-harvesting chlorophyll *a*/*b*-binding protein), LHCB2, and LHCB3, as well as monomeric antenna proteins LHCB4, LHCB5, and LHCB6 (Ballottari et al., 2012). The OEC in cyanobacteria consists of five extrinsic proteins: PsbO, PsbP-like, PsbQ-like, PsbU, and PsbV (Hankamer et al., 2001; Thornton et al., 2004; Bricker et al., 2012). The OEC in green algae and land plants only has three proteins: PsbO, PsbP and PsbQ (Hankamer et al., 2001; Thornton et al., 2004; Bricker et al., 2012). PsbU and PsbV were lost during the evolution of green algae and land plants (Thornton et al., 2004).

Photosynthetic species are subject to a wide range of environmental stresses, such as drought, flood, high salinity, extreme temperature, and to the main interest of this work, suboptimal light intensities. In oxygenic photosynthetic organisms, a major consequence from high light exposure is damage to PSII core proteins, especially PSII reaction-center protein D1 (Demmig-Adams and Adams, 1992; Aro et al., 1993). To minimize photodamage and photoinhibition, photosynthetic organisms have evolved photoprotection and repair strategies, such as increased thermal dissipation [e.g., non-photochemical quenching (NPQ)] at the antennae level and accelerated PSII repair at the reaction-center level (Liu et al., 2019). NPQ mechanisms differ among cyanobacteria, algae, and land plants (Gorbunov et al., 2011; Kirilovsky and Kerfeld, 2016; Misumi et al., 2016). In land plants, the major NPQ component is energy-dependent quenching mediated by the xanthophyll cycle (Demmig-Adams and Adams, 1996). Algae have diverse antennae systems, thus different algal species have different mechanisms of energy-dependent quenching (Goss and Lepetit, 2015). Cyanobacteria do not have the xanthophyll cycle (Demmig-Adams et al., 1990; Campbell et al., 1998). NPQ in cyanobacteria is mediated by the orange carotenoid protein (OCP), a soluble stromal protein that acts as a homodimer (Kerfeld et al., 2003; Wilson et al., 2010; Gupta et al., 2019). Strong white (or blue-green) light was found to cause OCP photoactivation and binding to phycobilisomes, which induces OCP-mediated NPQ (Kirilovsky, 2007; Kirilovsky, 2015; Kirilovsky and Kerfeld, 2016). The N-terminal effector domain and the C-terminal regulator domain of monomeric OCP contain two and one cysteine residues, respectively; and the cysteine residue in the C-terminal domain was found to be critical for dimerization and activation of OCP (Moldenhauer et al., 2017; Muzzopappa et al., 2017). Although NPQ avoids photodamage and photoinhibition, it occurs at the cost of reduced photosynthetic efficiency. Thus, down regulation and fine tuning of NPQ is a target of improving photosynthetic efficiency (Berteotti et al., 2016; Kromdijk et al., 2016; Perozeni et al., 2019).

Unlike NPQ, major steps of the damage, repair, and reassembly cycle of PSII are highly conserved among cyanobacteria, algae, and land plants (Mulo et al., 2008; Nixon et al., 2010; Nickelsen and Rengstl, 2013; Nickelsen and Zerges, 2013; Rast et al., 2015; Lu, 2016). This process occurs under low or moderate light intensity as well, although at a slower speed (Aro et al., 1993; Foyer and Shigeoka, 2011). In brief, the inactive PSII complexes with photodamaged D1 are partially dissembled to facilitate the degradation of photodamaged D1 and the co-translational insertion of the nascent D1 protein. After the replacement of D1, the PSII complexes are re-assembled to restore function. It was proposed that folding, disassembly, and re-assembly of PSII proteins and complexes may involve transient formation and breakage of inter- and/or intra-molecular disulfide bonds between cysteine residues (Zhang and Aro, 2002; Shimada et al., 2007; Karamoko et al., 2011; Lu et al., 2011). Interestingly, a number of PSII proteins contain cysteine residues, including hydrophobic PSII core subunits D1, D2, CP43, and CP47, as well as hydrophilic OEC subunits PsbO, PsbP, and PsbQ (Shimada et al., 2007). Exploiting the PSII repair and reassembly cycle is another target of improving photosynthetic efficiency (Liu et al., 2019).

The elaborate PSII repair and reassembly cycle requires auxiliary proteins of different functions, such as D1 C-terminal processing, thiol/disulfide-modulating, peptidylprolyl isomeration, phosphorylation, and dephosphorylation (Mulo et al., 2008; Nixon et al., 2010; Nickelsen and Rengstl, 2013; Lu, 2016). Although some auxiliary proteins are unique to land plants, algae, or cyanobacteria, most auxiliary proteins exist ubiquitously in oxygenic photosynthetic organisms (Komenda et al., 2012; Nickelsen and Rengstl, 2013). One example of thiol/disulfide-modulating auxiliary proteins that exist ubiquitously in oxygenic phyotosynthetic organisms is Lumen Thiol Oxidoreductase 1 (LTO1). *Arabidopsis thaliana* LTO1 and its cyanobacterial homologs were found to catalyze disulfide bond formation in lumenal and lumen-exposed proteins, thus regulating PSII assembly and redox homeostasis (Singh et al., 2008a; Furt et al., 2010; Li et al., 2010; Feng et al., 2011; Karamoko et al., 2011; Lu et al., 2013). LTO1 contains an N-terminal vitamin K epoxide reductase (VKOR)-like domain with five transmembrane segments and a C-terminal thioredoxin-like domain. The thioredoxin-like domain in LTO1 was found to interact with lumen-exposed PSII OEC proteins PsbO1 and PsbO2 and a thylakoid lumenal

peptidyl-prolyl isomerase FKBP13 [FK506 (tacrolimus)-binding protein 13] (Karamoko et al., 2011; Lu et al., 2013). The LTO1 homolog in the green alga *Chlamodonas reinhardtii*, which is encoded by Cre12.g493150, has not been characterized (Nickelsen and Rengstl, 2013).

In comparison to algae and cyanobacteria, land plants are subject to more extensive high light stress, due to the difference in mobility and environmental conditions (Lu, 2011; Nickelsen and Rengstl, 2013; Wessendof, 2017). Aquatic algae and cyanobacteria can vary their depth in lakes and oceans to avoid the damaging effects of exposure to high light, while land plants do not have the capability of escaping. Land plants evolved additional thiol/disulfide-modulating proteins, such as CYO1/SCO2 (Shiyou1/Snowy Cotyledon2) (Shimada et al., 2007; Albrecht et al., 2008; Muranaka et al., 2012; Tanz et al., 2012) and LQY1 (Low Quantum Yield of PSII 1) (Lu, 2011; Lu et al., 2011), to aid in the repair and reassembly cycle of PSII. LQY1 homologs are present in land plants (e.g., AtLQY1 in *Arabidopsis thaliana*) but are not found in the sequenced genomes of aquatic algae and cyanobacteria, suggesting that LQY1 may play a role in plant adaptations to life on land (Lu, 2011). AtLQY1 is a small thylakoid zinc-finger protein with four CXXCXGXG repeats and an N-terminal transmembrane domain anchoring the protein to the thylakoid membrane from the stromal side (Lu et al., 2011). Inductively coupled plasma-mass spectrometry analysis of affinity-purified recombinant AtLQY1 protein showed that each LQY1 peptide contains two zinc ions, coordinately by the cysteine residues in four CXXCXGXG repeats (Lu et al., 2011). The zinc-finger domain of AtLQY1 also demonstrated protein disulfide isomerase activity (i.e., thiol/disulfide-modulating activity) towards thiol/disulfide-containing protein substrates. Thus, LQY1 was proposed to participate in folding, disassembly, and/or assembly of cysteine-containing PSII subunits in land plants (Lu, 2016).

Loss-of-function *Atlqy1* mutants were more sensitive to light stress than the wild type, had higher *NPQ* values, and accumulated more reactive oxygen species (ROS) than the wild type after the high light treatment (Lu et al., 2011). Under elevated light conditions, the *Atlqy1* mutants had fewer PSII-LHCII supercomplexes and lower PSII maximum efficiency than the wild type. In line with these observations, AtLQY1 was found to be associated with the PSII core monomer and the CP43-less PSII monomer (a marker for ongoing PSII repair and reassembly; Boehm et al., 2012). The proportion of PSII monomer-associated AtLQY1 increased substantially after prolonged high light treatment. Furthermore, cysteine-containing PSII core subunits CP47 and C43 were found to co-immunoprecipitate with the anti-AtLQY1 antibody. Therefore, it was concluded that LQY1 may regulate PSII repair and reassembly by forming transient disulfide bonds with cysteine-containing PSII subunits and regulate redox homeostasis by reducing ROS accumulation (Lu, 2011; Lu et al., 2011).

In this study, we introduced AtLQY1 into the model cyanobacterium *Synechocystis* sp. PCC6803 (*Synechocystis*), performed a series of biochemical and physiological assays on AtLQY1-expressing *Synechocystis*, and compared with the empty-vector control. We are particularly interested in knowing whether AtLQY1 expression improves PSII photochemical efficiency in *Synechocystis*.

MATERIALS AND METHODS

Introducing AtLQY1 Into *Synechocystis*

The coding sequence of full-length AtLQY1 ($AtLQY1^{1\text{-}154}$) (Lu et al., 2011) was amplified by PCR using primers Nde1_LQY1_F and Hpa1_LQY1_R (**Supplementary Table S1**). The resulting PCR product was AT-cloned into the pGEM-T Easy Vector and sequenced with primers M13_Forward and_M13 Reverse (**Supplementary Table S1**) to confirm the absence of PCR errors. Nde1/Hpa1-digested *AtLQY1* fragment was subcloned into the *Synechocystis* expression vector pSL2035. The resulting construct was sequenced to confirm correct insertion and absence of errors. Thirty milliliters of wild-type *Synechocystis* was grown continuously at 50 μmol photons m^{-2} s^{-1} to an optical density of 0.60 at 730 nm (i.e., OD_{730} = 0.60), in a 125-ml Erlenmeyer flask containing BG-11 liquid medium. To minimize cell damage, *Synechocystis* cells were gently harvested via centrifugation at 2,760 g for 10 min at 4°C. The cell pellet was washed twice with 5 ml of fresh BG-11 medium. The washed cell pellet was resuspended in 1.5 ml of fresh BG-11 medium. pSL2035-AtLQY1 and the empty pSL2035 vector constructs were mixed with *Synechocystis* cell suspensions to the concentration of 1 μg/ml in a 300-μl final volume. Cells were incubated at 28°C at 50 μmol photons m^{-2} s^{-1} for 5 h, and were gently inverted every hour. The resulting cultures were plated on a piece of autoclaved filter paper on BG-11 solid medium supplemented with 25 μg/ml kanamycin and examined for colonies in two weeks. Candidate transformants (colonies) were genotyped with the Nde1_LQY1_F forward primer and the psbA1d_100_down_R and psbA1d_200_down_R reverse primers (**Supplementary Table S1**) to ensure proper insertion of exogenous DNA. Confirmed transformants were streaked to fresh BG-11 plates supplemented with 50 μg/ml kanamycin to ensure a more homoplasmidic state.

Culture Growth Conditions

Synechocystis cultures transformed with pSL2035-AtLQY1 or the empty pSL2035 vector were grown in BG-11 liquid medium or on BG-11 plates supplemented with 25 μg/ml kanamycin (Varman, 2010; Eaton-Rye, 2011; Ermakova et al., 2016). All liquid cultures (30 ml) were grown in 125-ml Erlenmeyer flasks with a culture depth of 1 cm on a VWR mini shaker set at 140 rpm in a growth chamber (Percival). The temperature was set to 28°C and the light intensity set to 25 or 50 μmol photons m^{-2} s^{-1} at the surface of the flasks. The Percival reach-in chamber used in this study was equipped with a mixed array of fluorescent and incandescent lamps designed to produce a broader spectral range: eight 25-W T8 standard fluorescent tube light bulbs (Philips F25TB/TLB841) and four 100-W incandescent light bulbs (Westinghouse Commercial Service). For 25 and 50 μmol photons m^{-2} s^{-1} light intensities, six 25-W T8 standard fluorescent tube light bulbs and two 100-W incandescent light bulbs were used and the difference between two light intensities was achieved by adjusting the distance between the shelf and the light fixture. To ensure

uniform light quality and quantity, all bulbs were replaced before they reached the end of their lifetime. Solid cultures were grown on a growth station with similar growth conditions. Samples were collected from liquid cultures at the mid-log phase (OD_{730} = 0.50 to 0.70) for all downstream assays unless otherwise stated.

Total Protein Extraction

Mid-log phase *Synechocystis* cultures (10 ml) were harvested via centrifugation at 3,220 g for 20 min at 4°C. The pellets were resuspended in 400 µl of lysis buffer (0.1 M NaOH, 0.025 M EDTA, 2% SDS, 1 mM DTT) and incubated at 60°C for 10 min. The lysed cells were neutralized with 10 µl of 4 M acetic acid, and mixed thoroughly by vortexing for 30 s. The resuspended samples were centrifuged at 14,000 g for 2 min, after which the supernatant was collected. The total protein concentration in the supernatant was determined with the DC protein assay kit (Bio-Rad). Protein samples were diluted into an equal final total protein concentration (4 µg/ml) and an appropriate volume of 5X loading buffer (0.025 M EDTA, 0.25 M Tris-HCl, pH = 6.8, 50% glycerol, 39 mM DTT, 0.05% bromophenolblue) was added. The resulting protein samples were used for SDS-Urea-PAGE and immunoblot analysis.

SDS-Urea-PAGE and Immunoblot Analysis

Total protein samples were loaded on an equal culture OD_{730} basis and separated by SDS-Urea-PAGE (15% polyacrylamide, 6 M urea). Proteins were then transferred to a polyvinylidene difluoride membrane in a Trans-Blot electrophoresis transfer cell (Bio-Rad). The membrane was blocked in a blocking solution (5% nonfat dry milk, 0.1% Tween-20 in 1X Tris Buffered Saline), and then incubated in diluted antibody solutions (Lu et al., 2011). The anti-AtLQY1 antibody was made by Open Biosystems (Lu et al., 2011); the anti-PsaA, anti-D1 (C-terminus of D1), anti-D2, anti-APC, and anti-PC antibodies were purchased from Agrisera. Immunodetection was achieved with the SuperSignal west pico rabbit immunoglobulin G detecting kit (Thermo Fisher) and the Gel Logic 1500 Imaging System (Kodak), as described previously (Hackett et al., 2017).

Chlorophyll *a* and Carotenoid Content Measurements

Chlorophyll (Chl) *a* and carotenoids are extracted as previously described (Zavřel et al., 2015). In brief, *Synechocystis* cultures (1 ml) were harvested at an OD_{730} of ~0.7 via centrifugation at 15,000 g for 7 min at 4°C. The pellets were resuspended in 1 ml of pre-chilled (4°C) methanol. After 4-s vortexing to obtain homogenization, samples were incubated in the dark at 4°C for 20 min. To remove cell residues, samples were centrifuged at 15,000 g for 7 min at 4°C. The optical densities of the supernatants were measured at 470, 665, and 720 nm with a BioMate 3S spectrophotometer (Thermo Fisher). The Chl *a* content (µg/ml) was calculated as: $12.9447 * (OD_{665} - OD_{720})$ (Ritchie, 2006); the carotenoid content (µg/ml) was calculated as: $(1{,}000 * (OD_{470} - OD_{720}) - 2.86 * Chl\ a\ [\mu g/ml])/ 221$ (Wellburn, 1994). It should be noted that cyanobacteria such as *Synechocystis* do not produce Chl *b*.

Phycobilisome Pigment Measurements

The contents of phycobilisome pigments APCB, PCB, and PEB were determined as previously described (Hsieh et al., 2014), with some modifications explained in von der Haar (2007). Pellets from Chl *a* and carotenoid extraction were washed twice with 1 ml of 6 mM EDTA (pH 8.0). Washed pellets were resuspended with 50 µl of 6 mM EDTA (pH 8.0) and 700 µg/ml lysozyme, and incubated at 37°C for one hour with one shake at 30 min. Next, 50 µl of 4 M sodium hydroxide was added to each sample and all the samples were incubated at room temperature for 5 min. After re-pelleting, the supernatants were transferred to new centrifuge tubes and 100 µl of 1.5 M TRIS-HCl (pH 6.8) was added as a neutralizer to re-establish pigmentation of the samples. Samples were loaded on a 96-well flat bottom plate (Greiner). The optical densities of the samples were measured at 562 nm, 615 nm, and 652 nm on an Epoch microplate spectrophotometer (BioTek) equipped with the Gen5 software. APCB was calculated as: $(OD_{652} - 0.208 * OD_{615}) / 5.09$, PCB was calculated as: $(OD_{615} - 0.474 * OD_{652}) / 5.34$ and PEB was calculated as: $(OD_{652} - 2.41 * PCB\ [\mu g/ml] - 0.849 * APCB\ [\mu g/ml]) / 9.62$ (Hsieh et al., 2014).

Measurements of Fluorescence Parameters

Measurements of minimal fluorescence (F_o), maximal fluorescence (F_m), variable fluorescence (F_v), F_v/F_m (a relative measure of PSII maximum photochemical efficiency), light response curves of PSII operating efficiency (Φ_{PSII}), and electron transport rate (ETR_{PSII}) in *Synechocystis* cultures were performed as described previously (Sauer et al., 2001; Barthel et al., 2013), with minor modifications. *Synechocystis* cultures (2 ml) were harvested at an OD_{730} of ~0.7 and dark adapted for 5 min in the quartz cuvette of the DUAL-PAM-100 measuring system (Walz, Germany). Cultures were resuspended, exposed to a saturation pulse (2,000 µmol photons m^{-2} s^{-1}) to determine F_o and F_m of dark-adapted cultures, and then illuminated for 30 s at the following light intensities: 0, 8, 13, 20, 46, 82, 105, 161, 236, and 422 µmol photons m^{-2} s^{-1}. A saturation pulse (2,000 µmol photons m^{-2} s^{-1}) was applied at the end of each 30-s illumination to determine fluorescence parameters of illuminated cultures. F_v and F_v/F_m of dark-adapted cultures were calculated using the following equations: $F_v = F_m - F_o$; $F_v/F_m = (F_m - F_o)/F_m$. Φ_{PSII} was calculated using the following equation: $\Phi_{PSII} = (F_m' - F)/F_m'$, where F_m' and F are maximal and current fluorescence. ETR_{PSII} was calculated as: $\Phi_{PSII} * PAR * A_{culture} * Fraction_{PSII}$, where PAR is incident photosynthetic active radiation, $A_{culture}$ is the ratio of incident photons absorbed by cultures (0.84) and $Fraction_{PSII}$ is the ratio of absorbed photons distributed to PSII. Depending on the quality and intensity of growth light, the PSI:PSII ratio in cyanobacteria varies between 5:1 and 2:1 (Shen et al., 1993; Murakami et al., 1997; Luimstra et al., 2018). Under a growth light of 10-65 µmol photons m^{-2} s^{-1} with a broader spectral range, the PSI:PSII ratio is ~2.5:1 in *Synechocystis* (Fraser et al., 2013). Therefore, a $Fraction_{PSII}$ of 0.29 (i.e., 1/3.5) was used to calculate ETR_{PSII} in the empty-vector control grown at 25 µmol photons m^{-2} s^{-1}. The $Fraction_{PSII}$ of AtLQY1-expressing

Synechocystis grown at 25 and 50 μmol photons m^{-2} s^{-1} (0.34 and 0.27, respectively) and the empty-vector control grown at 50 μmol photons m^{-2} s^{-1} (0.25) was estimated from the abundance of the PsaA and D1 proteins.

NPQ Measurements

NPQ was measured with a DUAL-PAM-100 measuring system (Waltz), as described previously (Gorbunov et al., 2011). Cultures were harvested at an OD_{730} of ~0.7. After a 5-min dark adaption, cultures were resuspended, and a saturation pulse (2,000 μmol photons m^{-2} s^{-1}) was applied to determine F_o and F_m of dark-adapted cultures. Cultures were pre-illuminated under a measuring light of 2 μmol photons m^{-2} s^{-1} for 3 min, with saturating pulses at 30-s intervals. After the 3-min pre-illumination, blue actinic light (422 μmol photons m^{-2} s^{-1}) was applied for 8 min with saturating pulses at 20-s intervals. Recovery was monitored under a measuring light of 2 μmol photons m^{-2} s^{-1} for 18 min, with exponentially increasing intervals between saturating pulses. *NPQ* was calculated using the following equation: $(F_m - F_m')/F_m'$, where F_m is maximal fluorescence of dark-adapted cultures and F_m' is maximal fluorescence near the end of blue actinic illumination.

High Light Treatment

High light treatment was performed according to Singh et al. (2008b) with some modifications (Singh et al., 2008b). *Synechocystis* cultures used for high light experiments were grown in the Percival growth chamber at 50 μmol photons m^{-2} s^{-1} till mid-log phase (OD_{730} of ~0.7). Prior to the high light treatment, an aliquot (2 ml) of cultures was harvested and dark-adapted for chlorophyll fluorescent measurements of F_v/F_m. The remaining cultures were left in the growth chamber and the light intensity was increased to a moderately high intensity of 250 μmol photons m^{-2} s^{-1}, while all other conditions in the growth chamber remained constant. After the 90-min high light treatment, another aliquot (2 ml) of cultures was harvested and dark-adapted for F_v/F_m measurements.

ROS Measurements

The total amount of ROS was determined by using the ROS indicator 2',7'-dichlorodihydro fluorescin diacetate (DCHF-DA), as previously described (Singh and Montgomery, 2012; Lea-Smith et al., 2013). The DCHF-DA probe is cell permeable and becomes highly fluorescent when oxidized to dichloroflurescin (DCF) by intracellular ROS, such as H_2O_2, hydroxyl and peroxyl radicals, and peeroxynitrite (Kalyanaraman et al., 2012; Lea-Smith et al., 2013). *Synechocystis* cultures (3 ml) were harvested at an OD_{730} of ~0.7, twice washed and resuspended with 1X TES buffer (pH 8.2), to reduce background noise from BG-11 media. DCHF-DA was dissolved in N,N-dimethylformamide and added to appropriate cell samples at a final concentration of 50 μM. After a 30-min dark incubation, fluorescence in all samples was measured on a fluorescence spectrophotometer (Varian Cary Eclipse) with an excitation wavelength of 485 nm and emission wavelengths from 500 to 600 nm in a 96-well plate. Measurements were taken at four wavelengths (520 nm, 525 nm, 530 nm, and 535 nm) and were normalized to OD_{730}. TES buffer containing the DCHF-DA probe was used as the negative control; the positive control consisted of cells treated with 100 μM methyl viologen (Thomas et al., 1998). Fluorescence in cell samples not treated with DCHF-DA was subtracted from cells samples treated with DCHF-DA.

Transmission Electron Microscopy

Synechocystis cells were prepared for transmission electron microscopy (TEM) analysis as described in Tsang et al. (2013), with some modifications. *Synechocystis* cultures (30 ml) were harvested at an OD_{730} of ~0.7. Cells were gently pelleted by centrifugation at 2,000 g for 10 min at 4°C. The supernatant was removed and the cells were re-suspended in a fixative solution (formaldehyde/glutaraldehyde, 2.5% each in 0.1 M sodium cacodylate buffer, pH 7.4). After primary fixation, samples were washed with 0.1 M cacodylate buffer and postfixed with 1% osmium tetroxide in 0.1 M cacodylate buffer, dehydrated in a gradient series of acetone and infiltrated and embedded in Spurr's resin. 70-nm thin sections were obtained with a Power Tome Ultramicrotome (RMC Boeckeler Instruments) and post-stained with uranyl acetate and lead citrate. Images were taken with JEOL 100CX Transmission Electron Microscope (Japan Electron Optics Laboratory, Japan) at an accelerating voltage of 100 kV at the Michigan State University Center for Advance Microscopy.

Thylakoid membrane spacing distances were measured from the TEM images and calibrated with the pixel size of TEM images as described previously (Schindelin et al., 2012; Liberton et al., 2013; Majumder et al., 2017). Approximately three measurements were taken on each cell for ten cells per cell type per growth condition.

Accession Numbers

Sequences data of related genes/proteins can be found in the GenBank/EMBL databases under the following accession numbers: AtLQY1, At1g75690.

RESULTS

Expression of AtLQY1 in *Synechocystis*

To introduce AtLQY1 into *Synechocystis*, the coding region of full-length AtLQY1 (Lu, 2011; Lu et al., 2011) was subcloned into the *Synechocystis* expression vector pSL2035. The pSL2035 vector is designed to integrate a gene of interest into the *psbA1* gene site in the *Synechocystis* genome, using homologous double recombination. The *psbA1* gene site in wild-type *Synechocystis* is silent under most conditions (Varman, 2010). Expression of the gene of interest is controlled by the *PsbA2* promoter (Varman, 2010). The integration of the *PsbA2* promoter and the gene of interest to the *psbA1* gene site allows overexpression of the gene of interest without causing untargeted physiological effects. pSL2035-AtLQY1 and the empty pSL2035 vector were transformed into wild-type *Synechocystis*, as described previously (Varman, 2010; Varman et al., 2013). Candidate transformants were genotyped to confirm successful transformation and were streaked to fresh BG-11 plates supplemented with 50 μg/ml kanamycin to achieve

homoplasmidity. Before *Synechocystis* transformants were used in detailed phenotypic characterization, we tested the expression level of AtLQY1 with SDS-Urea-PAGE and immunoblot analysis. The result confirmed successful expression of AtLQY1 in *Synechocystis* transformants (**Figure 1A**). The AtLQY1 protein level in *Synechocystis* transformants grown at 50 μmol photons m^{-2} s^{-1} was significantly higher than that in *Synechocystis* transformants grown at 25 μmol photons m^{-2} s^{-1} (**Figure 1B**, **Supplementary Table S2**). This observation is consistent with the use of the light-inducible *psbA2* promoter to express the exogenous *AtLQY1* gene (Mohamed and Jansson, 1989; Lindberg et al., 2010).

Cell Counts in AtLQY1-Expressing *Synechocystis*

The cell count in AtLQY1-expressing *Synechocystis* and the empty-vector control was comparable at both growth light intensities (**Table 1**). As the growth light intensity increased from 25 to 50 μmol photons m^{-2} s^{-1}, the cell count in both AtLQY1-expressing *Synechocystis* and the empty-vector control doubled (**Table 1**).

Chl *a* and Carotenoid Contents in AtLQY1-Expressing *Synechocystis*

At a growth light of 25 μmol photons m^{-2} s^{-1}, AtLQY1-expressing *Synechocystis* and the empty-vector control had a similar Chl *a* content (**Table 1**). As the growth light intensity increased from 25 to 50 μmol photons m^{-2} s^{-1}, the Chl *a* content in the empty-vector control decreased significantly (20%), while the Chl *a* content in AtLQY1-expressing *Synechocystis* only slightly decreased (8%,). Consequently, the Chl *a* content in AtLQY1-expressing *Synechocystis* was slightly (11%) higher than that in the empty-vector control, at 50 μmol photons m^{-2} s^{-1} (**Table 1**).

At 25 μmol photons m^{-2} s^{-1}, AtLQY1-expressing *Synechocystis* and the empty-vector control had a similar carotenoid content (**Table 1**). As the growth light intensity increased from 25 to 50 μmol photons m^{-2} s^{-1}, the carotenoid content in the empty-vector control did not change. The carotenoid content in AtLQY1-expressing *Synechocystis* grown at 50 μmol photons m^{-2} s^{-1} increased slightly (19%) (**Table 1**). Carotenoids have been shown to protect photosynthetic apparatus from photo-oxidation, especially under elevated light intensities (Steiger et al., 1999).

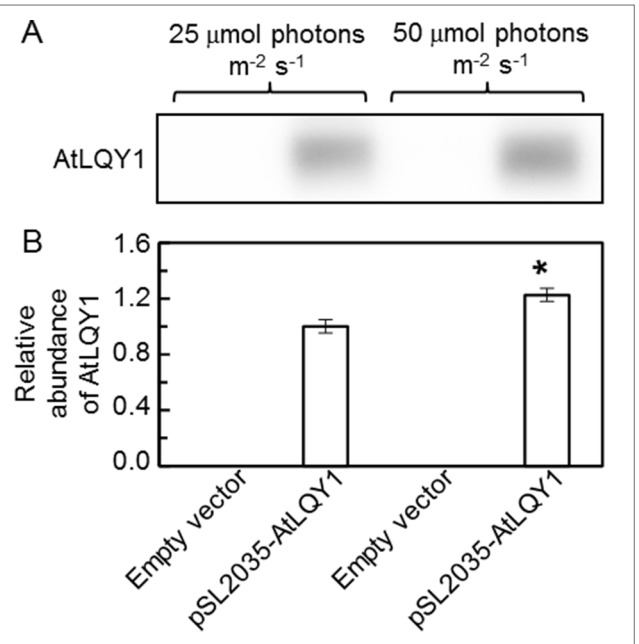

FIGURE 1 | Immunoblot analysis of AtLQY1 expression in *Synechocystis* cultures grown at 25 and 50 μmol photons m^{-2} s^{-1}. **(A)** Representative immunoblot of AtLQY1. Total protein samples were loaded on an equal culture OD_{730} basis. **(B)** Relative abundance of AtLQY1. Data are presented as mean ± SE (n = 4 independent biological replicates). The asterisks indicate significant differences between AtLQY1–expressing *Synechocystis* grown at 25 and 50 μmol photons m^{-2} s^{-1} (Student's *t*-test; *, $p < 0.05$).

Phycobilisome Pigment Contents in AtLQY1-Expressing *Synechocystis*

At a growth light of 25 μmol photons m^{-2} s^{-1}, the APCB pigment content in AtLQY1-expressing *Synechocystis* was significantly (25%) lower than that in the empty-vector control (**Table 1**). As the growth light intensity increased from 25 to 50 μmol photons m^{-2} s^{-1}, the APCB level in the empty-vector control and AtLQY1-expressing *Synechocystis* showed a 58% and 41% decrease, respectively (**Table 1**). Therefore, at 50 μmol photons m^{-2} s^{-1}, the APCB content in AtLQY1-expressing *Synechocystis* was similar to that in the empty-vector control (**Table 1**).

At 25 μmol photons m^{-2} s^{-1}, the PCB pigment content in AtLQY1-expressing *Synechocystis* was significantly (26%) lower than that in the empty-vector control (**Table 1**). As the growth light intensity increased from 25 to 50 μmol photons m^{-2} s^{-1}, the PCB level in the empty-vector control decreased slightly (13%) while the PCB level in AtLQY1-expressing *Synechocystis* increased slightly (15%). Thus, the PCB content in the empty-vector control and AtLQY1-expressing *Synechocystis* was comparable at 50 μmol photons m^{-2} s^{-1} (**Table 1**).

Compared to APCB and PCB, the level of PEB pigment in *Synechocystis* was much lower (Hsieh et al., 2014). At 25 μmol photons m^{-2} s^{-1}, the PEB content in AtLQY1-expressing *Synechocystis* was slightly (23%) lower than that in the empty-vector control (**Table 1**). As the growth light intensity increased from 25 to 50 μmol photons m^{-2} s^{-1}, the PE level in both AtLQY1-expressing *Synechocystis* and the empty-vector control became negligible (**Table 1**). These light-dependent changes in *Synechocystis* pigment contents (APCB, PCB, and PEB) have been observed in previous studies (Hsieh et al., 2014).

The PCB/APCB ratio is a good indicator of the rod lengths of phycobilisomes (Chenu et al., 2017). *Synechocystis* may change the PCB/APCB ratio as an adaption response to different light intensities (Chenu et al., 2017). Therefore, we calculated the PCB/APCB ratio for *Synechocystis* cultures grown at different light intensities (**Table 1**). AtLQY1-expressing *Synechocystis* and the empty-vector control had a PCB/APCB ratio of ~2.70 when grown at 25 μmol photons m^{-2} s^{-1} (**Table 1**). As the growth light intensity increased from 25 to 50 μmol photons m^{-2} s^{-1}, the PCB/APCB ratio in the empty-vector control and AtLQY1-expressing *Synechocystis* increased by 111% and 97%, respectively (**Table 1**). Consequently, the PCB/APCB ratio in AtLQY1-expressing *Synechocystis* was

TABLE 1 | Cell counts, pigment contents and chlorophyll fluorescence parameters.

Parameter	25 µmol photons m^{-2} s^{-1}		50 µmol photons m^{-2} s^{-1}	
	Empty vector	pSL2035-AtLQY1	Empty vector	pSL2035-AtLQY1
Cell count (10^6/ml)	1.40 ± 0.05^{B}	1.41 ± 0.13^{B}	2.76 ± 0.08^{A}	2.56 ± 0.07^{A}
Chl *a* (µg/ml)	4.14 ± 0.24^{A}	4.00 ± 0.25^{AB}	3.31 ± 0.32^{B}	3.69 ± 0.25^{AB}
Carotenoid (µg/ml)	1.79 ± 0.12^{A}	1.72 ± 0.12^{A}	1.74 ± 0.21^{A}	2.05 ± 0.11^{A}
Chl *a*/carotenoid	2.32 ± 0.06^{A}	2.33 ± 0.02^{A}	1.92 ± 0.06^{B}	1.79 ± 0.03^{B}
APCB (µg/ml)	21.65 ± 1.08^{A}	16.26 ± 1.81^{B}	9.05 ± 0.96^{C}	9.54 ± 0.92^{C}
PCB (µg/ml)	58.25 ± 1.63^{A}	43.18 ± 2.70^{B}	50.65 ± 3.93^{AB}	49.84 ± 3.37^{AB}
PEB (µg/ml)	3.66 ± 0.35^{A}	2.82 ± 0.64^{A}	Negligible	Negligible
PCB/APCB	2.70 ± 0.06^{B}	2.69 ± 0.19^{B}	5.70 ± 0.47^{A}	5.30 ± 0.39^{A}
F_v/F_m	0.261 ± 0.003^{B}	0.259 ± 0.008^{B}	0.281 ± 0.010^{B}	0.344 ± 0.007^{A}
F_o	0.154 ± 0.007^{B}	0.180 ± 0.013^{A}	0.110 ± 0.003^{C}	0.170 ± 0.003^{AB}
F_m	0.209 ± 0.010^{B}	0.243 ± 0.019^{AB}	0.153 ± 0.004^{C}	0.260 ± 0.008^{A}
F_v	0.055 ± 0.003^{BC}	0.063 ± 0.006^{B}	0.043 ± 0.002^{C}	0.090 ± 0.004^{A}
NPQ	0.695 ± 0.017^{A}	0.695 ± 0.020^{A}	0.562 ± 0.023^{B}	0.381 ± 0.010^{C}

Measurements for cell counts, pigment contents, and fluorescence parameters were performed on Synechocystis cultures grown at 25 and 50 µmol photons m^{-2} s^{-1}. Data are normalized to 1 ml of culture and are presented as mean ± SE (n = 3–4 independent biological replicates). Values not connected by the same letter are significantly different (Student's t-test, $p < 0.05$).

slightly (7%) lower than that in the empty-vector control at 50 µmol photons m^{-2} s^{-1} (**Table 1**). This suggests that AtLQY1-expressing *Synechocystis* may have slightly shorter phycobilisome rods than the empty-vector control, at 50 µmol photons m^{-2} s^{-1}.

AtLQY1-Expressing *Synechocystis* Had Significantly Higher F_v/F_m Than the Empty-Vector Control at 50 µmol Photons m^{-2} s^{-1}

To analyze whether expressing AtLQY1 in *Synechocystis* is beneficial to PSII, we determined F_v/F_m of dark-adapted cultures. At a growth light of 25 µmol photons m^{-2} s^{-1}, AtLQY1-expressing *Synechocystis* and the empty-vector control had similar F_v/F_m: 0.26 (**Table 1**). In cyanobacteria, the F_v/F_m value is typically ~0.3 instead of ~0.8 in higher plants. One reason for this difference is that cyanobacteria have very high PSI:PSII ratios (e.g., 2:1 to 5:1), while higher plants have a PSI:PSII ratio close to 1:1 (Shen et al., 1993; Murakami et al., 1997; Luimstra et al., 2018). Another reason is that fluorescence from phycobilisomes also contributes to F_o (Campbell et al., 1998). However, the fluorescence contribution from phycobilisomes to F_o is fairly constant during a measurement; thus, F_v/F_m is still a useful relative measure of PSII maximum photochemical efficiency in cyanobacteria, if neither the PSI:PSII ratio nor the phycobilisome amount is changed (Campbell et al., 1998). As the growth light intensity increased from 25 to 50 µmol photons m^{-2} s^{-1}, F_v/F_m in AtLQY1-expressing *Synechocystis* displayed a significant increase (33%). Consequently, F_v/F_m in AtLQY1-expressing *Synechocystis* was significantly (22%) higher than that in the empty-vector control, at a growth light of 50 µmol photons m^{-2} s^{-1} (**Table 1**). This observation suggests that AtLQY1 expression in *Synechocystis* is beneficial to PSII at 50 µmol photons m^{-2} s^{-1}.

A high F_v/F_m [$(F_v/F_m = (F_m - F_o)/F_m = 1 - F_o/F_m)$] value could be the result of a low F_o or a high F_v value. To identify the causal parameter(s) for increased F_v/F_m in AtLQY1-expressing *Synechocystis*, we determined F_o, F_m, and F_v of dark-adapted cultures. At a growth light of 25 µmol photons m^{-2} s^{-1}, the F_o, F_m, and F_v values in dark-adapted AtLQY1-expressing *Synechocystis* were approximately 15-17% higher than those in the dark-adapted empty-vector control (**Table 1**). Due to the coordinated increases in these three parameters, F_v/F_m in AtLQY1-expressing *Synechocystis* was similar to that in the empty-vector control, at 25 µmol photons m^{-2} s^{-1} (**Table 1**). At a growth light of 50 µmol photons m^{-2} s^{-1}, the F_o, F_m, and F_v values in dark-adapted AtLQY1-expressing *Synechocystis* were 55%, 70%, and 109% higher than those in the empty-vector control, respectively (**Table 1**). This suggests that the high F_v/F_m value in AtLQY1-expressing *Synechocystis* grown at 50 µmol photons m^{-2} s^{-1} is mostly the effect of high F_v. In cyanobacteria as well as land plants, F_v arises essentially from PSII; thus a higher F_v value is indicative of a high ability of PSII to perform primary photochemistry (Campbell et al., 1998; Baker et al., 2007).

We also subjected *Synechocystis* cultures grown at 50 µmol photons m^{-2} s^{-1} to a 90-min moderately high light treatment at 250 µmol photons m^{-2} s^{-1} and determined F_v/F_m before and after the high light treatment (**Figure 2**, **Supplementary Table S2**). We found that F_v/F_m in AtLQY1-expressing *Synechocystis* was significantly (~16%) higher than that in the empty-vector control before and after the high light treatment at 250 µmol photons m^{-2} s^{-1}. This suggests that AtLQY1-expressing *Synechocystis* outperforms the empty-vector control at higher growth light intensities.

AtLQY1-Expressing *Synechocystis* Grown at 50 µmol Photons m^{-2} s^{-1} Had Significantly Higher Φ_{PSII} and ETR_{PSII} Than the Empty-Vector Control Under High Measuring Light Intensities

To further investigate the benefits of AtLQY1 expression in *Synechocystis*, we determined the light response curves of Φ_{PSII} and ETR_{PSII} (**Figure 3**; **Supplementary Table S2**). AtLQY1-expressing *Synechocystis* and the empty-vector control grown at 25 µmol photons m^{-2} s^{-1} had no statistically significant difference in Φ_{PSII} or ETR_{PSII}, under all the measuring light intensities tested (**Figures 3A**, **C**). When grown at 50 µmol photons m^{-2} s^{-1}, AtLQY1-expressing *Synechocystis* and the empty-vector control

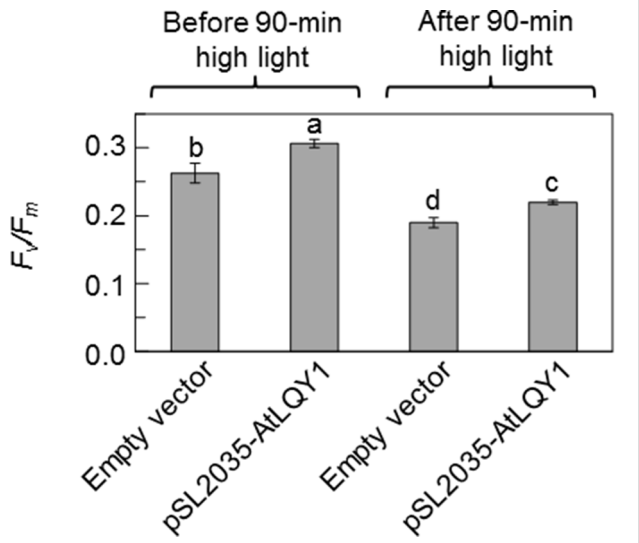

FIGURE 2 | F_v/F_m values before and after a 90-min moderately high light treatment at 250 µmol photons m^{-2} s^{-1}. Prior to high light the treatment, *Synechocystis* cultures were grown at 50 µmol photons m^{-2} s^{-1}. Data are presented as mean ± SE (n = 4 independent biological replicates). Values not connected by the same lowercase letter are significantly different (Student's *t*-test, $p < 0.05$).

had statistically similar Φ_{PSII} and ETR_{PSII} under low measuring light intensities, such as 8, 13, 20, and 46 µmol photons m^{-2} s^{-1} (**Figures 3B**, **D**). The initial slope of ETR_{PSII} light response curves is a measure of PSII antenna size, i.e., light harvesting capacity (Sauer et al., 2001; Yamazaki et al., 2005). The identical initial slope of the two ETR_{PSII} light response curves (**Figure 3D**) suggests that PSII antenna size in AtLQY1-expressing *Synechocystis* is similar to that in the empty-vector control. AtLQY1-expressing *Synechocystis* started to show slight but statistically insignificant advantages at the measuring light intensities of 82 µmol photons m^{-2} s^{-1} (**Figures 3B**, **D**). Under high measuring light intensities, i.e., 161, 236, and 422 µmol photons m^{-2} s^{-1}, AtLQY1-expressing *Synechocystis* displayed significantly higher Φ_{PSII} and ETR_{PSII} than the empty-vector control: Φ_{PSII} in AtLQY1-expressing *Synechocystis* was 21%, 35%, and 64% higher than that in the empty-vector control whereas ETR_{PSII} in AtLQY1-expressing *Synechocystis* was 32%, 45%, and 77% higher than that in the empty-vector control (**Figures 3B, D**). ETR_{PSII} in the empty-vector control plateaued at the measuring light of 236 µmol photons m^{-2} s^{-1} while ETR_{PSII} in AtLQY1-expressing *Synechocystis* continued to increase as the measuring light intensity increased. This indicates that AtLQY1-expressing *Synechocystis* devotes a higher percentage of excitation energy into photochemistry than the empty-vector control, under high light intensities.

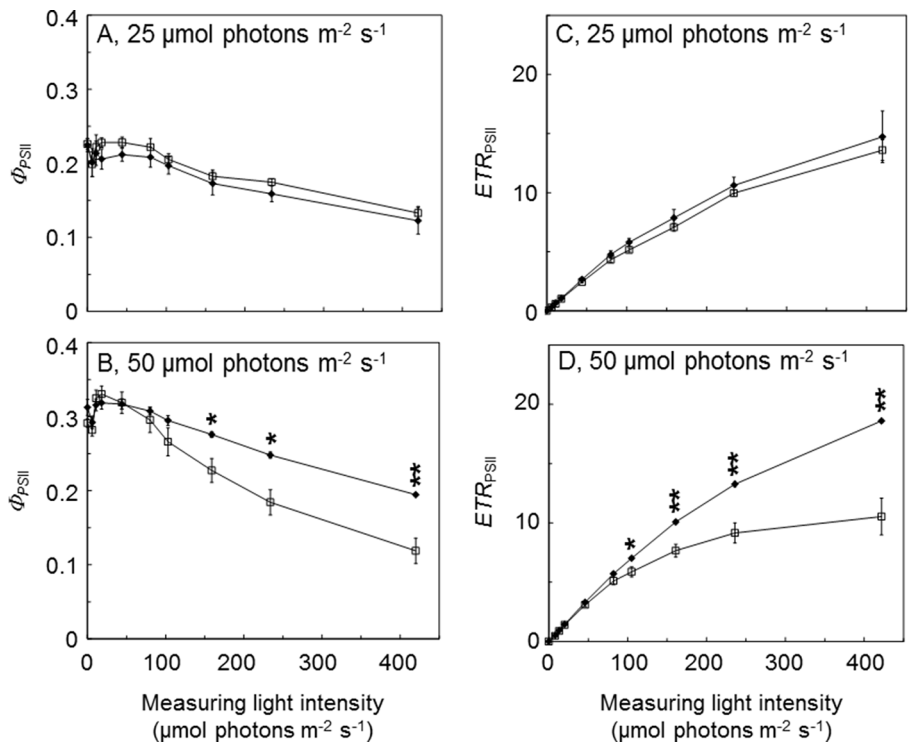

FIGURE 3 | Light response curves of PSII operating efficiency and electron transport rate. **(A**, **B)** Light response curves of PSII operating efficiency (Φ_{PSII}) in the empty-vector control (white squares) and AtLQY1-expressing *Synechocystis* (black diamonds) grown at 25 **(A)** and 50 **(B)** µmol photons m^{-2} s^{-1}. **(C**, **D)** Light response curves of PSII electron transport rate (ETR_{PSII}) in the empty-vector control and AtLQY1-expressing *Synechocystis* grown at 25 **(C)** and 50 **(D)** µmol photons m^{-2} s^{-1}. Initial cultures were started at an optical density of 0.05 at 730 nm. The light response curves were determined on mid-log phase cultures after a 5-min dark adaption. During the measurement, cultures were exposed for 30 s at a wide range of light intensities (0, 8, 13, 20, 46, 82, 105, 161, 236, and 422 µmol photons m^{-2} s^{-1}). Data are presented as mean ± SE (n = 4 independent biological replicates). Asterisks indicate significant differences between AtLQY1-expressing *Synechocystis* and the empty-vector control (Student's *t*-test; *, $p < 0.05$; **, $p < 0.01$).

AtLQY1-Expressing *Synechocystis* Had a Significantly Lower *NPQ* Value Than the Empty-Vector Control at 50 μmol Photons m^{-2} s^{-1}

In photosynthetic organisms, excess excitation energy can be coped with by mechanisms such as thermal dissipation (Campbell and Oquist, 1996; Campbell et al., 1998; Müller et al., 2001; Gorbunov et al., 2011; Jahns and Holzwarth, 2012; Kress and Jahns, 2017). Although cyanobacteria lack the xanthophyll-cycle-mediated energy-dependent quenching, they can regulate excitation energy via state transitions and NPQ, which is mediated by the orange carotenoid protein (Campbell and Oquist, 1996; Campbell et al., 1998; Gorbunov et al., 2011). Therefore, we measured NPQ in AtLQY1-expressing *Synechocystis* and the empty-vector control. At a growth light of 25 μmol photons m^{-2} s^{-1}, AtLQY1-expressing *Synechocystis* and the empty-vector control had a similar *NPQ* value (**Table 1**). Both AtLQY1-expressing *Synechocystis* and the empty-vector control displayed reduced *NPQ* values as the growth light intensity increased from 25 to 50 μmol photons m^{-2} s^{-1}. This concave dependence of *NPQ* on actinic light intensities has been previously reported in *Synechocystis* and other cyanobacterial species (Campbell and Oquist, 1996; Misumi et al., 2016; Ogawa and Sonoike, 2016; Misumi and Sonoike, 2017). As the growth light intensity increased from 25 to 50 μmol photons m^{-2} s^{-1}, *NPQ* in the empty-vector control showed a 19% reduction whereas AtLQY1-expressing *Synechocystis* displayed a 45% reduction. As a result, *NPQ* in AtLQY1-expressing *Synechocystis* was significantly (32%) lower than that in the empty-vector control, at a growth light of 50 μmol photons m^{-2} s^{-1} (**Table 1**). This observation suggests that AtLQY1 expression in *Synechocystis* may reduce NPQ at certain growth light conditions, such as 50 μmol photons m^{-2} s^{-1}.

AtLQY1-Expressing *Synechocystis* Had a Significantly Lower Amount of ROS Than the Empty-Vector Control at 50 μmol Photons m^{-2} s^{-1}

The light response curves of ETR_{PSII} suggested that AtLQY1-expressing *Synechocystis* allocates a higher ratio of excitation energy into photochemistry than the empty-vector control, under higher light intensities. It is commonly known that there is more oxidative damage to photosynthetic organisms at higher light intensities. This prompted us to measure the amount of ROS in *Synechocystis* cultures at both growth light intensities (**Figure 4**, **Supplementary Table S2**). At a growth light of 25 μmol photons m^{-2} s^{-1}, AtLQY1-expressing *Synechocystis* and the empty-vector control had a similar total ROS content (**Figure 4**). As the growth light intensity increased from 25 to 50 μmol photons m^{-2} s^{-1}, the amount of ROS in the empty-vector control increased significantly (32%) whereas the ROS content in AtLQY1-expressing *Synechocystis* did not change (**Figure 4**). Consequently, at a growth light of 50 μmol photons m^{-2} s^{-1}, the ROS level in AtLQY1-expressing *Synechocystis* was 16% lower than that in the empty-vector control (**Figure 4**). This observation suggests that AtLQY1 expression in *Synechocystis* may reduce ROS accumulation at certain growth light conditions, such as 50 μmol photons m^{-2} s^{-1}.

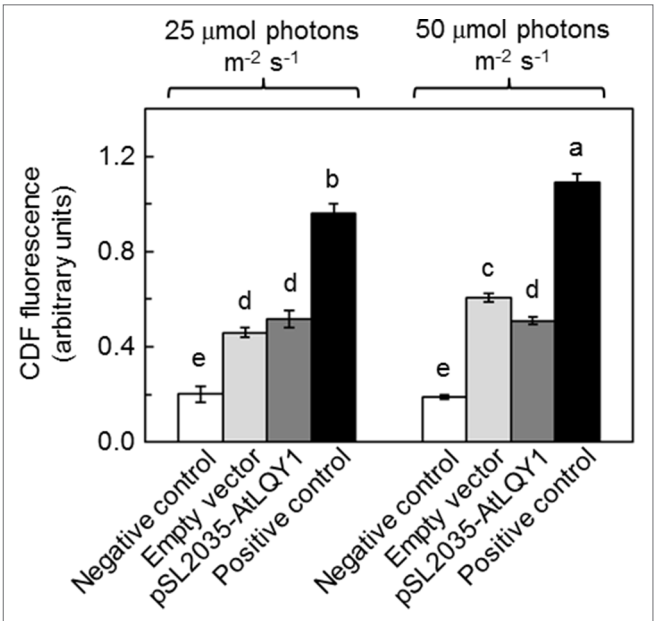

FIGURE 4 | Measurement of ROS accumulation in *Synechocystis* cultures grown at 25 and 50 μmol photons m^{-2} s^{-1}. Data are presented as mean ± SE (n = 4 independent biological replicates). Values not connected by the same lowercase letter are significantly different (Student's *t*-test, $p < 0.05$).

The Amounts of Cysteine-Containing Proteins in AtLQY1-Expressing *Synechocystis*

Recombinant AtLQY1 protein displayed thiol/disulfide-modulating activity towards thiol/disulfide-containing protein substrates (Lu et al., 2011). Therefore, we determined the amounts of representative cysteine-containing PSI and PSII core proteins in AtLQY1-expressing *Synechocystis* and the empty-vector control (**Figure 5**, **Supplementary Table S2**). PSI core protein PsaA in *Synechocystis* contains four cysteine residues. The abundance of PsaA in AtLQY1-expressing *Synechocystis* was statistically similar to that in the empty-vector control at both growth light intensities (**Figure 5B**). PSII core protein D1 in *Synechocystis* contains four cysteine residues. The abundance of D1 in AtLQY1-expressing *Synechocystis* was slightly (16%) higher than that in the empty-vector control under both growth light conditions (**Figure 5C**). This observation is consistent with the proposed role of AtLQY1 in the PSII repair and reassembly cycle. PSII core protein D2 in *Synechocystis* contains two cysteine residues. Interestingly, the amount of D2 was slightly higher than that in the empty-vector control under both growth light intensities: 33% higher at 25 μmol photons m^{-2} s^{-1} and 18% higher at 50 μmol photons m^{-2} s^{-1} (**Figure 5D**).

Phycobilisome proteins APC, PC, and PE also contain conserved cysteine residues, to which phycobilisome chromophores APCB, PCB, and PEB, are covalently attached (Zhao et al., 2006). Therefore, we determined the amounts of APC and PC proteins (**Figure 5**, **Supplementary Table S2**). The APC content in the empty-vector control and AtLQY1-expressing *Synechocystis* was similar at 25 μmol photons m^{-2} s^{-1} (**Figure 5E**). As the growth light intensity increased from 25 to 50 μmol photons m^{-2} s^{-1}, the APC level in

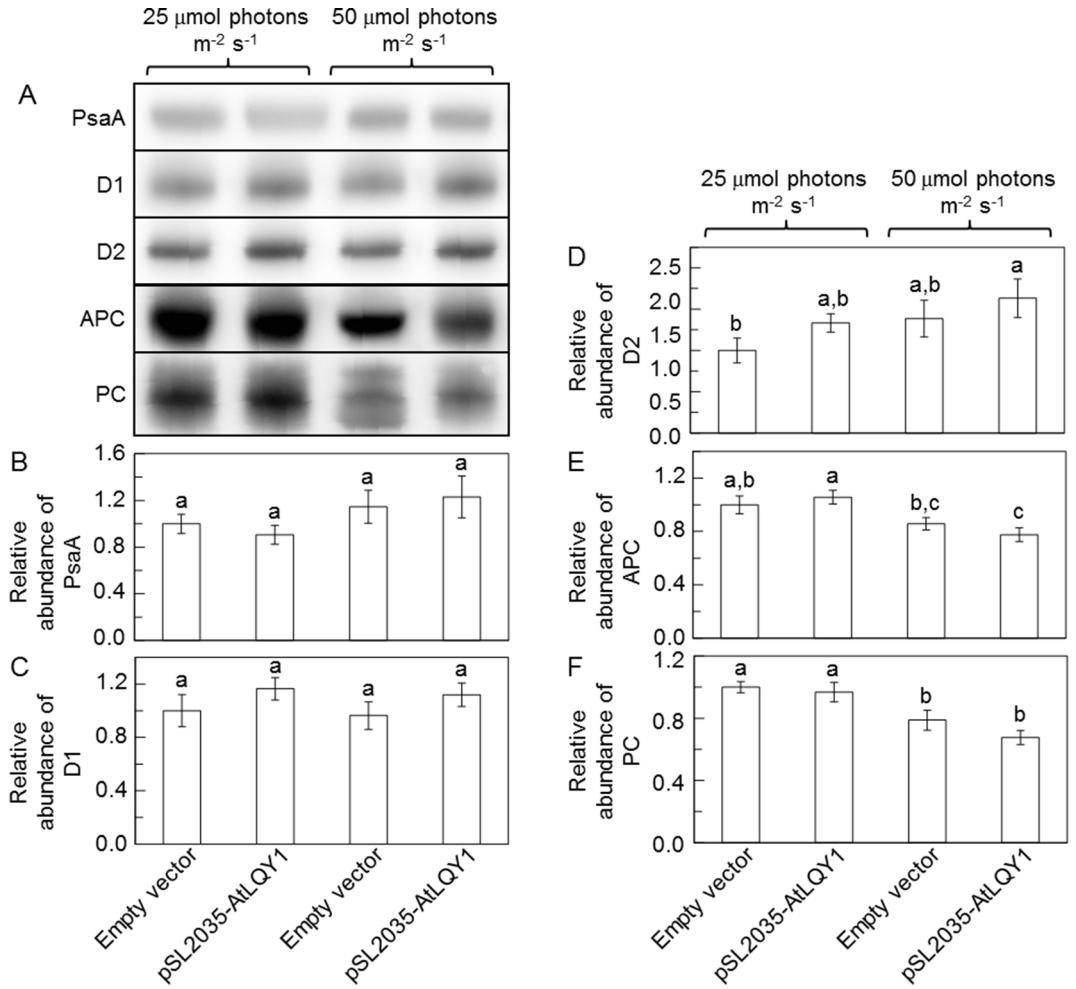

FIGURE 5 | Immunoblot analysis of protein abundances in *Synechocystis* cultures grown at 25 and 50 μmol photons m^{-2} s^{-1}. **(A)** Representative immunoblots of PSI core protein PsaA, PSII core proteins D1 and D2, and phycobilisome proteins APC and PC. Total protein samples were loaded on an equal culture OD_{730} basis. **(B–F)** Relative abundances of PsaA, D1, D2, APC, and PC proteins. Data are presented as mean ± SE (n = 3 independent biological replicates). Values not connected by the same lowercase letter are significantly different (Student's *t*-test, $p < 0.05$).

the empty-vector control and AtLQY1-expressing *Synechocystis* reduced by 14% and 27%, respectively (**Figure 5E**). Consequently, the APC amount in AtLQY1-expressing *Synechocystis* was slightly (10%) lower than that in the empty-vector control at 50 μmol photons m^{-2} s^{-1} (**Figure 5E**). The PC content displayed a similar pattern as APC (**Figure 5F**).

Thylakoid Structures of AtLQY1-Expressing *Synechocystis*

We analyzed thylakoid structures of AtLQY1-expressing *Synechocystis* and the empty-vector control with TEM (**Figure 6**). The overall cell morphology of AtLQY1-expressing *Synechocystis* and the empty-vector control was quite similar, with visible thylakoid membranes and carboxysomes, at both growth light intensities (**Figures 6A–D**). It was previously found that in cyanobacteria, thylakoid membrane spacing distance depends on the presence and size of extrinsic phycobilisomes and that light induces the expansion of thylakoid membrane spacing distance (Olive et al., 1997; Nagy et al., 2011; Collins et al., 2012; Liberton et al., 2013; Stingaciu et al., 2016; Majumder et al., 2017). Therefore, we measured thylakoid membrane spacing distances in TEM images of *Synechocystis* grown at different light intensities (**Figures 6E–H**). The empty-vector control grown at 25 μmol photons m^{-2} s^{-1} had an average thylakoid membrane spacing distance of 475 ± 10 Å (i.e., 47.5 ± 1.0 nm) (**Figure 6I**, **Supplementary Table S2**), which is comparable to wild-type *Synechocystis* grown under the same conditions (white light at 25 μmol photons m^{-2} s^{-1}) (Liberton et al., 2013). AtLQY1-expressing *Synechocystis* grown at 25 μmol photons m^{-2} s^{-1} had an average thylakoid membrane spacing distance of 494 ± 11 Å, statistically similar to the empty-vector control (**Figure 6I**). As the growth light intensity increased from 25 to 50 μmol photons m^{-2} s^{-1}, the thylakoid membrane spacing distance in the empty-vector control and AtLQY1-expressing *Synechocystis* increased by 18% and 6% respectively, both of which are statistically significant (**Figure 6I**). Consequently, at a growth light intensity of 50 μmol photons m^{-2} s^{-1}, the thylakoid membrane spacing distance in AtLQY1-expressing *Synechocystis*

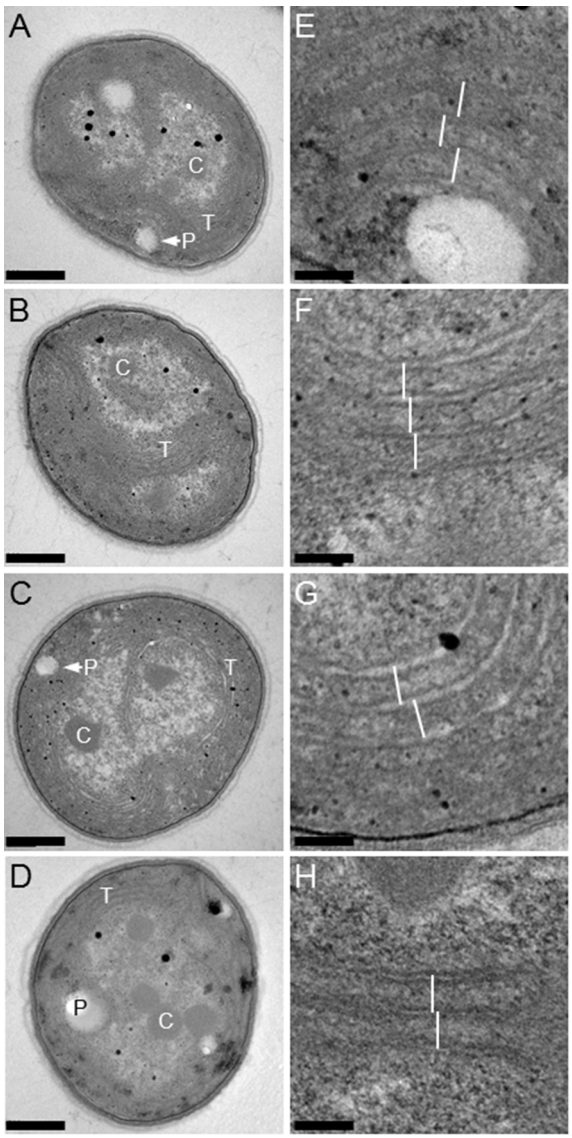

FIGURE 6 | Continued

FIGURE 6 | Transmission electron micrographs of the empty-vector control and AtLQY1-expressing *Synechocystis*. **(A–D)** Whole cell images of the empty-vector control **(A, C)** and AtLQY1-expressing *Synechocystis* **(B**, **D)** grown at 25 **(A**, **B)** and 50 **(C**, **D)** µmol photons m^{-2} s^{-1}. C, carboxysomes; P, polyphosphate bodies or holes left by polyphosphate bodies; T, thylakoid membranes. Scale bars in A-D: 400 nm. **(E–H)** Enlargements of the empty-vector control **(E**, **G)** and AtLQY1-expressing *Synechocystis* **(F**, **H)** grown at 25 **(E**, **F)** and 50 **(G**, **H)** µmol photons m^{-2} s^{-1}. White lines depict thylakoid membrane spacing distances. Scale bars in **E–H**: 80 nm. **(I)** Thylakoid membrane spacing distances. Data are presented as mean ± SE (n = 30 independent biological replicates). Values not connected by the same lowercase letter are significantly different (Student's *t*-test, $p < 0.05$).

was significantly (6%) lower than that in the empty-vector control (**Figure 6I**). This observation suggests that AtLQY1 expression in *Synechocystis* may reduce light-induced expansion of thylakoid membrane spacing distance at certain growth light conditions, such as 50 µmol photons m^{-2} s^{-1}. This is consistent with the slightly lower PCB/APCB ratio, which is indicative of phycobilisome rod lengths, in AtLQY1-expressing *Synechocystis* grown at 50 µmol photons m^{-2} s^{-1} (**Table 1**).

DISCUSSION

Measurements of different photosynthetic parameters consistently showed that AtLQY1 expression improves PSII photochemical efficiency in *Synechocystis* cells grown at 50 µmol photons m^{-2} s^{-1}. In higher plants, F_v/F_m is well established as the indicator of the maximum quantum efficiency of PSII photochemistry (Campbell et al., 1998; Baker et al., 2007). In cyanobacteria, F_v/F_m is still a useful relative measure of the maximum photochemical efficiency of PSII (Campbell et al., 1998; Sauer et al., 2001). When grown at 50 µmol photons m^{-2} s^{-1}, AtLQY1-expressing *Synechocystis* had significantly (22%) higher F_v/F_m than the empty-vector control (**Table 1**), suggesting that introducing AtLQY1 into *Synechocystis* may increase the maximum photochemical efficiency of PSII. At 50 µmol photons m^{-2} s^{-1}, the amount of PSII core protein D1 increased in AtLQY1-expressing *Synechocystis* by ~16% (**Figure 5C**), while the amount of PSI core protein PsaA remained relatively unchanged (**Figure 5B**). Therefore, the increase in F_v/F_m most likely comes from the increased amount of PSII. Further analysis of chlorophyll fluorescence parameters showed that AtLQY1-expressing *Synechocystis* grown at 50 µmol photons m^{-2} s^{-1} also had higher F_v than the empty-vector control. In both cyanobacteria and land plants, F_v comes mostly from PSII (Campbell et al., 1998; Baker et al., 2007); thus, the increase of PSII relative to PSI can explain the increase of F_v/F_m and also of F_v. In oxygenic photosynthetic organisms such as plants, algae, and cyanobacteria, Φ_{PSII} and ETR_{PSII} estimate the efficiency of PSII photochemistry and the rate of non-cyclic electron transport through PSII at given light intensities (Sauer et al., 2001; Baker et al., 2007; Barthel et al., 2013). Interestingly, AtLQY1-expressing *Synechocystis* grown at 50 µmol photons m^{-2} s^{-1} also had higher Φ_{PSII} and ETR_{PSII} than the empty-vector control, at high measuring light intensities (e.g., 161-422 µmol photons m^{-2} s^{-1}, **Figure 3**). This suggests that AtLQY1 expression in *Synechocystis* may improve PSII operating efficiency and electron transport rate under higher light intensities. AtLQY1-expressing *Synechocystis* grown at 50 µmol

photons m^{-2} s^{-1} was also found to have lower *NPQ* and ROS levels than the corresponding empty-vector control (**Table 1**, **Figure 4**). This indicates that AtLQY1 expression in *Synechocystis* may reduce NPQ and ROS accumulation at certain light intensities, such as 50 μmol photons m^{-2} s^{-1}.

Many phenotypic advantages of AtLQY1-expressing *Synechocystis* grown at 50 μmol photons m^{-2} s^{-1} were not seen when the *Synechocystis* cells were grown at 25 μmol photons m^{-2} s^{-1}. According to Trautmann et al. (2016), the growth of S*ynechocystis* transits from light-limited to light-saturated at around 46 μmol photons m^{-2} s^{-1}. When the light intensity is below 46 μmol photons m^{-2} s^{-1}, S*ynechocystis* growth is light-limited and the growth rate is proportional directly to the light intensity (Trautmann et al., 2016). When the light intensity exceeds 46 μmol photons m^{-2} s^{-1}, S*ynechocystis* growth transits to light-saturated (Trautmann et al., 2016). Consistent with these findings, AtLQY1-expressing *Synechocystis* grown at 50 μmol photons m^{-2} s^{-1} displayed advantages in PSII operating efficiency and electron transport rate (**Figures 3B, D**). Taken together, although AtLQY1 expression does not improve the efficiency of PSII photochemistry of S*ynechocystis* under light-limited conditions, it significantly improves PSII photochemical efficiency, when the light intensity exceeds the threshold value of 46 μmol photons m^{-2} s^{-1}.

As discussed above, AtLQY1-expressing *Synechocystis* had significantly higher F_v, F_v/F_m, Φ_{PSII}, and ETR_{PSII}, lower *NPQ* and ROS levels, and a shorter thylakoid membrane spacing distance than the empty-vector control, when grown at 50 μmol photons m^{-2} s^{-1}. It is possible that AtLQY1 exerts these effects by participating in the folding, disassembly, and assembly of cysteine-containing PSII subunits, and reducing ROS accumulation. Consistent with this possibility, AtLQY1-expressing *Synechocystis* had a slightly higher amount of cysteine-containing PSII core protein D1 as well as an opposite phenotype of loss-of-function Arabidopsis mutants of AtLQY1, which was proposed to assist in the repair and reassembly cycle of PSII and redox homeostasis in Arabidopsis (Lu, 2011; Lu et al., 2011). It's possible that AtLQY1 exerts these effects by reducing OCP-mediated NPQ, potentially via modulating the redox status of thiol-containing cysteine residues in OCP homodimers. In line with this possibility, AtLQY1-expressing *Synechocystis* had a lower *NPQ* value than the empty-vector control, when grown at 50 μmol photons m^{-2} s^{-1}. AtLQY1 may also influence phycobilisome assembly, and/or association between phycobilisome proteins and their respective chromophores. Consistent with this possibility, AtLQY1-expressing *Synechocystis* had a shorter thylakoid membrane spacing distance and a slightly lower PCB/APCB ratio (indicative of shorter phycobilisome rod lengths) than the empty-vector control, when grown at 50 μmol photons m^{-2} s^{-1}. Further studies are needed to unveil the mechanisms behind the observed phenotypes, in AtLQY1-expressing *Synechocystis*.

Photochemistry, NPQ, and photoinhibition are competing processes in photosynthetic organisms (Arsalane et al., 1994; Horton et al., 1996; Müller et al., 2001; Lambrev et al., 2012; Berteotti et al., 2016; Pathak et al., 2019). NPQ evolved as a photoprotective mechanism to minimize photodamage and photoinhibition. Therefore, reductions in NPQ are often associated with increases in ROS accumulation. For example, NPQ in green algae is mediated by LHC-like proteins known as LHCSRs (Bonente et al., 2011; Berteotti et al., 2016; Correa-Galvis et al., 2016; Tibiletti et al., 2016; Perozeni et al., 2019). Disruption of all three *lhcsr* genes resulted in enhanced ROS production (Berteotti et al., 2016; Perozeni et al., 2019). However, enhanced ROS accumulation can also be accompanied by increases in NPQ. For example, loss-of-function *Atlqy1* and *hypersensitive to high light1* (*hhl1*) Arabidopsis mutants displayed simultaneous increases in NPQ and ROS under high light conditions (Lu, 2011; Lu et al., 2011; Jin et al., 2014). Therefore, it is conceivable to observe simultaneous decreases in NPQ and ROS in AtLQY1-expressing *Synechocystis.* Furthermore, because NPQ reduces photodamage and photoinhibition at the cost of reduced photosynthetic efficiency, down regulation of NPQ was recently found to be a suitable strategy to improve photosynthetic efficiency in land plants and green algae (Berteotti et al., 2016; Kromdijk et al., 2016; Perozeni et al., 2019).

Synechocystis has a set of endogenous chloroplastic thiol/disulfide-modulating proteins (Nixon et al., 2010; Mulo et al., 2012; Nickelsen and Rengstl, 2013; Lu, 2016). Loss-of-function mutations in genes encoding these chloroplastic thiol/disulfide-modulating proteins were found to have pleiotropic effects, e.g., reductions in F_v/F_m, increases in NPQ, increased photoinhibition, enhanced ROS accumulation, and deficiencies in the assembly and stability of photosynthetic apparatus (Karamoko et al., 2011; Calderon et al., 2013; Wang et al., 2013). One example is thylakoid membrane-anchored LTO1 (encoded by slr0565 in *Synechocystis*). As mentioned in the introduction, *Synechocystis* and *Arabidopsis* homologs of this protein were reported to catalyze disulfide bond formation in lumenal and lumen-exposed proteins, such as FKBP13, PsbO1, and PsbO2 (Singh et al., 2008a; Furt et al., 2010; Li et al., 2010; Feng et al., 2011; Karamoko et al., 2011; Lu et al., 2013). The *lto1* mutant showed reduced F_v/F_m, increased NPQ, increased photoinhibition, and deficient PSII assembly (Karamoko et al., 2011). A second example is thylakoid membrane-anchored rubredoxin 1 (RBD1, encoded by slr2033 in *Synechocystis*). *Synechocystis*, *Chlamodonas reinhardtii*, and *Arabidopsis* homologs of this protein were found to be necessary for PSII activity and were therefore proposed to play a role in promoting PSII assembly and stability (Calderon et al., 2013). The *rbd1* mutant displayed very low F_v/F_m and severely impaired PSII accumulation (Calderon et al., 2013). A third example is chloroplast stromal m-type thioredoxin (trx-M, encoded by slr0623 in *Synechocystis*). Although the role of *Synechocystis* trx-M in PSII assembly and repair has not been reported, its Arabidopsis homologs (TRX-M1, TRX-M2, and TRX-M4) were found to participate in the assembly of CP47 into PSII (Cain et al., 2009; Wang et al., 2013). Disruption of all three *trx-m* genes resulted in reduced F_v/F_m, increased NPQ, enhanced ROS production, and reduced PSII stability (Wang et al., 2013). Therefore, it is conceivable to observe that AtLQY1 expression in *Synechocystis* had pleiotropic effects (e.g., increased F_v/F_m, Φ_{PSII}, and ETR_{PSII}, reduced NPQ, and decreased ROS content).

Unlike LQY1, these three thiol/disulfide-modulating proteins are present ubiquitously in cyanobacteria, algae, and land plants (Lu, 2016). It is interesting that introducing AtLQY1, an Arabidopsis thylakoid membrane-anchored thiol/disulfide-modulating protein, into *Synechocystis*, which contains three endogenous chloroplastic

thiol/disulfide-modulating proteins, is still beneficial to the organism. One possibility is that these four proteins target different thiol/disulfide-containing proteins, depending on the locations of these thiol/disulfide-modulating proteins in the chloroplast. For instance, LTO1 may target lumenal and lumen-exposed thiol/disulfide–containing proteins (Singh et al., 2008a; Furt et al., 2010; Li et al., 2010; Feng et al., 2011; Karamoko et al., 2011; Lu et al., 2013); Trx-M may target soluble thiol/disulfide–containing proteins in the chloroplast stroma (Cain et al., 2009; Wang et al., 2013). In Arabidopsis, LQY1 is a thylakoid membrane protein with its N-terminal transmembrane domain anchored in thylakoid membranes and its C-terminal zinc-finger domain in the stroma (Lu et al., 2011). Therefore, LQY1 has the potential to target thiol/disulfide–containing proteins in thylakoid membranes and stroma in land plants. Although further studies are needed to determine the subcellular location of AtLQY1 in AtLQY1-expressing *Synechocystis*, the amphipathic property of this protein suggests that AtLQY1 may target both membrane and soluble proteins.

To sum up, this study showed that introducing a land plant-derived thylakoid thiol/disulfide-modulating protein, AtLQY1, into a cyanobacterium significantly improved overall PSII efficiency of the organism. Cyanobacteria have great potential as biofuel producers, making efforts to enhance the productivity of these organisms is valuable to society (Machado and Atsumi, 2012; Nozzi et al., 2013; Varman et al., 2013; Allahverdiyeva et al., 2014; Lea-Smith and Howe, 2017; Cheregi et al., 2019). Introducing LQY1, or other land plant-derived thiol/disulfide-modulating proteins, may be a strategy to optimize cyanobacterial growth under light-saturated conditions.

DATA AVAILABILITY STATEMENT

The datasets generated for this study are available on request to the corresponding author.

AUTHOR CONTRIBUTIONS

RW performed the experiments, analyzed the data, and edited the manuscript. YL conceived the project, analyzed the data, and wrote and edited the manuscript.

FUNDING

This work was financially supported by the U.S. National Science Foundation (grant number MCB-1244008) and the Western Michigan University Faculty Research and Creative Activities Award (grant number W2016-023).

ACKNOWLEDGMENTS

The authors thank Himadri B. Pakrasi, Yinjie J. Tang, and Arul M. Varman at the Washington University for sharing the pSL2035 vector; Beronda Montgomery at Michigan State University for sharing the wild-type *Synechocystis* sp. PCC6803 strain and comments on TEM images; Alicia Withrow at Michigan State University for TEM sample preparation and imaging; James P. O'Donnell, Manasa B. Satyanarayan, Amy T. Kobylarz, and Sianoush B. Fereidani for technical assistance; Christopher D. Jackson for growth chamber management; and Todd J. Barkman, Jian Yao, and Silvia Rossbach for comments on experimental design.

SUPPLEMENTARY MATERIAL

The Supplementary Material for this article can be found online at: https://www.frontiersin.org/articles/10.3389/fpls.2019.01284/full#supplementary-material

REFERENCES

Albrecht, V., Ingenfeld, A., and Apel, K. (2008). *Snowy cotyledon 2*: the identification of a zinc finger domain protein essential for chloroplast development in cotyledons but not in true leaves. *Plant Mol. Biol.* 66, 599–608. doi: 10.1007/s11103-008-9291-y

Allahverdiyeva, Y., Aro, E. M., and Kosourov, S. N. (2014). "Chapter 21 - Recent developments on cyanobacteria and green algae for biohydrogen photoproduction and its importance in CO2 reduction," in *Bioenergy Research: Advances and Applications*. Eds. V. K. Gupta, M. G. Tuohy, C. P. Kubicek, J. Saddler, and F. Xu (Amsterdam: Elsevier), 367–387. doi: 10.1016/B978-0-444-59561-4.00021-8

Allen, J. F., de Paula, W. B., Puthiyaveetil, S., and Nield, J. (2011). A structural phylogenetic map for chloroplast photosynthesis. *Trends Plant Sci.* 16, 645–655. doi: 10.1016/j.tplants.2011.10.004

Aro, E. M., McCaffery, S., and Anderson, J. M. (1993). Photoinhibition and D1 protein degradation in peas acclimated to different growth irradiances. *Plant Physiol.* 103, 835–843. doi: 10.1104/pp.103.3.835

Arsalane, W., Rousseau, B., and Duval, J.-C. (1994). Influence of the pool size of the xanthophyll cycle on the effects of light stress in a diatom: competition between photoprotection and photoinhibition. *Photochem. Photobiol.* 60, 237–243. doi: 10.1111/j.1751-1097.1994.tb05097.x

Baker, N. R., Harbinson, J., and Kramer, D. M. (2007). Determining the limitations and regulation of photosynthetic energy transduction in leaves. *Plant Cell Environ.* 30, 1107–1125. doi: 10.1111/j.1365-3040.2007.01680.x

Ballottari, M., Girardon, J., Dall'Osto, L., and Bassi, R. (2012). Evolution and functional properties of Photosystem II light harvesting complexes in eukaryotes. *Biochim. Biophys. Acta* 1817, 143–157. doi: 10.1016/j.bbabio.2011.06.005

Barthel, S., Bernát, G., Seidel, T., Rupprecht, E., Kahmann, U., and Schneider, D. (2013). Thylakoid membrane maturation and PSII activation are linked in greening *Synechocystis* sp. PCC 6803 cells. *Plant Physiol.* 163, 1037–1046. doi: 10.1104/pp.113.224428

Berteotti, S., Ballottari, M., and Bassi, R. (2016). Increased biomass productivity in green algae by tuning non-photochemical quenching. *Sci. Rep.* 6, 21339. doi: 10.1038/srep21339

Boehm, M., Yu, J., Reisinger, V., Beckova, M., Eichacker, L. A., Schlodder, E., et al. (2012). Subunit composition of CP43-less Photosystem II complexes of *Synechocystis* sp. PCC 6803: implications for the assembly and repair of Photosystem II. *Phil. Trans. R. Soc. B* 367, 3444–3454. doi: 10.1098/rstb.2012.0066

Bonente, G., Ballottari, M., Truong, T. B., Morosinotto, T., Ahn, T. K., Fleming, G. R., et al. (2011). Analysis of LhcSR3, a protein essential for feedback de-excitation in the green alga *Chlamydomonas reinhardtii*. *PLoS Biol.* 9, e1000577. doi: 10.1371/journal.pbio.1000577

Bricker, T. M., Roose, J. L., Fagerlund, R. D., Frankel, L. K., and Eaton-Rye, J. J. (2012). The extrinsic proteins of Photosystem II. *Biochim. Biophys. Acta* 1817, 121–142. doi: 10.1016/j.bbabio.2011.07.006

Cain, P., Hall, M., Schroder, W. P., Kieselbach, T., and Robinson, C. (2009). A novel extended family of stromal thioredoxins. *Plant Mol. Biol.* 70, 273–281. doi: 10.1007/s11103-009-9471-4

Calderon, R. H., García-Cerdán, J. G., Malnoë, A., Cook, R., Russell, J. J., Gaw, C., et al. (2013). A conserved rubredoxin is necessary for Photosystem II accumulation in diverse oxygenic photoautotrophs. *J. Biol. Chem.* 288, 26688–26696. doi: 10.1074/jbc.M113.487629

Campbell, D., and Oquist, G. (1996). Predicting light acclimation in cyanobacteria from nonphotochemical quenching of photosystem II fluorescence, which reflects state transitions in these organisms. *Plant Physiol.* 111, 1293–1298. doi: 10.1104/pp.111.4.1293

Campbell, D., Hurry, V., Clarke, A. K., Gustafsson, P., and Öquist, G. (1998). Chlorophyll fluorescence analysis of cyanobacterial photosynthesis and acclimation. *Microbiol. Mol. Biol. Rev.* 62, 667–683.

Chenu, A., Keren, N., Paltiel, Y., Nevo, R., Reich, Z., and Cao, J. (2017). Light adaptation in phycobilisome antennas: influence on the rod length and structural arrangement. *J. Phys. Chem. B* 121, 9196–9202. doi: 10.1021/acs.jpcb.7b07781

Cheregi, O., Ekendahl, S., Engelbrektsson, J., Stromberg, N., Godhe, A., and Spetea, C. (2019). Microalgae biotechnology in Nordic countries - the potential of local strains. *Physiol. Plant.* 166, 438–450. doi: 10.1111/ppl.12951

Collins, A. M., Liberton, M., Jones, H. D. T., Garcia, O. F., Pakrasi, H. B., and Timlin, J. A. (2012). Photosynthetic pigment localization and thylakoid membrane morphology are altered in *Synechocystis* 6803 phycobilisome mutants. *Plant Physiol.* 158, 1600–1609. doi: 10.1104/pp.111.192849

Correa-Galvis, V., Redekop, P., Guan, K., Griess, A., Truong, T. B., Wakao, S., et al. (2016). Photosystem II subunit PsbS is involved in the induction of LHCSR protein-dependent energy dissipation in *Chlamydomonas reinhardtii*. *J. Biol. Chem.* 291, 17478–17487. doi: 10.1074/jbc.M116.737312

Demmig-Adams, B., Adams, W. W., Czygan, F. C., Schreiber, U., and Lange, O. L. (1990). Differences in the capacity for radiationless energy dissipation in the photochemical apparatus of green and blue-green algal lichens associated with differences in carotenoid composition. *Planta* 180, 582–589. doi: 10.1007/BF02411457

Demmig-Adams, B., and Adams, W. W. (1992). Photoprotection and other responses of plants to high light stress. *Annu. Rev. Plant Physiol. Plant Mol. Biol.* 43, 599–626. doi: 10.1146/annurev.pp.43.060192.003123

Demmig-Adams, B., and Adams, W. W. (1996). The role of xanthophyll cycle carotenoids in the protection of photosynthesis. *Trends Plant Sci.* 1, 21–26. doi: 10.1016/S1360-1385(96)80019-7

Eaton-Rye, J. J. (2011). "Construction of gene interruptions and gene deletions in the cyanobacterium *Synechocystis* sp. strain PCC 6803," in *Photosynthesis Research Protocols*. Ed. R. Carpentier (Totowa, NJ: Humana Press), 295–312. doi: 10.1007/978-1-60761-925-3_22

Ermakova, M., Huokko, T., Richaud, P., Bersanini, L., Howe, C. J., Lea-Smith, D. J., et al. (2016). Distinguishing the roles of thylakoid respiratory terminal oxidases in the cyanobacterium *Synechocystis* sp. PCC 6803. *Plant Physiol.* 171, 1307–1319. doi: 10.1104/pp.16.00479

Feng, W.-K., Wang, L., Lu, Y., and Wang, X.-Y. (2011). A protein oxidase catalysing disulfide bond formation is localized to the chloroplast thylakoids. *FEBS J.* 278, 3419–3430. doi: 10.1111/j.1742-4658.2011.08265.x

Foyer, C. H., and Shigeoka, S. (2011). Understanding oxidative stress and antioxidant functions to enhance photosynthesis. *Plant Physiol.* 155, 93–100. doi: 10.1104/pp.110.166181

Fraser, J. M., Tulk, S. E., Jeans, J. A., Campbell, D. A., Bibby, T. S., and Cockshutt, A. M. (2013). Photophysiological and photosynthetic complex changes during iron starvation in *Synechocystis* sp. PCC 6803 and *Synechococcus elongatus* PCC 7942. *PLoS ONE* 8, e59861. doi: 10.1371/journal.pone.0059861

Furt, F., Oostende, C., Widhalm, J. R., Dale, M. A., Wertz, J., and Basset, G. J. (2010). A bimodular oxidoreductase mediates the specific reduction of phylloquinone (vitamin K(1)) in chloroplasts. *Plant J.* 64, 38–46. doi: 10.1111/j.1365-313X.2010.04305.x

Gorbunov, M. Y., Kuzminov, F. I., Fadeev, V. V., Kim, J. D., and Falkowski, P. G. (2011). A kinetic model of non-photochemical quenching in cyanobacteria. *Biochim. Biophys. Acta* 1807, 1591–1599. doi: 10.1016/j.bbabio.2011.08.009

Goss, R., and Lepetit, B. (2015). Biodiversity of NPQ. *J. Plant Physiol.* 172, 13–32. doi: 10.1016/j.jplph.2014.03.004

Gupta, S., Sutter, M., Remesh, S. G., Dominguez-Martin, M. A., Bao, H., Feng, X. A., et al. (2019). X-ray radiolytic labeling reveals the molecular basis of orange carotenoid protein photoprotection and its interactions with fluorescence recovery protein. *J. Biol. Chem.* 294, 8848–8860. doi: 10.1074/jbc.RA119.007592

Hackett, J. B., Shi, X., Kobylarz, A. T., Lucas, M. K., Wessendorf, R. L., Hines, K. M., et al. (2017). An organelle RNA recognition motif protein is required for photosystem II subunit *psbF* transcript editing. *Plant Physiol.* 173, 2278–2293. doi: 10.1104/pp.16.01623

Hankamer, B., Morris, E., Nield, J., Carne, A., and Barber, J. (2001). Subunit positioning and transmembrane helix organisation in the core dimer of Photosystem II. *FEBS Lett.* 504, 142–151. doi: 10.1016/S0014-5793(01)02766-1

Horton, P., Ruban, A. V., and Walters, R. G. (1996). Regulation of light harvesting in green plants. *Annu. Rev. Plant Physiol. Plant Mol. Biol.* 47, 655–684. doi: 10.1146/annurev.arplant.47.1.655

Hsieh, P., Pedersen, J. Z., and Bruno, L. (2014). Photoinhibition of cyanobacteria and its application in cultural heritage conservation. *Photochem. Photobiol.* 90, 533–543. doi: 10.1111/php.12208

Jahns, P., and Holzwarth, A. R. (2012). The role of the xanthophyll cycle and of lutein in photoprotection of photosystem II. *Biochim. Biophys. Acta* 1817, 182–193. doi: 10.1016/j.bbabio.2011.04.012

Jin, H., Liu, B., Luo, L., Feng, D., Wang, P., Liu, J., et al. (2014). hypersensitive to high light1 interacts with low quantum yield of photosystem II1 and functions in protection of Photosystem II from photodamage in *Arabidopsis*. *Plant Cell* 26, 1213–1229. doi: 10.1105/tpc.113.122424

Kalyanaraman, B., Darley-Usmar, V., Davies, K. J., Dennery, P. A., Forman, H. J., Grisham, M. B., et al. (2012). Measuring reactive oxygen and nitrogen species with fluorescent probes: challenges and limitations. *Free Radic. Biol. Med.* 52, 1–6. doi: 10.1016/j.freeradbiomed.2011.09.030

Karamoko, M., Cline, S., Redding, K., Ruiz, N., and Hamel, P. P. (2011). Lumen Thiol Oxidoreductase1, a disulfide bond-forming catalyst, is required for the assembly of Photosystem II in *Arabidopsis*. *Plant Cell* 23, 4462–4475. doi: 10.1105/tpc.111.089680

Kerfeld, C. A., Sawaya, M. R., Brahmandam, V., Cascio, D., Ho, K. K., Trevithick-Sutton, C. C., et al. (2003). The crystal structure of a cyanobacterial water-soluble carotenoid binding protein. *Structure* 11, 55–65. doi: 10.1016/S0969-2126(02)00936-X

Kirilovsky, D. (2007). Photoprotection in cyanobacteria: the orange carotenoid protein (OCP)-related non-photochemical-quenching mechanism. *Photosynth. Res.* 93, 7. doi: 10.1007/s11120-007-9168-y

Kirilovsky, D. (2015). Modulating energy arriving at photochemical reaction centers: orange carotenoid protein-related photoprotection and state transitions. *Photosynth. Res.* 126, 3–17. doi: 10.1007/s11120-014-0031-7

Kirilovsky, D., and Kerfeld, C. A. (2016). Cyanobacterial photoprotection by the orange carotenoid protein. *Nat. Plants* 2, 16180. doi: 10.1038/nplants.2016.180

Komenda, J., Sobotka, R., and Nixon, P. J. (2012). Assembling and maintaining the Photosystem II complex in chloroplasts and cyanobacteria. *Curr. Opin. Plant Biol.* 15, 245–251. doi: 10.1016/j.pbi.2012.01.017

Kress, E., and Jahns, P. (2017). The dynamics of energy dissipation and xanthophyll conversion in Arabidopsis indicate an indirect photoprotective role of zeaxanthin in slowly inducible and relaxing components of non-photochemical quenching of excitation energy. *Front. Plant Sci.* 8, 2094. doi: 10.3389/fpls.2017.02094

Kromdijk, J., Głowacka, K., Leonelli, L., Gabilly, S. T., Iwai, M., Niyogi, K. K., et al. (2016). Improving photosynthesis and crop productivity by accelerating recovery from photoprotection. *Science* 354, 857–861. doi: 10.1126/science.aai8878

Lambrev, P. H., Miloslavina, Y., Jahns, P., and Holzwarth, A. R. (2012). On the relationship between non-photochemical quenching and photoprotection of Photosystem II. *Biochim. Biophys. Acta* 1817, 760–769. doi: 10.1016/j.bbabio.2012.02.002

Lea-Smith, D. J., Ross, N., Zori, M., Bendall, D. S., Dennis, J. S., Scott, S. A., et al. (2013). Thylakoid terminal oxidases are essential for the cyanobacterium *Synechocystis* sp. PCC 6803 to survive rapidly changing light intensities. *Plant Physiol.* 162, 484–495. doi: 10.1104/pp.112.210260

Lea-Smith, D. J., and Howe, C. J. (2017). "The use of cyanobacteria for biofuel production," in *Biofuels and Bioenergy*. Eds. J. Love and J. A. Bryant (Chichester, West Sussex: Wiley-Blackwell), 143–155. doi: 10.1002/9781118350553.ch9

Li, W., Schulman, S., Dutton, R. J., Boyd, D., Beckwith, J., and Rapoport, T. A. (2010). Structure of a bacterial homologue of vitamin K epoxide reductase. *Nature* 463, 507. doi: 10.1038/nature08720

Liberton, M., Page, L. E., O'Dell, W. B., O'Neill, H., Mamontov, E., Urban, V. S., et al. (2013). Organization and flexibility of cyanobacterial thylakoid membranes examined by neutron scattering. *J. Biol. Chem.* 288, 3632–3640. doi: 10.1074/jbc.M112.416933

Lindberg, P., Park, S., and Melis, A. (2010). Engineering a platform for photosynthetic isoprene production in cyanobacteria, using *Synechocystis* as the model organism. *Metab. Eng.* 12, 70–79. doi: 10.1016/j.ymben.2009.10.001

Liu, J., Lu, Y., Hua, W., and Last, R. L. (2019). A new light on Photosystem II maintenance in oxygenic photosynthesis. *Front. Plant Sci,* 1-10. 10. doi: 10.3389/fpls.2019.00975

Lu, Y. (2011). The occurrence of a thylakoid-localized small zinc finger protein in land plants. *Plant Signal. Behav.* 6, 1181–1185. doi: 10.4161/psb.6.12.18022

Lu, Y., Hall, D. A., and Last, R. L. (2011). A small zinc finger thylakoid protein plays a role in maintenance of Photosystem II in *Arabidopsis thaliana. Plant Cell* 23, 1861–1875. doi: 10.1105/tpc.111.085456

Lu, Y., Wang, H.-R., Li, H., Cui, H.-R., Feng, Y.-G., and Wang, X.-Y. (2013). A chloroplast membrane protein LTO1/AtVKOR involving in redox regulation and ROS homeostasis. *Plant Cell Rep.* 32, 1427–1440. doi: 10.1007/s00299-013-1455-9

Lu, Y. (2016). Identification and roles of Photosystem II assembly, stability, and repair factors in Arabidopsis. *Front. Plant Sci.* 7, 168. doi: 10.3389/fpls.2016.00168

Luimstra, V. M., Schuurmans, J. M., Verschoor, A. M., Hellingwerf, K. J., Huisman, J., and Matthijs, H. C. P. (2018). Blue light reduces photosynthetic efficiency of cyanobacteria through an imbalance between photosystems I and II. *Photosynth. Res.* 138, 177–189. doi: 10.1007/s11120-018-0561-5

Machado, I. M. P., and Atsumi, S. (2012). Cyanobacterial biofuel production. *J. Biotechnol.* 162, 50–56. doi: 10.1016/j.jbiotec.2012.03.005

Majumder, E. L.-W., Wolf, B. M., Liu, H., Berg, R. H., Timlin, J. A., Chen, M., et al. (2017). Subcellular pigment distribution is altered under far-red light acclimation in cyanobacteria that contain chlorophyll f. *Photosynth. Res.* 134, 183–192. doi: 10.1007/s11120-017-0428-1

Misumi, M., Sonoike, K., Katoh, H., and Tomo, T. (2016). Relationship between photochemical quenching and non-photochemical quenching in six species of cyanobacteria reveals species difference in redox state and species commonality in energy dissipation. *Plant Cell Physiol.* 57, 1510–1517. doi: 10.1093/pcp/pcv185

Misumi, M., and Sonoike, K. (2017). Characterization of the influence of chlororespiration on the regulation of photosynthesis in the glaucophyte *Cyanophora paradoxa. Sci. Rep.* 7, 46100. doi: 10.1038/srep46100

Mohamed, A., and Jansson, C. (1989). Influence of light on accumulation of photosynthesis-specific transcripts in the cyanobacterium *Synechocystis* 6803. *Plant Mol. Biol.* 13, 693–700. doi: 10.1007/BF00016024

Moldenhauer, M., Sluchanko, N. N., Buhrke, D., Zlenko, D. V., Tavraz, N. N., Schmitt, F. J., et al. (2017). Assembly of photoactive orange carotenoid protein from its domains unravels a carotenoid shuttle mechanism. *Photosynth. Res.* 133, 327–341. doi: 10.1007/s11120-017-0353-3

Müller, P., Li, X. P., and Niyogi, K. K. (2001). Non-photochemical quenching. A response to excess light energy. *Plant Physiol.* 125, 1558–1566. doi: 10.1104/125.4.1558

Mulo, P., Sirpiö, S., Suorsa, M., and Aro, E. M. (2008). Auxiliary proteins involved in the assembly and sustenance of Photosystem II. *Photosynth. Res.* 98, 489–501. doi: 10.1007/s11120-008-9320-3

Mulo, P., Sakurai, I., and Aro, E. M. (2012). Strategies for psbA gene expression in cyanobacteria, green algae and higher plants: from transcription to PSII repair. *Biochim. Biophys. Acta* 1817, 247–257. doi: 10.1016/j.bbabio.2011.04.011

Murakami, A., Kim, S. J., and Fujita, Y. (1997). Changes in photosystem stoichiometry in response to environmental conditions for cell growth observed with the cyanophyte Synechocystis PCC 6714. *Plant Cell Physiol.* 38, 392–397. doi: 10.1093/oxfordjournals.pcp.a029181

Muranaka, A., Watanabe, S., Sakamoto, A., and Shimada, H. (2012). Arabidopsis cotyledon chloroplast biogenesis factor CYO1 uses glutathione as an electron donor and interacts with PSI (A1 and A2) and PSII (CP43 and CP47) subunits. *J. Plant Physiol.* 169, 1212–1215. doi: 10.1016/j.jplph.2012.04.001

Muzzopappa, F., Wilson, A., Yogarajah, V., Cot, S., Perreau, F., Montigny, C., et al. (2017). Paralogs of the C-terminal domain of the cyanobacterial orange carotenoid protein are carotenoid donors to helical carotenoid proteins. *Plant Physiol.* 175, 1283–1303. doi: 10.1104/pp.17.01040

Nagy, G., Posselt, D., Kovacs, L., Holm, J. K., Szabo, M., Ughy, B., et al. (2011). Reversible membrane reorganizations during photosynthesis in vivo: revealed by small-angle neutron scattering. *Biochem. J.* 436, 225–230. doi: 10.1042/BJ20110180

Nickelsen, J., and Rengstl, B. (2013). Photosystem II assembly: from cyanobacteria to plants. *Annu. Rev. Plant Biol.* 64, 609–635. doi: 10.1146/annurev-arplant-050312-120124

Nickelsen, J., and Zerges, W. (2013). Thylakoid biogenesis has joined the new era of bacterial cell biology. *Front. Plant Sci.* 4, 458. doi: 10.3389/fpls.2013.00458

Nixon, P. J., Michoux, F., Yu, J., Boehm, M., and Komenda, J. (2010). Recent advances in understanding the assembly and repair of Photosystem II. *Ann. Bot.* 106, 1–16. doi: 10.1093/aob/mcq059

Nozzi, N., Oliver, J., and Atsumi, S. (2013). Cyanobacteria as a platform for biofuel production. *Front. Bioeng. Biotechnol.* 1, 1–6. doi: 10.3389/fbioe.2013.00007

Ogawa, T., and Sonoike, K. (2016). Effects of bleaching by nitrogen deficiency on the quantum yield of photosystem II in *Synechocystis* sp. PCC 6803 revealed by Chl fluorescence measurements. *Plant Cell Physiol.* 57, 558–567. doi: 10.1093/pcp/pcw010

Olive, J., Ajlani, G., Astier, C., Recouvreur, M., and Vernotte, C. (1997). Ultrastructure and light adaptation of phycobilisome mutants of Synechocystis PCC 6803. *Biochim. Biophys. Acta* 1319, 275–282. doi: 10.1016/S0005-2728(96)00168-5

Pathak, J., Ahmed, H., Singh, P. R., Singh, S. P., Häder, D.-P., and Sinha, R. P. (2019). "Mechanisms of photoprotection in cyanobacteria," in *Cyanobacteria*. Eds. A. K. Mishra, D. N. Tiwari, and A. N. Rai (Cambridge: Academic Press), 145–171. doi: 10.1016/B978-0-12-814667-5.00007-6

Perozeni, F., Cazzaniga, S., and Ballottari, M. (2019). *In vitro* and *in vivo* investigation of chlorophyll binding sites involved in non-photochemical quenching in Chlamydomonas reinhardtii. *Plant Cell Environ.* 42, 2522–2535. doi: 10.1111/pce.13566

Rast, A., Heinz, S., and Nickelsen, J. (2015). Biogenesis of thylakoid membranes. *Biochim. Biophys. Acta* 1847, 821–830. doi: 10.1016/j.bbabio.2015.01.007

Ritchie, R. J. (2006). Consistent sets of spectrophotometric chlorophyll equations for acetone, methanol and ethanol solvents. *Photosynth. Res.* 89, 27–41. doi: 10.1007/s11120-006-9065-9

Sauer, J., Schreiber, U., Schmid, R., Völker, U., and Forchhammer, K. (2001). Nitrogen starvation-induced chlorosis in *Synechococcus* PCC 7942. Low-level photosynthesis as a mechanism of long-term survival. *Plant Physiol.* 126, 233–243. doi: 10.1104/pp.126.1.233

Schindelin, J., Arganda-Carreras, I., Frise, E., Kaynig, V., Longair, M., Pietzsch, T., et al. (2012). Fiji: an open-source platform for biological-image analysis. *Nat. Methods* 9, 676–682. doi: 10.1038/nmeth.2019

Shen, G., Boussiba, S., and Vermaas, W. F. (1993). *Synechocystis* sp PCC 6803 strains lacking photosystem I and phycobilisome function. *Plant Cell* 5, 1853–1863. doi: 10.1105/tpc.5.12.1853

Shimada, H., Mochizuki, M., Ogura, K., Froehlich, J. E., Osteryoung, K. W., Shirano, Y., et al. (2007). Arabidopsis cotyledon-specific chloroplast biogenesis factor CYO1 is a protein disulfide isomerase. *Plant Cell* 19, 3157–3169. doi: 10.1105/tpc.107.051714

Singh, A. K., Bhattacharyya-Pakrasi, M., and Pakrasi, H. B. (2008a). Identification of an atypical membrane protein involved in the formation of protein disulfide bonds in oxygenic photosynthetic organisms. *J. Biol. Chem.* 283, 15762–15770. doi: 10.1074/jbc.M800982200

Singh, A. K., Elvitigala, T., Bhattacharyya-Pakrasi, M., Aurora, R., Ghosh, B., and Pakrasi, H. B. (2008b). Integration of carbon and nitrogen metabolism with energy production is crucial to light acclimation in the cyanobacterium Synechocystis. *Plant Physiol.* 148, 467–478. doi: 10.1104/pp.108.123489

Singh, S. P., and Montgomery, B. L. (2012). Reactive oxygen species are involved in the morphology-determining mechanism of *Fremyella diplosiphon* cells during complementary chromatic adaptation. *Microbiology* 158, 2235–2245. doi: 10.1099/mic.0.060475-0

Stadnichuk, I. N., Krasilnikov, P. M., and Zlenko, D. V. (2015). Cyanobacterial phycobilisomes and phycobiliproteins. *Microbiology* 84, 101–111. doi: 10.1134/S0026261715020150

Steiger, S., Schäfer, L., and Sandmann, G. (1999). High-light-dependent upregulation of carotenoids and their antioxidative properties in the cyanobacterium *Synechocystis* PCC 6803. *J. Photochem. Photobiol. B: Biol.* 52, 14–18. doi: 10.1016/S1011-1344(99)00094-9

Stingaciu, L.-R., O'Neill, H., Liberton, M., Urban, V. S., Pakrasi, H. B., and Ohl, M. (2016). Revealing the dynamics of thylakoid membranes in living cyanobacterial cells. *Sci. Rep.* 6, 19627. doi: 10.1038/srep19627

Tanz, S. K., Kilian, J., Johnsson, C., Apel, K., Small, I., Harter, K., et al. (2012). The SCO2 protein disulphide isomerase is required for thylakoid biogenesis and interacts with LHCB1 chlorophyll a/b binding proteins which affects chlorophyll biosynthesis in Arabidopsis seedlings. *Plant J.* 69, 743–754. doi: 10.1111/j.1365-313X.2011.04833.x

Thomas, D. J., Avenson, T. J., Thomas, J. B., and Herbert, S. K. (1998). A cyanobacterium lacking iron superoxide dismutase is sensitized to oxidative stress induced with methyl viologen but is not sensitized to oxidative stress induced with norflurazon. *Plant Physiol.* 116, 1593–1602. doi: 10.1104/pp.116.4.1593

Thornton, L. E., Ohkawa, H., Roose, J. L., Kashino, Y., Keren, N., and Pakrasi, H. B. (2004). Homologs of plant PsbP and PsbQ proteins are necessary for regulation

of Photosystem II activity in the cyanobacterium *Synechocystis* 6803. *Plant Cell* 16, 2164–2175. doi: 10.1105/tpc.104.023515

Tibiletti, T., Auroy, P., Peltier, G., and Caffarri, S. (2016). *Chlamydomonas reinhardtii* PsbS protein is functional and accumulates rapidly and transiently under high light. *Plant Physiol.* 171, 2717–2730. doi: 10.1104/pp.16.00572

Trautmann, A., Watzer, B., Wilde, A., Forchhammer, K., and Posten, C. (2016). Effect of phosphate availability on cyanophycin accumulation in *Synechocystis* sp. PCC 6803 and the production strain BW86. *Algal Res.* 20, 189–196. doi: 10.1016/j.algal.2016.10.009

Tsang, T. K., Roberson, R. W., and Vermaas, W. F. (2013). Polyhydroxybutyrate particles in *Synechocystis* sp. PCC 6803: facts and fiction. *Photosynth. Res* 118, 37–49. doi: 10.1007/s11120-013-9923-1

Varman, A. M. (2010). *An Improved plasmid vector system for genetic engineering of Synechocystis sp PCC 6803. Master's thesis*. (St. Louis: Washington University).

Varman, A. M., Xiao, Y., Pakrasi, H. B., and Tang, Y. J. (2013). Metabolic engineering of *Synechocystis* sp. strain PCC 6803 for isobutanol production. *Appl. Environ. Microbiol.* 79, 908–914. doi: 10.1128/AEM.02827-12

von der Haar, T. (2007). Optimized protein extraction for quantitative proteomics of yeasts. *PLoS ONE* 2, e1078. doi: 10.1371/journal.pone.0001078

Wang, P., Liu, J., Liu, B., Feng, D., Da, Q., Shu, S., et al. (2013). Evidence for a role of chloroplastic m-type thioredoxins in the biogenesis of Photosystem II in Arabidopsis. *Plant Physiol.* 163, 1710–1728. doi: 10.1104/pp.113.228353

Wellburn, A. R. (1994). The spectral determination of chlorophyll *a* and chlorophyll *b*, as well as total carotenoids, using various solvents with spectrophotometers of different resolution. *J. Plant Physiol.* 144, 307–313. doi: 10.1016/S0176-1617(11)81192-2

Wessendof, R. L. (2017). *Evolution of a thylakoid zinc-finger protein and effects of introducing this protein into Synechocystis sp. PCC 6803. Master of Science*. Kalamazoo, MI: Western Michigan University.

Wilson, A., Kinney, J. N., Zwart, P. H., Punginelli, C., D'Haene, S., Perreau, F., et al. (2010). Structural determinants underlying photoprotection in the photoactive orange carotenoid protein of cyanobacteria. *J. Biol. Chem.* 285, 18364–18375. doi: 10.1074/jbc.M110.115709

Yamazaki, J.-y., Suzuki, T., Maruta, E., and Kamimura, Y. (2005). The stoichiometry and antenna size of the two photosystems in marine green algae, *Bryopsis maxima* and *Ulva pertusa*, in relation to the light environment of their natural habitat. *J. Exp. Bot.* 56, 1517–1523. doi: 10.1093/jxb/eri147

Zavřel, T., Sinetova, M. A., and Červený, J. (2015). Measurement of chlorophyll a and carotenoids concentration in cyanobacteria. *Bio-protocol* 5, e1467. doi: 10.21769/BioProtoc.1467

Zhang, L., and Aro, E.-M. (2002). Synthesis, membrane insertion and assembly of the chloroplast-encoded D1 protein into photosystem II. *FEBS Lett.* 512, 13–18. doi: 10.1016/S0014-5793(02)02218-4

Zhao, K. H., Wu, D., Zhang, L., Zhou, M., Böhm, S., Bubenzer, C., et al. (2006). Chromophore attachment in phycocyanin: Functional amino acids of phycocyanobilin - α-phycocyanin lyase and evidence for chromophore binding. *FEBS J.* 273, 1262–1274. doi: 10.1111/j.1742-4658.2006.05149.x

Conflict of Interest: The authors declare that the research was conducted in the absence of any commercial or financial relationships that could be construed as a potential conflict of interest.

frontiers in Plant Science

PERSPECTIVE
published: 30 October 2019
doi: 10.3389/fpls.2019.01403

Arabidopsis thaliana Leaf Epidermal Guard Cells: A Model for Studying Chloroplast Proliferation and Partitioning in Plants

Makoto T. Fujiwara[1], Alvin Sanjaya[1] and Ryuuichi D. Itoh[2]*

[1] *Department of Materials and Life Sciences, Faculty of Science and Technology, Sophia University, Tokyo, Japan,*
[2] *Department of Chemistry, Biology and Marine Science, Faculty of Science, University of the Ryukyus, Nishihara, Japan*

The existence of numerous chloroplasts in photosynthetic cells is a general feature of plants. Chloroplast biogenesis and inheritance involve two distinct mechanisms: proliferation of chloroplasts by binary fission and partitioning of chloroplasts into daughter cells during cell division. The mechanism of chloroplast number coordination in a given cell type is a fundamental question. Stomatal guard cells (GCs) in the plant shoot epidermis generally contain several to tens of chloroplasts per cell. Thus far, chloroplast number at the stomatal (GC pair) level has generally been used as a convenient marker for identifying hybrid species or estimating the ploidy level of a given plant tissue. Here, we report that *Arabidopsis thaliana* leaf GCs represent a useful system for investigating the unexploited aspects of chloroplast number control in plant cells. In contrast to a general notion based on analyses of leaf mesophyll chloroplasts, a small difference was detected in the GC chloroplast number among three *Arabidopsis* ecotypes (Columbia, Landsberg *erecta*, and Wassilewskija). Fluorescence microscopy often detected dividing GC chloroplasts with the FtsZ1 ring not only at the early stage of leaf expansion but also at the late stage. Compensatory chloroplast expansion, a phenomenon well documented in leaf mesophyll cells of chloroplast division mutants and transgenic plants, could take place between paired GCs in wild-type leaves. Furthermore, modest chloroplast number per GC as well as symmetric division of guard mother cells for GC formation suggests that *Arabidopsis* GCs would facilitate the analysis of chloroplast partitioning, based on chloroplast counting at the individual cell level.

Keywords: chloroplast, guard cell, plastid development, organelle inheritance, organelle partitioning, stoma

OPEN ACCESS

Edited by:
Hongbo Gao,
Beijing Forestry University, China

Reviewed by:
Chanhong Kim,
Shanghai Institutes for Biological Sciences (CAS), China
Susanne Hoffmann-Benning,
Michigan State University, United States

****Correspondence:***
Makoto T. Fujiwara
mtf1@mac.com

Specialty section:
This article was submitted to Plant Physiology, a section of the journal Frontiers in Plant Science

Received: *25 July 2019*
Accepted: *10 October 2019*
Published: *30 October 2019*

Citation:
Fujiwara MT, Sanjaya A and Itoh RD (2019) Arabidopsis thaliana Leaf Epidermal Guard Cells: A Model for Studying Chloroplast Proliferation and Partitioning in Plants. Front. Plant Sci. 10:1403. doi: 10.3389/fpls.2019.01403

INTRODUCTION

Chloroplasts represent a structural feature of plant cells and support plant survival *via* their primary metabolism and high-level functions (Kirk and Tilney-Bassett, 1978; Mullet, 1988; López-Juez and Pyke, 2005). During plant vegetative growth, leaf cells contain a highly homogeneous population of chloroplasts with respect to size and shape. The number of chloroplasts per cell is achieved by binary fission of pre-existing organelles and partitioning into two daughter cells during cell division (Birky, 1983; Possingham and Lawrence, 1983). Thus, regulation of the chloroplast number in a given cell type is crucial for the cellular function and genetic inheritance of chloroplasts.

To investigate the nature of chloroplast number determination in plant cells, leaf mesophyll cells of representative species have played a major role [*e.g.*, Boasson and Laetsch, 1969 (for tobacco, *Nicotiana tabacum*); Honda et al., 1971 (for spinach, *Spinacia oleracea*); Boffey et al., 1979 (for wheat, *Triticum aestivum*); Lamppa et al., 1980 (for pea, *Pisum sativum*); and Pyke and Leech, 1991 (for *Arabidopsis thaliana*)]. These cells are physiologically important for photosynthesis and show a high degree of structural and functional homogeneity. Early systematic observation analyses of isolated tissues and cells (Boasson and Laetsch, 1969; Possingham and Saurer, 1969; Boffey et al., 1979; Lamppa et al., 1980; Thomas and Rose, 1983; Pyke and Leech, 1991) provided much useful information on chloroplast number determination, including the notion that chloroplasts (plastids) are not synthesized *de novo* but replicate by division and the observation that leaf mesophyll chloroplast number is sensitive to various environmental and plant-endogenous factors. With respect to the latter, in spinach, light has a positive impact on chloroplast division during leaf disc culture compared with dim or dark conditions (Possingham and Lawrence, 1983). In the first leaves of wheat, cell volume is positively correlated with chloroplast proliferation (Ellis and Leech, 1985; Pyke and Leech, 1987). In *Arabidopsis*, the genetic background affects chloroplast proliferation; the average chloroplast number per cell in first leaves is 121 in the Landsberg *erecta* (L*er*) ecotype and 83 in the Wassilewskija (Ws) ecotype (Pyke and Leech, 1994; Pyke et al., 1994). Leaf mesophyll cells have also contributed to understanding the genetic control of chloroplast division; for instance, screening mutants impaired in chloroplast proliferation and characterizing gene functions involved in chloroplast division have revealed over 20 genes encoding chloroplast division machinery components or chloroplast regulatory factors (Gao and Gao, 2011; Miyagishima et al., 2011; Basak and Møller, 2013; Osteryoung and Pyke, 2014; Li et al., 2017).

By contrast, studies on the replication of chloroplasts in non-mesophyll cells (*e.g.*, pavement cells in leaf epidermis; Itoh et al., 2018) are scarce. Recently, the regulation of chloroplast division has been reported to differ between leaf tissues (Fujiwara et al., 2018; Itoh et al., 2018), although the detailed mechanism remains unknown. Additionally, while the analyses of suspension-cultured BY-2 cells and leaf mesophyll protoplasts in tobacco and shoot apical meristem and leaf primordial cells in *Arabidopsis* (Nebenführ et al., 2000; Sheahan et al., 2004; Seguí-Simarro and Staehelin, 2009) have provided major insights, how chloroplast (plastid) partitioning is regulated in plants is still unclear. Thus, despite considerable effort, fundamental questions in chloroplast research remain, such as (i) how is chloroplast number per cell coordinated in plant tissues and (ii) how is chloroplast partitioning regulated at cell division.

HISTORY OF RESEARCH ON GUARD CELL CHLOROPLAST NUMBER

Stomatal GCs in the shoot epidermis generally contain chloroplasts and control gas exchange between the leaf mesophyll and the atmosphere (Sachs, 1875; Taiz et al., 2015; see **Figure 1A**). The first investigation of GC chloroplast number in leaves was performed over a century ago in naturally grown *Drosera* plants (Macfarlane, 1898). This study demonstrated that, like other plant and cell structural features, GC chloroplast number per cell in a putative hybrid derived from a cross between *Drosera filiformis* and *Drosera intermedia* was intermediate between the two species, implying that GC chloroplast number could be used to determine the genetic makeup of a plant. Important observations were subsequently reported on the differences in GC chloroplast number among plant species (Sakisaka, 1929) and the relatively stable chloroplast number in GCs in the leaf epidermis of mulberry (*Morus* spp.; Hamada and Baba, 1930) and in mature leaves of several *Brassica* species (Iura, 1934). Furthermore, analysis of autopolyploid sugar beet (*Beta vulgaris*) plants revealed that the GC chloroplast number in leaves is positively correlated with the nuclear ploidy level of plants (Mochizuki and Sueoka, 1955). More in-depth and comprehensive analyses were then conducted using various plant samples to investigate the relationship of chloroplast number and stomatal size with the ploidy level (*e.g.*, Frandsen, 1968). In these analyses, chloroplast counting at the stomatal (GC pair) level was frequently adopted, which excluded the effect of biased chloroplast distribution between paired GCs (*e.g.*, Mochizuki and Sueoka, 1955; Frandsen, 1968), revealing that the average GC chloroplast number in leaves or cotyledons in approximately 80 species, variants, or hybrids ranged from 2.8 to 40.0 in diploids (2×) and 5.0 to 73.5 in tetraploids (4×). In addition, whole-genome duplication events in plants (*i.e.*, 1× to 2×, 2× to 4×, etc.) caused an approximately 1.7-fold increase in GC chloroplast number with high fidelity (reviewed in Butterfass, 1973). These results encouraged investigations into ploidy level in various tissues and plants obtained *via* tissue culture, crossing, or natural cultivation, in combination with chemical (*e.g.*, colchicine) or radiation treatments (*e.g.*, Jacobs and Yoder, 1989; Singsit and Veilleux, 1991; Qin and Rotino, 1995). While GC chloroplast number has been studied in stomatal biology (Lawson, 2009) and cytology to understand chloroplast multiplication (Butterfass, 1979; see below), it has largely served as a reliable and convenient marker for the detection of hybrids, species, and variants and for the estimation of ploidy levels of target plant tissues.

UTILITY OF LEAF GUARD CELLS FOR THE ANALYSIS OF CHLOROPLAST NUMBER CONTROL

Leaf mesophyll cells have long been employed as a primary model for the analysis of chloroplast number. While they have advantages for the study of the effects of environmental conditions on chloroplast division (*e.g.*, the light-cytokinin signaling; Boasson and Laetsch, 1969; Possingham and Lawrence, 1983; Okazaki et al., 2009; Chiang et al., 2012), they are limited in some respects. Firstly, leaf mesophyll cells vary in size and shape and are distributed deep within the leaf, which makes it difficult to manipulate intact tissues. Secondly, the susceptibility of leaf mesophyll chloroplast

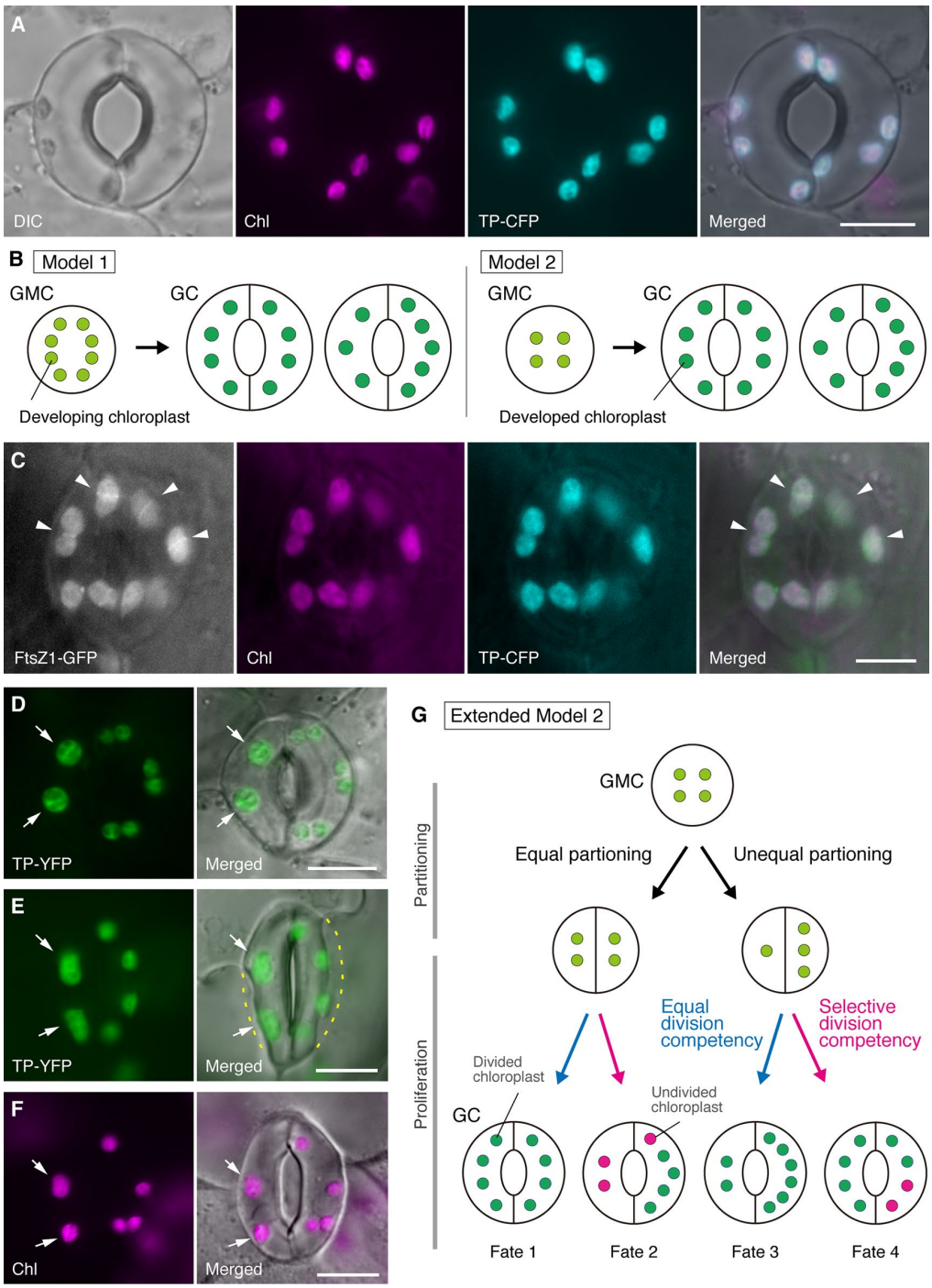

FIGURE 1 | Simplified models and microscopy evidence for the control of chloroplast number in stomatal guard cells (GCs). **(A)** A typical stoma (GC pair) in abaxial epidermis of the *Arabidopsis* leaf blade expressing a stoma-targeted fusion of the transit peptide (TP) with cyan fluorescent protein (CFP; TP-CFP). **(B)** Two models of chloroplast number determination in GCs, involving either chloroplast partitioning (model 1) or both chloroplast proliferation and partitioning (model 2) during GC development from guard mother cells (GMCs). **(C)** A GC pair in adaxial epidermis of *Arabidopsis* leaf petiole expressing TP-CFP and FtsZ1 fused to the green fluorescent protein (GFP; FtsZ1-GFP). **(D–F)** GC pairs in abaxial epidermis of *Arabidopsis* leaf blade with **(D**, **E)** or without **(F)** the expression of TP fused to the yellow fluorescent protein (YFP; TP-YFP). **(F)** Chlorophyll autofluorescence (Chl) was used as a chloroplast marker. **(G)** Extended model 2, representing the involvement of equal and unequal chloroplast partitioning following GMC division and subsequent division of GC chloroplasts with equal (blue line) or selective (red line) division competency, which would result in four types of chloroplast number determination (Fates 1–4) during late stomatal development of *Arabidopsis* leaves. **(A**, **C–F)** Epifluorescence microscopy was performed with an Olympus IX71 inverted microscope using plant materials as previously described (Fujiwara et al., 2017, Fujiwara et al., 2018). Fluorescence signals of chlorophyll, CFP, GFP, and YFP are pseudo-colored in magenta, cyan, green (in merged image only), and green, respectively. Indications in panels are as follows: arrowhead, the FtsZ1 ring; arrow, enlarged GC chloroplast; dashed line, cell shape. Scale bar = 10 μm.

proliferation to environmental stress and plant growth conditions can prevent reliable comparisons between studies. The leaf mesophyll chloroplast number per cell in *Arabidopsis* Columbia (Col) ecotype has been reported variously as 76 (Kinsman and Pyke, 1998), 80–100 (Stokes et al., 2000), 70 (Tirlapur and König, 2001), 41 (Yoder et al., 2007), 40–60 (Okazaki et al., 2009), and 30–40 (Kawade et al., 2013). Furthermore, it is almost impossible to assess the contribution of chloroplast partitioning to final chloroplast number per mesophyll cell during leaf development, although this is thought to be determined by the balance between the rate of cell division and rate of chloroplast division. To uncover the mechanism of chloroplast number control in vegetative leaf cells, a model system that overcomes the above issues is required.

Stomatal GCs (see **Figure 1A**) exhibit the characteristics of a model system for understanding the mechanism of chloroplast number control. GCs are highly uniform in size and shape within a tissue, and their scattered but dense distribution in the outermost layer of shoots facilitates their detection by light and fluorescence microscopy. GCs are also derived from protodermal cells in the shoot apical meristem or from embryonic epidermal cells, and their developmental sequence through meristemoids (a stomatal precursor with meristematic activity) and guard mother cells (GMCs; a precursor of GC pairs) is established in detail (Zhao and Sack, 1999; Nadeau and Sack, 2002; Kalve et al., 2014). Late stomatal development involves a single round of symmetric GMC division, which enables the assessment of chloroplast distribution and partitioning before and after cytokinesis. From the perspective of practical experiments, leaf GCs are suitable for microscopy. It was previously shown that chloroplast number per cell in leaf GCs of *Sinapis alba* was less affected by different light conditions than that in leaf mesophyll cells (Wild and Wolf, 1980). Additionally, the difference in GC chloroplast number in leaf petioles is relatively minor among the three *Arabidopsis* ecotypes Col, L*er*, and Ws (Fujiwara et al., 2018). Furthermore, endoreduplication, which impacts the development of leaf mesophyll, pavement, and trichome cells, has not been detected in *Arabidopsis* leaf GCs (Melaragno et al., 1993), which would assure the interpretations of chloroplast number data at the 2C level of cells. Together, these reports suggest that leaf GCs are potentially an excellent model for the systematic analysis of chloroplast number dynamics in a particular cell lineage.

ARABIDOPSIS LEAF GUARD CELLS AS A MODEL FOR STUDYING THE CONTROL OF CHLOROPLAST NUMBER

In the history of GC chloroplast research, chloroplast counting at the stomatal (GC pair) level has served an equally important role in determining the chloroplast number as counting at the individual GC level. Both methods produce the same mean chloroplast number (Butterfass, 1973). When the variation in chloroplast distribution in paired GCs and its underlying mechanism is a subject of focus, detailed information of chloroplasts at the individual cell level, *i.e.*, their size, shape, and intracellular localization, is essential. Chloroplast (plastid) proliferation during the GMC–GC differentiation was previously investigated in several plant species (Butterfass, 1973, Butterfass 1979). These studies proposed two models for determining the terminal chloroplast number in GCs in different plant species (**Figure 1B**): one (model 1; sugar beet) involves only chloroplast partitioning at GMC division, and the other [model 2; alsike clover (*Trifolium hybridum*)] involves not only chloroplast partitioning but also chloroplast proliferation during GC development.

In the era of molecular genetics, genomics, cell imaging, and other interdisciplinary analyses, there are many possibilities for the further characterization of the chloroplast partitioning mechanism. *Arabidopsis* leaf GCs may be one of the best model systems for this purpose. Several studies have examined the GC chloroplast number in the leaves or cotyledons of *Arabidopsis* (Hoffmann, 1968; Pyke and Leech, 1994; Pyke et al., 1994; Robertson et al., 1995; Keech et al., 2007; Chen et al., 2009; Yu et al., 2009; Higaki et al., 2012; Fujiwara et al., 2018). These GCs exhibit a modest number of chloroplasts, ranging from 3.5 to 5.5 on average. To date, no studies have examined the alterations in chloroplast (plastid) number during stomatal development. However, microscopic evidence from stomatal development analyses (*e.g.*, Zhao and Sack, 1999; Hachez et al., 2011) and our preliminary observations indicate that GMCs may contain smaller numbers of developing chloroplasts than GCs and that chloroplast proliferation may occur during GC differentiation. To test this, the formation of the chloroplast division machinery in GCs was monitored with the probe FtsZ1 fused to the green fluorescent protein (FtsZ1-GFP) (Fujiwara et al., 2008). A transgenic line, simultaneously expressing a transit peptide (TP)-fused CFP and FtsZ1-GFP to visualize the stroma and FtsZ1 ring, respectively, was examined by epifluorescence microscopy (Fujiwara et al., 2017). Expanding leaf petioles (fifth leaves of 4-week-old seedlings) were employed. As a result, GCs with symmetrically constricting chloroplasts were detected (**Figure 1C**). These chloroplasts formed the FtsZ1 ring, a chloroplast division ring on the stromal surface of the inner envelope membrane in leaf mesophyll and pavement cells (Vitha et al., 2001; Fujiwara et al., 2008), at the equatorial constriction site. Consistent with the stomatal patterning in *Arabidopsis* leaf development (Donnelly et al., 1999; Andriankaja et al., 2012), dividing chloroplasts were detected at the late, as well as early, stage of leaf expansion. Thus, model 2 is most likely the best fit for *Arabidopsis* leaf GCs.

RELATIONSHIP BETWEEN CHLOROPLAST PROLIFERATION AND EXPANSION IN *ARABIDOPSIS* LEAF GUARD CELLS

Furthermore, an unexpected phenotype of GC chloroplast morphogenesis was observed in mature GCs (**Figures 1D, E**). When epidermal peels of fully expanded leaves (third–fourth leaf blades of 4-week-old seedlings) from a TP-fused yellow fluorescent protein (YFP) line were microscopically characterized

(FL6-5 line; Fujiwara et al., 2018), some stomata showed unequal chloroplast distribution patterns in GC pairs, while most leaf stomata showed equal or similar chloroplast distribution patterns (Robertson et al., 1995; Fujiwara et al., 2018). Within the GC pair of a stoma, the size of chloroplasts in the GC containing smaller numbers of chloroplasts was larger than in the other GCs in the pair containing larger numbers of chloroplasts (**Figures 1D**, **E**). In this way, GCs probably maintain the total chloroplast volume per cell at a constant level during cell growth. Enlarged chloroplasts represented the terminal phenotype and could no longer divide in expanded leaves. These results were confirmed in several independent experiments, irrespective of the expression of a TP-fused fluorescent protein for stroma labeling (**Figure 1F**).

This GC chloroplast phenotype is interpreted as a compensation mechanism for chloroplast expansion, which was well documented in leaf mesophyll cells defective in the control of chloroplast division (Pyke and Leech, 1994; Pyke et al., 1994). To date, only one study (Ellis and Leech, 1985) has reported a negative correlation between chloroplast number and chloroplast size in leaf mesophyll cells of wheat, whereas many studies have reported a positive correlation between cell volume and chloroplast number in normal leaf mesophyll cells (Leech and Pyke, 1988; Pyke, 1997). Whereas imbalances in GC chloroplast number occur at low frequency (Fujiwara et al., 2018), chloroplast heterogeneity in GC pairs indicates that unequal chloroplast partitioning could trigger differential chloroplast growth between wild-type leaf cells in *Arabidopsis*, despite symmetric cell division.

The chloroplast compensation effect in GCs may be less strict than in leaf mesophyll cells. GCs might be able to withstand scarcity or complete loss of total chloroplast volume per cell in severely impaired chloroplast division mutants, such as in *Arabidopsis arc6* and *atminE1* and tomato *suffulta*, whereas many mutant GCs showed reduced chloroplast number and enlarged chloroplast size similarly to the leaf mesophyll cells (Robertson et al., 1995; Forth and Pyke, 2006; Chen et al., 2009; Fujiwara et al., 2018). In a late chloroplast division mutant, *arc5*, the reduction in GC chloroplast number was not associated with a significant increase in chloroplast size, unlike in leaf mesophyll cells (Pyke and Leech, 1994). A lower degree of chloroplast expansion in GCs than in mesophyll cells (Pyke and Leech, 1994; Barton et al., 2016), and the variation in chloroplast expansion among GCs, might underlie such a wide permissible range of total chloroplast volume per GC. Furthermore, the timing of chloroplast division during GMC–GC differentiation might significantly affect the terminal GC chloroplast phenotype. Although further detailed characterization is required to address this issue, it seems plausible that *Arabidopsis* leaf GCs represent a system to investigate the unexploited aspects of chloroplast number control in plant cells.

A WORKING MODEL FOR CHLOROPLAST NUMBER DETERMINATION IN *ARABIDOPSIS* LEAF GUARD CELLS

On the basis of the above, we propose a working model (an extended model 2) for the analysis of chloroplast number in GCs (**Figure 1G**). The final chloroplast number per GC is determined by chloroplast partitioning at GMC division and chloroplast proliferation in GCs. During GMC division, chloroplasts may undergo either equal or unequal partitioning. During chloroplast proliferation, GC chloroplasts will proliferate with either equal (blue line) or selective (magenta line) division competency. For example, if equally partitioned chloroplasts possess equivalent division competency, equal chloroplast numbers will occur in the GC pair (Fate 1). If unequally partitioned chloroplasts possess equivalent division competency, chloroplasts will increase at the same rate within the GC pair (Fate 3). If selective chloroplast division occurs in GCs, the balance of chloroplast number in the GC pair will change after GMC division (Fates 2 and 4). It is currently difficult to find support for "selective chloroplast division," but if Fates 1 and 4 actually predominate in GCs, then they might possess a mechanism that controls total chloroplast volume per cell, as in leaf mesophyll cells. The model raises two issues: (i) Are GC chloroplasts properly partitioned into daughter cells and how do they partition? And (ii) is division competency of GC chloroplasts coordinately regulated?

Regarding issue (i), whether chloroplast inheritance occurs by random distribution of multiple chloroplasts in the cytoplasm or by positive chloroplast partitioning mechanism(s) has been a long-standing concern (Butterfass, 1969; Birky, 1983; Hennis and Birky, 1984; Nebenführ, 2007; Sheahan et al., 2016). Intriguingly, in *Arabidopsis arc6*, leaf or cotyledon GCs have zero to three chloroplasts, and in chloroplast-deficient GCs, non-photosynthetic plastids still exist in vesicular to elongated forms (Robertson et al., 1995; Chen et al., 2009; Fujiwara et al., 2018). No GCs devoid of plastids *per se* have been found in *arc6*, and no explanation for this has been forthcoming, despite the disruption of the chloroplast division apparatus (Vitha et al., 2003). Accordingly, it will be important to examine the replication and morphology of *arc6* chloroplasts in stomatal lineage studies. *Arabidopsis* mutant research may also give another clue for this issue. The observation that 18% of cotyledon GCs in the *crumpled leaf* (*crl*) mutant contain no plastidic structures in the cytoplasm, while 100% of the leaf mesophyll cells contain one to four enlarged chloroplasts (Asano et al., 2004; Chen et al., 2009), is of great importance. CRL is a chloroplast outer-envelope protein with an unknown function. Understanding CRL protein function may provide insights into the mechanism(s) of chloroplast partitioning. The analysis of chloroplast proliferation and partitioning in leaf mesophyll cells in *Arabidopsis arc* mutants and other transgenic lines has promoted research into the proliferation and partitioning of non-mesophyll plastids. Likewise, results obtained in GCs may be transferrable to other cell systems.

FINAL REMARK

The GC model opens many prospects for the development of chloroplast biology. For example, while cytoskeletal systems are known to regulate chloroplast morphology, movement, and partitioning (Sheahan et al., 2016; Wada, 2016; Erickson and Schattat, 2018), the role of each regulatory gene in chloroplast

proliferation and partitioning in plants has received little attention. On the other hand, once it becomes possible to impair GC chloroplast number or morphology *via* various experimental strategies, new insights into the molecular control of chloroplast morphogenesis in stomatal lineage cells may be provided. Additionally, in conjunction with quantitative analyses of chloroplast number during stomatal development, mathematical modeling may offer a new avenue for these investigations. This paper presents current knowledge of how GC chloroplast number is controlled and highlights the potential usefulness of *Arabidopsis* leaf GCs for understanding chloroplast proliferation and partitioning.

DATA AVAILABILITY STATEMENT

All datasets for this study are included in the article/ supplementary material.

AUTHOR CONTRIBUTIONS

MF conceived the study and wrote the manuscript. MF and AS conducted the experiments. AS and RI conducted the analyses. All authors read and approved the final manuscript.

FUNDING

This work was supported by the Ministry of Education, Culture, Science and Technology of Japan under KAKENHI (grant nos. 19K05831 to MF and 18K06314 to RI).

ACKNOWLEDGMENTS

The authors thank Dr. Nobuyuki Kanzawa (Sophia University) for advice on the work.

REFERENCES

Andriankaja, M., Dhondt, S., De Bodt, S., Vanhaeren, H., Coppens, F., De Milde, L., et al (2012). *Dev. Cell* 22, 64–78. doi: 10.1016/j.devcel.2011.11.011.

Asano, T., Yoshioka, Y., Kurei, S., Sakamoto, W., Sodmergen, and Machida, Y. (2004). A mutation of the CRUMPLED LEAF gene that encodes a protein localized in the outer envelope membrane of plastids affects the pattern of cell division, cell differentiation, and plastid division in *Arabidopsis*. *Plant J.* 38, 448–459. doi: 10.1111/j.1365-313X.2004.02057.x

Barton, K. A., Schattat, M. H., Jakob, T., Hause, G., Wilhelm, C., Mckenna, J. F., et al (2016). Epidermal pavement cells of *Arabidopsis* have chloroplasts. *Plant Physiol.* 171, 723–726. doi: 10.1104/pp.16.00608

Basak, I., and Møller, S. G. (2013). Emerging facets of plastid division regulation. *Planta* 237, 389–398. doi: 10.1007/s00425-012-1743-6

Birky, C. W. Jr. (1983). The partitioning of cytoplasmic organelles at cell division. *Int. Rev. Cytol.* 15, 49–86.

Boasson, R., and Laetsch, W. M. (1969). Chloroplast replication and growth in tobacco. *Sci.* 166, 749–751. doi: 10.1126/science.166.3906.749

Boffey, S. A., Ellis, J. R., Selldén, G., and Leech, R. M. (1979). Chloroplast division and DNA synthesis in light-grown wheat leaves. *Plant Physiol.* 64, 502–505. doi: 10.1104/pp.64.3.502

Butterfass, T. (1969). Die Plastidenverteilung bei der Mitose der Schließzellenmutterzellen von haploidem Schwedenklee (Trifolium hybridum L.). *Planta* 84, 230–234. doi: 10.1007/BF00388108

Butterfass, T. (1973). Control of plastid division by means of nuclear DNA amount. *Protoplasma* 76, 167–195. doi: 10.1007/BF01280696

Butterfass, T. (1979). "Patterns of chloroplast reproduction," in *A developmental approach to protoplasmic plant anatomy* (Wien: Springer-Verlag). doi: 10.1007/978-3-7091-8561-2

Chen, Y., Asano, T., Fujiwara, M. T., Yoshida, S., Machida, Y., and Yoshioka, Y. (2009). Plant cells without detectable plastids are generated in the crumpled leaf mutant of *Arabidopsis thaliana*. *Plant Cell Physiol.* 50, 956–969. doi: 10.1093/pcp/pcp047

Chiang, Y.-H., Zubo, Y. O., Tapken, W., Kim, H. J., Lavanway, A. M., Howard, L., et al (2012). Functional characterization of the GATA transcription factors GNC and CGA1 reveals their key role in chloroplast development, growth, and division in *Arabidopsis*. *Plant Physiol.* 160, 332–348. doi: 10.1104/pp.112.198705

Donnelly, P. M., Bonetta, D., Tsukaya, H., Dengler, R. E., and Dengler, N. G. (1999). Cell cycling and cell enlargement in developing leaves of *Arabidopsis*. *Dev. Biol.* 215, 407–419. doi: 10.1006/dbio.1999.9443

Ellis, J. R., and Leech, R. M. (1985). Cell size and chloroplast size in relation to chloroplast replication in light-grown wheat leaves. *Planta* 165, 120–125. doi: 10.1007/BF00392220

Erickson, J. L., and Schattat, M. H. (2018). Shaping plastid stromules – principles of *in vitro* membrane tubulation applied in planta. *Curr. Opin. Plant Biol.* 46, 48–54. doi: 10.1016/j.pbi.2018.07.003

Forth, D., and Pyke, K. A. (2006). The *suffulta* mutation in tomato reveals a novel method of plastid replication during fruit ripening. *J. Exp. Bot.* 57, 1971–1979. doi: 10.1093/jxb/erj14

Frandsen, N. (1968). Die Plastidenzahl als Merkmal bei der Kartoffel. *Theor. Appl. Genet.* 38, 153–167. doi: 10.1007/BF00933811

Fujiwara, M. T., Hashimoto, H., Kazama, Y., Abe, T., Yoshida, S., Sato, N., et al (2008). The assembly of the FtsZ ring at the mid-chloroplast division site depends on a balance between the activities of AtMinE1 and ARC11/AtMinD1. *Plant Cell Physiol.* 49, 345–361. doi: 10.1093/pcp/pcn012

Fujiwara, M. T., Yasuzawa, M., Kojo, K. H., Niwa, Y., Abe, T., Yoshida, S., et al (2018). The *Arabidopsis* arc5 and arc6 mutations differentially affect plastid morphology in pavement and guard cells in the leaf epidermis. *PLOS ONE* 13, e0192380. doi: 10.1371/journal.pone.0192380

Fujiwara, M. T., Yasuzawa, M., Sasaki, S., Nakano, T., Niwa, Y., Yoshida, S., et al (2017). The *Arabidopsis minD* mutation causes aberrant FtsZ1 ring placement and moderate heterogeneity of chloroplasts in the leaf epidermis. *Plant Signal. Behav.* 12, e1343776. doi: 10.1080/15592324.2017.1343776

Gao, H., and Gao, F. (2011). Evolution of the chloroplast division machinery. *Front. Biol.* 6, 398–413. doi: 10.1007/s11515-011-1139-1

Hachez, C., Ohashi-Ito, K., Dong, J., and Bergmann, D. C. (2011). Differentiation of *Arabidopsis* guard cells: analysis of the networks incorporating the basic helix-loop-helix transcription factor, FAMA. *Plant Physiol.* 155, 1458–1472. doi: 10.1104/pp.110.167718

Hamada, S., and Baba, H. (1930). On the number of chloroplasts in the guard cells in mulberry (translated in English by Butterfass (1973)). *J. Sericult. Sci. Japan* 1, 305–309. doi: 10.11416/kontyushigen1930.1.4_305

Hennis, A., and Birky, C. W. Jr. (1984). Stochastic partitioning of chloroplasts at cell division in the alga Olisthodiscus, and compensating control of chloroplast replication. *J. Cell Sci.* 70, 1–15.

Higaki, T., Kutsuna, N., Hosokawa, Y., Akita, K., Ebine, K., Ueda, T., et al (2012). Statistical organelle dissection of Arabidopsis guard cells using image database LIPS. *Sci. Rep.* 2, 405. doi: 10.1038/srep00405

Hoffmann, P. (1968). "Zur Physiologie der Photosynthese bei höheren Pflanzen," in *Botanische Studien*, vol. 18. (Verlag, Jena: Gustav Fischer).

Honda, S. I., Hongladarom-Honda, T., and Kwanyuen, P. (1971). Interpretations on chloroplast reproduction derived from correlations between cells and chloroplasts. *Planta* 97, 115. doi: 10.1007/BF00388401

Itoh, R. D., Ishikawa, H., Nakajima, K. P., Moriyama, S., and Fujiwara, M. T. (2018). Isolation and analysis of a stromule-overproducing *Arabidopsis* mutant suggest

the role of *PARC6* in plastid morphology maintenance in the leaf epidermis. *Physiol. Plant.* 162, 479–494. doi: 10.1111/ppl.12648

Iura, M. (1934). On the size of the guard cells, as well as the number of chloroplasts in them in the leaf of Brassica. *Jap. J. Genet.* 9, 239–245. doi: 10.1266/jjg.9.239

Jacobs, J. P., and Yoder, J. I. (1989). Ploidy levels in transgenic tomato plants determined by chloroplast number. *Plant Cell Rep.* 7, 662–664. doi: 10.1007/BF00272055

Kalve, S., De Vos, D., and Beemster, G. T. S. (2014). Leaf development: a cellular perspective. *Front. Plant Sci.* 5, 1–25. doi: 10.3389/fpls.2014.00362

Kawade, K., Horiguchi, G., Ishikawa, N., Hirai, M. Y., and Tsukaya, H. (2013). Promotion of chloroplast proliferation upon enhanced post-mitotic cell expansion in leaves. *BMC Plant Biol.* 13, 143. doi: 10.1186/1471-2229-13-143

Keech, O., Pesquet, E., Ahad, A., Askne, A., Nordvall, D., Vodnala, S. M., et al (2007). The different fates of mitochondria and chloroplasts during dark-induced senescence in Arabidopsis leaves. *Plant Cell Environ.* 30, 1523–1534. doi: 10.1111/j.1365-3040.2007.01724.x

Kinsman, E. A., and Pyke, K. A. (1998). Bundle sheath cells and cell-specific plastid development in *Arabidopsis* leaves. *Dev.* 125, 1815–1822.

Kirk, J. T. O., and Tilney-Bassett, R. A. E. (1978). "The Plastids – Their Chemistry, Structure, Growth and Inheritance" (Amsterdam, The Netherlands: Elsevier/North- Holland).

Lamppa, G. K., Elliot, L. V., and Bendich, A. J. (1980). Changes in chloroplast number during pea leaf development. *Planta* 148, 437–443. doi: 10.1007/BF00552656

Lawson, T. (2009). Guard cell photosynthesis and stomatal function. *New Phytol.* 181, 13–34. doi: 10.1111/j.1469-8137.2008.02685.x

Leech, R. M., and Pyke, K. A. (1988). "Chloroplast division in higher plants with particular reference to wheat," in *In Division and Segregation of Organelles*. Eds. Boffey, S. A., and Lloyd, D. (Cambridge: Cambridge University Press), 39–62.

Li, Y., Wang, L., Wang, G., Feng, Y., and Liu, X. (2017). AT2G21280 only has a minor role in chloroplast division. *Front. Plant Sci.* 8, 2095. doi: 10.3389/fpls.2017.02095

López-Juez, E., and Pyke, K. A. (2005). Plastids unleashed: their development and their integration in plant development. *Int. J. Dev. Biol.* 49, 557–577. doi: 10.1387/ijdb.051997el

Macfarlane, J. M. (1898). Observations on some hybrids between Drosera filiformis and D. intermedia. *Trans. Proc. Bot. Soc. Penn.* 1, 87–99.

Melaragno, J. E., Mehrotra, B., and Coleman, A. (1993). Relationship between endopolyploidy and cell size in epidermal tissue of *Arabidopsis*. *Plant Cell* 5, 1661–1668. doi: 10.1105/tpc.5.11.1661

Miyagishima, S., Nakanishi, H., and Kabeya, Y. (2011). Structure, regulation, and evolution of the plastid division machinery. *Int. Rev. Cell Mol. Biol.* 291, 115–153. doi: 10.1016/B978-0-12-386035-4.00004-5

Mochizuki, A., and Sueoka, N. (1955). Genetic studies on the number of plastid in stomata I. Effects of autopolyploidy in sugar beets. *Cytologia* 20, 358–366. doi: 10.1508/cytologia.20.358

Mullet, J. E. (1988). Chloroplast development and gene expression. *Ann. Rev. Plant Physiol. Plant Mol. Biol.* 39, 475–502. doi: 10.1146/annurev.pp.39.060188.002355

Nadeau, J. A., and Sack, F. D. (2002). Stomatal development in *Arabidopsis*. *The Arabidopsis Book* 1, e0066. doi: 10.1199/tab.0066

Nebenführ, A. (2007). "Organelle dynamics during cell division," in *Cell Division Control in Plants Plant Monographs*, vol. 9. Eds. Verma, D. P. S., and Hong, Z. (Springer, Berlin, Heidelberg), 195–206. doi: 10.1007/7089_2007_129.

Nebenführ, A., Frohlick, J. A., and Staehelin, L. A. (2000). Redistribution of Golgi stacks and other organelles during mitosis and cytokinesis in plant cells. *Plant Physiol.* (Springer-Verlag) 124, 135–151. doi: 10.1104/pp.124.1.135

Okazaki, K., Kabeya, Y., Suzuki, K., Mori, T., Ichikawa, T., Matsui, M., et al (2009). The PLASTID DIVISION1 and 2 components of the chloroplast division machinery determine the rate of chloroplast division in land plant cell differentiation. *Plant Cell* 21, 1769–1780. doi: 10.1105/tpc.109.067785

Osteryoung, K. W., and Pyke, K. A. (2014). Division and dynamic morphology of plastids. *Annu. Rev. Plant. Biol.* 65, 443–472. doi: 10.1146/annurev-arplant- 050213-035748

Possingham, J. V., and Lawrence, M. E. (1983). Controls to plastid division. *Int. Rev. Cytol.* 84, 1–56. doi: 10.1016/S0074-7696(08)61014-1

Possingham, J. V., and Saurer, W. (1969). Changes in chloroplast number per cell during leaf development in spinach. *Planta* 86, 186–194. doi: 10.1007/BF00379826

Pyke, K. A. (1997). Plastid division and development. *Am. J. Bot.* 84, 1017–1027. doi: 10.2307/2446145

Pyke, K. A., and Leech, R. M. (1987). The control of chloroplast number in wheat mesophyll cells. *Planta* 170, 416–420. doi: 10.1007/BF00395035

Pyke, K. A., and Leech, R. M. (1991). Rapid image analysis screening procedure for identifying chloroplast number mutants in mesophyll cells of *Arabidopsis* thaliana (L.) Heynh. *Plant Physiol.* 96, 1193–1195. doi: 10.1104/pp.96.4.1193

Pyke, K. A., and Leech, R. M. (1994). A genetic analysis of chloroplast division and expansion in *Arabidopsis thaliana*. *Plant Physiol.* 104, 201–207. doi: 10.1104/pp.104.1.201

Pyke, K. A., Rutherford, S. M., Robertson, E. J., and Leech, R. M. (1994). arc6, a fertile *Arabidopsis* mutant with only two mesophyll cell chloroplasts. *Plant Physiol.* 106, 1169–1177. doi: 10.1104/pp.106.3.1169

Qin, X., and Rotino, G. L. (1995). Chloroplast number in guard cells as ploidy indicator of *in vitro*-grown androgenic pepper plantlets. *Plant Cell Tissue Organ Cult.* 41, 145–149. doi: 10.1007/BF00051583

Robertson, E. J., Pyke, K. A., and Leech, R. M. (1995). arc6, an extreme chloroplast division mutant of *Arabidopsis* also alters proplastid proliferation and morphology in shoot and root spices. *J. Cell Sci.* 108, 2937–2944.

Sachs, J. (1875). *Textbook of Botany*. Oxford: Clarendon Press.

Sakisaka, M. (1929). On the number of chloroplasts in the guard cells of seed plants. *Bot. Mag.* 43, 46–48. doi: 10.15281/jplantres1887.43.46

Seguí-Simarro, J. M., and Staehelin, L. A. (2009). Mitochondrial reticulation in shoot apical meristem cell provides a mechanism for homogeneization of mtDNA prior to gamete formation. *Plant Signal. Behavior.* 4, 168–171. doi: 10.4161/psb.4.3.7755

Sheahan, M. B., McCurdy, D. W., and Rose, R. J. (2016). "Mechanisms of organelle inheritance in dividing plant cells," in *Molecular Cell Biology of the Growth and Differentiation of Plant Cells*. Ed. Rose, R. J. (Boca Raton: FL: CRC Press), 66–85. doi: 10.1201/b20316

Sheahan, M. B., Rose, R. J., and McCurdy, D. W. (2004). Organelle inheritance in plant cell division: the actin cytoskeleton is required for unbiased inheritance of chloroplasts, mitochondria and endoplasmic reticulum in dividing protoplasts. *Plant J.* 37, 379–390. doi: 10.1046/j.1365-313X.2003.01967.x

Singsit, C., and Veilleux, R. E. (1991). Chloroplast density in guard cells of leaves of anther-derived potato plants grown *in vitro* and *in vivo*. *HortScience* 26, 592–594. doi: 10.21273/HORTSCI.26.5.592

Stokes, K. D., McAndrew, R. S., Figueroa, R., Vitha, S., and Osteryoung, K. W. (2000). Chloroplast division and morphology are differentially affected by overexpression of FtsZ1 and FtsZ2 genes in *Arabidopsis*. *Plant Physiol.* 124, 1668–1677. doi: 10.1104/pp.124.4.1668

Taiz, L., Zeiger, E., Møller, I. M., and Murphy, A. (2015). *Plant Physiology and Development, Sixth Ed*. Sunderland, MA: Sinauer Associates Inc.

Thomas, M. R., and Rose, R. J. (1983). Plastid number and plastid structural changes associated with tobacco mesophyll protoplast culture and plant regeneration. *Planta* 158, 329–338. doi: 10.1007/BF00397335

Tirlapur, U. K., and König, K. (2001). Femtosecond near-infrared lasers as a novel tool for non-invasive real-time high-resolution time-lapse imaging of chloroplast division in living bundle sheath cells of *Arabidopsis*. *Planta* 214, 1–10. doi: 10.1007/s004250100597

Vitha, S., McAndrew, R. S., and Osteryoung, K. W. (2001). FtsZ ring formation at the chloroplast division site in plants. *J. Cell Biol.* 153, 111–120. doi: 10.1083/jcb.153.1.111

Vitha, S., Froehlich, J. E., Koksharova, O., Pyke, K. A., van Erp, H., and Osteryoung, K. W. (2003). ARC6 is a J-domain plastid division protein and an evolutionary descendant of the cyanobacterial cell division protein Ftn2. *Plant Cell* 15, 1918–1933. doi: 10.1105/tpc.013292

Wada, M. (2016). Chloroplast and nuclear photorelocation movements. *Proc. Jpn. Acad. Ser. B Phys. Biol. Sci.* 92, 387–411. doi: 10.2183/pjab.92.387

Wild, A., and Wolf, G. (1980). The effect of different light intensities on the frequency and size of stomata, the size of cells, the number, size and chlorophyll content of chloroplasts in the mesophyll and the guard cells during the ontogeny of primary leaves of Sinapis alba. *Z. Pflanzenphysiol. Bd.* 97, 325–342. doi: 10.1016/S0044-328X(80)80006-7

Yoder, D. W., Kadirjan-Kalbach, D., Olson, B. J. S. C., Miyagishima, S., DeBlasio, S. L., Hangarter, R. P., et al (2007). Effects of mutations in *Arabidopsis* FtsZ1 on plastid division, FtsZ ring formation and positioning, and FtsZ filament morphology in vivo. *Plant Cell Physiol.* 48, 775–791. doi: 10.1093/pcp/pcm049

Yu, Z., Haage, K., Streit, V. E., Gierl, A., and Torres-Ruiz, R. A. (2009). A large number of tetraploid *Arabidopsis thaliana* lines, generated by a rapid strategy, reveal high stability of neo-tetraploids during consecutive generations. *Theor. Appl. Genet.* 118, 1107–1119. doi: 10.1007/s00122-009-0966-9

Zhao, L., and Sack, F. D. (1999). Ultrastructure of stomatal development in *Arabidopsis* (Brassicaceae) leaves. *Am. J. Bot.* 86, 929–939. doi: 10.2307/2656609

Conflict of Interest: The authors declare that the research was conducted in the absence of any commercial or financial relationships that could be construed as a potential conflict of interest.

frontiers in Plant Science

ORIGINAL RESEARCH
published: 08 November 2019
doi: 10.3389/fpls.2019.01401

Membrane-Specific Targeting of Tail-Anchored Proteins SECE1 and SECE2 Within Chloroplasts.

*Stacy A. Anderson, Rajneesh Singhal† and Donna E. Fernandez**

Department of Botany, University of Wisconsin-Madison, Madison, WI, United States

Membrane proteins that are imported into chloroplasts must be accurately targeted in order to maintain the identity and function of the highly differentiated internal membranes. Relatively little is known about the targeting information or pathways that direct proteins with transmembrane domains to either the inner envelope or thylakoids. In this study, we focused on a structurally simple class of membrane proteins, the tail-anchored proteins, which have stroma-exposed amino-terminal domains and a single transmembrane domain within 30 amino acids of the carboxy-terminus. SECE1 and SECE2 are essential tail-anchored proteins that function as components of the dual SEC translocases in chloroplasts. SECE1 localizes to the thylakoids, while SECE2 localizes to the inner envelope. We have used transient expression in Arabidopsis leaf protoplasts and confocal microscopy in combination with a domain-swapping strategy to identify regions that contain important targeting determinants. We show that membrane-specific targeting depends on features of the transmembrane domains and the short C-terminal tails. We probed the contributions of these regions to targeting processes further through site-directed mutagenesis. We show that thylakoid targeting still occurs when changes are made to the tail of SECE1, but changing residues in the tail of SECE2 abolishes inner envelope targeting. Finally, we discuss possible parallels between sorting of tail-anchored proteins in the stroma and in the cytosol.

Keywords: chloroplast, inner envelope membrane, thylakoid, organelle biogenesis, SEC translocase, tail-anchored protein, targeting

OPEN ACCESS

Edited by:
Rebecca L. Roston, University of Nebraska-Lincoln, United States

Reviewed by:
Hsou-min Li, Academia Sinica, Taiwan
Carole Dabney-Smith, Miami University, United States

****Correspondence:***
Donna E. Fernandez
dfernand@wisc.edu

†Present address:
Rajneesh Singhal, Department of Plant Biology, Michigan State University, East Lansing, MI, United States

Specialty section:
This article was submitted to Plant Physiology, a section of the journal Frontiers in Plant Science

Received: *03 June 2019*
Accepted: *10 October 2019*
Published: *08 November 2019*

Citation:
Anderson SA, Singhal R and Fernandez DE (2019) Membrane-Specific Targeting of Tail-Anchored Proteins SECE1 and SECE2 Within Chloroplasts. Front. Plant Sci. 10:1401. doi: 10.3389/fpls.2019.01401

INTRODUCTION

For biogenesis and maintenance of a functional chloroplast, proteins must be localized in the correct compartments. Most chloroplast proteins are encoded by nuclear genes. Therefore, targeting is a multi-step process, involving delivery of newly synthesized precursor proteins to the import apparatus in the envelope membranes, translocation through the outer and inner envelopes, and subsequent sub-organellar targeting of the imported proteins (for recent reviews, see Lee et al., 2017; Richardson et al., 2017). Imported proteins have five possible destinations: soluble proteins may reside in the stroma, in the thylakoid lumen, or in the intermembrane space, while membrane proteins may function either in the inner envelope or the thylakoid membranes.

Membrane proteins that are imported present a special challenge: although most membrane proteins are targeted co-translationally in the cyanobacterial ancestors of chloroplasts, they must be

Abbreviations: GFP, green fluorescent protein; GRAVY, grand average of hydropathy; TA, tail-anchored; TMD, transmembrane domain

targeted in a post-translational fashion within the organelle. Many of these proteins have highly hydrophobic domains and must be shielded from the aqueous environment to prevent aggregation while they are being targeted and integrated. Despite their importance for photosynthesis, biosynthesis, and transport, we know relatively little about the targeting information and systems that direct them to particular membranes. For example, we do not yet have a reliable strategy for directing novel or engineered membrane proteins to the inner envelope (Rolland et al., 2017).

To further our understanding of membrane-specific targeting in chloroplasts, we have studied targeting of the membrane components of the two SEC translocases in chloroplasts. We previously reported on a study of the SCY components (homologs of bacterial SecY proteins) with 10 transmembrane domains (TMDs) (Singhal and Fernandez, 2017). We identified sequences within the N-terminal leader and characteristics of the TMDs as important determinants for membrane-specific targeting, and performed experiments that implicated the chloroplast Signal Recognition Particle (SRP) pathway in the targeting of thylakoid-localized SCY1. In the present study, we have focused on the SECE components (homologs of bacterial SecE proteins). Previous studies have shown that SECE1 is confined to the thylakoids (Schuenemann et al., 1999), while SECE2 is primarily associated with the inner envelope (Li et al., 2015). Both proteins have a single TMD followed by a tail of 30 amino acids or fewer, and belong to a special class of proteins known as tail-anchored (TA) proteins. Because they share a similar structure, we were able to swap different domains without perturbing the overall topology of the proteins. To identify regions important for targeting, we expressed and localized fluorescently tagged chimeric proteins in transfected protoplasts. We learned that targeting determinants are located in the TMD and tail regions, rather than the stroma-exposed N-terminal regions. Physicochemical properties of the TMDs and tails appear to dictate which pathway the TA protein will enter and whether it will insert into the target membrane or remain in a stromal pool. The position and nature of these determinants are fundamentally different than anything previously described in studies of membrane targeting inside chloroplasts. They may, however, include some characteristics that mirror those of cytosolically targeted TA proteins. We suggest that targeting pathways novel to the chloroplast may be involved.

MATERIALS AND METHODS

Sequence Analysis and Definition of SECE Protein Regions

Putative SECE1 and SECE2 protein sequences from multiple plant species were acquired by homology searches using the blastp algorithm of BLAST (https://blast.ncbi.nlm.nih.gov/Blast.cgi) (Altschul et al., 1990) and the predicted protein sequence of *Arabidopsis thaliana* SECE1 (At4g14870) or SECE2 (At4g38490). Protein sequences were acquired from TAIR (https://www.arabidopsis.org/index.jsp). Sequences used for alignments were chosen based on the availability of complete protein sequences for both SECE1 and SECE2 in a given species and to reflect species diversity. Sequences were aligned using the M-Coffee algorithm (Wallace et al., 2006) (http://tcoffee.crg.cat/apps/tcoffee/index.html). The resulting alignment files were submitted to BoxShade (https://embnet.vital-it.ch/software/BOX_form.html) to create the alignment figures.

Different regions of SECE1 and SECE2 were defined based on a combination of topological features and protein sequence alignments. The signature, linker and TMD, and tail regions of SECE2 were previously defined in Li et al. (2015) and comparable regions of SECE1 regions were identified using sequence alignments. The N region was defined as everything N-terminal to the signature region. The N region was further subdivided such that the N1 region contained the predicted transit peptide, the GFP insertion site, and 5–9 amino acids C-terminal to that site. The N2 region included amino acid sequences that showed a moderate degree of conservation in alignments and were predicted to have a helical secondary structure, when analyzed using the JPred4 algorithm (http://www.compbio.dundee.ac.uk/jpred/) (Drozdetskiy et al., 2015). The TMDs were identified using consensus transmembrane domain prediction programs (ConPred_v2 and AramTmCon) available through the Aramemnon database (http://aramemnon.uni-koeln.de/) (Schwacke et al., 2003) or the topology prediction in UniProt (https://www.uniprot.org/) (TheUniprot Consortium, 2019).

The helical propensity, hydrophobicity scores of the TMDs, and hydrophobicity plots were calculated using various web-based tools. Helical propensity was calculated using the Agadir algorithm (http://agadir.crg.es/) (Muñoz and Serrano, 1997) with conditions pH 7.5, 298 K, and ionic strength 0.15 M. The grand average of hydropathy (GRAVY) scores were calculated using the GRAVY calculator (http://www.gravy-calculator.de/) (Kyte and Doolittle, 1982). Hydrophobicity plots for the C-terminal regions (starting with the conserved E-W-P motif) of SECE1 and SECE2 were created using the ProtScale tool in ExPASy (https://web.expasy.org/protscale/) (Gasteiger et al., 2005). The "Hydrophob./Kyte & Doolittle" amino acid scale, a window size of 9, relative weight of 100%, linear weight variation model, and "no normalization of the scale" were used.

Generation of GFP-Fusion Constructs

Generation of the GFP-SECE2 construct was described previously (Li et al., 2015). For amplification of SECE1 sequence, cDNA prepared from Arabidopsis (Wassilewskija ecotype) seedling RNA or, because SECE1 has no introns, a previously described Columbia ecotype SECE1 genomic clone (Skalitzky et al., 2011) were used as templates. The GFP-SECE1 construct was assembled by amplifying a fragment encoding the putative transit peptide plus the first 33 amino acids of the mature protein, a second fragment encoding GFP, and a third fragment encoding the rest of the protein, and then connecting the fragments using overlap-extension PCR. The final PCR product was then introduced into the vector pML94 (Bionda et al., 2010) between the Kpn1 and BamHI restriction sites by sequence- and ligation-independent cloning (Jeong et al., 2012). pML94 includes sequence encoding the promoter for the 35S gene of cauliflower mosaic virus, which should confer high level constitutive expression *in planta*. All other SECE1–SECE2 chimeric constructs were generated from the GFP-SECE1 and GFP-SECE2 clones using primers that spanned

the SECE1–SECE2 junctions. Individual fragments were joined by overlap-extension PCR and the complete coding sequence was introduced into pML94 by sequence- and ligation-independent cloning. All plasmids used for imaging were verified by sequencing.

Protoplast Isolation and Transfection

For protoplast preparation, *Arabidopsis thaliana* (Columbia ecotype) plants were grown using a 12 h light/12 h dark cycle at 22°C as described in Singhal and Fernandez (2017). Leaves were removed from plants that were 4–5 weeks old and still in the vegetative phase. Protoplasts were isolated using a tape sandwich method as described in Wu et al. (2009) except that more leaves (~25) were used so that transfections could be performed on a higher number of cells. PEG-mediated transfections of 100,000–500,000 cells were performed as described in Yoo et al. (2007) except that buffer W1 was eliminated and replaced by an equal volume of W5 buffer. Transfections were performed using 10 μg DNA for all plasmids encoding SECE constructs or 6 μg of the TIC20-mCherry plasmid, which was previously described in Singhal and Fernandez (2017). Protoplasts were incubated in the dark for 12–16 h.

Microscopy and Image Analysis

Transfected protoplasts that had been incubated overnight were transferred to μ-Slide Angiogenesis slides (Ibidi, https://ibidi.com/) and imaged using Zeiss LSM 710 and LSM 780 Confocal microscopes (Zeiss, https://www.zeiss.com/microscopy/us). A 488-nm laser was used for GFP excitation and a 561-nm laser for chlorophyll excitation and mCherry excitation. GFP emission was recorded at 499–526 nm, chlorophyll autofluorescence was recorded at 655–735 nm, and mCherry emission was recorded at 589–636 nm. For each construct, at least three to five transfected protoplasts were imaged in each of three independent experiments.

Co-localization analysis and calculation of Pearson's correlation coefficients were performed on 16 protoplasts using the Coloc2 plugin of the ImageJ software. Although similar distributions of fluorescent proteins were observed regardless of the position of the chloroplast within the protoplast or its orientation, for fluorescence intensity plots, we chose chloroplasts angled such that distinct thylakoid and stromal regions were visible. Appropriate linear regions were selected and the pixel intensity values were recorded from the GFP and chlorophyll or mCherry channels. Intensity measurements were performed in ImageJ (Version 2.0.0-rc-68/1.52g, NIH, https://imagej.nih.gov). A minimum of three fluorescence intensity plots, one each from three different protoplasts, were generated and compared for each construct. The protoplasts and scans shown are representative images.

RESULTS

SECE1 and SECE2 Localize to Distinct Compartments When Transiently Expressed in Protoplasts

To localize SECE1 and SECE2 in chloroplasts, we imaged fluorescent fusion proteins in transfected Arabidopsis leaf protoplasts. Localizations to the stroma, thylakoids, or envelope membranes can be easily distinguished using this assay system (**Figure S1**). To localize SECE1 and SECE2, sequence encoding GFP was added downstream of the predicted transit peptide cleavage site, such that GFP would be in the N-terminal domain of the predicted mature protein and exposed in the stroma. SECE1 has been previously shown by fractionation to be confined to the thylakoids (Schuenemann et al., 1999). For GFP-SECE1 (construct I, **Figure 1A**), the GFP fluorescence occupied most of the interior of the chloroplast, showing strong co-localization (Pearson's R value = 0.84 ± 0.05) with chlorophyll autofluorescence (**Figure 1B**). However, we also saw some association with interior regions without chlorophyll, which suggests that transfer of the fusion protein from a stromal pool to the thylakoids is less than 100% efficient under our incubation conditions. The relative amounts of GFP-SECE1 in membrane and soluble fractions prepared from chloroplasts isolated from transfected protoplasts are consistent with this conclusion (**Figure S2C**). To demonstrate that GFP-SECE1 is not associated with the inner envelope, constructs encoding GFP-SECE1 and TIC20-mCherry, an inner envelope marker, were co-transfected. The profile of TIC20-mCherry shows two peaks in linear scans, indicating envelope localization, and was spatially separate from the GFP-SECE1 signal (**Figure 1D**). For GFP-SECE2 (construct II), GFP fluorescence was confined to the periphery of the chloroplasts, producing a profile of two distinct peaks in linear scans of individual chloroplasts (**Figure 1C**). The chlorophyll autofluorescence signal showed a very different profile, occupying a more central location to the inside of the GFP-SECE2 peaks. The peripheral localization of GFP-SECE2 is consistent with localization in the inner envelope, which was previously established by demonstrating interactions between SECE2 and the inner envelope integral membrane protein SCY2, as well as co-localization of GFP-SECE2 and TIC20-mCherry in transfected protoplasts (Li et al., 2015). We found that GFP-SECE2 fusion proteins were associated exclusively with the membrane fraction in chloroplasts isolated from transfected protoplasts (**Figure S2D**). We conclude that the distribution of GFP fusion proteins accurately reflects the localization of the chloroplast SECE proteins in different chloroplast compartments.

SECE1 and SECE2 Have Conserved Structures But Different Sequences

Because SECE1 and SECE2 have similar domain structures and topologies, individual domains can be swapped without perturbing the overall structure of the proteins. We undertook a series of domain-swapping experiments in order to identify regions responsible for differential targeting of SECE1 and SECE2. As a first step, we analyzed and aligned SECE1 and SECE2 sequences in different plant species (**Figures 2** and **3**) and identified four regions of interest, which we designated as the N-terminal region (subdivided into N1 and N2), the signature domain, the linker and TMD region, and the C-terminal region (tail). The amino acids included in each region are shown in **Figure 1E**.

The N-terminal region is the region that is least conserved between species, and the SECE1 and SECE2 N-terminal regions cannot be easily aligned. This region is likely to be fully exposed

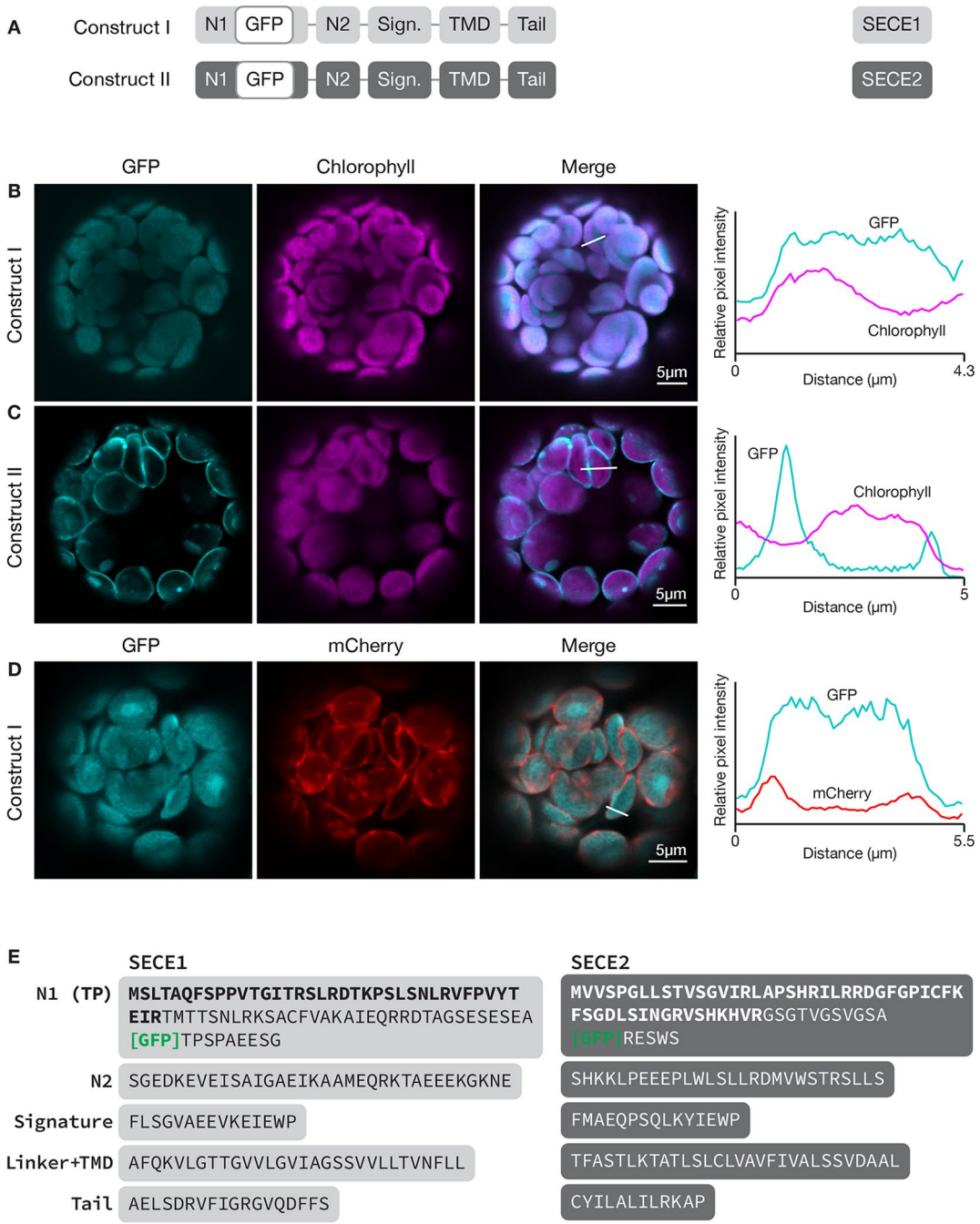

FIGURE 1 | Localization of GFP-SECE1 and GFP-SECE2 in transfected protoplasts and designation of protein domains in SECE1 and SECE2. **(A)** Diagrams depicting constructs I and II. SECE1 sequences are indicated with light gray and SECE2 sequences with dark gray; N1 and N2: N-terminal regions; GFP: green fluorescent protein; Sign.: signature domain; TMD: linker plus transmembrane domain; Tail: C-terminal tail. **(B–D)** Leaf protoplasts from 4–5 week old wildtype (Columbia ecotype) plants were transfected with **(B)** construct I, **(C)** construct II, or **(D)** construct I plus a TIC20-mCherry construct. The images show GFP fluorescence (cyan), chlorophyll fluorescence (magenta) or TIC20-mCherry fluorescence (red), merged images, and relative pixel intensity diagrams that correspond with the white lines on the merged images. **(E)** Amino acid sequences that correspond to the individual domains of SECE1 and SECE2. Predicted transit peptides (TP) are shown in bold text and the GFP insertion site is indicated. TMD, transmembrane domain.

to the stroma following membrane insertion of the TMD. For experimental purposes, we subdivided the N-terminal region into two unequal halves. The region designated as N1 includes the transit peptide and the GFP insertion site. This region lacks any predicted secondary structure according to the JPred4 algorithm (http://www.compbio.dundee.ac.uk/jpred/) (Drozdetskiy et al., 2015). The region designated as N2 includes amino acid sequence predicted to form a helix in both SECE1 and SECE2 (data not shown).

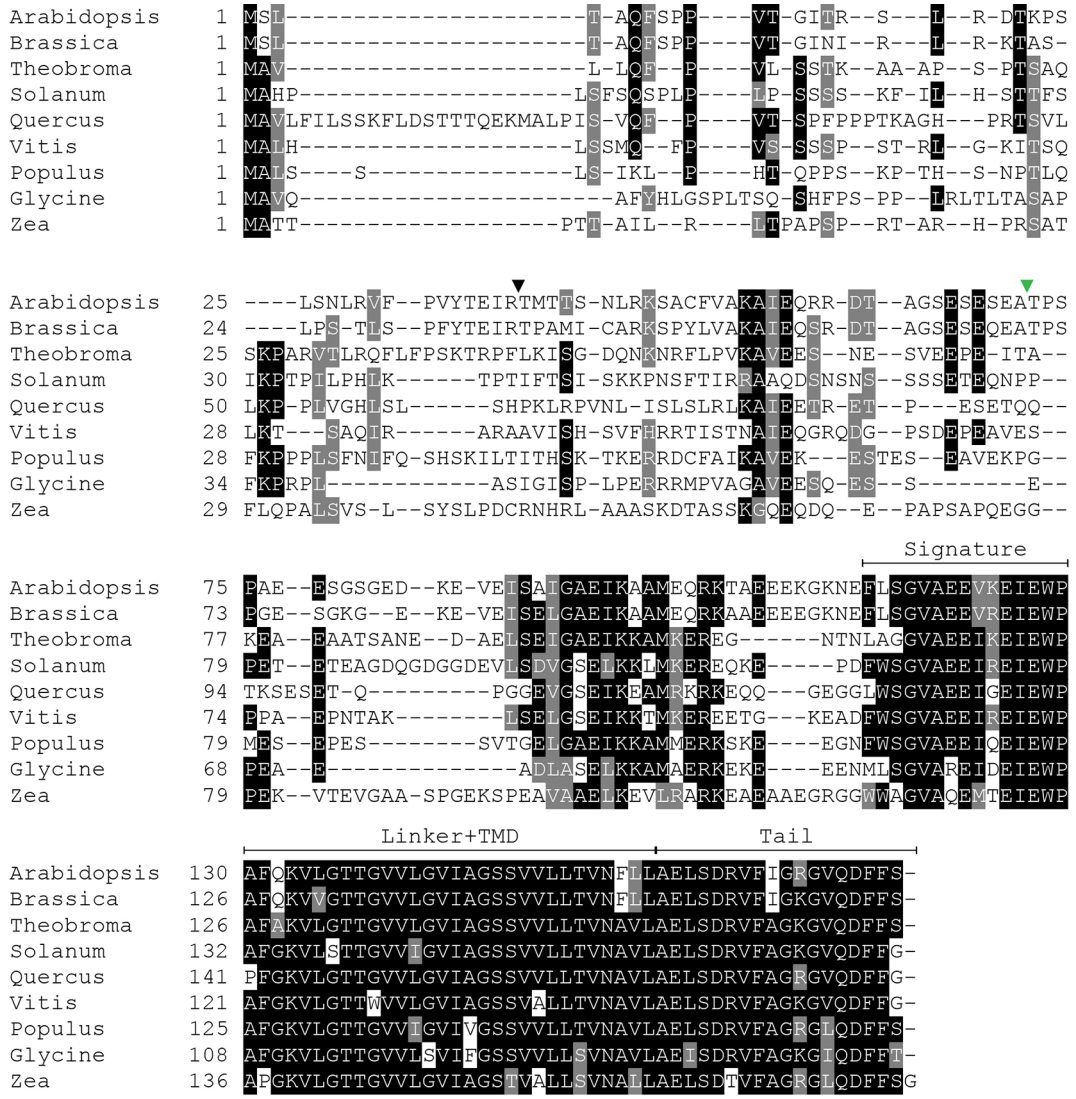

FIGURE 2 | Multiple sequence alignment of SECE1 from a variety of plant species. The predicted transit peptide cleavage site in Arabidopsis is indicated with a black triangle. The GFP insertion site is indicated by a green triangle. Signature, signature region; TMD, transmembrane domain; Tail, C-terminal tail.

Following the N-terminal region, SECE1 and SECE2 each has a 15-amino acid region designated as the signature domain. When SECE1 and SECE2 are considered separately, the signature domain is highly conserved between different species (**Figures 2** and **3**); however, when SECE1 and SECE2 are compared, their signature domains are quite different. This region ends with the amino acid motif E-W-P, which are the only invariant amino acids in both proteins. A short linker sequence connects the signature region with the predicted TMD. The linker sequences were included with the TMD as a single domain. The TMD is followed by a short region, which we designated as the tail region. We designated the final 18 amino acids as the SECE1 tail and the final 12 amino acids as the SECE2 tail. With three acidic and two basic residues, the SECE1 tail has an overall charge that is slightly negative, while the SECE2 tail has two adjacent basic residues and is positively charged.

Targeting Determinants Are Associated With the TMDs and C-Terminal Tails

To define the minimal region required to target a protein to the inner envelope, we started with full-length GFP-SECE2 and replaced individual regions with the corresponding SECE1 sequence, progressing from the N-terminus to C-terminus of SECE2 (**Figure 4A**). When the N1 and N2 regions of SECE2 were replaced with the corresponding SECE1 sequence, most of the chimeric proteins were still associated with the envelope (construct III, **Figure 4B**). A similar pattern was seen when the N1 region, N2 region, and the signature domain of SECE2 were replaced (construct IV, **Figure 4C**). We concluded that the domains that are predicted to be stroma-exposed after integration were unlikely to contain important determinants for envelope targeting.

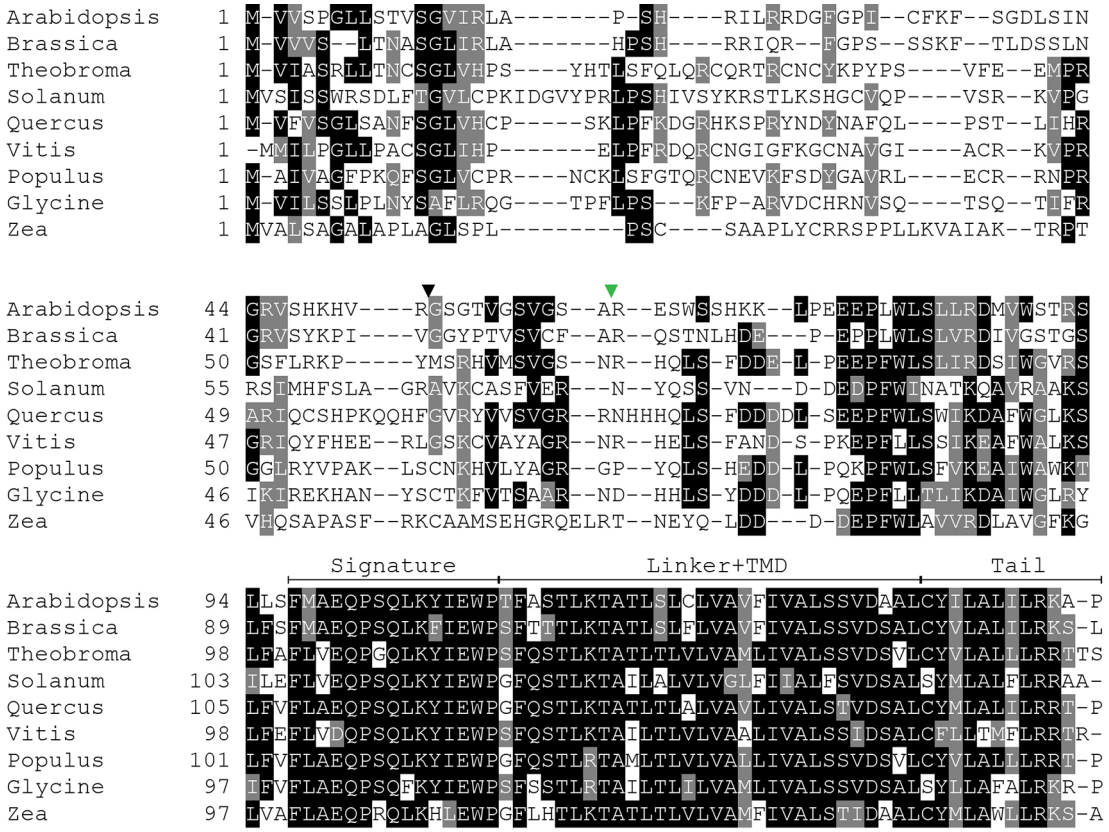

FIGURE 3 | Multiple sequence alignment of SECE2 from a variety of plant species. The predicted transit peptide cleavage site in Arabidopsis is indicated with a black triangle. The GFP insertion site is indicated by a green triangle. Signature, signature region; TMD, transmembrane domain; Tail, C-terminal tail.

When the TMD region of SECE2, in addition to N1 region, N2 region, and the signature domain, was replaced, leaving SECE2 sequence only in the tail (construct V), the chimeric proteins were displaced from the envelope and accumulated in the interior of the chloroplasts (**Figure 4D**). The overlap between GFP fluorescence and chlorophyll autofluorescence, as shown in the fluorescence intensity diagram, suggests that this chimeric protein is associated with the thylakoid membranes. This series of experiments indicated that important inner envelope targeting determinants are associated with the TMD of SECE2.

To probe this further, we wanted to conduct the inverse experiment, progressively replacing SECE2 sequences with SECE1 sequences starting at the C-terminus. However, we learned in preliminary experiments that chimeric proteins with the N1 region, N2 region, and signature domain of SECE2, and the TMD and tail of SECE1, failed to import into the chloroplast (data not shown). We found that if we modified the constructs such that they included the N1 region of SECE1, the chimeric proteins were successfully imported. Therefore, we started this series of experiments with a construct that encoded most of the mature SECE2 protein but included the N1 region of SECE1 (construct VI, **Figure 5**). The chimeric protein encoded by this construct was primarily associated with the envelope (**Figure 5B**). We observed some fluorescent foci, which we suspect reflects a limited degree of protein aggregation. Despite these visible foci, this protein retained the overall localization pattern of full length SECE2. When we replaced the SECE2 tail with the SECE1 tail (construct VII), the chimeric protein showed stromal accumulation rather than envelope localization (**Figure 5C**). Chimeric proteins that included both the SECE1 TMD and tail (construct VIII) also accumulated primarily in the stroma (**Figure 5D**). We conclude that the SECE2 tail is also necessary for envelope targeting.

Next, we asked whether the sequences in the TMD and tail must be located at the C-terminus in order to function appropriately as targeting determinants. To test this, we fused sequence encoding GFP to the 3' end of the coding sequence for full-length SECE1 and SECE2, creating SECE1-GFP and SECE2-GFP (constructs IX and X, **Figure 5A**). When SECE1-GFP was expressed in protoplasts, it was efficiently imported and accumulated in the stroma (**Figure 5E**). Similar results were obtained with SECE2-GFP (**Figure 5F**). From these experiments, we concluded that the targeting determinants associated with the TMD and tail are context-dependent, i.e., they must be near the C-terminus to successfully target a TA protein to the appropriate target membrane.

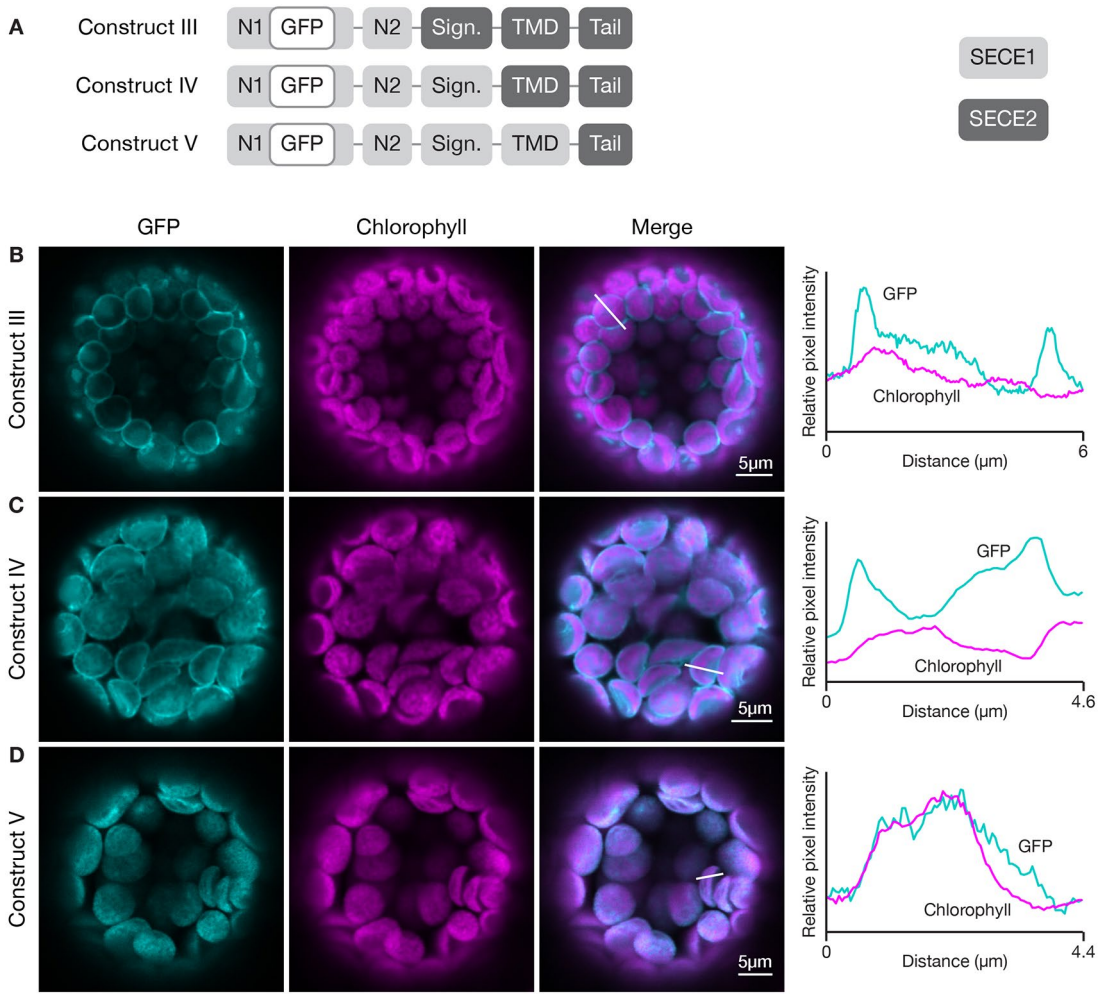

FIGURE 4 | Localization of fluorescent chimeric proteins containing N-terminal SECE1 regions and C-terminal SECE2 regions in transfected protoplasts. **(A)** Diagrams depicting constructs III, IV, and V. SECE1 sequences are indicated with light gray and SECE2 sequences with dark gray; N1 and N2: N-terminal region; GFP: green fluorescent protein; Sign.: signature domain; TMD: linker plus transmembrane domain; Tail: C-terminal tail. **(B–D)** Leaf protoplasts from 4–5 week old wildtype (Columbia ecotype) plants were transfected with **(B)** construct III, **(C)** construct IV, or **(D)** construct V. The images show GFP fluorescence (cyan), chlorophyll fluorescence (magenta), merged images, and relative pixel intensity diagrams that correspond with the white lines on the merged images.

TMD Regions Alone Are Not Sufficient to Confer Either Envelope or Thylakoid Targeting

Studies of cytosolic TA proteins indicated that physicochemical features of the C-terminal regions, such as TMD hydrophobicity, helical propensity, and charges in the tail region, are important for targeting (Hwang et al., 2004; Kriechbaumer et al., 2009; Rao et al., 2016; Teresinski et al., 2019; reviewed in Chio et al., 2017). If TA protein targeting within chloroplasts depends on the same features, we might expect the TMDs of SECE1 and SECE2 to differ significantly with regard to at least one of these parameters. Because TMD sequence predictions depend on the algorithm used, we analyzed three different predicted TMD sequences for each protein (**Table 1**). These were obtained either using the ConPred_v2 and AramTmCon algorithms [available through the Aramemnon database (http://aramemnon.uni-koeln.de/)] or the topology prediction in the UniProt database (https://www.uniprot.org/). The latter predicts a TMD of 21 amino acids for SECE1 and a longer TMD of 30 amino acids for SECE2. Grand Average of Hydropathy (GRAVY) scores were obtained using the GRAVY calculator (http://www.gravy-calculator.de/). GRAVY scores for the TMD of SECE1 varied from 1.776 to 2.31, while GRAVY scores for the TMD of SECE2 varied from 2.2 to 2.38. Both proteins would be considered to have moderate hydrophobicity when compared to the values obtained with cytosolic TA proteins in yeast, whose GRAVY scores vary from 0.87 to 3.73 (Rao et al., 2016) Therefore, despite possible differences in length, the TMDs of SECE1 and SECE2 do not appear to differ significantly in overall hydrophobicity.

Another parameter that is useful for comparing different TMDs is the helical propensity, calculated as Agadir scores (http://agadir.crg.es/about.jsp), which reflect the relative tendency to

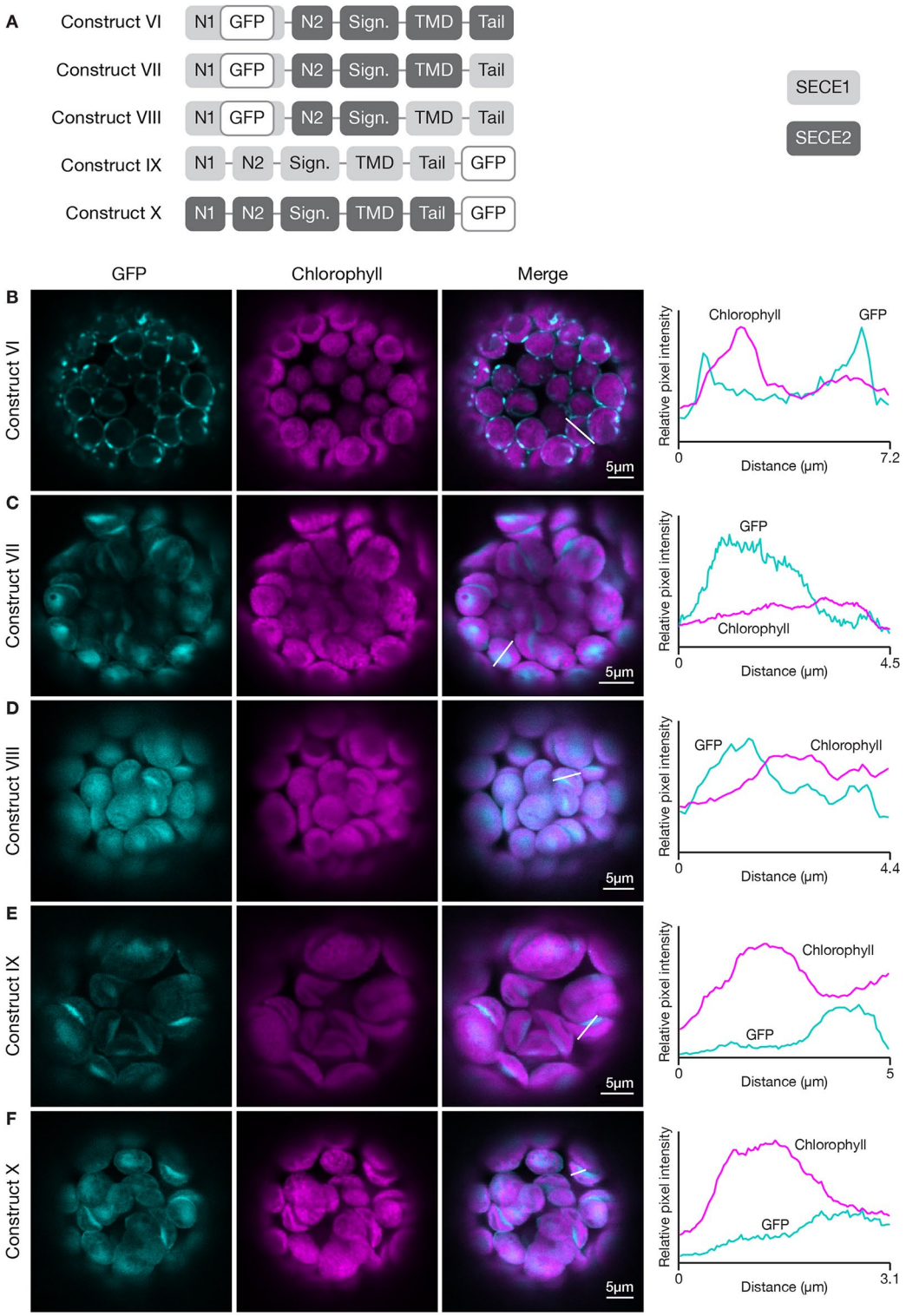

FIGURE 5 | Localization of fluorescent chimeric SECE1 and SECE2 proteins in transfected protoplasts. The SECE1 N1-region is included in constructs VI–VIII to facilitate chloroplast import. **(A)** Diagrams depicting constructs VI, VII, VIII, IX, and X. SECE1 sequences are indicated with light gray and SECE2 sequences with dark gray; N1 and N2: N-terminal region; GFP: green fluorescent protein; Sign.: signature domain; TMD: linker plus transmembrane domain; Tail: C-terminal tail. **(B–F)** Leaf protoplasts from 4–5 week old wildtype (Columbia ecotype) plants were transfected with **(B)** construct VI, **(C)** construct VII, **(D)** construct VIII, **(E)** construct IX, or **(F)** construct X. The images show GFP fluorescence (cyan), chlorophyll fluorescence (magenta), merged images, and relative pixel intensity diagrams that correspond with the white lines on the merged images.

TABLE 1 | Grand Average of Hydropathy (GRAVY) and helical propensity (Agadir) scores for predicted transmembrane domains (TMDs) of SECE1 and SECE2.

Prediction method	SECE1 predicted TMD At4g14870/O23342-1	GRAVY score	Agadir score
ConPredv2	GVVLGVIAGSSVVLLTVNFLL	2.205	0.29
AramTmCon	TTGVVLGVIAGSSVVLLTVNF	1.776	0.26
UniProt	VVLGVIAGSSVVLLTVNFLLA	2.31	0.27
Prediction method	**SECE2 At4g38490/Q940H5-1**	**GRAVY score**	**Agadir score**
ConPredv2	TLSLCLVAVFIVALSSVDAAL	2.2	2.12
AramTmCon	LCLVAVFIVALSSVDAALCYI	2.362	2.04
UniProt	ATLSLCLVAVFIVALSSVDAALCYILALIL	2.38	6.12

ConPredv2 and AramTmCon predictions were obtained by submitting the gene locus number to the Aramemnon database (http://aramemnon.uni-koeln.de/). The UniProt prediction was obtained by submitting the UniProt ID number to the UniProt database (http://www.uniprot.org). GRAVY scores for each predicted TMD were obtained using the GRAVY calculator (http://www.gravy-calculator.de/), and Agadir scores reflecting helical propensity were obtained using the Agadir algorithm (http://agadir.crg.es/).

form helices in aqueous solution. The Adagir score of SECE1's TMD varies from 0.26 to 0.29, while the Agadir score of SECE2's TMD varies from 2.04 to 6.12 (**Table 1**). The Agadir scores of cytosolic TA proteins in yeast vary from 0.13 to 74.40. Lower Agadir scores are typically associated with TA proteins targeted to the mitochondrial outer envelope, while higher Agadir scores are typically associated with TA proteins targeted to the ER (Rao et al., 2016). Although the TMD of SECE2 appears to have a slightly higher helical propensity than the TMD of SECE1, the Agadir scores for SECE1 and SECE2 TMDs are both on the low end of the scale.

Finally, we compared the hydrophobicity profiles of the TMD and tail regions of SECE1 and SECE2 (**Figure 6**). SECE1's TMD shows fairly uniform hydrophobicity throughout its length and is followed by a tail with low hydrophobicity. The TMD and tail regions of SECE2, on the other hand, have two "peaks" of higher than average hydrophobicity separated by a "valley" of lower than average hydrophobicity, which is centered around the charged amino acid in the TMD. Therefore, although the GRAVY scores of the TMDs of the two proteins are similar, the hydrophobicity profiles are very different.

How does the character of the TMD affect targeting? To determine this, we generated a construct encoding a chimeric protein where the TMD of SECE1 was placed in the context of SECE2 (construct XI, **Figure 7A**) and another where the TMD of SECE2 was placed in the context of SECE1 (construct XII, **Figure 7A**). These changes resulted in significant alterations in the hydrophobicity profiles of the TMD and tail regions (compare **Figures 7B, C** to **Figures 6A, B**). The chimeric protein encoded by construct XI had uniform moderate hydrophobicity throughout the TMD and tail regions (**Figure 7B**). When protoplasts were transfected with this construct, only weak fluorescence was seen (**Figure 7E**). The chimeric protein did not appear to show any specificity and low-level fluorescence was associated with multiple locations, including the thylakoid, stroma, and envelope. For the chimeric protein encoded by construct XII, the first peak of higher hydrophobicity associated with SECE2's TMD was retained but the second peak was eliminated (**Figure 7C**). The chimeric protein produced by this construct primarily accumulated in the stroma (**Figure 7F**). We conclude that the TMD regions alone are not sufficient to confer either envelope or thylakoid targeting, possibly because physiochemical features of

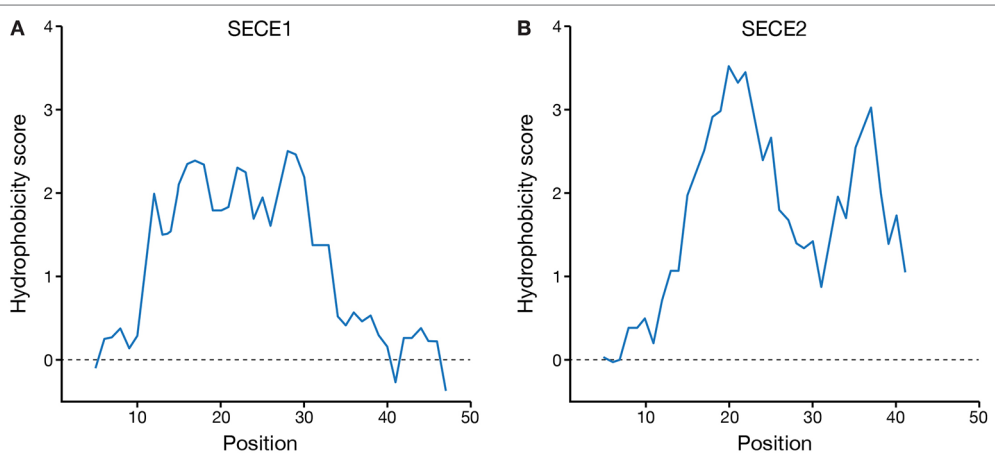

FIGURE 6 | Hydrophobicity profiles of the C-terminal regions of SECE1 and SECE2. Profiles were generated through ExPASy ProtScale (https://web.expasy.org/protscale/) using the Kyte & Doolittle amino acid scale with a window size of 9. Each profile represents the linker, TMD, and tail regions beginning with the E-W-P motif. **(A)** Hydrophobicity profile of SECE1's C-terminal regions, corresponding to residues 127–177 of the full-length protein. **(B)** Hydrophobicity profile of SECE2's C-terminal regions, corresponding to residues 109–153 of the full-length protein.

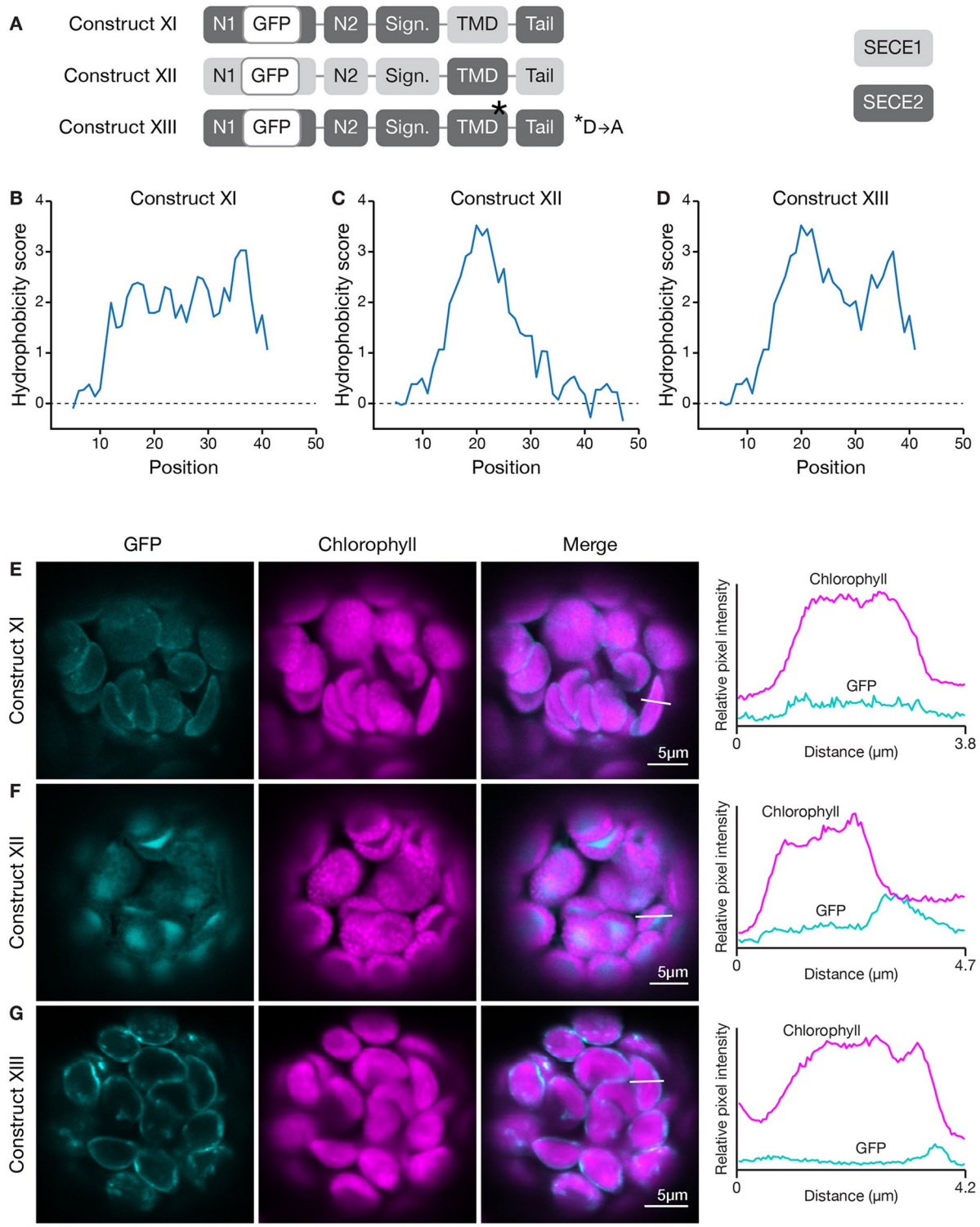

FIGURE 7 | Localization of fluorescent chimeric SECE1 and SECE2 proteins with alterations in the TMD region. **(A)** Diagrams depicting constructs XI, XII, and XIII. SECE1 sequences are indicated with light gray and SECE2 sequences with dark gray; N1 and N2: N-terminal regions; GFP: green fluorescent protein; Sign.: signature domain; TMD: linker plus transmembrane domain; Tail: C-terminal tail. The asterisk indicates the location of a D to A amino acid substitution. **(B–D)** Hydrophobicity profiles of the linker, TMD, and tail regions of the proteins encoded by **(B)** construct XI, **(C)** construct XII, and **(D)** construct XIII. **(E–G)** Leaf protoplasts from 4–5 week old wildtype (Columbia ecotype) plants were transfected with **(E)** construct XI, **(F)** construct XII, or **(G)** construct XIII. The images show GFP fluorescence (cyan), chlorophyll fluorescence (magenta), merged images, and relative pixel intensity diagrams that correspond with the white lines on the merged images.

the C-terminal region are shaped by contributions from both the TMDs and tail regions.

The valley between the two peaks in the hydrophobicity profile of SECE2 is centered on a charged residue (aspartic acid). We tested whether changing this amino acid has an impact on targeting. We generated a GFP-SECE2 construct in which the aspartic acid was replaced by an alanine residue (construct XIII, **Figure 7A**). This amino acid substitution results in minimal change to the hydrophobicity profile. The floor of the valley between the two high peaks of hydrophobicity associated with SECE2 is raised but the valley is not eliminated (compare **Figure 7D** to **Figure 6B**). When protoplasts were transfected with this construct, the fluorescent mutant protein was targeted primarily to the envelope (**Figure 7G**). Thus, having a charged residue in this position may be less important for envelope targeting than the overall hydrophobicity profile.

C-Terminal Tail Characteristics Play a Role in Membrane-Specific Targeting

The results of the first two sets of domain swap experiments suggested that the character of the tail region was more important for envelope-directed targeting than for thylakoid-directed targeting. Substitution of SECE1's tail for the tail of SECE2 blocked association of SECE2 with the envelope membrane, while substitution of SECE2's tail for the tail of SECE1 was tolerated. The net charge of the tail has been shown to be an important factor for sorting cytosolic tail-anchored proteins (reviewed in Moog, 2019 and Pedrazzini, 2009). The SECE1 tail has three acidic and two basic residues, while the SECE2 tail has two adjacent basic residues. All of the charged residues are highly conserved. We performed several different experiments to test whether changes in the amino acid composition of the SECE2 tail would affect localization to the envelope. First, we generated a construct encoding a SECE2 protein where the final 12 amino acids were changed to alanine residues (construct XIV, **Figure 8A**). When protoplasts were transfected with this construct, the fluorescent mutant protein accumulated in the stroma (**Figure 8B**). Next, we tested a construct where the dibasic R-K motif was changed to A-A (construct XV, **Figure 8A**). This fluorescent mutant protein also accumulated in the stroma (**Figure 8C**). Similar results were obtained with constructs encoding proteins where either the first six residues in the tail were changed to alanines or the last six residues (including the R-K motif) were changed to alanines (data not shown). We conclude that there are stringent requirements for particular tail sequences for efficient envelope-directed SECE2 targeting.

We also tested the effect of alterations in the amino acid composition of the tail on thylakoid-directed targeting. A construct was generated that encoded a SECE1 protein where the entire tail was replaced by 12 alanine residues (construct XVI, **Figure 8A**). In transfected protoplasts, the fluorescent mutant protein was associated with the thylakoids (**Figure 8D**). Therefore, the native tail, including its two positive and three negative charged residues, is clearly not required in the context of full-length SECE1. In fact, in contrast to envelope-directed SECE2 targeting, we could not detect any requirements for particular tail sequences for thylakoid-directed SECE1 targeting.

In summary, these experiments show that, just as in the cytosolic targeting systems for TA proteins, targeting of TA proteins to internal chloroplast membranes depends on determinants associated with the TMD and tail regions. Targeting to the thylakoids and targeting to the inner envelope have somewhat different requirements. For envelope targeting, the TMD and tail regions are both important, and adjacent basic residues or some other feature of the tail may be necessary for high fidelity targeting. For thylakoid targeting, the TMD and tail regions are also important; however, in the context of full-length SECE1, the requirement for the native tail is relaxed.

DISCUSSION

Summary Model

TA proteins that are imported and localized in either the inner envelope or thylakoid membranes of chloroplasts require a number of targeting signals for accurate delivery and successful integration. Our studies show that membrane specificity depends primarily on signals located at the C-terminus, in the TMD and tail regions. In **Figure 9**, we present a multistep model for how the nuclear-encoded imported chloroplast TA proteins are targeted.

In step 1, precursor TA proteins are synthesized in the cytosol with transit peptides. The newly synthesized precursors evade the cytosolic TA protein targeting systems and are delivered to the TOC-TIC import apparatus of the chloroplast. Following import of the N-terminus, the transit peptide of the precursor protein is removed in the stroma.

In step 2, TA proteins are recruited into an inner envelope-directed pathway or a thylakoid-directed pathway, based on characteristics of their TMD and tail regions. Inner envelope TA proteins have two possible routes: translocation may be arrested during import and the protein may be released laterally from the TIC. Alternatively, they may take a post-import route, as do thylakoid TA proteins. According to our model, fully imported TA proteins would be recruited to the appropriate pathway through interactions with stromal factors as the TMD and tail regions exit the TIC.

In step 3, the TA proteins are integrated into the target membranes. Insertion may be spontaneous or it may be catalyzed by a specific translocase. The efficiency of integration may also depend on the characteristics of the TMD and tail regions.

Pre- and Post-Import Targeting Features Are Located on Distinct Termini

Targeting of internal chloroplast TA proteins involves at least two sets of targeting determinants: one set at the N-terminus for delivery to the chloroplast import machinery and one set close to the C-terminus for localization within the chloroplast. The N-terminal determinants appear to be dominant in the cytosol, perhaps because this region is exposed first during synthesis, while the C-terminal regions are still in the ribosome tunnel. Interactions between cytosolic factors and transit peptide sequences that result in the precursor proteins being directed to the TOC-TIC import apparatus have been extensively studied (May and Soll, 2000; Qbadou et al., 2006; Bölter and Soll, 2016).

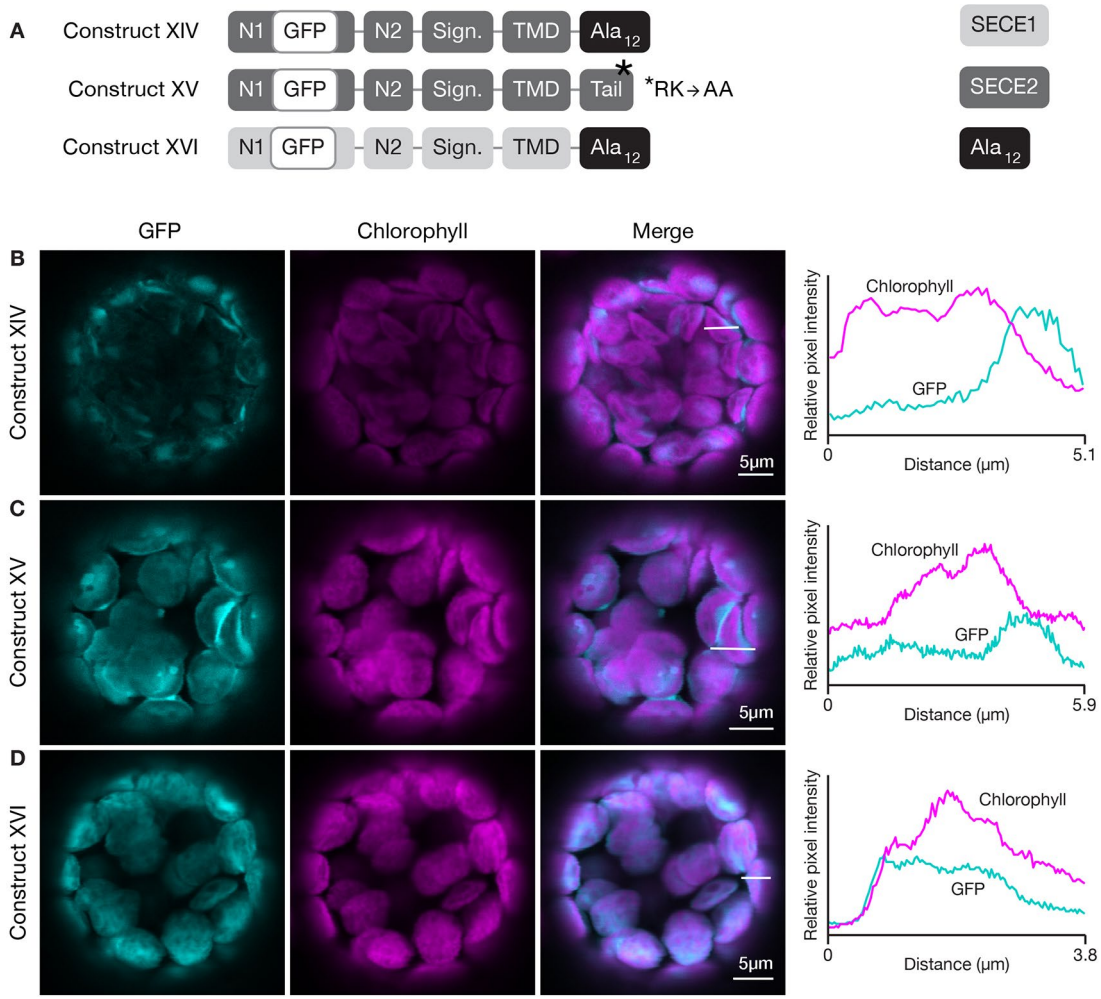

FIGURE 8 | Localization of fluorescent chimeric SECE1 and SECE2 proteins with alterations in the C-terminal tail regions. **(A)** Diagrams depicting constructs XIV, XV, and XVI. SECE1 sequences are indicated with light gray and SECE2 sequences with dark gray; N1 and N2: N-terminal regions; GFP: green fluorescent protein; Sign.: signature domain; TMD: linker plus transmembrane domain; Tail: C-terminal tail. The black rectangles with Ala_{12} indicate a substitution of the entire native tail with 12 alanine residues. The asterisk indicates the location of an R-K to A-A amino acid substitution. **(B–D)** Leaf protoplasts from 4–5 week old wildtype (Columbia ecotype) plants were transfected with **(B)** construct XIV, **(C)** construct XV, or **(D)** construct XVI. The images show GFP fluorescence (cyan), chlorophyll fluorescence (magenta), merged images, and relative pixel intensity diagrams that correspond with the white lines on the merged images.

Following import and removal of the transit peptide, determinants near the C-terminus become important, just as they are in the cytosolic TA protein targeting systems. Both SECE1 and SECE2 have TMDs with moderate hydrophobicity, but the tails of SECE1 and SECE2 are quite different. Both tails lack the RK/ST-enriched sequences associated with the tails of many chloroplast outer envelope TA proteins (Teresinski et al., 2019). In the case of SECE2, the tail region most closely resembles the targeting sequence of a mitochondrial outer envelope TA protein. Mitochondrial TA proteins tend to have tails with a more positive net charge and often contain a dibasic R-R/K/H-X (X≠E) motif (Hwang et al., 2004; Marty et al., 2014). In Arabidopsis and other species, the sequence R-R/K-X, where X tends to be either A, T, or S, is highly conserved in SECE2's tail (**Figure 3**). We showed that changing the R-K motif to A-A disrupts targeting of SECE2 to the inner envelope.

In the case of SECE1, the tail region most closely resembles the targeting sequence of ER-directed TA proteins, which often contain a R/H-X-Y/F motif and have a slightly positive net charge (Moog, 2019). SECE1's tail has a slightly negative net charge instead, but it contains the highly conserved R-V-F motif in all species we examined aside from *Zea*, where the sequence is T-V-F (**Figure 2**). Because replacing the tail with A residues or substituting SECE2's tail for the SECE1 tail does not block the thylakoid localization of SECE1, these residues may be dispensable for targeting.

We are not suggesting that the inner envelope is equivalent to the mitochondrial outer envelope, nor are the thylakoids equivalent to the ER. However, the parallelism is curious and raises the possibility that physicochemical features that contribute to discrimination between different pathways in the cytosol might serve a similar purpose in the stroma.

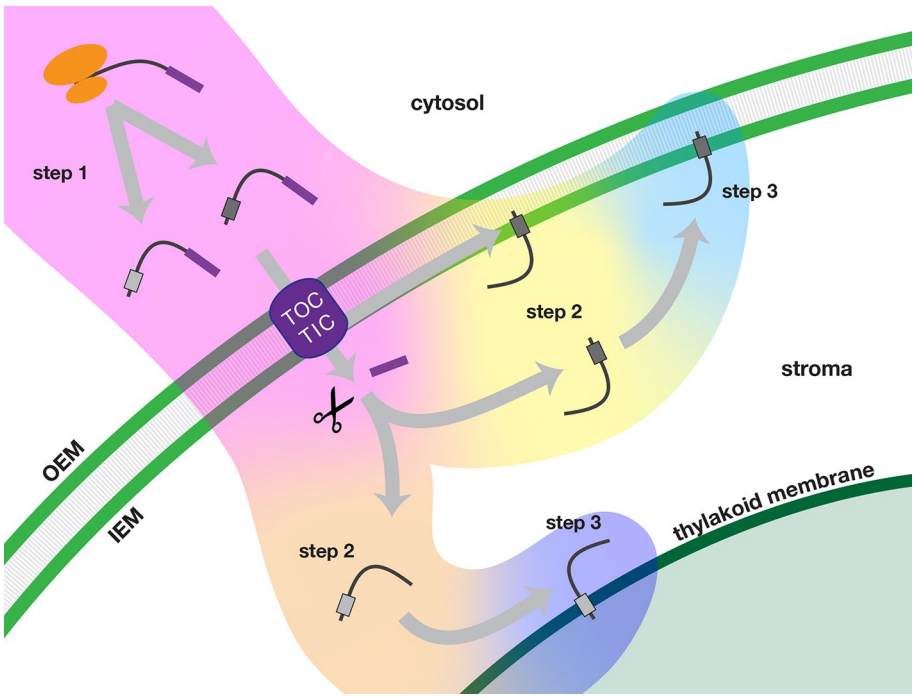

FIGURE 9 | Multi-step model of targeting nuclear-encoded TA proteins to the inner envelope or thylakoid membranes of chloroplasts. In step 1 (pink background color), the TA protein is synthesized in the cytosol and delivered to the chloroplast. In step 2, the TA proteins are sorted either in an inner envelope-directed (yellow background color) or thylakoid-directed (peach background color) pathway. In step 3, the TA proteins are integrated either into the inner envelope membrane (light blue background color) or the thylakoid membrane (dark blue background). Scissors indicate stromal processing peptidase activity. IEM, inner envelope membrane; OEM, outer envelope membrane; TOC/TIC, Translocons of the Outer and Inner Envelope membranes of the chloroplast.

Post-Import Sorting Events

Following import into the stroma and removal of the transit peptide, the TA proteins are sorted into different targeting pathways. For thylakoid-directed proteins, interaction with one or more stromal factors is likely necessary to prevent aggregation and aid in delivery to the thylakoids. Based on the observation that SECE1 can integrate into isolated thylakoids in the absence of stromal extracts and an energy source (Steiner et al., 2002), SECE1 is often considered to be a client of the "spontaneous" pathway. However, given the similar lipid composition of the thylakoids and inner envelope (Benning, 2009), it is hard to reconcile a protein-free targeting process with the membrane specificity that is observed *in vivo*. We suggest that targeting to the thylakoid is more likely to be protein-mediated. Based on its sequence, SECE1 does not appear to be a good candidate for either the SEC, ΔpH, or SRP pathways. It lacks the N-terminal sequences that resemble signal peptides often found in clients of the SEC and ΔpH pathways, and it lacks the D-P-L-G motif used to recruit proteins to the SRP pathway (DeLille et al., 2000). Given the resemblance of SECE1's tail to those of ER-directed TA proteins, which are delivered *via* the cytosolic Guided Entry of Tail-anchored proteins (GET) system, we speculate that targeting of thylakoid TA proteins might be a possible role for GET3B, the recently discovered chloroplast homolog of the GET3 targeting factor (Duncan et al., 2013; Xing et al., 2017).

For inner envelope TA proteins, there are two possible targeting pathways. The final topology, with a stroma-exposed N-terminus, would be compatible with a stop transfer mechanism, which involves arrest of translocation and lateral release of the TMD from the TIC. Features previously identified as being associated with stop transfer TMDs include absence of proline residues, a relatively high content of clustered tryptophan and phenylalanine residues, and G-X_3-G or G-X_4-G motifs (Froehlich and Keegstra, 2011). SECE2's TMD lacks proline residues, but it does not have any other feature that would suggest it functions as a stop transfer TMD. Our experiments have shown that SECE2's TMD must be combined with the appropriate tail to be an effective targeting determinant (compare constructs VII, XII, and XIV to construct II). Therefore, it is unlike the single-span inner envelope protein ARC6, whose stop transfer TMD is sufficient to confer inner envelope localization (Froehlich and Keegstra, 2011). We found that full-length SECE2 proteins with GFP fused at their C-terminus and several different mutant SECE2 proteins with amino acid changes in the tail region accumulate in the stroma (constructs X, XIV, XV). It is possible that the amino acid changes interfere with the arrest of translocation or some other aspect of the stop transfer mechanism. However, it is equally possible that SECE2 normally fully transits the TIC, and the C-terminal extensions and/or alterations alter the dynamics of the normally transient stromal pool, perhaps by

slowing or preventing integration from the stromal side of the inner envelope.

If both SECE2 and SECE1 use post-import pathways, what features of the TMDs and tails might contribute to sorting? As discussed in the previous section, the tails of SECE1 and SECE2 carry different net charges. The tail appears to be more important for inner envelope targeting than for thylakoid targeting. The TMDs of SECE1 and SECE2 are similar in that they have moderate hydrophobicity; however, they differ in several regards: First, SECE1's TMD has a lower helical propensity than SECE2's TMD. Helical propensity differences were previously shown to be strongly correlated with the efficacy of targeting of TA proteins to different target membranes in the cytosol (Rao et al., 2016). Second, SECE1's TMD, but not SECE2's TMD, has features that are often associated with the TMDs of thylakoid proteins, namely clustered leucine residues and a relatively high alanine (A), valine (V), and glycine (G) content (Froehlich and Keegstra, 2011). Finally, we note that while the average hydrophobicities of SECE1's and SECE2's TMDs are similar, the hydrophobicity profiles are very different: SECE1's TMD shows fairly uniform hydrophobicity throughout its length, and is followed by a tail with multiple charged residues and low hydrophobicity. The TMD and tail regions of SECE2, on the other hand, are marked by two regions of higher hydrophobicity separated by a region of lower hydrophobicity that includes a charged amino acid. Changing the aspartic acid to alanine had no apparent effect on targeting (construct XIII); however, the change also did not completely eliminate the region of lower hydrophobicity in the hydrophobicity profile (compare **Figure 7D** to **Figure 6B**). The difference in SECE1 and SECE2's profiles could be significant if stromal factors discriminate between clients on this basis. For example, a stromal factor with a hydrophobic groove that accommodates SECE1's TMD might be unable to accommodate SECE2's TMD because of the region of lower hydrophobicity or the nearby charges in the tail. Additional experiments will be needed to test which of the many differences between SECE1 and SECE2's TMD and tail regions are significant.

Membrane Integration

After successful recruitment into the appropriate pathway and delivery to the target membrane, the TA protein must be integrated. Integration involves partitioning of the hydrophobic TMD into the lipid bilayer and transfer of the tail region across the lipid bilayer. The thylakoids contain a variety of different translocases, any of which could at least theoretically be involved in this process. Because thylakoids are an energized membrane, transfer also might be aided by the proton-motive force. Therefore, thylakoids clearly have the capacity to transfer a small protein domain such as a short C-terminal tail across the membrane. Indeed, it was reported previously that SECE1 can insert into isolated thylakoid membranes without stromal extracts or an energy source (Steiner et al., 2002) and we observed that successful integration can occur with a variety of different short tails (construct V and XVI). For inner envelope proteins, transfer of the tail across a membrane only becomes a concern for TA proteins that integrate by a post-import mechanism. In this case, we imagine that TA proteins are brought in close proximity to the membrane by targeting complexes, allowing integration to occur. This might happen spontaneously, *via* the SEC2 translocase, or *via* some as-yet-unidentified translocase. The lack of a protonmotive force and more limited capacity for transfer might explain why we see a more stringent requirement for a particular tail with SECE2.

In summary, we have shown that membrane-specific targeting of TA proteins within chloroplasts depends on features of their TMDs and short C-terminal tails. We propose that physicochemical features of the TMDs and tail regions are important in two ways. First, they dictate whether a given tail-anchored protein is recruited to either a thylakoid- or an inner envelope-targeting pathway. Second, after delivery to the target membrane, attributes of the TMDs and tail regions may influence membrane insertion.

DATA AVAILABILITY STATEMENT

All datasets generated for this study are included in the article.

AUTHOR CONTRIBUTIONS

SA, RS, and DF designed and performed the research. SA and DF wrote the manuscript. All authors contributed to manuscript revision, and read and approved the submitted version.

FUNDING

Support for this research was provided by the United States National Science Foundation (DGE1747503 to SA, MCB1158173 to DF) and the University of Wisconsin-Madison Office of the Vice Chancellor for Research and Graduate Education with funding from the Wisconsin Alumni Research Foundation.

ACKNOWLEDGMENTS

The authors thank Dr. Sarah Swanson for microscopy assistance, Dr. Enrico Scheiff for providing the pML94 vector, Dr. Cullen Vens for contributing to construct generation, and Sarah Friedrich for figure preparation. Confocal imaging was performed at the Newcomb Imaging Center, Department of Botany, University of Wisconsin-Madison.

SUPPLEMENTARY MATERIAL

The Supplementary Material for this article can be found online at: https://www.frontiersin.org/articles/10.3389/fpls.2019.01401/full#supplementary-material

REFERENCES

Altschul, S. F., Gish, W., Miller, W., Myers, E. W., and Lipman, D. J. (1990). Basic local alignment search tool. *J. Mol. Biol.* 3, 403–410. doi: 10.1016/S0022-2836(05)80360-2

Benning, C. (2009). Mechanisms of lipid transport involved in organelle biogenesis in plant cells. *Annu. Rev. Cell Dev. Biol.* 25, 71–91. doi: 10.1146/annurev.cellbio.042308.113414

Bionda, T., Tillmann, B., Simm, S., Beilstein, K., Ruprecht, M., and Schleiff, E. (2010). Chloroplast import signals: The length requirement for translocation *in vitro* and *in vivo*. *J. Mol. Biol.* 402, 510–523. doi: 10.1016/j.jmb.2010.07.052

Bölter, B., and Soll, J. (2016). Once upon a time – chloroplast protein import research from infancy to future challenges. *Mol. Plant* 9, 798–812. doi: 10.1016/j.molp.2016.04.014

Chio, U. S., Cho, H., and Shan, S. (2017). Mechanisms of tail-anchored membrane protein targeting and insertion. *Annu. Rev. Cell Dev. Biol.* 33, 417–438. doi: 10.1146/annurev-cellbio-100616-060839

DeLille, J., Peterson, E. C., Johnson, T., Moore, M., Kight, A., and Henry, R. (2000). A novel precursor recognition element facilitates posttranslational binding to the signal recognition particle in chloroplasts. *Proc. Natl. Acad. Sci.* 97, 1926–1931. doi: 10.1073/pnas.030395197

Drozdetskiy, A., Cole, C., Procter, J., and Barton, G. J. (2015). JPred4: A protein secondary structure prediction server. *Nucleic Acids Res.* 43, W389–W394. doi: 10.1093/nar/gkv332

Duncan, O., van der Merwe, M. J., Daley, D. O., and Whelan, J. (2013). The outer mitochondrial membrane in higher plants. *Trends Plant Sci.* 18, 207–217. doi: 10.1016/j.tplants.2012.12.004

Froehlich, J. E., and Keegstra, K. (2011). The role of the transmembrane domain in determining the targeting of membrane proteins to either the inner envelope or thylakoid membrane. *Plant J.* 68, 844–856. doi: 10.1111/j.1365-313X.2011.04735.x

Gasteiger, E., Hoogland, C., Gattiker, A., Duvaud, S., Wilkins, M. R., Appel, R. D., et al. (2005). "Chapter 52: Protein Identification and Analysis Tools on the ExPASy Server" in *The Proteomics Protocols Handbook,* ed. J.M. Walker (Totowa, NJ: Humana Press Inc.), 571-607. doi: 10.1385/1592598900

Hwang, Y. T., Pelitire, S. M., Henderson, M. P. A., Andrews, D. W., Dyer, J. M., and Mullen, R. T. (2004). Novel targeting signals mediate the sorting of different isoforms of the tail-anchored membrane protein cytochrome b5 to either endoplasmic reticulum or mitochondria. *Plant Cell* 16, 3002–3019. doi: 10.1105/tpc.104.026039

Jeong, J.-Y., Yim, H.-S., Ryu, J.-Y., Lee, H. S., Lee, J.-H., Seen, D.-S., et al. (2012). One-step sequence- and ligation-independent cloning as a rapid and versatile cloning method for functional genomics studies. *Appl. Environ. Microbiol.* 78, 5440–5443. doi: 10.1128/aem.00844-12

Kriechbaumer, V., Shaw, R., Mukherjee, J., Bowsher, C. G., Harrison, A. M., and Abell, B. M. (2009). Subcellular distribution of tail-anchored proteins in arabidopsis. *Traffic* 10, 1753–1764. doi: 10.1111/j.1600-0854.2009.00991.x

Kyte, J., and Doolittle, R. F. (1982). A simple method for displaying the hydropathic character of a protein. *J. Mol. Biol.* 157, 105–132. doi: 10.1016/0022-2836(82)90515-0

Lee, D. W., Lee, J., and Hwang, I. (2017). Sorting of nuclear-encoded chloroplast membrane proteins. *Curr. Opin. Plant Biol.* 40, 1–7. doi: 10.1016/j.pbi.2017.06.011

Li, Y., Singhal, R., Taylor, I. W., McMinn, P. H., Chua, X. Y., Cline, K., et al. (2015). The Sec2 translocase of the chloroplast inner envelope contains a unique and dedicated SECE2 component. *Plant J.* 84, 647-658. doi: 10.1111/tpj.13028

Marty, N. J., Teresinski, H. J., Hwang, Y. T., Clendening, E. A., Gidda, S. K., Sliwinska, E., et al. (2014). New insights into the targeting of a subset of tail-anchored proteins to the outer mitochondrial membrane. *Front. Plant Sci.* 5, 1–20. doi: 10.3389/fpls.2014.00426

May, T., and Soll, J. (2000). 14-3-3 Proteins Form a Guidance Complex with Chloroplast Precursor Proteins in Plants. *Plant Cell* 12, 53. doi: 10.2307/3871029

Moog, D. (2019). Higher complexity requires higher accuracy: tail-anchored protein targeting to the outer envelope membrane of plant plastids *via a* specific c-terminal motif. *Plant Cell Physiol.* 60, 489–491. doi: 10.1093/pcp/pcz021

Muñoz, V., and Serrano, L. (1997). Development of the multiple sequence approximation within the AGADIR model of alpha-helix formation: comparison with Zimm-Bragg and Lifson-Roig formalisms. *Biopolymers* 41, 495–509. doi: 3.0.CO;2-H

Pedrazzini, E. (2009). Tail-Anchored proteins in plants. *J. Plant Biol.* 52, 88–101. doi: 10.1007/s12374-009-9014-1

Qbadou, S., Becker, T., Mirus, O., Tews, I., Soll, J., and Schleiff, E. (2006). The molecular chaperone Hsp90 delivers precursor proteins to the chloroplast import receptor Toc64. *EMBO J.* 25, 1836–1847. doi: 10.1038/sj.emboj.7601091

Rao, M., Okreglak, V., Chio, U. S., Cho, H., Walter, P., and Shan, S.-O. (2016). Multiple selection filters ensure accurate tail-anchored membrane protein targeting. *Elife* 5, 1–24. doi: 10.7554/eLife.21301

Richardson, L. G. L., Singhal, R., and Schnell, D. J. (2017). The integration of chloroplast protein targeting with plant developmental and stress responses. *BMC Biol.* 15, 118. doi: 10.1186/s12915-017-0458-3

Rolland, V., Rae, B. D., and Long, B. M. (2017). Setting sub-organellar sights: Accurate targeting of multi-transmembrane-domain proteins to specific chloroplast membranes. *J. Exp. Bot.* 68, 5013–5016. doi: 10.1093/jxb/erx351

Schuenemann, D., Amin, P., Hartmann, E., and Hoffman, N. E. (1999). Chloroplast secY is complexed to secE and involved in the translocation of the 33-kDa but not the 23-kDa subunit of the oxygen-evolving complex. *J. Biol. Chem.* 274, 12177–12182. doi: 10.1074/jbc.274.17.12177

Schwacke, R., Schneider, A., van der Graaff, E., Fischer, K., Catoni, E., Desimone, M., et al. (2003). Aramemnon, a novel database for Arabidopsis integral membrane proteins *Plant Physiol.* 131, 16–26. doi: 10.1104/pp.011577.that

Singhal, R., and Fernandez, D. E., (2017). Sorting of SEC translocase SCY components to different membranes in chloroplasts. *J. Exp. Bot.* 68, 5029–5043. doi: 10.1093/jxb/erx318

Skalitzky, C. A., Martin, J. R., Harwood, J. H., Beirne, J. J., Adamczyk, B. J., Heck, G. R., et al. (2011). Plastids contain a second sec translocase system with essential functions. *Plant Physiol.* 155, 354–369. doi: 10.1104/pp.110.166546

Steiner, J. M., Köcher, T., Nagy, C., and Löffelhardt, W. (2002). Chloroplast SecE: Evidence for spontaneous insertion into the thylakoid membrane. *Biochem. Biophys. Res. Commun.* 293, 747–752. doi: 10.1016/S0006-291X(02)00285-1

Teresinski, H. J., Gidda, S. K., Nguyen, T. N. D., Howard, N. J. M., Porter, B. K., Grimberg, N., et al. (2019). An RK/ST c-terminal motif is required for targeting of OEP7.2 And a subset of other arabidopsis tail-anchored proteins to the plastid outer envelope membrane. *Plant Cell Physiol.* 0, 1–22. doi: 10.1093/pcp/pcy234

The Uniprot Consortium. (2019). UniProt : a worldwide hub of protein knowledge. *Nucleic Acids Res.* 47, D506–D515. doi: 10.1093/nar/gky1049

Wallace, I. M., Sullivan, O. O., Higgins, D. G., and Notredame, C., (2006). M-Coffee : combining multiple sequence alignment methods with T-Coffee. *Nucleic Acids Res.* 34, 1692–1699. doi: 10.1093/nar/gkl091

Wu, F. H., Shen, S. C., Lee, L. Y., Lee, S. H., Chan, M. T., and Lin, C. S. (2009). Tape-arabidopsis sandwich - A simpler arabidopsis protoplast isolation method. *Plant Methods* 5, 1–10. doi: 10.1186/1746-4811-5-16

Xing, S., Mehlhorn, D. G., Wallmeroth, N., Asseck, L. Y., Kar, R., Voss, A., et al. (2017). Loss of GET pathway orthologs in *Arabidopsis thaliana* causes root hair growth defects and affects SNARE abundance. *Proc. Natl. Acad. Sci.* 114, E1544–E1553. doi: 10.1073/pnas.1619525114

Yoo, S., Cho, Y., and Sheen, J. (2007). Arabidopsis mesophyll protoplasts: a versatile cell system for transient gene expression analysis. *Nat. Protoc.* 2, 1565–1572. doi: 10.1038/nprot.2007.199

Conflict of Interest: The authors declare that the research was conducted in the absence of any commercial or financial relationships that could be construed as a potential conflict of interest.

frontiers in Plant Science

REVIEW
published: 21 November 2019
doi: 10.3389/fpls.2019.01500

Functional Implications of Multiple IM30 Oligomeric States

*Carmen Siebenaller†, Benedikt Junglas† and Dirk Schneider**

Department of Pharmacy and Biochemistry, Johannes Gutenberg University Mainz, Mainz, Germany

The inner membrane-associated protein of 30 kDa (IM30), also known as the vesicle-inducing protein in plastids 1 (Vipp1), is essential for photo-autotrophic growth of cyanobacteria, algae and higher plants. While its exact function still remains largely elusive, it is commonly accepted that IM30 is crucially involved in thylakoid membrane biogenesis, stabilization and/or maintenance. A characteristic feature of IM30 is its intrinsic propensity to form large homo-oligomeric protein complexes. 15 years ago, it has been reported that these supercomplexes have a ring-shaped structure. However, the *in vivo* significance of these ring structures is not finally resolved yet and the formation of more complex assemblies has been reported. We here present and discuss research on IM30 conducted within the past 25 years with a special emphasis on the question of why we potentially need IM30 supercomplexes *in vivo*.

Keywords: IM30, Vipp1, PspA, thylakoid membrane, membrane fusion, membrane stabilization, membrane dynamics, heat shock proteins

OPEN ACCESS

Edited by:
Luning Liu,
University of Liverpool,
United Kingdom

Reviewed by:
Radek Kana,
Institute of Microbiology, Czechia
Wataru Sakamoto,
Okayama University, Japan

****Correspondence:***
Dirk Schneider
Dirk.Schneider@uni-mainz.de

†These authors have contributed equally to this work

Specialty section:
This article was submitted to Plant Physiology, a section of the journal Frontiers in Plant Science

Received: *21 August 2019*
Accepted: *29 October 2019*
Published: *21 November 2019*

Citation:
Siebenaller C, Junglas B and Schneider D (2019) Functional Implications of Multiple IM30 Oligomeric States. Front. Plant Sci. 10:1500. doi: 10.3389/fpls.2019.01500

IM30 IS INVOLVED IN TM PROTECTION AND REMODELING

The thylakoid membranes (TMs) of chloroplasts and cyanobacteria harbor the complexes of the photosynthetic electron transfer chain. The emergence of TMs in cyanobacteria is evolutionary coupled to the development of the inner membrane-associated protein of 30 kDa (IM30)/vesicle-inducing protein in plastids 1 (Vipp1)-protein (Vothknecht et al., 2012), and while Vipp1/IM30 is clearly linked to the biogenesis/maintenance of TMs, its exact physiological function still is unclear. As this protein appears to be essential for proper development of a functional TM system and therefore the whole photosynthetic apparatus, clarifying the involvement of Vipp1/IM30 in TM biogenesis/maintenance is vital to understand and eventually reconstruct the photosynthetic machinery, which is the major energy source for life on earth.

The inner membrane-associated protein of 30 kDa (IM30) was first described in 1994 as a protein with a dual localization at the inner envelope (IE) and at TMs in *Pisum sativum* chloroplasts (Li et al., 1994). In 2001, homologs of this protein have been identified and characterized in *Arabidopsis thaliana* and the cyanobacterium *Synechocystis* sp. PCC 6803 (from now on: *Synechocystis*) (Kroll et al., 2001; Westphal et al., 2001). Due to an apparent deficiency in vesicle formation at low temperatures of *Arabidopsis* Vipp1 depletion mutants, IM30 was renamed to *vesicle inducing proteins in plastids* 1 (Vipp1) (Kroll et al., 2001). In recent years, IM30/Vipp1 has been found to be essential for TM formation and IM30/Vipp1 was suggested to be involved in many processes linked to TM maintenance and/or biogenesis (summarized in Heidrich et al., 2017). As the proposed involvement in vesicle formation was not supported by any additional data, we here name the protein as originally proposed, *i.e.* IM30.

IM30 proteins are conserved amongst almost all photosynthetic organisms (Westphal et al., 2001; Vothknecht et al., 2012), and phylogenetic analyses have revealed that IM30 proteins potentially

evolved *via* gene duplication from the bacterial phage shock protein A (PspA) during evolution (Westphal et al., 2001). Although sequence identity (~30%) and similarity (~50%) are not too high between PspA and IM30 proteins (Bultema et al., 2010), both proteins appear to share a highly conserved (predicted) secondary structure with an N-terminal core structure of about 220 amino acids consisting of six α-helices (the so-called PspA-like domain, **Figure 1A**). A major structural difference between PspA and IM30 is an extra C-terminal α-helix in IM30 proteins that is connected to the PspA domain *via* an extended linker region (Westphal et al., 2001; Otters et al., 2013). This extra domain of 20–30 aa possibly discriminated PspA from IM30 proteins and potentially causes the specialized functions of IM30 during TM biogenesis/maintenance, which cannot be accomplished by PspA (Westphal et al., 2001; Aseeva et al., 2004; Bultema et al., 2010; Vothknecht et al., 2012). In contrast, IM30 can functionally replace PspA in *E. coli pspA* null mutants (DeLisa et al., 2004; Zhang et al., 2012), suggesting a conserved function of the PspA domain and a more specific function of the C-terminal IM30 domain in TM biogenesis/maintenance gained during evolution. Nevertheless, due to their similarities, PspA and IM30 together form the PspA/IM30 protein family, together with LiaH, a phage shock protein homolog (Wolf et al., 2010).

An outstanding feature of all members of the PspA/IM30 protein family is their ability to organize into large ring-shaped homo-oligomeric (super)complexes (as further discussed below), which have first been described 15 years ago for both, PspA and IM30 (Aseeva et al., 2004; Hankamer et al., 2004) and were later on also identified for LiaH (Wolf et al., 2010). Interestingly, the occurrence of these IM30 supercomplexes appears to depend on

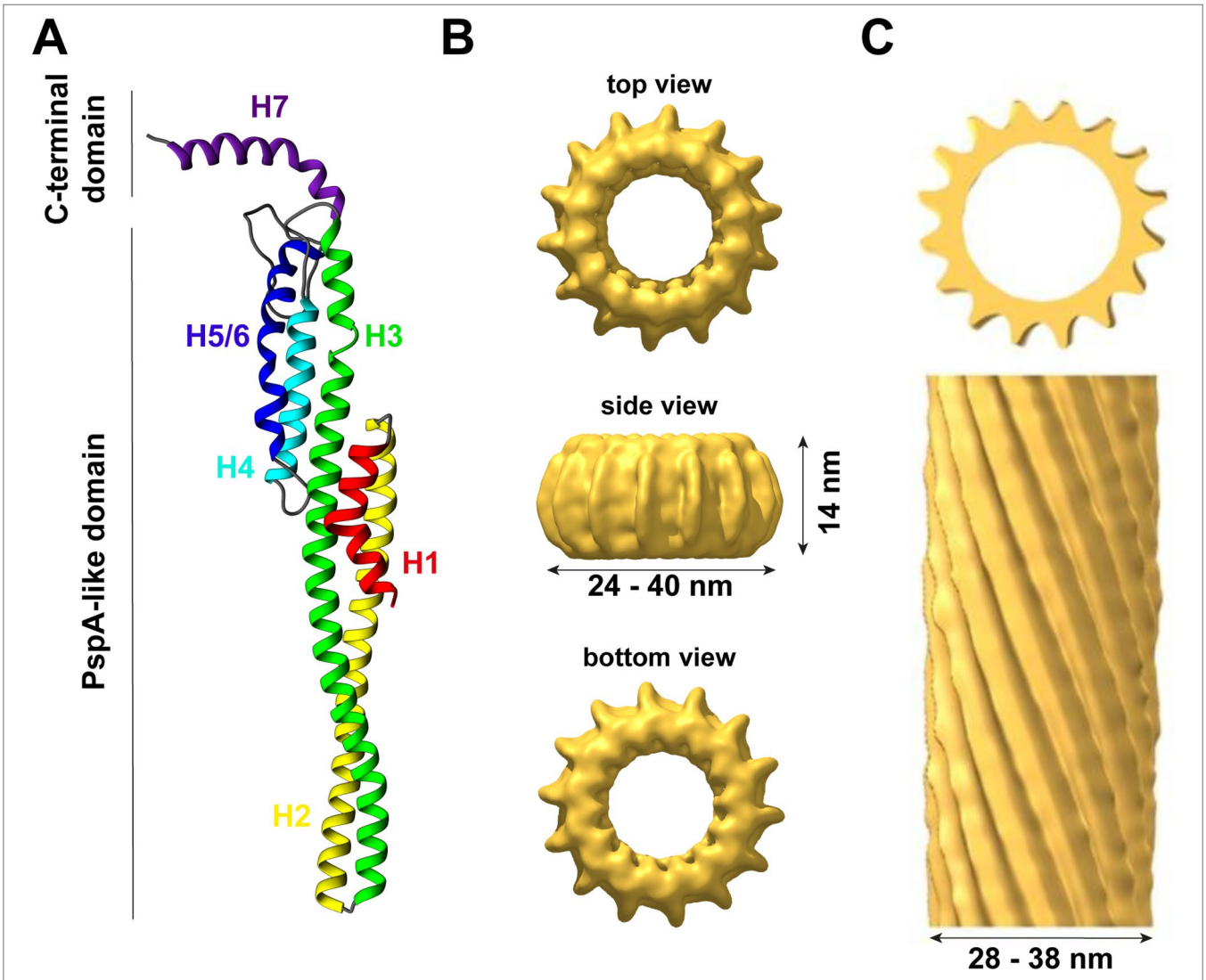

FIGURE 1 | The structure of IM30. **(A)** IM30 is a predominantly α-helical protein with seven helices. Helix 1–6 form the PspA-like domain. IM30 can be discriminated from PspA by a C-terminal extension, which includes an additional helix. **(B)** IM30 forms ring-like homo-oligomers with diameters ranging from 24 to 40 nm and a height of 14 nm (EMDB:3740). **(C)** IM30 forms rod-like structures with typical diameters of 28–38 nm [adapted from (Theis et al., 2019); open-access license http://creativecommons.org/licenses/by/4.0/].

the presence of chaperones/chaperonins, which are likely involved in assembly and disassembly of the IM30 supercomplexes (at least *ex vivo*) (Liu et al., 2005; Liu et al., 2007; Gao et al., 2015).

The exact physiological function of IM30 monomers and/or oligomers is still not finally resolved yet. In recent years, potential *in vivo* functions of IM30 have mainly been studied using IM30 depleted or deleted cyanobacteria, algae, or plants. In fact, most studies were performed in the cyanobacterium *Synechocystis* sp. PCC 6803, the green alga *Chlamydomonas reinhardtii* or the higher plant *Arabidopsis thaliana* (**Table 1**). Yet, results obtained after protein depletion were not entirely conclusive. While depleting IM30 in the cyanobacteria *Synechococcus* sp. PCC 7002 or *Synechocystis* sp. PCC 6803 (Westphal et al., 2001; Fuhrmann et al., 2009b; Zhang et al., 2014) as well as in *Arabidopsis* chloroplasts (Aseeva et al., 2007; Vothknecht et al., 2012) resulted in reduced TM networks and a disturbed TM morphology, depleting the protein in *Chlamydomonas* did not affect the TM structure (Nordhues et al., 2012). However, *Chlamydomonas* contains two IM30 paralogs (named Vipp1 and Vipp2), and in Nordhues *et al.* solely expression of one paralog was reduced. Yet, depletion of this paralog resulted already in an altered photosynthetic activity in *Chlamydomonas,* as has also been observed in cyanobacteria, but not in *Arabidopsis*, with photosystem II being affected in *Chlamydomonas* and photosystem I in cyanobacteria (Aseeva et al., 2007; Fuhrmann et al., 2009a; Nordhues et al., 2012; Vothknecht et al., 2012). Noteworthy, in contrast to most other studies, Gao *et al.* describe that depletion of IM30 in *Synechocystis* did lead to a generally reduced photosynthetic activity but not to TM reduction (Gao and Xu, 2009). While these results could indicate different roles of IM30 in different species, even results obtained in the same strain are not conclusive (Gao and Xu, 2009; Fuhrmann et al., 2009b). We believe that the major activity of IM30 remained conserved throughout evolution and that differences were observed due to other species-specific features, e.g., in some photosynthetic organisms certain lipids are essential whereas these can be replaced by other lipids in other species. This has e.g. been well studied in case of sulfoquinovosyldiacylglycerol (SQDG), which can be replaced by phosphatidylglycerol (PG) to some extent in *Synechococcus*, but not in *Synechocystis* or *Arabidopsis* (Aoki et al., 2004; Kobayashi et al., 2015). As IM30 likely interacts with defined lipids and as lipids are crucial building blocks of TMs as well as part of photosystems, the observed differences could be explained by this. Yet, also other species-specific factors are described to be exclusively involved in TM and/or photosystem biogenesis in chloroplasts or cyanobacteria (Anbudurai et al., 1994; Guskov et al., 2009; Umena et al., 2011; Heinz et al., 2016). Yet, within the last 25 years, besides many others (Kroll et al., 2001; Benning et al., 2006; Göhre et al., 2006; Fuhrmann et al., 2009b; Nordhues et al., 2012; Rütgers and Schroda, 2013; Zhang et al., 2014; Walter et al., 2015) (reviewed in more detail in (Heidrich et al., 2017)), two major physiological functions of IM30 have been suggested, which we briefly introduce here:

(i) Membrane protection:

PspA, the major effector of the bacterial phage shock system, is known to have a membrane stabilizing/protecting function, and binding of PspA to membrane surfaces helps to maintain the proton motive force (PMF) (Kleerebezem et al., 1996; Kobayashi et al., 2007; Joly et al., 2010). Due to the high similarity of PspA and IM30, it appears reasonable to speculate that IM30 also has a membrane-stabilizing/-protecting function (Vothknecht et al., 2012; Zhang et al., 2012; Zhang and Sakamoto, 2013; Zhang and Sakamoto, 2015). Indeed, both, PspA and IM30, bind to negatively charged lipid membranes in a curvature dependent manner *in vitro* (Kobayashi et al., 2007; Hennig et al., 2015; McDonald et al., 2015; Heidrich et al., 2016) and IM30 potentially increases the lipid order upon membrane binding (Hennig et al., 2015; Heidrich et al., 2016). While this suggests that the protein preferentially binds to ordered membrane regions (*i.e.* gel-phase membranes), further experimental proof is missing. Besides these *in vitro* observations, it has been observed that heterologous expression of IM30 from *Synechocystis* and *Arabidopsis* can complement deficiencies in a bacterial Δ*pspA* mutant (DeLisa et al., 2004; Zhang et al., 2012) and that IM30 overexpression can increase the heat stress tolerance in *Arabidopsis* (Zhang et al., 2016). As small IM30 oligomers bind with higher affinity to negatively charged membranes than the large oligomeric ring structures (Heidrich et al., 2016), it has been hypothesized that IM30 and PspA rings disassemble on membranes and function as membrane chaperones by forming a membrane protective structure upon membrane binding (Thurotte et al., 2017; Junglas and Schneider, 2018).

(ii) Membrane remodeling:

While IM30 appears to share its membrane-stabilizing/-protecting activity with PspA, IM30 clearly must have acquired additional functions in cyanobacteria and chloroplasts, as PspA is not able to replace IM30 (Westphal et al., 2001; Aseeva et al., 2004; Bultema et al., 2010; Vothknecht et al., 2012). Expression of IM30 appears to be of special importance when cyanobacterial

TABLE 1 | The IM30 supercomplex structures in different species.

Organism	Ultrastructure *in vitro*	Diameter	Ultrastructure *in vivo*	Size
Synechocystis sp. PCC 6803	Mostly rings, (rods) [1,2]	25–33 nm [2]	At membranes: dynamic and static punctae [8,9] In the cytoplasm: diffuse particles [8,9]	100–300 GFP molecules estimated: 100 ± 25 nm [8]
Arabidopsis thaliana	Mostly rings, (rods) [3,4]	40 nm [3]	At membranes: static clusters [4,10] In the stroma: mobile IM30 particles [4,10]	<0.2–1.5 μm [4]
Chlamydomonas reinhardtii	Mostly rods, rings [5,6]	28–37 nm [5]	*n.a.*	*n.a.*
Triticum urartu	Mostly rings, (rods) [7]	~30 nm [7]	*n.a.*	*n.a.*

[1] (Fuhrmann et al., 2009a), [2] (Saur et al., 2017), [3] (Aseeva et al., 2004), [4] (Zhang et al., 2016), [5] (Liu et al., 2007), [6] (Theis et al., 2019), [7] (Gao et al., 2017) [8] (Bryan et al., 2014), [9] (Gutu et al., 2018), [10] (Zhang et al., 2012). n.a. = data not available.

cells are shifted from dark to light growth conditions (Gutu et al., 2018), where photosynthetic organisms need to adapt their photosynthetic apparatus to account for the changing light intensities by dynamic rearrangement of the TM system (Chuartzman et al., 2008; Nagy et al., 2011; Liberton et al., 2013). Such TM rearrangements require extensive membrane remodeling, and a likely candidate catalyzing TM remodeling is IM30. IM30 can induce fusion of liposomal membranes, at least *in vitro* (Hennig et al., 2015; Thurotte and Schneider, 2019), a process that appears to be controlled by the cytosolic Mg^{2+} concentration, as Mg^{2+} directly binds to IM30 and thereby triggers the fusion process (Hennig et al., 2015; Heidrich et al., 2018; Thurotte and Schneider, 2019). This is of special importance in TM-containing organisms, as the cytosolic Mg^{2+} concentration varies in the dark *vs.* light and depends on the photosynthetic activity (Pohland and Schneider, 2019). Thus, the IM30-specific membrane remodeling activity appears to be (indirectly) controlled by light. Besides light, GTP binding and hydrolysis were recently suggested to control the IM30 membrane remodeling function (Ohnishi et al., 2018), although IM30 does not contain a canonical G-domain and GTP is not required *per se* for membrane binding and liposome fusion (Hennig et al., 2015). Noteworthy, the suggested membrane-stabilizing and the membrane-remodeling activity of IM30 on the first view contradict each other, at least in part, as membrane fusion processes typically involve membrane destabilization. However, both functions might be relevant *in vivo,* as Mg^{2+}-release or binding to IM30 could control the respective activities (Junglas and Schneider, 2018).

IM30 STRUCTURE: WHAT DO WE (NOT) KNOW SO FAR?

The Monomer Structure

Thus far, the structure of the IM30 monomer is still elusive. The monomer is supposed to have a highly α-helical structure (~80% α-helix) with six helices separated by short linker regions (Fuhrmann et al., 2009a; Gao et al., 2015). Additionally, helix 7 is separated from the PspA(-like) domain by an extended flexible linker (Otters et al., 2013). All these assumptions are based on secondary structure predictions but are supported by CD-spectroscopy and FTIR measurements (Fuhrmann et al., 2009a; Gao et al., 2015; Heidrich et al., 2018). Recently, a model of the IM30 monomer has been reported (see **Figure 1A**) that is based on the X-ray structure of a PspA fragment (amino acids 1–144) (Osadnik et al., 2015) and homology modeling (Saur et al., 2017). The X-ray structure of the PspA fragment revealed that helix 2 and 3 form an extended hairpin coiled-coil structure (Osadnik et al., 2015), which appears to form the structural core of the PspA domain. Suggested structural and functional roles of each helix were discussed in more detail recently (Heidrich et al., 2017). Studying truncated IM30 variants allowed to deduce the involvement of individual helices in protein oligomerization (Otters et al., 2013; Gao et al., 2015; Thurotte and Schneider, 2019). Based on these analyses, helix 2 and 3 form the structural core of IM30 that is crucial for supercomplex formation, but by itself does exclusively form monomers (Thurotte and Schneider, 2019). Adding helix 1 and 4 to the structural core enables the formation of dimers (Thurotte and Schneider, 2019) or intermediate-sized oligomers (800 kDa) (Gao et al., 2015), but not of ring-shaped supercomplexes. At minimum, helices 2–6 are required for the formation of stable ring/supercomplex structures (Thurotte and Schneider, 2019). Hence, the helix 2/3 coiled-coil apparently interacts with helix 4 and/or 5/6 in the supercomplexes.

Small Oligomers

In solution, isolated IM30 has a strong tendency to spontaneously form homo-oligomeric supercomplexes, as further discussed below. Yet, a minor fraction of the protein still forms small oligomers (mostly tetramers and dimers), and also the basic building block of the ring complex appears to be an IM30 tetramer (Liu et al., 2007; Fuhrmann et al., 2009a; Saur et al., 2017). Although some low-resolution data of the structure of the supercomplexes are available, essentially nothing is known about the structure of the small oligomers. Thus far, solely a hypothetical model describing the organization of the monomers in the ring structure, including the tetrameric building block, was suggested (Saur et al., 2017) (**Figure 1A**).

IM30 Supercomplexes

In 2004, PspA (Hankamer et al., 2004) and IM30 (Aseeva et al., 2004) were reported to form homo-oligomeric supercomplexes with ring-like structures and molecular masses exeeding 1 MDa. In the following 15 years, one main aspect of the research on IM30 was to analyze the structure and implications of these large supercomplexes.

In various experiments, involving size exclusion chromatography (SEC), BN-PAGE, and sucrose gradient centrifugation, members of the PspA/IM30 family were found to mainly organize into high molecular mass complexes in solution, besides a small fraction of dimers/tetramers (Aseeva et al., 2004; Liu et al., 2005; Liu et al., 2007; Fuhrmann et al., 2009a; Gao et al., 2015; Heidrich et al., 2016; Saur et al., 2017). This has been observed for IM30 in cellular extracts of cyanobacteria and chloroplasts of green algae or vascular plants, but also for heterologously expressed and purified proteins (Aseeva et al., 2004; Liu et al., 2005; Liu et al., 2007; Fuhrmann et al., 2009a; Gao et al., 2015; Heidrich et al., 2016; Gao et al., 2017; Saur et al., 2017). As no other proteins appear to be necessary for IM30 oligomerization, the complexes identified in cellular extracts likely represent homo-oligomeric assemblies.

The size of the *EcoPspA* complex was determined via SEC to be ~1 MDa, indicating that the complex contains 36–37 subunits (Hankamer et al., 2004). For isolated IM30, the molecular mass was determined to be >1 MDa for *Arabidopsis* IM30 (*Ara*IM30) (Aseeva et al., 2004; Otters et al., 2013), for *Chlamydomonas* IM30 (*Cr*IM30) (Liu et al., 2007; Gao et al., 2015) as well as for two IM30 paralogs encoded in Tricum urartu (Gao et al., 2017). The size of *Synechocystis* IM30 (*Syn*IM30) was estimated via SEC to be about 1600–2000 kDa (or even higher) (Fuhrmann et al., 2009a). For the homologous LiaH protein of *B. subtillis*, a molecular mass of at least 1.25 MDa was determined via SEC (Wolf et al., 2010). As these high molecular mass supercomplexes elute in the void volume or close to the void volume in most SEC experiments and as a compact

globular shape is assumed in SEC analyzes, which deviates from the partially hollow ring structure of IM30/PspA rings, the determined masses have to be taken with caution. In fact, from a recent 3D-reconstruction of IM30-rings, a molecular mass of about 1.5–2.5 MDa could be roughly estimated by using the volume/shape of the complex (Saur et al., 2017). However, the low resolution of this 3D-reconstruction makes it difficult to set the correct contour level for an exact determination of the volume and thus the exact mass.

Ring-shaped supercomplexes have been observed multiple times via negative stain electron microscopy for purified PspA (Hankamer et al., 2004), LiaH (Wolf et al., 2010) and IM30 from different organisms, involving *Arabidopsis*, *Chlamydomonas* and *Synechocystis* (Aseeva et al., 2004; Liu et al., 2007; Fuhrmann et al., 2009a; Gao et al., 2015). Thus far, the prevailing thesis is that PspA rings solely occur with 9-fold rotational symmetry (from *E. coli*), indicating a 4x9 (= 36 monomers) structure, which is in agreement with the molecular mass estimated via SEC. These *Eco*PspA rings have a diameter of about 20 nm and a height of 8–11 nm (Hankamer et al., 2004). However, *Eco*PspA rings with different diameters have also been observed, although they have not been further characterized (Male et al., 2014). The symmetry and number of monomers of the LiaH rings were identical with the PspA rings described by Hankamer et al. (2004); yet a ring diameter of 25 nm has been determined (Wolf et al., 2010).

In contrast to the supposedly homogeneous PspA and LiaH supercomplex structures, the IM30 ring dimensions are clearly highly variable. The first electron micrographs of heterologously expressed *Ara*IM30 revealed ring-shaped particles with a diameter of about 40 nm and a height of about 14 nm (**Figure 1B**) (Aseeva et al., 2004). Subsequent more detailed analysis of *Cr*IM30 and *Syn*IM30 revealed a heterogeneous size distribution with rings having diameters of at least 28–37 nm (*Cr*IM30) (Liu et al., 2007) and 25–33 nm (*Syn*IM30), respectively, resulting in a calculated number of monomers per ring ranging from 48–72 (Fuhrmann et al., 2009a; Saur et al., 2017). While the ring diameter clearly is variable, a constant height of 13–15 nm was observed for all *Syn*IM30 ring structures (Saur et al., 2017). Most electron micrographs of IM30 exhibit a pronounced spike architecture, giving rise to a very well defined rotational symmetry (at least 7 up to 22fold) (Saur et al., 2017). Interestingly, the 3D-reconstructions of the *Syn*IM30 rings suggest that the rings are polar and have two distinct sides (ring top and bottom side) (**Figure 1B**), with the monomers likely being ordered unidirectional in the ring structure (Saur et al., 2017), possibly enabling the rings to interact with two different interaction partners. This perfectly supports the idea of IM30 rings beeing able to bind/fuse two different membrane surfaces, e.g. different TM sheets or the cyanobacterial cytoplasmic membrane (CM) with the TM (Saur et al., 2017).

Rod-Like Structures

Besides isolated rings, in electron micrographs of purified IM30 and PspA also double rings and elongated rod-like structures were identified (**Figure 1C**), the latter appear to form via stacking of multiple IM30/PspA rings (Liu et al., 2007; Fuhrmann et al., 2009a; Male et al., 2014; Gao et al., 2015; Saur et al., 2017; Thurotte and Schneider, 2019).

While the formation of rod-like structures is a common feature of IM30/PspA family members, the preference for rings vs. rod-like structures appears to depend on the species (see **Table 1**). *Syn*IM30, the most intensely studied member of the IM30/PspA family in terms of protein structure, does only occasionally form rod-like structures (Fuhrmann et al., 2009a; Saur et al., 2017). Yet, formation of double ring structures is induced by Mg2+-binding to IM30, which alters the surface properties of individual IM30 rings (Heidrich et al., 2018). Additionally, increased formation of rod-like structures has been observed upon removal of the C-terminal helix 7 from *Syn*IM30 (Hennig et al., 2017). This observation suggests that PspA (and/or the PspA core of IM30 proteins) might be more prone to the formation of rod-like structures as they do not contain the (IM30-specific) C-terminal extension. PspA rings were initially observed and analyzed in the presence of chaotropic salts (Hankamer et al., 2004), which might hinder rod formation or disassemble PspA rods. In fact, extensive formation of rod-like structures has recently been reported for *Eco*PspA (Male et al., 2014). Furthermore, truncation of the *Syn*IM30 helix 1 also resulted in an increased formation of rod-like structures (Thurotte and Schneider, 2019), suggesting that helix 1 and helix 7 negatively control rod-formation in *Syn*IM30. Indeed, the removal of helix 1 and helix 7 in combination resulted in the exclusive formation of rod-like structures in the case of *Syn*IM30 (Thurotte and Schneider, 2019). This might be due to the removal of steric barriers inhibiting rod-formation of the wt protein. Interestingly, helix 7 is known to protrude out of the ring core structure (Otters et al., 2013; Heidrich et al., 2018) and thereby may hinder ring-ring contacts at one side of the ring. However, both helix 1 and 7 seem to have an intrinsic propensity to be unstructured (Osadnik et al., 2015; Zhang et al., 2016; Hennig et al., 2017; McDonald et al., 2017). Thus, they occupy a large conformational space, which might explain why they can create a steric hindrance for ring/supercomplex formation.

Notably, while *Ara*IM30, as well as the two IM30 paralogs of *Triticum urartu*, also appear to have a rather weak tendency to form rod-like structures (to the best of our knowledge, as the experimental evidence on these structures is limited (Otters et al., 2013; Zhang et al., 2016; Gao et al., 2017)), *Cr*IM30 has a pronounced tendency to form rods (Liu et al., 2005; Liu et al., 2007; Theis et al., 2019) (**Table 1**).

Also, deletion of helix 1 has different effects on the ultrastructure of IM30 from different species: While deletion of helix 1 in *Syn*IM30 clearly induced rod formation, deleting helix 1 from *Eco*PspA (Jovanovic et al., 2014) as well as from *Ara*IM30 (Otters et al., 2013; Ohnishi et al., 2018) did even abolish formation of large oligomers (including rings and rods), and thus here helix 1 appears to be essential for the formation of large oligomers as well as rings or rods. In contrast, removal of helix 1 from *Cr*IM30 did not abolish formation of large oligomers, albeit the oligomers appear not to have the prototypical ring structures anymore (Gao et al., 2015). Thus, the exact role of helix 1 for supercomplex formation appears to be species-dependent and has to be analyzed in more detail. Nevertheless, helix 1 and 7 are crucially involved in (de)stabilization of IM30 supercomplexes.

However, while also the physiological relevance of the rod-like structures is not at all clear yet, it has been hypothesized

that they might be part of cytoskeleton-like elements with microtubule-like structures (Liu et al., 2007; Rütgers and Schroda, 2013). Recently, it has been shown that *Cr*IM30 rods can engulf phosphatidylinositol phosphate-containing membranes (Theis et al., 2019), and thus, the rod-like structures could well be part of the membrane remodeling machinery of IM30.

THE STRUCTURE OF IM30 CHANGES DYNAMICALLY *IN VIVO*

The *in vivo* structure of IM30 is still enigmatic. It has been shown via fluorescence microscopy that GFP-tagged IM30 forms large clusters close to the TMs in chloroplasts and cyanobacterial cells, seen as punctae (Bryan et al., 2014). These punctae are called "functional Vipp1 particles" (FVPs) in chloroplasts (Zhang et al., 2016) (see **Table 1**). Additionally, GFP-tagged IM30 has also been identified at the CM and in the cytoplasm of *Synechocystis* (Bryan et al., 2014). Importantly, the localization of IM30 in *Synechocystis* changes when cells are transferred from low-light (LL, 8 μE m-2 s-1 intensity) to high-light (HL, (600 μE m-2 s-1 intensity) conditions. At LL, the majority of IM30 clusters were found at the cyanobacterial CM, whereas under HL conditions the total number of IM30 puncta strongly increased and the IM30 puncta preferentially form at the TM (Bryan et al., 2014). This dynamic relocalization of IM30 in *Synechocystis* has been investigated more extensively by Gutu et al. At standard light conditions (100 μE m-2 s-1 intensity), *Syn*IM30 was identified in two fractions: (i) a diffuse uniformly distributed fraction and (ii) short-lived puncta closely associated with highly curved TM regions. Yet, at HL conditions, IM30 puncta stably form at and associate with TMs (Gutu et al., 2018), and potential implications of this relocalization were discussed in more detail recently (Junglas and Schneider, 2018). A similar mobility of FVPs has also been observed in chloroplasts when protoplasts from *Arabidopsis* were treated with hypotonic stress (Zhang et al., 2016). As all members of the IM30/PspA family appear to be localized in discrete punctae associated with (probably stressed) cellular membranes (Engl et al., 2009; Yamaguchi et al., 2013; Domínguez-Escobar et al., 2014) the transient formation of clusters at defined membrane regions might be linked to the primordial PspA-function, *i.e.* membrane protection/maintenance.

However, the question arises, how IM30 is structured in these clusters? Unfortunately, the resolution of conventional fluorescence microscopy is limited to roughly 200 nm. Thus, single IM30 rings with typical diameters of 30 to 40 nm will be hardly detectable. Nevertheless, it has been suggested that the so-called FVPs in chloroplasts represent IM30 rings or clusters of IM30 rings (Zhang et al., 2016). In fact, the observed clusters have estimated maximal diameters of <0.2–1.5 μm (Zhang et al., 2016) and are thus too large for single IM30 rings and may consist of assemblies of multiple IM30 rings (**Table 1**). Notably, the IM30 puncta observed in *Synechocystis* are much smaller than the FVPs (100 ± 25 nm) and contain about 100–300 IM30 molecules (Bryan et al., 2014) (**Table 1**). Thus, they would consist of at least two to five rings, assuming an average monomer content of the rings of about 60. Taking into account the roughly estimated shape of these puncta, it is rather unlikely that they are formed by rod-like structures, but by multiple IM30 rings sitting next to each other (Junglas and Schneider, 2018). However, it is hard to imagine how membrane attached IM30 rings can stabilize lipid bilayers. Yet, as small IM30 oligomers and/or monomers have a higher membrane binding affinity than rings (Heidrich et al., 2016), it is reasonable to assume that IM30 rings disassemble upon membrane binding. Monomers or small oligomers may then form a protein network on membrane surfaces, similar to the clathrin-like structure that has been described for *Eco*PspA (Standar et al., 2008; Thurotte et al., 2017; Junglas and Schneider, 2018). The assumption that IM30 does not remain ring-structured upon membrane binding is further supported by the recent notion that IM30 rings were not found by template matching in tomograms of *Synechocystis* cells at or close to the highly curved TM ends (Rast et al., 2019), *i.e.* at the regions where the clusters have been identified via fluorescence microscopy. Furthermore, while not being genuine proof, up to the present day IM30 rings have, to the best of our knowledge, never been observed in any study of isolated TMs via electron microscopy or atomic force microscopy, despite the large ring dimensions (Olive et al., 1981; Kirchhoff et al., 2004; Kirchhoff et al., 2008b; Engel et al., 2015; Kowalewska et al., 2016; Casella et al., 2017; MacGregor-Chatwin et al., 2019; Wietrzynski et al., 2019). Hence, we conclude that the observed clusters most likely are not formed from IM30 rings sitting on membrane surfaces. However, the diffuse particles observed by Gutu et al. potentially represent single IM30 rings in solution (Gutu et al., 2018). Unfortunately, for the diffuse particles, no dimensions were given, possibly because the diffuse particles were too small and too mobile.

DYNAMIC (DIS)ASSEMBLY OF IM30 IS MEDIATED BY CHAPERONES

As observed in the before mentioned *in vivo* studies, the oligomeric state of IM30 appears to be highly dynamic. This dynamic behavior likely involves the activity of chaperones, which have been identified to interact with IM30 proteins (**Figure 2**). In *Chlamydomonas rheinhardtii*, IM30 was shown to associate with HSP70 chaperones and the co-chaperones CDJ2 and CGE1 in ATP-depleted cell extracts (Liu et al., 2005; Liu et al., 2007). These interactions were thereafter confirmed in solubilized membrane fractions (Heide et al., 2009). Additionally, HSP90 was identified as a supplementary interaction partner of the IM30/HSP70 complex in *Chlamydomonas* (Heide et al., 2009) and in *Arabidopsis* chloroplasts (Feng et al., 2014). In *Synechocystis*, the two HSP70 chaperones DnaK2 and DnaK3 (Rupprecht et al., 2007; Rupprecht et al., 2008; Rupprecht et al., 2010), as well as the HSP60 chaperonin GroL1, were shown to interact with IM30 (Bryan et al., 2014).

Interaction of IM30 with different chaperones significantly impacts the oligomeric state of IM30 (**Figure 2**). Although

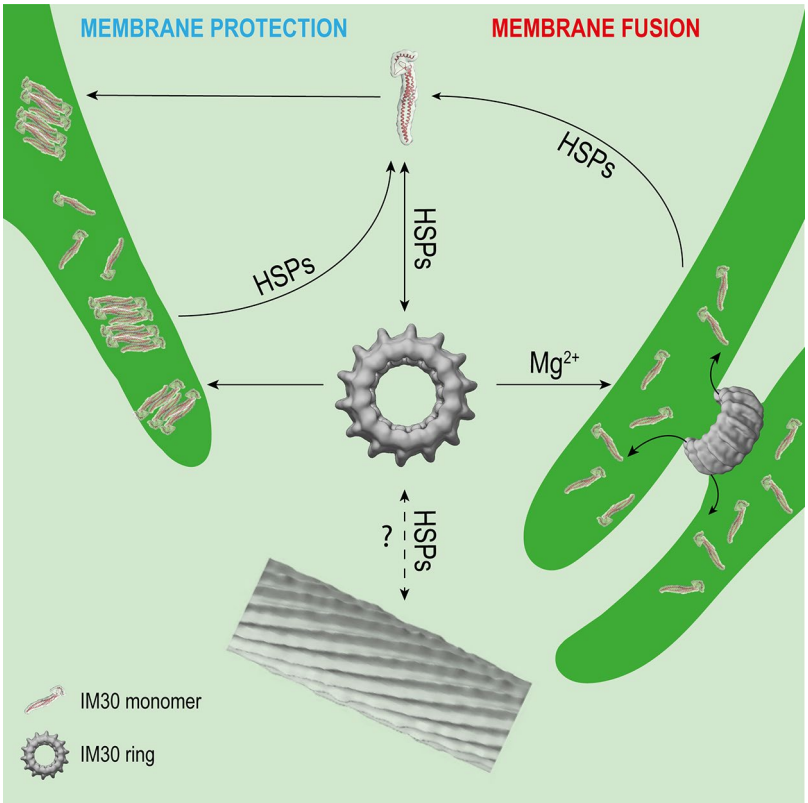

FIGURE 2 | Potential interactions of IM30 with membrane and HSPs. IM30 interacts with the TM as a ring and/or monomer. The monomers possibly rearrange on the TM to form a membrane-protecting structure. In presence of high amounts of Mg^{2+}, the IM30 ring is able to fuse adjacent membranes, which might involve dissociation of the ring into membrane-bound small oligomers/monomers. HSPs may detach the monomers from the membrane and trigger homo-oligomerization and ring formation. The physiological relevance of IM30 rod-like structures is unclear so far. However, HSPs have been shown to disassemble IM30 rods in the presence of ATP *in vitro*. (Rod structure adapted from (Theis et al., 2019); open-access license http://creativecommons.org/licenses/by/4.0/).

IM30 was found in the IM30/CDJ2 complex in a high- and low-molecular-weight fraction (> > 670 kDa and <230 kDa) in ATP-depleted *Chlamydomonas* cell extracts, it was only part of an intermediate-size molecular-weight fraction (about 670 kDa) in ATP-supplemented cell extracts (Liu et al., 2007), clearly suggesting an ATP-dependent assembly and/or disassembly, as expected when ATP-dependent chaperones are involved. Further analyses showed that also heterologously expressed IM30 can be assembled and disassembled by the HSP70-chaperone machinery in an ATP-dependent manner (Liu et al., 2007). Interestingly, the rod-like structures formed by *Cr*IM30 were also disassembled into IM30 rings and possibly smaller oligomers by the HSP70/CDJ2/CGE1 system when ATP was present (Liu et al., 2007). The bacterial HSP70 *Eco*DnaK was able to replace the *Cr*HSP70 protein in presence of CDJ2 and CGE1 (Liu et al., 2007). Interaction of the *Eco*DnaK protein with the *Cr*IM30 full-length protein was observed directly upon induction of heterologous expression of *Cr*IM30 in *E. coli* cells, suggesting that HSP70s generally recognize and stabilize IM30 monomers and assist in the formation of IM30 oligomers and supercomplexes. Likely, HSP70s shield IM30 domains to prevent unspecific aggregation. In fact, *Eco*DnaK binds with high affinity to truncated versions of the *Cr*IM30 proteins that form smaller oligomers but no ring structure anymore (Gao et al., 2015). In intact *Synechocystis* cells, GFP-labeled DnaK2, DnaK3, and IM30 were observed via fluorescence microscopy to colocalize in specific TM regions under HL-conditions, but not under LL-conditions (Bryan et al., 2014). Thus, under (HL) stress conditions, IM30 is potentially recruited to DnaK2 and/or DnaK3-enriched regions close to the membrane that activate IM30 via catalyzing assembly/disassembly (Bryan et al., 2014). Such relocalization of proteins under stress conditions has also been observed for PspA of *Yersinia enterocolitica* which can be found in the cytoplasm and at the CM under normal conditions, whereas it forms large static complexes at the CM under stress conditions (Yamaguchi et al., 2013).

In an *Arabidopsis* mutant lacking *Ara*HSP90.5, the ratio of monomeric IM30 to higher molecular weight-oligomers of IM30 (>1000 kDa) was shifted to the oligomeric form, indicating that HSP90.5 is also involved in disassembly of IM30 supercomplexes, possibly together with HSP70 (Feng et al., 2014).

Taken together, IM30 clearly has an intrinsic propensity to spontaneously form large oligomeric structures. HSP70 and HSP90 chaperones have been shown to catalyze disassembly, but also the assembly of IM30 oligomers (**Figure 2**), at

least *ex vivo* and *in vitro*. The chaperones may be required for removal of membrane-bound small IM30 oligomers (**Figure 2**), as has been described for the uncoating of clathrin complexes by auxilin and HSP70 (Ungewickell et al., 1995). Membrane-associated chaperones are potential candidates for this process. After removal from the membrane, small oligomers may then assemble into oligomers in the cytosol, to finally form the typical ring-shaped IM30 structures and complete the recycling process (**Figure 2**). Yet, it remains to be shown which physiological conditions trigger the interaction of IM30 with the chaperones.

WHY DO WE NEED A RING?

In several models, a need for the formation of IM30 rings and/or rod-like structures to fulfill their physiological function(s) is implicated. However, the existence and relevance of IM30 supercomplexes *in vivo* still need to be shown, especially because IM30 rings have never been observed in an *in vivo* context so far. But, are IM30 rings really indispensable for the proposed IM30 functions?

The IM30 Ring Structure Enables Efficient Membrane Chaperoning

Formation of IM30/PspA rings is probably not necessary for the proteins´ membrane chaperoning function, as small oligomers bind with higher affinity to membrane surfaces (Heidrich et al., 2016). This observation has triggered the suggestion that IM30 rings disassemble into smaller oligomers (or monomers) upon/during membrane binding. It has been hypothesized that PspA/IM30 family proteins act as membrane chaperones by forming a stabilizing network on the membrane surface, as discussed above (Thurotte et al., 2017; Junglas and Schneider, 2018). Possibly, such structures have been imaged via GFP-tagged IM30 in living cells as large IM30 assemblies located at the TM (Zhang et al., 2012; Bryan et al., 2014; Zhang et al., 2016; Gutu et al., 2018; Junglas and Schneider, 2018). Also, the oligomeric PspA structures identified by Standar et al., described as a clathrin-like scaffold (Standar et al., 2008), potentially represent *E. coli* membrane patches coated with PspA.

So, what might the ring structure then be good for, especially in the case of PspA and LiaH proteins that are the main effector proteins of the *psp*/*lia* membrane-stress response system, where their major task is to maintain membranes? Homo-oligomeric protein complexes can provide a highly ordered structure and high stability due to the compactness and cooperativity of highly packed monomers. This might protect the monomeric protein against proteolysis and degradation under harsh conditions, which is especially beneficial for stress-response proteins. Indeed, IM30 rings (more precisely the ring core) are relatively protease-resistant and resistant against chemical and thermal denaturation compared to small oligomers (Gao et al., 2015; Heidrich et al., 2018; Thurotte and Schneider, 2019). Furthermore, the surface of a higher-ordered oligomer is relatively small compared to the monomer. This could be a mechanism to control the IM30 activity, as amphiphilic helices, which are prone to interact with membrane surfaces, are exposed solely when the complexes dissociate. Consequently, the IM30 ring could be a storage form of smaller, active IM30 oligomers/monomers to prevent a continuous need for shielding the hydrophobic surfaces by chaperones. Additionally, preformation of a highly ordered homo-oligomeric supercomplex ensures a high avidity and an immediate high local concentration of the active small oligomers (or monomers) upon membrane binding, which is likely necessary for membrane attachment and rapid formation of protein networks on membrane surfaces involved in membrane repair and/or protection. The orientation of the monomers in the ring could support e.g. membrane binding if the interacting amino acid residues are positioned in a favorable orientation to the membrane.

The IM30 Ring Is Crucial for Membrane Fusion

Besides the involvement of the IM30 ring structure in membrane protection, the ring seems to be mandatory for the membrane fusion activity of IM30. A membrane fusion protein requires strict control of its activity, as any uncontrolled fusion event is potentially detrimental for the cell because it could e.g. result in a loss of electrical and/or chemical gradients. This is especially relevant for the TM, as any leak by misdirected fusion reduces the proton gradient and the photosynthetic efficiency. Therefore, control of the IM30 activity *via* oligomer formation might be a potential solution. Another regulation mechanism is the dependence of the fusion process on Mg^{2+}, which seems to activate IM30 rings (Heidrich et al., 2018).

The structural features of the IM30 ring structure seem to support the fusion mechanism directly. An oligomeric ring exposes two distinct sides of the monomers, which are orientated unidirectional, as suggested for IM30 (Saur et al., 2017). The opposing sides of the ring can consequently interact *e.g.* with two membranes, as it would be necessary for a membrane fusion activity. This would also be possible with a cylindrically shaped protein, but the hole inside the ring might be important for the formation of a fusion pore(-like structure). A recent model for the IM30-mediated membrane fusion suggests that fusion is initiated by the ring (Heidrich et al., 2017). As the protein binds negatively charged lipids (Hennig et al., 2015), IM30 might recruit such lipids when binding as a ring to a membrane surface. In the center of the ring, the concentration of the non-bilayer forming lipid MGDG becomes locally high, which might result in disruption of an ordered bilayer structure and initial fusion of two interacting membranes. Dissociation of the ring could then lead to lipid mixing, allowing the formation of a stable, now fused membrane (Heidrich et al., 2017). Moreover, a large protein complex would clearly facilitate the formation of a fusion pore at the TM. As the membrane is completely crowded with integral and peripheral membrane proteins (Kirchhoff et al., 2008a; Casella et al., 2017; MacGregor-Chatwin et al., 2019; Wietrzynski et al., 2019), it is hard to imagine that binding of a small protein could provide enough space needed for membrane-membrane contacts and subsequent membrane fusion. Instead, binding of a

large ring complex that finally dissociates could generate a fusion platform on the membrane. We, therefore, suggest that the IM30 ring structure is mandatory for the membrane fusion function.

Taken together, the formation of IM30 rings might prevent uncontrolled membrane binding and simultaneously prealigns IM30 monomers for efficient membrane binding. Furthermore, IM30 rings are directly involved in membrane fusion, where Mg^{2+} binding is an additional activation step that renders the rings fusion competent.

WHERE AND WHEN TO FIND IM30 RINGS?

As discussed above, IM30 rings are indispensable for controlled membrane remodeling but are probably also generally useful to ensure proper activity of IM30, *i.e.* increase the local concentration of active small oligomers/monomers or shield them from unwanted interactions when not bound to the membrane. An intriguing question that arises from these assumptions is: When such rings are so important, why do we not see them *in vivo*? While IM30 clusters have been observed on TMs in cyanobacteria and chloroplasts (Zhang et al., 2012; Bryan et al., 2014; Zhang et al., 2016; Gutu et al., 2018), the supramolecular organization of IM30 within these structures is still enigmatic, and rings "sitting" on TMs have not been observed yet. The problem probably is not that IM30 rings are hard to find because of their size and shape. Other proteins of similar or even smaller size have been identified in cryo-TEM tomograms of *Synechocystis* recently (Rast et al., 2019). So the question probably is more: Where and when to find IM30 rings in living cells?

IM30 appears to be a protein with (at least) a dual function, *i.e.* a membrane remodeling and a membrane stabilizing/protecting function. These functions have to be separated spatiotemporally, as they would otherwise cancel out each other. Assuming that both functions have different requirements on the protein structure (as discussed above), IM30 rings are very short-living and can probably only be found on a membrane under certain specific conditions. However, both processes, membrane chaperoning and remodeling, potentially involve binding of IM30 rings to the membrane and ring dissociation, resulting in small membrane-bound oligomers or even monomers (**Figure 2**). Thus, chances to find IM30 rings on membrane surfaces are probably low. Only at the initial phase of a fusion event, *i.e.* when two adjacent membranes meet each other, rings may be found to connect these (**Figure 2**). This may only be observed at TM convergence zones under conditions where membrane remodeling is needed, e.g. when cells are shifted from the dark to light. Under HL/stress conditions, IM30 monomers and/or small oligomers will be found on the TM (Thurotte et al., 2017; Gutu et al., 2018; Junglas and Schneider, 2018) (**Figure 2**), so chances to find rings are also low. Yet, as discussed above, the oligomeric state of IM30 depends on the activity of molecular chaperones, which likely control assembly and disassembly of IM30 oligomers (**Figure 2**). Indeed, IM30 supercomplexes have been detected in cellular extracts of *Chlamydomonas rheinhardtii* chloroplasts when ATP was depleted (Liu et al., 2007). Thus, IM30 rings might only exist in detectable amounts under conditions of low ATP, e.g. as periodically observed at the (diurnal) dark to light transition in cyanobacteria and chloroplasts (Konno et al., 2012; Saha et al., 2016; Voon et al., 2018). During dark to light transition, where IM30 is necessary for unimpaired growth (Gutu et al., 2018), IM30 rings might be needed for TM remodeling. However, the oligomeric state of IM30 is probably also controlled by altered expression of chaperones, as observed e.g. for DnaK2 under HL, heat, hyperosmotic and salt stress in *Synechococcus elongatus* PCC 7942 and *Synechocystis* sp. PCC 6803 (Sato et al., 2007; Rupprecht et al., 2008). Under normal growth conditions (no increased chaperone expression), IM30 rings could display an inactive cytosolic storage form. These possibly represent the diffuse particles observed by Gutu et al. (2018). Thus, the cellular ATP levels will likely have only minor effects on the oligomeric state of IM30 when chaperones are not induced.

In summary, we believe that IM30 rings can barely be found on membranes in living cells as they likely represent a short-lived IM30 structure. Assembly and disassembly of the supercomplexes likely are highly controlled and meetcellular demands.

AUTHOR CONTRIBUTIONS

All authors wrote the manuscript.

FUNDING

This work was funded by the Max-Planck graduate center at the Max Planck institutes and the University of Mainz.

ACKNOWLEDGMENTS

We thank Anne-Christin Pohland, Lucas Gewehr, and Hildegard Pearson for carefully reading the manuscript.

REFERENCES

Anbudurai, P. R., Mor, T. S., Ohad, I., Shestakov, S. V., and Pakrasi, H. B. (1994). The ctpA gene encodes the C-terminal processing protease for the D1 protein of the photosystem II reaction center complex. *Proc. Natl. Acad. Sci. U. S. A.* 91, 8082–8086. doi: 10.1073/pnas.91.17.8082

Aoki, M., Sato, N., Meguro, A., and Tsuzuki, M. (2004). Differing involvement of sulfoquinovosyl diacylglycerol in photosystem II in two species of unicellular cyanobacteria. *Eur. J. Biochem.* 271, 685–693. doi: 10.1111/j.1432-1033.2003.03970.x

Aseeva, E., Ossenbühl, F., Eichacker, L. A., Wanner, G., Soll, J., and Vothknecht, U. C. (2004). Complex formation of Vipp1 depends on its alpha-helical PspA-like domain. *J. Biol. Chem.* 279, 35535–35541. doi: 10.1074/jbc.M401750200

Aseeva, E., Ossenbühl, F., Sippel, C., Cho, W. K., Stein, B., and Eichacker, L. A. (2007). Vipp1 is required for basic thylakoid membrane formation but not for the assembly of thylakoid protein complexes. *Plant Physiol. Biochem.* 45, 119–128. doi: 10.1016/J.PLAPHY.2007.01.005

Benning, C., Xu, C., and Awai, K. (2006). Non-vesicular and vesicular lipid trafficking involving plastids. *Curr. Opin. Plant Biol.* 9, 241–247. doi: 10.1016/j.pbi.2006.03.012

Bryan, S. J., Burroughs, N. J., Shevela, D., Yu, J., Rupprecht, E., and Liu, L. N. (2014). Localisation and interactions of the Vipp1 protein in cyanobacteria. *Mol. Microbiol.* 94, 1179–1195. doi: 10.1111/mmi.12826

Bultema, J. B., Fuhrmann, E., Boekema, E. J., and Schneider, D. (2010). Vipp1 and PspA. *Commun. Integr. Biol.* 3, 162–165. doi: 10.4161/cib.3.2.10529

Casella, S., Huang, F., Mason, D., Zhao, G.-Y., Johnson, G. N., and Mullineaux, C. W. (2017). Dissecting the native architecture and dynamics of cyanobacterial photosynthetic machinery. *Mol. Plant* 10, 1434–1448. doi: 10.1016/j.molp.2017.09.019

Chuartzman, S. G., Nevo, R., Shimoni, E., Charuvi, D., Kiss, V., and Ohad, I. (2008). Thylakoid membrane remodeling during state transitions in Arabidopsis. *Plant Cell* 20, 1029–1039. doi: 10.1105/tpc.107.055830

DeLisa, M. P., Lee, P., Palmer, T., and Georgiou, G. (2004). Phage shock protein PspA of Escherichia coli relieves saturation of protein export via the Tat pathway. *J. Bacteriol.* 186, 366–373. doi: 10.1128/JB.186.2.366-373.2004

Domínguez-Escobar, J., Wolf, D., Fritz, G., Höfler, C., Wedlich-Söldner, R., and Mascher, T. (2014). Subcellular localization, interactions and dynamics of the phage-shock protein-like Lia response in Bacillus subtilis. *Mol. Microbiol.* 92, 716–732. doi: 10.1111/mmi.12586

Engel, B. D., Schaffer, M., Kuhn Cuellar, L., Villa, E., Plitzko, J. M., and Baumeister, W. (2015). Native architecture of the Chlamydomonas chloroplast revealed by in situ cryo-electron tomography. *Elife* 4: e04889. doi: 10.7554/eLife.04889

Engl, C., Jovanovic, G., Lloyd, L. J., Murray, H., Spitaler, M., and Ying, L. (2009). In vivo localizations of membrane stress controllers PspA and PspG in Escherichia coli. *Mol. Microbiol.* 73, 382–396. doi: 10.1111/j.1365-2958.2009.06776.x

Feng, J., Fan, P., Jiang, P., Lv, S., Chen, X., and Li, Y. (2014). Chloroplast-targeted Hsp90 plays essential roles in plastid development and embryogenesis in Arabidopsis possibly linking with VIPP1. *Physiol. Plant* 150, 292–307. doi: 10.1111/ppl.12083

Fuhrmann, E., Bultema, J. B., Kahmann, U., Rupprecht, E., Boekema, E. J., and Schneider, D. (2009a). The vesicle-inducing protein 1 from Synechocystis sp. PCC 6803 organizes into diverse higher-ordered ring structures. *Mol. Biol. Cell* 20, 4620–4628. doi: 10.1091/mbc.E09-04-0319

Fuhrmann, E., Gathmann, S., Rupprecht, E., Golecki, J., and Schneider, D. (2009b). Thylakoid membrane reduction affects the photosystem stoichiometry in the cyanobacterium Synechocystis sp. PCC 6803. *Plant Physiol.* 149, 735–744. doi: 10.1104/pp.108.132373

Göhre, V., Ossenbühl, F., Crèvecoeur, M., Eichacker, L. A., and Rochaix, J. D. (2006). One of two Alb3 proteins is essential for the assembly of the photosystems and for cell survival in Chlamydomonas. *Plant Cell* 18, 1454–1466. doi: 10.1105/tpc.105.038695

Gao, H., and Xu, X. (2009). Depletion of Vipp1 in Synechocystis sp. PCC 6803 affects photosynthetic activity before the loss of thylakoid membranes. *FEMS Microbiol. Lett.* 292, 63–70. doi: 10.1111/j.1574-6968.2008.01470.x

Gao, F., Wang, W., Zhang, W., and Liu, C. (2015). α-Helical domains affecting the oligomerization of Vipp1 and its interaction with Hsp70/DnaK in Chlamydomonas. *Biochemistry* 54, 4877–4889. doi: 10.1021/acs.biochem.5b00050

Gao, F., Chen, B., Jiao, J., Jia, L., and Liu, C. (2017). Two novel vesicle-inducing proteins in plastids 1 genes cloned and characterized in *Triticum urartu*. *PloS One* 12, e0170439. doi: 10.1371/journal.pone.0170439

Guskov, A., Kern, J., Gabdulkhakov, A., Broser, M., Zouni, A., and Saenger, W. (2009). Cyanobacterial photosystem II at 2.9-Å resolution and the role of quinones, lipids, channels and chloride. *Nat. Struct. Mol. Biol.* 16, 334–342. doi: 10.1038/nsmb.1559

Gutu, A., Chang, F., and O'Shea, E. K. (2018). Dynamical localization of a thylakoid membrane binding protein is required for acquisition of photosynthetic competency. *Mol. Microbiol.* 108, 16–31. doi: 10.1111/mmi.13912

Hankamer, B. D., Elderkin, S. L., Buck, M., and Nield, J. (2004). Organization of the AAA+ Adaptor Protein PspA is an Oligomeric Ring. *J. Biol. Chem.* 279, 8862–8866. doi: 10.1074/JBC.M307889200

Heide, H., Nordhues, A., Drepper, F., Nick, S., Schulz-Raffelt, M., and Haehnel, W. (2009). Application of quantitative immunoprecipitation combined with knockdown and cross-linking to Chlamydomonas reveals the presence of vesicle-inducing protein in plastids 1 in a common complex with chloroplast HSP90C. *Proteomics* 9, 3079–3089. doi: 10.1002/pmic.200800872

Heidrich, J., Wulf, V., Hennig, R., Saur, M., Markl, J., and Sönnichsen, C. (2016). Organization into higher ordered ring structures counteracts membrane binding of IM30, a protein associated with inner membranes in chloroplasts and cyanobacteria. *J. Biol. Chem.* 291, 14954–14962. doi: 10.1074/JBC.M116.722686

Heidrich, J., Thurotte, A., and Schneider, D. (2017). Specific interaction of IM30/Vipp1 with cyanobacterial and chloroplast membranes results in membrane remodeling and eventually in membrane fusion. *Biochim. Biophys. Acta - Biomembr.* 1859, 537–549. doi: 10.1016/j.bbamem.2016.09.025

Heidrich, J., Junglas, B., Grytsyk, N., Hellmann, N., Rusitzka, K., and Gebauer, W. (2018). Mg2+ binding triggers rearrangement of the IM30 ring structure, resulting in augmented exposure of hydrophobic surfaces competent for membrane binding. *J. Biol. Chem.* 293, 8230–8241. doi: 10.1074/jbc.RA117.000991

Heinz, S., Liauw, P., Nickelsen, J., and Nowaczyk, M. (2016). Analysis of photosystem II biogenesis in cyanobacteria. *Biochim. Biophys. Acta* 1857, 274–287. doi: 10.1016/j.bbabio.2015.11.007

Hennig, R., Heidrich, J., Saur, M., Schmüser, L., Roeters, S. J., and Hellmann, N. (2015). IM30 triggers membrane fusion in cyanobacteria and chloroplasts. *Nat. Commun.* 6, 7018. doi: 10.1038/ncomms8018

Hennig, R., West, A., Debus, M., Saur, M., Markl, J., and Sachs, J. N. (2017). The IM30/Vipp1 C-terminus associates with the lipid bilayer and modulates membrane fusion. *Biochim. Biophys. Acta - Bioenerg.* 1858, 126–136. doi: 10.1016/j.bbabio.2016.11.004

Joly, N., Engl, C., Jovanovic, G., Huvet, M., Toni, T., and Sheng, X. (2010). Managing membrane stress: the phage shock protein (Psp) response, from molecular mechanisms to physiology. *FEMS Microbiol. Rev.* 34, 797–827. doi: 10.1111/j.1574-6976.2010.00240.x

Jovanovic, G., Mehta, P., McDonald, C., Davidson, A. C., Uzdavinys, P., and Ying, L. (2014). The N-terminal amphipathic helices determine regulatory and effector functions of phage shock protein A (PspA) in escherichia coli. *J. Mol. Biol.* 426, 1498–1511. doi: 10.1016/j.jmb.2013.12.016

Junglas, B., and Schneider, D. (2018). What is Vipp1 good for?. *Mol. Microbiol.* 108, 1–5. doi: 10.1111/mmi.13924

Kirchhoff, H., Tremmel, I., Haase, W., and Kubitscheck, U. (2004). Supramolecular photosystem II organization in grana thylakoid membranes: evidence for a structured arrangementt. *Biochemistry* 43, 9204–9213. doi: 10.1021/bi0494626

Kirchhoff, H., Haferkamp, S., Allen, J. F., Epstein, D. B. A., and Mullineaux, C. W. (2008a). Protein diffusion and macromolecular crowding in thylakoid membranes. *Plant Physiol.* 146, 1571–1578. doi: 10.1104/pp.107.115170

Kirchhoff, H., Lenhert, S., Büchel, C., Chi, L., and Nield, J. (2008b). Probing the organization of photosystem II in photosynthetic membranes by atomic force microscopy. *Biochemistry* 47, 431–440. doi: 10.1021/bi7017877

Kleerebezem, M., Crielaard, W., and Tommassen, J. (1996). Involvement of stress protein PspA (phage shock protein A) of Escherichia coli in maintenance of the protonmotive force under stress conditions. *EMBO J.* 15, 162–171. doi: 10.1128/JCM.43.1.19

Kobayashi, R., Suzuki, T., and Yoshida, M. (2007). Escherichia coli phage-shock protein A (PspA) binds to membrane phospholipids and repairs proton leakage of the damaged membranes. *Mol. Microbiol.* 66, 100–109. doi: 10.1111/j.1365-2958.2007.05893.x

Kobayashi, K., Fujii, S., Sato, M., Toyooka, K., and Wada, H. (2015). Specific role of phosphatidylglycerol and functional overlaps with other thylakoid lipids in Arabidopsis chloroplast biogenesis. *Plant Cell Rep.* 34, 631–642. doi: 10.1007/s00299-014-1719-z

Konno, H., Nakane, T., Yoshida, M., Ueoka-Nakanishi, H., Hara, S., and Hisabori, T. (2012). Thiol modulation of the chloroplast ATP synthase is dependent on the energization of thylakoid membranes. *Plant Cell Physiol.* 53, 626–634. doi: 10.1093/pcp/pcs018

Kowalewska, Ł., Mazur, R., Suski, S., Garstka, M., and Mostowska, A. (2016). Three-dimensional visualization of the Tubular-Lamellar transformation of the internal plastid membrane network during runner bean chloroplast biogenesis. *Plant Cell* 28, 875–891. doi: 10.1105/tpc.15.01053

Kroll, D., Meierhoff, K., Bechtold, N., Kinoshita, M., Westphal, S., and Vothknecht, U. C. (2001). VIPP1, a nuclear gene of Arabidopsis thaliana essential for thylakoid membrane formation. *Proc. Natl. Acad. Sci.* 98, 4238–4242. doi: 10.1073/PNAS.061500998

Li, H., Kaneko, Y., and Keegstra, K. (1994). Molecular cloning of a chloroplastic proteinassociated with both the envelope and thylakoid membranes. *Plant Mol. Biol.* 25, 619–632. doi: 10.1007/BF00029601

Liberton, M., Page, L. E., O'Dell, W. B., O'Neill, H., Mamontov, E., and Urban, V. S. (2013). Organization and flexibility of cyanobacterial thylakoid membranes examined by neutron scattering. *J. Biol. Chem.* 288, 3632–3640. doi: 10.1074/jbc.M112.416933

Liu, C., Willmund, F., Whitelegge, J. P., Hawat, S., Knapp, B., and Lodha, M. (2005). J-domain protein CDJ2 and HSP70B are a plastidic chaperone pair that

interacts with vesicle-inducing protein in plastids 1. *Mol. Biol. Cell* 16, 1165–1177. doi: 10.1091/mbc.E04-08-0736

Liu, C., Willmund, F., Golecki, J. R., Cacace, S., Heß, B., and Markert, C. (2007). The chloroplast HSP70B-CDJ2-CGE1 chaperones catalyse assembly and disassembly of VIPP1 oligomers in Chlamydomonas. *Plant J.* 50, 265–277. doi: 10.1111/j.1365-313X.2007.03047.x

MacGregor-Chatwin, C., Jackson, P. J., Sener, M., Chidgey, J. W., Hitchcock, A., and Qian, P. (2019). Membrane organization of photosystem I complexes in the most abundant phototroph on Earth. *Nat. Plants* 5, 879–889. doi: 10.1038/s41477-019-0475-z

Male, A. L., Oyston, P. C. F., and Tavassoli, A. (2014). Self-assembly of Escherichia coli Phage Shock Protein A. *Adv. Microbiol.* 04, 353–359. doi: 10.4236/aim.2014.47042

McDonald, C., Jovanovic, G., Ces, O., and Buck, M. (2015). Membrane stored curvature elastic stress modulates recruitment of maintenance proteins PspA and Vipp1. *MBio* 6, e01188–e01115. doi: 10.1128/mbio.01188-15

McDonald, C., Jovanovic, G., Wallace, B. A., Ces, O., and Buck, M. (2017). Structure and function of PspA and Vipp1 N-terminal peptides: insights into the membrane stress sensing and mitigation. *Biochim. Biophys. Acta - Biomembr.* 1859, 28–39. doi: 10.1016/J.BBAMEM.2016.10.018

Nagy, G., Posselt, D., Kovács, L., Holm, J. K., Szabó, M., and Ughy, B. (2011). Reversible membrane reorganizations during photosynthesis in vivo: revealed by small-angle neutron scattering. *Biochem. J.* 436, 225–230. doi: 10.1042/bj20110180

Nordhues, A., Schottler, M. A., Unger, A.-K., Geimer, S., Schonfelder, S., and Schmollinger, S. (2012). Evidence for a role of VIPP1 in the structural organization of the photosynthetic apparatus in Chlamydomonas. *Plant Cell Online* 24, 637–659. doi: 10.1105/tpc.111.092692

Ohnishi, N., Zhang, L., and Sakamoto, W. (2018). VIPP1 involved in chloroplast membrane integrity has GTPase activity in vitro. *Plant Physiol.* 177, 328–338. doi: 10.1104/pp.18.00145

Olive, J., Wollman, F.-A., Bennoun, P., and Recouvreur, M. (1981). Ultrastructure of thylakoid membranes in C. reinhardtii: Evidence for variations in the partition coefficient of the light-harvesting complex-containing particles upon membrane fracture. *Arch. Biochem. Biophys.* 208, 456–467. doi: 10.1016/0003-9861(81)90532-4

Osadnik, H., Schöpfel, M., Heidrich, E., Mehner, D., Lilie, H., and Parthier, C. (2015). PspF-binding domain PspA1-144and the PspA·F complex: New insights into the coiled-coil-dependent regulation of AAA+ proteins. *Mol. Microbiol.* 98, 743–759. doi: 10.1111/mmi.13154

Otters, S., Braun, P., Hubner, J., Wanner, G., Vothknecht, U. C., and Chigri, F. (2013). The first α-helical domain of the vesicle-inducing protein in plastids 1 promotes oligomerization and lipid binding. *Planta* 237, 529–540. doi: 10.1007/s00425-012-1772-1

Pohland, A.-C., and Schneider, D. (2019). Mg2+ homeostasis and transport in cyanobacteria – at the crossroads of bacterial and chloroplast Mg2+ import. *Biol. Chem.* 400, 1289–1301. doi: 10.1515/hsz-2018-0476

Rütgers, M., and Schroda, M. (2013). A role of VIPP1 as a dynamic structure within thylakoid centers as sites of photosystem biogenesis? *Plant Signal. Behav.* 8, e27037. doi: 10.4161/psb.27037

Rast, A., Schaffer, M., Albert, S., Wan, W., Pfeffer, S., and Beck, F. (2019). Biogenic regions of cyanobacterial thylakoids form contact sites with the plasma membrane. *Nat. Plants* 5, 436–446. doi: 10.1038/s41477-019-0399-7

Rupprecht, E., Gathmann, S., Fuhrmann, E., and Schneider, D. (2007). Three different DnaK proteins are functionally expressed in the cyanobacterium Synechocystis sp. PCC 6803. *Microbiology* 153, 1828–1841. doi: 10.1099/mic.0.2007/005876-0

Rupprecht, E., Fuhrmann, E., and Schneider, D. (2008). "Stress Regulated DnaK Expression in Synechocystis sp. PCC 6803" in *Photosynthesis. Energy from the Sun* (Dordrecht: Springer Netherlands), 1327–1330. doi: 10.1007/978-1-4020-6709-9_286

Rupprecht, E., Duppre, E., and Schneider, D. (2010). Similarities and Singularities of Three DnaK Proteins from the Cyanobacterium Synechocystis sp. PCC 6803. *Plant Cell Physiol.* 51, 1210–1218. doi: 10.1093/pcp/pcq074

Saha, R., Liu, D., Hoynes-O'Connor, A., Liberton, M., Yu, J., and Bhattacharyya-Pakrasi, M. (2016). Diurnal regulation of cellular processes in the Cyanobacterium Synechocystis sp. Strain PCC 6803: insights from transcriptomic, fluxomic, and physiological analyses. *MBio* 7, e00464–e00416. doi: 10.1128/mBio.00464-16

Sato, M., Nimura-Matsune, K., Watanabe, S., Chibazakura, T., and Yoshikawa, H. (2007). Expression analysis of multiple dnaK genes in the cyanobacterium Synechococcus elongatus PCC 7942. *J. Bacteriol.* 189, 3751–3758. doi: 10.1128/JB.01722-06

Saur, M., Hennig, R., Young, P., Rusitzka, K., Hellmann, N., and Heidrich, J. (2017). A Janus-Faced IM30 Ring Involved in Thylakoid Membrane Fusion Is Assembled from IM30 Tetramers. *Structure* 25, 1380–1390.e5. doi: 10.1016/J.STR.2017.07.001

Standar, K., Mehner, D., Osadnik, H., Berthelmann, F., Hause, G., and Lünsdorf, H. (2008). PspA can form large scaffolds in Escherichia coli. *FEBS Lett.* 582, 3585–3589. doi: 10.1016/j.febslet.2008.09.002

Theis, J., Gupta, T. K., Klingler, J., Wan, W., Albert, S., and Keller, S. (2019). VIPP1 rods engulf membranes containing phosphatidylinositol phosphates. *Sci. Rep.* 9, 8725. doi: 10.1038/s41598-019-44259-3

Thurotte, A., and Schneider, D. (2019). The fusion activity of IM30 rings involves controlled unmasking of the fusogenic core. *Front. Plant Sci.* 10, 108. doi: 10.3389/fpls.2019.00108

Thurotte, A., Brüser, T., Mascher, T., and Schneider, D. (2017). Membrane chaperoning by members of the PspA/IM30 protein family. *Commun. Integr. Biol.* 10, e1264546. doi: 10.1080/19420889.2016.1264546

Umena, Y., Kawakami, K., Shen, J. R., and Kamiya, N. (2011). Crystal structure of oxygen-evolving photosystem II at a resolution of 1.9Å. *Nature* 473, 55–60. doi: 10.1038/nature09913

Ungewickell, E., Ungewickell, H., Holstein, S. E. H., Lindner, R., Prasad, K., and Barouch, W. (1995). Role of auxilin in uncoating clathrin-coated vesicles. *Nature* 378, 632–635. doi: 10.1038/378632a0

Voon, C. P., Guan, X., Sun, Y., Sahu, A., Chan, M. N., and Gardeström, P. (2018). ATP compartmentation in plastids and cytosol of Arabidopsis thaliana revealed by fluorescent protein sensing. *Proc. Natl. Acad. Sci. U. S. A.* 115, E10778–E10787. doi: 10.1073/pnas.1711497115

Vothknecht, U. C., Otters, S., Hennig, R., and Schneider, D. (2012). Vipp1: a very important protein in plastids? *J. Exp. Bot.* 63, 1699–1712. doi: 10.1093/jxb/err357

Walter, B., Hristou, A., Nowaczyk, M. M., and Schünemann, D. (2015). In vitro reconstitution of co-translational D1 insertion reveals a role of the cpSec–Alb3 translocase and Vipp1 in photosystem II biogenesis. *Biochem. J.* 468, 315–324. doi: 10.1042/BJ20141425

Westphal, S., Heins, L., Soll, J., and Vothknecht, U. C. (2001). Vipp1 deletion mutant of Synechocystis: a connection between bacterial phage shock and thylakoid biogenesis? *Proc. Natl. Acad. Sci. U. S. A.* 98, 4243–4248. doi: 10.1073/pnas.061501198

Wietrzynski, W., Schaffer, M., Tegunov, D., Albert, S., Kanazawa, A., and Plitzko, J. M. (2019). Charting the native architecture of thylakoid membranes with single-molecule precision [Preprint]. *bioRxiv*, 759001. doi: 10.1101/759001

Wolf, D., Kalamorz, F., Wecke, T., Juszczak, A., Mäder, U., and Homuth, G. (2010). In-depth profiling of the LiaR response of Bacillus subtilis. *J. Bacteriol.* 192, 4680–4693. doi: 10.1128/JB.00543-10

Yamaguchi, S., Reid, D. A., Rothenberg, E., and Darwin, A. J. (2013). Changes in Psp protein binding partners, localization and behaviour upon activation of the Yersinia enterocolitica phage shock protein response. *Mol. Microbiol.* 87, 656–671. doi: 10.1111/mmi.12122

Zhang, L., and Sakamoto, W. (2013).). Possible function of VIPP1 in thylakoids: Protection but not formation? *Plant Signal. Behav.* 8: e22860. doi: 10.4161/psb.22860

Zhang, L., and Sakamoto, W. (2015). Possible function of VIPP1 in maintaining chloroplast membranes. *Biochim. Biophys. Acta* 1847: 831–837. doi: 10.1016/j.bbabio.2015.02.013

Zhang, L., Kato, Y., Otters, S., Vothknecht, U. C., and Sakamoto, W. (2012). Essential role of VIPP1 in chloroplast envelope maintenance in Arabidopsis. *Plant Cell* 24, 3695–3707. doi: 10.1105/tpc.112.103606

Zhang, S., Shen, G., Li, Z., Golbeck, J. H., and Bryant, D. A. (2014). Vipp1 is essential for the biogenesis of Photosystem I but not thylakoid membranes in Synechococcus sp. PCC 7002. *J. Biol. Chem.* 289, 15904–15914. doi: 10.1074/jbc.M114.555631

Zhang, L., Kondo, H., Kamikubo, H., Kataoka, M., and Sakamoto, W. (2016). VIPP1 has a disordered C-Terminal tail necessary for protecting photosynthetic membranes against stress. *Plant Physiol.* 171, 1983–1995. doi: 10.1104/pp.16.00532

Conflict of Interest: The authors declare that the research was conducted in the absence of any commercial or financial relationships that could be construed as a potential conflict of interest.

frontiers in Plant Science

ORIGINAL RESEARCH
published: 15 January 2020
doi: 10.3389/fpls.2019.01665

Arabidopsis PARC6 Is Critical for Plastid Morphogenesis in Pavement, Trichome, and Guard Cells in Leaf Epidermis

Hiroki Ishikawa[1†], Mana Yasuzawa[1†], Nana Koike[1†], Alvin Sanjaya[1], Shota Moriyama[1], Aya Nishizawa[1], Kanae Matsuoka[1], Shun Sasaki[1], Yusuke Kazama[2], Yoriko Hayashi[2], Tomoko Abe[2], Makoto T. Fujiwara[1,2] and Ryuuichi D. Itoh[3]*

[1] Department of Materials and Life Sciences, Faculty of Science and Technology, Sophia University, Tokyo, Japan, [2] Nishina Center for Accelerator-Based Science, RIKEN, Wako, Japan, [3] Department of Chemistry, Biology and Marine Science, Faculty of Science, University of the Ryukyus, Okinawa, Japan

OPEN ACCESS

Edited by:
Luning Liu,
University of Liverpool,
United Kingdom

Reviewed by:
Zhong-Nan Yang,
Shanghai Normal University,
China
Kevin Andrew Pyke,
University of Nottingham,
United Kingdom

***Correspondence:**
Ryuuichi D. Itoh
ryuitoh@sci.u-ryukyu.ac.jp

[†]These authors have contributed equally to this work

Specialty section:
This article was submitted to Plant Physiology, a section of the journal Frontiers in Plant Science

Received: 20 July 2019
Accepted: 26 November 2019
Published: 15 January 2020

Citation:
Ishikawa H, Yasuzawa M, Koike N, Sanjaya A, Moriyama S, Nishizawa A, Matsuoka K, Sasaki S, Kazama Y, Hayashi Y, Abe T, Fujiwara MT and Itoh RD (2020) Arabidopsis PARC6 Is Critical for Plastid Morphogenesis in Pavement, Trichome, and Guard Cells in Leaf Epidermis. Front. Plant Sci. 10:1665. doi: 10.3389/fpls.2019.01665

Recently, a recessive *Arabidopsis thaliana* mutant with abundant stromules in leaf epidermal pavement cells was visually screened and isolated. The gene responsible for this mutant phenotype was identified as *PARC6*, a chloroplast division site regulator gene. The mutant allele *parc6-5* carried two point mutations (G62R and W700stop) at the N- and C-terminal ends of the coding sequence, respectively. Here, we further characterized *parc6-5* and other *parc6* mutant alleles, and showed that *PARC6* plays a critical role in plastid morphogenesis in all cell types of the leaf epidermis: pavement cells, trichome cells, and guard cells. Transient expression of PARC6 transit peptide (TP) fused to the green fluorescent protein (GFP) in plant cells showed that the G62R mutation has no or little effect on the TP activity of the PARC6 N-terminal region. Then, plastid morphology was microscopically analyzed in the leaf epidermis of wild-type (WT) and *parc6* mutants (*parc6-1*, *parc6-3*, *parc6-4* and *parc6-5*) with the aid of stroma-targeted fluorescent proteins. In *parc6* pavement cells, plastids often assumed aberrant grape-like morphology, similar to those in severe plastid division mutants, *atminE1,* and *arc6*. In *parc6* trichome cells, plastids exhibited extreme grape-like aggregations, without the production of giant plastids (>6 μm diameter), as a general phenotype. In *parc6* guard cells, plastids exhibited a variety of abnormal phenotypes, including reduced number, enlarged size, and activated stromules, similar to those in *atminE1* and *arc6* guard cells. Nevertheless, unlike *atminE1* and *arc6*, *parc6* exhibited a low number of mini-chloroplasts (< 2 μm diameter) and rarely produced chloroplast-deficient guard cells. Importantly, unlike *parc6*, the chloroplast division site mutant *arc11* exhibited WT-like plastid phenotypes in trichome and guard cells. Finally, observation of *parc6* complementation lines expressing a functional PARC6-GFP protein indicated that PARC6-GFP formed a ring-like structure in both constricting and non-constricting chloroplasts, and that PARC6 dynamically changes its configuration during the process of chloroplast division.

Keywords: chloroplast, leucoplast, plastid development, stromule, stoma

INTRODUCTION

Plastids represent a diverse group of double membrane-bound organelles, with the ability to transdifferentiate, depending on the tissue type and environmental stimuli (Kirk and Tilney-Bassett, 1978; Mullet, 1988; Pyke, 2007; Pyke, 2009). Leaf cells contain a homogeneous population of round to spherical chloroplasts (photosynthetic plastids; 5–10 μm in diameter) that vary in number from several tens to hundreds per cell (López-Juez and Pyke, 2005). Besides these general features, chloroplasts display varied morphology, depending on the cell type and plant species (Kirk and Tilney-Bassett, 1978; Pyke, 2009; Barton et al., 2016). For example, leaf mesophyll cells develop expanded chloroplasts, with a high degree of inner membrane systems. Mesophyll chloroplasts proliferate by binary fission to sufficiently cover the cell surface (Leech and Pyke, 1988). Chloroplasts in leaf bundle sheath cells contain developed thylakoids and granas; in *Arabidopsis thaliana*, leaf bundle sheath chloroplasts are relatively small in size and lower in number than mesophyll chloroplasts (Kinsman and Pyke, 1998; Kandasamy and Meagher, 1999; Tirlapur and König, 2001). In many plant species, leaf pavement cell chloroplasts are structurally underdeveloped and low in density compared with mesophyll chloroplasts (Pyke and Leech, 1994; Barton et al., 2016; Erickson et al., 2017). Furthermore, leaf stomatal guard cells contain small-sized chloroplasts at a high density, with fewer thylakoids but more starch grains, compared with mesophyll cells (Sachs, 1875; Zhao and Sack, 1999; Lawson, 2009).

Leaf epidermis is ideal for studying plastid morphogenesis not only because of the wide variation in chloroplast morphology observed among leaf epidermal cells but also because plastids in leaf epidermal cells can be readily detected by fluorescence microscopy and developmentally tracked in the L1 layer during leaf development. In *Arabidopsis*, three different types of plastids have been reported, including pavement cell chloroplasts, trichome leucoplasts, and guard cell chloroplasts, all of which originate from proplastids in the shoot apical meristem, or more strictly, protodermal plastids with poor thylakoids (early differentiating chloroplasts) in leaf primordia (Pyke and Leech, 1994; Robertson et al., 1995; Barton et al., 2018). The number, shape, distribution, and dynamics of plastids have been relatively well-studied using pavement cell chloroplasts (Pyke and Leech, 1994; Schattat and Klösgen, 2011; Schattat et al., 2011; Schattat et al., 2012; Higa et al., 2014; Fujiwara et al., 2015; Erickson et al., 2017; Fujiwara et al., 2017; Fujiwara et al., 2018), while stomata physiology has long been investigated in guard cell chloroplasts (Lawson, 2009; Taiz et al., 2015). However, fewer studies have been conducted on the morphological aspects of epidermal plastids than on mesophyll chloroplasts. Thus, the regulation of epidermal plastid development and morphology remains largely unknown (Pyke, 1999; Barton et al., 2018).

Leaf epidermal plastids are also suitable for studying stromule biology. Stromules are thin, tubular structures derived from the plastid surface that dynamically extend from or retract back to the plastid bodies at the second level (reviewed in Gray et al., 2001; Kwok and Hanson, 2004; Natesan et al., 2005; Schattat et al., 2015; Hanson and Hines, 2018; Erickson and Schattat, 2018). Stromules are surrounded by double envelope membranes containing the stroma and are effectively visualized using various stroma-targeted fluorescent proteins (e.g., Köhler et al., 1997; Köhler and Hanson, 2000; Haswell and Meyerowitz, 2006; Schattat et al., 2012; Delfosse et al., 2016). Although stromules have been detected in most plastid types, their abundance is higher in plastids of non-photosynthetic tissues such as petals, roots, endosperms, and bulbs or shoot epidermal tissues such as hypocotyl and leaf epidermis (Kwok and Hanson, 2004; Waters et al., 2004; Erickson et al., 2017). Stromule development is responsive to various abiotic and biotic stimuli, such as light, heat, reactive oxygen species, phytohormones, sugars, and pathogens. Stromule biogenesis also involves interactions with the cytoskeleton and other organelles (reviewed in Erickson and Schattat, 2018; Hanson and Hines, 2018). Furthermore, inhibition of chloroplast division causes excessive production of stromules in various tissues, as shown in tomato (*Solanum lycopersicum*) *suffulta* mutant and Arabidopsis *arc3*, *arc5*, *arc6*, *crl*, and *atminE1* mutants (Forth and Pyke, 2006; Holzinger et al., 2008; Chen et al., 2009; Kojo et al., 2009; Fujiwara et al., 2015; Fujiwara et al., 2018). These studies indicate the importance of stromules in plant cells; however, the mechanism of the origin of stromules and their functions in plant cells remains largely unknown (Hanson and Hines, 2018).

Previously, we screened an ethyl methanesulfonate (EMS)-mutagenized population of Arabidopsis FL4-4 plants co-expressing a plastid stroma-targeted cyan fluorescent protein (CFP) and mitochondrial matrix-targeted yellow fluorescent protein (YFP) and isolated two independent recessive mutant lines, *stromule biogenesis altered1* (*suba1*) and *suba2*, with abundant stromules in pavement cells (Itoh et al., 2018). Analysis of *suba2* revealed that the causal gene responsible for the mutant phenotype was *PARC6* (*CDP1*/*ARC6H*), a known chloroplast division-regulator gene (Glynn et al., 2009; Zhang et al., 2009; Ottesen et al., 2010). The PARC6 protein is inserted in the chloroplast inner envelope membrane and functions as a component of the chloroplast division machinery (Zhang et al., 2016; Chen et al., 2018a). The N-terminal region of PARC6 functions as a transit peptide (TP) (Glynn et al., 2009), and the subsequent region is exposed to the stroma, allowing interaction with a chloroplast division site regulator ARC3 (Shimada et al., 2004; Maple et al., 2007; Glynn et al., 2009). The C-terminal region of PARC6 is exposed to the intermembrane space, where it interacts with an outer envelope-localized division protein PDV1 (Miyagishima et al., 2006; Zhang et al., 2016). In *parc6*, the spatial control of FtsZ ring formation (the first event of chloroplast division; Miyagishima et al., 2011) is perturbed, resulting in asymmetric or multiple chloroplast divisions in leaf mesophyll cells (Glynn et al., 2009; Zhang et al., 2009; Ottesen et al., 2010). The *parc6* allele in *suba2*, termed as *parc6-5*, carries two nucleotide substitutions, resulting in G62R and W700stop mutations at the translation level. The G62R mutation is located in the TP of PARC6 (Glynn et al., 2009), whereas the W700stop mutation is present in the C-terminal

region. Additionally, mutant analysis indicated that the enlarged size and excessive stromule proliferation phenotypes of *parc6-5* pavement cell plastids are similar to those of other *parc6* alleles, including *parc6-1*, *parc6-3*, and *parc6-4* (Itoh et al., 2018). Our results also indicated that PARC6 interacts with AtMinD1 (also known as ARC11), another chloroplast division site regulator in mesophyll and pavement cells (Marrison et al., 1999; Colletti et al., 2000; Vitha et al., 2003; Fujiwara et al., 2004; Fujiwara et al., 2008; Fujiwara et al., 2009b; Fujiwara et al., 2017). However, unlike *parc6*, *arc11* shows fairly modest pavement cell chloroplast phenotypes (Fujiwara et al., 2017; Itoh et al., 2018).

Isolation of the *parc6-5* (*suba2*) mutant from leaf pavement cells (Itoh et al., 2018) provided us with an opportunity to comprehensively study plastid morphology in the leaf epidermis. Our initial investigation (Itoh et al., 2018) raised several questions. In this paper, we attempted to complement our former study and comprehensively understand PARC6-mediated plastid morphologies in the leaf epidermis. The objectives of this study were three-fold: 1) evaluate the effect of G62R and W700stop mutations in *parc6-5*; 2) conduct a detailed investigation of plastid morphologies during epidermal cell development; and 3) examine the intraplastidic behavior of PARC6.

MATERIALS AND METHODS

Plant Materials and Growth Conditions

A. thaliana (L.) Heynh. plants were mainly used in this study to investigate plastid morphologies in leaf epidermal cells. Seeds of plastid division mutants, *parc6-1* (SALK_100009; Glynn et al., 2009; Zhang et al., 2009; Ottesen et al., 2010; generated by Alonso et al., 2003), *parc6-3* (Glynn et al., 2009), *parc6-4* (SALK_138043; Zhang et al., 2009; generated by Alonso et al., 2003), *arc6-3* (CS288; Pyke et al., 1994), and *arc11-1* (CS281; Marrison et al., 1999) were obtained from the Arabidopsis Biological Resource Center (ABRC), Ohio State University, Columbus, OH, USA. Two transgenic Arabidopsis lines [FL4-4 and FL6-4; Columbia (Col) background] expressing organelle-targeted fluorescent proteins as well as offspring derived from crosses between the transgenic lines and mutants (*parc6-1* × FL4-4, *parc6-3* × FL4-4, *parc6-4* × FL4-4, *arc11-1* × FL4-4, and *arc6-3* × FL6-4) were used (Chen et al., 2009; Itoh et al., 2010; Fujiwara et al., 2018; Itoh et al., 2018; see summary in **Table 1**). The *parc6-5* (*suba2*) mutant was isolated from EMS-treated FL4-4 seeds carrying two nucleotide substitutions in the *PARC6* coding sequence, resulting in G62R and W700stop mutations at the protein level (Itoh et al., 2018). The *parc6-1* mutant was crossed with FL6-4 transgenic line in this study. To analyze plastid division mutants, Col, FL4-4, or FL6-4 plants were correspondingly used as the wild type (WT). Seeds were germinated and grown under daily irradiation from 5:00 to 21:00, as described previously (Fujiwara et al., 2009b), unless otherwise specified.

Tobacco (*Nicotiana tabacum* L. cv. Samsun NN) and onion (*Allium cepa* L.) plants were employed for particle bombardment experiments (described below). Tobacco seeds were germinated and grown in soil under continuous white light at 25°C. Onion bulbs were purchased from a local supermarket in Tokyo.

TABLE 1 | List of transgenic *Arabidopsis thaliana* lines[1] used for organelle labeling experiments in this study.

Plant line	Transgene	Organelle labeling confirmed	Reference
FL4-4[2]	CaMV35Sp::*TP$_{FtsZ1-1}$-CFP*::NOSt, CaMV35Sp::*Pre$_{mtHSP60}$-YFP*::NOSt	Plastid-targeted CFP, mitochondria-targeted YFP	Itoh et al. (2010)
FL6-4[2,3]	CaMV35Sp::*TP$_{FtsZ1-1}$-YFP*::NOSt, CaMV35Sp::*NLS$_{cry2}$-CFP*::NOSt	Plastid-targeted YFP	Chen et al. (2009)
parc6-1 × FL4-4	Identical to FL4-4	Plastid-targeted CFP, mitochondria-targeted YFP	Itoh et al. (2018)
parc6-1 × FL6-4	Identical to FL6-4	Plastid-targeted YFP	This study
parc6-3 × FL4-4	Identical to FL4-4	Plastid-targeted CFP, mitochondria-targeted YFP	Itoh et al. (2018)
parc6-4 × FL4-4	Identical to FL4-4	Plastid-targeted CFP, mitochondria-targeted YFP	Itoh et al. (2018)
parc6-5 (parent: FL4-4)	Identical to FL4-4	Plastid-targeted CFP, mitochondria-targeted YFP	Itoh et al. (2018)
arc11-1 × FL4-4	Identical to FL4-4	Plastid-targeted CFP, mitochondria-targeted YFP	Fujiwara et al. (2017)
arc6-3 × FL6-4	Identical to FL6-4	Plastid-targeted YFP	Fujiwara et al. (2018)

[1]*See also Materials and Methods.*
[2]*Both FL4-4 and FL6-4 were transformed with T-DNAs carrying two expression cassettes in tandem.*
[3]*FL6-4 showed almost no CFP but strong YFP signals in leaf cells.*

Transient Expression Analysis

To examine the effect of G62R mutation on the function of PARC6 TP (N-terminal 76 amino acids; Glynn et al., 2009), green fluorescent protein (GFP) was used as a reporter (Chiu et al., 1996). The TP-coding sequence was PCR amplified from the total DNA of Col and *parc6-5* plants using sequence-specific primers containing restriction sites (underlined), H6-17 (5′-AGCGTCGACGCAATGCCAGTAGCTTACAC-3′) and H6-18 (5′-GCGCCATGGCGACGACATGGATACCACCAC-3′). The PCR product (0.25 kb) was treated with *Sal*I and *Nco*I and cloned into the CaMV35S-sGFP(S65T)-nos vector (Isono et al., 1997; provided by Dr. Yasuo Niwa, University of Shizuoka, Japan) under the control of the cauliflower mosaic virus *35S* promoter (CaMV35Sp) to generate two expression constructs, p35S-H-TP$_{wt}$-GFP and p35S-H-TP$_{G62R}$-GFP. These constructs, as well as the undigested vector, were introduced into the epidermal cells of tobacco leaves and onion bulbs *via* particle bombardment using 0.4-μm gold particles (InBio Gold, Hurstbridge VIC, Australia) and the Biolistic PDS-1000/He system (Bio-Rad, Hercules, CA, USA). Bombardments were conducted at 1,100-psi He pressure, with 27-inch vacuum of

Hg in the chamber and 6-cm distance to the target tissue. After the bombardment, samples were incubated at 23°C for 6 or 24 h and then observed by fluorescence microscopy, as described below.

Fluorescence Stereomicroscopy and Epifluorescence Microscopy

Basal parts of leaves including petioles were excised from Arabidopsis seedlings using tweezers. Based on previous observations (e.g., Fujiwara et al., 2004; Fujiwara et al., 2008; Fujiwara et al., 2009a; Fujiwara et al., 2009b; Itoh et al., 2010; Fujiwara et al., 2015; Fujiwara et al., 2017; Fujiwara et al., 2018; Itoh et al., 2018), the adaxial surface of the leaf epidermis in the upper petiole region was used to analyze leaf pavement, trichome, and guard cells in Arabidopsis, unless otherwise specified.

Fluorescence stereomicroscopy was performed using Leica MZ10 F fluorescence microscope (Leica Microsystems, Heidelberg, Germany) equipped with a color CCD camera (model DP26; Olympus, Tokyo, Japan). Fluorescence signals were detected through optical filters using the 0.63× objective lens (Leica Microsystems).

Epifluorescence microscopy was performed using inverted microscopes, IX71 and IX73 (Olympus), equipped with a CMOS camera (model ORCA-flash2.8; Hamamatsu Photonics, Hamamatsu, Japan) and a color CCD camera (model DP73; Olympus), respectively. Emission of fluorescence signals was detected through optical filters, FF01-483/32 (Semrock, Rochester, NY, USA) for CFP, BA510-550 (Olympus) or FF01-545/55 (Semrock) for GFP, FF01-545/55 (Semrock) for YFP, and BA610IF or BA575IF (Olympus) for chlorophyll using 60× [numerical aperture (N.A.) 1.20], 40× (N.A. 1.25), and 20× (N.A. 0.75) objective lenses. Bright field images were obtained with DIC optics.

Fluorescence images of CFP, GFP, YFP, and chlorophyll autofluorescence as well as bright field images were processed using Adobe Photoshop (Adobe Systems, San Jose, CA, USA), as described previously (Fujiwara et al., 2015).

Measurement of Stomatal Guard Cells and Plastids

Stomatal guard cells were measured as described previously (Fujiwara et al., 2018), except that leaves were sampled from 15:00 to 17:45 in this study. All samples were examined under the same conditions. Depending on the size, chloroplasts in guard cells were categorized as giant chloroplasts, (>6 μm), normal-sized chloroplasts (2–6 μm), and mini-chloroplasts (<2 μm). All chloroplast counting and measurement experiments were performed using at least three biological replicates (i.e., independent leaves).

Transmission Electron Microscopy (TEM)

TEM was performed by Tokai Electron Microscopy Inc. (Nagoya, Japan), as described previously (Itoh et al., 2018). Briefly, primary leaves of 10-day-old Col, FL4-4, *parc6-1*, and *parc6-5*/*suba2* seedlings were sampled from 10:30 to 12:00 and fixed in 2% paraformaldehyde and 2% formaldehyde in 0.05 M cacodylate buffer (pH 7.4) at 4°C. The fixed leaf samples were washed with 0.05 M cacodylate buffer, postfixed with 2% osmium tetroxide in 0.05 M cacodylate buffer, and dehydrated in a graded ethanol series (50, 70, 90, and 100%). Samples were then embedded in a 70:30 mixture of propylene oxide and Quetol-651 resin (Nisshin EM, Tokyo, Japan). Ultrathin (80 nm thick) sections were prepared using a diamond knife and then stained with 2% uranyl acetate and lead staining solution (Sigma-Aldrich, Tokyo, Japan). Grids were observed using a JEM-1400Plus electron microscope (JEOL, Tokyo, Japan) equipped with a CCD camera (model EM-14830RUBY2, JEOL).

Complementation of *parc6* Mutant Phenotype With *PARC6-GFP*

A multiple cloning site of pT7Blue (Novagen, Merck-Millipore, Burlington, MA, USA) was ligated into the *Hin*dIII and *Sac*I sites of the pSMAB704 vector (Igasaki et al., 2002; provided Dr. Hiroaki Ichikawa, NIAS, Japan) by simultaneously removing the vector-derived CaMV35Sp and *uidA* gene to yield pSMAB704-T7. A 1.0 kb fragment of the CaMV35S-sGFP (S65T)-nos vector (Isono et al., 1997; provided by Dr. Yasuo Niwa), comprising the full-length *sGFP*(*S65T*) gene and *nos* terminator (NOSt), was ligated to the *Xba*I and *Eco*RI sites of pSMAB704-T7 by simultaneously removing the vector-derived NOSt to yield pSMAB704-T7-GFP. A 3.4-kb DNA fragment comprising 1.0 kb sequence upstream of *PARC6* and the complete coding sequence of *PARC6* was PCR amplified from the pSMAB704-T7-H vector (Itoh et al., 2018) using sequence-specific primers containing restriction sites (underlined), H6-12 (5′-AGTCTAGACGAGCTGCGCGAAGCTAAAC-3′) and H6-8 (5′-GATCTAGACTTCTGTATTTGAATATCGCTTTG-3′). The PCR product was cloned into the pSMAB704-T7-GFP vector at the *Xba*I site using *Escherichia coli* HST04 strain as a host. The resulting binary vector pSMAB-T7-H-GFP was transformed into *Agrobacterium tumefaciens* C58 strain using the freeze-thaw method. An *Agrobacterium* transformant was employed for T-DNA-mediated nuclear transformation of Arabidopsis *parc6-1* (Glynn et al., 2009) and *parc6-4* (Zhang et al., 2009; Itoh et al., 2018) mutants using the floral dip method (Clough and Bent, 1998). A total of 12 transformed seedlings were selected on Murashige and Skoog (MS) medium containing bialaphos (10 μg/mL) and carbenicillin (100 μg/mL). Transgenic plants in the T_1, T_2, and T_3 generations were characterized by epifluorescence microscopy, as described above.

RESULTS

Effect of the G62R Mutation on the Subcellular Localization of PARC6

We investigated which of the two mutations (G62R and W700stop) in the N- and C-terminal coding sequence of *parc6-5* mutant allele in the recessive Arabidopsis *suba2* mutant (Itoh et al., 2018) were responsible for excessive stromule formation (*suba* phenotype) in pavement cells of mature leaves. Although it has been previously shown that

Gly62 is located within the experimentally confirmed TP region of PARC6 (Glynn et al., 2009), *in silico* analysis of *parc6-5* mutant allele with several protein localization predictors unanimously predicted that PARC6^{G62R} would be located inside the chloroplasts, similar to the WT PARC6 (Itoh et al., 2018). However, experimental evidence to support this finding was lacking. Moreover, prediction programs are not designed to predict a reduction in the chloroplast protein import efficiency (and the resulting accumulation of precursor proteins in the cytosol) and its possible dependency on the plastid type.

To determine the effect of the G62R mutation on the subcellular localization of PARC6, we generated constructs expressing translational fusions of GFP with the mutated PARC6 TP (TP_{G62R}-GFP) and its WT counterpart (TP-GFP) or expressing GFP alone (control) under the control of the constitutive CaMV35S promoter. These constructs were introduced into the epidermal cells of tobacco leaves and onion bulbs *via* particle bombardment, and the import of GFP into chloroplasts and leucoplasts, respectively, was monitored. At 24 h post-bombardment, GFP localization was observed by epifluorescence microscopy. The results showed that unfused GFP accumulated in the cytoplasm and nucleoplasm of tobacco pavement cells and guard cells and onion bulb epidermal cells (**Figure 1A**). Fluorescence of TP-GFP fusion protein was detected as particular bodies dispersed throughout the cytoplasm, which overlapped with chlorophyll autofluorescence in tobacco guard cells and thin stromule-like protrusions (distinctive structures of non-green plastids) in onion bulb epidermis (**Figure 1B**). These data support the localization of TP-GFP within the plastid stroma, regardless of the plastid type. Moreover, TP_{G62R}-GFP showed the same subcellular localization pattern as the TP-GFP in all cell types (**Figures 1B**, **C**). To investigate the difference in plastid import efficiency between TP-GFP and TP_{G62R}-GFP, we further observed GFP localization at 6

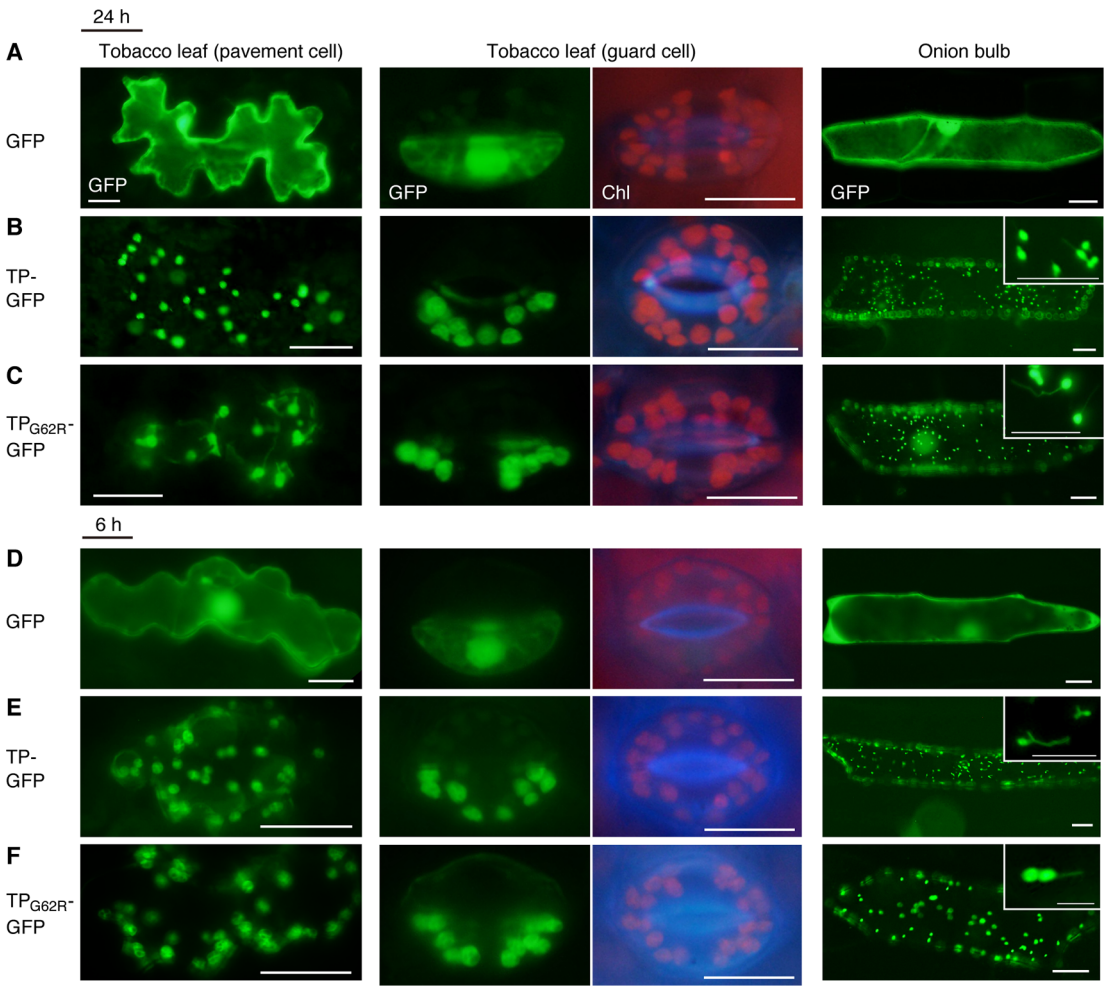

FIGURE 1 | Localization analysis of GFP fused to the mutant transit peptide of PARC6 (TP_{G62R}-GFP). GFP with or without a PARC6 transit peptide (TP) sequence from Col or *parc6-5* (TP_{G62R}) was transiently expressed in tobacco and onion cells by particle bombardment. **(A–F)** Epifluorescence microscopy images of tobacco leaf pavement cells and guard cells and onion epidermal cells at 24 h **(A–C)** or 6 h **(D–F)** post-bombardment. GFP fluorescence, chlorophyll autofluorescence (Chl), and merged images are shown. Scale bars: 20 μm (all guard cells and insets); 50 μm (others).

h post-bombardment. The localization patterns of the unfused and fused GFPs at 6 h were similar to those of the unfused and fused GFPs, respectively, at 24 h, and no significant difference was detected between the signal intensities (plastid/cytoplasm ratios) of TP-GFP and TP_{G62R}-GFP (**Figures 1D–F**). Based on these results, we conclude that the G62R substitution in PARC6 encoded by the *parc6-5* mutant allele has no or little effect on the plastid import efficiency of PARC6.

Plastids in Pavement Cells of *parc6* Mutants

To complement and complete our previous study (Itoh et al., 2018), we extended our observation of chloroplasts in pavement cells to *parc6* mutants. In the previous study, we used the first and second leaves of 3-week-old seedlings (Itoh et al., 2018), suitable for the analysis of mature pavement cells. In the present study, we used the third and fourth leaves of 2-week-old seedlings, as these are suitable for monitoring the dividing chloroplasts as well as the growing stromules. While stromules in *parc6* pavement cells were excessively elongated compared with those in WT pavement cells, perinuclear stromule attachment, previously reported for WT plants (Erickson et al., 2017; Kumar et al., 2018), was also often detected in *parc6* pavement cells (**Figures 2A**, **B**). Additionally, pavement cell chloroplasts of all *parc6* mutants examined in this study displayed autofluorescence over the entire chloroplast, except the stromule region (see inset in **Figure 2B**), indicating that hyperelongated stromules in *parc6* pavement cells maintained their general properties. Other morphological features of stromules (e.g., branching and preferential elongation along the longitudinal axis of cells) and plastid bodies (e.g., enlargement, heterogeneous size and shape, and multiple constrictions) described previously (Itoh et al., 2018) were also observed in the current study (data not shown). Intriguingly, although at a low frequency, pavement cells exclusively containing relatively normal-sized chloroplasts showed symmetric binary fission (**Figure 2C**; cells surrounded by the yellow dotted line). Although *parc6* mutants are generally recognized as "chloroplast division site" mutants, the present data imply that *parc6* mutants maintain, to some degree, a mechanism for mid-

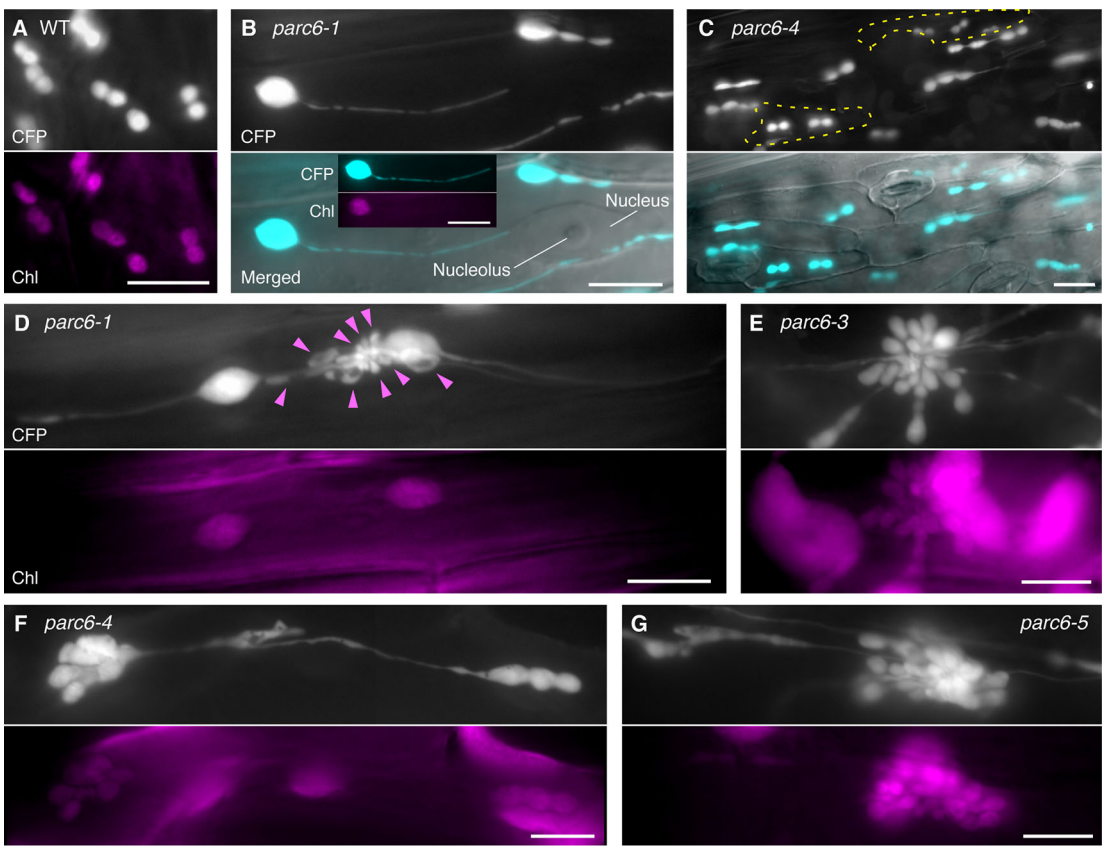

FIGURE 2 | Morphology of plastids in leaf epidermal pavement cells of *parc6* mutants. **(A–G)** Images of pavement cells in the 3rd and 4th leaf petioles of 2-week-old wild-type (WT) **(A)**, *parc6-1* **(B**, **D)**, *parc6-3* **(E)**, *parc6-4* **(C**, **F)**, and *parc6-5* **(G)** seedlings. Images of stroma-targeted CFP, chlorophyll autofluorescence, or differential interference contrast (DIC), and merged images of CFP and DIC **(B**, **C)** are shown. Inset in **(B)** indicates chlorophyll autofluorescence in a stromule-producing pavement cell chloroplast. Yellow regions in **(C)** indicate pavement cells with symmetric chloroplast division. Arrowheads in **(D)** indicate chlorophyll-less plastids or bulges. Scale bar = 10 μm.

plastid recognition, instead of completely randomly selecting plastid division sites, at least in pavement cells.

All *parc6* mutants showed grape-like clusters of plastids in pavement cells (**Figures 2D–G**). Although grape-like clusters showed a widely variable morphology, these clusters were commonly found in *parc6* pavement cells, regardless of the mutant type. Some of the clusters consisted of spherical, ovoid, and amorphous shaped bulges or blobs devoid of chlorophyll (arrowheads in **Figure 2D**); however, other clusters emitted chlorophyll autofluorescence over the whole body, and the majority of chloroplasts in these clusters showed one or more constriction sites each (**Figures 2E–G**). These plastids or chloroplasts either developed radially from a single nucleation point or were generated by the accumulation of spherical and ovoid stroma-containing blobs at a single local region. A more careful observation of the latter type revealed that a single cluster included two kinds of blobs, one with and another without chlorophyll autofluorescence, and smaller blobs tended to lack the autofluorescence signal. The morphology of pavement cell chloroplasts in the WT (FL4-4 line; **Figures 2A**, **S1A**) and *arc11* mutant (**Figure S1B**) at the same stage as for *parc6* analysis (**Figures 2B–G**) was similar to that observed at the later stage in the WT and *arc11*, respectively, in our previous report (Fujiwara et al., 2017). Chloroplasts in *arc11* pavement cells were seemingly undergoing either symmetric or asymmetric binary fission or multiple fissions (**Figure S1B**); however, no grape-like clusters were detected. In *parc6* pavement cells, we observed both mitochondria and grape-like plastid clusters simultaneously in the same field of view (**Figure S1C**). During the period of observation, blobs in grape-like clusters as well as physically distinct plastids showed motility and shape change. Some mitochondria were stuck and almost immobile in the space between the blobs within the clusters, suggesting occasional attachment between mitochondria and plastid-derived blobs in the clusters.

Plastids in Trichome Cells of *parc6* Mutants

Next, we focused on the morphology of leucoplasts in trichome cells of *parc6* mutants. In WT Arabidopsis plants, leaf trichome leucoplasts are smaller than pavement cell chloroplasts and assume an elongated or irregular shape (Barton et al., 2018). Leaf trichome leucoplasts differentiate from chlorophyll-bearing chloroplasts in the epidermal layer of expanding leaves. As well as at the initiation of trichomes (Barton et al., 2018), rounded chloroplasts were detected during cell growth until the primary branching stage (**Figures 3A**, **B**). Leucoplasts in Arabidopsis trichomes were also examined in the *atminE1* mutant and *AtMinE1* overexpressor line in our previous study (Fujiwara et al., 2009b), which was the only study that observed trichome leucoplasts in chloroplast division mutants.

Consistent with the earlier observation of Barton et al. (2018), trichome leucoplasts in WT Arabidopsis plants emitted no detectable chlorophyll autofluorescence (**Figure 3C**). A single giant mature trichome cell in the upper petiole (and at the junction between petiole and lamina) possibly contained over 100 leucoplasts, although accurate counting was not possible. This number is much larger than the number of leucoplasts in an early developing trichome cell (~30 in **Figure 3B**). The leucoplasts were distributed over the entire trichome cell, including both stalk and branch regions (Folkers et al., 1997). A subset of trichome leucoplasts showed a single or multiple constriction(s) (**Figure 3C**). Some of these plastid constrictions seemed stable and were unaffected by the shape change of the whole organelle (data not shown). Trichome leucoplasts were often found to produce longer stromules than pavement cell chloroplasts. Sometimes trichome leucoplasts surrounded the nucleus (**Figure 3D**), a phenomenon known for chloroplasts in normal pavement cells. Although we were able to determine the location of the nucleus using bright field illumination, fluorescence visualization of the nucleus (CFP) and leucoplasts (YFP) in the FL6-4 transgenic line facilitated more reliable identification of both organelles (**Figure 3D**). Another notable feature of trichome leucoplasts was the amoeba-like deformation. **Figure 3E** shows the process of shape change that occurred within 5 min. Consistent with this observation, we found various shapes of leucoplasts in trichome cells, such as spherical, ovoid, filamentous, amoeboid, dumbbell-shaped, and multiple-arrayed forms (**Figures 3C–F**).

Next, we examined the morphology of trichome leucoplasts in *parc6* mutants (**Figures 3G–J**, **S2B–D**). The following three alterations in plastid morphology were common to the trichomes of *parc6-1*, *parc6-3*, *parc6-4*, and *parc6-5* mutants. First, grape-like clusters of plastids were detected in *parc6* trichomes, most of which were more highly developed than those in *parc6* pavement cells. We frequently observed the grape-like clusters juxtaposed against the cell nucleus (**Figure 3J**), implying a possible link between the behavior of the nucleus (Mathur et al., 1999) and formation and/or location of the plastid clusters. Nevertheless, this was negated by the presence of clusters in the branch and stalk regions of trichomes (**Figures 3H, I**) and at a distant location from the nucleus (**Figure S2C**). Generally, within a grape-like cluster, plastids showed three-dimensional aggregation (**Supplementary Movies 1**, **2**). Although plastids within a cluster showed a wide variability in size, their shape was relatively uniform and spherical, as revealed by the image from a slightly squashed trichome cell (**Figure S2B**) and two-dimensional projection image of a plastid aggregate (**Figure S2D**). Second, leucoplasts in *parc6* trichomes exhibited a striking formation of stromules. Longer exposure time than that required to obtain images of grape-like clusters revealed extended stromules (**Figures 3G**, **S2C**). Third, the maximum diameter of the main body of a leucoplast in *parc6* trichomes was approximately 5 μm (e.g., 5.1 μm in **Figure 3H** and 4.8 μm in **Figure S2C**). Previously, we defined giant plastids as plastids with a diameter exceeding 6 μm (Fujiwara et al., 2018). In *parc6* trichomes, we did not find spherical leucoplasts that met the criterion for giant plastids. However, *parc6* trichome cells contained filamentous leucoplasts over 6 μm in length, as if their entire bodies were stromules themselves.

Next, we took a closer look at the occurrence of grape-like plastid clusters in *parc6* trichomes. We counted the number of

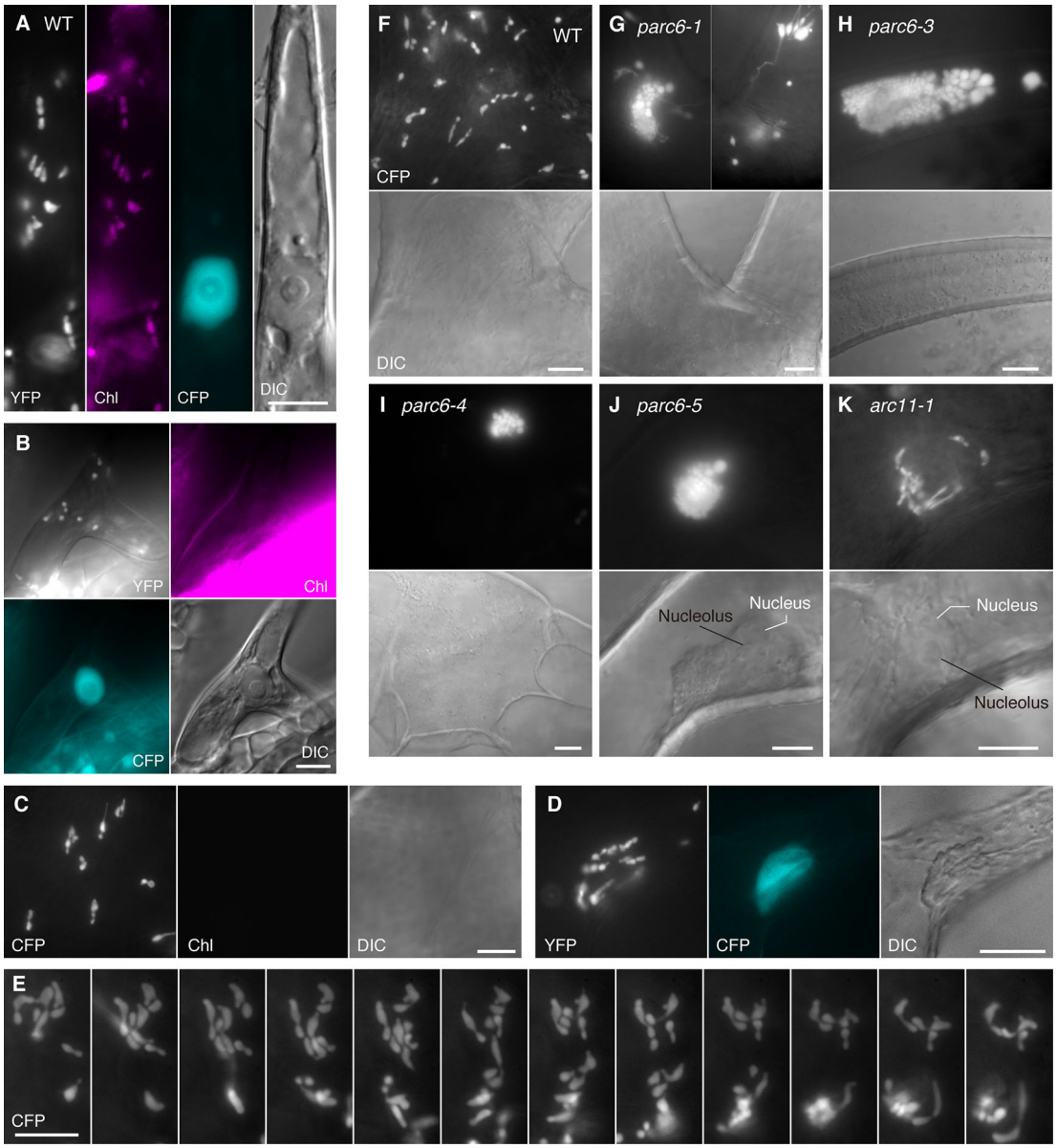

FIGURE 3 | Morphology of plastids in leaf trichome cells of *parc6* and *arc11* mutants. **(A–K)** Images of trichomes in leaf petioles of WT **(A–F)**, *parc6-1* **(G)**, *parc6-3* **(H)**, *parc6-4* **(I)**, *parc6-5* **(J)**, and *arc11-1* **(K)** seedlings. The 3rd and 4th leaves of 2-week-old seedlings were mainly observed **(A–C, F–K)**. Images of stroma-targeted CFP or YFP (black-and-white), chlorophyll autofluorescence (magenta) **(A–C)**, nucleus-targeted CFP (cyan) **(A**, **B**, **D)**, or DIC are shown. Time-lapse observation was performed for 5 min in **(E)**. Scale bar = 10 μm.

trichomes with and without the clusters in leaf petiole-blade regions. Among the 60 trichomes examined in *parc6-1*, 48 trichomes contained the grape-like plastid clusters. In the other *parc6* mutants, the frequency of clusters in trichomes was even higher: 100% (50/50) in *parc6-3* and *parc6-5* mutants and 98% (49/50) in *parc6-4*. In WT trichomes, the frequency of clusters was 8% (4/50). Because plastids constituting a "cluster" in WT were observed around the nucleus and showed less dense aggregation than those in *parc6* mutants (data not shown), the "cluster" in WT trichomes probably originated from the preferential localization of plastids at the periphery of the nucleus (e.g., Köhler and Hanson, 2000; Kwok and Hanson, 2004; Delfosse et al., 2016) and hence was considered to be a qualitatively different entity than the true cluster in *parc6*. Therefore, the formation of the grape-like plastid clusters in trichomes was recognized as a major cytological characteristic of *parc6* mutants. This was in contrast to the *parc6* pavement cells, where the occurrence of clusters was more sporadic. The number of vesicular plastids per cluster in *parc6* trichomes widely varied from 12 (**Figure 3I**) to approximately 200 (**Figure S2B**).

In contrast to those plastid phenotypes, mitochondria in *parc6* trichomes appeared similar to those in WT trichomes (**Figures S2A**, **D**).

Plastids in Guard Cells of *parc6* Mutants

Next, we examined plastid morphology in the guard cells of *parc6* mutants. In WT Arabidopsis leaves, chloroplasts in guard cells are smaller and less developed than those in pavement cells (Pyke and Leech, 1994; Barton et al., 2016), and there are little differences in chloroplast morphology, number, and pigmentation among guard cells. In some mesophyll chloroplast division mutants such as *arc3*, *arc5*, *arc6*, and *atminE1*, the morphology of plastids in guard cells was clearly distinct from that of plastids in mesophyll cells and pavement cells of the same plants. Moreover, guard cell plastids in these mutants were also unique with respect to the phenotypic differences among individual cells; while guard cell plastids showed diverse morphology among cells within a single tissue sample, mesophyll chloroplasts were relatively uniform. For instance, in the Arabidopsis mutant of *ARC6*, which encodes a key regulator protein of chloroplast division in mesophyll cells, occasional lack of chloroplasts (Robertson et al., 1995) and occurrence of non-photosynthetic plastids (Chen et al., 2009) were observed in guard cells. We previously showed that these non-photosynthetic plastids in *arc6* guard cells proliferate and elongate vigorously (Fujiwara et al., 2018).

In accordance with our earlier work, guard cell chloroplasts in the WT were relatively uniform in size and shape and often produced stromules (**Figure 4A**). On the contrary, guard cell plastids in *parc6-5* and other *parc6* mutants displayed variable phenotypes (**Figures 4B–G**). The first phenotype was the decrease in number and a complementary increase in size of

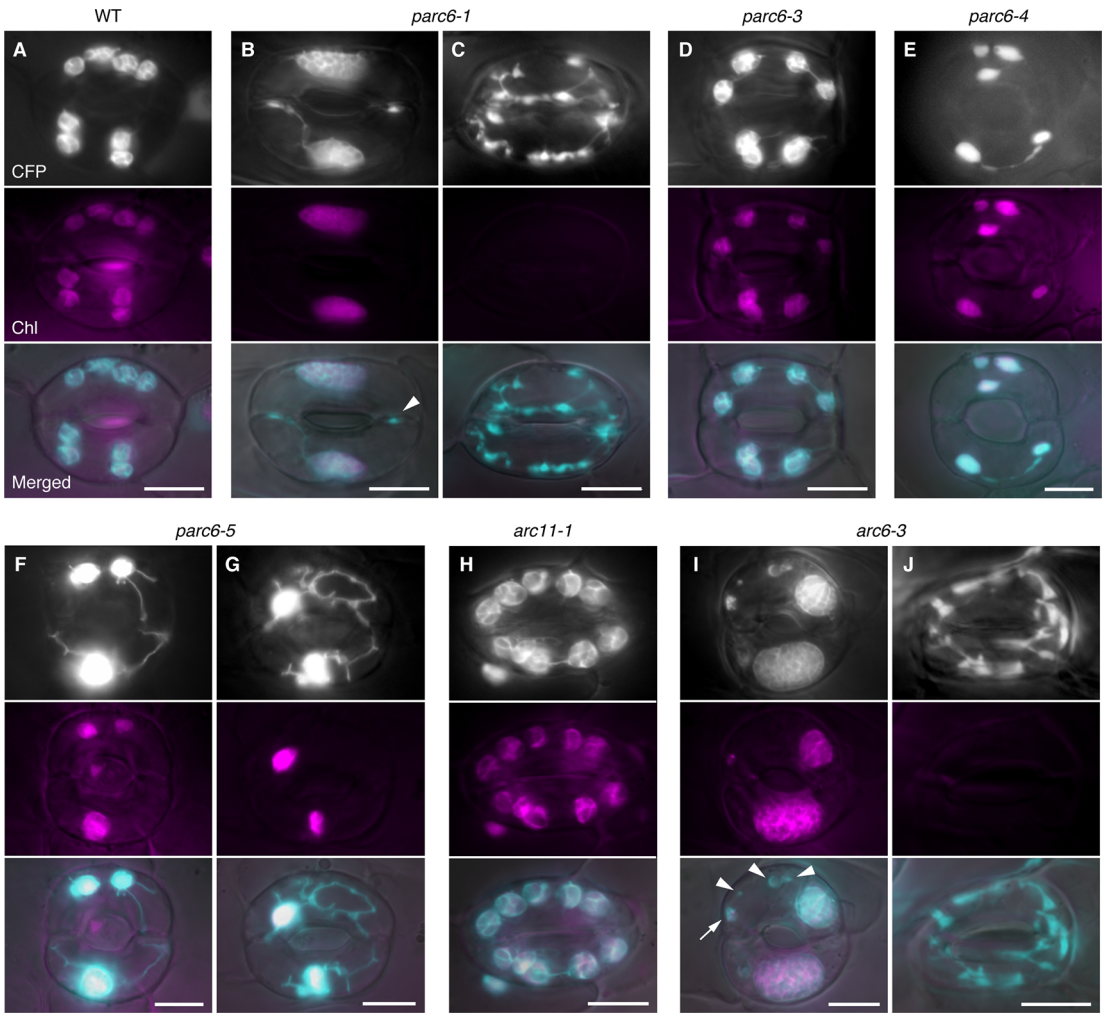

FIGURE 4 | Morphology of plastids in leaf stomatal guard cells of *parc6* and other plastid division mutants. **(A–J)** Images of guard cells in the 3rd and 4th leaf petioles of 4-week-old WT **(A)**, *parc6-1* **(B, C)**, *parc6-3* **(D)**, *parc6-4* **(E)**, *parc6-5* **(F, G)**, *arc11-1* **(H)**, and *arc6-3* **(I, J)** seedlings. Fluorescence images of stroma-targeted CFP (black-and-white or cyan-colored in 'merged' panels), chlorophyll (magenta), and merged images of CFP/YFP, chlorophyll and DIC are shown. Arrow and arrowheads indicate plastids with and without chlorophyll, respectively. Scale bar = 10 μm.

chloroplasts (**Figures 4B**, **F**, and **G**), a characteristic of mesophyll cell chloroplasts in *parc6*. The increase in chloroplast size in *parc6* guard cells was generally more modest than that in *parc6* pavement cells (**Figures S3A**, **2B–G**). The second phenotype was the existence of normally sized and shaped chloroplasts in *parc6* guard cells (**Figures 4D–F**). The third phenotype was the hyperproduction of stromules (**Figures 4B**, **F**, **G**), which is typically seen in pavement cells of mutants in which chloroplast division in mesophyll cells is severely inhibited. The extent of stromule development in guard cells was more limited than that in pavement cells as a whole (**Figures 4B–G**, **S3A**, and **B** vs. **Figures 3B–G**). The fourth phenotype was the formation of poorly developed plastids, devoid of chlorophyll autofluorescence (arrowheads in **Figures 4B**, **I**). The fifth and final phenotype was the disappearance of chloroplasts from guard cells (**Figure 4C**), which is typically seen in guard cells of mutants in which chloroplast division in mesophyll cells is severely inhibited. The above five features were commonly observed among all *parc6* mutants used in this study. The type(s) of feature observed in a given guard cell seemed to be independent of the location of the guard cell in the entire leaf and rather appeared to be selected randomly (**Figure S3A**). Additionally, the normally sized and shaped chloroplasts observed in *parc6* guard cells (second phenotype) sometimes displayed more prominent formation of stromules than those in WT guard cells. We also noticed that *parc6* guard cells without chloroplasts (fifth phenotype) were identical to class III guard cells, defined previously as guard cells containing "populations of numerous minute plastids, which were colorless (chlorophyll-less)" (Fujiwara et al., 2018), observed in guard cells of *arc5*, *arc6*, and *atminE1* mutants. In some cases, such colorless class III guard cells in *parc6* mutants outnumbered chloroplasts in WT guard cells on a per cell basis, although accurate counting of plastids in *parc6* guard cells was not feasible owing to their intricate morphology (**Figure 4C**). In *parc6*, we did not find class IV guard cells, defined as guard cells possessing "web-like structures consisting of chlorophyll-less plastids" (Fujiwara et al., 2018). No differences were detected in the morphology of mitochondria between WT and *parc6* guard cells, based on the fluorescence signal of mitochondrion-targeted YFP (**Figure S3A**), similar to the mitochondria in pavement cells (Itoh et al., 2018).

Next, we attempted to quantify and compare the phenotypes of guard cell plastids among different *parc6* mutants. We counted the number of chloroplasts in guard cells, both on a per stoma basis (i.e., pair of guard cells) and per guard cell basis. Among the four different *parc6* mutants examined, the number of chloroplasts (both per stoma and per guard cell) was similar (**Figures 5A**, **B**). Plastid partitioning between paired guard cells of each stoma was also similar among the *parc6* mutants (**Figures 5A**, **B**). The mean chloroplast number per guard cell was 5.0 in the WT (FL4-4 line) and ranged from 1.7 to 2.0 in *parc6* mutants. Furthermore, the number of chloroplasts per guard cell ranged from 0–4 among all *parc6* mutants but from 2–9 in the WT. Guard cells devoid of chloroplasts in *parc6* mutants occurred at a frequency of <2%; in a few measurements of *parc6-1* and *parc6-4* mutants, no chloroplast-lacking guard cells were detected (**Figures 5A**, **B**). Additionally, we generated two independent lines using the T-DNA insertion (knockout) mutant *parc6-1*; in one of these lines (*parc6-1* × FL4-4), plastid stroma was labeled with CFP, whereas in the other line (*parc6-1* × FL6-4), plastid stroma was labeled with YFP. Both of these lines showed similar chloroplast number per stoma and per guard cell (**Figure 5B**, **Table 1**). This further supports that the defective allele of *PARC6*, and not the other effects brought on by crossing, is responsible for the decrease in chloroplast number per guard cell and occasional occurrence of chloroplast-devoid guard cells. The results of counting (**Figures 5A**, **B**) also verified that the plastid phenotype observed in *parc6-5*/*suba2* leaf epidermis (Itoh et al., 2018) is quantitatively equivalent to that observed in the other known *parc6* mutants.

Since the guard cell plastid phenotypes were similar among *parc6* mutants and not affected by the fluorescently labeled transgenic line used in crossing, we chose the progeny of *parc6-1* × FL6-4 as a representative *parc6* line in the following experiment. Indeed, we confirmed that the morphology of YFP-labeled guard cell plastids in *parc6-1* × FL6-4 progeny was equivalent to that of CFP-labeled guard cell plastids in *parc6-1* × FL4-4 progeny (**Figure S3B**). We classified guard cells based on the length of guard cell chloroplasts (**Table 2**, **Figure 5C**). Taking into account our previous data on *arc5*, *arc6*, and *atminE1* mutants (Fujiwara et al., 2018), we conclude the following: 1) with regard to the frequency of guard cells containing giant chloroplasts, *parc6* was relatively similar to *arc6* and, to a lesser extent, to *atminE1* (**Figure 5C**); 2) with regard to the frequency of guard cells without chloroplasts, *parc6* was relatively similar to *arc5* (**Figure 5C**); and 3) with regard to the length variation of guard cell chloroplasts, *parc6* showed an intermediate phenotype between *arc5* (shorter guard cell chloroplasts) and *arc6*/*atminE1* (longer guard cell chloroplasts) (**Table 2**).

Plastids in Trichome and Guard Cells of *arc11* Mutants

Arabidopsis *arc11* is a loss-of-function mutant of *AtMinD1*; in *arc11*, the level of AtMinD1 protein is greatly reduced, and the mutant AtMinD1 protein (A296G) does not localize at the division site or at punctate structures in the chloroplasts, unlike the WT MinD1 protein, as shown by immunofluorescence microscopy (Nakanishi et al., 2009). The mesophyll cells of *arc11* and *parc6* mutants display an abnormal spatial control of stromal FtsZ ring formation, resulting in variable sized chloroplasts within a single cell (Marrison et al., 1999; Fujiwara et al., 2008; Glynn et al., 2009; see **Figure S4**). Previously, we reported the plastid phenotype in pavement cells of *arc11* (Fujiwara et al., 2017; Itoh et al., 2018). To gain further insight into the functional difference between the mesophyll chloroplast FtsZ ring positioning factors PARC6 and MinD1 and its tissue-dependency, we examined the phenotype of plastids in trichome and guard cells of *arc11* using the *arc11-1* × FL4-4 line, whose plastids could be visualized with fluorescence from stroma-targeted CFP. The trichomes of *arc11-1* contained

A

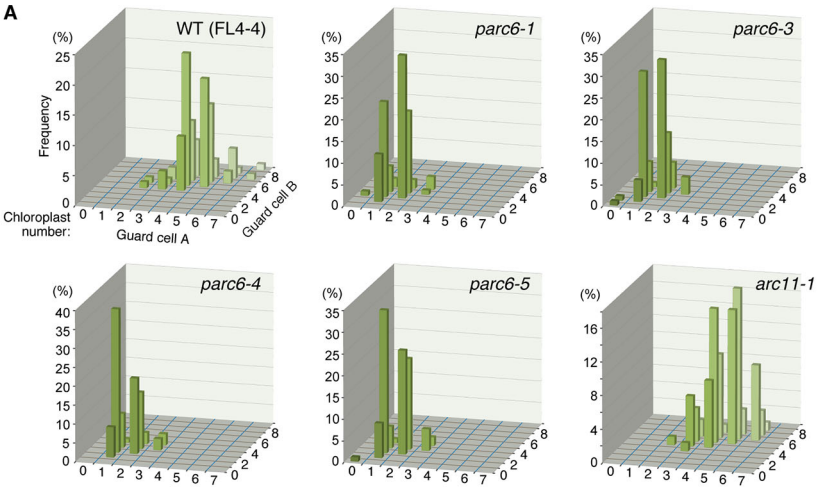

B

Plant (Background)		WT (FL4-4)	WT (FL6-4)	*parc6-1* (FL4-4)	*parc6-1* (FL6-4)	*parc6-3* (FL4-4)	*parc6-4* (FL4-4)	*parc6-5* (FL4-4)	*arc11-1* (FL4-4)
Chloroplast number per stoma [GC pair]	Mean ± S.D.	10.0 ± 1.6	9.9 ± 1.7	3.9 ± 1.1	3.5 ± 1.1	3.9 ± 1.1	3.8 ± 1.2	3.9 ± 1.2	9.9 ± 1.6
	Max.	16	14	7	7	6	7	7	14
	Min.	6	6	2	0	0	2	0	6
	n	100	100	100	100	100	100	100	100
per GC	Mean ± S.D.	5.0 ± 1.1	4.9 ± 1.0	2.0 ± 0.8	1.7 ± 0.7	1.9 ± 0.8	1.9 ± 0.8	1.9 ± 0.7	4.9 ± 1.0
	Max.	9	8	4	4	4	4	4	8
	Min.	2	3	0	0	0	1	0	2
	n	200	200	200	200	200	200	200	200

C

Plant (Background)		GC with giant chloroplasts	GC with chloroplasts	GC without chloroplasts	Total number	Chloroplastic GC pair			Hybrid GC pair		Chloroplast-less GC pair	Total number	Reference
WT	(FL4-4, FL6-5, FL6-4)	0	200	0	200	0	0	100	0	0	0	100	Fujiwara et al. (2018); This study
arc5-1	(FL6-4)	10	186	4	200	2	6	90	0	0	2	100	Fujiwara et al. (2018)
arc6-3	(FL6-4)	85	72	43	200	24	33	19	4	1	19	100	Fujiwara et al. (2018)
parc6-1	(FL6-4)	62	138	0	200	13	36	51	0	0	0	100	This study
arc11-1	(FL4-4)	0	200	0	200	0	0	100	0	0	0	100	This study
atminE1-1	(FL6-5)	142	41	17	200	55	28	6	4	1	6	100	Fujiwara et al. (2018)

FIGURE 5 | Distribution of chloroplasts in leaf stomatal guard cells of Arabidopsis *parc6* and other plastid division mutants. **(A, B)** Measurements of chloroplast number in arbitrarily selected 100 guard cell (described as "GC" in this figure) pairs ("cell A" and "cell B") of WT, *parc6-1*, *parc6-3*, *parc6-4*, *parc6-5* and *arc11-1* seedlings in graph **(A)** and table **(B)** form. All plants were derived from the FL4-4 line, and the 3rd and 4th leaf petioles of 4-week-old seedlings were examined. **(C)** Frequency of guard cells with giant, normal-sized, or no chloroplasts in *parc6-1*, *arc11-1*, and other mutant plants, based on results in the present study and previous study (Fujiwara et al., 2018). The fluorescence assays were representative of several measurements. Three to five independent leaves were used for each measurement.

leucoplasts, which were almost indistinguishable from the leucoplasts in trichomes of the WT, in terms of the size, shape, subcellular distribution, and chlorophyll autofluorescence signal (**Figure 3**; data not shown). Similarly, chloroplasts in guard cells of *arc11-1* were almost indistinguishable from those in guard cells of the WT (**Figure 4H**). To verify this observation quantitatively, we measured the morphological traits of guard cell plastids in *arc11* using the same method as that used to measure the guard cells of *parc6* mutants (**Figure 5**). The chloroplast number per stoma and per guard cell and guard cell classification, based on the presence or absence of plastids (**Figure 5**), reinforce our view that *arc11-1* is almost indistinguishable from the WT, at least with respect to the guard cell plastid phenotype.

Ultrastructural Analysis of Guard Cell Plastids in *parc6*

To reveal more detailed structural features of plastids in the leaf epidermis of *parc6*, we performed TEM analysis. Previously, we reported the TEM images of chloroplasts in mesophyll and

TABLE 2 | Measurement of chloroplast length in leaf stomatal guard cells of WT and *parc6-1* seedlings[1].

Chloroplast characteristics	WT (FL6-4)	*parc6-1* (FL6-4)
Frequency of chloroplasts		
Giant chloroplast	0 (0.0%)	30 (30.0%)
Normal-sized chloroplast	100 (100.0%)	69 (69.0%)
Mini-chloroplast	0 (0.0%)	1 (1.0%)
Chloroplast length (μm)		
Mean ± standard deviation	4.3 ± 0.7	5.4 ± 1.8
Maximum	5.6	10.9
Minimum	2.6	1.9
Total number of chloroplasts examined	100	100

[1]*For details of the experiment, see Materials and Methods.*

pavement cells of *parc6* mutants (*parc6-3* and *parc6-5*) (Itoh et al., 2018). In the present study, we focused on the ultrastructure of plastids in *parc6* guard cells. Generally, guard cells are smaller than mesophyll and pavement cells; therefore, the chloroplast density is relatively higher in guard cells than in mesophyll and pavement cells. We expected that this feature of guard cells would be more advantageous for TEM analysis of the whole structure of the variable and complexly shaped *parc6* plastids (**Figure 4**), which had been a difficult task for mesophyll and pavement cells (Itoh et al., 2018). We also compared the plastid ultrastructures of different plant lines (WT and *parc6*$^{-/-}$ backgrounds) with and without the transgene expressing the stroma-targeted fluorescent protein. To the best of our knowledge, no studies have reported a secondary effect of stroma-localized fluorescent protein on plastid ultrastructures in any plastid division mutants. In this experiment, we used *parc6-1* (Col background) and *parc6-5* [a mutant obtained from an EMS-mutagenized population of FL4-4 (Col background), in which plastids and mitochondria are labeled with CFP and YFP, respectively].

We examined guard cells in the adaxial surface of petioles of the first and second leaves of 10-day-old seedlings of *parc6-1* and *parc6-5* mutants and their respective parental strains, WT (Col) and WT (FL4-4). All four lines showed the previously described characteristics of cellular and subcellular structures of guard cells (Zhao and Sack, 1999), except for plastids in *parc6* mutants (**Figure 6A**). The two symmetrical guard cells showed a large central vacuole(s) occupying most of the cell volume, cell nucleus located near the stomatal aperture, and mitochondria distributed throughout the cytoplasm in all lines. Additionally, chloroplasts in all lines showed well-developed starch grains in the stroma, less organized thylakoid membranes with few grana stacks, and plastoglobules (**Figure 6B**). Comparison between WT (Col) and WT (FL4-4) lines showed no major difference in the size, shape, and internal structure of chloroplasts. Similarly, both *parc6-1* and *parc6-5* mutant lines contained variably sized chloroplasts (normal to giant), within a similar size range. Another characteristic of the *parc6* guard cell plastids was the frequent formation of stromules, surrounded by two envelope membranes (**Figure 6B**). The size and internal structure of mitochondria also showed no major differences among the four lines examined (**Figure 6C**), which was consistent with the fluorescence microscopy images (**Figure S3A**).

Localization of PARC6-GFP in Petiole Cells

Lastly, we investigated the subcellular localization of PARC6 using GFP as a reporter. Glynn et al. (2009) demonstrated the complementation of the Arabidopsis *parc6-1* mutant with the WT *PARC6* transgene fused to *GFP* gene under the control of the constitutive CaMV35S promoter and intraplastidic localization of PARC6-GFP in young leaf epidermal cells in this complementation line. Nonetheless, it remains elusive how PARC6 behaves during the entire process of chloroplast division. In the present study, we constructed a chimeric construct consisting of the upstream region of the *PARC6* gene, full-length *PARC6* cDNA, and *GFP* and introduced this construct into Arabidopsis *parc6-1* and *parc6-4* mutants. This construct was able to fully rescue the division defect in both *parc6* mutants (data not shown). Using these complementation lines, we observed cortical and epidermal cells in leaf petioles, which correspond to mesophyll and pavement cells in leaf blades, respectively.

In the *parc6-1* complementation line, PARC6-GFP was localized at the constricting neck of dividing chloroplasts as a filamentous or punctate pattern in cortex cells starting from the initial to the final stages of chloroplast division (**Figures 7A–E**). When we shifted the focal plane of the microscope from the top to the bottom of dumbbell-shaped chloroplasts at the middle stage of division, the GFP signal appeared as a filament over the constricting neck in the top and bottom focal planes but as two dots at opposite sides of the neck in the intermediate plane (**Figures 7F**, **G**). At the final stage of chloroplast division, the GFP signal was detected as a single focus (**Figure 7E**). These data suggest that PARC6 forms a ring surrounding the constricting neck of dividing chloroplasts. Moreover, at the early stage of chloroplast division, the GFP signal appeared as short filaments aligned discontinuously, like a dashed line, along the equatorial division plane of chloroplasts (**Figures 7H**, **I**). On the contrary, at later stages when chloroplasts were more deeply constricted, the GFP signal was detected as a continuous filament at the same position (**Figures 7B–D**). These observations imply that during the early to middle stages of constriction formation in dividing chloroplasts, PARC6 ring changes its configuration from a discontinuous array of short fragments to a continuous ring, possibly by gradual polymerization of PARC6 initiated at multiple sites along the circumference of the constriction. We further compared the signal intensities of the ring-like structures of PARC6 at different stages of chloroplast division under the same conditions of excitation and image acquisition (**Figures 7J**, **K**). The GFP signal was faint at the early stage, modest at the intermediate stage, and relatively strong at the late and final stages. This suggests that as chloroplast division proceeds, the PARC6 ring becomes denser by maintaining the number of PARC6 proteins within it, despite the progressive decrease in its diameter. Even after the complete separation of chlorophyll autofluorescence derived from the thylakoids of daughter chloroplasts, the PARC6 ring persisted at the original neck region between them (**Figure 7L**). The PARC6 rings were often detected between two attached but apparently separate

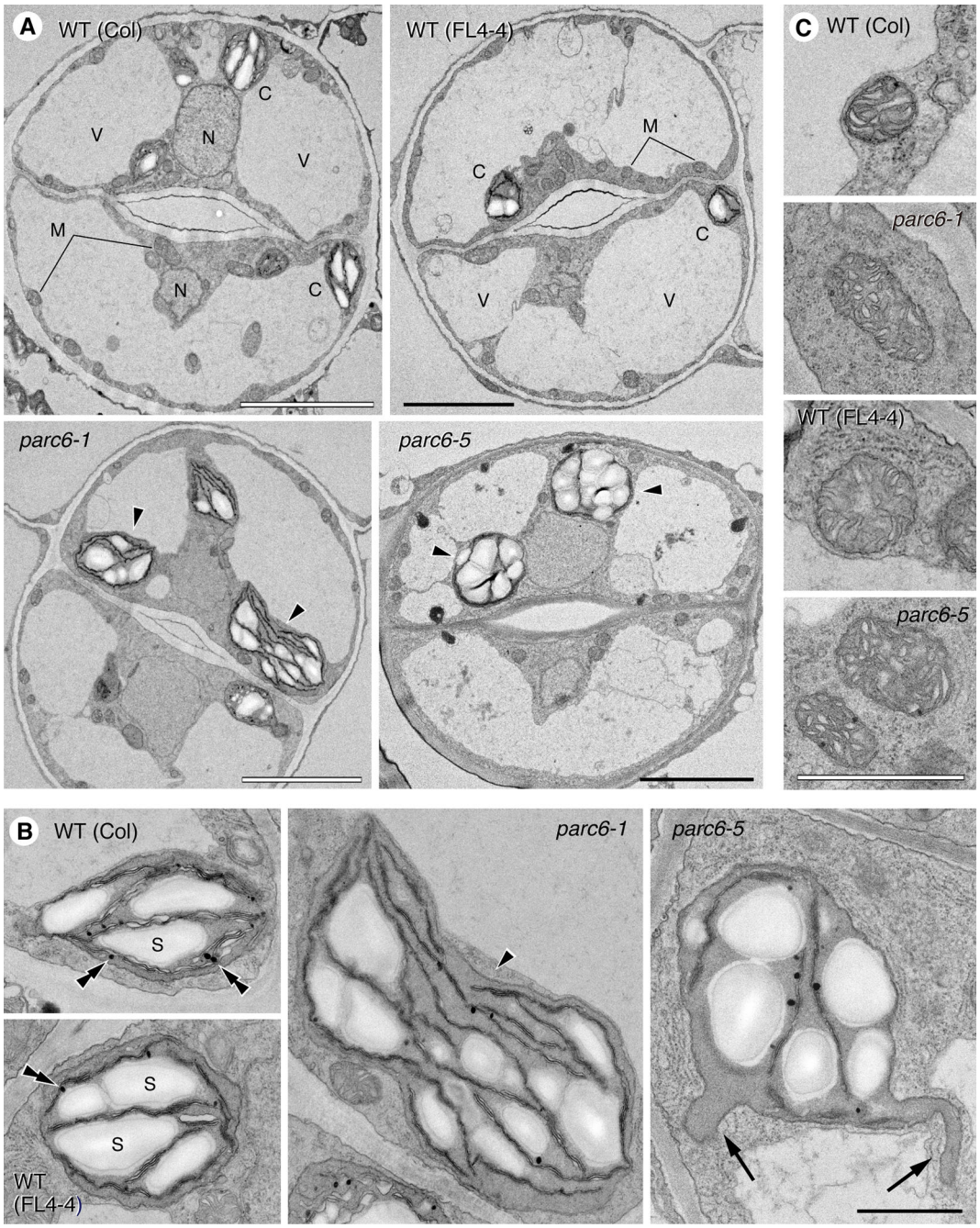

FIGURE 6 | Ultrastructure of plastids and mitochondria in leaf stomatal guard cells of *parc6* mutants. **(A)** Guard cells. **(B)** Plastids. **(C)** Mitochondria. Adaxial epidermis of the first leaf of 10-day-old WT (Col), WT (FL4-4 line), *parc6-1* (Col-derived), and *parc6-5* (FL4-4-derived) seedlings. Arrowheads, arrows, and double arrowheads indicate enlarged chloroplasts, stromules, and plastoglobules, respectively. Scale bars: 5 μm **(A)**; 1 μm **(B**, **C)**.

chloroplasts, based on the bright field images. **Figures 7M–O** show the localization of PARC6-GFP in chloroplasts of the epidermal cells. Because the chloroplasts in the epidermis were immature, detailed tracing of the behavior of PARC6 during chloroplast division was difficult. Nevertheless, the results (**Figures 7M–O**) were consistent with the abovementioned results of the cortex cells and thus support the notion that the localization pattern and behavior of PARC6 are largely conserved between cortex and epidermal cells. Additionally, the present results of epidermal cells were also consistent with the earlier report (Glynn et al., 2009). We also examined the *parc6-4* complementation line in the same manner as the *parc6-1*

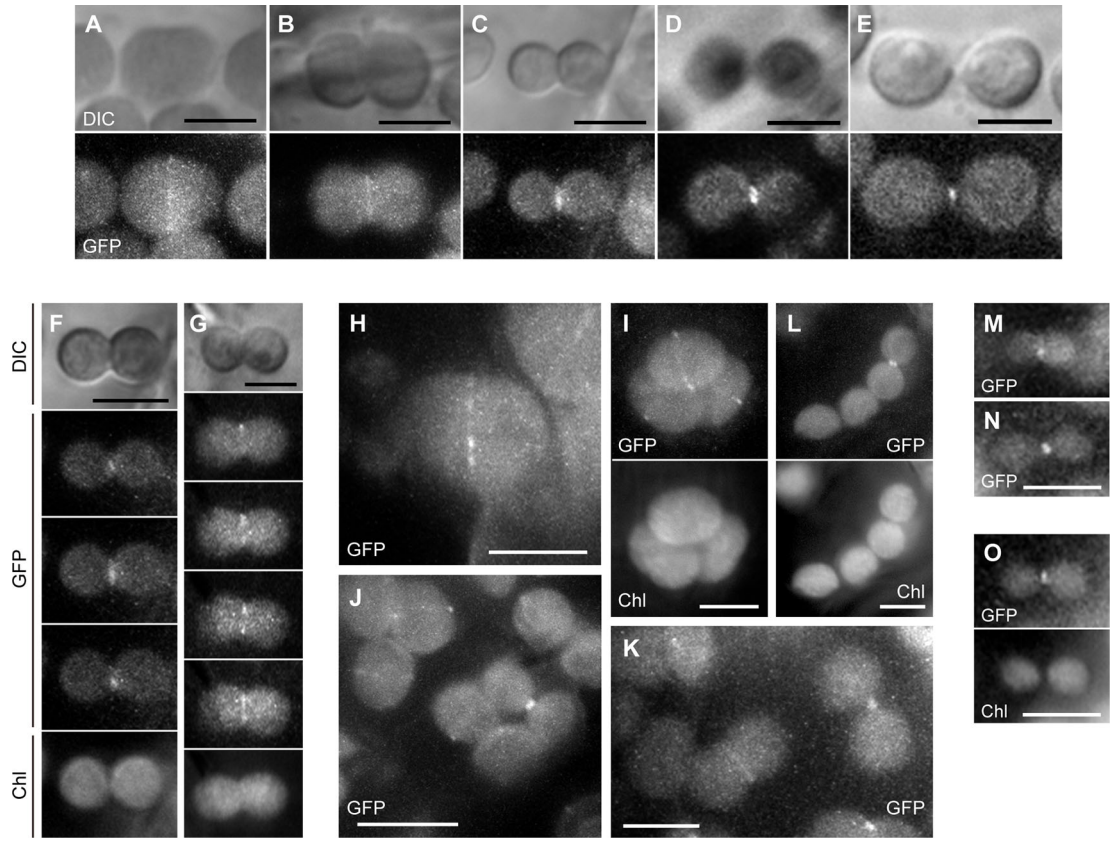

FIGURE 7 | Analysis of PARC6-GFP localization in leaf cortex and pavement cells. **(A–O)** Images of chloroplasts in leaf petioles of 1–3-week-old seedlings of *parc6-1* complementation lines. Images of full-length PARC6-GFP, chlorophyll, or DIC in cortex **(A–K)** and pavement cells **(M–O)** are shown. Scale bars: 10 μm **(J)**; 5 μm (others).

complementation line and obtained similar results (**Figure S5**; only a subset of data is shown). Taken together, these data indicate that the ring-like structure of PARC6 changes its configuration with the progression of chloroplast division.

DISCUSSION

Probable Causal Mutation in *parc6-5/suba2*

In this study, we further characterized the *parc6-5*/*suba2* mutant (Itoh et al., 2018) and other *parc6* alleles of Arabidopsis, while focusing on the role of *PARC6* in morphology maintenance of non-mesophyll plastids in the leaf epidermis. First, the effect of G62R, one of two mutations in *parc6-5*, on the plastid protein import efficiency was evaluated (**Figure 1**). In model plant species such as Arabidopsis, transient expression of a reporter gene, such as *GUS* and *GFP*, can be visually detected usually within 2 to 4 days after plasmid delivery using biolistics (Ueki et al., 2009). In our experiments, no difference was detected in the spatial distribution of fluorescence signals in cells (particularly in terms of the accumulation in plastids and staying in the cytoplasm) between TP-GFP and TP_{G62R}-GFP, irrespective of the types of bombarded cells, including tobacco pavement and guard cells containing chloroplasts and onion bulb epidermal cells containing leucoplasts, at the relatively early time points (6–24 h post-bombardment) (**Figures 1B**, **C**, **E**, **F**). It is possible that at later time points, saturated GFP signal from plastids would mask the putative difference in the protein import rate. Our results at 6–24 h indicate therefore that TP_{G62R} functions as efficiently as the WT TP. Thus, by a process of elimination, it is likely that the W700stop nonsense mutation is responsible for the phenotype of *suba2*/*parc6-5*. Accordingly, it was suggested that the C-terminal 120-amino acid region (amino acids 700–819) of PARC6 is critical for its function. This conclusion is in agreement with an earlier report that showed a chloroplast division defect in another Arabidopsis *parc6* mutant, *arc6h* (Ottesen et al., 2010), harboring a frameshift mutation, causing V697stop mutation and eventually a C-terminal truncation of PARC6, quite similar to that in *parc6-5*. The C-terminal 223-amino acid region (amino acids 597–819) of PARC6 is exposed in the intermembrane space, as shown by biochemical analysis, which facilitates the interaction of PARC6 with PDV1, as shown

by the yeast two-hybrid assay (Zhang et al., 2016). PDV1 and its paralog PDV2 are outer envelope membrane proteins of plastids, which recruit a dynamin-related protein DRP5B (ARC5) from the cytosol to the plastid surface (Miyagishima et al., 2006). Our results suggest that C-terminal 120-amino acid region of PARC6 exposed within the intermembrane space is indispensable for its function, probably because of its association with PDV1 and the resultant recruitment of DRP5B, although precise functions of PDV1 and DRP5B and their physical and functional association with PARC6 are currently unknown in non-mesophyll plastids.

Significance of *PARC6* in Plastid Replication and Morphology Maintenance in the Leaf Epidermis

Building on our previous results (Itoh et al., 2018), but by examining younger leaves of *parc6* mutants, we obtained additional insights into the involvement of *PARC6* in chloroplast morphology maintenance in pavement cells. The most remarkable discovery was the occurrence of the grape-like plastid clusters in pavement cells (**Figures 2D–G**, **S1C**). Similarly, in trichome cells, the occurrence of the grape-like clusters was the most striking cytological feature of *parc6* mutants (**Figures 3G–J**, **S2B–D**). This is the first report of the three-dimensional structure of plastid clusters (**Supplementary Movies 1**, **2**). Furthermore, to the best of our knowledge, this is the first report describing the morphology and distribution pattern of plastids (leucoplasts) in the trichomes of any chloroplast division mutants. Overall, in *parc6* mutants, the phenotype of plastids in trichomes (**Figure 3**) was unique compared with that of plastids in mesophyll cells, pavement cells, and guard cells. We believe that the data reported in this study offer a basis for probing the mechanisms of replication and morphology maintenance (including stromule formation) in non-mesophyll plastids and the change of mechanisms during cell differentiation, which are largely unknown at present (Pyke, 2010; Pyke, 2013; Pyke, 2016). Since the developmental process of trichomes in Arabidopsis is well understood and can be readily traced because of their large size and unicellular nature (Hülskamp, 2019), trichomes might be a potential experimental system for resolving the above issues.

The present study showed a significant decrease in the number of chloroplasts in guard cells of *parc6* mutants (**Figures 5A**, **B**). Previously, we performed similar analyses on other chloroplast division mutants including *arc5*, *arc6*, and *atminE1* (F_2 siblings derived from a cross between the original mutant and FL6-4 or FL6-5) (Fujiwara et al., 2018) and presented the results of guard cell chloroplast counting as integer values, which makes the direct comparison with the present results of *parc6* mutants difficult. When compared in a unified manner, the chloroplast numbers on a per guard cell basis were as follows: WT, 4.6 ± 1.0, max. 7, min. 3 [5 ± 1 in Fujiwara et al., 2018 (the same hereafter)]; *arc5-1*, 3.9 ± 1.3, max. 9, min. 0 (4 ± 1); *arc6-3*, 2.5 ± 1.6, max. 7, min. 0 (2 ± 2); *atminE1-1*, 2.6 ± 1.3, max. 6, min 0. (3 ± 1); *parc6-1*, 1.7 ± 0.7, max. 4, min. 0. This direct comparison suggests that among the examined genes, *PARC6* exhibits the most effective control of chloroplast number in guard cells. By contrast, phenotypic analysis of these mutants, based on the classification of guard cells by size and presence/absence of chloroplasts in them (**Figure 5C**, **Table 2**), suggests that the importance of *PARC6* is intermediate between that of *ARC6*/*AtMinE1* (higher importance) and *ARC5* (lower importance) in terms of chloroplast morphology and differentiation in guard cells.

During leaf development in WT Arabidopsis plants, chloroplasts in pavement cells undergo symmetric binary fission, as mediated by the FtsZ1 ring formation at the equatorial plane (Fujiwara et al., 2015). By contrast, chloroplasts in *arc11-1* pavement cells exhibited aberrant assembly of the FtsZ1 ring(s) at a non-equatorial site or multiple sites, which is consistent with our previous report (Fujiwara et al., 2017). Nonetheless, chloroplasts that initiated such asymmetric or multiple divisions were likely to complete the division process, eventually assuming a morphology that was largely indistinguishable from WT chloroplasts. Thus, the "terminal" phenotype of pavement cells in mature *arc11* leaves was slight heterogeneity in chloroplast size. Chloroplasts in both trichomes and guard cells of *arc11* appeared similar to those in their WT counterparts (**Figures 3K**, **4H**, and **5**), which further underlines the difference in epidermal plastid phenotype between *arc11* and *parc6*. Although AtMinD1 (ARC11) and PARC6 function in the same process of chloroplast division (namely, division site placement) in mesophyll cells, our previous (Fujiwara et al., 2017; Itoh et al., 2018) and present results suggest that the known role and importance of both proteins are modified and differentiated upon morphogenesis of leaf epidermal plastids. AtMinD1 and PARC6 were previously demonstrated to interact with each other in the yeast two-hybrid system (Itoh et al., 2018). It remains uncertain, however, whether they actually interact with each other *in vivo*, i.e., in chloroplasts and other types of plastids. It is possible that the mode and extent of AtMinD1–PARC6 interaction vary with the type of plastids, thereby giving rise to a variety of mechanisms that control plastid division.

Although *suba2*/*parc6-5* was originally identified as one of the two stromule-overproducing mutants by fluorescence microscopy-based screening of leaf epidermal tissues, we failed to detect stromules in the leaf epidermis at the ultrastructural level in our previous study (Itoh et al., 2018). Here, we presented ultrastructural evidence for the active production of stromules in *parc6* guard cells (**Figure 6B**), substantiating the abovementioned speculation that guard cells are suitable for the ultrastructural analysis of complexly shaped plastids, often accompanied by highly developed stromules, in chloroplast division mutants. At the ultrastructural level, guard cell plastids in *parc6-5* were morphologically equivalent to those in *parc6-1*, further supporting the results of fluorescence microscopy (**Figures 4** and **5A**, **B**). Our TEM investigations of WT and *parc6* plants with and without the expression of stroma-targeted CFP and matrix-targeted YFP (**Figures 6B**, **C**) also address the question whether the accumulation of a fluorescent protein in a particular organelle affects the internal and external structures of that organelle. It is widely believed that GFP and its

derivatives are not cytotoxic to plants (Stewart Jr, 2001), although the possible effects of these reporter proteins on organelles remain elusive in plants. Comparison of fluorescent protein-expressing and non-expressing plants in an otherwise identical genetic background (WT or *parc6*$^{-/-}$ in Col background) unequivocally established that the accumulation of fluorescent protein in the stroma and matrix does not affect the structures of plastids and mitochondria, respectively, at least at a detectable level (**Figures 6B**, **C**).

At present, it remains an open question how a defect in PARC6 leads to a variety of abnormal plastid morphologies in leaf epidermal cells. One possibility is that PARC6 has an epidermis-specific function in plastid morphogenesis, in addition to its established function in the division of mesophyll cell chloroplasts, as discussed in our previous report (Itoh et al., 2018). Another possibility is that an arrest of plastid division due to the lack of functional PARC6 secondarily causes abnormal plastid phenotypes during the differentiation of epidermal cells, but in a different and more complicated manner than in mesophyll cells, which consistently show simple phenotypes (i.e., increase in chloroplast size and decrease in chloroplast number). A prerequisite for the latter possibility is that plastids divide at least once during epidermis development. In flowering plants, cells in the outermost cell layer of the shoot apical meristem, namely, the L1 layer, undergo anticlinal cell division and eventually differentiate into pavement, trichome, and stomatal guard cells constituting the epidermis (Glover et al., 2016). While cells in the shoot apical meristem contain undifferentiated proplastids, pavement, trichome, and guard cells contain poorly developed chloroplasts, leucoplasts converted from chloroplasts, and well-developed chloroplasts, respectively (Pyke, 2009; Barton et al., 2016; Barton et al., 2018). In the pavement cells of Arabidopsis, we have previously shown that peanut-shaped chloroplasts associated with the mid-plastid FtsZ1 accumulation, implying that these chloroplasts are in the process of FtsZ1 ring-mediated binary division (Fujiwara et al., 2015). Leucoplasts in trichomes seemed to increase in number during the development of trichome cells in Arabidopsis, as inferred from a rough comparison between early developing trichomes (containing ~30 leucoplasts; **Figures 3A**, **B**) and mature trichomes (containing >100 leucoplasts; **Figure 3F**), although leucoplasts in trichomes could not be accurately counted in this study because of the difficulty imposed by the extremely large size of trichomes. Supporting this notion, in our preliminary experiments, we observed FtsZ1 ring-associated, constricted leucoplasts in Arabidopsis trichomes (Fujiwara, unpublished data). Similarly, in Arabidopsis guard cells, our data suggest FtsZ1 ring-mediated division of chloroplasts (Fujiwara et al., 2019). We cannot, therefore, exclude the latter possibility mentioned above. To determine how a mutation in *PARC6* leads to abnormal plastid morphology in leaf epidermal cells, further investigation of the *parc6* mutant is needed to understand the processes during which the morphological phenotypes of plastids become apparent along the lineage of each type of epidermal cell and to determine the activity (evaluated by plastid counting) and mode (e.g., symmetric vs. asymmetric, binary vs. multiple) of plastid division in differentiating and differentiated epidermal cells.

Dynamics of PARC6 at the Plastid Division Site

Previously, a functional PARC6-GFP fusion protein was shown to localize to mid-plastid puncta in ovoid and partially constricted chloroplasts, a mid-plastid spot in deeply constricted chloroplasts, and a polar spot at the surface of round, probably post-dividing chloroplasts, which appeared to be the remnant of mid-plastid spots, in the epidermis of young expanding leaves of 14-day-old transgenic Arabidopsis seedlings (Glynn et al., 2009). In the current study, we employed similar methodology as that used by Glynn et al. (2009) but used both cortical and epidermal tissues in the leaf petioles to provide more detailed information on the subplastidic dynamics of PARC6. The PARC6-GFP proteins localized to the middle of pre-dividing and dividing chloroplasts as well as to a single polar spot in post-dividing chloroplasts (**Figure 7**), as described above. However, we noted two aspects of PARC6 localization: 1) formation of a PARC6 ring surrounding the constricting neck of dividing chloroplasts (**Figures 7A–G**), and 2) discontinuous nature of the PARC6 ring at the early stage of chloroplast division (**Figures 7H**, **I**). Although the formation of a PARC6 ring around the dividing chloroplasts was formerly hinted at by Glynn et al. (2009), direct evidence for this has been lacking to date. More importantly, the discontinuous nature of the PARC6 ring early during chloroplast division observed in this study is in contrast to the progressive concentration of PARC6 in a single spot at the isthmus of highly constricted chloroplasts at the final stage of division [Glynn et al., 2009; this study (**Figure 7E**)]. To the best of our knowledge, PARC6 is the first protein reported to form an array of short filaments at the chloroplast division site at the early division stage. Among the known mid-plastid-localizing proteins, DRP5B (ARC5) and PDV1 clearly show a discontinuous, "array-of-dot"-like localization pattern surrounding the division site, as revealed by GFP tagging (for DRP5B and PDV1) and immunofluorescence microcopy (for DRP5B) (Miyagishima et al., 2006; Okazaki et al., 2009; Miyagishima et al., 2011). Components of the chloroplast division site-determining Min system, including AtMinD1, AtMinE1, and MCD1 (Osteryoung and Pyke, 2014), also appear to exhibit a punctate pattern, as revealed by immunofluorescence microcopy (Nakanishi et al., 2009; Fujiwara et al., 2009a; Miyagishima et al., 2011; Chen et al., 2018b). Nevertheless, the observed punctate signals of AtMinD1, AtMinE1, and MCD1 were generally smaller, more varied in size, and more irregularly aligned along the division plane than those of DRP5B and PDV1 (e.g., Figure 4.3 in Miyagishima et al., 2011). The discontinuous localization pattern of PARC6-GFP (**Figures 7H**, **I**) seems to bear a greater resemblance to that of GFP-DRP5B (see Figure 4G in Miyagishima et al., 2006) and GFP-PDV1 (see Figures 4A, C in Miyagishima et al., 2006) in unconstricted chloroplasts rather than to that of AtMinD1,

AtMinE1, and MCD1. This might imply partial colocalization of PARC6 with PDV1 and DRP5B in the early stage of chloroplast division. In fact, regions of PARC6 and PDV1 in the intermembrane space were shown to interact with each other in yeast two-hybrid and pull-down assays (Zhang et al., 2016). Additionally, DRP5B and the cytosolic region of PDV1 were also demonstrated to interact with each other by both yeast two-hybrid and bimolecular fluorescence complementation assays (Holtsmark et al., 2013), thereby enabling the recruitment of DRP5B from the cytosol to the outer envelope surface of chloroplasts at the division site (Miyagishima et al., 2006). This suggests that PARC6, PDV1, and DRP5B might act together during a certain period of chloroplast division initiation. However, at a later stage of chloroplast division, when chloroplasts were clearly constricted, GFP-PDV1 and GFP-DRP5B still showed an "array-of-dot"-like localization (see Figures 4D, H in Miyagishima et al., 2006), whereas PARC6-GFP appeared to form a continuous ring in similarly constricted chloroplasts (**Figure 7C**). This highlights the differential dynamics of PARC6 and PDV1/DRP5B upon the constriction of chloroplasts.

In the PARC6 localization experiment, the fluorescence signal of PARC6-GFP in chloroplasts was detected only in young, emerging leaves (shorter in length than several millimeters). Thus, it remains unknown whether the above-described PARC6 dynamics commonly exists in chloroplasts of mesophyll and pavement cells at every developmental stage. Moreover, because the fluorescence signal of PARC6-GFP was quite faint, a long exposure time was needed to capture the GFP signal, making it impossible to obtain GFP images in trichome and guard cells in the current study (not shown). Despite such technical difficulties, change in the expression and possibly localization of PARC6 during leaf development deserves future investigation because GFP-PDV1 (and GFP-PDV2) expressed by their respective promoters were also detected in young, emerging leaves but not in older, expanding leaves (Okazaki et al., 2009), similar to PARC6. Simultaneous labeling and imaging of PARC6 and PDV1 would be particularly important for the elucidation of the assembly process of the plastid division machinery and its possible dependency on the developmental stage and differentiation state of the leaf cell.

DATA AVAILABILITY STATEMENT

The datasets generated for this study are available on request to the corresponding author.

AUTHOR CONTRIBUTIONS

RI designed the study. HI, MY, NK, AS, SM, AN, KM, SS, YK, YH, MF, and RI performed the experiments. HI, MY, NK, MF, and RI interpreted the data. AS, MF, and RI wrote the paper. YK, TA, MF, and RI contributed reagents, materials, and/or analytical tools.

FUNDING

This work was supported by the Ministry of Education, Culture, Science and Technology of Japan under KAKENHI (grant nos. 22780087, 25450136, and 19K05831 to MF; 25292009 to YK; and 26440152 and 18K06314 to RI) and by the Uruma Fund for the Promotion of Science (to RI).

ACKNOWLEDGMENTS

We thank the ABRC, Dr. Yasuo Niwa, and Dr. Hiroaki Ichikawa for providing resources, Tokai Electron Microscopy Inc. and Olympus Biomedical Science Sales Inc. for technical support, and Dr. Kensuke Hayashi, Dr. Kei H. Kojo, Ayaka Yoshino (Sophia University), Dr. Tadashi Kambara, Dr. Ryouhei Morita, Sumie Ohbu, and Sachiko Usuda (RIKEN) for experimental support and discussion.

SUPPLEMENTARY MATERIAL

The Supplementary Material for this article can be found online at: https://www.frontiersin.org/articles/10.3389/fpls.2019.01665/full#supplementary-material

REFERENCES

Alonso, J. M., Stepanova, A. N., Leisse, T. J., Kim, C. J., Chen, H., Shinn, P., et al. (2003). Genome-wide insertional mutagenesis of *Arabidopsis thaliana*. *Science* 301, 653–657. doi: 10.1126/science.1086391

Barton, K. A., Schattat, M. H., Jakob, T., Hause, G., Wilhelm, C., Mckenna, J. F., et al. (2016). Epidermal pavement cells of *Arabidopsis* have chloroplasts. *Plant Physiol.* 171, 723–726. doi: 10.1104/pp.16.00608

Barton, K. A., Wozny, M. R., Mathur, N., Jaipargas, E. A., and Mathur, J. (2018). Chloroplast behaviour and interactions with other organelles in *Arabidopsis thaliana* pavement cells. *J. Cell Sci.* 131, jcs202275. doi: 10.1242/jcs.202275

Chen, Y., Asano, T., Fujiwara, M. T., Yoshida, S., Machida, Y., and Yoshioka, Y. (2009). Plant cells without detectable plastids are generated in the crumpled leaf mutant of *Arabidopsis thaliana*. *Plant Cell Physiol.* 50, 956–969. doi: 10.1093/pcp/pcp047

Chen, C., MacCready, J. S., Ducat, D. C., and Osteryoung, K. W. (2018a). The molecular machinery of chloroplast division. *Plant Physiol.* 176, 138–151. doi: 10.1104/pp.17.01272

Chen, L., Sun, B., Gao, W., Zhang, Q.-Y., Yuan, H., and Zhang, M. (2018b). MCD1 associates with FtsZ filaments via the membrane-tethering protein ARC6 to guide chloroplast division. *Plant Cell* 30, 1807–1823. doi: 10.1105/tpc.18.00189

Chiu, W., Niwa, Y., Zeng, W., Hirano, T., Kobayashi, H., and Sheen, J. (1996). Engineered GFP as a vital reporter in plants. *Curr. Biol.* 6, 325–330. doi: 10.1016/S0960-9822(02)00483-9

Clough, S. J., and Bent, A. F. (1998). Floral dip: a simplified method for *Agrobacterium*-mediated transformation of *Arabidopsis thaliana*. *Plant J.* 16, 735–743. doi: 10.1046/j.1365-313x.1998.00343.x

Colletti, K. S., Tattersall, E. A., Pyke, K. A., Froelich, J. E., Stokes, K. D., and Osteryoung, K. W. (2000). A homologue of the bacterial cell division site-determining factor MinD mediates placement of the chloroplast division apparatus. *Curr. Biol.* 10, 507–516. doi: 10.1016/S0960-9822(00)00466-8

Delfosse, K., Wozny, M. R., Jaipargas, E. A., Barton, K. A., Anderson, C., and Mathur, J. (2016). Fluorescent protein aided insights on plastids and their extensions: a critical appraisal. *Front. Plant Sci.* 6, 1253. doi: 10.3389/fpls.2015.01253

Erickson, J. L., and Schattat, M. H. (2018). Shaping plastid stromules – principles of *in vitro* membrane tubulation applied *in planta*. *Curr. Opin. Plant Biol.* 46, 48–54. doi: 10.1016/j.pbi.2018.07.003

Erickson, J. L., Kantek, M., and Schattat, M. H. (2017). Plastid-nucleus distance alters the behavior of stromules. *Front. Plant Sci.* 8, 1135. doi: 10.3389/fpls.2017.01135

Folkers, U., Berger, J., and Hülskamp, M. (1997). Cell morphogenesis of trichomes in *Arabidopsis*: differential control of primary and secondary branching by branch initiation regulators and cell growth. *Development* 124, 3779–3786.

Forth, D., and Pyke, K. A. (2006). The *suffulta* mutation in tomato reveals a novel method of plastid replication during fruit ripening. *J. Exp. Bot.* 57, 1971–1979. doi: 10.1093/jxb/erj14

Fujiwara, M. T., Nakamura, A., Itoh, R., Shimada, Y., Yoshida, S., and Møller, S. G. (2004). Chloroplast division site placement requires dimerization of the ARC11/AtMinD1 protein in *Arabidopsis*. *J. Cell Sci.* 117, 2399–2410. doi: 10.1242/jcs.01092

Fujiwara, M. T., Hashimoto, H., Kazama, Y., Abe, T., Yoshida, S., Sato, N., et al. (2008). The assembly of the FtsZ ring at the mid-chloroplast division site depends on a balance between the activities of AtMinE1 and ARC11/AtMinD1. *Plant Cell Physiol.* 49, 345–361. doi: 10.1093/pcp/pcn012

Fujiwara, M. T., Li, D., Kazama, Y., Abe, T., Uno, T., Yamagata, H., et al. (2009a). Further evaluation of the localization and functionality of hemagglutinin epitope- and fluorescent protein-tagged AtMinD1 in *Arabidopsis thaliana*. *Biosci. Biotechnol. Biochem.* 73, 1693–1697. doi: 10.1271/bbb.90309

Fujiwara, M. T., Sekine, K., Yamamoto, Y. Y., Abe, T., Sato, N., and Itoh, R. D. (2009b). Live imaging of chloroplast FtsZ1 filaments, rings, spirals, and motile dot structures in the *AtMinE1* mutant and overexpressor of *Arabidopsis thaliana*. *Plant Cell Physiol.* 50, 1116–1126. doi: 10.1093/pcp/pcp063

Fujiwara, M. T., Kojo, K. H., Kazama, Y., Sasaki, S., Abe, T., and Itoh, R. D. (2015). The *Arabidopsis minE* mutation causes new plastid and FtsZ1 localization phenotypes in the leaf epidermis. *Front. Plant Sci.* 6, 823. doi: 10.3389/fpls.2015.00823

Fujiwara, M. T., Yasuzawa, M., Sasaki, S., Nakano, T., Niwa, Y., Yoshida, S., et al. (2017). The *Arabidopsis minD* mutation causes aberrant FtsZ1 ring placement and moderate heterogeneity of chloroplasts in the leaf epidermis. *Plant Signal. Behav.* 12, e1343776. doi: 10.1080/15592324.2017.1343776

Fujiwara, M. T., Yasuzawa, M., Kojo, K. H., Niwa, Y., Abe, T., Yoshida, S., et al. (2018). The *Arabidopsis arc5* and *arc6* mutations differentially affect plastid morphology in pavement and guard cells in the leaf epidermis. *PLoS One* 13, e0192380. doi: 10.1371/journal.pone.0192380

Fujiwara, M. T., Sanjaya, A., and Itoh, R. D. (2019). *Arabidopsis thaliana* leaf epidermal guard cells: a model for studying chloroplast proliferation and partitioning in plants. *Front. Plant Sci.* 10, 1403. doi: 10.3389/fpls.2019.01403

Glover, B. J., Airoldi, C. A., and Moyroud, E. (2016). "Epidermis: outer cell layer of the plant," in *eLS* (Chichester: John Wiley & Sons, Ltd). doi: 10.1002/9780470015902.a0002072.pub3

Glynn, J. M., Yang, Y., Vitha, S., Schmitz, A. J., Hemmes, M., Miyagishima, S., et al. (2009). PARC6, a novel chloroplast division factor, influences FtsZ assembly and is required for recruitment of PDV1 during chloroplast division in Arabidopsis. *Plant J.* 59, 700–711. doi: 10.1111/j.1365-313X.2009.03905.x

Gray, J. C., Hansen, M. R., Shaw, D. J., Graham, K., Dale, R., Smallman, P., et al. (2001). Stromules: mobile protrusions and interconnections between plastids. *Plant Biol.* 3, 223–233. doi: 10.1055/2-2001-15204

Hülskamp, M. (2019). Trichomes. *Curr. Biol.* 29, R273–R274. doi: 10.1016/j.cub.2019.02.010

Hanson, M. R., and Hines, K. M. (2018). Stromules: probing formation and function. *Plant Physiol.* 176, 128–137. doi: 10.1104/pp.17.01287

Haswell, E. S., and Meyerowitz, E. M. (2006). MscS-like proteins control plastid size and shape in *Arabidopsis thaliana*. *Curr. Biol.* 16, 1–11. doi: 10.1016/j.cub.2005.11.044

Higa, T., Suetsugu, N., Kong, S.-G., and Wada, M. (2014). Actin-dependent plastid movement is required for motive force generation in directional nuclear movement in plants. *Proc. Natl. Acad. Sci. U.S.A.* 111, 4327–4331. doi: 10.1073/pnas.1317902111

Holtsmark, I., Lee, S., Lunde, K. A., Auestad, K., Maple-Grødem, J., and Møller, S. G. (2013). Plastid division control: the PDV proteins regulate DRP5B dynamin activity. *Plant Mol. Biol.* 82, 255–266. doi: 10.1007/s11103-013-0059-7

Holzinger, A., Kwok, E. Y., and Hanson, M. R. (2008). Effects of *arc3*, *arc5* and *arc6* mutations on plastid morphology and stromule formation in green and nongreen tissues of *Arabidopsis thaliana*. *Photochem. Photobiol.* 84, 1324–1335. doi: 10.1111/j.1751-1097.2008.00437.x

Igasaki, T., Ishida, Y., Mohri, T., Ichikawa, H., and Shinohara, K. (2002). Transformation of *Populus alba* and direct selection of transformants with the herbicide bialaphos. *Bull. FFPRI* 1, 235–240.

Isono, K., Shimizu, M., Yoshimoto, K., Niwa, Y., Satoh, K., Yokota, A., et al. (1997). Leaf-specifically expressed genes for polypeptides destined for chloroplasts with domains of σ^{70} factors of bacterial RNA polymerases in *Arabidopsis thaliana*. *Proc. Natl. Acad. Sci. U.S.A.* 94, 14948–14953. doi: 10.1073/pnas.94.26.14948

Itoh, R. D., Yamasaki, H., Septiana, A., Yoshida, S., and Fujiwara, M. T. (2010). Chemical induction of rapid and reversible plastid filamentation in *Arabidopsis thaliana* roots. *Physiol. Plant.* 139, 144–158. doi: 10.1111/j.1399-3054.2010.01352.x

Itoh, R. D., Ishikawa, H., Nakajima, K. P., Moriyama, S., and Fujiwara, M. T. (2018). Isolation and analysis of a stromule-overproducing *Arabidopsis* mutant suggest the role of *PARC6* in plastid morphology maintenance in the leaf epidermis. *Physiol. Plant.* 162, 479–494. doi: 10.1111/ppl.12648

Köhler, R. H., and Hanson, M. R. (2000). Plastid tubules of higher plants are tissue- specific and developmentally regulated. *J. Cell Sci.* 113, 81–89.

Köhler, R. H., Cao, J., Zipfel, W. R., Webb, W. W., and Hanson, M. R. (1997). Exchange of protein molecules through connections between higher plant plastids. *Science* 276, 2039–2042. doi: 10.1126/science.276.53212039

Kandasamy, M., and Meagher, R. B. (1999). Actin-organelle interaction: association with chloroplast in *Arabidopsis* leaf mesophyll cells. *Cell Motil. Cytoskeleton* 44, 110–118. doi: 10.1002/(SICI)1097-0169(199910)44:2<110::AID-CM3>3.0.CO;2-O

Kinsman, E. A., and Pyke, K. A. (1998). Bundle sheath cells and cell-specific plastid development in *Arabidopsis* leaves. *Development* 125, 1815–1822.

Kirk, J. T. O., and Tilney-Bassett, R. A. E. (1978). *The plastids* (Amsterdam, The Netherlands: Elsevier/North-Holland).

Kojo, K. H., Fujiwara, M. T., and Itoh, R. D. (2009). Involvement of *AtMinE1* in plastid morphogenesis in various tissues of *Arabidopsis thaliana*. *Biosci. Biotechnol. Biochem.* 73, 2632–2639. doi: 10.1271/bbb.90473

Kumar, A. S., Park, E., Nedo, A., Alqarni, A., Ren, L., Hoban, K., et al. (2018). Stromule extension along microtubules coordinated with actin-mediated anchoring guides perinuclear chloroplast movement during innate immunity. *eLife* 7, 1098. doi: 10.7554/eLife.23625

Kwok, E. Y., and Hanson, M. R. (2004). Stromules and dynamic nature of plastid morphology. *J. Microsc.* 214, 124–137. doi: 10.1111/j.0022-2720.2004.01317.x

López-Juez, E., and Pyke, K. A. (2005). Plastids unleashed: their development and their integration in plant development. *Int. J. Dev. Biol.* 49, 557–577. doi: 10.1387/ijdb.051997el

Lawson, T. (2009). Guard cell photosynthesis and stomatal function. *New Phytol.* 181, 13–34. doi: 10.1111/j.1469-8137.2008.02685.x

Leech, R. M., and Pyke, K. A. (1988). "Chloroplast division in higher plants with particular reference to wheat," in *Division and Segregation of Organelles*. Eds. S. A. Boffey and D. Lloyd (Cambridge: Cambridge University Press), 39–62.

Maple, J., Vojta, L., Soll, J., and Møller, S. G. (2007). ARC3 is a stromal Z-ring accessory protein essential for plastid division. *EMBO Rep.* 8, 293–299. doi: 10.1038/sj.embor.7400902

Marrison, J. L., Rutherford, S. M., Robertson, E. J., Lister, C., Dean, C., and Leech, R. M. (1999). The distinctive roles of five different *ARC* genes in the chloroplast division process in *Arabidopsis*. *Plant J.* 18, 651–662. doi: 10.1046/j.1365-313x.1999.00500.x

Mathur, J., Spielhofer, P., Kost, B., and Chua, N. (1999). The actin cytoskeleton is required to elaborate and maintain spatial patterning during trichome cell morphogenesis in *Arabidopsis thaliana*. *Development* 126, 5559–5568.

Miyagishima, S., Froehlich, J. E., and Osteryoung, K. W. (2006). PDV1 and PDV2 mediate recruitment of the dynamin-related protein ARC5 to the plastid division site. *Plant Cell* 18, 2517–2530. doi: 10.1105/tpc.106.045484

Miyagishima, S., Nakanishi, H., and Kabeya, Y. (2011). Structure, regulation, and evolution of the plastid division machinery. *Int. Rev. Cell Mol. Biol.* 291, 115–153. doi: 10.1016/B978-0-12-386035-4.00004-5

Mullet, J. E. (1988). Chloroplast development and gene expression. *Annu. Rev. Plant Physiol. Plant Mol. Biol.* 39, 475–502. doi: 10.1146/annurev.pp.39.060188.002355

Nakanishi, H., Suzuki, K., Kabeya, Y., and Miyagishima, S. (2009). Plant-specific protein MCD1 determines the site of chloroplast division in concert with bacteria-derived MinD. *Curr. Biol.* 19, 151–156. doi: 10.1016/j.cub.2008.12.018

Natesan, S. K. A., Sullivan, J. A., and Gray, J. C. (2005). Stromules: a characteristic cell-specific feature of plastid morphology. *J. Exp. Bot.* 56, 787–797. doi: 10.1093/jxb/eri088

Okazaki, K., Kabeya, Y., Suzuki, K., Mori, T., Ichikawa, T., Matsui, M., et al. (2009). The PLASTID DIVISION1 and 2 components of the chloroplast division machinery determine the rate of chloroplast division in land plant cell differentiation. *Plant Cell* 21, 1769–1780. doi: 10.1105/tpc.109.067785

Osteryoung, K. W., and Pyke, K. A. (2014). Division and dynamic morphology of plastids. *Annu. Rev. Plant Biol.* 65, 443–472. doi: 10.1146/annurev-arplant-050213-035748

Ottesen, E., Zhong, R., and Lamppa, G. K. (2010). Identification of a chloroplast division mutant coding for ARC6H, an ARC6 homolog that plays a nonredundant role. *Plant Sci.* 178, 114–122. doi: 10.1016/j.plantsci.2009.10.009

Pyke, K. A., and Leech, R. M. (1994). A genetic analysis of chloroplast division and expansion in *Arabidopsis thaliana*. *Plant Physiol.* 104, 201–207. doi: 10.1104/pp.104.1.201

Pyke, K. A., Rutherford, S. M., Robertson, E. J., and Leech, R. M. (1994). *arc6*, a fertile *Arabidopsis* mutant with only two mesophyll cell chloroplasts. *Plant Physiol.* 106, 1169–1177. doi: 10.1104/pp.106.31169

Pyke, K. A. (1999). Plastid division and development. *Plant Cell* 11, 549–556. doi: 10.1105/tpc.11.4.549

Pyke, K. (2007). "Plastid biogenesis and differentiation," in *Cell and Molecular Biology of Plastids (Topics in Current Genetics, vol 19)*. Ed. R. Bock (Berlin and Heidelberg: Springer), 1–28. doi: 10.1007/4735_2007_0226

Pyke, K. A. (2009). *Plastid Biology* (Cambridge, UK: Cambridge University Press). doi: 10.1017/CBO9780511626715

Pyke, K. A. (2010). Plastid division. *AoB Plants* 2010, plq016. doi: 10.1093/aobpla/plq016

Pyke, K. A. (2013). Divide and shape: an endosymbiont in action. *Planta* 237, 381–387. doi: 10.1007/s00425-012-1739-2

Pyke, K. A. (2016). "Plastid division," in *Molecular Cell Biology of the Growth and Differentiation of Plant Cells*. Ed. R. J. Rose (Boca Raton, FL: CRC Press), 37–50. doi: 10.1201/b20316

Robertson, E. J., Pyke, K. A., and Leech, R. M. (1995). *arc6*, an extreme chloroplast division mutant of *Arabidopsis* also alters proplastid proliferation and morphology in shoot and root apices. *J. Cell Sci.* 108, 2937–2944.

Sachs, J. (1875). *Textbook of Botany* (Oxford: Clarendon Press).

Schattat, M. H., and Klösgen, R. B. (2011). Induction of stromule formation by extracellular sucrose and glucose in epidermal leaf tissue of *Arabidopsis thaliana*. *BMC Plant Biol.* 11, 115. doi: 10.1186/1471-2229-11-115

Schattat, M. H., Barton, K., Baudisch, B., Klösgen, R. B., and Mathur, J. (2011). Plastid stromule branching coincides with contiguous endoplasmic reticulum dynamics. *Plant Physiol.* 155, 1667–1677. doi: 10.1104/pp.110.170480

Schattat, M. H., Griffiths, S., Mathur, N., Barton, K., Wozny, M. R., Dunn, N., et al. (2012). Differential coloring reveals that plastids do not form networks for exchanging macromolecules. *Plant Cell* 24, 1465–1477. doi: 10.1105/tpc.111.095398

Schattat, M. H., Barton, K. A., and Mathur, J. (2015). The myth of interconnected plastids and related phenomena. *Protoplasma* 252, 359–371. doi: 10.1007/s00709-014-0666-4

Shimada, H., Koizumi, M., Kuroki, K., Mochizuki, M., Fujimoto, H., Ohta, H., et al. (2004). ARC3, a chloroplast division factor, is a chimera of prokaryotic FtsZ and part of eukaryotic phosphatidylinositol-4-phosphate 5-kinase. *Plant Cell Physiol.* 45, 960–967. doi: 10.1093/pcp/pch130

Stewart, C. N.Jr. (2001). The utility of green fluorescent protein in transgenic plants. *Plant Cell Rep.* 20, 376–382. doi: 10.1007/s002990100346

Taiz, L., Zeiger, E., Møller, I. M., and Murphy, A. (2015). *Plant Physiology and Development, Sixth Ed* (Sunderland, MA: Sinauer Associates Inc.).

Tirlapur, U. K., and König, K. (2001). Femtosecond near-infrared lasers as a novel tool for non-invasive real-time high-resolution time-lapse imaging of chloroplast division in living bundle sheath cells of *Arabidopsis*. *Planta* 214, 1–10. doi: 10.1007/s004250100597

Ueki, S., Lacroix, B., Krichevsky, A., Lazarowitz, S. G., and Citovsky, V. (2009). Functional transient genetic transformation of *Arabidopsis* leaves by biolistic bombardment. *Nat. Protoc.* 4, 71–77. doi: 10.1038/nprot.2008.217

Vitha, S., Froehlich, J. E., Koksharova, O., Pyke, K. A., van Erp, H., and Osteryoung, K. W. (2003). ARC6 is a J-domain plastid division protein and an evolutionary descendant of the cyanobacterial cell division protein Ftn2. *Plant Cell* 15, 1918–1933. doi: 10.1105/tpc.013292

Waters, M. T., Fray, R. G., and Pyke, K. A. (2004). Stromule formation is dependent upon plastid size, plastid differentiation status and the density of plastids within the cell. *Plant J.* 39, 655–667. doi: 10.1111/j.1365-313X.2004.02164.x

Zhang, M., Hu, Y., Jia, J., Li, D., Zhang, R., Gao, H., et al. (2009). CDP1, a novel component of chloroplast division site positioning system in *Arabidopsis*. *Cell Res.* 19, 877–886. doi: 10.1038/cr.2009.78

Zhang, M., Chen, C., Froehlich, J. E., TerBush, A. D., and Osteryoung, K. W. (2016). Roles of Arabidopsis PARC6 in coordination of the chloroplast division complex and negative regulation of FtsZ assembly. *Plant Physiol.* 170, 250–262. doi: 10.1104/pp.15.01460

Zhao, L., and Sack, F. D. (1999). Ultrastructure of stomatal development in *Arabidopsis* (Brassicaceae) leaves. *Amer. J. Bot.* 86, 929–939. doi: 10.2307/2656609

Conflict of Interest: The authors declare that the research was conducted in the absence of any commercial or financial relationships that could be construed as a potential conflict of interest.

frontiers in Plant Science

ORIGINAL RESEARCH
published: 22 January 2020
doi: 10.3389/fpls.2019.01719

Two Arabidopsis Chloroplast GrpE Homologues Exhibit Distinct Biological Activities and Can Form Homo- and Hetero-Oligomers

Pai-Hsiang Su[1,2]*, *Hsuan-Yu Lin*[2] *and Yen-Hsun Lai*[2]

[1] Agricultural Biotechnology Research Center, Academia Sinica, Taipei, Taiwan, [2] Biotechnology Center in Southern Taiwan, Academia Sinica, Tainan, Taiwan

OPEN ACCESS

Edited by:
Yan Lu,
Western Michigan University,
United States

Reviewed by:
Long-Liu Lin,
National Chiayi University,
Taiwan
Toshifumi Tomoyasu,
Tokushima University,
Japan
Cuimin Liu,
Chinese Academy of Sciences,
China

***Correspondence:**
Pai-Hsiang Su
kennedy@gate.sinica.edu.tw

Specialty section:
This article was submitted to Plant Physiology, a section of the journal Frontiers in Plant Science

Received: 30 September 2019
Accepted: 06 December 2019
Published: 22 January 2020

Citation:
Su P-H, Lin H-Y and Lai Y-H (2020) Two Arabidopsis Chloroplast GrpE Homologues Exhibit Distinct Biological Activities and Can Form Homo- and Hetero-Oligomers. Front. Plant Sci. 10:1719. doi: 10.3389/fpls.2019.01719

Flowering plants have evolved two distinct clades of chloroplast GrpE homologues (CGEs), which are the nucleotide exchange factor for Hsp70. In Arabidopsis, they are named AtCGE1 (At5g17710) and AtCGE2 (At1g36390). Characterization of their corresponding T-DNA insertion mutants revealed that there is no visible change in phenotype except a defect in protein import in an *AtCGE2*-knockout mutant under normal growth conditions. However, the embryo development of an *AtCGE1*-knockout mutant was arrested early at the globular stage. An *AtCGE1*-knockdown mutant, harboring a T-DNA insertion in the 5′-UTR region, exhibited growth retardation and protein import defect, and its mutant phenotypes became more severe when *AtCGE2* was further knocked out. Sub-organellar distribution implied that AtCGE2 might be important for membrane biology due to its preferential association with chloroplast membranes. Biochemical studies and complementation tests showed that only AtCGE1, but not AtCGE2, can effectively rescue the heat-sensitive phenotype of *Escherichia coli grpE* mutant and robustly stimulate the refolding of denatured luciferase by DnaK. Interestingly, AtCGE1 and AtCGE2 are tending to form heterocomplexes, which exhibit comparable co-chaperone activity to AtCGE1 homocomplexes. Our data indicate that AtCGE1 is the principle functional homologue of GrpE. The possibility that AtCGE2 has a subsidiary or regulatory function through homo- and/or hetero-oligomerization is discussed.

Keywords: chloroplast GrpE homologue (CGE), embryo lethal, Hsp70, DnaK, luciferase refolding assay, oligomerization

INTRODUCTION

Almost all living organisms have 70-kD heat shock proteins (Hsp70) in most cellular compartments, including the cytoplasm, endoplasmic reticulum (ER), mitochondria, and chloroplasts. In addition to the general function of assisting protein folding, emerging roles of Hsp70 are being reported in animal cells, including gene regulation, protein translocation and degradation, signal transduction, and cell apoptosis (Mayer and Bukau, 2005; Joly et al., 2010;

Kampinga and Craig, 2010). However, experimental evidence to support the biological functions of Hsp70 in the plant system is still scarce. Sung and Guy (2003) showed that the cytosolic Hsp70 overexpression can enhance the heat tolerance of Arabidopsis under certain conditions. Leborgne-Castel et al. (1999) reported that overexpressing ER-localized Hsp70 (Bip) in tobacco plants alleviated ER stress and increased drought tolerance, but no effect on heat tolerance was observed. In green algae, it has been shown that chloroplast Hsp70 may be involved in the protection of the photosystem and repair after photoinhibition (Schroda et al., 1999; Yokthongwattana et al., 2001). In *Chlamydomonas*, chloroplast Hsp70 mediates the assembly of vesicle inducing protein in plastid 1 (VIPP1), which may facilitate the biogenesis and maintenance of thylakoid membrane (Liu et al., 2007). However, whether chloroplast Hsp70 in flowering plants also exhibits similar functions to its algal counterparts is still uncertain. Recently it has been demonstrated that plastid Hsp70s are essential for chloroplast and plant development and are important for seed basal thermotolerance in Arabidopsis (Su and Li, 2008; Latijnhouwers et al., 2010). Genetic and biochemical analyses revealed that plastid Hsp70s function as the molecular motor driving precursor proteins into chloroplasts in moss, pea, and Arabidopsis (Shi and Theg, 2010; Su and Li, 2010; Liu et al., 2014).

The chloroplast Hsp70 chaperone system is derived from the cyanobacterial endosymbiotic ancestor. In general the system is composed of three core members: Hsp70, DnaJ, and GrpE homologues. In Arabidopsis, there are two chloroplast Hsp70s (cpHsc70-1 and cpHsc70-2), two chloroplast GrpE homologues (AtCGE1 and AtCGE2), and 19 chloroplast DnaJ homologues (Su and Li, 2008; Hu et al., 2012; Chiu et al., 2013). The functions of individual co-chaperone family members are still largely unknown. It has been shown that small J proteins (AtJ8, AtJ11, and AtJ20) may contribute to the optimization of photosynthesis (Chen et al., 2010). In *Chlamydomonas*, CGE1 cooperates with Hsp70 to mediate the assembly of VIPP1 protein complex (Liu et al., 2007) and the formation of Hsp70/Hsp90 multichaperone complex (Willmund et al., 2008). *Physcomitrella* CGE proteins play a crucial role in protein import (Shi and Theg, 2010). In recent, de Luna-Valdez et al. (2019) proposed that land plants have evolved two independent groups of CGE proteins with distinguishable variations in conserved short motifs. It is suggested that AtCGE1 is involved in specific physiological phenomena in Arabidopsis, such as the chloroplast response to heat stress, and the correct oligomerization of photosynthesis-related LHCII complex (de Luna-Valdez et al., 2019). However, the physiological significance of AtCGE2 and the difference in co-chaperone activities between AtCGE1 and AtCGE2 are still unknown.

From genomic survey and phylogenetic analysis, we revealed that flowering plants have evolved two distinct clades of CGE homologues prior to the divergence of monocot and dicot lineages. To understand the functional differences between these two clades of CGEs in flowering plants, we performed genetic and biochemical analyses of the two Arabidopsis CGEs. Our data show that two AtCGEs exhibit different co-chaperone activities. AtCGE1 functions as a bona fide GrpE homologue with an essential function in embryo development, and AtCGE2 seems to be subsidiary or have a regulatory function to diversify the CGE co-chaperone activities.

MATERIALS AND METHODS

Data Mining and Phylogenetic Analysis

Genomic resources were obtained from National Center for Biotechnology Information (NCBI), Ensembl_Plants, the DOE Joint Genome Institute, and the Rice Genome Annotation Project through the web sites listed in **Table S1**. Sequences which were ambiguous due to poor sequencing data were not used for further analysis. Finally, a total of 62 CGE protein sequences from 34 sequenced genomes were adopted for the construction of a phylogenetic tree by ClustalW alignment and the neighbor-joining method in MEGA6 software (Tamura et al., 2013).

Plant Growth Conditions

For plate culture, Arabidopsis seeds were sterilized with 1.5% sodium hyperchloride for 10 min, washed with sterile water 5 times, and plated on 0.3% gellan gum-solidified 1× Murashige and Skoog (MS) medium containing 2% sucrose. After a 3-d cold stratification, seeds were grown in a growth chamber under 16-h photoperiod with a light intensity around 70 μmol m^{-2} s^{-1} at 22°C. For soil culture, Arabidopsis seeds were imbibed and cold-stratified for 3 d in a refrigerator and sowed on a 9:1:1 mixture of peat, vermiculite, and perlite under a 16-h photoperiod with a light intensity approximately 100 μmol m^{-2} s^{-1} at 24°C.

Identification and Characterization of the T-DNA Insertion Mutants of *CGE*s

The candidate T-DNA insertion mutants were searched by the SIGnAL T-DNA Express platform (http://signal.salk.edu/cgi-bin/tdnaexpress). Seeds of candidate lines, FLAG_136H03 (*atcge2-1*), FLAG_079G12 (*atcge1-3*), SALK_004126 (*atcge2-2*), SALK_005391 (*atcge1-2*), and WiscDxLoxHs045_03B (*atcge1-1*) were obtained from ABRC (Arabidopsis Biological Resource Center) and INRA (French National Institute for Agricultural Research) (Brunaud et al., 2002; Alonso et al., 2003; Woody et al., 2007) and confirmed by genomic PCR with specific primers. For amplifying the wild-type copy of *AtCGE2*, primer pairs of CGE2P-S and CGE2t-AS were used. Primer pairs of CGE2P-S and Tag5 were used for amplifying the *atcge2-1* specific T-DNA copy, and primer pairs of LBa1-2 and CGE2t-AS were used for identifying the *atcge2-2*. For amplifying the wild-type copy of *AtCGE1*, primer pairs of CGE1P-S + CGE1I2-AS or CGE1E1-S + CGE1t-AS were used. Primer pairs of CGE1P-S and pDs-LoxHs-L4' were used for amplifying the *atcge1-1* specific T-DNA copy; primer pairs of LBa1-2 and CGE2t-AS were used for identifying the *atcge1-2*; and primer pairs of CGE1P-S and Tag5 were used for identifying the *atcge1-3*. The T-DNA insertion sites were verified by sequencing the PCR products. Primers pairs used for

checking *AtCGE2* and *AtCGE1* transcripts by reverse transcription-polymerase chain reaction (RT-PCR) were CGE2-S + CGE2-AS and CGE1E1-S + CGE1-AS, respectively. Individual insertion mutants were back crossed to their relative wild type to select their single insertion mutants for phenotype characterization, crossing, and functional analyses. Total chlorophyll was determined by the method described by Lichtenthaler (Lichtenthaler, 1987). Sequences of oligonucleotide primers are listed in **Table S2**.

In Vitro Translation and Protein Import Assay

[^{35}S]-Methione-labeled prRBCS were *in vitro* transcribed/translated with TNT® Coupled Wheat Germ Extract System driven by SP6 promoter (Promega). Chloroplasts were isolated from 24-d-old seedlings grown on MS medium containing 2% sucrose. Import assays were conducted as described in Perry et al. (1991), except the grinding buffer was modified to 50 mM HEPES-KOH (pH 8.0), 330 mM sorbitol, 2 mM EDTA, and 0.5% bovine serum albumin. After import, intact chloroplasts were re-isolated through 40% Percoll cushion for SDS-PAGE analysis (NuPAGE 4–12% Bis-Tris gel, Invitrogen), and import was visualized by radiography with intensifying screens or by phosphor-imaging. Quantification of gel bands was performed using the Typhoon Trio phosphor-imager and ImageQuant TL software (GE Healthcare).

Sub-Organellar Fractionation

Intact Arabidopsis chloroplasts were isolated from 21-d-old plate-grown seedlings of wild type, and suspended in import buffer. Lysis of chloroplasts was performed by resuspending pelleted intact chloroplasts in hypotonic buffer [50 mM HEPES-KOH (pH 8.0), 50 mM NaCl, and 5 mM $MgCl_2$], or in alkaline extraction buffer containing 0.1 M Na_2CO_3 (pH 11.5). Lysis mixture was incubated at 4°C for 30 min with mild vortex and then frozen overnight in −20°C freezer. Thereafter, the thawed samples were separated into membranes and soluble fractions by ultracentrifugation at 100,000 g for 45 min, and repeated once to ensure a sufficient fractionation. Total chloroplast protein, lysed supernatant, and pellet (membrane fraction) were then resolved on PAGE, transferred onto polyvinylidene fluoride (PVDF) membrane, and decorated with Western blotting against AtCGE2 and AtCGE1 antibodies, respectively. The CBR-stained LHCB and RBCS were used as the controls of membrane and stromal fraction, respectively.

Expression of Recombinant CGE Proteins and Antibody Preparation

Using proofreading Phusion DNA polymerase, the coding sequences of mature regions of *AtCGE2* and *AtCGE1* were amplified by PCR with specific primer pairs, CGE2-NdeI-S + CGE2-XhoI-AS and CGE1-NdeI-S + CGE1-XhoI-AS, respectively. The amplified DNA fragments were cut with *Nde*I and *Xho*I, and subcloned onto pET22b (Novagen) expression vectors trimmed with the same restriction enzymes to generate the 6xHis-tagged recombinant constructs, designated as pET22b-AtCGE2 and pET22b-AtCGE1, respectively. After being confirmed by DNA sequencing, the recombinant plasmids were transformed into *Escherichia coli*. BL21 (DE3) for IPTG (Isopropyl β-D-1-thiogalactopyranoside) induced overexpression. Recombinant AtCGE proteins were affinity-purified by Talon beads (Clontech Laboratories) for chaperone activity assay and customer antibody production (GeneTex). To generate the V294A mutation of AtCGE1 on pET22b, site-directed mutagenesis was conducted with mutated primer pairs, CGE1-V294A-S + CGE1-V294A-AS. To express AtCGE1/2 heterodimer, the coding sequence of mature AtCGE1 was amplified by PCR with primer pairs XhoI-CGE1-S and XhoI-CGE1-AS, and then subcloned onto *Xho*I-cut pET22b-Ptac-AtCGE2 plasmid (see below) to generate a polycistronic cassette named as pET22b-Ptac-AtCGE2-CGE1, in which AtCGE1 is tagged with 6xHis and AtCGE2 was tag-free. Purification procedure of mutated AtCGE1 and AtCGE1/2 heterodimer was was according to the user's manual of Talon metal affinity resins (Clontech Laboratories).

Functional Complementation of *E. coli grpE* Mutant

The heat-sensitive *E. coli* DA16 harbors a *grpE280* mutation (Johnson et al., 1989). Because DA16 lacks the λDE3 fragment for inducible expression of T7 RNA polymerase, the expression cassette driven by T7 promoter on the pET22b vector could not be turned on by IPTG. Therefore, we replaced the T7 promoter with *tac* promoter to generate the pET22b-Ptac vector, which enables IPTG-induced overexpression in DA16. Then the coding sequences of *grpE* and the mature regions of *AtCGE2* and *AtCGE1* were subcloned onto this vector as described above. The resulting plasmids were named as pET22b-Ptac-GrpE, -AtCGE2, and -AtCGE1, respectively. For complementation test, wild-type *grpE* construct tagged with 6xHis was used as a positive control. After 2-h induction by a serial concentration of IPTG at 30°C on solid agar plates, the transformed bacteria were heat challenged at high temperature as indicated. The overnight cultured plates were photographed by digital camera to record the results of complementation. To co-express both AtCGEs in DA16 mutant, the T7 promoter of pCOLA vector (Novagen) was replaced by *tac* promoter to generate pCOLA-Ptac vector, then the coding sequence of *AtCGE2* was subcloned on this vector to generate pCOLA-Ptac-AtCGE2 plasmid with S-tag in frame. Finally, pCOLA-Ptac-AtCGE2 and pET22b-Ptac-AtCGE1 were co-transformed into *E. coli* DA16.

Luciferase Refolding Assay

Using the pJKE7 plasmid (Takara Bio), which harbors *dnaK*, *dnaJ*, and *grpE* genes, as template DNA, the protein-coding sequences of *dnaK*, *dnaJ*, and *grpE* were amplified by PCR, and were respectively subcloned onto the expression vectors of pACYC-T7, pET21d, and pET22b-Ptac. Their resulting plasmids were named pACYC-T7-DnaK, pET21d-DnaJ, and pET22b-Ptac-GrpE and were transformed into *E. coli* for overexpression. All recombinant proteins of DnaK, DnaJ, GrpE, and AtCGEs were fused with a 6xHis tag and were

affinity purified by Talon metal affinity beads according to the user's manual (Clontech Laboratories). The *E. coli* BL21(DE3) strain was used for IPTG-induced overexpression of DnaJ, GrpE, and AtCGE proteins, and the KRX strain (Promega) was used for rhamnose-controlled overexpression of DnaK. Purified proteins underwent dialysis in common buffer [25 mM Hepes-KOH (pH 7.8), 5 mM $MgCl_2$, and 5 mM DTT] containing 100 mM NaCl and were quantified by BCA protein assay kit (Pierce), then stored in −80°C deepfreezer at 100 μM concentration in small aliquot. Refolding of denatured firefly luciferase was modified from Sugimoto et al. (2007). Briefly, luciferase was chemically denatured in 6 M guanidine hydrochloride for 30 min at 25°C. Refolding was conducted by adding denatured luciferase into common buffer containing 100 mM KCl, chaperone mixture, and 3 mM ATP, mixing well, and incubating for 30 min at 25°C. The protein concentrations used are DnaK (5 μM), DnaJ (1 μM), and luciferase (100 nM). For GrpE and AtCGEs, serial concentrations from 0.5 to 32 μM were used as indicated in the figures. After reaction, 10 μl of refolding mixture was sampled for luciferase activity assay in a final 125 μl common buffer containing 1 mM ATP and 0.25 mM D-luciferin. The luminescence was measured by a luminometer (Victor X2 multilabel plate reader, PerkinElmer). Activity of native luciferase was assayed as a positive control.

Crosslinking of Purified AtCGEs by Glutaraldehyde

Crosslinking experiment was modified from Wu et al. (1996). Five micromolar proteins in common buffer were crosslinked with glutaraldehyde at 0.05, 0.1, and 0.2% for 10 min. After crosslinking, their oligomeric states were visualized by PAGE analysis and CBR staining.

RESULTS

Phylogenetic Analysis Revealed That Flowering Plants Have Evolved Two Distinct Clades of CGEs

Survey of sequenced plant genomes revealed that most flowering plants contain at least two copies of *CGE* homologues, instead of a single genomic copy as found in cyanobacteria, algae, and *Selaginella*. To understand their evolutionary relationship, a phylogenetic tree was constructed with 62 CGE protein sequences from 34 sequenced genomes using the MEGA6 program (Tamura et al., 2013). As shown in **Figure 1**, flowering plants have evolved two distinct clades of CGEs, which were grouped into CGE1 and CGE2 homologues, respectively, with a bootstrap value (74% of 1,000 replicates). It was shown that two CGEs of *Amborella*, which is an ancient plant diverging near the base of flowering plant lineages, were also grouped into CGE1 and CGE2 clades respectively, indicating that these two CGE clades of flowering plants may have evolved prior to the divergence of monocot and dicot lineages. There are duplicated copies in the same clade in some species with more recent whole genome duplication or polyploidy, such as *Brassica rapa*, *Triticum aestivum*, and *Zea mays*. Notably, *Physcomitrella patens* also has two CGEs, which seem to be derived from a more recent duplication based on their high similarity with 85% sequence identity in mature proteins, and are grouped into the same clade. In *Chlamydomonas*, two CGE isoforms (namely CGE1a and CGE1b) with only a two-amino acid difference are encoded by a single gene with an alternative splicing of mRNA (Schroda et al., 2001).

Characterizations of Arabidopsis *atcge1* and *atcge2* Mutants

To understand the biological significance of having two clades of CGE homologues, we conducted further studies using Arabidopsis CGEs. Data mining of a microarray database revealed that there is not a large difference in RNA expression patterns and levels between *AtCGE2* and *AtCGE1* (access through Arabidopsis eFP browser at http://bar.utoronto.ca/efp_arabidopsis/cgi-bin/efpWeb.cgi), implying possible functional redundancy. *AtCGE* T-DNA insertion mutants were further isolated for characterization (**Figure 2** and **Figure S1**). The actual T-DNA insertion sites after being re-confirmed by genomic PCR and DNA sequencing are illustrated in **Figure 2A**. Knockout mutations of *AtCGE1* (*atcge1-1* and *atcge1-2*) caused an embryo lethal phenotype. During seed development, approximately one quarter of the seeds produced from the heterozygous *atcge1-1* mutant showed bleaching color at the torpedo stage and brown aborted seeds at the mature green stage (**Figure 2B**). Differential interference contrast (DIC) microscopic observation of developing seeds at the torpedo stage revealed that embryogenesis of these bleaching seeds was arrested at the early globular stage (**Figure 2C**). It is surprising that *AtCGE2* cannot compensate the defect of *AtCGE1* although their RNA expression patterns and levels are quite similar, suggesting that the two proteins may have different functions or activities. We also isolated a viable *AtCGE1*-knockdown mutant, *atcge1-3*, which has a T-DNA insertion in the 5′-UTR region and produces almost no detectable AtCGE1 protein (**Figure 2D**). To avoid the uncertain effect caused by different ecotypes, *atcge1-3* and *atcge2-1* (both are of WS4 ecotype) were selected for further analysis. There was no visible mutant phenotype in *AtCGE2*-knockout plants (*atcge2-1*) under normal growth conditions (**Figure 2E**). The *atcge1-3* mutant exhibited a growth retardation phenotype (**Figure 2E**). In 21-d soil-grown seedlings, the above-ground tissue fresh weight of *atcge1-3* only reached 60% of that of the wild type (**Figure 2F**). When *atcge1-3* was crossed to *atcge2-1*, their double mutant progeny showed more severe growth retardation (**Figures 2E, F**). The fresh weight and chlorophyll content of *atcge1-3 atcge2-1* were reduced to 40% and 80% of that of the wild type, respectively (**Figures 2F, G**). Taken together these results show that AtCGE1 is essential for embryogenesis, and important for plant growth. In contrast, AtCGE2 is dispensable under normal growth conditions, but becomes important when AtCGE1 is knocked down. AtCGE2 may be partially functionally redundant to AtCGE1 or may mediate AtCGE1 function under some conditions.

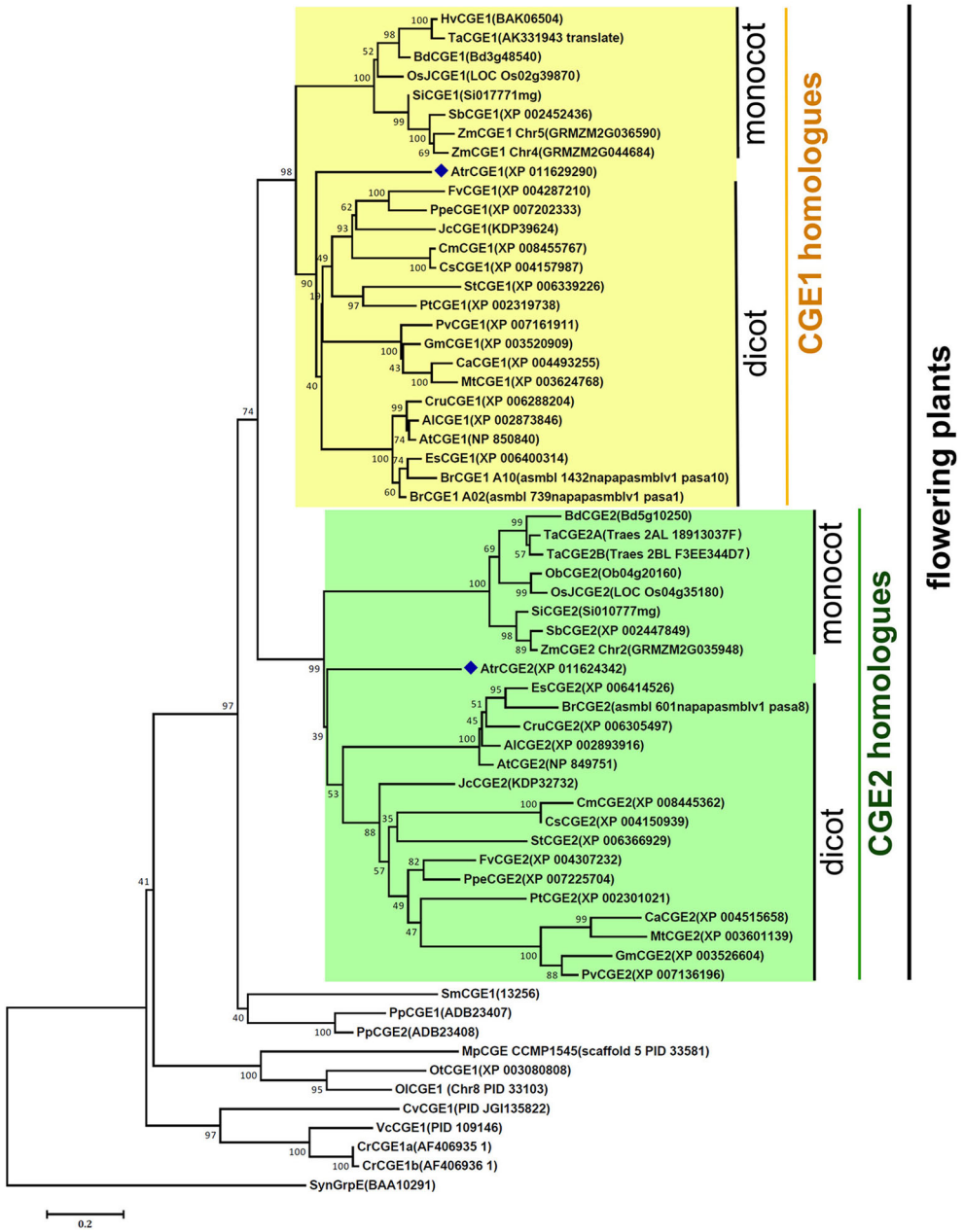

FIGURE 1 | A phylogenetic tree of species CGE proteins. The tree was constructed by using the neighbor-joining method in MEGA6 (19) with 62 CGE proteins (see aligned sequences in **Data S1**). Bootstrap Values are shown as a percentage of 1,000 replicates. The evolutionary distances were computed using the Dayhoff matrix based method and are in the units of the number of amino acid substitutions per site. The rate variation among sites was modeled with a gamma distribution (shape parameter = 2). All ambiguous positions were removed for each sequence pair. Al, *Arabidopsis lyrata*; At, *Arabidopsis thaliana*; Atr, *Amborella trichopoda*; Bd, *Brachypodium distachyon*; Br, *Brassica rapa*; Ca, *Cicer arietinum*; Cm, *Cucumis melo*; Cr, *Chlamydomonas reinhardtii*; Cru, *Capsella rubella*; Cs, Cucumis sativus; Cv, *Chlorella variabilis*; Es, *Eutrema salsugineum*; Fv, *Fragaria vesca*; Gm, *Glycine max*; Hv, *Hordeum vulgare*; Jc, *Jatropha curcas*; Mp, *Micromonas pusilla*; Mt, *Medicago truncatula*; Ob, *Oryza brachyantha*; OsJ, *Oryza sativa* Japonica Group; Ol, *Ostreococcus lucimarinus*; Ot, *Ostreococcus tauri*; Pp, *Physcomitrella patens*; Ppe, *Prunus persica*; Pt, *Populus trichocarpa*; Pv, *Phaseolus vulgaris*; Sb, *Sorghum bicolor*; Si, *Setaria italica*; Sm, *Selaginella moellendorffii*; St, *Solanum tuberosum*; Syn, *Synechocystis*; Ta, *Triticum aestivum*; Vc, *Volvox carteri*; Zm, *Zea mays*.

The *atcge* Mutants Defect in Chloroplast Protein Import

It has been shown that chloroplast Hsp70 is engaged in chloroplast protein import in *Physcomitrella*, Arabidopsis, and pea (Shi and Theg, 2010; Su and Li, 2010), and *Physcomitrella* CGEs are important for efficient protein import (Shi and Theg, 2010). To investigate whether flowering plant CGEs are also involved in this essential process, *in vitro* protein import of [^{35}S]-

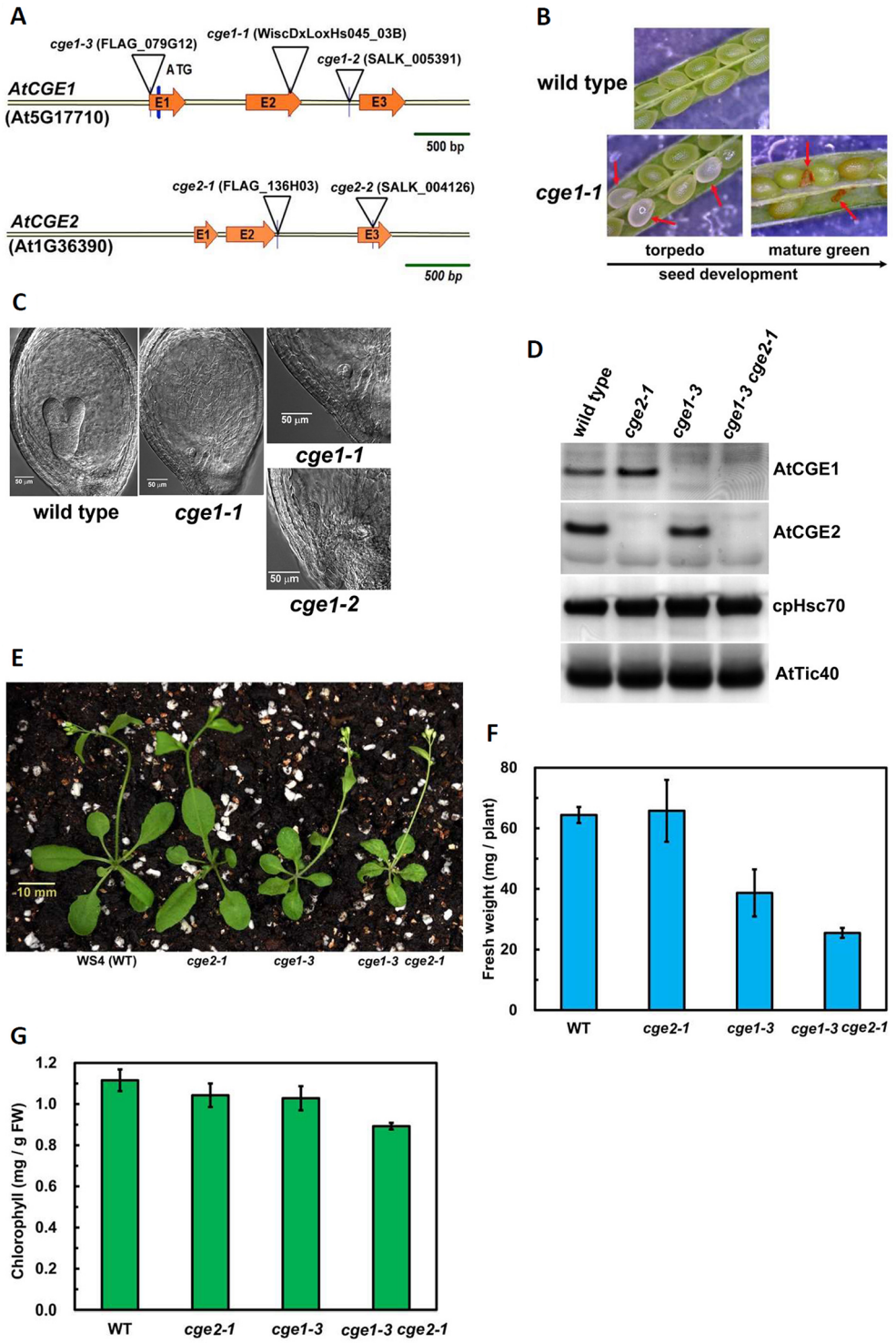

FIGURE 2 | Characterization of *atcge* mutants. **(A)** Illustration of T-DNA insertion sites in the genomic fragments of *AtCGE1* (At5g17710) and *AtCGE2* (At1g36390). Both AtCGE1 and AtCGE2 contain three exons, designated as E1, E2, and E3. **(B)** Observing aborted seeds of *atcge1-1* mutant in the siliques at the torpedo and the mature green stages under dissecting microscopy. **(C)** Microscopic observation of embryogenesis in wild type and *atcge* mutants at the torpedo stage. **(D)** Western blot of total chloroplast proteins isolated from wild type and *atcge* mutants. Samples were loaded with equal chlorophyll. Antibodies used are indicated on the right sides of blots. **(E)** Photograph of 21-d-old soil-grown seedlings. Fresh weight **(F)** and chlorophyll content **(G)** of the above-ground part of wild type and *atcge* mutants. Data are the means ± SD of three replicates.

methione-labeled precursor to the small subunit of Rubisco (prRBCS) was assayed. The *atcge1-3* chloroplasts showed a severe import defect, and their imported RBCS only reached to about a half of that of wild-type chloroplasts after a 16-min import (**Figure 3** and **Figure S2**). It was noticeable that *atcge2-1* chloroplasts also exhibited a remarkable import defect, but to a quite milder degree compared to *atcge1-3* (**Figure 3** and **Figure S2**), although the *atcge2-1* plant did not show visible mutant appearance under normal growth conditions (**Figure 2E**). The *atcge1-3 atcge2-1* double mutant seemed to display a more severe import defect than both single mutants (**Figure 3** and **Figure S2**). These results indicated that AtCGE2 might still be important for plant vigor under normal conditions. It is noted that the steady-state level of AtCGE1 protein seems to be increased in *atcge2-1* mutant (**Figure 2D**), possibly implying the loss of AtCGE2 may have a consequential effect on plant physiology. In summary, both AtCGEs may contribute to chloroplast protein import by mediating the action of chloroplast Hsp70s.

Sub-Organellar Fractionation of AtCGEs

We next analyzed the sub-organellar fractionation of AtCGEs. As shown in **Figure 4**, we found that AtCGE1 is exclusively located in the soluble part either fractionated by hypotonic buffer or the alkaline extraction method. In comparison, a portion of AtCGE2 did associate with chloroplast membranes fractionated by hypotonic buffer, but not by alkaline extraction, indicating a possible role of AtCGE2 by peripheral membrane association, such as in protein import (**Figure 3**).

Functional Complementation of *E. coli grpE* Mutant

E. coli DA16 (*grpE280*) is a heat-sensitive mutant carrying a G122D missense mutation in GrpE, which impairs interaction of GrpE with DnaK and the ADP/ATP-exchange activity of GrpE (Ang et al., 1986; Grimshaw et al., 2005). For complementation test, mature AtCGE1 and AtCGE2, in which transit peptides were removed, were expressed in DA16 mutant to determine the degree of thermotolerance. Chloroplast transit peptides (cTP) of AtCGEs were surveyed through the PPDB database (http://ppdb.tc.cornell.edu) (Sun et al., 2009) and predicted by the ChloroP program (Emanuelsson et al., 1999) (**Figure 5A**). Additionally AtCGE1 has a predicted lumen transit peptide (lTP) (the boxed region in **Figure 5A**) annotated in the PPDB database. Therefore, we also constructed an lTP-deleted clone, named AtCGE1ΔlTP. Notably, the current proteomic study indicates that AtCGE1 is a stromal protein (Peltier et al., 2006), and AtCGE1 was not identified in the lumen proteome of Arabidopsis chloroplasts (Schubert et al., 2002). It was found that AtCGE1 (with or without lTP) can efficiently complement the heat-sensitive phenotype of DA16 after IPTG induction. Although AtCGE2 was highly expressed in DA16, no obvious complementation ability could be detected at either 40°C or 42°C (**Figures 5B, C**). It was noted that, for unknown reason, there were two induced protein bands in the AtCGE1ΔlTP construct (**Figure 5C**), and both of them can be recognized by an anti-AtCGE1 antibody

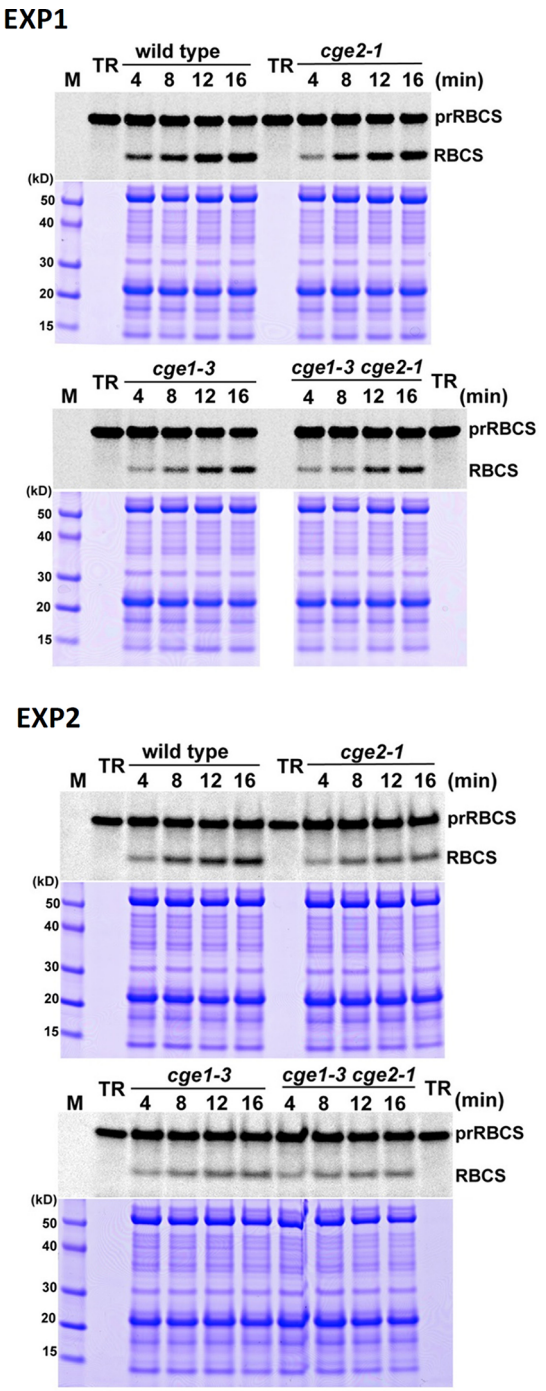

FIGURE 3 | The *atcge* mutants had defects in chloroplast protein import. The prRBCS import into chloroplasts isolated from wild-type and mutant seedlings grown on MS medium for 24 d. *In vitro* import assays were conducted for 4 to 16 min with [^{35}S]Methionine-labeled prRBCS. After import, intact chloroplasts were reisolated and analyzed by PAGE. The gels were stained with Coomassie blue, scanned, and then dried for phosphoimaging. The region of each stained gel between the endogenous large and small subunits of Rubisco is shown below the phosphoimage. Two independent experiments (EXP1 and EXP2) are shown. TR, *in vitro*–translated [^{35}S]Met-prRBCS before the import reactions.

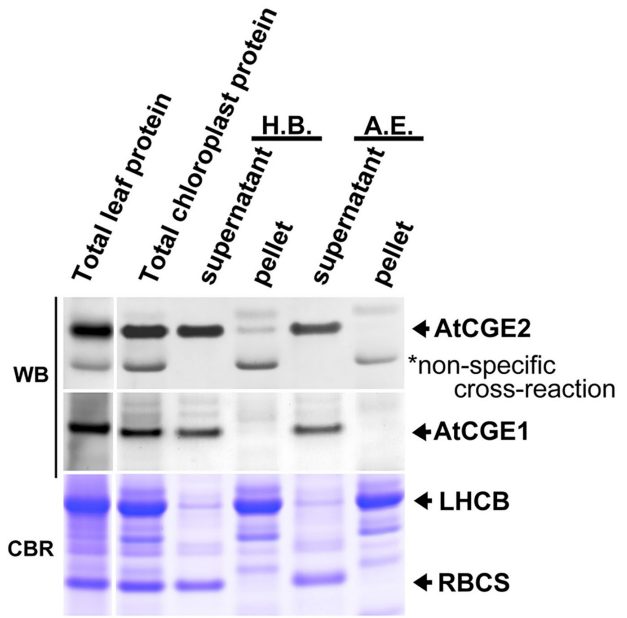

FIGURE 4 | Sub-organellar distribution of AtCGEs. Total chloroplast proteins were fractionated by ultracentrifugation after being lysed with hypotonic buffer (H.B.) or alkaline extraction (A.E.). Samples were resolved by PAGE and visualized by Western blot (WB). Coomassie Blue R-250 (CBR) stained light-harvesting chlorophyll a/b binding (LHCB) proteins and the small subunit of Rubisco (RBCS) were used as membrane and stromal protein control, respectively. Samples were loaded with equal proportion.

(**Figure S3**). It is interesting that *E. coli* GrpE can complement the DA16 mutant even before IPTG induction due to a leaky expression and its complementation ability actually decreased after a higher expression level was induced at a higher IPTG concentration (**Figures 5B, C**). This observation supports the notion that a proper GrpE/DnaK ratio is critical for adequate chaperone activity as described in Sugimoto et al. (2008). Therefore we cannot exclude the possibility that the inability of AtCGE2 to complement the DA16 mutant may be due to its excess expression.

In Vitro Luciferase Refolding Assay

Functional complementation assay revealed that only AtCGE1, and not AtCGE2, can complement the heat-sensitive DA16 mutant. To further confirm whether the complementation ability is really directly correlated with their co-chaperone activity, their stimulation of luciferase refolding by DnaK/J was analyzed. Recombinant DnaK, DnaJ, GrpE, AtCGE2, and AtCGE1 with His-tag were purified with high purity as shown in **Figure 6A**. Chemically denatured luciferase was refolded by 5 μM Dnak plus 1 μM DnaJ and stimulated by GrpE homologues from 0.5 to 32 μM. Data was represented as percentage luciferase activity recovery. It has been shown that a proper ratio of GrpE to DnaK is critical for chaperone activity of DnaK system (Sugimoto et al., 2008). Results of our GrpE control were consistent with those previously reported. Refolding of luciferase was stimulated at lower GrpE concentration and inhibited by higher GrpE/DnaK ratio (**Figure 6B**). There was no obvious stimulation by AtCGE2 at tested concentrations. AtCGE1 exhibited a concentration-dependent increase in stimulation of luciferase refolding (**Figure 6B**). Even in higher AtCGE1/DnaK ratio, there is no inhibitory effect on DnaK refolding activity, implying that although AtCGE1 has a good co-chaperone activity to DnaK, it may harbor distinct regulatory mechanism to GrpE. Further analyses of reciprocal exchange in chaperone/co-chaperone pairs between DnaK/GrpE and Hsp70/CGE may be needed to clarify this issue in the future. Next, to clarify whether the detected co-chaperone activity of AtCGE1 really originated from our target protein, we tried to make loss-of function mutations on two conserved Val residues of AtCGE1 by site-directed mutagenesis. It is noted that a Val-Lys-Val tri-residue motif is conserved in all plant CGE proteins. Instead, *E. coli* GrpE has a Val-Thr-Val (residues 190–192) tri-residue motif, which is located in the β-domain. Gelinas et al. (2004) have shown that the V192A mutation of GrpE destabilizes the GrpE β-domain and losses its ability to interact with DnaK. The Val294 and Val296 of AtCGE1 are respectively corresponding to the Val190 and Val192 of GrpE. Finally, we only got the V294A mutation of AtCGE1. *In vitro* refolding assay revealed that the co-chaperone activity of AtCGE1^{V294A} was almost totally abolished (**Figure 6C**). *In vivo* complementation test also showed that AtCGE1^{V294A} almost lost its complementation ability (**Figure 6D**). It convinces the important role of the Val294 residue on the co-chaperone activity of AtCGE1 proteins. Taken together, these results support the notion that the detected activity is truly conferred by the co-chaperone activity of AtCGE1, and not caused by contamination of other co-purified proteins with chaperone/co-chaperone activities during purification. Therefore, we suggest that AtCGE1 is a bona fide functional GrpE homologue based on its *in vivo* complementation ability and *in vitro* co-chaperone activity, although it may have evolved different co-chaperone properties from GrpE to cope with the need of chloroplast Hsp70 system. Furthermore, no detectable co-chaperone activity by AtCGE2 implies that its inability to complement the DA16 mutant is most probably due to the lack of co-chaperone activity, and not caused by its excess expression.

AtCGE1 and AtCGE2 Can Form a Heterocomplex With Co-Chaperone Activity

To test whether AtCGE1 and AtCGE2 can form a heterocomplex, we co-expressed AtCGE1 and AtCGE2 in *E. coli* BL21(DE3). We tagged AtCGE1 with 6xHis. As shown in **Figure 7A**, the crude protein extract (see the "input" lane) contained a high AtCGE2/AtCGE1 ratio due to higher expression level of AtCGE2 as observed previously (**Figure 5C**). Following Talon-bead binding, the flow-through sample had no visible AtCGE1 band, implying most AtCGE1 was bound to beads. After stringent wash, AtCGE2 was co-eluted with His-tagged AtCGE1 with a molar ratio approximately 1:1, indicating a robust formation of heterocomplex between AtCGE1 and

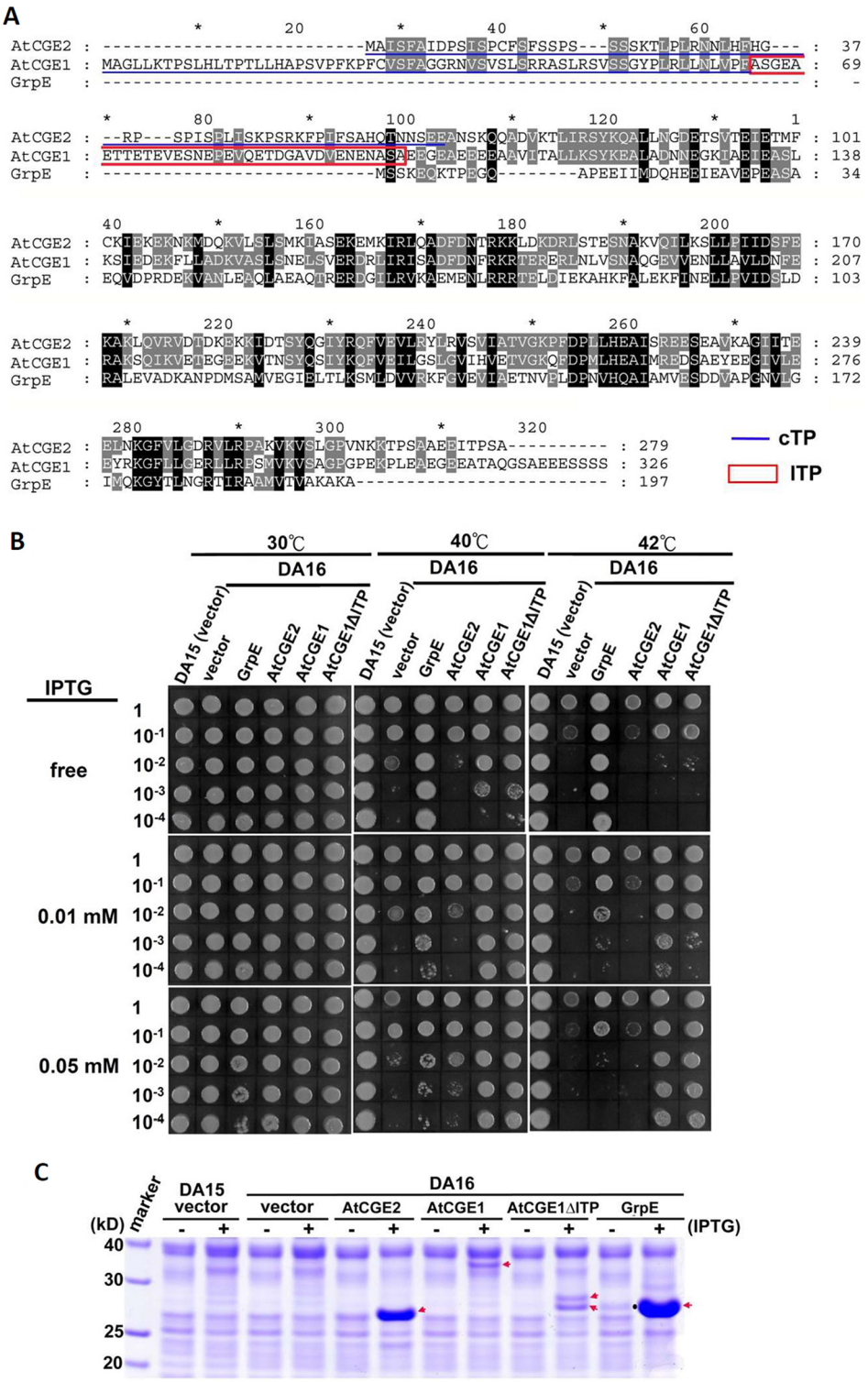

FIGURE 5 | Functional complementation of *E. coli grpE* mutant (DA16) by *AtCGE*s. **(A)** Alignment of GrpE homologues. Underlines represent predicted chloroplast transit peptide (cTP), and a boxed region indicates a putative lumen transit peptide (ITP). **(B)** Complementation of the DA16 mutant by expressing AtCGEs. Overnight liquid culture of DA16 mutant harboring GrpE, AtCGE1, or AtCGE2 was refreshed in LB, and grown to OD_{600} about 0.8. A serial dilution of bacterial suspension (4 μl) was dropped on IPTG-free or -containing LB agar plates for 2 h pre-induction at 30°C, then challenged with different heat shock condition as indicated. DA15 is the wild counterpart of DA16 mutant. **(C)** Induction test of GrpE homologues. Arrows indicates the protein bands induced by IPTG. A dot in GrpE/IPTG-free lane indicates the leaky-expressed GrpE.

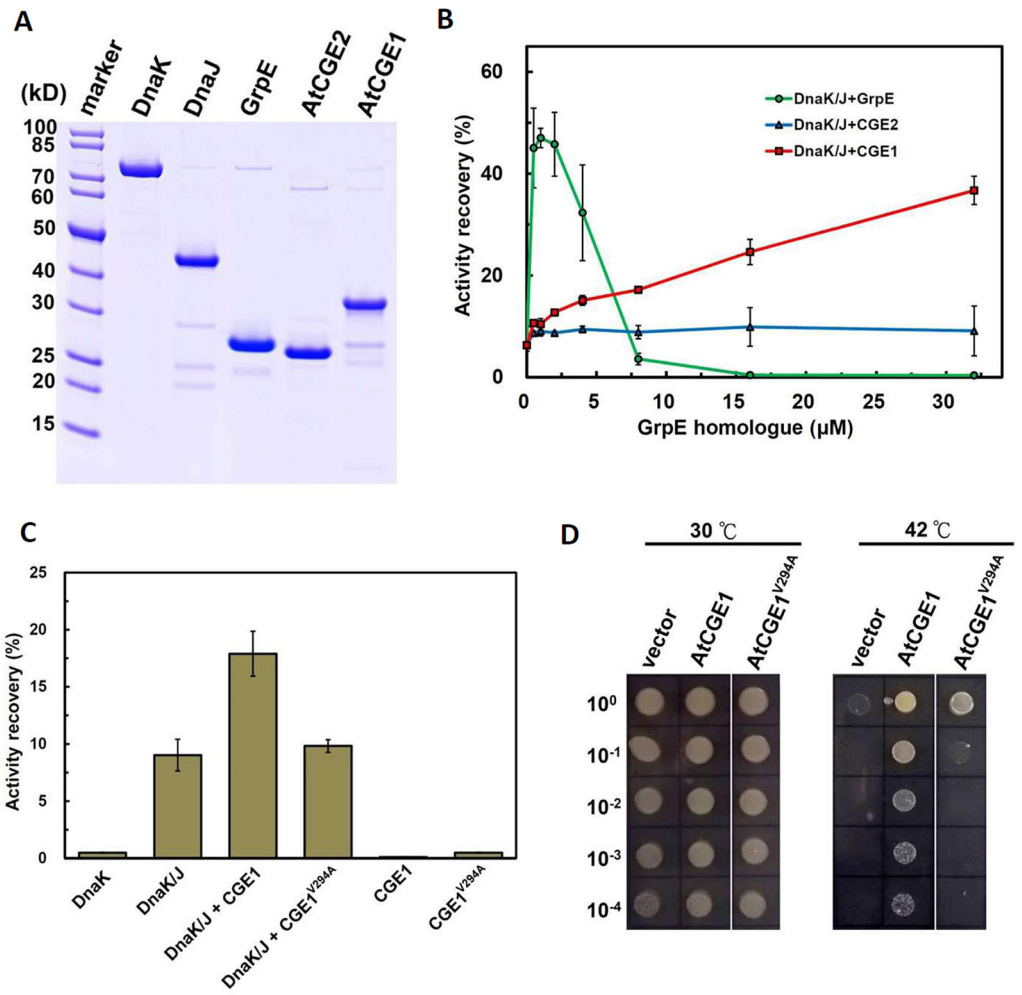

FIGURE 6 | AtCGE1, but not AtCGE2, exhibited GrpE-like cochaperone activity. **(A)** Recombinant proteins of Dnak, DnaJ, GrpE, and AtCGEs were affinity purified, resolved on PAGE, and stained by CBR. **(B)** A dosage response of GrpE homologues on stimulating the luciferase refolding by DnaK/J machinery. DnaK and DnaJ concentrations are 5 and 1 μM, respectively. **(C)** Activity recovery of chemically denatured luciferase by DnaK/J machinery with the stimulation of wild-type or mutated AtCGE1 as indicated. The concentration of DnaK, DnaJ, and AtCGE1 are 5, 1, and 16 μM, respectively. **(D)** *E. coli* DA16 complementation by wild-type and mutated AtCGE1. After 2 h pre-induction on LB plate containing 0.05 mM IPTG at 30°C, the bacteria were challenged at 42°C for overnight.

AtCGE2. *In vitro* luciferase refolding assays demonstrated that AtCGE1/2 heterocomplex efficiently stimulated DnaK/J-mediated luciferase refolding with comparable activity to that of AtCGE1 homocomplex (**Figure 7B**). Further, *in vivo* complementation assays also showed that co-expressed AtCGE1/2 functioned similarly to AtCGE1 in rescuing the DA16 heat-sensitive phenotype (**Figures 7C, D**).

AtCGE1 and AtCGE2 Undergo Homo- and Hetero-Oligomerization

In bacteria, GrpE is known to form a functional homodimer and to further oligomerize into tetramer, hexamer, and high molecular mass oligomers upon the increase of concentration (Wu et al., 1996; Harrison et al., 1997). It has been shown that Arabidopsis CGE1 and CGE2 can form homo- and hetero-dimers *in vivo* by BiFC experiments (de Luna-Valdez et al., 2019). To determine the oligomeric state of Arabidopsis CGE proteins, 5 μM each of purified AtCGE1, AtCGE2, and AtCGE1/2 were crosslinked by glutaraldehyde at 0.05 to 0.2% for 10 min. As shown in **Figure 8**, AtCGE2 was prone to aggregate to form unusually high molecular mass oligomers, with only a few dimers and tetramers. Monomers were nearly undetectable. This tendency to aggregation may be one of the reasons that AtCGE2 was inactive in co-chaperone activity assays (**Figures 6B, C**). AtCGE1 was detected largely in a dimeric homocomplex, with a small proportion in the monomeric form. Interestingly, when AtCGE1 and 2 were co-expressed, they formed dimers and tetramers. The size of the dimers was in between the AtCGE1 homodimer and the AtCGE2 homodimer (**Figure 8**), suggesting that they were AtCGE1/2 heterodimers. The size of the tetramers was also in between the AtCGE1 homotetramer and the AtCGE2 homotetramer, and the aggregation of AtCGE2 at the high molecular mass region was no longer observed. This result was in

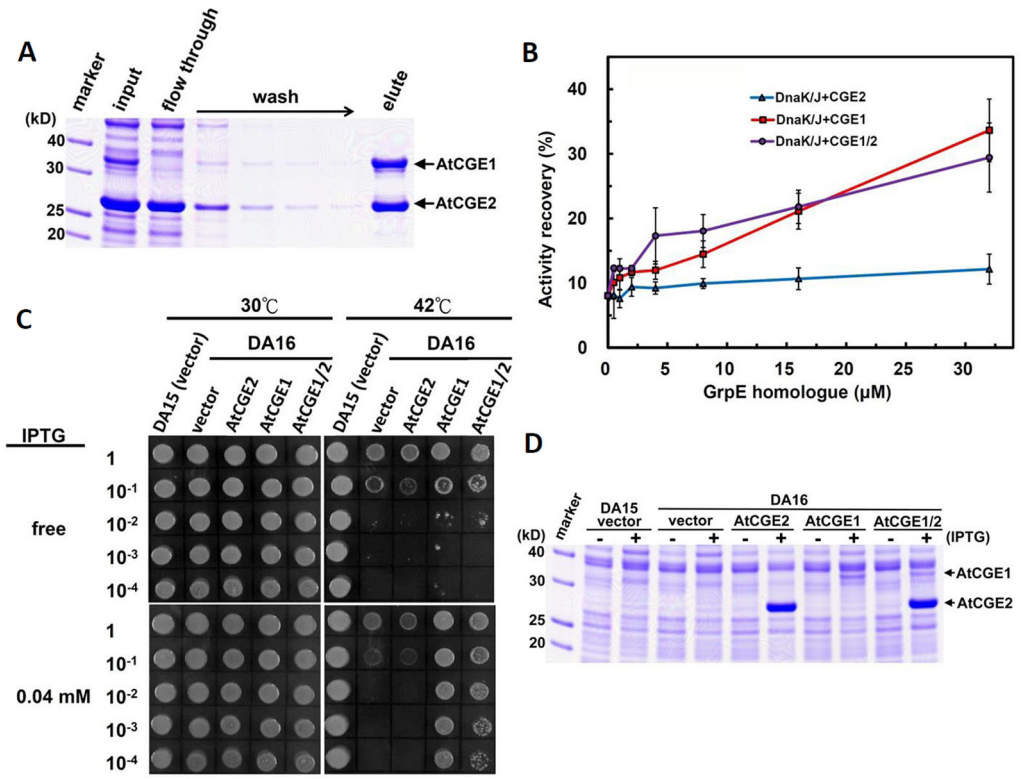

FIGURE 7 | AtCGE1/2 heterocomplex exhibited a comparable cochaperone activity with AtCGE1. **(A)** Affinity purification of AtCGE1/2 heterocomplex. The eluted sample contained AtCGE1 and AtCGE2-6xHis with approximately 1:1 ratio. **(B)** A dosage response of ACGEs on stimulating the luciferase refolding by DnaK/J machinery. DnaK and DnaJ concentrations are 5 and 1 μM, respectively. For AtCGE1/2 heterocomplex, 1 μM protein concentration equals to approximately 0.5 μM each. **(C)** Complementation of *E. coli* DA16 mutant by AtCGEs. **(D)** Induction of AtCGEs by IPTG. Protein bands corresponding to AtCGE1 and AtCGE2 are indicated.

agreement with the result of AtCGE2 binding to AtCGE1 at a molar ratio of approximately 1:1 (**Figure 7A**) and both results suggest that AtCGE1 and AtCGE2 have a high propensity to form heterocomplexes. To sum up, both *in vivo* BiFC (de Luna-Valdez et al., 2019) and our *in vitro* crosslinking analyses support that AtCGE1 and AtCGE2 can form homo- and hetero-oligomers, although further fractionation of different homo- and hetero-oligomers to correlate their biological activities and in combination with a more precise way to determine their oligomeric status (such as analytical ultracentrifuge) may be needed to clarify every detail.

DISCUSSION

Gene and genome duplications are the major driving forces of gene diversification and evolution (Lynch and Conery, 2000). de Luna-Valdez et al. (2019) recently reported that the CGE protein sequences from embryophytes form a monophyletic group that further divides into two subgroups, naming type A and type B. The two subgroups of CGEs can be distinguished from each other by variations in short motifs conserved in CGE proteins. Our phylogenetic analysis showed that flowering plants did evolved two distinct clades of CGE homologues prior to the divergence of monocot and dicot lineages, and functional characterizations suggest that two Arabidopsis CGE proteins have gained diversified activities during evolution. Although the early diverging land plant, *Physcomitrella patens*, also has two copies of CGE proteins, these two CGEs are highly similar with 85% sequence identity in their mature protein regions, and are grouped into the same clade. Shi and Theg (Shi and Theg, 2010) reported that single *Physcomitrella cge1* and *cge2* mutants are viable on phototrophic media but displayed similar slow growth phenotypes and are delayed in development of leafy shoots compared with the wild type. Their further characterizations revealed that *cge1 cge2* double-knockout mutant is lethal, indicating the functional redundancy between these two CGE proteins in moss. These two moss CGE proteins might have originated from a large-scale gene duplication event, possibly involving the whole genome, occurring in *Physcomitrella patents* (Rensing et al., 2008). But green algae and the lycophyte *Selaginella moellendorffii* generally have fewer genes per shared gene family when compared to angiosperm species. It is interesting that most flowering plants have also evolved at least two mitochondrial GrpE homologues (MGEs), for which duplication occurred independently after the divergence of many distantly related plant species. In Arabidopsis, it has been demonstrated that the two MGE homologues (AtMGE1 and AtMGE2) are derived from a recent gene

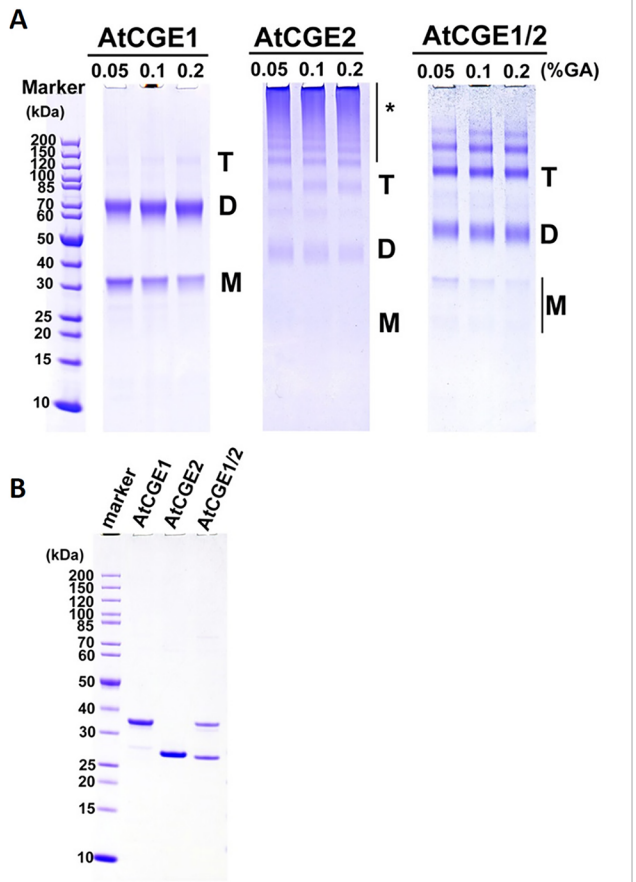

FIGURE 8 | Oligomeric states of AtCGEs. **(A)** 5 μM proteins in common buffer were crosslinked with glutaraldehyde (GA) at 0.05, 0.1, and 0.2% for 10 min. After crosslinking, their oligomeric states were visualized by 4–12% SDS-PAGE analysis and CBR staining. **(B)** Purified AtCGE proteins were mock incubation in common buffer, and were resolved on SDS-PAGE as uncrosslinked controls. For each lane, 1 μg protein was loaded. Asterisk (*) indicates high molecular mass oligomers.

duplication and AtMGE2 is sub-functionalized to confer thermotolerance to chronic heat shock (Hu et al., 2012). In comparison to the nature of the single GrpE homologue in bacteria and yeast mitochondria, we suggest that there is a convergent trend in gene duplication and functional/activity diversification both in mitochondria and chloroplasts of flowering plants, which should be beneficial to accommodate the changing environment on the land; although two CGE clades are derived from an ancient duplication, two MGE homologues were duplicated more recently.

GrpE homologues are nucleotide exchange factors, which stimulate the exchange of Hsp70/DnaK-bound ADP with ATP to complete the ATP-dependent binding and release of polypeptides (Young, 2010). Unlike DnaJ homologues, which can broaden the functions of the Hsp70 machinery by presenting the machinery with different client proteins (Kampinga and Craig, 2010), there is no substrate specificity mediated by GrpE homologues. It is unclear how a duplicated GrpE homologue confers diversified biological functions and co-chaperone activities in the organelles of flowering plants. One of the likely means is through different spatial or temporal expression patterns of the duplicated homologue. This might happen in plant mitochondrial *MGE*s, which are differentially induced by heat shock and UV-B irradiation (Hu et al., 2012). However, two *CGEs* are expressed in a similar pattern without large differences during development or upon abiotic stress, except in dry seeds and in recovering heated roots (see microarray database by Arabidopsis eFP browser at http://bar.utoronto.ca/efp_arabidopsis/cgi-bin/efpWeb.cgi). Our biochemical analyses suggested that the two distinct clades of plant CGEs may modulate Hsp70 machinery by diversified co-chaperone activity and membrane association. According to *grpE* complementation and luciferase refolding assays, we showed that only AtCGE1, but not AtCGE2, can complement the heat-sensitive phenotype of a *grpE* mutant, and significantly stimulate the luciferase refolding mediated by the DnaK/J machinery. These results indicate that AtCGE1 functions as the principle GrpE homologue. Although AtCGE2 homocomplex shows no obvious co-chaperone activity, its hetero-oligomers complexed with AtCGE1 exhibit a comparable co-chaperone activity to the AtCGE1 homocomplex. For this reason *AtCGE2* is dispensable under normal growth conditions, but becomes more important when *AtCGE1* is knocked down. Furthermore the unique properties of AtCGE2 may offer a way to fine-tune the balance of ATP/ADP-bound state of Hsp70. Indeed, it has been shown that a proper ratio of GrpE to DnaK is important for the chaperone activity both *in vitro* and *in vivo* (Sugimoto et al., 2008). Overexpression of DnaK or GrpE alone will disturb the balance between the ATP-bound (low affinity to substrate) and the ADP-bound state (high affinity to substrate) of DnaK, leading to inefficient chaperone activity (Blum et al., 1992; Sugimoto et al., 2008). To avoid the negative effect caused by a high dosage of GrpE homologues, flowering plants may have evolved a fine-tuned mediator of CGE homologues. It is possible that AtCGE1 homocomplex takes charge of the principle role in stimulating the ATP cycles of chloroplast Hsp70, and inactive AtCGE2 may become active through hetero-oligomerization with AtCGE1 in a certain conditions.

Recently it has been shown that chloroplast Hsp70 is important for protein import into chloroplasts (Shi and Theg, 2010; Su and Li, 2010), and *Physcomitrella* CGE proteins are involved in the process possibly by mediating the release of precursor proteins from Hsp70 (Shi and Theg, 2010). Our *in vitro* import assays showed that AtCGE1 is required for protein import into chloroplasts, and AtCGE2 could have a similar function at a quite lower level. Furthermore, our sub-organellar fractionations found that AtCGE2, but not AtCGE1, can associate with chloroplast membranes to some degree. Although the mechanism for membrane association of AtCGE2 is still not known, it can be imagined that AtCGE2 may have a more important role in chloroplast membrane biology. Considering the nature of protein import, in which Hsp70 may hold the newly imported precursors near the inner envelope membrane for a longer time to avoid their sliding back to the cytosol, membrane associated AtCGE2 with a low ADP/ATP exchange activity may

be beneficial for keeping chloroplast Hsp70 in a high-affinity ADP-bound state. Once the precursor proteins reach the stroma, AtCGE1 may efficiently promote their release from Hsp70s by its highly-active co-chaperone activity. However, the detailed mechanism will require further investigation, especially in providing a direct *in vivo* evidence for Hsp70/CGE interaction.

Our mutant studies showed that embryo development of atcge*1* was arrested at an early globular stage, indicating the essential role of AtCGE1. Our result is consistent with the data in the SeedGenes database (http://www.seedgenes.org) based on the study of essential genes in Arabidopsis conducted by Meinke et al. (2008), in which AtCGE1 mutant was designated as *emb1241*. This again emphasizes the pivotal function of chloroplast Hsp70 machinery. Our previous report showed that chloroplast Hsp70 is essential for plant development, and *cphsc70-1 cphsc70-2* double mutation is lethal to embryos (Su and Li, 2008). It is of interest why chloroplast Hsp70 machinery is vital at such an early stage of development. Recently, non-randomly distributed chloroplast-containing cells were found as early as the globular stage of embryogenesis in Arabidopsis by the observation of chlorophyll fluorescence (Tejos et al., 2010), and well-developed chloroplasts with grana stacks were seen in the peripheral endosperm of developing seeds (Belmonte et al., 2013). Through data mining of transcriptomic profiles of Arabidopsis developing seeds generated by Belmonte et al. (2013), we found that *AtCGE1* was highly expressed from the preglobular to the heart stage, particularly in the peripheral endosperm of developing embryos (Figure S4). In addition, the embryogenesis of the chloroplast protein import mutants, *tic110* and *toc75-III*, cannot proceed beyond the globular stage (Baldwin et al., 2005; Kovacheva et al., 2005), suggesting that the cessation of embryo development caused by *atcge1* mutation may also mainly be due to the defect of protein import, leading to hindrance of plastid/chloroplast biogenesis. A further proteomic study on identify the client proteins chaperoned by Hsp70/CGE machinery will be helpful to screen the putative molecules related to the embryo lethality of *atcge1* mutant.

DATA AVAILABILITY STATEMENT

All datasets generated for this study are included in the article/ **Supplementary Material**.

AUTHOR CONTRIBUTIONS

P-HS and H-YL conducted the biochemical analyses. P-HS and Y-HL contributed to the isolation and characterization of Arabidopsis mutants. P-HS designed the experiments and wrote the manuscript.

FUNDING

This work was supported by the funding of Ministry of Science and Technology (Grant NSC100-2311-B-001-029) and Academia Sinica to P-HS.

ACKNOWLEDGMENTS

We thank Dr. Hsou-min Li for critical reading of the manuscript and comments, Dr. Yee-yung Charng for kindly providing the DA16 mutant, and Ms. Miranda Loney for English editing. We thank the Arabidopsis Biological Resource Center and the French National Institute for Agricultural Research for providing the Arabidopsis T-DNA insertion lines.

SUPPLEMENTARY MATERIAL

The Supplementary Material for this article can be found online at: https://www.frontiersin.org/articles/10.3389/fpls.2019.01719/full#supplementary-material

REFERENCES

Alonso, J. M., Stepanova, A. N., Leisse, T. J., Kim, C. J., Chen, H., Shinn, P., et al. (2003). Genome-wide insertional mutagenesis of Arabidopsis thaliana. *Science* 301 (5633), 653–657. doi: 10.1126/science.1086391

Ang, D., Chandrasekhar, G. N., Zylicz, M., and Georgopoulos, C. (1986). Escherichia coli grpE gene codes for heat shock protein B25.3, essential for both lambda DNA replication at all temperatures and host growth at high temperature. *J. Bacteriol.* 167 (1), 25–29. doi: 10.1128/jb.167.1.25-29.1986

Baldwin, A., Wardle, A., Patel, R., Dudley, P., Park, S. K., Twell, D., et al. (2005). A molecular-genetic study of the Arabidopsis Toc75 gene family. *Plant Physiol.* 138 (2), 715–733. doi: 10.1104/pp.105.063289

Belmonte, M. F., Kirkbride, R. C., Stone, S. L., Pelletier, J. M., Bui, A. Q., Yeung, E. C., et al. (2013). Comprehensive developmental profiles of gene activity in regions and subregions of the Arabidopsis seed. *Proc. Natl. Acad. Sci. U.S.A.* 110 (5), E435–E444. doi: 10.1073/pnas.1222061110

Blum, P., Ory, J., Bauernfeind, J., and Krska, J. (1992). Physiological consequences of DnaK and DnaJ overproduction in Escherichia coli. *J. Bacteriol.* 174 (22), 7436–7444. doi: 10.1128/jb.174.22.7436-7444.1992

Brunaud, V., Balzergue, S., Dubreucq, B., Aubourg, S., Samson, F., Chauvin, S., et al. (2002). T-DNA integration into the Arabidopsis genome depends on sequences of pre-insertion sites. *EMBO Rep.* 3 (12), 1152–1157. doi: 10.1093/embo-reports/kvf237

Chen, K. M., Holmstrom, M., Raksajit, W., Suorsa, M., Piippo, M., and Aro, E. M. (2010). Small chloroplast-targeted DnaJ proteins are involved in optimization of photosynthetic reactions in Arabidopsis thaliana. *BMC Plant Biol.* 10, 43. doi: 10.1186/1471-2229-10-43

Chiu, C. C., Chen, L. J., Su, P. H., and Li, H. M. (2013). Evolution of chloroplast J proteins. *PloS One* 8 (7), e70384. doi: 10.1371/journal.pone.0070384

de Luna-Valdez, L. A., Villasenor-Salmeron, C. I., Cordoba, E., Vera-Estrella, R., Leon-Mejia, P., and Guevara-Garcia, A. A. (2019). Functional analysis of the Chloroplast GrpE (CGE) proteins from Arabidopsis thaliana. *Plant Physiol. Biochem.* 139, 293–306. doi: 10.1016/j.plaphy.2019.03.027

Emanuelsson, O., Nielsen, H., and von Heijne, G. (1999). ChloroP, a neural network-based method for predicting chloroplast transit peptides and their cleavage sites. *Protein Sci.* 8 (5), 978–984. doi: 10.1110/ps.8.5.978

Gelinas, A. D., Toth, J., Bethoney, K. A., Stafford, W. F., and Harrison, C. J. (2004). Mutational analysis of the energetics of the GrpE.DnaK binding interface: equilibrium association constants by sedimentation velocity analytical ultracentrifugation. *J. Mol. Biol.* 339 (2), 447–458. doi: 10.1016/j.jmb.2004.03.074

Grimshaw, J. P., Siegenthaler, R. K., Zuger, S., Schonfeld, H. J., Z'Graggen, B. R., and Christen, P. (2005). The heat-sensitive Escherichia coli grpE280

phenotype: impaired interaction of GrpE(G122D) with DnaK. *J. Mol. Biol.* 353 (4), 888–896. doi: 10.1016/j.jmb.2005.08.069

Harrison, C. J., Hayer-Hartl, M., Di Liberto, M., Hartl, F., and Kuriyan, J. (1997). Crystal structure of the nucleotide exchange factor GrpE bound to the ATPase domain of the molecular chaperone DnaK. *Science* 276 (5311), 431–435. doi: 10.1126/science.276.5311.431

Hu, C., Lin, S. Y., Chi, W. T., and Charng, Y. Y. (2012). Recent gene duplication and subfunctionalization produced a mitochondrial GrpE, the nucleotide exchange factor of the Hsp70 complex, specialized in thermotolerance to chronic heat stress in Arabidopsis. *Plant Physiol.* 158 (2), 747–758. doi: 10.1104/pp.111.187674

Johnson, C., Chandrasekhar, G. N., and Georgopoulos, C. (1989). Escherichia coli DnaK and GrpE heat shock proteins interact both in vivo and in vitro. *J. Bacteriol.* 171 (3), 1590–1596. doi: 10.1128/jb.171.3.1590-1596.1989

Joly, A. L., Wettstein, G., Mignot, G., Ghiringhelli, F., and Garrido, C. (2010). Dual role of heat shock proteins as regulators of apoptosis and innate immunity. *J. Innate Immun.* 2 (3), 238–247. doi: 10.1159/000296508

Kampinga, H. H., and Craig, E. A. (2010). The HSP70 chaperone machinery: J proteins as drivers of functional specificity. *Nat. Rev. Mol. Cell Biol.* 11 (8), 579–592. doi: 10.1038/nrm2941

Kovacheva, S., Bedard, J., Patel, R., Dudley, P., Twell, D., Rios, G., et al. (2005). In vivo studies on the roles of Tic110, Tic40 and Hsp93 during chloroplast protein import. *Plant J.* 41 (3), 412–428. doi: 10.1111/j.1365-313X.2004.02307.x

Latijnhouwers, M., Xu, X. M., and Moller, S. G. (2010). Arabidopsis stromal 70-kDa heat shock proteins are essential for chloroplast development. *Planta* 232 (3), 567–578. doi: 10.1007/s00425-010-1192-z

Leborgne-Castel, N., Jelitto-Van Dooren, E. P., Crofts, A. J., and Denecke, J. (1999). Overexpression of BiP in tobacco alleviates endoplasmic reticulum stress. *Plant Cell* 11 (3), 459–470. doi: 10.1105/tpc.11.3.459

Lichtenthaler, H. K. (1987). Chlorophylls and carotenoids: pigments of photosynthetic biomembranes. *Methods Enzymol.* 148, 350–382. doi: 10.1016/0076-6879(87)48036-1

Liu, C., Willmund, F., Golecki, J. R., Cacace, S., Hess, B., Markert, C., et al. (2007). The chloroplast HSP70B-CDJ2-CGE1 chaperones catalyse assembly and disassembly of VIPP1 oligomers in Chlamydomonas. *Plant J.* 50, 265–277. doi: 10.1111/j.1365-313X.2007.03047.x

Liu, L., McNeilage, R. T., Shi, L. X., and Theg, S. M. (2014). ATP requirement for chloroplast protein import is set by the Km for ATP hydrolysis of stromal Hsp70 in Physcomitrella patens. *Plant Cell* 26 (3), 1246–1255. doi: 10.1105/tpc.113.121822

Lynch, M., and Conery, J. S. (2000). The evolutionary fate and consequences of duplicate genes. *Science* 290 (5494), 1151–1155. doi: 10.1126/science.290.5494.1151

Mayer, M. P., and Bukau, B. (2005). Hsp70 chaperones: cellular functions and molecular mechanism. *Cell. Mol. Life Sci.* 62 (6), 670–684. doi: 10.1007/s00018-004-4464-6

Meinke, D., Muralla, R., Sweeney, C., and Dickerman, A. (2008). Identifying essential genes in Arabidopsis thaliana. *Trends Plant Sci.* 13 (9), 483–491. doi: 10.1016/j.tplants.2008.06.003

Peltier, J.-B., Cai, Y., Sun, Q., Zabrouskov, V., Giacomelli, L., Rudella, A., et al. (2006). The Oligomeric Stromal Proteome of Arabidopsis thaliana Chloroplasts. *Mol. Cell. Proteomics* 5 (1), 114–133. doi: 10.1074/mcp.M500180-MCP200

Perry, S. E., Li, H. M., and Keegstra, K. (1991). In vitro reconstitution of protein transport into chloroplasts. *Methods Cell Biol.* 34, 327–344. doi: 10.1016/s0091-679x(08)61688-x

Rensing, S. A., Lang, D., Zimmer, A. D., Terry, A., Salamov, A., Shapiro, H., et al. (2008). The Physcomitrella genome reveals evolutionary insights into the conquest of land by plants. *Science* 319 (5859), 64–69. doi: 10.1126/science.1150646

Schroda, M., Vallon, O., Wollman, F. A., and Beck, C. F. (1999). A chloroplast-targeted heat shock protein 70 (HSP70) contributes to the photoprotection and repair of photosystem II during and after photoinhibition. *Plant Cell* 11 (6), 1165–1178.

Schroda, M., Vallon, O., Whitelegge, J. P., Beck, C. F., and Wollman, F. A. (2001). The chloroplastic GrpE homolog of Chlamydomonas: two isoforms generated by differential splicing. *Plant Cell* 13 (12), 2823–2839. doi: 10.1105/tpc.010202

Schubert, M., Petersson, U. A., Haas, B. J., Funk, C., Schroder, W. P., and Kieselbach, T. (2002). Proteome map of the chloroplast lumen of Arabidopsis thaliana. *J. Biol. Chem.* 277 (10), 8354–8365. doi: 10.1074/jbc.M108575200

Shi, L. X., and Theg, S. M. (2010). A stromal heat shock protein 70 system functions in protein import into chloroplasts in the moss Physcomitrella patens. *Plant Cell* 22 (1), 205–220. doi: 10.1105/tpc.109.071464

Su, P. H., and Li, H. M. (2008). Arabidopsis stromal 70-kD heat shock proteins are essential for plant development and important for thermotolerance of germinating seeds. *Plant Physiol.* 146 (3), 1231–1241. doi: 10.1104/pp.107.114496

Su, P. H., and Li, H. M. (2010). Stromal Hsp70 is important for protein translocation into pea and Arabidopsis chloroplasts. *Plant Cell* 22, 1516–1531. doi: 10.1105/tpc.109.071415

Sugimoto, S., Higashi, C., Saruwatari, K., Nakayama, J., and Sonomoto, K. (2007). A gram-negative characteristic segment in Escherichia coli DnaK is essential for the ATP-dependent cooperative function with the co-chaperones DnaJ and GrpE. *FEBS Lett.* 581 (16), 2993–2999. doi: 10.1016/j.febslet.2007.05.055

Sugimoto, S., Saruwatari, K., Higashi, C., and Sonomoto, K. (2008). The proper ratio of GrpE to DnaK is important for protein quality control by the DnaK-DnaJ-GrpE chaperone system and for cell division. *Microbiology* 154 (Pt 7), 1876–1885. doi: 10.1099/mic.0.2008/017376-0

Sun, Q., Zybailov, B., Majeran, W., Friso, G., Olinares, P. D., and van Wijk, K. J. (2009). PPDB, the Plant Proteomics Database at Cornell. *Nucleic Acids Res.* 37 (Database issue), D969–D974. doi: 10.1093/nar/gkn654

Sung, D. Y., and Guy, C. L. (2003). Physiological and molecular assessment of altered expression of Hsc70-1 in Arabidopsis. Evidence pleiotropic consequences. *Plant Physiol.* 132 (2), 979–987. doi: 10.1104/pp.102.019398

Tamura, K., Stecher, G., Peterson, D., Filipski, A., and Kumar, S. (2013). MEGA6: Molecular Evolutionary Genetics Analysis version 6.0. *Mol. Biol. Evol.* 30 (12), 2725–2729. doi: 10.1093/molbev/mst197

Tejos, R. I., Mercado, A. V., and Meisel, L. A. (2010). Analysis of chlorophyll fluorescence reveals stage specific patterns of chloroplast-containing cells during Arabidopsis embryogenesis. *Biol. Res.* 43 (1), 99–111. doi: 10.4067/S0716-97602010000100012

Willmund, F., Dorn, K. V., Schulz-Raffelt, M., and Schroda, M. (2008). The chloroplast DnaJ homolog CDJ1 of Chlamydomonas reinhardtii is part of a multichaperone complex containing HSP70B, CGE1, and HSP90C. *Plant Physiol.* 148 (4), 2070–2082. doi: 10.1104/pp.108.127944

Woody, S. T., Austin-Phillips, S., Amasino, R. M., and Krysan, P. J. (2007). The WiscDsLox T-DNA collection: an arabidopsis community resource generated by using an improved high-throughput T-DNA sequencing pipeline. *J. Plant Res.* 120 (1), 157–165. doi: 10.1007/s10265-006-0048-x

Wu, B., Wawrzynow, A., Zylicz, M., and Georgopoulos, C. (1996). Structure-function analysis of the Escherichia coli GrpE heat shock protein. *EMBO J.* 15 (18), 4806–4816. doi: 10.1002/j.1460-2075.1996.tb00861.x

Yokthongwattana, K., Chrost, B., Behrman, S., Casper-Lindley, C., and Melis, A. (2001). Photosystem II damage and repair cycle in the green alga Dunaliella salina: involvement of a chloroplast-localized HSP70. *Plant Cell Physiol.* 42 (12), 1389–1397. doi: 10.1093/pcp/pce179

Young, J. C. (2010). Mechanisms of the Hsp70 chaperone system. *Biochem. Cell Biol.* 88 (2), 291–300. doi: 10.1139/o09-175

Conflict of Interest: The authors declare that the research was conducted in the absence of any commercial or financial relationships that could be construed as a potential conflict of interest.

frontiers in Plant Science

MINI REVIEW
published: 23 January 2020
doi: 10.3389/fpls.2019.01729

ROS-Driven Oxidative Modification: Its Impact on Chloroplasts-Nucleus Communication

Chanhong Kim *

Shanghai Center for Plant Stress Biology and Center of Excellence in Molecular Plant Sciences, Chinese Academy of Sciences, Shanghai, China

As a light-harvesting organelle, the chloroplast inevitably produces a substantial amount of reactive oxygen species (ROS) primarily through the photosystems. These ROS, such as superoxide anion, hydrogen peroxide, hydroxyl radical, and singlet oxygen, are potent oxidizing agents, thereby damaging the photosynthetic apparatus. On the other hand, it became increasingly clear that ROS act as beneficial tools under photo-oxidative stress conditions by stimulating chloroplast-nucleus communication, a process called retrograde signaling (RS). These ROS-mediated RS cascades appear to participate in a broad spectrum of plant physiology, such as acclimation, resistance, programmed cell death (PCD), and growth. Recent reports imply that ROS-driven oxidation of RS-associated components is essential in sensing and responding to an increase in ROS contents. ROS appear to activate RS pathways *via* reversible or irreversible oxidation of sensor molecules. This review provides an overview of the emerging perspective on the topic of "oxidative modification-associated retrograde signaling."

Keywords: reactive oxygen species, retrograde signalling, chloroplast, photosystem, oxidative modification

OPEN ACCESS

Edited by:
Hongbo Gao,
Beijing Forestry University, China

Reviewed by:
Pavel Pospíšil,
Palacký University Olomouc, Czechia
Aigen Fu,
Northwest University, China

***Correspondence:**
Chanhong Kim
chanhongkim@sibs.ac.cn

Specialty section:
This article was submitted to Plant Physiology, a section of the journal Frontiers in Plant Science

Received: *22 August 2019*
Accepted: *09 December 2019*
Published: *23 January 2020*

Citation:
Kim C (2020) ROS-Driven Oxidative Modification: Its Impact on Chloroplasts-Nucleus Communication. Front. Plant Sci. 10:1729. doi: 10.3389/fpls.2019.01729

The post-translational modifications (PTMs) are essential in initiating intra- and inter-cellular signaling cascades. Such PTMs, including acetylation, phosphorylation/de-phosphorylation, ubiquitination, sumoylation, and redox-related protein modifications, are ubiquitous cellular events dynamically deployed in signaling network under various developmental and stress conditions (Schweppe et al., 2003; Apel and Hirt, 2004; Jensen, 2004; Buchanan and Balmer, 2005; Stulemeijer and Joosten, 2008). Unlike extraplastidic signaling cascades where the protein modifications have been extensively investigated, the current understanding of the potential impact of PTMs in triggering chloroplast-to-nucleus retrograde signaling pathways is mostly limited in the context of the reversible redox modifications (Tikkanen et al., 2012; Dietz et al., 2016). Even though chloroplasts are prime subcellular organelles producing reactive oxygen species (ROS), reactive electrophile species (RES) mainly through lipid peroxidation (Girotti and Kriska, 2004; Mueller et al., 2008), and stress hormones under both biotic and abiotic stress, the converging PTM events in stress-related proteins are mostly unexplored. In particular, oxidative PTMs by ROS and its interconnection with other PTMs, which may function in protein turnover, signaling, and metabolism, are poorly understood. Given that chloroplasts produce harmful reactive species, in this review paper, the current understanding of oxidative PTMs and its associated retrograde

signaling pathways are mainly discussed, which may provide a new prospect in the field of chloroplast-to-nucleus retrograde signaling research.

TWO SINGLET OXYGEN SENSORS UNDERGO OXIDATIVE MODIFICATION

The first breakthrough which has changed the classical view of ROS from toxic to signaling-associated agents arose from the identification of *fluorescent* (*flu*) mutant of *Arabidopsis thaliana* (Meskauskiene et al., 2001). Given that the FLU protein negatively regulates the Mg-branch of tetrapyrrole synthesis, overaccumulation of protochlorophyllide (Pchlide, end product in the dark) in the absence of light is inevitable in the *flu* mutant plants. The increase of free Pchlide, a photosensitizer, results in the generation of singlet oxygen ($^1O_2$) upon illumination, leading to rapid cell death in young seedlings and growth inhibition in mature plants (op den Camp et al., 2003). $^1O_2$-associated global transcriptome analyses reveal that a substantial number of nuclear genes (mostly related to stress responses) become upregulated upon $^1O_2$ release in chloroplasts. The gene expression changes precede the onset of cell death (op den Camp et al., 2003; Kim et al., 2012). At first glance, the rapid expression of nuclear-encoded stress-related genes was thought of as a consequence of $^1O_2$ cytotoxicity. However, the subsequent forward genetic screen has provided a clue that the $^1O_2$-associated transcriptome, as well as the cell death in young seedlings (or grown inhibition in mature plants) are likely to be mediated *via* activation of chloroplast-to-nucleus retrograde signaling (hereafter RS) (Wagner et al., 2004; Kim et al., 2008). The nuclear-encoded plastid protein EXECUTER (EX) 1 and its close homolog EX2 appear to mediate the stress responses in both young seedlings and mature plants of *flu* (Lee et al., 2007). Therefore, the genetic inactivation of EX1 and EX2 nearly abrogates $^1O_2$-triggered stress responses, including nuclear gene expression changes (Lee et al., 2007). This indicates that chloroplasts lacking both EX1 and EX2 become insensitive to $^1O_2$ generated in the *flu* mutant plants upon a dark-to-light shift. While EX1 plays a significant role in $^1O_2$ signaling, EX2 acts as a modulator. The loss of EX2 in *flu* only alters the $^1O_2$-associated nuclear transcriptome, but neither cell death nor growth inhibition (Kim et al., 2012). Besides, the absence of developmental defects in *ex1ex2* mutant plants (Kim et al., 2012) suggests that EXs are essentially functioning under photo-oxidative stress conditions in which chloroplasts enhance the level of $^1O_2$.

Mostly based on the genetic and transcriptome studies, EX1 has long been considered as a putative $^1O_2$ sensor (**Figure 1A**). The first mechanistic insight on how EX1 mediates $^1O_2$ signaling was only recently attained (Wang et al., 2016; Dogra et al., 2019b). Interestingly, membrane-bound FtsH2 protease participates in $^1O_2$ signaling by promoting EX1 degradation upon release of $^1O_2$ (Wang et al., 2016). FtsH2 is a major subunit of the hetero-hexameric FtsH complex, which functions in the proteolysis of damaged photosystem II (PSII) reaction center (RC) proteins. Inactivation of FtsH2 thus substantially attenuates $^1O_2$ signaling and its related stress responses in *flu*, like in the *flu ex1* mutant (Dogra et al., 2017).

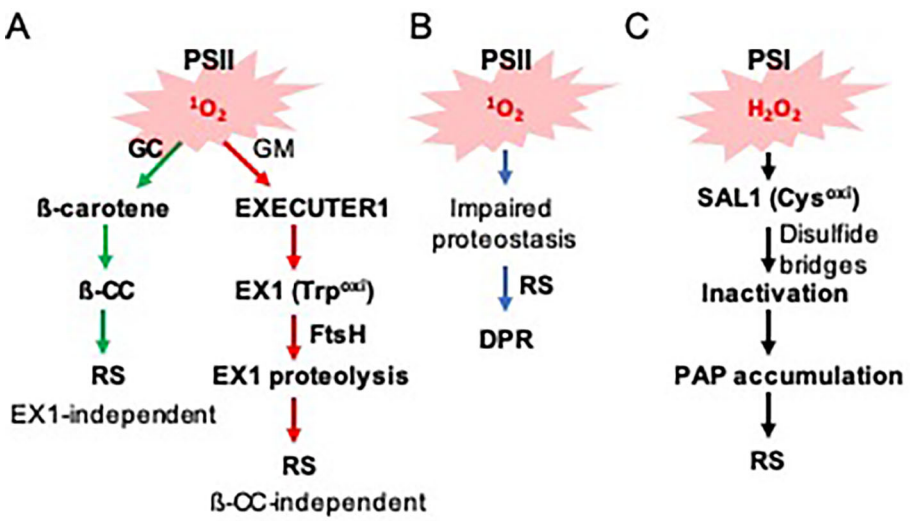

FIGURE 1 | Photosystems-driven ROS trigger distinct RS pathways. **(A)** PSII-associated $^1O_2$ sensors beta-carotene and EX1 mediate RS in the grana core (GC) and grana margins (GMs), respectively. $^1O_2$ oxidizes ß-carotene and EX1, resulting in the generation of ß-CC and EX1($Trp643^{oxi}$). While ß-CC serves as a volatile RS molecule, it is unclear how EX1($Trp643^{oxi}$) degradation alters the expression of $^1O_2$-responsive nuclear genes. **(B)** $^1O_2$ constantly damages PSII core proteins, which leads to the accumulation of damaged proteins in the chloroplasts of the *var2* mutant. The impaired proteostasis triggers a DPR *via* an EX1-independent pathway. **(C)** PSI-driven ROS (such as H_2O_2) inactivate the SAL1 enzyme *via* intra- and/or inter-disulfide bond formation, leading to the accumulation of its substrate PAP. PAP then mediates RS.

This finding also suggested that EX1 might undergo post-translational modification, thereby promoting EX1 degradation. Consistent with the notion, it appears that the tryptophan-643 residue (Trp643) undergoes $^1O_2$-dependent oxidation (Dogra et al., 2019b). Oxidation of the indole side chain of Trp leads to the production of different Trp variants, such as keto-amino-hydroxy derivative oxindolylalanine (Oia), dihydro-hydroxy derivative N-formylkynurenine (NFK), and kynurenine with the corresponding mass shifts of + 16, + 32, and + 4 Da, respectively (Anderson et al., 2002; Dogra et al., 2019b). A substitution of Trp643 with $^1O_2$-insensitive amino acid residues, such as Alanine and Leucine, completely inactivates EX1. However, the modified EX1 proteins appear to be unexpectedly unstable and fail to accumulate despite the abundance of the cognate mRNA transcripts. Presumably, they failed to localize in the grana margin or become misfolded, facilitating their degradation. Because of this instability, it is unclear which of the assumptions, or even both, are responsible for the impaired $^1O_2$ signaling. However, this finding suggests that the accumulation of EX1 in the grana margins, wherein it associates with various proteins, and its FtsH-dependent proteolysis upon $^1O_2$ burst, are pivotal in initiating $^1O_2$ signaling (**Figure 1A**).

The deletion of DUF3506 (the domain of unknown function 3506; now dubbed singlet oxygen sensor [SOS] domain) containing Trp643 also impairs $^1O_2$ signaling with remaining EX1 stability in response to $^1O_2$. In 2004, Klaus Apel and his coworkers reported two independent *ex1* alleles, each of which contains a missense mutation in the SOS domain resulting in Phenylalanine-528-Cysteine and Glycine-646-Aspartic acid, respectively. It turned out that these mutated EX1 proteins cannot undergo Trp643 oxidation, underpinning the essential role of Trp643 in sensing $^1O_2$ and initiating cognate signaling (Dogra et al., 2019b). In fact, earlier studies found that amongst the $^1O_2$-sensitive amino acid residues, only Trp can scavenge $^1O_2$ *via* both physical quenching and chemical reactions. Thus, Trp is highly susceptible and reacts rapidly with $^1O_2$ (Davies, 2003; Pattison et al., 2012).

Another $^1O_2$ sensor, ß-carotene, also undergoes oxidation *via* $^1O_2$ under light stress conditions (**Figure 1A**). EX1 mediates $^1O_2$ signaling in the grana margin (non-appressed), while ß-carotene functions in the grana core (appressed) (Dogra et al., 2018). These two signaling cascades are distinct, as evident in the substantial difference of downstream target genes (Dogra et al., 2017; Dogra et al., 2018). Excess light-generated $^1O_2$ oxidizes ß-carotene, which leads to the production of its volatile compounds such as ß-cyclocitral (ß-CC) which belongs to the RES. ß-CC then induces numerous nuclear-encoded genes independently of EX1 and EX2 (Ramel et al., 2012; Ramel et al., 2013b; Ramel et al., 2013a). Given that excess light results in the generation of ß-CC in PSII RC where ß-carotene acts as a $^1O_2$ scavenger, it is tempting to suggest that there might be a certain threshold level of ß-CC required for initiating RS. While the source of $^1O_2$ for ß-carotene oxidation is evident, the source of EX1 oxidation is yet unclear. Considering the exclusive localization of EX1 in the grana margin and the extremely short lifespan of $^1O_2$ (Apel and Hirt, 2004; Asada, 2006), it is difficult to suggest that $^1O_2$ generated in PSII in the grana core moves to the grana margin wherein EX1 senses it. Perhaps, as suggested recently (Dogra et al., 2018), the impaired reassembly process of PSII in the grana margin may cause the generation of $^1O_2$ under photo-oxidative stress conditions. In the grana margin, EX1 is associated with PSII RC proteins, FtsH protease, chlorophyll synthesis enzymes, and proteins of the chloroplast translation apparatus (Wang et al., 2016). These proteins are all implicated in PSII reassembly. Since PSII reassembly requires newly synthesized chlorophyll molecules, it is possible that, by any chance, free chlorophyll or its precursors released under stress generate $^1O_2$. EX1 may sense such $^1O_2$ generated in the grana margin. However, at present, we cannot exclude a possibility that any oxidized products (including RES) by $^1O_2$ oxidizes EX1 protein (Dogra et al., 2018; Dogra et al., 2019b). Therefore, finding the source of EX1 oxidation would shed light on the underlying mechanism of EX1 oxidation further.

DAMAGED/UNFOLDED/MISFOLDED PROTEIN RESPONSES *VIA* RS

$^1O_2$ is a prime ROS causing photodamage in PSII RC proteins (Apel and Hirt, 2004; Yamamoto et al., 2013). Especially the D1 protein has been implicated as a major target of $^1O_2$ because of its proximity to the chlorophyll a molecule (called P680) in PSII RC. It is known that the excited triplet state of P680 serves as a photosensitizer. Earlier studies demonstrated that high light stress results in Trp oxidation in the D1 protein, not in all but certain Trp residues (Dreaden et al., 2011; Dreaden Kasson et al., 2012). Dogra et al., (2019b) also confirmed that these Trp residues in D1 undergo oxidation, resulting in the generation of oxidized Trp variants, including NFK. Nonetheless, photodamage in PSII RC proteins facilitates a process called PSII repair, which involves a series of steps: 1) migration of damaged PSII RC from the grana core to the grana margin; 2) degradation *via* the FtsH protease; 3) reassembly *via* protein *de novo* synthesis; and 4) re-migration from the grana margin to the grana core (Kato and Sakamoto, 2018). The hetero-hexameric FtsH protease comprises four subunits, FtsH1, 2, 5, and 8. Among them, FtsH2 and FtsH5 are pivotal for establishing a functional FtsH protease, as evident in the emergence of leaf variegation in the cognate mutant plants (Yu et al., 2005). Besides, the loss of FtsH2 results in the accumulation of damaged PSII proteins relative to wild-type plants and in the failure of survival under very mild light stress conditions wherein wild-type plants can rapidly acclimate (Duan et al., 2019).

Not only PSII proteins but also other chloroplast proteins appear to accumulate in the chloroplasts of *var2* mutant lacking FtsH2. Interestingly, a substantial number of proteins, which are known to function in protein quality control (PQC), are accumulating in *var2* (Dogra et al., 2019a). These proteins include heat shock proteins and heat shock transcription factors as well as a suite of proteases (such as the ATP-

dependent caseinolytic protease Clp). Besides, detoxification- and redox-related proteins were found to accumulate in *var2*, coinciding with an increase in ROS in the chloroplasts (Kato et al., 2009). The resulting global transcriptome analysis of *var2* versus wild-type plants revealed that the accumulation of PQC-related proteins seems to be transcriptionally controlled *via* RS (Dogra et al., 2019a). This molecular phenotype (upregulation of a suite of proteins involved in PQC) resembles one so-called unfolded/misfolded protein response, namely UPR (Walter and Ron, 2011). Considering the plausible interrelation between the accumulation of damaged chloroplast proteins and the induction of PQC/detoxification/redox-related nuclear genes, we dubbed this UPR-like response as a damaged protein response (DPR) (**Figure 1B**).

The UPR was first characterized in the endoplasmic reticulum (ER) and is an ubiquitously conserved cellular system eliminating misfolded/unfolded proteins, thereby maintaining proteostasis (Kozutsumi et al., 1988). A presence of chloroplast-mediated UPR (cpUPR) was first reported in the green unicellular alga *Chlamydomonas reinhardtii* lacking ClpP, a plastid-encoded catalytic subunit of the Clp complex (Ramundo and Rochaix, 2014; Ramundo et al., 2014). Like the chloroplasts of *var2*, the ClpP-deficient chloroplasts of *C. reinhardtii* accumulate PQC-related proteins. Even though chloroplast proteome changes induced by the loss of Clp and FtsH2 are largely comparable, there is also an apparent difference. For instance, while chloroplast-encoded proteins remain almost unchanged in *clp*, loss of FtsH2 affects their abundances relative to wild-type plants (Zybailov et al., 2009; Dogra et al., 2019a). At present, it is unclear whether cpUPR has resulted from the general defect in chloroplast proteostasis or if the inactivation of the independent protease triggers a unique RS pathway.

Intriguingly, one *var2* allele, *var2-9*, was found to upregulate not only a suite of genes involved in PQC but also salicylic acid-responsive genes (SRGs) (Duan et al., 2019). *var2-9* mutant plants express dysfunctional FtsH2, which specifically impairs the substrate unfolding activity. This defect leads to a higher accumulation of damaged/oxidized PSII core proteins, including D1, D2, CP43, and CP47 as compared to those in *var2* null mutant plants. In addition to genes involved in PQC, *var2-9* mutant plants exhibit a significant upregulation of SRGs. It turned out that SA accumulation in *var2-9* depends on the chloroplast-established isochorismate (ICS) pathway in the absence of transcriptional upregulation of ICS-associated genes. This result suggests that the impaired proteostasis leading to the accumulation of damaged proteins may directly activate ICS enzymes to accumulate SA without transcriptional regulation. This also indicates that impaired ROS homeostasis may stimulate the ICS pathway, perhaps by altering chloroplast redox status and that the slightly accumulated SA may facilitate appropriate stress responses. Collectively, it is reasonable to propose that the ROS- (or redox)-and SA-mediated RS pathways may coordinate stress responses in response to cold, high light, and pathogen attack in which ROS and/or SA are known to accumulate.

EITHER OXIDATIVE MODIFICATION OR PROTEOLYSIS INVOLVES RS PATHWAYS

Besides EX1, another chloroplastic oxidative stress sensor, namely 3′-phosphoadenosine 5′-phosphate (PAP) phosphatase SAL1, undergoes oxidation at specific Cysteine (Cys) residues in response to the increased level of hydrogen peroxide (H_2O_2) (Estavillo et al., 2011; Chan et al., 2016). In contrast to $^1O_2$ mainly generated in PSII, H_2O_2 is released *via* PSI. This fact suggests that while ß-carotene and EX1 are PSII-associated ROS sensors, SAL1 is a PSI-associated ROS sensor. The Cys residue is a target of ROS since it contains a reactive thiol group, which also plays an essential role in structural modification of proteins *via* intra- and/or inter-disulfide bond formation in response to redox changes. It appears that under photo-oxidative stress conditions, specific Cys residues form inter- and intra-disulfide bonds, leading to the inactivation of SAL1 and an increase of its substrate PAP (**Figure 1C**). The PAP migrates from the chloroplasts to the nucleus to modulate the expression of a group of stress-related genes.

In contrast to EX1, Genomes Uncoupled 1 (GUN1), an integrator of multiple retrograde signals, is being stabilized under specific conditions wherein GUN1 is required to mediate RS (Wu et al., 2018; Wu et al., 2019). Given the considerable amount of *GUN1* transcripts but nearly undetectable levels of this protein, chloroplasts seem to avoid the accumulation of GUN1, perhaps because of its negative impact on chloroplast integrity under normal growth conditions (Wu et al., 2018). On the contrary, GUN1 is crucial to mediate chloroplasts-nucleus communication under certain stress conditions. As suggested for EX1, GUN1 may also facilitate RS by affecting its associated components involved in RS. Therefore, finding GUN1-associated proteins and distinguishing their molecular function seem to be essential to elucidate the mode of action of GUN1. It is important to note that it is better to reveal the GUN1 interactome under a condition where the *gun1* mutant exhibits a distinct phenotype relative to wild-type plants. This concern also can be applied for EX1 protein.

CONCLUSIONS AND REMARKS

The past years of studies on chloroplast-mediated RS have unveiled different oxidative stress sensors mediating distinct RS pathways. These signaling molecules include the $^1O_2$ sensors ß-carotene and EX1 (perhaps also EX2), and the moonlighting protein SAL1. The oxidative modifications of these sensor molecules are a prerequisite to initiating the RS pathways. Such modifications directly result from an increase in ROS levels and changes in redox status in chloroplasts. Indeed, it became apparent that chloroplasts rapidly accumulate ROS in response to various stress factors. Most likely, these sensor molecules reside close to the site of ROS production, thereby efficiently sensing the degree of stress and responding appropriately *via* RS. Even though a genuine signaling

molecule acting in EX1-mediated RS remains elusive, it is rational to assume that EX1-associated proteins or EX1 per se (e.g., EX1 fragments) may release signaling molecules upon EX1 proteolysis. Besides, it is unclear: (i) how many chloroplast proteins act as ROS/redox sensors under ROS-generating stress conditions; (ii) which different stress factors activate which different ROS/redox sensor; and (iii) if ROS activate RS pathways *via* inactivation or activation of chloroplast metabolism? Resolving these questions may provide real insights for understanding the role of chloroplasts as environmental sensors in land plants.

AUTHOR CONTRIBUTIONS

The author confirms being the sole contributor of this work and has approved it for publication.

ACKNOWLEDGMENTS

This work was supported by the Strategic Priority Research Program from the Chinese Academy of Sciences (Grant No. XDB27040102).

REFERENCES

Anderson, L. B., Maderia, M., Ouellette, A. J., Putnam-Evans, C., Higgins, L., Krick, T., et al. (2002). Posttranslational modifications in the CP43 subunit of photosystem II. *Proc. Natl. Acad. Sci. U.S.A.* 99, 14676–14681. doi: 10.1073/pnas.232591599

Apel, K., and Hirt, H. (2004). Reactive oxygen species: metabolism, oxidative stress, and signal transduction. *Annu. Rev. Plant Biol.* 55, 373–399. doi: 10.1146/annurev.arplant.55.031903.141701

Asada, K. (2006). Production and scavenging of reactive oxygen species in chloroplasts and their functions. *Plant Physiol.* 141, 391–396. doi: 10.1104/pp.106.082040

Buchanan, B. B., and Balmer, Y. (2005). Redox regulation: a broadening horizon. *Annu. Rev. Plant Biol.* 56, 187–220. doi: 10.1146/annurev.arplant.56.032604.144246

Chan, K. X., Mabbitt, P. D., Phua, S. Y., Mueller, J. W., Nisar, N., Gigolashvili, T., et al. (2016). Sensing and signaling of oxidative stress in chloroplasts by inactivation of the SAL1 phosphoadenosine phosphatase. *Proc. Natl. Acad. Sci. U.S.A.* 113, E4567–E4576. doi: 10.1073/pnas.1604936113

Davies, M. J. (2003). Singlet oxygen-mediated damage to proteins and its consequences. *Biochem. Biophys. Res. Commun.* 305, 761–770. doi: 10.1016/s0006-291x(03)00817-9

Dietz, K. J., Turkan, I., and Krieger-Liszkay, A. (2016). Redox- and reactive oxygen species-dependent signaling into and out of the photosynthesizing chloroplast. *Plant Physiol.* 171, 1541–1550. doi: 10.1104/pp.16.00375

Dogra, V., Duan, J., Lee, K. P., Lv, S., Liu, R., and Kim, C. (2017). FtsH2-Dependent Proteolysis of EXECUTER1 is essential in mediating singlet oxygen-triggered retrograde signaling in arabidopsis thaliana. *Front. Plant Sci.* 8, 1145. doi: 10.3389/fpls.2017.01145

Dogra, V., Rochaix, J. D., and Kim, C. (2018). Singlet oxygen-triggered chloroplast-to-nucleus retrograde signalling pathways: an emerging perspective. *Plant Cell Environ.* 41, 1727–1738. doi: 10.1111/pce.13332

Dogra, V., Duan, J., Lee, K. P., and Kim, C. (2019a). Impaired PSII proteostasis triggers a UPR-like response in the var2 mutant of Arabidopsis. *J. Exp. Bot.* 70, 3075–3088. doi: 10.1093/jxb/erz151

Dogra, V., Li, M., Singh, S., Li, M., and Kim, C. (2019b). Oxidative post-translational modification of EXECUTER1 is required for singlet oxygen sensing in plastids. *Nat. Commun.* 10, 2834. doi: 10.1038/s41467-019-10760-6

Dreaden, T. M., Chen, J., Rexroth, S., and Barry, B. A. (2011). N-formylkynurenine as a marker of high light stress in photosynthesis. *J. Biol. Chem.* 286, 22632–22641. doi: 10.1074/jbc.M110.212928

Dreaden Kasson, T. M., Rexroth, S., and Barry, B. A. (2012). Light-induced oxidative stress, N-formylkynurenine, and oxygenic photosynthesis. *PloS One* 7, e42220. doi: 10.1371/journal.pone.0042220

Duan, J., Lee, K. P., Dogra, V., Zhang, S., Liu, K., Caceres-Moreno, C., et al. (2019). Impaired PSII proteostasis promotes retrograde signaling *via* salicylic acid. *Plant Physiol.* 180, 2182–2197. doi: 10.1104/pp.19.00483

Estavillo, G. M., Crisp, P. A., Pornsiriwong, W., Wirtz, M., Collinge, D., Carrie, C., et al. (2011). Evidence for a SAL1-PAP chloroplast retrograde pathway that functions in drought and high light signaling in Arabidopsis. *Plant Cell* 23, 3992–4012. doi: 10.1105/tpc.111.091033

Girotti, A. W., and Kriska, T. (2004). Role of lipid hydroperoxides in photo-oxidative stress signaling. *Antioxid. Redox Sign* 6, 301–310. doi: 10.1089/152308604322899369

Jensen, O. N. (2004). Modification-specific proteomics: characterization of post-translational modifications by mass spectrometry. *Curr. Opin. Chem. Biol.* 8, 33–41. doi: 10.1016/j.cbpa.2003.12.009

Kato, Y., and Sakamoto, W. (2018). FtsH Protease in the thylakoid membrane: physiological functions and the regulation of protease activity. *Front. Plant Sci.* 9, 855. doi: 10.3389/fpls.2018.00855

Kato, Y., Miura, E., Ido, K., Ifuku, K., and Sakamoto, W. (2009). The variegated mutants lacking chloroplastic FtsHs are defective in D1 degradation and accumulate reactive oxygen species. *Plant Physiol.* 151, 1790–1801. doi: 10.1104/pp.109.146589

Kim, C., Meskauskiene, R., Apel, K., and Laloi, C. (2008). No single way to understand singlet oxygen signalling in plants. *EMBO Rep.* 9, 435–439. doi: 10.1038/embor.2008.57

Kim, C., Meskauskiene, R., Zhang, S., Lee, K. P., Lakshmanan Ashok, M., Blajecka, K., et al. (2012). Chloroplasts of Arabidopsis are the source and a primary target of a plant-specific programmed cell death signaling pathway. *Plant Cell* 24, 3026–3039. doi: 10.1105/tpc.112.100479

Kozutsumi, Y., Segal, M., Normington, K., Gething, M. J., and Sambrook, J. (1988). The presence of malfolded proteins in the endoplasmic reticulum signals the induction of glucose-regulated proteins. *Nature* 332, 462–464. doi: 10.1038/332462a0

Lee, K. P., Kim, C., Landgraf, F., and Apel, K. (2007). EXECUTER1- and EXECUTER2-dependent transfer of stress-related signals from the plastid to the nucleus of Arabidopsis thaliana. *Proc. Natl. Acad. Sci. U.S.A.* 104, 10270–10275. doi: 10.1073/pnas.0702061104

Meskauskiene, R., Nater, M., Goslings, D., Kessler, F., op den Camp, R., and Apel, K. (2001). FLU: a negative regulator of chlorophyll biosynthesis in Arabidopsis thaliana. *Proc. Natl. Acad. Sci. U.S.A.* 98, 12826–12831. doi: 10.1073/pnas.221252798

Mueller, S., Hilbert, B., Dueckershoff, K., Roitsch, T., Krischke, M., Mueller, M. J., et al. (2008). General detoxification and stress responses are mediated by oxidized lipids through TGA transcription factors in Arabidopsis. *Plant Cell* 20, 768–785. doi: 10.1105/tpc.107.054809

op den Camp, R. G., Przybyla, D., Ochsenbein, C., Laloi, C., Kim, C., Danon, A., et al. (2003). Rapid induction of distinct stress responses after the release of singlet oxygen in Arabidopsis. *Plant Cell* 15, 2320–2332. doi: 10.1105/tpc.014662

Pattison, D. I., Rahmanto, A. S., and Davies, M. J. (2012). Photo-oxidation of proteins. *Photochem. Photobiol. Sci.* 11, 38–53. doi: 10.1039/c1pp05164d

Ramel, F., Birtic, S., Ginies, C., Soubigou-Taconnat, L., Triantaphylides, C., and Havaux, M. (2012). Carotenoid oxidation products are stress signals that mediate gene responses to singlet oxygen in plants. *Proc. Natl. Acad. Sci. U.S.A.* 109, 5535–5540. doi: 10.1073/pnas.1115982109

Ramel, F., Mialoundama, A. S., and Havaux, M. (2013a). Nonenzymic carotenoid oxidation and photooxidative stress signalling in plants. *J. Exp. Bot.* 64, 799–805. doi: 10.1093/jxb/ers223

Ramel, F., Ksas, B., Akkari, E., Mialoundama, A. S., Monnet, F., Krieger-Liszkay, A., et al. (2013b). Light-induced acclimation of the Arabidopsis chlorina1 mutant to singlet oxygen. *Plant Cell* 25, 1445–1462. doi: 10.1105/tpc.113.109827

Ramundo, S., and Rochaix, J. D. (2014). Chloroplast unfolded protein response, a new plastid stress signaling pathway? *Plant Signal Behav.* 9, e972874. doi: 10.4161/15592316.2014.972874

Ramundo, S., Casero, D., Muhlhaus, T., Hemme, D., Sommer, F., Crevecoeur, M., et al. (2014). Conditional depletion of the Chlamydomonas Chloroplast ClpP protease activates nuclear genes involved in autophagy and plastid protein quality control. *Plant Cell* 26, 2201–2222. doi: 10.1105/tpc.114.124842

Schweppe, R. E., Haydon, C. E., Lewis, T. S., Resing, K. A., and Ahn, N. G. (2003). The characterization of protein post-translational modifications by mass spectrometry. *Acc. Chem. Res.* 36, 453–461. doi: 10.1021/ar0201431

Stulemeijer, I. J., and Joosten, M. H. (2008). Post-translational modification of host proteins in pathogen-triggered defence signalling in plants. *Mol. Plant Pathol.* 9, 545–560. doi: 10.1111/j.1364-3703.2008.00468.x

Tikkanen, M., Gollan, P. J., Suorsa, M., Kangasjarvi, S., and Aro, E. M. (2012). STN7 Operates in retrograde signaling through controlling redox balance in the electron transfer chain. *Front. Plant Sci.* 3, 277. doi: 10.3389/fpls.2012.00277

Wagner, D., Przybyla, D., Op den Camp, R., Kim, C., Landgraf, F., Lee, K. P., et al. (2004). The genetic basis of singlet oxygen-induced stress responses of Arabidopsis thaliana. *Science* 306, 1183–1185. doi: 10.1126/science.1103178

Walter, P., and Ron, D. (2011). The unfolded protein response: from stress pathway to homeostatic regulation. *Science* 334, 1081–1086. doi: 10.1126/science.1209038

Wang, L., Kim, C., Xu, X., Piskurewicz, U., Dogra, V., Singh, S., et al. (2016). Singlet oxygen- and EXECUTER1-mediated signaling is initiated in grana margins and depends on the protease FtsH2. *Proc. Natl. Acad. Sci. U.S.A.* 113, E3792–E3800. doi: 10.1073/pnas.1603562113

Wu, G. Z., Chalvin, C., Hoelscher, M., Meyer, E. H., Wu, X. N., and Bock, R. (2018). Control of retrograde signaling by rapid turnover of GENOMES UNCOUPLED1. *Plant Physiol.* 176, 2472–2495. doi: 10.1104/pp.18.00009

Wu, G. Z., Meyer, E. H., Richter, A. S., Schuster, M., Ling, Q., Schottler, M. A., et al. (2019). Control of retrograde signalling by protein import and cytosolic folding stress. *Nat. Plants* 5, 525–538. doi: 10.1038/s41477-019-0415-y

Yamamoto, Y., Hori, H., Kai, S., Ishikawa, T., Ohnishi, A., Tsumura, N., et al. (2013). Quality control of Photosystem II: reversible and irreversible protein aggregation decides the fate of Photosystem II under excessive illumination. *Front. Plant Sci.* 4, 433. doi: 10.3389/fpls.2013.00433

Yu, F., Park, S., and Rodermel, S. R. (2005). Functional redundancy of AtFtsH metalloproteases in thylakoid membrane complexes. *Plant Physiol.* 138, 1957–1966. doi: 10.1104/pp.105.061234

Zybailov, B., Friso, G., Kim, J., Rudella, A., Rodriguez, V. R., Asakura, Y., et al. (2009). Large scale comparative proteomics of a chloroplast Clp protease mutant reveals folding stress, altered protein homeostasis, and feedback regulation of metabolism. *Mol. Cell Proteomics* 8, 1789–1810. doi: 10.1074/mcp.M900104-MCP200

Conflict of Interest: The author declares that the research was conducted in the absence of any commercial or financial relationships that could be construed as a potential conflict of interest.

frontiers in Plant Science

ORIGINAL RESEARCH
published: 27 February 2020
doi: 10.3389/fpls.2020.00157

Crystal Structure of the Chloroplastic Glutamine Phosphoribosylpyrophosphate Amidotransferase GPRAT2 From *Arabidopsis thaliana*

Xueli Cao[1†], Bowen Du[1†], Fengjiao Han[1†], Yu Zhou[2], Junhui Ren[1], Wenhe Wang[1], Zeliang Chen[1,3] and Yi Zhang[1]*

[1] Beijing Advanced Innovation Center for Soft Matter Science and Engineering, Beijing Key Laboratory of Bioprocess, Beijing University of Chemical Technology, Beijing, China, [2] Department of Computational Chemistry, National Institute of Biological Sciences, Beijing, China, [3] Key Laboratory of Livestock Infectious Diseases in Northeast China, Ministry of Education, College of Animal Science and Veterinary Medicine, Shenyang Agricultural University, Shenyang, China

OPEN ACCESS

Edited by:
Yan Lu,
Western Michigan University,
United States

Reviewed by:
Lin Liu,
Anhui University, China
Xiaochun Li,
UT Southwestern Medical Center,
United States

***Correspondence:**
Yi Zhang
zhangyishirly@hotmail.com

†These authors have contributed equally to this work

Specialty section:
This article was submitted to Plant Physiology, a section of the journal Frontiers in Plant Science

Received: *20 December 2019*
Accepted: *31 January 2020*
Published: *27 February 2020*

Citation:
Cao X, Du B, Han F, Zhou Y, Ren J, Wang W, Chen Z and Zhang Y (2020) Crystal Structure of the Chloroplastic Glutamine Phosphoribosylpyrophosphate Amidotransferase GPRAT2 From Arabidopsis thaliana. Front. Plant Sci. 11:157. doi: 10.3389/fpls.2020.00157

Chloroplastic glutamine phosphoribosylpyrophosphate amidotransferase (GPRATase) catalyzes the first committed step of *de novo* purine biosynthesis in *Arabidopsis thaliana*, and DAS734 is a direct and specific inhibitor of AtGPRAT, with phytotoxic effects similar to the leaf beaching phenotypes of known AtGPRAT genetic mutants, especially *cia1* and *atd2*. However, the structure of AtGPRAT and the inhibition mode of DAS734 still remain poorly understood. In this study, we solved the structure of AtGPRAT2, which revealed structural differences between AtGPRAT2 and bacterial enzymes. Kinetics assay demonstrated that DAS734 behaves as a competitive inhibitor for the substrate phosphoribosyl pyrophosphate (PRPP) of AtGPRAT2. Docking studies showed that DAS734 forms electrostatic interactions with R264 and hydrophobic interactions with several residues, which was verified by binding assays. Collectively, our study provides important insights into the inhibition mechanism of DAS734 to AtGPRAT2 and sheds light on future studies into further development of more potent herbicides targeting *Arabidopsis* GPRATases.

Keywords: chloroplastic glutamine phosphoribosylpyrophosphate amidotransferase, herbicide, X-ray crystallography, competitive inhibition, Arabidopsis thaliana, DAS734

INTRODUCTION

De novo purine nucleotide biosynthesis is important for plant growth and development. This essential pathway in plant metabolism plays series of key roles, including providing purine precursors for DNA and RNA, B-class vitamins, and plant hormones (Senecoff et al., 1996; Herz et al., 2000; Moffatt and Ashihara, 2002). In addition, several vital coenzymes, such as NAD, FAD, and FMN, are derived from this pathway and phosphoribosylpyrophosphate (PRPP) is utilized in the biosynthesis of all these coenzymes. (Hanson and Gregory, 2002; Boldt and Zrenner, 2003; Zrenner et al., 2006; Hove-Jensen et al., 2017). As the key regulatory enzyme in the pathway,

researches into the glutamine phosphoribosylpyrophosphate amidotransferase (GPRATase) of *Arabidopsis thaliana* have shown the important role of *de novo* purine biosynthesis in chloroplast development or function as well as cell division (Hung et al., 2004; Yang et al., 2015).

GPRATase catalyzes the first committed step of purine biosynthesis (Smith et al., 1994; Smith and Atkins, 2002), transforming phosphoribosylpyrophosphate (PRPP) to phosphoribosylamine (PRA) with amide group of glutamine as nitrogen source. The entire catalytic reaction is shown in **Figure S1** (Walsh et al., 2007). Ten enzymatic reactions are required in the purine biosynthesis pathway to generate inosine monophosphate (IMP). Out of these ten enzymatic transformations, six enzymes including GPRATase are common, and four steps could be catalyzed by different enzymes in various organisms (Zhang et al., 2008). Two aminotransferases are involved in this pathway, GPRATase with an N-terminal nucleophile-glutaminase and PurLQS with a triad glutaminase activity, respectively (Zhang et al., 2008). GPRATase is also subjected to feed-back inhibition by purine nucleotides and thus forms the important control over *de novo* purine biosynthesis (Walsh et al., 2007). Genes encoding GPRATase have been found in bacteria, Eukarya, and Archaea. However, only the enzymes from *Escherichia coli* (*E. coli*) and *Bacillus subtilis* (*B. subtilis*) have been characterized through structural and biochemical studies (Smith, 1998). The two enzymes are both homo-tetramers and are representative of two classes of GPRATases. The *B. subtilis* GPRATase (BsGPRAT) is synthesized with an N-terminal propeptide and an Fe-S center, whereas the *E. coli* GPRATase (EcGPRAT) has neither of them. Three homologs of GPRATases (AtGPRAT1-3) exist in the Arabidopsis genome with differentially expression pattern in various plant tissues (Ito et al., 1994; Boldt and Zrenner, 2003; Hung et al., 2004; van der Graaff et al., 2004; Woo et al., 2011), which is quite different from most of the other enzymes in purine biosynthesis present with a single isoform (Boldt and Zrenner, 2003). Previous biochemical and genetic studies have confirmed that AtGPRAT2 (At4g34740) is the major isoform expressing in leaves (Hung et al., 2004).

AtGPRAT2 was localized in the stroma of chloroplasts in *Arabidopsis* leaf cells (Hung et al., 2004), and recently was further confirmed in the nucleoid of chloroplasts (Yang et al., 2015). The AtGPRAT2-deficient mutants *cia1* (chloroplast import apparatus1), *dov1* (differential development of vascular associated cells 1), *dg169* (delayed greening 169), *alx13* (altered APX2 expression 13), and knock out mutant *atd2* (amidotransferase-deficient2) showed growth retardation and bleached seedling phenotype which was also regarded as leaf chlorosis, but could survive under low light condition (Hung et al., 2004; van der Graaff et al., 2004; Woo et al., 2011; Rosar et al., 2012; Yang et al., 2015). The bleached new leaves imply damage by photooxidative effects or harmful effects on chloroplast biogenesis. The phenotype could be restored to wild-type by the addition of AMP or IMP, but not cytokinin or nicotinamide adenine dinucleotide (NADH), to the medium (Hung et al., 2004; van der Graaff et al., 2004). The leave number of *cia1* mutant is only half of wild-type plants, while with slightly smaller cell size. In addition, the protein-import efficiency of the chloroplasts isolated from *cia1* mutant is only less than 50% compared with wild-type chloroplasts, but the import efficiency cannot be rescued by adding ATP and GTP. These phenotypes suggested that *de novo* purine biosynthesis is also vital for cell division and chloroplast biogenesis. A recent research into *dg169* mutant indicated AtGPRAT2 featured in early chloroplast development through maintaining PEP (plastid-encoded RNA polymerases) function, thus sustaining normal transcription and translation (Yang et al., 2015).

Currently, very few small molecules have been known to act directly and specifically on the important purine biosynthetic pathway, especially in the initial reactions of the pathway, while the novel phenyltriazole acetic acid [5-(4-chlorophenyl)-1-isopropyl-1H-[1,2,4]triazol-3-yl]-acetic acid (DAS734) compound is an exception in contrast to nonspecific inhibitors such as azaserine, acivicin, and 6-diazo-5-oxo-L-norleucine (Lyons et al., 1990). DAS734 shows herbicidal activity on the seedlings of a variety of dicotyledonous weeds, producing bleaching of newly emerged leaves and root inhibition, phenocopying *AtGPRAT2* mutants with variegated bleached-white appearance (Hung et al., 2004; van der Graaff et al., 2004). However, the phenotype it induced is different from many other herbicidal inhibitors of primary metabolism. It is lethal when *Arabidopsis* seedlings were treated with more than 5 μM DAS734. In particular, DAS734 is effective on Arabidopsis, but with no inhibitory activity on *E. coli*, cyanobacteria, green algae, or yeasts. The phytotoxic effects of DAS734 can be alleviated only by the end product adenine and its derivatives (Walsh et al., 2007), similar to the phenotypes of GPRATase mutants. The combination of genetic and biochemical study has confirmed that the phytotoxicity of DAS734 results from direct inhibition of AtGPRATases. Therefore, treatment by DAS734 is equal to knockout mutants lacking *AtGPRAT2* and *AtGPRAT3* or even all GPRAT activity, thus overcoming GPRAT genetic redundancy. Therefore, DAS734 has been established as a specific biochemical probe for plant purine biosynthesis and especially useful in analyzing how the disrupted GPRATases impose influences on impaired chloroplast biogenesis and new leaf bleaching. In addition, DAS734 could also be used as a novel bleaching herbicide (Walsh et al., 2007). Despite the importance of plant GPRATases and its inhibitor DAS734, studies into the structure of plant GPRATases and inhibition mechanism of DAS734 have been enigmatic.

Here, we report the crystal structure of AtGPRAT2 and investigate the binding mode of DAS734 through molecular biochemical and docking studies. Our results indicated that AtGPRAT2 folds more like BsGPRAT than EcGPRAT. Compared with bacterial enzymes, AtGPRAT2 also exhibits different features in the conformations of active site loops. Molecular docking and kinetics studies suggested that DAS734 inhibits AtGPRAT2 through a competitive manner with respect to PRPP. Together, our study offers insights into the inhibition mechanism of DAS734 on AtGPRAT2 and will facilitate further development of more potent herbicides targeting *Arabidopsis* GPRATases.

MATERIALS AND METHODS

Materials

The pfu polymerase, the two restriction enzymes Nde I and Xho I and T4 DNA ligase were all purchased from Thermo Fisher. Ni-NTA beads were purchased from QIAGEN and the Superdex-200 column was purchased from GE Healthcare. DAS734 was synthesized as described in Walsh et al. (2007).

Cloning, Expression, and Purification

The gene of AtGPRAT2 was amplified from the complementary DNA (cDNA) of *Arabidopsis thaliana* and sub-cloned into the bacterial expression vector pET22b, to produce a C-terminal His-tagged fusion protein. The AtGPRAT2 mutants were generated by two-step PCR and were subcloned, overexpressed and purified in the same way as wild-type protein. The protein was expressed in *E. coli* strain BL21 and induced by 0.2 mM isopropyl-β-D-thiogalactopyranoside (IPTG) when the cell density reached an OD_{600nm} of 1.0. After growth at 16°C for 18 h, the cells were harvested, re-suspended in lysis buffer (50 mM Tris pH 8.0, 10 mM imidazole, and 300 mM NaCl) and lysed by sonication. Recombinant His-tagged protein was purified by Ni-affinity column chromatography and was further subjected to gel filtration chromatography (Superdex-200 column) in buffer containing 10 mM Tris-HCl pH 8.0, 200 mM NaCl, 5 mM dithiothreitol (DTT). The purified protein was analyzed by sodium dodecyl sulfate polyacrylamide gel electrophoresis (SDS–PAGE). The fractions containing the target protein were pooled and concentrated to 20 mg/ml.

Crystallization, Data Collection, Processing, and Structure Determination

Crystallization screening was performed by the sitting-drop vapor-diffusion method at 291 K. 1 μl protein solution (20 mg/ml) was mixed with an equal volume of reservoir solution in 48-well plates and the drops were equilibrated against 80 μl reservoir solution. Crystals appeared from several conditions, out of which HR2-110 No. 11 from Hampton Research was further taken to do crystal optimization. Crystals of the best diffraction quality appeared in about 1 week, which were used for data collection. The final optimized condition was 0.1 M Sodium citrate tribasic pH 5.6, 1.5 M ammonium phosphate monobasic, and 0.1 M citric acid pH 3.4.

All the data were collected at SSRF beamline BL17U1 and BL19U1, integrated and scaled using the HKL2000 package (Otwinowski, 1997). The initial model was solved by molecular replacement by the PHASER program from the CCP4 suite (Collaborative Computational Project, 1994) and refined manually using COOT (Emsley and Cowtan, 2004). The structure was further refined with PHENIX (Adams et al., 2002) using non-crystallographic symmetry and stereochemistry information as restraints. The final structure was obtained through several rounds of refinement.

Docking Studies

The inhibitor DAS734 was docked onto AtGPRAT2 using UCSF DOCK 3.7 (Coleman et al., 2013). The binding site was defined as the set of protein residues which have at least one heavy atom within 10 Å of the residue R264. A flexible-receptor docking protocol was applied to treat binding-site side-chain flexibility (Li et al., 2019). Multiple poses were generated for structural filtering and conformational clustering (Peng et al., 2013). All the survived poses were then submitted for MM-GB/SA refining and rescoring with OPLS all-atom force field (Banks et al., 2005) using UCSF PLOP (Jacobson et al., 2004). The conformation of 472-477 loop was rebuilt and minimized along with the ligand considering its ambiguous electron density.

AtGPRAT2 Enzymatic Activity Assay

Purified wild-type and mutant AtGPRAT2s were desalted to a buffer containing 10 mM Tris pH 7.8, 200 mM NaCl, 5 mM $MgCl_2$, and 10 mM DTT. AtGPRAT2 activity was assayed by measuring the production of Glu from Gln. Glu production was determined by coupling the glutamate dehydrogenase (GDH) reaction (Messenger and Zalkin, 1979), in which Glu was oxidized and NAD^+ was simultaneously reduced to NADH. Then, we continuously monitored NADH produced at 340 nm every 1 second, using a UV-VIS SPECTROPHOTOMETER UV-2450 (SHIMADZU). The standard assay for enzymatic activity measurement contained 37.5 mM NAD^+, 10 mM Gln, 2.5 mM PRPP, 247.5 units/ml GDH, 110 mM potassium phosphate buffer pH 8.0, and about 0.125 mg/ml AtGPRAT2 in a total volume of 300 μl. The reaction was initiated by the addition of AtGPRAT2 and the enzymatic activities were determined utilizing extinction coefficient for NADH of 6,220 cm^{-1} M^{-1} at 340 nm. For calculating the kinetic constants K_m and V_{max}, we held the Gln concentration constant at 10 mM, and fitted the data to the appropriate equations using GraphPad Prism software with mixed inhibition model. Effects of inhibition by DAS734 were determined by the standard assay in which DAS734 at concentration of 0, 10, 20, and 40 μM was added respectively. Then we calculated the *K*i using the GraphPad Prism software with mixed inhibition model.

Isothermal Titration Calorimetry Binding Assay

The dissociation constants of binding reactions of wild-type and mutants of AtGPRAT2 with DAS734 were determined by isothermal titration calorimetry (ITC) using a MicroCal ITC200 calorimeter. Proteins were desalted into the working buffer [20 mM 4-(2-hydroxyethyl)-1-piperazineethanesulfonic acid (HEPES) pH 7.5, 200 mM NaCl]. The titration was carried out with 19 successive injections of 2 μl DAS734 at the 0.3 mM concentration, spaced 125 s apart, into the sample cell containing AtGPRAT2 at the 0.04 mM concentration at 25°C. The Origin software was used for baseline correction, integration, and curve fitting to a single site binding model.

RESULTS

Overall Structure of AtGPRAT2

We solved the crystal structure of a recombinant $AtGPRAT2^{75-561}$ without the predicted chloroplast transit peptide at 3.07 Å

resolution (**Figure 1A** and **Table S1**). This recombinant protein exhibited high GPRATase activity which was measured by the enzymatic assay (**Figure 2C** and **Table S2**). The crystal belonged to the P3121 space group and two AtGPRAT2 molecules were found in the asymmetric unit, each with a 4Fe-4S cofactor. However, the PISA (Proteins, Interfaces, Structures and Assemblies) server (Krissinel and Henrick, 2007) indicated that AtGPRAT2 exists as a homo-tetramer in crystal as other members of this family (**Figure 1B**). It was known that all eukaryotic and many microbial GPRATs harbor a short N-terminal propeptide, which is autocatalytically cleaved to yield a conserved N-terminal Cys. Walsh et al. also showed that in recombinant AtGPRAT2 expressed in *E. coli*, the propeptide was removed to expose the N-terminal catalytic Cys87 (Walsh et al., 2007). Consistent with this, in the AtGPRAT2 structure, the first residue with interpretable electron density was the predicted N-terminal Cys87, the mutation of which abolished the activity of the enzyme (**Figure 2C**). Moreover, the visible electron density corresponded to the AtGPRAT2 fragment spanning residues from 87 to 546. Similar to members of this family, the overall structure of AtGPRAT2 folds into an N-terminal glutaminase (Glnase) domain (residues 87-320) and a C-terminal phosphoribosyltransferase (PRTase) domain (residues 321-546) (**Figures 1A, C**). Structural comparison indicated that AtGPRAT2 adopts an inactive, open conformation as compared to the structures of the EcGPRAT in the presence or absence of the PRPP analog carboxylic PRPP (cPRPP), which represent the active and inactive state, respectively (**Figure S2**).

Structural Comparison With Other GPRATases

The reaction catalyzed by GPRATases is carried out as two half-reactions by two separate domains, in tight allosteric communication between each other (Smith, 1998; Bera et al., 2000). One is the Glnase domain where Gln is hydrolyzed to yield ammonia. And then, the ammonia is transferred through a ~20-Å hydrophobic channel to a distal PRTase domain, in which PRA is synthesized from PRPP and ammonia. Formation of the ammonia channel is a characteristic of the glutamine amidotransferases, which catalyze the synthesis of different aminated products (Mouilleron and Golinelli-Pimpaneau, 2007). Unlike the carbamoyl-phosphate synthetase (CPS) and asparagine synthetase B (AsnB), in which the channel forms in the absence of an acceptor, the

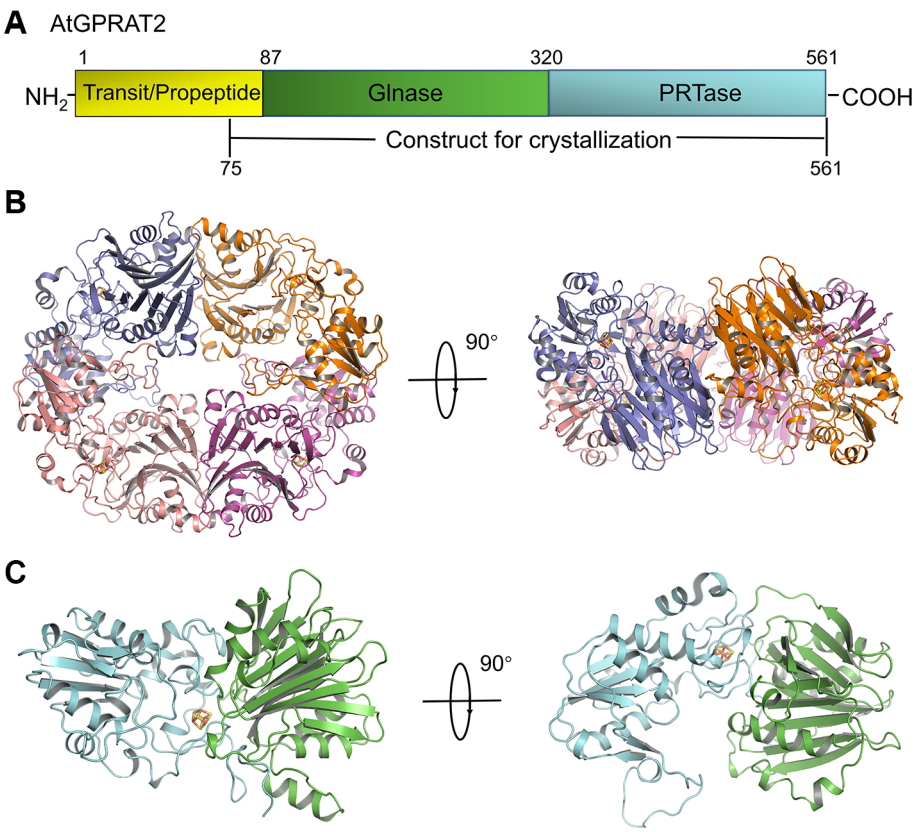

FIGURE 1 | Overview of AtGPRAT2. **(A)** The domain architecture of AtGPRAT2, and the construct for crystallization is indicated in the bottom. **(B)** Cartoon model of the tetramer conformation of AtGPRAT2. The protomers are shown in different colors and the 4Fe-4S cofactor is shown in sticks. Two views are shown. **(C)** Cartoon model of one protomer of AtGPRAT2. The Glnase domain and PRTase domain are colored in green and cyan, respectively. Two views are shown.

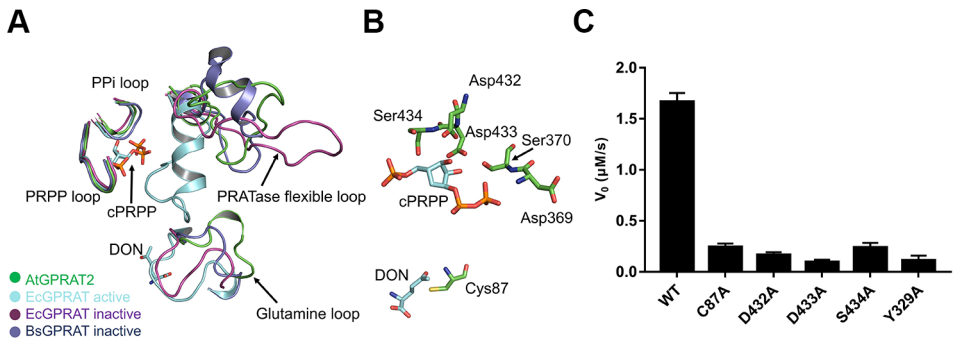

FIGURE 2 | Active site of AtGPRAT2. **(A)** Structural superimposition of AtGPRAT2, EcGPRAT in the active [Protein Data Bank (PDB): 1ECC] and inactive (PDB: 1ECF) conformation, and *Bacillus subtilis* glutamine phosphoribosylpyrophosphate amidotransferase (BsGPRAT) in the inactive conformation (PDB: 1GPH). Only the indicated loop regions are shown in cartoon models. The ligands in 1ECC are shown as sticks. cPRPP, carbocyclic phosphoribosyl pyrophosphate (PRPP). DON, 6-diazo-5-oxo-L-*nor*-leucine, is an analog of substrate glutamine. The conserved loop regions are marked. **(B)** An enlarged view of the active site of AtGPRAT2. Several active site residues (green) and the substrate analogs cPRPP and DON in the aligned structure of EcGPRAT in the active conformation (PDB: 1ECC) are shown in sticks. **(C)** Activity assay with the wildtype and several active site mutants of AtGPRAT2. Error bars are standard error of the mean (SEM) values of three independent experiments.

formation of the channel in AtGPRAT2 requires the binding of acceptor and closing of the PRTase flexible loop, similar as EcGPRAT and BsGPRAT (**Figure S2**). Whereas the exact shape of the channel still awaits the structure of AtGPRAT2 complexed with PRPP or cPRPP, one can get information from that of EcGPRAT based on the high identity of the channel-lining residues between the two proteins (Bera et al., 2000) (**Figure S3**). Then we compared the structures of the essential catalytic motifs of the two domains between AtGPRAT2 and bacterial enzymes (**Figure 2A**). In the Glnase domain, a conserved glutamine loop binds glutamine during the first half reaction. In contrary to the glutamine loop of EcGPRAT, which is in a closed conformation no matter glutamine binds or not, the glutamine loop of AtGPRAT2 exhibits an open conformation more similar to that of BsGPRAT (**Figure 2A**). Nevertheless, the glutamine loop of AtGPRAT2 opens to an extent larger than that of BsGPRAT, and forms a 3_{10} helix (**Figure 2A**). In the PRTase domain, three loops in core fold are important for PRPP binding and catalysis (**Figure S3**). The "PRPP loop" binds the ribose-5-phosphate group of PRPP and the adjacent "PPi loop" interacts with the pyrophosphate of PRPP. The PRTase flexible loop undergoes remarkable conformational change during the catalysis, which closes over the active site as a helix when PRPP binds and is generally open when the substrate binding site is free. Structural superimposition indicated that both PRPP and PPi loops exhibit highly conserved folds, and single mutations of three residues Asp432, Asp433 and S434 within the PRPP loop all markedly decreased the activities of AtGPRAT2 (**Figure 2C**). The PRTase flexible loops of AtGPRAT and bacterial enzymes display different open conformations, consistent with the disordered feature of this loop. This is also confirmed by the high B-factors of the PRTase flexible loop region of AtGPRAT2 (**Figure S4A**). The C-terminal helix (residues 471-492 in EcGPRAT) is also an important feature of EcGPRAT (**Figure S2**) (Smith, 1998). However, similar as BsGPRAT, AtGPRAT2 does not contain the helix and the corresponding region folds as a flexible loop (**Figures S2** and **S4**).

DAS734 Inhibits AtGPRAT2 in a Competitive Manner With Respect to Phosphoribosyl Pyrophosphate

Studies into GPRATases from bacteria and eukaryotes found that the enzyme undergoes feedback inhibition by the end products of the purine biosynthetic pathway, such as AMP, GMP, ADP, and GDP (Chen et al., 1997). Recently, the growth regulator, guanosine tetraphosphate (ppGpp) was also shown to inhibit EcGPRAT in a competitive manner (Wang et al., 2019). DAS734 has been shown to be a slow, tight-binding inhibitor for both AtGPRAT2 and AtGPRAT3 (Walsh et al., 2007). To characterize the inhibition mode of DAS734, we performed *in vitro* enzymatic kinetics assay of AtGPRAT2. In the study of Walsh et al. they determined the *K*m for glutamine as 1.34 mM. Here in this study, we set up a coupled-enzyme reaction with AtGPRAT2 and glutamate dehydrogenase to monitor the production of glutamate by AtGPRAT2 continuously. Using this system, we determined the K_m of AtGPRAT2 for PRPP as 0.35 mM (**Figure S5**). And then, the kinetics of AtGPRAT2 was tested under different concentrations of DAS734. The inhibition kinetics (**Figure 3A** and **Table S3**) showed that DAS734 behaves like a competitive inhibitor with respect to PRPP with a *K*i of 5.293 μM.

The Binding Site of DAS734

Two inhibitor binding sites are located in the PRTase domain, an A (allosteric) site and a C (catalytic) site (**Figure 3B**) (Chen et al., 1997). The A site overlaps the site for the pyrophosphate of PRPP, and the C site overlaps the site for the ribose-5-phosphate part of PRPP. Synergistic inhibition of GPRATases was also

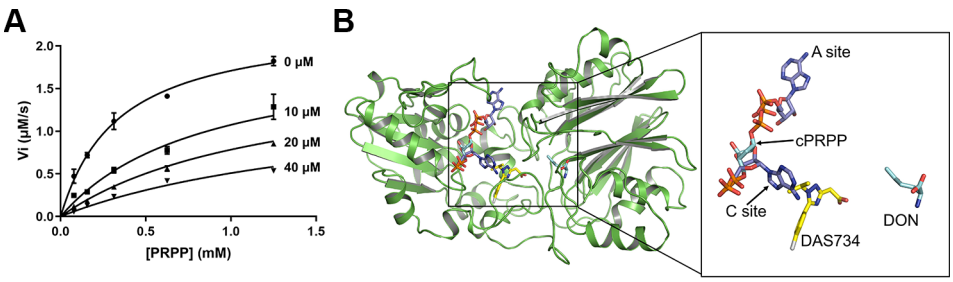

FIGURE 3 | The inhibition mode of DAS734 on AtGPRAT2. **(A)** Inhibition kinetics showing that DAS734 is a competitive AtGPRAT2 inhibitor with respect to phosphoribosyl pyrophosphate (PRPP). The labels indicate different DAS734 concentrations. The data was fitted to the mixed inhibition model in GraphPad Prism software, and the alpha value of 12.56 calculated by this model indicated a competitive inhibition. Error bars are standard error of the mean (SEM) values of three independent experiments. **(B)** Structural superimposition of AtGPRAT2 with docked DAS734, EcGPRAT in the active [Protein Data Bank (PDB): 1ECC] and BsGPRAT in the inactive conformation (PDB: 1GPH). The cPRPP and 6-diazo-5-oxo-L-*nor*-leucine (DON) in the structure of 1ECC are shown as cyan sticks. The two AMP molecules in the A and C sites are shown as slate sticks. The docked DAS734 is shown in yellow sticks with the chlorine atom colored in gray.

observed by a combination of adenine and guanine nucleotides (Chen et al., 1997; Smith, 1998). However, ppGpp was found to bind at the interface between the Glnase domains of two protomers within the tetramer in a ratio of 1:2 (ppGpp to EcGPRAT), a position totally different from the known A and C sites (Wang et al., 2019).

To get insights into the binding site of DAS734 within AtGPRAT2, we attempted to get the complex structure of AtGPRAT2 with DAS734 but still failed. Therefore, we turned to docking assays to analyze the binding sites of DAS734. Previous studies have shown that the R264K mutation of AtGPRAT2 will render the enzyme highly insensitive to DAS734 (Walsh et al., 2007). Therefore, the docking region was set around R264 of AtGPRAT2. The results showed that the binding site of DAS734 partially overlaps with the known C site in the PRTase domain (**Figure 3B**).

The binding of DAS734 to AtGPRAT2 was found to involve both hydrophilic and hydrophobic interactions (**Figure 4A**). The guanidyl group of R264 forms electrostatic interactions with the carboxyl group of the acetate moiety. Moreover, the oxygen atom of the carboxyl group also forms a hydrogen bond with the amide nitrogen atom of V473. In addition, the sidechains of F325, Y329, F330, and I465 form hydrophobic interactions with DAS734 (**Figure 4A**). To validate the docking results, we performed the isothermal titration calorimetry (ITC) assay with wildtype, R264K and Y329A mutants of AtGPRAT2. The results showed that the R264K mutation abolished the binding of DAS734 to AtGPRAT2, but the Y329A mutation

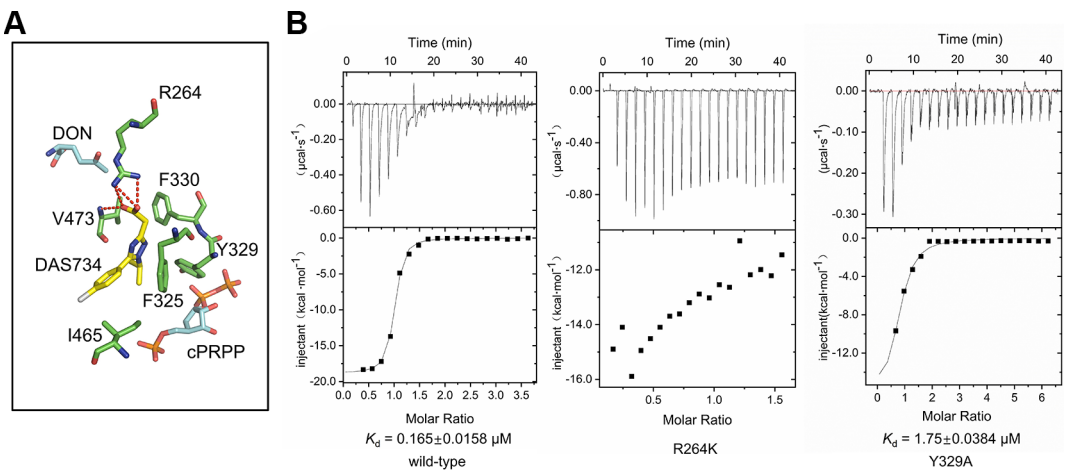

FIGURE 4 | The binding site of DAS734. **(A)** Structural superimposition of AtGPRAT2 with docked DAS734 and EcGPRAT in the active [Protein Data Bank (PDB): 1ECC] conformation. The AtGPRAT2 residues involved in DAS734 binding are shown as sticks. The carbocyclic phosphoribosyl pyrophosphate (cPRPP) and 6-diazo-5-oxo-L-*nor*-leucine (DON) molecules in EcGPRAT are colored as in **Figure 3B**. Electrostatic interactions and hydrogen bonds are shown as red dashed lines. **(B)** Interaction of AtGPRAT2 mutants and DAS734 as detected by isothermal titration calorimetry (ITC). The ITC curves are shown. The calculated K_d mean ± SE values are indicated. The top plots represent time, and the bottom plots represent molar ratio. These experiments were performed twice with equivalent results.

only slightly decreased DAS734 binding (**Figure 4B**). This suggested that the electrostatic interactions from R264 contribute much to the binding of DAS734, while the hydrophobic interaction from Y329 may play a minor role. In the previous study, P476S, P265S, and G371S mutations could also confer resistance to DAS734 at levels of around 60, 6, and 5-fold, respectively. We also analyzed these three sites in the structure of AtGPRAT2 docked with DAS734 (**Figure S6**). P476 is adjacent to the binding pocket of DAS734 and on the same loop with V473, whose amide nitrogen atom forms a hydrogen bond with the carboxyl group of the acetate moiety of DAS734. P265S mutation may affect the location of R264, thus interfering with DAS734 binding. G371 is in the PRTase domain and away from the binding pocket of DAS734. The G371S mutation may confer resistance to DAS734 through allosteric communications between the two domains.

DISCUSSION

GPRATase catalyzes the first committed step of *de novo* purine biosynthesis. Although genes encoding GPRATase have been found in bacteria, Eukarya, and Archaea, only the GPRATase from *E. coli* and *B. subtilis* have been characterized through structural and biochemical studies. AtGPRAT2 is the primary isoform among the three homologs of GPRATases (AtGPRAT1-3) in *Arabidopsis thaliana*. To our knowledge, the 3.07 Å crystal structure of AtGPRAT2 in this study offered the first description of the structure of GPRATases in plants, with several structural differences, especially in the catalytic motifs, when compared with bacterial enzymes.

Combined with GPRATase kinetic assay, ITC and molecular docking, we showed that DAS734 behaved as a competitive inhibitor for PRPP and proposed the binding site of DAS734. Notably, the binding site of DAS734 does not interfere with the interface between each monomer in the tetrameric structure (**Figure S7**). Interestingly, the docking site of DAS734 does not directly overlaps the binding site of PRPP (**Figure 3B**), raising the question of how DAS734 behaves its competitive function with respect to PRPP. We proposed that the binding of DAS734 might induce conformational changes surrounding it, thus influencing the binding of PRPP. Supporting this notion, Y329 is a highly conserved residue among GPRATases and its counterpart in EcGPRAT, Y258, interacts with the pyrophosphate group of PRPP (Krahn et al., 1997). Consistently, the Y329A mutation almost abolished the activity of AtGPRAT2 (**Figure 2C**). In contrast, the EcGPRAT counterparts of the interacting residues of DAS734 do not contribute to glutamine binding (data not shown). Walsh et al. also showed that DAS734 is a noncompetitive inhibitor with respect to glutamine (Walsh et al., 2007). Therefore, the binding of DAS734 to AtGPRAT2 might cause movements of its surrounding residues, especially Y329, thus preventing PRPP binding. However, this still needs to be tested in the future studies.

DAS734 could be used not only as a specific biochemical probe to help analyze how disruption of GPRATases damage the chloroplast development or function and lead to the leaf bleaching, but also as a novel bleaching herbicide(Walsh et al., 2007). In the future, more efforts should be made in the development of more potent herbicides targeting *Arabidopsis* GPRATases according to the inhibition mechanism of DAS734 to AtGPRAT2.

DATA AVAILABILITY STATEMENT

The coordinate and structure factors for AtGPRAT2 have been deposited in the Protein Data Bank (PDB) under the accession code: 6LBP. All other data are available from the corresponding author upon reasonable request.

AUTHOR CONTRIBUTIONS

YiZ conceived, designed and supervised the project. XC, BD, FH, JR, WW and ZC purified the proteins, grew and optimized the crystals, collected the diffraction data, solved the structure and performed enzymatic analysis. YuZ performed docking studies. YiZ analyzed the data and wrote the paper with the help of all the authors.

FUNDING

This work was supported by the National Natural Science Foundation of China (31822012), and the Fundamental Research Funds for the Central Universities (XK1802-8 and ZY1934).

ACKNOWLEDGMENTS

We thank Song Xue for the discussions about the inhibition mechanisms of DAS734, Yue Feng and Jianwei Zeng for structure refinement. We would like to thank the staff at beamline BL17U1 and BL19U1 of the Shanghai Synchrotron Radiation Facility for their assistance with data collection. We would like to thank the Tsinghua University Branch of China National Center for Protein Sciences Beijing and Shilong Fan for providing facility support for X-ray diffraction of the crystal samples.

SUPPLEMENTARY MATERIAL

The Supplementary Material for this article can be found online at: https://www.frontiersin.org/articles/10.3389/fpls.2020.00157/full#supplementary-material

REFERENCES

Adams, P. D., Grosse-Kunstleve, R. W., Hung, L. W., Ioerger, T. R., McCoy, A. J., Moriarty, N. W., et al. (2002). PHENIX: building new software for automated crystallographic structure determination. *Acta Crystallogr. D Biol. Crystallogr.* 58, 1948–1954. doi: 10.1107/S0907444902016657

Banks, J. L., Beard, H. S., Cao, Y. X., Cho, A. E., Damm, W., Farid, R., et al. (2005). Integrated modeling program, applied chemical theory (IMPACT). *J. Comput. Chem.* 26, 1752–1780. doi: 10.1002/jcc.20292

Bera, A. K., Smith, J. L., and Zalkin, H. (2000). Dual role for the glutamine phosphoribosylpyrophosphate amidotransferase ammonia channel. Interdomain signaling and intermediate channeling. *J. Biol. Chem.* 275, 7975–7979. doi: 10.1074/jbc.275.11.7975

Boldt, R., and Zrenner, R. (2003). Purine and pyrimidine biosynthesis in higher plants. *Physiol. Plant* 117, 297–304. doi: 10.1034/j.1399-3054.2003.00030.x

Chen, S., Tomchick, D. R., Wolle, D., Hu, P., Smith, J. L., Switzer, R. L., et al. (1997). Mechanism of the synergistic end-product regulation of Bacillus subtilis glutamine phosphoribosylpyrophosphate amidotransferase by nucleotides. *Biochemistry* 36, 10718–10726. doi: 10.1021/bi9711893

Coleman, R. G., Carchia, M., Sterling, T., Irwin, J. J., and Shoichet, B. K. (2013). Ligand pose and orientational sampling in molecular docking. *PloS One* 8, e75992. doi: 10.1371/journal.pone.0075992

Collaborative Computational Project, N (1994). The CCP4 suite: programs for protein crystallography. *Acta Crystallogr. D Biol. Crystallogr.* 50, 760–763. doi: 10.1107/S0907444994003112

Emsley, P., and Cowtan, K. (2004). Coot: model-building tools for molecular graphics. *Acta Crystallogr. D Biol. Crystallogr.* 60, 2126–2132. doi: 10.1107/S0907444904019158

Hanson, A. D., and Gregory, J. F.3rd (2002). Synthesis and turnover of folates in plants. *Curr. Opin. Plant Biol.* 5, 244–249. doi: 10.1016/S1369-5266(02)00249-2

Herz, S., Eberhardt, S., and Bacher, A. (2000). Biosynthesis of riboflavin in plants. The ribA gene of Arabidopsis thaliana specifies a bifunctional GTP cyclohydrolase II/3,4-dihydroxy-2-butanone 4-phosphate synthase. *Phytochemistry* 53, 723–731. doi: 10.1016/S0031-9422(00)00013-3

Hove-Jensen, B., Andersen, K. R., Kilstrup, M., Martinussen, J., Switzer, R. L., and Willemoes, M. (2017). Phosphoribosyl diphosphate (PRPP): biosynthesis, enzymology, utilization, and metabolic significance. *Microbiol Mol. Biol. Rev.* 81, 42–57. doi: 10.1128/MMBR.00040-16

Hung, W. F., Chen, L. J., Boldt, R., Sun, C. W., and Li, H. M. (2004). Characterization of Arabidopsis glutamine phosphoribosyl pyrophosphate amidotransferase-deficient mutants. *Plant Physiol.* 135, 1314–1323. doi: 10.1104/pp.104.040956

Ito, T., Shiraishi, H., Okada, K., and Shimura, Y. (1994). Two amidophosphoribosyltransferase genes of Arabidopsis thaliana expressed in different organs. *Plant Mol. Biol.* 26, 529–533. doi: 10.1007/BF00039565

Jacobson, M. P., Pincus, D. L., Rapp, C. S., Day, T. J. F., Honig, B., Shaw, D. E., et al. (2004). A hierarchical approach to all-atom protein loop prediction. *Proteins* 55, 351–367. doi: 10.1002/prot.10613

Krahn, J. M., Kim, J. H., Burns, M. R., Parry, R. J., Zalkin, H., and Smith, J. L. (1997). Coupled formation of an amidotransferase interdomain ammonia channel and a phosphoribosyltransferase active site. *Biochemistry* 36, 11061–11068. doi: 10.1021/bi9714114

Krissinel, E., and Henrick, K. (2007). Inference of macromolecular assemblies from crystalline state. *J. Mol. Biol.* 372, 774–797. doi: 10.1016/j.jmb.2007.05.022

Li, G., Li, W., Xie, Y., Wan, X., Zheng, G., Huang, N., et al. (2019). Discovery of novel pim-1 kinase inhibitors with a flexible-receptor docking protocol. *J. Chem. Info. Modeling* 59, 4116–4119. doi: 10.1021/acs.jcim.9b00494

Lyons, S. D., Sant, M. E., and Christopherson, R. I. (1990). Cytotoxic mechanisms of glutamine antagonists in mouse L1210 leukemia. *J. Biol. Chem.* 265, 11377–11381.

Messenger, L. J., and Zalkin, H. (1979). Glutamine phosphoribosylpyrophosphate amidotransferase from Escherichia coli. Purification and properties. *J. Biol. Chem.* 254, 3382–3392.

Moffatt, B. A., and Ashihara, H. (2002). Purine and pyrimidine nucleotide synthesis and metabolism. *Arabidopsis Book* 1, e0018. doi: 10.1199/tab.0018

Mouilleron, S., and Golinelli-Pimpaneau, B. (2007). Conformational changes in ammonia-channeling glutamine amidotransferases. *Curr. Opin. Struct. Biol.* 17, 653–664. doi: 10.1016/j.sbi.2007.09.003

Otwinowski, Z. „. M. W. (1997). Processing of X-ray diffraction data collected in oscillation mode. *Macromol. Crystallogr.* Pt A, 307–326. doi: 10.1016/S0076-6879(97)76066-X

Peng, S. M., Zhou, Y., and Huang, N. (2013). Improving the accuracy of pose prediction in molecular docking *via* structural filtering and conformational clustering. *Chin. Chem. Lett.* 24, 1001–1004. doi: 10.1016/j.cclet.2013.06.016

Rosar, C., Kanonenberg, K., Nanda, A. M., Mielewczik, M., Brautigam, A., Novak, O., et al. (2012). The leaf reticulate mutant dov1 is impaired in the first step of purine metabolism. *Mol. Plant* 5, 1227–1241. doi: 10.1093/mp/sss045

Senecoff, J. F., McKinney, E. C., and Meagher, R. B. (1996). De novo purine synthesis in Arabidopsis thaliana. II. The PUR7 gene encoding 5'-phosphoribosyl-4-(N-succinocarboxamide)-5-aminoimidazole synthetase is expressed in rapidly dividing tissues. *Plant Physiol.* 112, 905–917. doi: 10.1104/pp.112.3.905

Smith, P. M., and Atkins, C. A. (2002). Purine biosynthesis. Big in cell division, even bigger in nitrogen assimilation. *Plant Physiol.* 128, 793–802. doi: 10.1104/pp.010912

Smith, J. L., Zaluzec, E. J., Wery, J. P., Niu, L., Switzer, R. L., Zalkin, H., et al. (1994). Structure of the allosteric regulatory enzyme of purine biosynthesis. *Science* 264, 1427–1433. doi: 10.1126/science.8197456

Smith, J. L. (1998). Glutamine PRPP amidotransferase: snapshots of an enzyme in action. *Curr. Opin. Struct. Biol.* 8, 686–694. doi: 10.1016/S0959-440X(98)80087-0

van der Graaff, E., Hooykaas, P., Lein, W., Lerchl, J., Kunze, G., Sonnewald, U., et al. (2004). Molecular analysis of "*de novo*" purine biosynthesis in solanaceous species and in Arabidopsis thaliana. *Front. Biosci* 9, 1803–1816. doi: 10.2741/1344

Walsh, T. A., Bauer, T., Neal, R., Merlo, A. O., Schmitzer, P. R., Hicks, G. R., et al. (2007). Chemical genetic identification of glutamine phosphoribosylpyrophosphate amidotransferase as the target for a novel bleaching herbicide in Arabidopsis. *Plant Physiol.* 144, 1292–1304. doi: 10.1104/pp.107.099705

Wang, B., Dai, P., Ding, D., Del Rosario, A., Grant, R. A., Pentelute, B. L., et al. (2019). Affinity-based capture and identification of protein effectors of the growth regulator ppGpp. *Nat. Chem. Biol.* 15, 141–150. doi: 10.1038/s41589-018-0183-4

Woo, N. S., Gordon, M. J., Graham, S. R., Rossel, J. B., Badger, M. R., and Pogson, B. J. (2011). A mutation in the purine biosynthetic enzyme ATASE2 impacts high light signalling and acclimation responses in green and chlorotic sectors of Arabidopsis leaves. *Funct. Plant Biol.* 38, 401–419. doi: 10.1071/FP10218

Yang, Z., Shang, Z., Wang, L., Lu, Q., Wen, X., Chi, W., et al. (2015). Purine biosynthetic enzyme ATase2 is involved in the regulation of early chloroplast development and chloroplast gene expression in Arabidopsis. *Photosynth Res.* 126, 285–300. doi: 10.1007/s11120-015-0131-z

Zhang, Y., Morar, M., and Ealick, S. E. (2008). Structural biology of the purine biosynthetic pathway. *Cell Mol. Life Sci.* 65, 3699–3724. doi: 10.1007/s00018-008-8295-8

Zrenner, R., Stitt, M., Sonnewald, U., and Boldt, R. (2006). Pyrimidine and purine biosynthesis and degradation in plants. *Annu. Rev. Plant Biol.* , 57 805–836. doi: 10.1146/annurev.arplant.57.032905.105421

Conflict of Interest: The authors declare that the research was conducted in the absence of any commercial or financial relationships that could be construed as a potential conflict of interest.

frontiers in Plant Science

MINI REVIEW
published: 11 March 2020
doi: 10.3389/fpls.2020.00186

Chloroplast Calcium Signaling in the Spotlight

Lorella Navazio[1,2†], *Elide Formentin*[1,2†], *Laura Cendron*[1] *and Ildikò Szabò*[1,2*]

[1] Department of Biology, University of Padova, Padova, Italy, [2] Botanical Garden, University of Padova, Padova, Italy

Calcium has long been known to regulate the metabolism of chloroplasts, concerning both light and carbon reactions of photosynthesis, as well as additional non photosynthesis-related processes. In addition to undergo Ca^{2+} regulation, chloroplasts can also influence the overall Ca^{2+} signaling pathways of the plant cell. Compelling evidence indicate that chloroplasts can generate specific stromal Ca^{2+} signals and contribute to the fine tuning of cytoplasmic Ca^{2+} signaling in response to different environmental stimuli. The recent set up of a toolkit of genetically encoded Ca^{2+} indicators, targeted to different chloroplast subcompartments (envelope, stroma, thylakoids) has helped to unravel the participation of chloroplasts in intracellular Ca^{2+} handling in resting conditions and during signal transduction. Intra-chloroplast Ca^{2+} signals have been demonstrated to occur in response to specific environmental stimuli, suggesting a role for these plant-unique organelles in transducing Ca^{2+}-mediated stress signals. In this mini-review we present current knowledge of stimulus-specific intra-chloroplast Ca^{2+} transients, as well as recent advances in the identification and characterization of Ca^{2+}-permeable channels/transporters localized at chloroplast membranes. In particular, the potential role played by cMCU, a chloroplast-localized member of the mitochondrial calcium uniporter (MCU) family, as component of plant environmental sensing is discussed in detail, taking into account some specific structural features of cMCU. In summary, the recent molecular identification of some players of chloroplast Ca^{2+} signaling has opened new avenues in this rapidly developing field and will hopefully allow a deeper understanding of the role of chloroplasts in shaping physiological responses in plants.

Keywords: chloroplasts, organellar calcium signaling, calcium-permeable channels, calcium transporters, calcium binding proteins, genetically encoded calcium indicators, chloroplast calcium uniporter

OPEN ACCESS

Edited by:
Jürgen Soll, Ludwig Maximilian University of Munich, Germany

Reviewed by:
Markus Teige, University of Vienna, Austria
Cornelia Spetea, University of Gothenburg, Sweden

***Correspondence:**
Ildikò Szabò
ildiko.szabo@unipd.it

[†]These authors have contributed equally to this work

Specialty section:
This article was submitted to Plant Physiology, a section of the journal Frontiers in Plant Science

Received: *09 December 2019*
Accepted: *07 February 2020*
Published: *11 March 2020*

Citation:
Navazio L, Formentin E, Cendron L and Szabò I (2020) Chloroplast Calcium Signaling in the Spotlight. Front. Plant Sci. 11:186. doi: 10.3389/fpls.2020.00186

INTRODUCTION

Calcium is a fundamental intracellular messenger involved in a wide range of different signaling pathways in all eukaryotes. In plants, Ca^{2+} has been shown to participate in the transduction of a large variety of environmental stimuli of both abiotic and biotic nature (Dodd et al., 2010). A complex Ca^{2+} homeostatic and signaling machinery allows for a tight regulation of the intracellular concentration of the ion ($[Ca^{2+}]$) and its variations during signal transduction (Kudla et al., 2018). Plant organellar Ca^{2+} signaling is a rapidly expanding field of investigation, also thanks to the

increasing availability of novel genetically encoded Ca^{2+} indicators, specifically targeted to different intracellular compartments (Costa et al., 2018). In addition to the vacuole, considered as the main stimulus-releasable Ca^{2+} store in the plant cell, other organelles, *i.e.* chloroplasts, have recently come to the fore. The detection of stimulus-specific intra-chloroplast Ca^{2+} signals in response to different environmental cues has highlighted the contribution of chloroplasts to shaping cytosolic Ca^{2+} signatures. In this mini-review we present the most recent research works dealing with the monitoring of chloroplast Ca^{2+} concentration and its changes during signal transduction events. Moreover, we focus on the recently reported identification and biochemical characterization of some molecular players involved in chloroplast Ca^{2+} handling. Current evidence for a crucial role of chloroplasts as stress sensors and future avenues of investigation in this promising field are also discussed.

THE EMERGING ROLE OF CHLOROPLAST CALCIUM SIGNALING IN THE TRANSDUCTION OF BIOTIC AND ABIOTIC STRESS SIGNALS

Chloroplasts have long been known to be involved in intracellular Ca^{2+} homeostasis and signaling. The regulatory role played by these organelles on intracellular Ca^{2+} handling is two-fold: i) a tight control of intra-organellar [Ca^{2+}] is essential for the proper functioning of the chloroplast physiology, *e.g.* the regulation of photosynthesis, as well as other chloroplast-localized processes (Stael et al., 2012b; Rocha and Vothknecht, 2012; Nomura and Shiina, 2014; Hochmal et al., 2015); ii) transient changes in stromal [Ca^{2+}] ([Ca^{2+}]$_{str}$), evoked in response to different stress stimuli, in turn can shape intracellular Ca^{2+} signals, thereby affecting Ca^{2+}-mediated signaling circuits.

After the pioneering work conducted by Johnson et al. (Johnson et al., 1995) and Sai and Johnson (Sai and Johnson, 2002), who monitored [Ca^{2+}] in the chloroplast stroma by means of a chloroplast-targeted aequorin chimera, precise measurements of Ca^{2+} levels inside the different chloroplast subcompartments have been lacking for a long time. However, in the last few years the increasing availability of specifically targeted Ca^{2+} reporters has rapidly expanded the possibility of accurately monitoring organellar Ca^{2+} dynamics. The set up of a toolkit of aequorin-based probes targeted to the different subcompartments of chloroplasts (outer and inner envelope membranes, stroma, thylakoids) has allowed for the elucidation of stimulus-specific intra-organellar Ca^{2+} signals and their contribution to fine-tuning cytosolic Ca^{2+} signatures (Mehlmer et al., 2012; Sello et al., 2016; Sello et al., 2018). A complementary approach based on the design of a cameleon probe directed to the chloroplast stroma further permitted Ca^{2+} imaging in single chloroplasts, highlighting organelle-autonomous Ca^{2+} transients (Loro et al., 2016). The establishment of aequorin reporters targeted to the thylakoid lumen and thylakoid membrane highlighted the ability of thylakoids to store 3- to 5-fold higher [Ca^{2+}] with respect to the stroma (about 500 nM in the thylakoid lumen *versus* 100÷150 nM in the stroma, in resting conditions in the dark), as well as their contribution to the modulation of intra-chloroplast Ca^{2+} signals (Sello et al., 2018).

Chloroplast Ca^{2+} signals have been shown to be triggered by a large number of different stimuli of both biotic and abiotic nature. Elicitors of plant defence responses, such as the fungal-derived protein cryptogein and the plant cell wall-derived pectin fragments oligogalacturonides, were found to evoke transient Ca^{2+} elevations in the chloroplast stroma of *Nicotiana tabacum* and *Arabidopsis thaliana* plant cell suspension cultures (Manzoor et al., 2012; Sello et al., 2018). Moreover, the bacterial flagellin peptide flg22 was demonstrated to trigger a chloroplast Ca^{2+} response in the chloroplast stroma of Arabidopsis rosette leaves, peaking later than the cytosolic Ca^{2+} elevation (Nomura et al., 2012; Nomura and Shiina, 2014). In this latter work, a striking chloroplast-mediated transcriptional reprogramming during plant immune responses was demonstrated, uncovering an unanticipated link between chloroplast and nuclear plant innate immunity *via* ROS and Ca^{2+} signaling (Stael et al., 2015). The calcium-sensing receptor CAS, a thylakoid-localized protein of not yet well-defined function, was found to be involved in the generation of the flg22-induced stromal Ca^{2+} transient and chloroplast-mediated activation of defence gene expression (Nomura et al., 2012).

Different abiotic cues, such as cold, oxidative, salt and osmotic stresses were found to evoke stimulus-specific Ca^{2+} signals in the chloroplast stroma (Nomura et al., 2012; Sello et al., 2016; Sello et al., 2018; Teardo et al, 2019). Whereas these stimuli were shown to activate Ca^{2+} responses in both chloroplasts and non-green plastids (Sello et al., 2016), the light-to-dark transition was found to elicit a chloroplast-specific response (Sello et al., 2016; Loro et al., 2016). Although the precise mechanisms underlying dark-induced chloroplast Ca^{2+} fluxes remain to be unravelled, the circadian gating of dark-induced chloroplast and cytosolic Ca^{2+} elevations has recently been demonstrated (Martí Ruiz et al., 2020), uncovering an intriguing link between eukaryotic circadian clocks and chloroplasts.

In contrast to the above-mentioned stimuli, that have been demonstrated to trigger Ca^{2+} transients in both chloroplasts and the cytosol, increases in absolute temperature were found to evoke Ca^{2+} responses specific to chloroplasts, as no corresponding elevations were detected in the cytosol (Lenzoni and Knight, 2019). Interestingly, also in this case the chloroplast Ca^{2+} response was found to be partially dependent on CAS (Lenzoni and Knight, 2019).

Taken together, the above findings strongly highlight the ability of chloroplasts to perceive and transduce environmental signals in a Ca^{2+}-dependent manner. However, compared to the large amount of information progressively cumulating on the generation of chloroplast Ca^{2+} signals, information about Ca^{2+}-permeable channels/transporters localized at chloroplast membranes has long lagged behind.

CURRENT KNOWLEDGE OF THE MOLECULAR PLAYERS INVOLVED IN Ca^{2+} HANDLING IN CHLOROPLASTS

The extent, duration and frequency (*i.e.* signature) of free Ca^{2+} elevation in the cytosol ($[Ca^{2+}]_{cyt}$) acts as a signal to be implemented in the transducing machinery of the cell. Different stimuli are followed by different Ca^{2+} signatures, leading in turn to different specific responses, in terms of gene expression, protein activity and localization. The Ca^{2+} signature is shaped by the activity of Ca^{2+}-permeable channels and transporters regulating the ion entry into and exit from the cytosol, respectively. Ca^{2+}-permeable channels are grouped in five families: cyclic nucleotide-gated channels (CNGCs), glutamate receptors-like channels (GLRs), two-pore channels (TPCs), mechanosensitive channels (MCAs), hyperosmolality gated channels (OSCAs) (Demidchik et al., 2018). Ca^{2+} transport off the cytosol to restore the resting $[Ca^{2+}]_{cyt}$ is mediated by energy-driven pumps/transporters belonging to the P-type ATPases, such as P1B-type calcium/heavy metal cation-transporting ATPase (AtHMA1), P2A-type calcium cation-transporting ATPase (ECAs) and P2B-type calcium cation-transporting ATPase (ACAs) (García Bossi et al., 2020). Other Ca^{2+} transporters are grouped in the CaCA family (CAX-type proton:calcium cation exchanger, CCX-type cation:calcium cation exchanger, MHX-type proton:magnesium cation exchanger, NCL/EF-CAX-type cation exchanger, EF-CAX-type cation exchanger) (Pittman and Hirschi, 2016) and CaCA2 family (PAM71-type manganese/calcium cation transporter).

The transduction of the Ca^{2+} signal is mediated by Ca^{2+} -dependent/binding proteins. The Arabidopsis genome encodes for 250 proteins harbouring at least one Ca^{2+} binding domain (EF-hand), hence acting as putative Ca^{2+} sensors [*e.g.* (Ranty et al., 2016)]. Calmodulins (CaMs), calmodulin-like (CaMLs), calcineurin B-like proteins (CBLs) and Ca^{2+}-dependent protein kinases (CPKs) all harbour EF hand motifs. Ca^{2+} sensors directly (CPKs) or indirectly (CaMs, CaMLs, CBLs) [*e.g.* (Sanyal et al., 2015; Kudla et al., 2018)] modulate protein activity (*e.g.* ion channels, metabolic enzymes) and/or protein subcellular localization (*e.g.* transcription factors). The redundancy of sensor isoforms allows the discrimination between different signals and carry the specificity of the message brought by the Ca^{2+} signature.

To our knowledge, Ca^{2+}-binding proteins acting as buffers in the chloroplast have not yet been identified. Nevertheless, organellar Ca^{2+} buffering mechanisms are likely to play an essential role, generating heterogeneity in local Ca^{2+} concentrations inside chloroplasts. How Ca^{2+} is stored in the chloroplast remains an open question for future investigations, aimed to unravel whether Ca^{2+} interacts with specific Ca^{2+} binding proteins or with the thylakoid surface, which harbours a significant amount of phosphorylated proteins that have been suggested to bind calcium ions (Rocha and Vothknecht, 2012; Stael et al., 2012a; Stael et al., 2012b).

The major part of research carried out so far has focused on the analysis of the cytosolic Ca^{2+} signature, but the possibility to study Ca^{2+} dynamics in organelles by targeting Ca^{2+} probes to plastids has recently allowed the understanding of the existence of organellar Ca^{2+} transients in response to external stimuli. These findings pose the question of the identity of players involved in shaping and transducing the Ca^{2+} signal coming from organelles. The existence of peculiar and dedicated pathways for Ca^{2+} handling in organelles can be a possibility, and/or the machinery may comprise some already known players that may localize to chloroplasts as well (Finazzi et al., 2015; Pottosin and Shabala, 2015; Carraretto et al., 2016).

Recently, two proteins belonging to the family of the mitochondrial calcium uniporter (MCU) have been found to mediate Ca^{2+} transport across the mitochondria and chloroplast membranes, respectively AtMCU1 (Teardo et al, 2017) and AtMCU6 (later renamed AtcMCU (Teardo et al., 2019). In animal cells the only isoform, MCU (De Stefani et al., 2011; Baughman, 2011) is responsible for Ca^{2+} loading into mitochondria, thus helping recovery of resting $[Ca^{2+}]_{cyt}$. New evidence supports the involvement of MCU isoforms in shaping the organellar Ca^{2+} signatures in plants as well (Wagner et al., 2015; Teardo et al., 2017; Selles et al., 2018; Teardo et al., 2019). In particular, cMCU is involved in the generation of the stromal Ca^{2+} transient specific for the osmotic stress and mutants lacking cMCU showed an improved drought tolerance (Stael, 2019; Teardo et al., 2019).

It is now commonly acknowledged that a protein can localize to different cell compartments (Karniely and Pines, 2005), as it has been proven also for proteins involved in Ca^{2+} handling (**Table 1**). AtGLR3.4 and AtGLR3.5, two Ca^{2+} -permeable channels belonging to the GLR family, have a dual localization, at the plasma membrane and chloroplasts the former (Teardo et al., 2010; Teardo et al., 2011), in mitochondria and chloroplasts the latter (Teardo et al., 2015). Both seem to play a role in ABA signaling under abiotic stress (Cheng et al., 2018; Ju et al., 2020), although their direct involvement in organellar Ca^{2+} signaling under abiotic stress has to be investigated more in depth.

Querying the protein databases Uniprot (The UniProt Consortium, 2019), SUBA4 (Hooper et al., 2017) and Aramemnon (Schwacke et al., 2003) for *A. thaliana* records with plastidial localization and using "calcium" as keyword, 682 hits can be found in SUBA4, only 43 in Aramemnon and 42 in Uniprot. **Table 1** shows all those proteins belonging to the above-mentioned classes of channels/transporters, sensors and kinases involved in Ca^{2+} signature formation and signaling, whose plastidial localization has been predicted or demonstrated by MS/MS or by fusion to fluorescent proteins (FP).

23 out of 47 proteins belong to Ca^{2+} channels/transporters: 6 are confirmed to be located in plastid membranes either by biochemical and cell biology methods or by mass spectrometry. Among them, for AtcMCU, AtGLR3.4 and AtGLR3.5 a role in stress response was suggested. Altogether, these channels/transporters can be involved in the formation of the plastidial Ca^{2+} transients, along with the putative calcium-transporting protein PAM71/BICAT (Frank et al., 2019). However, this latter protein seems to play a prevalent role in manganese homeostasis rather than in calcium homeostasis (Schneider et al., 2016;

TABLE 1 | List of proteins involved in Ca^{2+} handling predicted to be located in plastids.

Gene ID	Protein Name	Description	Protein family	Predicted Localization (Aramemnon or SUBA4)	Experimental Localization (FP, MS/MS)	involved in	references
Ca^{2+} sensors							
At1g18890	AtCPK10	Calcium-dependent protein kinase 10	Calcium Dependent Protein Kinase	plastid, mitochondrion, cytosol, nucleus	nucleus	drought, ABA, stomatal closure	Zou et al., 2010; Liu et al., 2017
At1g35670	AtCPK11	Calcium-dependent protein kinase 11	Calcium Dependent Protein Kinase	plastid, mitochondrion, cytosol, nucleus	nucleus, cytosol, PM	pollen tube growth, salt and drought induced, salt and ABA signaling	Urao et al., 1994; Rodriguez Milla et al., 2006; Zhu et al., 2007; Benschop et al., 2007; Ito et al., 2011; Zhao et al., 2013
At2g17890	AtCPK16	Calcium-dependent protein kinase 16	Calcium Dependent Protein Kinase	plastid, mitochondrion, cytosol	PM		Dammann et al., 2003; Stael et al., 2011
At2g31500	AtCPK24	Calcium-dependent protein kinase 24	Calcium Dependent Protein Kinase	plastid, mitochondrion, cytosol, nucleus	nucleus, PM	pollen tube growth	Gutermuth et al., 2013; Zhao et al., 2013
At2g38910	AtCPK20	Calcium-dependent protein kinase 20	Calcium Dependent Protein Kinase	plastid, nucleus, membrane	plastid, PM		Dammann et al., 2003; Behrens et al., 2013; Gutermuth et al., 2013
At3g10660	AtCPK2	Calcium-dependent protein kinase 2	Calcium Dependent Protein Kinase	plastid, nucleus, mitochondrion, cytosol	PM		Gutermuth et al., 2013
At4g04695	AtCPK31	Calcium-dependent protein kinase 31	Calcium Dependent Protein Kinase	nucleus, plastid, cytosol, mitochondrion	plastid, PM	arsenite uptake	Helm et al., 2014; Ji et al., 2017
At4g04720	AtCPK21	Calcium-dependent protein kinase 21	Calcium Dependent Protein Kinase	PM, cytosol, mitochondrion, plastid, nucleus	PM	interacts with SLAC1, ABI1, SLAH3, GORK	Dammann et al., 2003; Alexandersson et al., 2004; Nelson et al., 2006; Benschop et al., 2007; Marmagne et al., 2007; Mitra et al., 2009; Keinath et al., 2010; Geiger et al., 2010; Zhang and Peck, 2011; Elmore et al., 2012; Nikolovski et al., 2012; Bernfur et al., 2013; Demir et al., 2013; Zargar et al., 2015; De Michele et al., 2016; van Kleeff et al., 2018
At4g09570	AtCPK4	Calcium-dependent protein kinase 4	Calcium Dependent Protein Kinase	cytosol, nucleus, mitochondrion, plastid	PM, cytosol, nucleus	ABA and salt response; interacts with plastid proteins	Dammann et al., 2003; Zhu et al., 2007; Mitra et al., 2009; Uno et al., 2009; Ito et al., 2011; Li et al., 2018
At4g21940	AtCPK15	Calcium-dependent protein kinase 15	Calcium Dependent Protein Kinase	cytosol, plastid, nucleus, mitochondrion	PM		Li et al., 2012; Bernfur et al., 2013
At4g23650	AtCPK3	Calcium-dependent protein kinase 3	Calcium Dependent Protein Kinase	plastid, mitochondrion, cytosol, nucleus	cytosol, nucleus, PM, Golgi, tonoplast	stomatal closure	Dammann et al., 2003; Alexandersson et al., 2004; Dunkley et al., 2006; Mori et al., 2006; Nelson et al., 2006; Benschop et al., 2007; Mitra et al., 2009; Keinath et al., 2010; Ito et al., 2011; Elmore et al., 2012; Li et al., 2012; Nikolovski et al., 2012; Latz et al., 2013; Zargar et al., 2015; Heard et al., 2015; De Michele et al., 2016
At4g36070	AtCPK18	Calcium-dependent protein kinase 18	Calcium Dependent Protein Kinase	plastid, mitochondrion, peroxisome, PM			
At5g04870	AtCPK1/ AtAK1	Calcium-dependent protein kinase 1	Calcium Dependent Protein Kinase	plastid, nucleus, cytosol, mitochondrion	peroxisome, MVB, cytosol, PM	salt and drought	Dammann et al., 2003; Chen et al., 2010; Drakakaki et al., 2012; De Michele et al., 2016; Huang et al., 2018
At5g12180	AtCPK17	Calcium-dependent protein kinase 17	Calcium Dependent Protein Kinase	cytosol, nucleus, mitochondrion, plastid	PM	pollen tube tip growth	Myers et al., 2009; Gutermuth et al., 2013; Bernfur et al., 2013

(Continued)

TABLE 1 | Continued

Gene ID	Protein Name	Description	Protein family	Predicted Localization (Aramemnon or SUBA4)	Experimental Localization (FP, MS/MS)	involved in	references
At5g12480	AtCPK7	Calcium-dependent protein kinase 7	Calcium Dependent Protein Kinase	plastid, mitochondrion, cytosol, nucleus	PM, Golgi	root hydraulic conductivity	Dammann et al., 2003; Marmagne et al., 2007; Benschop et al., 2007; Elmore et al., 2012; Heard et al., 2015; Li et al., 2015
At5g19360	AtCPK34	Calcium-dependent protein kinase 34	Calcium Dependent Protein Kinase	cytosol, nucleus, mitochondrion, plastid	PM	pollen tube tip growth	Myers et al., 2009; Gutermuth et al., 2013; Bernfur et al., 2013
At5g19450	AtCPK8	Calcium-dependent protein kinase 8	Calcium Dependent Protein Kinase	cytosol, nucleus, mitochondrion, plastid	PM	ABA signaling and H_2O_2 homeostasis in guard cells	Dammann et al., 2003; Nühse et al., 2003; Nühse et al., 2004; Benschop et al., 2007; Chen et al., 2010; Keinath et al., 2010; Zhang and Peck, 2011; Elmore et al., 2012; Zargar et al., 2015; Zou et al., 2015
At5g24430	AtCRK4	Calcium-dependent protein kinase 4	Calcium Dependent Protein Kinase	plastid, nucleus, cytosol, mitochondrion	PM		Benschop et al., 2007; Marmagne et al., 2007; Chen et al., 2010; Keinath et al., 2010; Zhang and Peck, 2011; Li et al., 2012; Szymanski et al., 2015; De Michele et al., 2016
At5g66210	AtCPK28	Calcium-dependent protein kinase 28	Calcium Dependent Protein Kinase	cytosol, plastid, mitochondrion, nucleus	PM	plant immunity	Dammann et al., 2003; Benschop et al., 2007; Elmore et al., 2012; Monaghan et al., 2014; Monaghan et al., 2015; Matschi et al., 2015; De Michele et al., 2016
At2g15680	AtCML30	Calmodulin-like protein 30	Calmodulin-like protein	plastid, mitochondrion, cytosol, PM	mitochondrion		Chigri et al., 2012
At2g41410	AtCML35	Probable calcium-binding protein CML35	Calmodulin-like protein	plastid, mitochondrion, nucleus, cytosol, PM	PM, vacuole	dark induced	Lee et al., 2005; Benschop et al., 2007; Whiteman et al., 2008; Elmore et al., 2012; Li et al., 2012; De Michele et al., 2016
At2g43290	AtCML5	Calmodulin-like protein 5	Calmodulin-like protein	plastid, mitochondrion, nucleus, cytosol, PM, ER, extracellular	ER, Golgi	dark and touch induced	Lee et al., 2005; Ruge et al., 2016
At3g10190	AtCML36	Calmodulin-like protein 36	Calmodulin-like protein	plastid, nucleus, mitochondrion, cytosol	PM	ACA8 activation	Benschop et al., 2007; Astegno et al., 2017
At3g29000	AtCML45	Calmodulin-like protein 45	Calmodulin-like protein	plastid, mitochondrion, Golgi, cytosol, PM, ER			
At3g50770	AtCML41	Probable calcium-binding protein CML41	Calmodulin-like protein	plastid, mitochondrion, cytosol			
At4g26470	AtCML21	Calmodulin-like protein 21		cytosol, PM, mitochondrion, nucleus, plastid	cell wall		Nguyen-Kim et al., 2016
At5g04170	AtCML50	Probable calcium-binding protein CML50	Calmodulin-like protein	plastid, extracellular space, ER, mitochondrion, PM, nucleus	cell wall		Nguyen-Kim et al., 2016
At5g39670	AtCML46	Calmodulin-like protein 46	Calmodulin-like protein	cytosol, plastid, mitochondrion, ER, Golgi, nucleus, extraellular			
At5g42380	AtCML37	Calcium-binding protein CML37	Calmodulin-like protein	plastid, nucleus, cytosol, PM, mitochondrion	cytosol, nucleus	drought, wounding	Vanderbeld and Snedden, 2007; Inzè et al., 2012; Scholz et al., 2014; Scholz et al., 2015
At4g32060	AtMICU	Calcium uptake protein, mitochondrial		PM, mitochondrion, plastid	mitochondrion	regulation of Ca^{2+} uniporters (MCUs)	Wagner et al., 2015; Teardo et al., 2017
At4g33000	AtCBL10	Calcineurin B-like protein 10	Calcineurin B-like protein	plastid, mitochondrion, PM, ER	PM, tonoplast	salt tolerance	Mitra et al., 2009; Ma et al., 2019; Yang et al., 2019

(Continued)

TABLE 1 | Continued

Gene ID	Protein Name	Description	Protein family	Predicted Localization (Aramemnon or SUBA4)	Experimental Localization (FP, MS/MS)	involved in	references
At5g23060	AtCAS	Calcium sensing receptor	Calcium sensing receptor	plastid, mitochondrion	plastid, thylakoid, Golgi, mitochondrion, nucleus	high light, stomatal regulation, drought tolerance	Vainonen et al., 2008; Weinl et al., 2008; Behrens et al., 2013; Helm et al., 2014; Tomizioli et al., 2014; Wang et al., 2014; Heard et al., 2015; Fakih et al., 2016; Fromm et al., 2016; Melonek et al., 2016; Senkler et al., 2017; Cutolo et al., 2019
Ca^{2+} transporters/channels							
At1g53210	AtNCL	Sodium/calcium exchanger	NCL/EF-CAX-type cation exchanger	plastid, mitochondrion, Golgi, cytosol, PM, ER	PM, tonoplast	flowering time, auxin signaling, salt stress	Nikolovski et al., 2012; Elmore et al., 2012; Li et al., 2016; Wang et al., 2012; Yoshida et al., 2013; Szymanski et al., 2015; Zargar et al., 2015; Li et al., 2016
At2g34020		Putative EF-CAX-type cation exchanger	EF-CAX-type cation exchanger	PM, plastid, mitochondrion, ER, Golgi			
At2g38170	AtCAX1	High-affinity calcium/proton cation exchanger	CAX-type proton:calcium cation exchanger	plastid, mitochondrion, Golgi, PM, tonoplast	tonoplast	Cd^{2+} tolerance; pH regulation; hormone signaling; guard cell dynamics; stress response	Cheng et al., 2003; Conn et al., 2011; Cho et al., 2012; Baliardini et al., 2015; Hocking et al., 2017
At3g14070	AtCCX3/ CAX9	Cation/calcium exchanger 3	CCX-type cation:calcium cation exchanger	plastid, mitochondrion, Golgi, PM, ER	endomembrane		Morris et al., 2008
At3g51860	AtCAX3	High-affinity calcium/proton cation exchanger	CAX-type proton:calcium cation exchanger	plastid, mitochondrion, Golgi, PM, tonoplast	tonoplast	pH regulation; hormone signaling; guard cell dynamics	Manohar et al., 2011; Cho et al., 2012; Hocking et al., 2017
At5g01490	AtCAX4	High-affinity calcium/proton cation exchanger	CAX-type proton:calcium cation exchanger	plastid, ER, PM, tonoplast	tonoplast	Cd^{2+} accumulation	Cheng et al., 2002; Mei et al., 2009
At2g23790	AtMCU3	Putative channel component of MCUC calcium uniporter complex	Component of MCU calcium uniporter complex	plastid, mitochondrion, nucleus	tonoplast		Yoshida et al., 2013
At4g36820	AtMCU4	Putative channel component of MCUC calcium uniporter complex	Component of MCU calcium uniporter complex	mitochondrion, chloroplast, nucleus	mitochondrion		Teardo et al., 2017
At5g66650	AtMCU6/ AtcMCU	Putative channel component of MCUC calcium uniporter complex	Component of MCU calcium uniporter complex	plastid, mitochondrion	plastid, mitochondrion	drought, hypoxia	Teardo et al., 2019; Lee and Bailey-Serres, 2019
At1g05200	AtGLR3.4	Putative GLR-type amino acid-gated calcium cation channel	GLR-type ligand-gated cation channel	PM, plastid, ER, Golgi, mitochondrion	plastid, PM	Ca^{2+} transport; salt and cold stress; ABA signaling; seed germination; lateral root development	Meyerhoff et al., 2005; Stephens et al., 2008; Teardo et al., 2011; Vincill et al., 2013; Cheng et al., 2018
At2g17260	AtGLR3.1	Putative GLR-type calcium cation-permeable channel	GLR-type ligand-gated cation channel	PM, plastid, ER, Golgi	endomembrane	stomatal closure	Cho et al., 2009; Kong et al., 2016; Nguyen et al., 2018a
At2g32390	AtGLR3.5	Putative GLR-type calcium cation-permeable channel	GLR-type ligand-gated cation channel	PM, plastid, mitochondrion, nucleus	mitochondrion, plastid	Ca^{2+} transport; ABA signaling; seed germination; stomatal closure	Teardo et al., 2015; Kong et al., 2016; Ju et al., 2020

(Continued)

TABLE 1 | Continued

Gene ID	Protein Name	Description	Protein family	Predicted Localization (Aramemnon or SUBA4)	Experimental Localization (FP, MS/MS)	involved in	references
At5g11210	AtGLR2.5	Putative GLR-type calcium cation-permeable channel	GLR-type ligand-gated cation channel	plastid, mitochondrion, PM	PM		Mitra et al., 2009
At1g69450	AtOSCA2.4	Early-responsive to dehydration stress protein (ERD4)	OSCA1/2/3-type Ca^{2+}-permeable hyperosmolality-gated channel	chloroplast, mitochondrion, PM, Golgi	PM		Yuan et al., 2014
At3g54510	AtOSCA2.5	Hyperosmolality-gated calcium-permeable channel	OSCA1/2/3-type Ca^{2+}-permeable hyperosmolality-gated channel	mitochondrion, plastid, nucleus, Golgi,ER, PM	ER, mitochondrion, plastid		Lee et al., 2011
At4g02900	AtOSCA1.7	Hyperosmolality-gated calcium-permeable channel	OSCA1/2/3-type Ca^{2+}-permeable hyperosmolality-gated channel	mitochondrion, plastid, nucleus, Golgi,ER, PM			
At4g35870	AtOSCA4.1/ AtGFS10	Calcium-permeable channel-like protein	OSCA4-type unspecified channel	chloroplast, mitochondrion, PM, Golgi, nucleus	Golgi		Heard et al., 2015
At4g37270	AtHMA1	Thapsigargin-sensitive calcium/ heavy metal cation-transporting P1B-type ATPase	P1B-type heavy metal cation-transporting ATPase	plastid, mitochondrion, PM	chloroplast envelope	photosynthesis	Seigneurin-Berny et al., 2006; Higuchi et al., 2009; Ferro et al., 2010; Nikolovski et al., 2012; Tomizioli et al., 2014
At1g27770	AtACA1	Calcium-transporting ATPase	P2B-type calcium cation-transporting ATPase	plasma membrane, plastid, cytosol, ER, mitochondrion, nucleus	plastid, ER, PM, tonoplast, microtubule		Huang et al., 1993; Dunkley et al., 2006; Benschop et al., 2007; Mitra et al., 2009; Zhang and Peck, 2011; Yoshida et al., 2013; Hamada et al., 2013
At3g21180	AtACA9	Calcium-transporting ATPase	P2B-type calcium cation-transporting ATPase	plasma membrane, plastid, cytosol, ER, mitochondrion, nucleus	plasma membrane, plastid, cytosol	pollen development,	Schiott et al., 2004; Tomizioli et al., 2014
At4g37640	AtACA2	Calcium-transporting ATPase	P2B-type calcium cation-transporting ATPase	PM, ER, plastid, mitochondrion, vacuole	Golgi, ER, PM	salt tolerance in yeast	Dunkley et al., 2006; Benschop et al., 2007; Anil et al., 2008; Zhang and Peck, 2011; Nikolovski et al., 2012; Heard et al., 2015
At5g53010		Calcium-transporting ATPase, putative	P2B-type calcium cation-transporting ATPase	mitochondrion, PM, ER	plastid		Tomizioli et al., 2014
At1g64150	AtBICAT1/ AtPAM71/ AtCCHA1	Putative calcium/ manganese cation transporter	PAM71-type manganese/ calcium cation transporter	plastid, mitochondrion	thylakoid membrane	Mn^{2+} homeostasis, phototropic growth, chloroplast Ca^{2+} homeostasis, photosynthesis	Wang et al., 2016; Schneider et al., 2016; Frank et al., 2019
At4g13590	AtBICAT2/ AtCMT1	Putative calcium/ manganese cation transporter	PAM71-type manganese/ calcium cation transporter	plastid, mitochondrion	chloroplast envelope	Mn^{2+} homeostasis, phototropic growth, chloroplast Ca^{2+} homeostasis, photosynthesis	Ferro et al., 2010; Zybailov et al., 2008; Ferro et al., 2010; Tomizioli et al., 2014; Eisenhut et al., 2018; Zhang et al., 2018; Frank et al., 2019
Others							
At1g64850			Calcium-binding EF hand family protein	vacuole, mitochondrion, plastid, nucleus, vacuole	plastid, peroxisome		Reumann et al., 2009; Ferro et al., 2010; Nikolovski et al., 2012

(Continued)

TABLE 1 | Continued

Gene ID	Protein Name	Description	Protein family	Predicted Localization (Aramemnon or SUBA4)	Experimental Localization (FP, MS/MS)	involved in	references
At2g42590	AtGRF9	14-3-3-like protein GF14 mu	14-3-3 protein	nucleus, cytosol, mitochondrion, PM	cytosol, plastid, vacuole, nucleus, PM, peroxisome, Golgi	root growth in water stress, leaf development,cold stress	Mayfield et al., 2012; He et al., 2015; Liu et al., 2017; Omidbakhshfard et al., 2018
At4g08810	AtSUB1		Calcium binding protein	plastid, nucleus, ER, Golgi,	Golgi	cryptochrome and phytochrome coaction	Guo et al., 2001; Parsons et al., 2012
At4g34070			Calcium-binding EF-hand family protein	plastid, mitochondrion, Golgi, ER, cytosol, extracellular			
At4g38810			Calcium-binding EF-hand family protein	plastid, nucleus, mitochondrion, cytosol			

The experimental determined localization comes from MS/MS analyses or fluorescent protein fusion (FP). Articles referring to the original data are reported. In bold proteins proved to be located in chloroplasts. In italics genes involved in stress response. PM, plasma membrane; ER, endoplasmic reticulum.

Zhang et al., 2018). In addition to Ca^{2+} channels and transporters, Ca^{2+} sensors, namely 21 proteins, are predicted to be located in plastids. However, only three have been confirmed so far: AtCPK20, AtCPK31, and AtCAS. It is worth to mention that CPK20, besides the plastidial localization that was confirmed by MS/MS approaches (Behrens et al., 2013), showed a plasma membrane localization when fused to reporter genes or co-expressed with other CPK members (Gutermuth et al., 2013). CPK31 has also been shown to localize at the plasma membrane when interacting with the arsenite transporter NIP1;1 (Ji et al., 2017). In addition, localization of many CPKs with chloroplast-targeting sequence can be affected by N-acylation. For example, AtCPK20 and 31 are located in the chloroplast, only if its N-acylation is prevented (Stael et al., 2011). Interestingly, AtGRF9, a Ca^{2+}-regulated 14-3-3 protein, although not predicted to be located in chloroplasts, has been demonstrated to be present in many compartments, including plastids. This regulatory protein is involved in root and leaf development under water stress (He et al., 2015) and leaf development in general (Omidbakhshfard et al., 2018), but its role in chloroplasts has not yet been explored.

The presence of members of protein families involved in Ca^{2+} transport/sensing supports the idea of a core-machinery determining the observed Ca^{2+} transients in the chloroplast stroma, and putatively in the thylakoid lumen as well. Ca^{2+} sensors are indeed present in plastids, although their activity in deciphering organellar Ca^{2+} signatures has not been fully demonstrated so far. Nevertheless, a recent work points to CAS as mediator of light response and photoacclimation (Cutolo et al., 2019).

The multiple localizations shown by some proteins in **Table 1** awaits further investigation. Recent evidence is pointing to the hypothesis of an inter-connection between organelles and nucleus for material exchanging or signal propagation (Kmiecik et al., 2016). The presence of the Ca^{2+} handling machinery in multiple positions can be part of the retrograde signaling in response to adverse environmental conditions (Pornsiriwong et al., 2017).

STRUCTURAL AND FUNCTIONAL COMPARISON BETWEEN MCU ISOFORMS FROM DIFFERENT ORGANISMS AND THE CHLOROPLAST-LOCALIZED HOMOLOGUE IN PLANTS

As mentioned above, AtcMCU is one of the very few molecular entities among the plastidial Ca^{2+} channels/transporters shown to work as a Ca^{2+}-permeable ion channel, to mediate indeed Ca^{2+} flux across chloroplast envelope and to participate in the drought stress response in Arabidopsis. While many organisms have only one MCU isoform (Bick et al., 2012), Arabidopsis harbours 6 different isoforms: 5 with clear predicted subcellular localization to mitochondria, whereas AtMCU6/At5g66650 has a predicted localization to either chloroplasts and/or to mitochondria. Localization prediction was confirmed for AtMCU1/At1g09575 (Teardo et al., 2017), AtMCU2/At1g57610 (Wagner et al., 2015; Selles et al., 2018), AtMCU3/At2g23790 (Carraretto et al., 2016). For AtMCU6 an interesting situation was observed: in tissues harbouring mature chloroplasts, AtMCU6 was efficiently targeted to these photosynthetic organelles, whereas in roots the protein was found in mitochondria (Teardo et al., 2019). Thus, either plastid-specific partners promote targeting of AtMCU6/AtcMCU or targeting depends on the metabolic state of a given cell. However, among the possible partners (https://string-db.org/network/3702.AT5G66650.1) no proteins with unique localization to chloroplasts are present. Thus, the mechanism by which dual localization occurs awaits clarification.

The N-terminal domain (NTD) of AtcMCU harbours motifs rich in acidic residues, one of which (107-118) playing a role in Ca^{2+} uptake by cMCU, as demonstrated by mutagenesis studies (D107A/E118K mutant) and Ca^{2+} uptake assays in an aequorin-based *E. coli* system (Teardo et al., 2019). Two groups independently set up the same system to study MCU activity,

namely that exploiting *E. coli* stably expressing aequorin (Teardo et al., 2019) or the fluorescent Ca^{2+} reporter GCaMP2 (Fan et al., 2018). This valuable tool allows a quick screening of the effect of MCU residues' mutations and of chemical modulators on the Ca^{2+} flux-mediating activity and may become a method of choice for further structure-function studies.

One common feature of MCU homologs from fungi and Arabidopsis is that they can function as Ca^{2+}-permeable channels on their own in contrast to vertebrates, where the uniporter is a complex (MCUC) consisting of multiple subunits, including: 1) the channel forming unit (MCU) with two transmembrane segments and a conserved DXXE sequence forming the Ca^{2+} selectivity filter (see **Figure 1**); 2) regulatory EF-hand proteins MICU1-3; 3) a small, single-pass transmembrane protein, EMRE (Essential MCU REgulator) [for review see *e.g.*(Wagner et al., 2016)]. The structure of MCU homologs from various organisms has been recently solved: 1) from *Fusarium graminearum* and *Metarhizium acridum* revealing a dimer assembly of MCU (Fan et al., 2018); 2) from *Neurospora crassa* (Yoo et al., 2018); 3) from *Neosartorya fischeri* (Nguyen et al., 2018b); and from 4) zebrafish and *Cyphellophora europaea* (Baradaran et al., 2018). All these homologues share high sequence similarity in their transmembrane domains, show a similar pore architecture and a high structural similarity of the NTDs (despite relatively low sequence homology). The amino acid sequence is more similar between Arabidopsis and *Dictyostelium discoideum* than between AtMCUs and human MCU (Teardo et al., 2017). This similarity apparently translates also to the tertiary structure of the two proteins, at least regarding the N-terminal domain, whose structure has been recently resolved for Dictyostelium MCU, proving its divergent evolution (doi: https://doi.org/10.1101/848002) (see **Figure 1**).

In plants and fungi, the pore-forming unit MCU alone is able to allow Ca^{2+} flux, without the need of EMRE, as confirmed by different groups (Tsai et al., 2016; Teardo et al., 2017; Fan et al., 2018; Teardo et al., 2019). In fact, homologs of EMRE are not present in these organisms. The cryo-EM structure of the human MCU-EMRE complex (Wang et al., 2019) suggests that NTD mediates the dimerization of two human MCU tetramers, thereby modulating the function of the channel [although deletion of NTD does not affect Ca^{2+} flux (Lee et al., 2015)]. In contrast to other MCUs, an (R/K)/Q/(R/K/D)/K/L motif is found in the L2 (Oxenoid et al., 2016) (now called CC2a for coiled-coiled domain 2a) (Wang et al., 2019) region of Arabidopsis, Dictyostelium and NfMCU (Teardo et al., 2017; Wang et al., 2019), all being able to form functional MCU without EMRE. It has been proposed that the extended side chain of HsMCU R297 (missing in the above MCUs) on CC2a connects the gate-forming juxtamembrane loop (JML) of MCU to EMRE by forming hydrogen bonds with the hydroxyl group of highly conserved T285 (on the JML of MCU) and a valine residue of EMRE. Interaction between CC2a and EMRE has been proposed as a crucial factor determining the conductivity of the channel formed by MCU tetramers. On the other hand, in the EMRE-independent Dictyostelium MCU, deletion of either CC1 or CC2

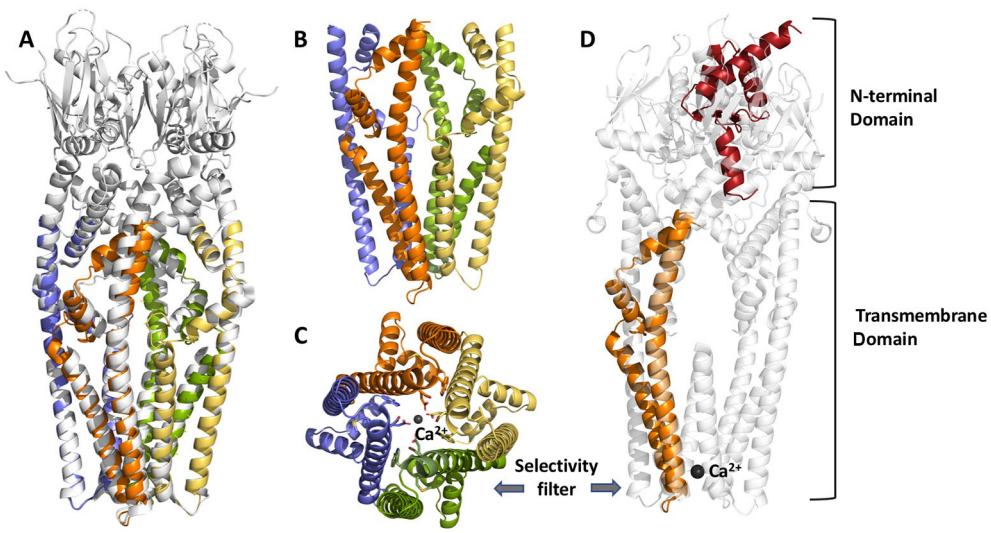

FIGURE 1 | Structural features of chloroplast MCU from *Arabidopsis thaliana*, modelled by Phyre V 2.0. From the left to the right: (panel **A**) cartoon view of the superposition of MCU structure from *Neurospora crassa* (cryoEM, 3.7 Å resolution, PDB:6DT0, grey), used as a reference, and predicted *A. thaliana* cMCU transmembrane tetrameric assembly (coloured chains); (panel **B, C**) details of the transmembrane (TM) and coiled-coil domain (CCD) tetrameric assembly and selectivity filter (panel **C**), where the four chains are shown in yellow, orange, pale violet and green. The key acidic residues within the highly conserved motif (WDXXEP, where X is any hydrophobic residue) of cMCU are highlighted in sticks, as well as the coordinated calcium ion, shown as dark grey sphere; (panel **D**) superposition of the model of one monomer of *A. thaliana* cMCU channel (orange and red) and *N. crassa* MCU tetramers (light grey); cMCU model shown here includes the transmembrane domain (TM), part of the coil-coiled region and the N-terminal domain (NTD), the last predicted according to our previous homology searches and its similarity toward *Dictyostelium discoideum* NTD (PDB:5Z2H, doi: https:/doi.org/10.1101/848002). The superposition underlines the divergence from metazoan NTDs and other structure-known fungal homologues such as NcMCU, CeMCU, MaMCU, and NfMCU.

caused the loss of function of MCU (Yamamoto et al., 2019), suggesting that these two domains are crucial for MCU function independently of their ability to bind EMRE. Altogether, determination of structural differences among various MCUs accounting for the requirement of EMRE for channel function requires further work.

CONCLUSIONS AND PERSPECTIVES

In these last few years there has been a surge of papers on Ca^{2+} signaling in chloroplasts, witnessing the crucial role increasingly attributed to these plant-unique organelles in the orchestration of the complex Ca^{2+} signaling network of the plant cell. We foresee that the newly available experimental tools to investigate the role of thylakoids in Ca^{2+}-mediated signal transduction, the molecular identification of Ca^{2+} channels/transporters in chloroplast membranes and the determination of the structure of transmembrane proteins by cryo-EM will lead to a rapid development of this exciting field of plant research. Future plant organellar Ca^{2+} signaling studies should also focus on non-photosynthetic plastids, which have recently been proposed to trigger tissue-specific signaling involved in mounting plant systemic stress response (Beltran et al., 2018). Furthermore, the potential interplay of chloroplasts with other intracellular Ca^{2+}-mobilizable stores should also be taken into consideration, in view of the well-known structural and functional interactions established by plastids with other organelles (Mathur et al., 2012).

AUTHOR CONTRIBUTIONS

LN, EF, and IS jointly contributed to the writing of this manuscript. LC designed the structural model of cMCU presented in **Figure 1**. All authors reviewed and approved the final version of the submitted manuscript.

FUNDING

This work was supported by HFSP RG0052 to IS and the University of Padova (PRID 2018, BIRD180317) to LN.

REFERENCES

Alexandersson, E., Saalbach, G., Larsson, C., and Kjellbom, P. (2004). Arabidopsis plasma membrane proteomics identifies components of transport, signal transduction and membrane trafficking. *Plant Cell Physiol.* 45, 1543–1556. doi: 10.1093/pcp/pch209

Anil, V. S., Rajkumar, P., Kumar, P., and Mathew, M. K. (2008). A plant Ca^{2+} pump, ACA2, relieves salt hypersensitivity in yeast. Modulation of cytosolic calcium signature and activation of adaptive Na+ homeostasis. *J. Biol. Chem.* 283 (6), 3497–3506. doi: 10.1074/jbc.M700766200

Astegno, A., Bonza, M. C., Vallone, R., La Verde, V., D'Onofrio, M., Luoni, L., et al. (2017). Arabidopsis calmodulin-like protein CML36 is a calcium Ca^{2+} sensor that interacts with the plasma membrane Ca(2+)-ATPase isoform ACA8 and stimulates its activity. *J. Biol. Chem.* 292, 15049–15061. doi: 10.1074/jbc.M117.787796

Baliardini, C., Meyer, C. L., Salis, P., Saumitou-Laprade, P., and Verbruggen, N. (2015). CATION EXCHANGER1 Cosegregates with Cadmium tolerance in the metal hyperaccumulator Arabidopsis halleri and plays a role in limiting oxidative stress in Arabidopsis Spp. *Plant Physiol.* 169, 549–559. doi: 10.1104/pp.15.01037

Baradaran, R., Wang, C., Siliciano, A. F., and Long, S. B. (2018). Cryo-EM structures of fungal and metazoan mitochondrial calcium uniporters. *Nature* 559, 580–584. doi: 10.1038/s41586-018-0331-8

Baughman, J. M. (2011). Integrative genomics identifies MCU as an essential component of the mitochondrial calcium uniporter. *Nature* 476, 341–345. doi: 10.1038/nature10234

Behrens, C., Blume, C., Senkler, M., Eubel, H., Peterhansel, C., and Braun, H. P. (2013). The 'protein complex proteome' of chloroplasts in Arabidopsis thaliana. *J. Proteomics* 91, 73–83. doi: 10.1016/j.jprot.2013.07.001

Beltran, J., Wamboldt, Y., Sanchez, R., Labrant, E. W., Kundariya, H., Virdi, K. S., et al. (2018). Specialized plastids trigger tissue-specific signaling for systemic stress response in plants. *Plant Physiol.* 178, 672–683. doi: 10.1104/pp.18.00804

Benschop, J. J., Mohammed, S., O'Flaherty, M., Heck, A. J., Slijper, M., and Menke, F. L. (2007). Quantitative phosphoproteomics of early elicitor signaling in Arabidopsis. *Mol. Cell Proteomics* 6, 1198–1214. doi: 10.1074/mcp.M600429-MCP200

Bernfur, K., Larsson, O., Larsson, C., and Gustavsson, N. (2013). Relative abundance of integral plasma membrane proteins in Arabidopsis leaf and root tissue determined by metabolic labeling and mass spectrometry. *PloS One* 8, e71206. doi: 10.1371/journal.pone.0071206

Bick, A. G., Calvo, S. E., and Mootha, V. K. (2012). Evolutionary diversity of the mitochondrial calcium uniporter. *Science* 336, 886. doi: 10.1126/science.1214977

Carraretto, L., Teardo, E., Checchetto, V., Finazzi, G., Uozumi, N., and Szabo, I. (2016). Ion channels in plant bioenergetic organelles chloroplast and mitochondria: from molecular identification to function. *Mol. Plant* 9, 371–395. doi: 10.1016/j.molp.2015.12.004

Chen, Y., Hoehenwarter, W., and Weckwerth, W. (2010). Comparative analysis of phytohormone-responsive phosphoproteins in Arabidopsis thaliana using TiO2-phosphopeptide enrichment and mass accuracy precursor alignment. *Plant J.* 63 (1), 1–17. doi: 10.1111/j.1365-313X.2010.04218.x

Cheng, N. H., Pittman, J. K., Shigaki, T., and Hirschi, K. D. (2002). Characterization of CAX4, an Arabidopsis H(+)/cation antiporter. *Plant Physiol.* 128, 1245–1254. doi: 10.1104/pp.010857

Cheng, N. H., Pittman, J. K., Barkla, B. J., Shigaki, T., and Hirschi, K. D. (2003). The Arabidopsis cax1 mutant exhibits impaired ion homeostasis, development, and hormonal responses and reveals interplay among vacuolar transporters. *Plant Cell* 15 (2), 347–364. doi: 10.1105/tpc.007385

Cheng, Y., Zhang, X., Sun, T., Tian, Q., and Zhang, W. H. (2018). Glutamate receptor Homolog3.4 is involved in regulation of seed germination under salt stress in Arabidopsis. *Plant Cell Physiol.* 59, 978–988. doi: 10.1093/pcp/pcy034

Chigri, F., Flosdorff, S., Pilz, S., Kolle, E., Dolze, E., Gietl, C., et al. (2012). The Arabidopsis calmodulin-like proteins AtCML30 and AtCML3 are targeted to mitochondria and peroxisomes, respectively. *Plant Mol. Biol.* 78, 211–222. doi: 10.1007/s11103-011-9856-z

Cho, D., Kim, S. A., Murata, Y., Lee, S., Jae, S. K., Nam, H. G., et al. (2009). De-regulated expression of the plant glutamate receptor homolog AtGLR3.1 impairs long-term Ca^{2+}-programmed stomatal closure. *Plant J.* 58 (3), 437–449. doi: 10.1111/j.1365-313X.2009.03789.x

Cho, D., Villiers, F., Kroniewicz, L., Lee, S., Seo, Y. J., Hirschi, K. D., et al. (2012). Vacuolar CAX1 and CAX3 influence auxin transport in guard cells via regulation of apoplastic pH. *Plant Physiol.* 160 (3), 1293–1302. doi: 10.1104/pp.112.201442

Conn, S. J., Gilliham, M., Athman, A., Schreiber, A. W., Baumann, U., Moller, I., et al. (2011). Cell-specific vacuolar calcium storage mediated by CAX1

regulates apoplastic calcium concentration, gas exchange, and plant productivity in Arabidopsis. *Plant Cell* 23, 240–257. doi: 10.1105/tpc.109.072769

Costa, A., Navazio, L., and Szabo, I. (2018). The contribution of organelles to plant intracellular Calcium signaling. *J. Exp. Bot.* 69, 4175–4193. doi: 10.1093/jxb/ery185

Cutolo, E., Parvin, N., Ruge, H., Pirayesh, N., Roustan, V., Weckwerth, W., et al. (2019). The high light response in Arabidopsis requires the Calcium sensor protein CAS, a target of STN7- and STN8-Mediated phosphorylation. *Front. Plant Sci.* 10, 974. doi: 10.3389/fpls.2019.00974

Dammann, C., Ichida, A., Hong, B., Romanowsky, S. M., Hrabak, E. M., Harmon, A. C., et al. (2003). Subcellular targeting of nine calcium-dependent protein kinase isoforms from Arabidopsis. *Plant Physiol.* 132, 1840–1848. doi: 10.1104/pp.103.020008

De Michele, R., McFarlane, H. E., Parsons, H. T., Meents, M. J., Lao, J., Gonzalez Fernandez-Nino, S. M., et al. (2016). Free-flow electrophoresis of plasma membrane vesicles enriched by two-phase partitioning enhances the quality of the proteome from arabidopsis seedlings. *J. Proteome Res.* 15, 900–913. doi: 10.1021/acs.jproteome.5b00876

De Stefani, D., Raffaello, A., Teardo, E., Szabo, I., and Rizzuto, R. (2011). A forty-kilodalton protein of the inner membrane is the mitochondrial calcium uniporter. *Nature* 476, 336–340. doi: 10.1038/nature10230

Demidchik, V., Shabala, S., Isayenkov, S., Cuin, T. A., and Pottosin, I. (2018). Calcium transport across plant membranes: mechanisms and functions. *New Phytol.* 220, 49–69. doi: 10.1111/nph.15266

Demir, F., Horntrich, C., Blachutzik, J. O., Scherzer, S., Reinders, Y., Kierszniowska, S., et al. (2013). Arabidopsis nanodomain-delimited ABA signaling pathway regulates the anion channel SLAH3. *Proc. Natl. Acad. Sci. U. S. A* 110, 8296–8301. doi: 10.1073/pnas.1211667110

Dodd, A. N., Kudla, J., and Sanders, D. (2010). The language of calcium signaling. *Annu. Rev. Plant Biol.* 61, 593–620. doi: 10.1146/annurev-arplant-070109-104628

Drakakaki, G., van de Ven, W., Pan, S., Miao, Y., Wang, J., Keinath, N. F., et al. (2012). Isolation and proteomic analysis of the SYP61 compartment reveal its role in exocytic trafficking in Arabidopsis. *Cell Res.* 22, 413–424. doi: 10.1038/cr.2011.129

Dunkley, T. P., Hester, S., Shadforth, I. P., Runions, J., Weimar, T., Hanton, S. L., et al. (2006). Mapping the Arabidopsis organelle proteome. *Proc. Natl. Acad. Sci. U. S. A* 103, 6518–6523. doi: 10.1073/pnas.0506958103

Eisenhut, M., Hoecker, N., Schmidt, S. B., Basgaran, R. M., Flachbart, S., Jahns, P., et al. (2018). The plastid envelope CHLOROPLAST MANGANESE TRANSPORTER1 is essential for manganese homeostasis in Arabidopsis. *Mol. Plant* 11 (7), 955–969. doi: 10.1016/j.molp.2018.04.008

Elmore, J. M., Liu, J., Smith, B., Phinney, B., and Coaker, G. (2012). Quantitative proteomics reveals dynamic changes in the plasma membrane during Arabidopsis immune signaling. *Mol. Cell Proteomics* 11, M111.014555. doi: 10.1074/mcp.M111.014555

Fakih, Z., Ahmed, M. B., Letanneur, C., and Germain, H. (2016). An unbiased nuclear proteomics approach reveals novel nuclear protein components that participates in MAMP-triggered immunity. *Plant Signal Behav.* 11, e1183087. doi: 10.1080/15592324.2016.1183087

Fan, C., Fan, M., Orlando, B. J., Fastman, N. M., Zhang, J., XU, Y., et al. (2018). X-ray and cryo-EM structures of the mitochondrial calcium uniporter. *Nature* 559, 575–579. doi: 10.1038/s41586-018-0330-9

Ferro, M., Brugiere, S., Salvi, D., Seigneurin-Berny, D., Court, M., Moyet, L., et al. (2010). AT_CHLORO, a comprehensive chloroplast proteome database with subplastidial localization and curated information on envelope proteins. *Mol. Cell Proteomics* 9 (6), 1063–1084. doi: 10.1074/mcp.M900325-MCP200

Finazzi, G., Petroutsos, D., Tomizioli, M., Flori, S., Sautron, E., Villanova, V., et al. (2015). Ions channels/transporters and chloroplast regulation. *Cell Calcium* 58, 86–97. doi: 10.1016/j.ceca.2014.10.002

Frank, J., Happeck, R., Meier, B., Hoang, M. T. T., Stribny, J., Hause, G., et al. (2019). Chloroplast-localized BICAT proteins shape stromal calcium signals and are required for efficient photosynthesis. *New Phytol.* 221, 866–880. doi: 10.1111/nph.15407

Fromm, S., Senkler, J., Eubel, H., Peterhansel, C., and Braun, H. P. (2016). Life without complex I: proteome analyses of an Arabidopsis mutant lacking the mitochondrial NADH dehydrogenase complex. *J. Exp. Bot.* 67 (10), 3079–3093. doi: 10.1093/jxb/erw165

García Bossi, J., Kumar, K., Barberini, M. L., Domínguez, G. D., Rondón Guerrero, Y. D. C., Marino-Buslje, C., et al. (2020). The role of P-type IIA and P-type IIB Ca^{2+}-ATPases in plant development and growth. *J. Exp. Bot.* 71, 1239–1248. doi: 10.1093/jxb/erz521

Geiger, D., Scherzer, S., Mumm, P., Marten, I., Ache, P., Matschi, S., et al. (2010). Guard cell anion channel SLAC1 is regulated by CDPK protein kinases with distinct Ca2+ affinities. *Proc. Natl. Acad. Sci. U. S. A* 107, 8023–8028. doi: 10.1073/pnas.0912030107

Guo, H., Mockler, T., Duong, H., and Lin, C. (2001). SUB1, an Arabidopsis Ca^{2+}-binding protein involved in cryptochrome and phytochrome coaction. *Science* 291, 487–490. doi: 10.1126/science.291.5503.487

Gutermuth, T., Lassig, R., Portes, M. T., Maierhofer, T., Romeis, T., Borst, J. W., et al. (2013). Pollen tube growth regulation by free anions depends on the interaction between the anion channel SLAH3 and calcium-dependent protein kinases CPK2 and CPK20. *Plant Cell* 25, 4525–4543. doi: 10.1105/tpc.113.118463

Hamada, T., Nagasaki-Takeuchi, N., Kato, T., Fujiwara, M., Sonobe, S., Fukao, Y., et al. (2013). Purification and characterization of novel microtubule-associated proteins from Arabidopsis cell suspension cultures. *Plant Physiol.* 163, 1804–1816. doi: 10.1104/pp.113.225607

He, Y., Wu, J., Lv, B., Li, J., Gao, Z., Xu, W., et al. (2015). Involvement of 14-3-3 protein GRF9 in root growth and response under polyethylene glycol-induced water stress. *J. Exp. Bot.* 66 (8), 2271–2281. doi: 10.1093/jxb/erv149

Heard, W., Sklenar, J., Tome, D. F., Robatzek, S., and Jones, A. M. (2015). Identification of Regulatory and Cargo Proteins of Endosomal and Secretory Pathways in Arabidopsis thaliana by Proteomic Dissection. *Mol. Cell Proteomics* 14, 1796–1813. doi: 10.1074/mcp.M115.050286

Helm, S., Dobritzsch, D., Rodiger, A., Agne, B., and Baginsky, S. (2014). Protein identification and quantification by data-independent acquisition and multi-parallel collision-induced dissociation mass spectrometry (MS(E)) in the chloroplast stroma proteome. *J. Proteomics* 98, 79–89. doi: 10.1016/j.jprot.2013.12.007

Higuchi, M., Ozaki, H., Matsui, M., and Sonoike, K. (2009). A T-DNA insertion mutant of AtHMA1 gene encoding a Cu transporting ATPase in Arabidopsis thaliana has a defect in the water-water cycle of photosynthesis. *J. Photochem. Photobiol. B.* 94 (3), 205–213. doi: 10.1016/j.jphotobiol.2008.12.002

Hochmal, A. K., Schulze, S., Trompelt, K., and Hippler, M. (2015). Calcium-dependent regulation of photosynthesis. *Biochim. Biophys. Acta* 1847, 993–1003. doi: 10.1016/j.bbabio.2015.02.010

Hocking, B., Conn, S. J., Manohar, M., Xu, B., Athman, A., Stancombe, M. A., et al. (2017). Heterodimerization of Arabidopsis calcium/proton exchangers contributes to regulation of guard cell dynamics and plant defense responses. *J. Exp. Bot.* 68, 4171–4183. doi: 10.1093/jxb/erx209

Hooper, C. M., Castleden, I. R., Tanz, S. K., Aryamanesh, N., and Millar, A. H. (2017). SUBA4: the interactive data analysis centre for Arabidopsis subcellular protein locations. *Nucleic Acids Res.* 45, D1064–d1074. doi: 10.1093/nar/gkw1041

Huang, L., Berkelman, T., Franklin, A. E., and Hoffman, N. E. (1993). Characterization of a gene encoding a Ca(2+)-ATPase-like protein in the plastid envelope. *Proc. Natl. Acad. Sci. U. S. A* 90 (21), 10066–10070. doi: 10.1073/pnas.90.21.10066

Huang, K., Peng, L., Liu, Y., Yao, R., Liu, Z., Li, X., et al. (2018). Arabidopsis calcium-dependent protein kinase AtCPK1 plays a positive role in salt/drought-stress response. *Biochem. Biophys. Res. Commun.* 498 (1), 92–98. doi: 10.1016/j.bbrc.2017.11.175

Inzè, A., Vanderauwera, S., Hoeberichts, F. A., Vandorpe, M., van Gaever, T., and van Breusegem, F. (2012). A subcellular localization compendium of hydrogen peroxide-induced proteins. *Plant Cell Environ.* 35, 308–320. doi: 10.1111/j.1365-3040.2011.02323.x

Ito, J., Batth, T. S., Petzold, C. J., Redding-Johanson, A. M., Mukhopadhyay, A., Verboom, R., et al. (2011). Analysis of the Arabidopsis cytosolic proteome highlights subcellular partitioning of central plant metabolism. *J. Proteome Res.* 10 (4), 1571–1582. doi: 10.1021/pr1009433

Ji, R., Zhou, L., Liu, J., Wang, Y., Yang, L., Zheng, Q., et al. (2017). Calcium-dependent protein kinase CPK31 interacts with arsenic transporter AtNIP1;1 and regulates arsenite uptake in Arabidopsis thaliana. *PloS One* 12, e0173681. doi: 10.1371/journal.pone.0173681

Johnson, C. H., Knight, M. R., Kondo, T., Masson, P., Sedbrook, J., Haley, A., et al. (1995). Circadian oscillations of cytosolic and chloroplastic free calcium in plants. *Science* 269, 1863–1865. doi: 10.1126/science.7569925

Ju, C., Kong, D., Lee, Y., Ge, G., Song, Y., Liu, J., et al. (2020). Methionine Synthase 1 Provides Methionine for Activating AtGLR3.5 Ca2+ Channel and Regulating Germination in Arabidopsis. *J. Exp. Bot.* 71, 178–187. doi: 10.1093/jxb/erz431

Karniely, S., and Pines, O. (2005). Single translation–dual destination: mechanisms of dual protein targeting in eukaryotes. *EMBO Rep.* 6, 420–425. doi: 10.1038/sj.embor.7400394

Keinath, N. F., Kierszniowska, S., Lorek, J., Bourdais, G., Kessler, S. A., Shimosato-Asano, H., et al. (2010). PAMP (pathogen-associated molecular pattern)-induced changes in plasma membrane compartmentalization reveal novel components of plant immunity. *J. Biol. Chem.* 285 (50), 39140–39149. doi: 10.1074/jbc.M110.160531

Kmiecik, P., Leonardelli, M., and Teige, M. (2016). Novel connections in plant organellar signaling link different stress responses and signaling pathways. *J. Exp. Bot.* 67, 3793–3807. doi: 10.1093/jxb/erw136

Kong, D., Hu, H. C., Okuma, E., Lee, Y., Lee, H. S., Munemasa, S., et al. (2016). L-Met Activates Arabidopsis GLR Ca(2+) Channels Upstream of ROS Production and Regulates Stomatal Movement. *Cell Rep.* 17 (10), 2553–2561. doi: 10.1016/j.celrep.2016.11.015

Kudla, J., Becker, D., Grill, E., Hedrich, R., Hippler, M., Kummer, U., et al. (2018). Advances and current challenges in calcium signaling. *New Phytol.* 218, 414–431. doi: 10.1111/nph.14966

Latz, A., Mehlmer, N., Zapf, S., Mueller, T. D., Wurzinger, B., Pfister, B., et al. (2013). Salt stress triggers phosphorylation of the Arabidopsis vacuolar K+ channel TPK1 by calcium-dependent protein kinases (CDPKs). *Mol. Plant* 6, 1274–1289. doi: 10.1093/mp/sss158

Lee, T. A., and Bailey-Serres, J. (2019). Integrative Analysis from the Epigenome to Translatome Uncovers Patterns of Dominant Nuclear Regulation during Transient Stress. *Plant Cell* 31, 2573–2595. doi: 10.1105/tpc.19.00463

Lee, D., Polisensky, D. H., and Braam, J. (2005). Genome-wide identification of touch- and darkness-regulated Arabidopsis genes: a focus on calmodulin-like and XTH genes. *New Phytol.* 165, 429–444. doi: 10.1111/j.1469-8137.2004.01238.x

Lee, J., Lee, H., Kim, J., Lee, S., Kim, D. H., Kim, S., et al. (2011). Both the hydrophobicity and a positively charged region flanking the C-terminal region of the transmembrane domain of signal-anchored proteins play critical roles in determining their targeting specificity to the endoplasmic reticulum or endosymbiotic organelles in Arabidopsis cells. *Plant Cell* 23 (4), 1588–1607. doi: 10.1105/tpc.110.082230

Lee, Y., Min, C. K., Kim, T. G., Song, H. K., Lim, Y., Kim, D., et al. (2015). Structure and function of the N-terminal domain of the human mitochondrial calcium uniporter. *EMBO Rep.* 16, 1318–1333. doi: 10.15252/embr.201540436

Lenzoni, G., and Knight, M. R. (2019). Increases in Absolute Temperature Stimulate Free Calcium Concentration Elevations in the Chloroplast. *Plant Cell Physiol.* 60, 538–548. doi: 10.1093/pcp/pcy227

Li, B., Takahashi, D., Kawamura, Y., and Uemura, M. (2012). Comparison of plasma membrane proteomic changes of Arabidopsis suspension-cultured cells (T87 Line) after cold and ABA treatment in association with freezing tolerance development. *Plant Cell Physiol.* 53 (3), 543–554. doi: 10.1093/pcp/pcs010

Li, G., Boudsocq, M., Hem, S., Vialaret, J., Rossignol, M., Maurel, C., et al. (2015). The calcium-dependent protein kinase CPK7 acts on root hydraulic conductivity. *Plant Cell Environ.* 38 (7), 1312–1320. doi: 10.1111/pce.12478

Li, P., Zhang, G., Gonzales, N., Guo, Y., Hu, H., Park, S., et al. (2016). Ca(2+) -regulated and diurnal rhythm-regulated Na(+) /Ca(2+) exchanger AtNCL affects flowering time and auxin signaling in Arabidopsis. *Plant Cell Environ.* 39 (2), 377–392. doi: 10.1111/pce.12620

Li, Z., Takahashi, Y., Scavo, A., Brandt, B., Nguyen, D., Rieu, P., et al. (2018). Abscisic acid-induced degradation of Arabidopsis guanine nucleotide exchange factor requires calcium-dependent protein kinases. *Proc. Natl. Acad. Sci. U. S. A* 115, E4522–e4531. doi: 10.1073/pnas.1719659115

Liu, N., Hake, K., Wang, W., Zhao, T., Romeis, T., and Tang, D. (2017). CALCIUM-DEPENDENT PROTEIN KINASE5 associates with the truncated nlr protein TIR-NBS2 to contribute to exo70B1-mediated immunity. *Plant Cell* 29, 746–759. doi: 10.1105/tpc.16.00822

Loro, G., Wagner, S., Doccula, F. G., Behera, S., Weinl, S., Kudla, J., et al. (2016). Chloroplast-specific in Vivo Ca2+ imaging using yellow cameleon fluorescent protein sensors reveals organelle-autonomous Ca2+ signatures in the Stroma. *Plant Physiol.* 171, 2317–2330. doi: 10.1104/pp.16.00652

Ma, X., Gai, W. X., Qiao, Y. M., Ali, M., Wei, A. M., Luo, D. X., et al. (2019). Identification of CBL and CIPK gene families and functional characterization of CaCIPK1 under Phytophthora capsici in pepper (Capsicum annuum L.). *BMC Genomics* 20, 775. doi: 10.1186/s12864-019-6125-z

Manohar, M., Shigaki, T., Mei, H., Park, S., Marshall, J., Aguilar, J., et al. (2011). Characterization of Arabidopsis Ca2+/H+ exchanger CAX3. *Biochemistry* 50, 6189–6195. doi: 10.1021/bi2003839

Manzoor, H., Chiltz, A., Madani, S., Vatsa, P., Schoefs, B., Pugin, A., et al. (2012). Calcium signatures and signaling in cytosol and organelles of tobacco cells induced by plant defense elicitors. *Cell Calcium* 51, 434–444. doi: 10.1016/j.ceca.2012.02.006

Marmagne, A., Ferro, M., Meinnel, T., Bruley, C., Kuhn, L., Garin, J., et al. (2007). A high content in lipid-modified peripheral roteins and integral receptor kinases features in the arabidopsis plasma membrane proteome. *Mol. Cell Proteomics* 6, 1980–1996. doi: 10.1074/mcp.M700099-MCP200

Martí Ruiz, M. C., Jung, H. J., and Webb, A. A. R. (2020). Circadian gating of dark-induced increases in chloroplast- and cytosolic-free calcium in Arabidopsis. *New Phytol.* 225, 1993–2005 doi: 10.1111/nph.16280

Mathur, J., Mammone, A., and Barton, K. A. (2012). Organelle extensions in plant cells. *J. Integr. Plant Biol.* 54, 851–867. doi: 10.1111/j.1744-7909.2012.01175.x

Matschi, S., Hake, K., Herde, M., Hause, B., and Romeis, T. (2015). The calcium-dependent protein kinase CPK28 regulates development by inducing growth phase-specific, spatially restricted alterations in jasmonic acid levels independent of defense responses in Arabidopsis. *Plant Cell* 27 (3), 591–606. doi: 10.1105/tpc.15.00024

Mayfield, J. D., Paul, A. L., and Ferl, R. J. (2012). The 14-3-3 proteins of Arabidopsis regulate root growth and chloroplast development as components of the photosensory system. *J. Exp. Bot.* 63 (8), 3061–3070. doi: 10.1093/jxb/ers022

Mehlmer, N., Parvin, N., Hurst, C. H., Knight, M. R., Teige, M., and Vothknecht, U. C. (2012). A toolset of aequorin expression vectors for in planta studies of subcellular calcium concentrations in Arabidopsis thaliana. *J. Exp. Bot.* 63, 1751–1761. doi: 10.1093/jxb/err406

Mei, H., Cheng, N. H., Zhao, J., Park, S., Escareno, R. A., Pittman, J. K., et al. (2009). Root development under metal stress in Arabidopsis thaliana requires the H+/cation antiporter CAX4. *New Phytol.* 183, 95–105. doi: 10.1111/j.1469-8137.2009.02831.x

Melonek, J., Oetke, S., and Krupinska, K. (2016). Multifunctionality of plastid nucleoids as revealed by proteome analyses. *Biochim. Biophys. Acta* 1864, 1016–1038. doi: 10.1016/j.bbapap.2016.03.009

Meyerhoff, O., Muller, K., Roelfsema, M. R., Latz, A., Lacombe, B., Hedrich, R., et al. (2005). AtGLR3.4, a glutamate receptor channel-like gene is sensitive to touch and cold. *Planta* 222, 418–427. doi: 10.1007/s00425-005-1551-3

Mitra, S. K., Walters, B. T., Clouse, S. D., and Goshe, M. B. (2009). An efficient organic solvent based extraction method for the proteomic analysis of Arabidopsis plasma membranes. *J. Proteome Res.* 8, 2752–2767. doi: 10.1021/pr801044y

Monaghan, J., Matschi, S., Shorinola, O., Rovenich, H., Matei, A., Segonzac, C., et al. (2014). The calcium-dependent protein kinase CPK28 buffers plant immunity and regulates BIK1 turnover. *Cell Host. Microbe* 16, 605–615. doi: 10.1016/j.chom.2014.10.007

Monaghan, J., Matschi, S., Romeis, T., and Zipfel, C. (2015). The calcium-dependent protein kinase CPK28 negatively regulates the BIK1-mediated PAMP-induced calcium burst. *Plant Signal Behav.* 10, e1018497. doi: 10.1080/15592324.2015.1018497

Mori, I. C., Murata, Y., Yang, Y., Munemasa, S., Wang, Y. F., Andreoli, S., et al. (2006). CDPKs CPK6 and CPK3 function in ABA regulation of guard cell S-type anion- and Ca(2+)-permeable channels and stomatal closure. *PloS Biol.* 4, e327. doi: 10.1371/journal.pbio.0040327

Morris, J., Tian, H., Park, S., Sreevidya, C. S., Ward, J. M., and Hirschi, K. D. (2008). AtCCX3 is an Arabidopsis endomembrane H+ -dependent K+ transporter. *Plant Physiol.* 148, 1474–1486. doi: 10.1104/pp.108.118810

Myers, C., Romanowsky, S. M., Barron, Y. D., Garg, S., Azuse, C. L., Curran, A., et al. (2009). Calcium-dependent protein kinases regulate polarized tip growth in pollen tubes. *Plant J.* 59, 528–539. doi: 10.1111/j.1365-313X.2009.03894.x

Nelson, C. J., Hegeman, A. D., Harms, A. C., and Sussman, M. R. (2006). A quantitative analysis of Arabidopsis plasma membrane using trypsin-catalyzed

(18)O labeling. *Mol. Cell Proteomics* 5 (8), 1382–1395. doi: 10.1074/mcp.M500414-MCP200

Nguyen, C. T., Kurenda, A., Stolz, S., Chetelat, A., and Farmer, E. E. (2018a). Identification of cell populations necessary for leaf-to-leaf electrical signaling in a wounded plant. *Proc. Natl. Acad. Sci. U. S. A* 115, 10178–10183. doi: 10.1073/pnas.1807049115

Nguyen, N. X., Armache, J. P., Lee, C., Yang, Y., Zeng, W., Mootha, V. K., et al. (2018b). Cryo-EM structure of a fungal mitochondrial calcium uniporter. *Nature* 559, 570–574. doi: 10.1038/s41586-018-0333-6

Nguyen-Kim, H., San Clemente, H., Balliau, T., Zivy, M., Dunand, C., Albenne, C., et al. (2016). Arabidopsis thaliana root cell wall proteomics: Increasing the proteome coverage using a combinatorial peptide ligand library and description of unexpected Hyp in peroxidase amino acid sequences. *Proteomics* 16, 491–503. doi: 10.1002/pmic.201500129

Nikolovski, N., Rubtsov, D., Segura, M. P., Miles, G. P., Stevens, T. J., Dunkley, T. P., et al. (2012). Putative glycosyltransferases and other plant Golgi apparatus proteins are revealed by LOPIT proteomics. *Plant Physiol.* 160, 1037–1051. doi: 10.1104/pp.112.204263

Nomura, H., and Shiina, T. (2014). Calcium signaling in plant endosymbiotic organelles: mechanism and role in physiology. *Mol. Plant* 7, 1094–1104. doi: 10.1093/mp/ssu020

Nomura, H., Komori, T., Uemura, S., Kanda, Y., Shimotani, K., Nakai, K., et al. (2012). Chloroplast-mediated activation of plant immune signaling in Arabidopsis. *Nat. Commun.* 3, 926. doi: 10.1038/ncomms1926

Nühse, T. S., Stensballe, A., Jensen, O. N., and Peck, S. C. (2003). Large-scale analysis of in vivo phosphorylated membrane proteins by immobilized metal ion affinity chromatography and mass spectrometry. *Mol. Cell Proteomics* 2 (11), 1234–1243. doi: 10.1074/mcp.T300006-MCP200

Nühse, T. S., Stensballe, A., Jensen, O. N., and Peck, S. C. (2004). Phosphoproteomics of the Arabidopsis plasma membrane and a new phosphorylation site database. *Plant Cell* 16 (9), 2394–2405. doi: 10.1105/tpc.104.023150

Omidbakhshfard, M. A., Fujikura, U., Olas, J. J., Xue, G. P., Balazadeh, S., and Mueller-Roeber, B. (2018). GROWTH-REGULATING FACTOR 9 negatively regulates arabidopsis leaf growth by controlling ORG3 and restricting cell proliferation in leaf primordia. *PloS Genet.* 14, e1007484. doi: 10.1371/journal.pgen.1007484

Oxenoid, K., Dong, Y., Cao, C., Cui, T., Sancak, Y., Markhard, A. L., et al. (2016). Architecture of the mitochondrial calcium uniporter. *Nature* 533, 269–273. doi: 10.1038/nature17656

Parsons, H. T., Christiansen, K., Knierim, B., Carroll, A., Ito, J., Batth, T. S., et al. (2012). Isolation and proteomic characterization of the Arabidopsis Golgi defines functional and novel components involved in plant cell wall biosynthesis. *Plant Physiol.* 159, 12–26. doi: 10.1104/pp.111.193151

Pittman, J. K., and Hirschi, K. D. (2016). CAX-ing a wide net: Cation/H(+) transporters in metal remediation and abiotic stress signaling. *Plant Biol. (Stuttg)* 18, 741–749. doi: 10.1111/plb.12460

Pornsiriwong, W., Estavillo, G. M., Chan, K. X., Tee, E. E., Ganguly, D., Crisp, P. A., et al. (2017). A chloroplast retrograde signal, 3'-phosphoadenosine 5'-phosphate, acts as a secondary messenger in abscisic acid signaling in stomatal closure and germination. *Elife* 6, e23361. doi: 10.7554/eLife.23361

Pottosin, I., and Shabala, S. (2015). Transport across chloroplast membranes: optimizing photosynthesis for adverse environmental conditions. *Mol. Plant* 9, 356–370. doi: 10.1016/j.molp.2015.10.006

Ranty, B., Aldon, D., Cotelle, V., Galaud, J. P., Thuleau, P., and Mazars, C. (2016). Calcium sensors as key hubs in plant responses to biotic and abiotic stresses. *Front. Plant Sci.* 7, 327. doi: 10.3389/fpls.2016.00327

Reumann, S., Quan, S., Aung, K., Yang, P., Manandhar-Shrestha, K., Holbrook, D., et al. (2009). In-depth proteome analysis of Arabidopsis leaf peroxisomes combined with *in vivo* subcellular targeting verification indicates novel metabolic and regulatory functions of peroxisomes. *Plant Physiol.* 150, 125–143. doi: 10.1104/pp.109.137703

Rocha, A. G., and Vothknecht, U. C. (2012). The role of calcium in chloroplasts–an intriguing and unresolved puzzle. *Protoplasma* 249, 957–966. doi: 10.1007/s00709-011-0373-3

Rodriguez Milla, M. A., Uno, Y., Chang, I. F., Townsend, J., Maher, E. A., Quilici, D., et al. (2006). A novel yeast two-hybrid approach to identify CDPK substrates: characterization of the interaction between AtCPK11 and AtDi19, a nuclear zinc finger protein. *FEBS Lett.* 580 (3), 904–911. doi: 10.1016/j.febslet.2006.01.013

Ruge, H., Flosdorff, S., Ebersberger, I., Chigri, F., and Vothknecht, U. C. (2016). The calmodulin-like proteins AtCML4 and AtCML5 are single-pass membrane proteins targeted to the endomembrane system by an N-terminal signal anchor sequence. *J. Exp. Bot.* 67, 3985–3996. doi: 10.1093/jxb/erw101

Sai, J., and Johnson, C. H. (2002). Dark-stimulated calcium ion fluxes in the chloroplast stroma and cytosol. *Plant Cell* 14, 1279–1291. doi: 10.1105/tpc.000653

Sanyal, S. K., Pandey, A., and Pandey, G. K. (2015). The CBL-CIPK signaling module in plants: a mechanistic perspective. *Physiol. Plant* 155, 89–108. doi: 10.1111/ppl.12344

Schiott, M., Romanowsky, S. M., Baekgaard, L., Jakobsen, M. K., Palmgren, M. G., and Harper, J. F. (2004). A plant plasma membrane Ca2+ pump is required for normal pollen tube growth and fertilization. *Proc. Natl. Acad. Sci. U. S. A* 101 (25), 9502–9507. doi: 10.1073/pnas.0401542101

Schneider, A., Steinberger, I., Herdean, A., Gandini, C., Eisenhut, M., Kurz, S., et al. (2016). The evolutionarily conserved protein PHOTOSYNTHESIS AFFECTED MUTANT71 is required for efficient manganese uptake at the Thylakoid Membrane in Arabidopsis. *Plant Cell* 28, 892–910. doi: 10.1105/tpc.15.00812

Scholz, S. S., Vadassery, J., Heyer, M., Reichelt, M., Bender, K. W., Snedden, W. A., et al. (2014). Mutation of the Arabidopsis calmodulin-like protein CML37 deregulates the jasmonate pathway and enhances susceptibility to herbivory. *Mol. Plant* 7, 1712–1726. doi: 10.1093/mp/ssu102

Scholz, S. S., Reichelt, M., Vadassery, J., and Mithofer, A. (2015). Calmodulin-like protein CML37 is a positive regulator of ABA during drought stress in Arabidopsis. *Plant Signal Behav.* 10 (6), e1011951. doi: 10.1080/15592324.2015.1011951

Schwacke, R., Schneider, A., van der Graaff, E., Fischer, K., Catoni, E., Desimone, M., et al. (2003). ARAMEMNON, a novel database for Arabidopsis integral membrane proteins. *Plant Physiol.* 131, 16–26. doi: 10.1104/pp.011577

Seigneurin-Berny, D., Gravot, A., Auroy, P., Mazard, C., Kraut, A., Finazzi, G., et al. (2006). HMA1, a new Cu-ATPase of the chloroplast envelope, is essential for growth under adverse light conditions. *J. Biol. Chem.* 281, 2882–2892. doi: 10.1074/jbc.M508333200

Selles, B., Michaud, C., Xiong, T. C., Leblanc, O., and Ingouff, M. (2018). Arabidopsis pollen tube germination and growth depend on the mitochondrial calcium uniporter complex. *New Phytol.* 219, 58–65. doi: 10.1111/nph.15189

Sello, S., Perotto, J., Carraretto, L., Szabo, I., Vothknecht, U. C., and Navazio, L. (2016). Dissecting stimulus-specific Ca2+ signals in amyloplasts and chloroplasts of Arabidopsis thaliana cell suspension cultures. *J. Exp. Bot.* 67, 3965–3974. doi: 10.1093/jxb/erw038

Sello, S., Moscatiello, R., Mehlmer, N., Leonardelli, M., Carraretto, L., Cortese, E., et al. (2018). Chloroplast Ca(2+) Fluxes into and across Thylakoids revealed by Thylakoid-Targeted Aequorin Probes. *Plant Physiol.* 177, 38–51. doi: 10.1104/pp.18.00027

Senkler, J., Senkler, M., Eubel, H., Hildebrandt, T., Lengwenus, C., Schertl, P., et al. (2017). The mitochondrial complexome of Arabidopsis thaliana. *Plant J.* 89, 1079–1092. doi: 10.1111/tpj.13448

Stael, S., Bayer, R. G., Mehlmer, N., and Teige, M. (2011). Protein N-acylation overrides differing targeting signals. *FEBS Lett.* 585, 517–522. doi: 10.1016/j.febslet.2011.01.001

Stael, S., Rocha, A. G., Wimberger, T., Anrather, D., Vothknecht, U. C., and Teige, M. (2012a). Cross-talk between calcium signaling and protein phosphorylation at the thylakoid. *J. Exp. Bot.* 63, 1725–1733. doi: 10.1093/jxb/err403

Stael, S., Wurzinger, B., Mair, A., Mehlmer, N., Vothknecht, U. C., and Teige, M. (2012b). Plant organellar calcium signaling: an emerging field. *J. Exp. Bot.* 63, 1525–1542. doi: 10.1093/jxb/err394

Stael, S., Kmiecik, P., Willems, P., van der Kelen, K., Coll, N. S., Teige, M., et al. (2015). Plant innate immunity–sunny side up? *Trends Plant Sci.* 20, 3–11. doi: 10.1016/j.tplants.2014.10.002

Stael, S. (2019). Chloroplast calcium signaling quenches a thirst. *Nat. Plants* 5, 559–560. doi: 10.1038/s41477-019-0435-7

Stephens, N. R., Qi, Z., and Spalding, E. P. (2008). Glutamate receptor subtypes evidenced by differences in desensitization and dependence on the GLR3.3 and GLR3.4 genes. *Plant Physiol.* 146, 529–538. doi: 10.1104/pp.107.108134

Szymanski, W. G., Zauber, H., Erban, A., Gorka, M., Wu, X. N., and Schulze, W. X. (2015). Cytoskeletal components define protein location to membrane

microdomains. *Mol. Cell Proteomics* 14, 2493–2509. doi: 10.1074/mcp.M114.046904

Teardo, E., Segalla, A., Formentin, E., Zanetti, M., Marin, O., Giacometti, G. M., et al. (2010). Characterization of a plant glutamate receptor activity. *Cell Physiol. Biochem.* 26, 253–262. doi: 10.1159/000320525

Teardo, E., Formentin, E., Segalla, A., Giacometti, G. M., Marin, O., Zanetti, M., et al. (2011). Dual localization of plant glutamate receptor AtGLR3.4 to plastids and plasmamembrane. *Biochim. Biophys. Acta* 1807, 359–367. doi: 10.1016/j.bbabio.2010.11.008

Teardo, E., Carraretto, L., de Bortoli, S., Costa, A., Behera, S., Wagner, R., et al. (2015). Alternative splicing-mediated targeting of the Arabidopsis GLUTAMATE RECEPTOR3.5 to mitochondria affects organelle morphology. *Plant Physiol.* 167, 216–227. doi: 10.1104/pp.114.242602

Teardo, E., Carraretto, L., Wagner, S., Formentin, E., Behera, S., de Bortoli, S., et al. (2017). Physiological characterization of a plant mitochondrial Calcium Uniporter in Vitro and in Vivo. *Plant Physiol.* 173, 1355–1370. doi: 10.1104/pp.16.01359

Teardo, E., Carraretto, L., Moscatiello, R., Cortese, E., Vicario, M., Festa, M., et al. (2019). A chloroplast-localized mitochondrial calcium uniporter transduces osmotic stress in Arabidopsis. *Nat. Plants* 5, 581–588. doi: 10.1038/s41477-019-0434-8

Tomizioli, M., Lazar, C., Brugiere, S., Burger, T., Salvi, D., Gatto, L., et al. (2014). Deciphering thylakoid sub-compartments using a mass spectrometry-based approach. *Mol. Cell Proteomics* 13, 2147–2167. doi: 10.1074/mcp.M114.040923

Tsai, M. F., Phillips, C. B., Ranaghan, M., Tsai, C. W., Wu, Y., Willliams, C., et al. (2016). Dual functions of a small regulatory subunit in the mitochondrial calcium uniporter complex. *Elife* 5, e15545. doi: 10.7554/eLife.15545

Uno, Y., Rodriguez Milla, M. A., Maher, E., and Cushman, J. C. (2009). Identification of proteins that interact with catalytically active calcium-dependent protein kinases from Arabidopsis. *Mol. Genet. Genomics* 281 (4), 375–390. doi: 10.1007/s00438-008-0419-1

Urao, T., Katagiri, T., Mizoguchi, T., Yamaguchi-Shinozaki, K., Hayashida, N., and Shinozaki, K. (1994). An Arabidopsis thaliana cDNA encoding Ca(2+)-dependent protein kinase. *Plant Physiol.* 105, 1461–1462. doi: 10.1104/pp.105.4.1461

Vainonen, J. P., Sakuragi, Y., Stael, S., Tikkanen, M., Allahverdiyeva, Y., Paakkarinen, V., et al. (2008). Light regulation of CaS, a novel phosphoprotein in the thylakoid membrane of Arabidopsis thaliana. *FEBS J.* 275, 1767–1777. doi: 10.1111/j.1742-4658.2008.06335.x

van Kleeff, P. J. M., Gao, J., Mol, S., Zwart, N., Zhang, H., Li, K. W., et al. (2018). The Arabidopsis GORK K(+)-channel is phosphorylated by calcium-dependent protein kinase 21 (CPK21), which in turn is activated by 14-3-3 proteins. *Plant Physiol. Biochem.* 125, 219–231. doi: 10.1016/j.plaphy.2018.02.013

Vanderbeld, B., and Snedden, W. A. (2007). Developmental and stimulus-induced expression patterns of Arabidopsis calmodulin-like genes CML37, CML38 and CML39. *Plant Mol. Biol.* 64, 683–697. doi: 10.1007/s11103-007-9189-0

Vincill, E. D., Clarin, A. E., Molenda, J. N., and Spalding, E. P. (2013). Interacting glutamate receptor-like proteins in Phloem regulate lateral root initiation in Arabidopsis. *Plant Cell* 25, 1304–1313. doi: 10.1105/tpc.113.110668

Wagner, S., Behera, S., de Bortoli, S., Logan, D. C., Fuchs, P., Carraretto, L., et al. (2015). The EF-Hand Ca2+ binding protein MICU choreographs mitochondrial Ca2+ dynamics in Arabidopsis. *Plant Cell* 27, 3190–3212. doi: 10.1105/tpc.15.00509

Wagner, S., de Bortoli, S., Schwarzlander, M., and Szabo, I. (2016). Regulation of mitochondrial calcium in plants versus animals. *J. Exp. Bot.* 67, 3809–3829. doi: 10.1093/jxb/erw100

Wang, P., Li, Z., Wei, J., Zhao, Z., Sun, D., and Cui, S. (2012). A Na+/Ca2+ exchanger-like protein (AtNCL) involved in salt stress in Arabidopsis. *J. Biol. Chem.* 287 (53), 44062–44070. doi: 10.1074/jbc.M112.351643

Wang, W. H., Chen, J., Liu, T. W., Chen, J., Han, A. D., Simon, M., et al. (2014). Regulation of the calcium-sensing receptor in both stomatal movement and photosynthetic electron transport is crucial for water use efficiency and drought tolerance in Arabidopsis. *J. Exp. Bot.* 65 (1), 223–234. doi: 10.1093/jxb/ert362

Wang, C., Xu, W., Jin, H., Zhang, T., Lai, J., Zhou, X., et al. (2016). A putative chloroplast-localized Ca(2+)/H(+) Antiporter CCHA1 is involved in calcium and pH Homeostasis and required for PSII function in Arabidopsis. *Mol. Plant* 9 (8), 1183–1196. doi: 10.1016/j.molp.2016.05.015

Wang, Y., Nguyen, N. X., She, J., Zeng, W., Yang, Y., Bai, X. C., et al. (2019). Structural mechanism of EMRE-dependent gating of the human mitochondrial Calcium Uniporter. *Cell* 177, 1252–1261.e13. doi: 10.1016/j.cell.2019.03.050

Weinl, S., Held, K., Schlücking, K., Steinhorst, L., Kuhlgert, S., Hippler, M., et al. (2008). A plastid protein crucial for Ca2+-regulated stomatal responses. *New Phytol.* 179, 675–686. doi: 10.1111/j.1469-8137.2008.02492.x

Whiteman, S. A., Serazetdinova, L., Jones, A. M., Sanders, D., Rathjen, J., Peck, S. C., et al. (2008). Identification of novel proteins and phosphorylation sites in a tonoplast enriched membrane fraction of Arabidopsis thaliana. *Proteomics* 8 (17), 3536–3547. doi: 10.1002/pmic.200701104

Yamamoto, T., Ozono, M., Watanabe, A., Maeda, K., Nara, A., Hashida, M., et al. (2019). Functional analysis of coiled-coil domains of MCU in mitochondrial calcium uptake. *Biochim. Biophys. Acta Bioenerg.* 1860, 148061. doi: 10.1016/j.bbabio.2019.148061

Yang, Y., Zhang, C., Tang, R. J., Xu, H. X., Lan, W. Z., Zhao, F., et al. (2019). Calcineurin B-Like proteins CBL4 and CBL10 mediate two independent salt tolerance pathways in Arabidopsis. *Int. J. Mol. Sci.* 20, pii: E2421. doi: 10.3390/ijms20102421

Yoo, J., Wu, M., Yin, Y., Herzik, M. A.Jr., Lander, G. C., and Lee, S. Y. (2018). Cryo-EM structure of a mitochondrial calcium uniporter. *Science* 361, 506–511. doi: 10.1126/science.aar4056

Yoshida, K., Ohnishi, M., Fukao, Y., Okazaki, Y., Fujiwara, M., Song, C., et al. (2013). Studies on vacuolar membrane microdomains isolated from Arabidopsis suspension-cultured cells: local distribution of vacuolar membrane proteins. *Plant Cell Physiol.* 54, 1571–1584. doi: 10.1093/pcp/pct107

Yuan, F., Yang, H., Xue, Y., Kong, D., Ye, R., Li, C., et al. (2014). OSCA1 mediates osmotic-stress-evoked Ca2+ increases vital for osmosensing in Arabidopsis. *Nature* 514, 367–371. doi: 10.1038/nature13593

Zargar, S. M., Kurata, R., Inaba, S., Oikawa, A., Fukui, R., Ogata, Y., et al. (2015). Quantitative proteomics of Arabidopsis shoot microsomal proteins reveals a cross-talk between excess zinc and iron deficiency. *Proteomics* 15, 1196–1201. doi: 10.1002/pmic.201400467

Zhang, Z. J., and Peck, S. C. (2011). Simplified enrichment of plasma membrane proteins for proteomic analyses in Arabidopsis thaliana. *Proteomics* 11, 1780–1788. doi: 10.1002/pmic.201000648

Zhang, B., Zhang, C., Liu, C., Jing, Y., Wang, Y., Jin, L., et al. (2018). Inner envelope CHLOROPLAST MANGANESE TRANSPORTER 1 supports manganese homeostasis and phototrophic growth in Arabidopsis. *Mol. Plant* 11, 943–954. doi: 10.1016/j.molp.2018.04.007

Zhao, L. N., Shen, L. K., Zhang, W. Z., Zhang, W., Wang, Y., and Wu, W. H. (2013). Ca2+-dependent protein kinase11 and 24 modulate the activity of the inward rectifying K+ channels in Arabidopsis pollen tubes. *Plant Cell* 25 (2), 649–661. doi: 10.1105/tpc.112.103184

Zhu, S. Y., Yu, X. C., Wang, X. J., Zhao, R., Li, Y., Fan, R. C., et al. (2007). Two calcium-dependent protein kinases, CPK4 and CPK11, regulate abscisic acid signal transduction in Arabidopsis. *Plant Cell* 19, 3019–3036. doi: 10.1105/tpc.107.050666

Zou, J. J., Wei, F. J., Wang, C., Wu, J. J., Ratnasekera, D., Liu, W. X., et al. (2010). Arabidopsis calcium-dependent protein kinase CPK10 functions in abscisic acid- and Ca2+-mediated stomatal regulation in response to drought stress. *Plant Physiol.* 154, 1232–1243. doi: 10.1104/pp.110.157545

Zou, J. J., Li, X. D., Ratnasekera, D., Wang, C., Liu, W. X., Song, L. F., et al. (2015). Arabidopsis CALCIUM-DEPENDENT PROTEIN KINASE8 and CATALASE3 function in abscisic acid-mediated signaling and H2O2 homeostasis in stomatal guard cells under drought stress. *Plant Cell* 27 (5), 1445–1460. doi: 10.1105/tpc.15.00144

Zybailov, B., Rutschow, H., Friso, G., Rudella, A., Emanuelsson, O., Sun, Q., et al. (2008). Sorting signals, N-terminal modifications and abundance of the chloroplast proteome. *PloS One* 3, e1994. doi: 10.1371/journal.pone.0001994

Conflict of Interest: The authors declare that the research was conducted in the absence of any commercial or financial relationships that could be construed as a potential conflict of interest.

frontiers in Plant Science

ORIGINAL RESEARCH
published: 15 April 2020
doi: 10.3389/fpls.2020.00432

Relationship Between Glycerolipids and Photosynthetic Components During Recovery of Thylakoid Membranes From Nitrogen Starvation-Induced Attenuation in *Synechocystis* sp. PCC 6803

Koichi Kobayashi[1†], Yuka Osawa[2†], Akiko Yoshihara[3], Mie Shimojima[4] and Koichiro Awai[2,5]*

[1] Faculty of Liberal Arts and Sciences, Osaka Prefecture University, Sakai, Japan, [2] Department of Biological Science, Faculty of Science, Shizuoka University, Shizuoka, Japan, [3] Department of Biological Sciences, School of Science, Osaka Prefecture University, Sakai, Japan, [4] School of Life Science and Technology, Tokyo Institute of Technology, Yokohama, Japan, [5] Research Institute of Electronics, Shizuoka University, Hamamatsu, Japan

OPEN ACCESS

Edited by:
Yan Lu,
Western Michigan University,
United States

Reviewed by:
Josef Komenda,
Institute of Microbiology, Academy of Sciences of the Czech Republic, Czechia
Gabor Bernat,
MTA Centre for Ecological Research, Hungary
Cornelia Spetea,
University of Gothenburg, Sweden
Dirk Schneider,
Johannes Gutenberg University Mainz, Germany

***Correspondence:**
Koichiro Awai
awai.koichiro@shizuoka.ac.jp

† These authors have contributed equally to this work and share first authorship

Specialty section:
This article was submitted to Plant Physiology, a section of the journal Frontiers in Plant Science

Received: 25 September 2019
Accepted: 24 March 2020
Published: 15 April 2020

Citation:
Kobayashi K, Osawa Y, Yoshihara A, Shimojima M and Awai K (2020) Relationship Between Glycerolipids and Photosynthetic Components During Recovery of Thylakoid Membranes From Nitrogen Starvation-Induced Attenuation in Synechocystis sp. PCC 6803. Front. Plant Sci. 11:432. doi: 10.3389/fpls.2020.00432

Thylakoid membranes, the site of photochemical and electron transport reactions of oxygenic photosynthesis, are composed of a myriad of proteins, cofactors including pigments, and glycerolipids. In the non-diazotrophic cyanobacterium *Synechocystis* sp. PCC 6803, the size and function of thylakoid membranes are reduced under nitrogen (N) starvation but are quickly recovered after N addition to the starved cells. To understand how the functionality of thylakoid membranes is adjusted in response to N status in *Synechocystis* sp. PCC 6803, we examined changes in thylakoid components and the photosynthetic activity during the N starvation and recovery processes. In N-starved cells, phycobilisome content, photosystem II protein levels and the photosynthetic activity substantially decreased as compared with those in N-sufficient cells. Although the content of chlorophyll (Chl) *a*, total protein and total glycerolipid also decreased under the N-starved condition based on OD_{730} reflecting cell density, when based on culture volume, the Chl *a* and total protein content remained almost constant and total glycerolipid content even increased during N starvation, suggesting that cellular levels of these components decrease under the N-starved condition mainly through dilution due to cell growth. With N addition, the photosynthetic activity quickly recovered, followed by full restoration of photosynthetic pigment and protein levels. The content of phosphatidylglycerol (PG), an essential lipid constituent of both photosystems, increased faster than that of Chl *a*, whereas the content of glycolipids, the main constituents of the thylakoid lipid bilayer, gradually recovered after N addition. The data indicate differential regulation of PG and glycolipids during the construction of the photosynthetic machinery and regeneration of thylakoid membranes. Of note, addition of PG to the growth medium slightly accelerated the Chl *a* accumulation in wild-type

cells during the recovery process. Because PG is required for the biosynthesis of Chl *a* and the formation of functional photosystem complexes, rapid PG biosynthesis in response to N acquisition may be required for the rapid formation of the photosynthetic machinery during thylakoid regeneration.

Keywords: cyanobacterium, nitrogen starvation, phosphatidylglycerol, photosystem, pulse amplitude modulation fluorometry (PAM), thylakoid membrane

INTRODUCTION

A typical cyanobacterial cell contains the thylakoid membrane in addition to the plasma membrane and the outer membrane. In the thylakoid membrane, photosystem II (PSII), cytochrome b_6f and photosystem I (PSI) are embedded in a lipid bilayer with ATP synthase and form photosynthetic electron transport chain, which, by harnessing light energy, creates an electrochemical proton gradient for ATP synthesis and a strong reductant capable of reducing $NADP^+$ (Lea-Smith et al., 2016; Liu, 2016). On the surface of the thylakoid membrane, phycobilisomes (PBSs) associate with PSII and PSI as the light-harvesting antenna and transfer absorbed light energy to chlorophyll (Chl) *a* in the photosystem complexes.

Proteins are the most abundant component of the thylakoid membrane and account for 50–70% of total thylakoid components by weight (Murata et al., 1981; Chapman et al., 1983; Omata and Murata, 1983). Nitrogen (N) starvation strongly affects protein homeostasis and thus thylakoid functions including the photosynthetic electron transport (Forchhammer and Schwarz, 2019). The most prominent alteration in proteome with N starvation is extensive degradation of PBSs, which are composed of phycobiliproteins with covalently bound phycobilins and non-pigmented linker proteins. The degradation of PBSs leads to chlorosis of the N-starved cell in combination with decreased Chl *a* content. Proteins in PBSs constitute up to 50% of total protein in the cyanobacterial cell under optimal growth conditions and thus can provide massive nutrients with degradation in response to N starvation (Collier and Grossman, 1992; Görl et al., 1998). Another objective of the active degradation of PBSs may be avoidance of photodamage caused by over reduction of photosynthetic electron carriers due to the low metabolic activity during N starvation (Forchhammer and Schwarz, 2019). The levels of photosystem proteins also decrease under N-starved conditions, with PSII subunits more strongly degraded than PSI subunits (Spät et al., 2018). Thylakoid membranes become almost absent after long-term N starvation, and instead, granules of glycogen and other storage compounds accumulate in the cytosol. However, in *Synechocystis* sp. PCC 6803 (hereafter *Synechocystis*), addition of nitrate to N-starved cells induces gradual re-formation of thylakoid membranes (Klotz et al., 2016). Chlorotic *Synechocystis* cells re-green and almost completely re-establish thylakoid membranes after 48 h of recovery from N starvation.

In addition to proteins and photosynthetic pigments, glycerolipids are major and essential constituents of the thylakoid membrane. The lipid composition of the thylakoid membrane is highly conserved among cyanobacteria and chloroplasts of algae and plants, with four major glycerolipids, monogalacto-syldiacylglycerol (MGDG), digalactosyldiacylglycerol (DGDG), sulfoquinovosyl-diacylglycerol (SQDG), and phosphatidylglycerol (PG) (Janero and Barrnett, 1981; Murata et al., 1981; Dorne et al., 1990). MGDG, which contains one galactose residue bound to diacylglycerol, is the most abundant lipid class in the thylakoid membrane, followed by DGDG formed from MGDG. Together with SQDG containing a sulfoquinovose in the polar head group, these glycolipids account for ∼90 mol% of total thylakoid lipids. The rest ∼10 mol% is composed of PG, the only phospholipid in cyanobacteria. These glycerolipids form a lipid bilayer of the thylakoid membrane, which avoids free diffusion of ions and allows for generating an electrochemical potential difference across the membrane for ATP synthesis. Besides providing a matrix embedded with protein–pigment complexes and ATP synthase, glycerolipids in thylakoids play essential roles in photosynthesis as structural and functional components of PSII, cytochrome b_6f and PSI (Kobayashi et al., 2016). Thus, biogenesis of the thylakoid membrane with the functional photosynthetic machinery needs coordinated synthesis and assembly of proteins, cofactors including Chls, and glycerolipids, as represented by essential roles of galactolipids in the thylakoid membrane organization during chloroplast development in *Arabidopsis thaliana* (Fujii et al., 2019b).

In *Synechocystis*, the size and function of thylakoid membranes are reduced under N starvation but are rapidly recovered after N addition (Klotz et al., 2016). However, during this process, how the amounts of glycerolipids and other thylakoid components are organized with the thylakoid functionality remains unknown. To understand the relationship between the membrane lipid metabolism and other thylakoid-associated processes during N starvation and recovery in *Synechocystis*, we investigated changes in the content of membrane lipids and other thylakoid components and the photosynthetic activity before and after N addition to the N-starved cells.

MATERIALS AND METHODS

Growth Conditions

Synechocystis cells were cultured in 1,000 ml Erlenmeyer flasks containing 500 ml of the BG11 medium (Stanier et al., 1971) for photoautotrophic growth at 30°C under continuous light (15 μmol photons m^{-2} s^{-1}) with rotary shaking at 100 rpm. For the N-starved growth, cells were first grown in BG11 medium for 7 days and collected by centrifugation (1,840 × *g*, 10 min). After a wash of the cell precipitates with N-free medium ($BG11_0$: BG11 without nitrate), cells were resuspended in $BG11_0$ to set OD_{730} = 0.4. For the recovery growth from

N starvation, cells grown in $BG11_0$ for 7 days were harvested (1,840 × *g*, 10 min) and resuspended in the BG11 medium to set OD_{730} = 0.6. The cell density was measured using a spectrophotometer (UV-2600, Shimadzu, Japan or V730BIO, JASCO, Japan). For PG supplementation, 40 mM dioleoyl-PG (Sigma-Aldrich) dissolved in 100% ethanol was added to growth media at a final concentration of 20 μM PG and 0.05% (v/v) ethanol. As the negative control of PG supplementation, 100% ethanol was added to growth media at a final concentration of 0.05% (v/v).

Determination of Absorption Spectra and Content of Chl *a* and Phycocyanin

For measurement of absorbance spectra of intact cells, an integrating sphere (ISR-2600, Shimadzu) was attached to the UV-2600 spectrophotometer (Shimadzu, Japan). Chl *a* and phycocyanin content was estimated from the absorbance of intact cells at 620 nm and 678 nm as described (Arnon et al., 1974). For accurate determination of Chl *a* content, pigments were extracted from cells with 100% methanol. Concentration of Chl *a* in the methanol extracts was calculated from the absorbance at 665 nm (Grimme and Boardman, 1972) or from the fluorescence emission at 670 nm under 435 nm excitation measured by a spectrofluorometer (RT-5300PC, Shimadzu, Japan). The Chl *a* standard sample of known concentration was used for the fluorometric determination of the Chl *a* content.

Determination of Oxygen Evolution Rates and PSI Activity

The oxygen consumption rate and evolution rate were measured in cell suspensions at OD_{730} of 0.6 with a Clark-type oxygen electrode (Hansatech Instruments Ltd., United Kingdom) and a LED lamp (CCS Inc., Japan). Oxygen consumption was measured in the absence of light and net oxygen evolution was measured with illumination of growth light (48 μmol photons m^{-2} s^{-1}). The data were normalized with the OD_{730} value. To determine the maximal photosynthetic activity, the oxygen evolution rate was measured under saturating light (1995 μmol photons m^{-2} s^{-1}) and the oxygen consumption rate in the dark was subtracted from the data. The gross oxygen evolution rates were normalized with Chl *a* content of each cell suspension sample. The oxidation kinetics of the PSI reaction center Chl (P700) was measured by a Dual-PAM system (Heinz Walz GmbH, Germany) in cell suspensions at OD_{730} of 0.5. The quantum yields of the PSI photochemistry [Y(I)], non-photochemical energy dissipation due to the acceptor-side limitation [Y(NA)], and that due to the donor-side limitation [Y(ND)] were measured after 2-min illumination of either low (34 μmol photons m^{-2} s^{-1}) or high actinic light condition (212 μmol photons m^{-2} s^{-1}). The maximum level of P700 (Pm) was measured with saturating light irradiation before the actinic light treatment.

Protein Extraction, SDS-PAGE, and Western Blot Analysis

For protein extraction, 20 ml of culture (OD_{730} = 0.5) was centrifuged at 1,840 × *g*, and the precipitated cells were frozen with liquid nitrogen. These cells were lysed six times by a homogenizer (Micro Smash MS-100R, TOMY, Japan) at 4,500 rpm for 20 s at 2°C. Then the powdered cells were suspended in 100 μl of the resuspend solution [1 mM phenylmethylsulfonyl fluoride and 5 mM 6-aminocaproic acid] (Barthel et al., 2013). For protein content analysis, aliquots of the suspended cells were mixed with the same volume of detergent solution [60 mM Tris-HCl (pH6.8), 2% SDS (w/v)]. A BCA Protein Assay Kit (Thermo Fisher Scientific, United States) was used with bovine serum albumin as a standard. For SDS-PAGE and Western blot analysis, 70 μl of the resuspended cell solution was mixed with the same volume of loading buffer [0.5 M Tris-HCl (pH6.8), 60% (w/v) glycerol, 10% (w/v) SDS, 350 mM dithiothreitol, 1 mg/ml bromophenol blue] and incubated at 37°C for 2 h to solubilize proteins with avoiding aggregation of membrane proteins. Then 10 μl of the resulted protein solution was loaded on polyacrylamide gels containing 10% (w/v) acrylamide to perform Laemmli SDS-PAGE (Laemmli, 1970). For visualization of protein bands, the gels were stained with Coomassie Brilliant Blue R-250 (CBB). Pre-stained Protein Markers (Broad Range) for SDS-PAGE (Nacalai Tesque, Japan) were used to calibrate the gels.

For immunodetection, rabbit antibodies against PsaA (AS06172), PsaB (AS10695), PsbC (AS111787, CP43), and RbcL (AS03037) (Agrisera, Sweden) were used at a 1:3,000 dilution. A polyclonal antibody against spinach PsbA/D (a gift from Dr. Masahiko Ikeuchi at The University of Tokyo) was used at the same dilution. These antibodies were detected with an anti-rabbit horseradish peroxidase-coupled antibody (ab97051, Abcam plc, United Kingdom) at a dilution of 1:10,000 followed by development with Western Lightning Plus-ECL (Perkin Elmer, United States).

Lipid Analysis

Lipids were extracted as described (Bligh and Dyer, 1959) and separated by TLC. For membrane lipid analysis, a solvent system of chloroform: methanol: 25% ammonium (65: 35: 5, v/v) (Sato and Murata, 1988) was used for separation. For quantitative analysis of fatty acids attached to lipids, each separated spot was scraped off and fatty acid methyl esters (FAMEs) were prepared. FAMEs were then analyzed by gas chromatography equipped with a flame ionization detector as described (Awai et al., 2014). From the FAME data, fatty acid composition and the amount of each lipid class were calculated by using pentadecanoic acid as internal standard.

Transmission Electron Microscopy

A 30 ml culture of *Synechocystis* cells (OD_{730} = 0.5) was harvested and fixed in 2% (w/v) glutaraldehyde/BG11 medium for 30 min at room temperature. Cells were centrifuged (1,840 × *g*, 20 min) and resuspended in the fixing buffer [2.5% (w/v) glutaraldehyde, 0.1 M sodium phosphate (pH7.2)] for 20 min at room temperature. Then the cells were harvested again (1,840 × *g*, 20 min), resuspended in the fixing buffer for 100 min at room temperature, and then stored at 4°C. Samples were then washed five times in the fixing buffer for 5 min each at room temperature, and post-fixed with 1%

(w/v) osmium tetroxide in 0.1 M sodium phosphate buffer (pH7.2) for 2 h at room temperature. The fixed samples were dehydrated in a graded ethanol series and embedded in epoxy resin mixture (Epon812 mixture: TAAB, EM Japan, Japan). Ultrathin 70 nm sections were cut on a diamond knife with an ultramicrotome (Leica EM UC7, Leica, Germany) and placed on copper grids. The sections were first stained with EM stainer (Nissin EM, Japan) for 60 min and then with lead citrate for 9 min. Samples were observed under a transmission electron microscope (JEM-1400Plus, JEOL, Japan) with accelerating voltage at 100 kV.

Quantification of total thylakoid length and total area of high electron-dense inclusions in a cross-section of a *Synechocystis* cell was carried out on the transmission micrographs with ImageJ software. Small spots with the area $<1{,}000$ nm^2 were eliminated from the analysis of the high electron-dense inclusions.

RESULTS

Rapid Changes in Pigment Content in Response to N Conditions

The availability of nitrogen strongly affects growth of non-diazotrophic cyanobacteria including *Synechocystis*. In *Synechocystis*, cell density represented by OD_{730} only slowly increased under the N-starved condition (**Figure 1A**), which agreed with a similar increase in cell number of *Synechocystis* during N starvation (Krasikov et al., 2012). After the growth in the absence of N source for 7 days, *Synechocystis* cells were transferred to the fresh BG11 medium containing nitrate as N source. The OD_{730} values slightly decreased at the early stage of recovery but began to increase after 18 h of N addition (**Figure 1B**). These data are consistent with the previous report in *Synechocystis* by Klotz et al. (2016), in which cells were starved for N for the longer term (>1 month). Then we analyzed changes of pigment content based on OD_{730} during N starvation and recovery. Previous studies reported that PBSs are subject to rapid degradation in response to N starvation (Collier and Grossman, 1992; Görl et al., 1998; Deschoenmaeker et al., 2014; Spät et al., 2018). In fact, our spectroscopic analysis of intact cells using an integrating sphere demonstrated that N starvation induced a rapid decrease in the absorbance around 626 nm mainly by PBSs (**Figure 1C**). The absorbance around 680 and 440 nm mainly by Chl *a* also decreased during N starvation, but to a lesser extent than that by PBSs, consistent with the gradual decrease of Chl *a* content during N starvation determined by the methanol extraction method (**Figure 1D**). Spectroscopic estimation of phycocyanin and Chl *a* content in intact cells further supported the rapid and moderate decrease in phycocyanin and Chl *a* content, respectively, at the early stage of N starvation (**Supplementary Figure S1A**). Phycocyanin began to accumulate from 6 h after transfer to the N-sufficient condition and the content rapidly increased between 12 and 24 h (**Figure 1E**). Chl *a* showed an accumulation pattern similar to phycocyanin, but with a lower increase rate than phycocyanin (**Figure 1F** and **Supplementary Figure S1B**).

Changes in Protein Content During the Recovery Process From N Starvation

To compare the changes of protein content with those of PBSs and Chl *a* in response to N status, we performed a time-course analysis of total protein content during N starvation and recovery. As did the Chl *a* content, the total protein content based on OD_{730} gradually decreased during N starvation (**Figure 2A**). The protein content increased during first 6 h after N addition to the starved cells, followed by a stationary phase between 6 and 12 h and then a rapid increase until 24 h (**Figure 2B**). SDS-PAGE analysis with CBB staining, in which loaded protein content was normalized to OD_{730}, revealed that the amounts of phycocyanin α (17.5 kDa) and phycocyanin β (21 kDa) substantially decreased with N starvation but rapidly increased between 6 and 24 h after transfer to the N-sufficient condition (**Figure 2C**), consistent with the spectroscopic data from intact cells. We also performed immunoblot analysis of photosynthesis-associated proteins during the recovery from N starvation (**Figure 2D**). The levels of reaction center proteins of PSII, PsbA, and PsbC (also called D1 and CP43, respectively), strongly decreased by N starvation, but with a small portion of them remained. By contrast, the levels of PSI reaction center proteins, PsaA and PsaB, only moderately changed in response to N starvation and recovery. The Rubisco large subunit (RbcL) also slightly decreased with N starvation and gradually increased during the recovery process, contrasting with the substantial loss of PBSs in N-starved cells and their dynamic accumulation during recovery from N starvation.

Oxygen Metabolism During the Recovery Process From N Starvation

To examine the energy metabolism during recovery from N starvation, we analyzed O_2 consumption and evolution rates in intact cells. First, O_2 consumption by respiration was examined in the dark (**Figure 3A**). The O_2 consumption rate in N-starved cells increased 1.8 times at 6 h after N addition. The high O_2 consumption continued until 18 h after N addition, and then rapidly decreased. After the transient increase, the O_2 consumption rate was maintained at lower levels similar to that in the N-starved cells.

Next we examined net O_2 evolution under the growth light condition during the recovery process (**Figure 3B**). Until 15 h after N addition, net O_2 evolution levels were <0, so the respiratory O_2 consumption was higher than the photosynthetic O_2 evolution. After 15 h, the net O_2 evolution rate was maintained at levels above the compensation point. To examine the functionality of the photosynthetic machinery during the recovery process, we measured gross O_2 evolution rates on a Chl *a* basis under saturating light (1995 μmol photons m^{-2} s^{-1}), in which O_2 consumption rates in the dark was subtracted (**Figure 3C**). The photosynthetic activity measured as the gross O_2 evolution rate was at the low level in N-starved cells and rapidly increased in response to N addition, with peaking at 18 h after N addition and maintaining high levels afterward.

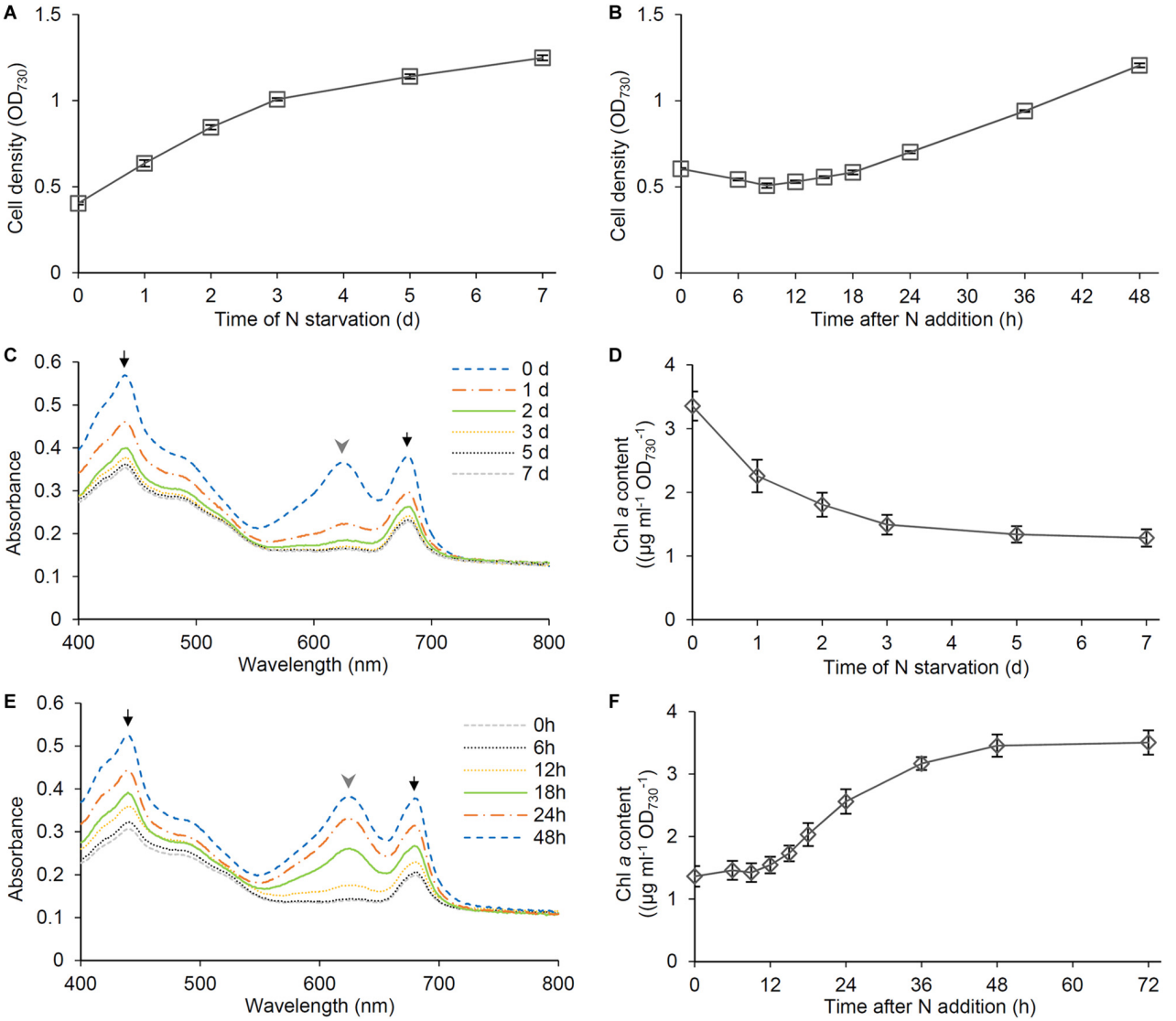

FIGURE 1 | Cell growth and pigment content during N starvation and the recovery after N addition. *Synechocystis* cells were grown in the N-free medium for 7 days and then were transferred to the N-containing medium and grown for 48 h. **(A,B)** Changes of OD_{730} values of the cell culture during **(A)** N starvation and **(B)** recovery. Data are means ± SE from three independent experiments. **(C)** Absorption spectra and **(D)** chlorophyll (Chl) *a* content of the cells grown under the N-starved condition for indicated times. **(E)** Absorption spectra and **(F)** Chl *a* content of the cells during recovery from N starvation. Data are means from two independent experiments for **(C,E)** and means ± SE from six independent experiments for **(D,F)**. Black arrows and gray arrowheads in **(C,E)** indicate absorption mainly by Chl *a* and phycobilisomes, respectively.

Changes in Photosynthetic Activity During the Recovery Process From N Starvation

To analyze the photosynthetic electron transport activity during recovery from N starvation, we examined the oxidation kinetics of P700. The Pm levels, which suggest the size of functional PSI reaction centers, gradually increased until 36 h after N addition, with a particular increase between 12 and 18 h (**Figure 4A**). In N-starved cells, Y(I) representing the quantum yield of the PSI photochemistry was substantially low under the low actinic light (34 μmol photons m^{-2} s^{-1}), whereas Y(ND) reflecting the donor-side limitation of PSI was high (**Figure 4B**). After N addition, Y(I) rapidly increased until 15 h, with Y(ND) inversely decreased. Y(NA) reflecting the acceptor-side limitation of PSI was maintained at the low level during the early recovery stage and then slightly increased at later stages. The contribution of Y(ND) was further enhanced under higher actinic light intensity (212 μmol photons m^{-2} s^{-1}) (**Figure 4C**). By contrast, under high actinic light, Y(I) was undetectable in N-starved cells and was maintained at low levels even after N addition for 9 h. However, Y(I) rapidly increased between 9 and 12 h and then gradually moved closer to a stationary level, with Y(ND) inversely

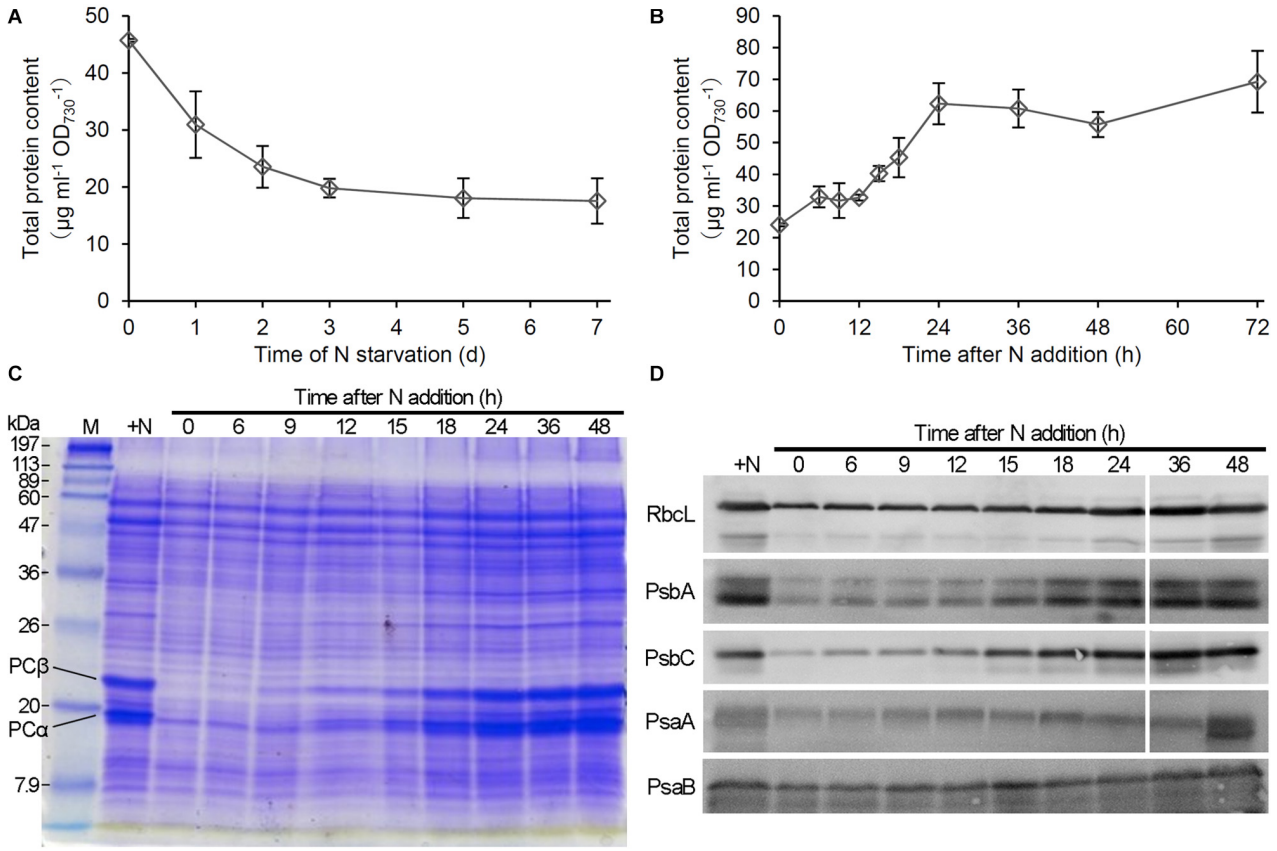

FIGURE 2 | Changes in protein levels during N starvation and recovery. **(A,B)** Changes of total protein content during **(A)** N starvation and **(B)** recovery. Data are means ± SE from three independent experiments. **(C)** Gel electrophoretic patterns of total protein from *Synechocystis* cells grown in the N-containing medium for indicated times after N starvation for 7 days. PCα and PCβ indicate the bands corresponding to phycocyanin α and phycocyanin β, respectively. + N indicates proteins from cells grown under the continuous N-sufficient condition. M; protein size markers. **(D)** Immunoblot analysis of reaction center proteins of PSII (PsbA and PsbC) and PSI (PsaA and PsaB) and the RuBisCO large subunit (RbcL) in recovering cells from N starvation.

decreased. Even under high actinic light, Y(NA) was maintained at lower levels.

Changes in Lipid and Fatty Acid Compositions During the Recovery Process From N Starvation

To assess whether the abundance of glycerolipids was changed in response to N conditions, we performed a time-course analysis of glycerolipid content during recovery from N starvation. In N-starved cells, total glycerolipid content based on OD_{730} decreased by half as compared with that in N-sufficient control (**Figure 5A**). The content gradually increased during the recovery process and reached to a steady-state level at 36 or 48 h after N addition. Of the four glycerolipids, PG showed the strongest increase in response to N addition, with its increasing kinetics being similar to or slightly faster than that of PBSs, Chl *a* and total proteins (**Figure 5B**). Other three lipids showed more gradual increases during the recovery process.

We also analyzed fatty acid compositions of glycerolipids in N-starved and recovered cells. In total glycerolipids from N-starved cells, proportions of 16:0 and 18:1 slightly increased and those of 18:2 and 18:3 decreased compared with those from N-sufficient control cells (**Figure 5C**). However, the fatty acid composition altered under N starvation reverted to the control level during the recovery process from N starvation. Changes in the fatty acid composition during the recovery process differed among glycerolipid classes; MGDG, SQDG, and PG showed transient modifications of their fatty acid compositions between 6 and 24 h after N addition with distinct patterns specific to each lipid class. Meanwhile, the fatty acid composition of DGDG was constant during recovery from N starvation (**Supplementary Figure S2**).

Changes in the Amounts of Thylakoid Components in Cell Culture

Our data showed that pigments (**Figure 1**), proteins (**Figure 2**), and glycerolipids (**Figure 5**) were all decreased in N-starved *Synechocystis* cells based on OD_{730}. To assess whether these components are actively degraded in response to N starvation or merely diluted due to cell growth, we calculated the amounts of these components based on culture volume. Whereas the amount of phycocyanin per milliliter of culture

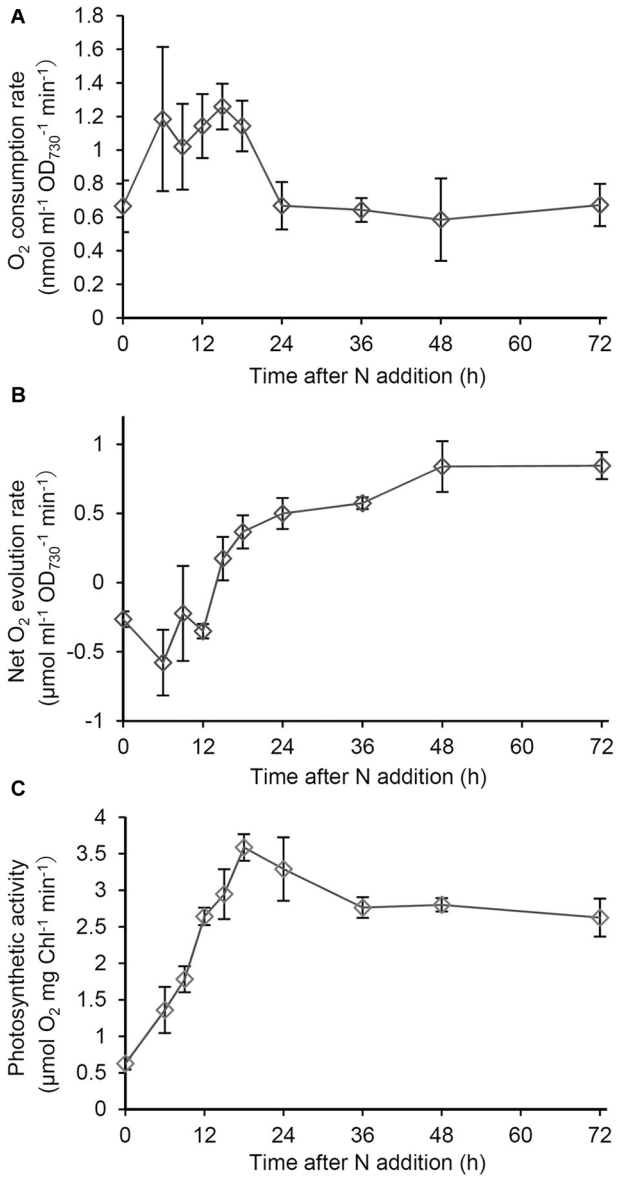

FIGURE 3 | Changes in respiratory and photosynthetic activities during recovery from N starvation. **(A)** O_2 consumption rate based on OD_{730} in the dark in *Synechocystis* cells grown in the N-containing medium for indicated times after N starvation for 7 days. **(B)** Net O_2 evolution rate based on OD_{730} under growth light (48 μmol photon m^{-2} s^{-1}) during the recovery process from N starvation. **(C)** Photosynthetic activity based on Chl *a* content, which was measured as gross O_2 evolution rate under saturating light (1995 μmol photon m^{-2} s^{-1}). Data are means ± SE from three independent experiments.

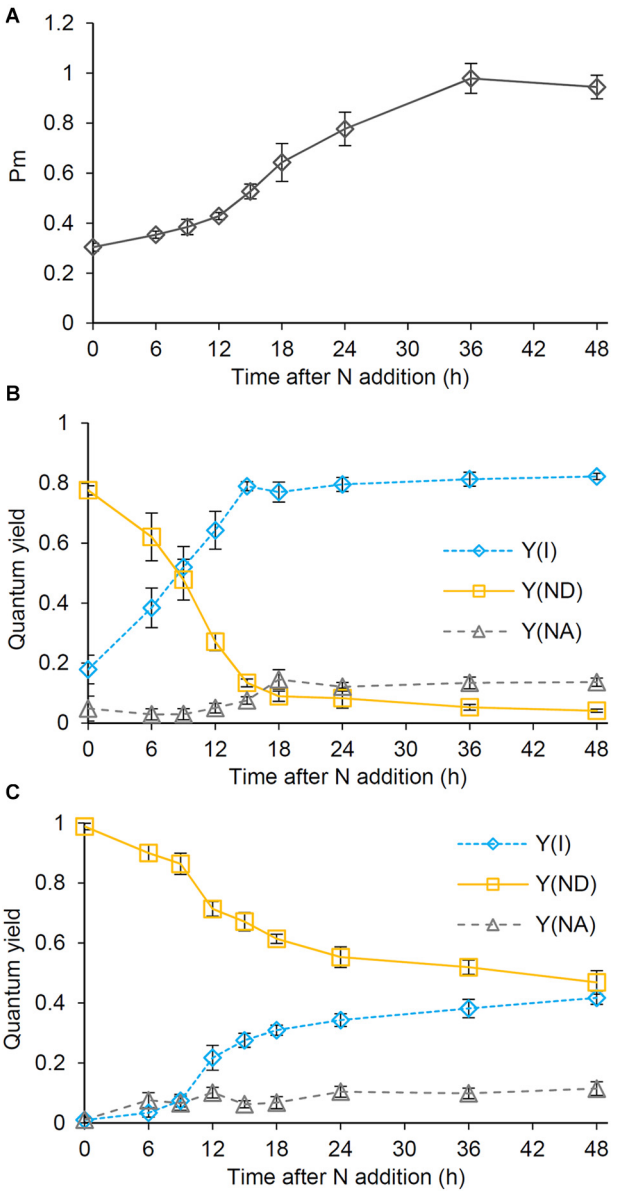

FIGURE 4 | Changes in the photosynthetic quantum yield of PSI during the recovery from N starvation. **(A)** The maximum level (Pm) of the oxidized PSI reaction center chlorophyll. **(B,C)** Photochemical [Y(I)] and non-photochemical quantum yields [Y(ND) and Y(NA)] of PSI under **(B)** low (34 μmol photon m^{-2} s^{-1}) and **(C)** high actinic light (212 μmol photon m^{-2} s^{-1}). Y(ND) and Y(NA) reflect limitations of PSI photochemistry at the donor side and the acceptor side, respectively. *Synechocystis* cells were grown under the N-starved condition for 7 days and then grown in the N-containing medium for indicated times. Data are means ± SE from six independent experiments.

substantially decreased during N starvation (**Supplementary Figure S3**), those of Chl *a* (**Figure 6A**) and total protein (**Figure 6B**) were almost constant and total lipid content (**Figure 6C**) even increased. Of four lipid classes in *Synechocystis*, MGDG, and DGDG particularly showed increased content during N starvation based on culture volume, whereas PG content per culture volume was unchanged after N starvation for 7 days.

Changes in Thylakoid Membrane Morphology During the Recovery Process From N Starvation

To examine the effect of N status on the thylakoid morphology, we compared the ultrastructure of *Synechocystis* cells grown under different N conditions (**Figure 7**). The cells grown under

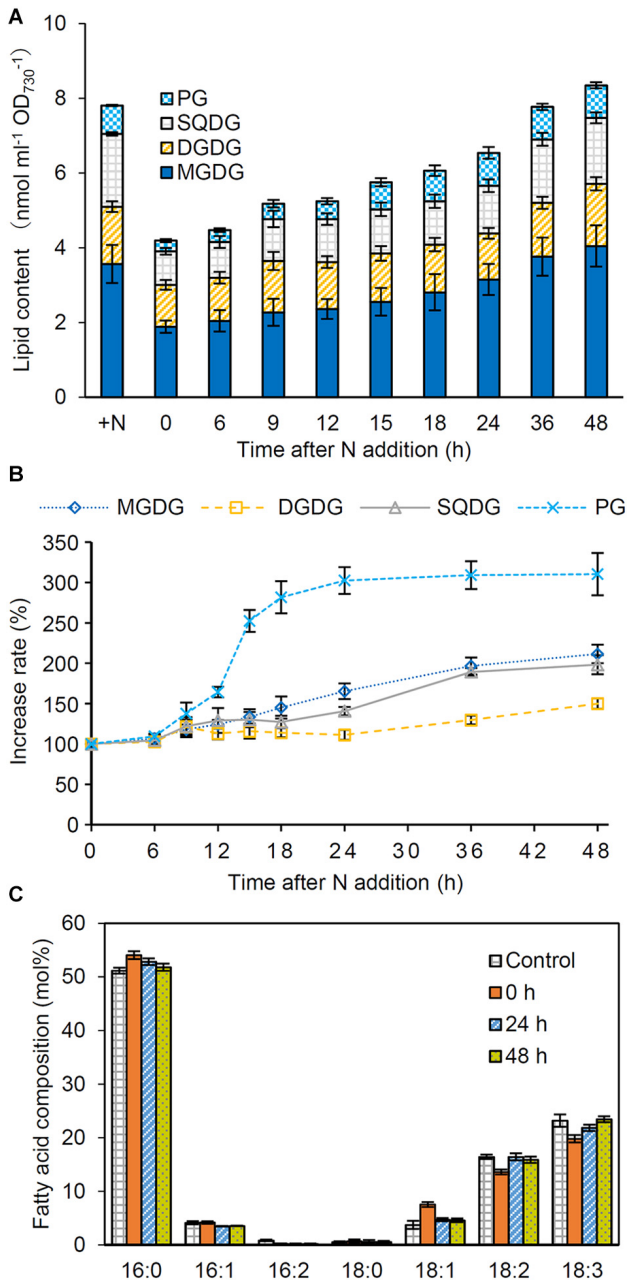

FIGURE 5 | Changes in lipid content during the recovery from N starvation. **(A)** Total and individual lipid content, **(B)** the increase rate of each lipid, and **(C)** the fatty acid composition of total glycerolipids after N addition. *Synechocystis* cells were grown under the N-starved condition for 7 days and then grown in the N-containing medium for indicated times. Data are means ± SE from four independent experiments. In **(B)**, increase rates of the each lipid content relative to the initial level before N addition (0 h) were shown as percentage.

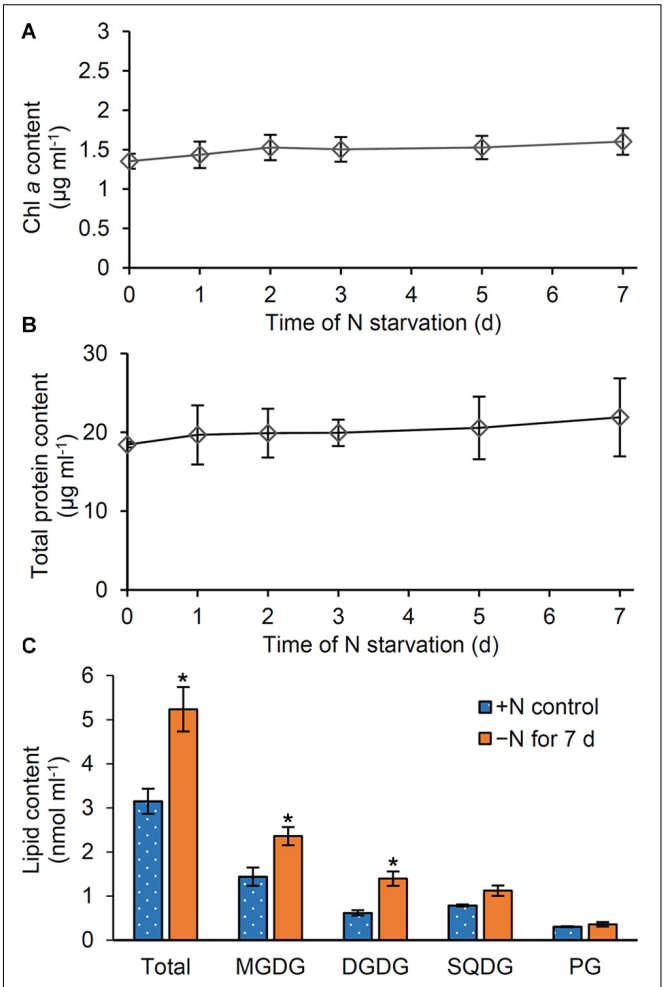

FIGURE 6 | Changes in pigment, protein and lipid content based on culture volume during N starvation. Content of **(A)** Chl *a*, **(B)** total proteins, and **(C)** glycerolipids per milliliter of culture of *Synechocystis* cells. Data in **Figure 1D** for Chl *a*, **Figure 2A** for total proteins, and **Figure 5A** for glycerolipids were recalculated with the OD_{730} data in **Figure 1A**. In **(C)**, lipid content in cells grown under the continuous N-sufficient (+ N) condition or the N-starved (−N) condition for 7 days was shown. Asterisks indicate significant differences from the + N control ($P < 0.05$, Welch's *t*-test).

the continuous N-sufficient condition developed thylakoids as parallel stacks of two to four membranes along the contour of the cell membrane. In addition, some parallel sheets of thylakoid membranes formed convergence zones in close contact with the plasma membrane (Rast et al., 2019).

By contrast, cells grown under the N-starved condition for 7 days had fewer thylakoid membranes and rarely formed convergence zones. In addition, N-starved cells accumulated many high electron-dense inclusions presumably lipid inclusions, cyanophycin granules, and/or polyphosphate granules. These observations were confirmed by the quantification of electron micrographs (**Figures 7B–D**). At 24 h after N addition, thylakoid morphology was heterogeneous: some cells showed largely or partially recovered thylakoid membranes and some severely lacked the membrane network. Two or three convergence zones were observed in cells with recovered thylakoid membranes. Many cells also contained high electron-dense inclusions. At 48 h after N addition, thylakoid membranes were fully developed in most cells. The total area of high electron-dense inclusions decreased.

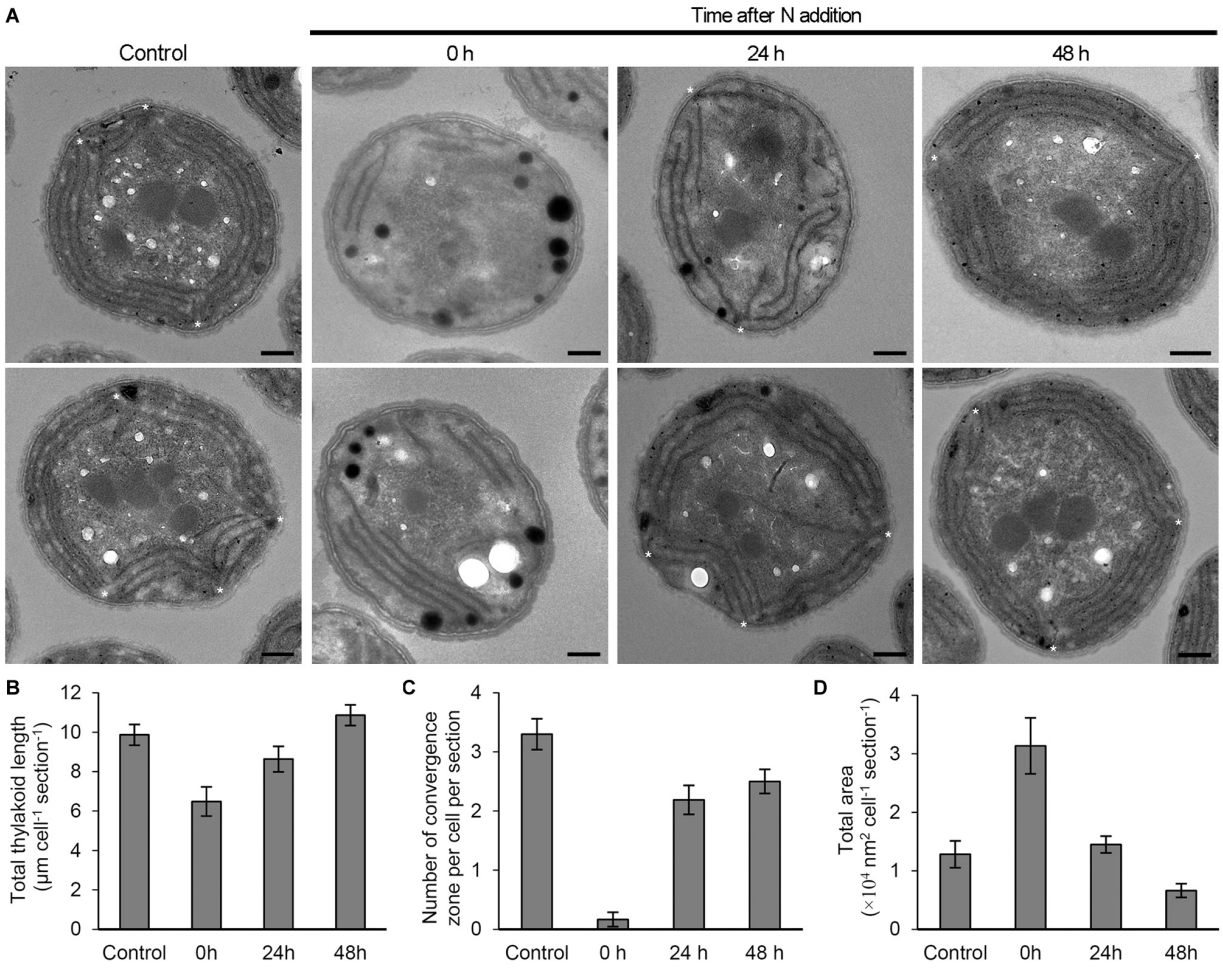

FIGURE 7 | Changes in the morphology of *Synechocystis* cells in response to N status. **(A)** Ultrastructure of *Synechocystis* cells grown in the N-containing medium for indicated times after 7 days N starvation was compared with N-sufficient control cells (Control) that were continuously grown in the N-containing medium. Two images of cell ultrastructure were shown for each condition. Asterisks indicate thylakoid convergence zones. Bars = 500 nm. **(B)** Total thylakoid length, **(C)** number of convergence zone and **(D)** total area of high electron-dense inclusions in a cross-section of a *Synechocystis* cell were quantified from the transmission electron micrographs for each condition. Data are means ± SE (n = 10 for Control, 11 for 0 h, 12 for 24 h, and 15 for 48 h in B; n = 10 for Control, 18 for 0 h, 16 for 24 h, and 16 for 48 h in C; n = 10 for Control, 16 for 0 h, 29 for 24 h, and 27 for 48 h in **D**).

Effect of PG Supplementation to N-Starved Synechocystis Cells

The biosynthesis of PG, which is required for Chl *a* biosynthesis in *Synechocystis* (Kopečná et al., 2015), occurred faster than that of Chl *a* after N addition (**Figures 1F**, **5B**). Because *Synechocystis* increases intracellular PG content by taking up external PG in the growth medium (Hagio et al., 2000), we tested whether external PG affects the Chl *a* metabolism during N starvation and recovery. We grew wild-type *Synechocystis* cells in the presence (+) or absence (−) of 20 μM PG and measured OD_{730} and Chl *a* content during N starvation and recovery. During N starvation, cell density represented by OD_{730} of +PG cells was comparable with that of −PG control (**Figure 8A**). In both +PG and −PG cells, Chl *a* content in culture was constant (**Figure 8B**), consistent with the data in **Figure 6A**. The data show that the presence of PG in growth media does not affect cell growth and Chl *a* metabolism during N starvation. After transfer to the N-sufficient medium, OD_{730} of −PG cells first slightly decreased and then increased (**Figure 8C**), as observed in **Figure 1B**. However, this initial decrease in OD_{730} was suppressed in +PG cells. Total Chl *a* content in culture began to increase after 9 h of N addition in −PG cells (**Figure 8D**). In +PG cells, Chl *a* content was higher than that in −PG cells at 9 and 18 h after N addition, but became similar to that in −PG cells at 27 h.

DISCUSSION

Disorganization of the Thylakoid Membrane Components by N Starvation

The rapid decrease in phycocyanin content per culture during N starvation (**Supplementary Figure S3**) suggests active degradation of PBSs, which would contribute to N recycling from the phycobiliproteins and also reducing the antenna size of

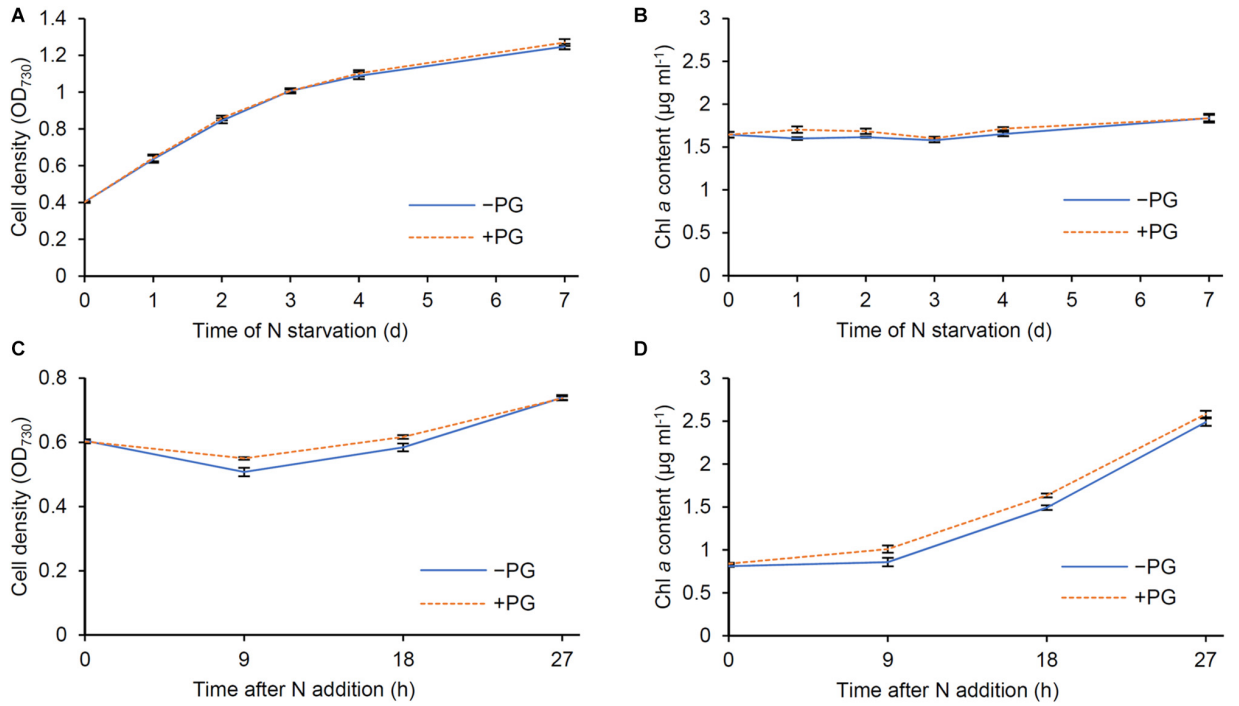

FIGURE 8 | Effect of phosphatidylglycerol (PG) supplementation to cells during N starvation and recovery. Changes of **(A,C)** OD_{730} and **(B,D)** Chl *a* content per milliliter of culture during **(A,B)** N starvation and **(C,D)** recovery were analyzed in the absence (−PG) and presence (+PG) of PG. Data are means ± SE from six independent experiments.

PSII. Meanwhile, total protein content per culture was unchanged during N starvation (**Figure 6B**). Thus, amino acids derived from degraded phycobiliproteins may be reused for the synthesis of other proteins or polypeptides in N-starved cells. Chl *a* content per culture was also constant during N starvation (**Figure 6A**), although the amounts of Chl *a* and total protein decreased when normalized by OD_{730} (**Figures 1D**, **2A**). The OD_{730} values themselves slightly increased similar to the increase in cell number (**Figure 1A**; Krasikov et al., 2012). These data suggest that Chl *a* and total protein content in a cell is decreased by dilution due to cell growth under the N-starved condition.

In N-starved cells, the levels of most proteins including RbcL moderately decreased compared with those in N-sufficient cells (**Figures 2C,D**), consistent with the gradual decrease in total protein content based on OD_{730} (**Figure 2A**). However, similar to phycobiliproteins, PSII protein levels strongly decreased in N-starved cells (**Figure 2D**), which was accompanied by a substantial decrease in the oxygen-evolving activity (**Figure 3C**). Consistent with our data, Ogawa and Sonoike (2016) determined the "true" maximum quantum yield of PSII (Fv/Fm) in *Synechocystis* by eliminating the interference from phycocyanin fluorescence and revealed that the Fv/Fm around 0.8, which was similar to the value observed in land plants, substantially decreased with N starvation. Inactivation of PSII may reduce a risk of photodamage from light energy that exceeds the photosynthetic capacity in N-starved cells with decreased cellular metabolism (Forchhammer and Schwarz, 2019).

In contrast to PSII proteins, PSI reaction center proteins PsaA and PsaB were relatively abundant even under N starvation (**Figure 2D**), which agrees with the proteomic data that PSI proteins are less degraded than PSII proteins with N starvation (Spät et al., 2018). Consistent with these results, Y(ND), which reflects the donor-side limitation of the PSI photochemistry, was remarkably high in N-starved cells, whereas the acceptor-side limitation represented by Y(NA) was negligible (**Figures 4B,C**). The data suggest that the linear electron transport from PSII to PSI is strongly downregulated in response to N starvation. In N-starved cells, the selective decrease of PSII components (**Figure 2D**) and the lowered PSII photochemical efficiency (Ogawa and Sonoike, 2016) would repress the linear electron transport to prevent over-reduction of PSI and consequent production of reactive oxygen species. Reduced thylakoid membranes with inactive PSII and active PSI were also observed in dark-grown *Synechocystis* cells (Barthel et al., 2013), implying an importance of the high PSI and low PSII activity in dormant *Synechocystis* cells. Low Y(NA) in N-starved cells suggests sufficient electron transport from P700 to downstream pathways including the cyclic electron transport system. Doello et al. (2018) revealed that the N-starved chlorotic cells maintain ATP levels to 20–25% of nutrient-sufficient cells. As discussed by Forchhammer and Schwarz (2019), the cyclic electron transport around PSI may be retained in N-starved cells to maintain ATP levels and cell viability during chlorosis.

During N starvation, the amount of membrane lipids also decreased based on OD_{730}, but with a smaller extent than those of Chl *a* and total protein content (**Figure 5A**). In fact, unlike Chl *a* and total protein, the amount of total membrane lipid per culture increased even under the N-starved condition (**Figure 6C**). Glycerolipids constitute the plasma membrane and the outer membrane besides thylakoids and thus a certain amount of lipids is constantly required to maintain cell integrity. Of note, lipid analysis in the cyanobacterium *Anacystis nidulans* revealed that the cytoplasmic membrane contained more galactolipids (MGDG and DGDG) and less anionic lipids (PG and SQDG) than the thylakoid membrane (Murata et al., 1981; Omata and Murata, 1983). Therefore, biosynthesis of membrane lipids, particularly galactolipids, may be partially maintained in N-starved cells to support their low growth activity. Under the N-starved condition, PG content decreased based on OD_{730}, but was unchanged on a culture basis. Thus, dilution due to cell growth may cause the decreased PG content in N-starved cells, as in the case of the Chl *a* and total protein content. Because external PG addition did not affect OD_{730} and Chl *a* content in N-starved cells (**Figures 8A,B**), the decreased PG content in N-starved cells would be independent of the suppression of cell growth and Chl *a* accumulation during N starvation.

Fatty acid compositions of membrane lipids also changed in response to N status; the proportions of 16:0 and 18:1 increased and those of 18:2 and 18:3 decreased with N starvation (**Figure 5C**). Gombos et al. (1987) reported that, in the cytoplasmic membrane of *A. nidulans*, the protein-to-lipid ratio decreased with N starvation. In parallel, the proportion of 16:1 decreased and that of 18:0 increased in all 4 glycerolipid classes in the cytoplasmic membrane of N-starved *A. nidulans*. They propose that the changes from shorter unsaturated fatty acids to longer saturated fatty acids in the cytoplasmic membrane would counteract the fluidizing effect due to the decreased protein-to-lipid ratio in the N-starved cells. The decreased polyunsaturation of fatty acids in *Synechocystis* may also contribute to maintaining a proper fluidity in membranes during N starvation, although fatty acid species used for membrane lipids are largely different between *Synechocystis* and *A. nidulans*.

Reconstruction of Thylakoid Membrane Systems After N Addition

After N addition to the starved cells, the oxygen evolving activity under saturating light rapidly increased (**Figure 3C**). Y(I) also quickly increased and Y(ND) inversely decreased after N addition (**Figures 4B,C**). These data suggest that the linear electron transport to PSI was rapidly improved after N addition to increase net photosynthetic activity. The increased amounts of PSII proteins and photosynthetic pigments after N addition would contribute to the improved linear electron transport. Of note, the respiratory activity was transiently enhanced by N addition (**Figure 3A**). The rapid decrease in Y(ND) under growth light between 0 and 15 h after N addition (**Figure 4B**), which coincided with the transient increase in the O_2 consumption rate (**Figure 3A**), may reflect electron donation from the respiratory flows to plastoquinone pools and the resulting relaxation of the donor-side limitation of P700. Doello et al. (2018) reported that glycogen breakdown is essential for N-starved cells to increase respiration after N addition and resuscitate from chlorotic growth. The transient increase in respiration and ATP concentration in response to N addition would help regenerate PSII and reconstruct the efficient linear photosynthetic electron transport system. However, considering that the change in oxygen evolving activity after N addition preceded the increases in the amounts of PSII proteins and pigments, other mechanisms may also be involved in the improved photosynthetic activity at the early recovery stage, particularly within 9 h after N addition.

In addition to the photosynthetic components, glycerolipid content increased in response to N addition to starved cells (**Figures 5A,B**). Whereas the increase in glycolipid (MGDG, DGDG and SQDG) content was gradual, that in PG content was rapid particularly between 9 and 24 h after N addition. This observation is consistent with the special importance of PG for the structure and function of photosystems (Kobayashi et al., 2016). Unlike glycolipids that are mostly used to form the lipid bilayer of thylakoid membranes, a large proportion of PG is allocated to photosystem complexes as a structural component (Kobayashi et al., 2017). Biosynthesis of PG, but not those of glycolipids, may be strictly co-regulated with those of other photosystem components. Considering that depletion of PG in the *Synechocystis* mutant lacking PG biosynthesis (*pgsA*) perturbed the structure and activity of PSII (Hagio et al., 2000; Sakurai et al., 2003, 2007; Itoh et al., 2012) and biosynthesis of Chl *a* (Kopečná et al., 2015), cellular PG content would be tightly associated with the PSII functionality and Chl *a* biosynthesis. Of note, addition of PG to PG-depleted *pgsA* mutants quickly recovered some impairment of the PSII activity (Hagio et al., 2000; Sakurai et al., 2003; Itoh et al., 2012). Furthermore, we observed that addition of PG to wild-type *Synechocystis* slightly accelerated Chl *a* accumulation during the recovery from N starvation (**Figure 8D**). Because the increase of PG content occurred faster than that of Chl *a* content after N addition, the rapid recovery of PG content may contribute to activating the Chl *a* biosynthesis and photosynthetic activity during recovery from N starvation. The OD_{730} kinetics during the recovery process was also affected by addition of PG to wild-type cells (**Figure 8C**). Although the mechanism for the transient decrease in OD_{730} between 9 and 18 h after N addition is unknown, increased PG content may somehow affect cellular processes that alter light scattering properties of recovering cells.

In N-starved cells, thylakoid convergence zones were rarely observed as compared with N-sufficient cells (**Figures 7A,C**). However, these zones regenerated after N addition to the starved cells. The analysis of *Synechocystis* mutant that lacks the small membrane-bending protein CurT suggests that the convergence zones formed by CurT function in the assembly and accumulation of PSII, but not PSI (Heinz et al., 2016). Moreover, *in situ* cryo-electron tomography of *Synechocystis* cells revealed that the convergence membranes have many membrane-associated ribosomes and may serve as the translation site (Rast et al., 2019). Thus, disappearance and reappearance of the convergence zones with N starvation and N addition,

respectively, are likely to be linked with the changes in the synthetic activity of PSII proteins under these conditions. Although membrane lipids strongly affect the architecture and functions of thylakoid membranes in plant chloroplasts (Hölzl et al., 2009; Kobayashi et al., 2013, 2015; Fujii et al., 2019a), whether specific lipids are involved in the formation and function of convergence zones in *Synechocystis* awaits future studies.

DATA AVAILABILITY STATEMENT

All datasets generated for this study are included in article/**Supplementary Material**.

AUTHOR CONTRIBUTIONS

YO and KA conceived the research. YO, KK, AY, and MS conducted the experiments. YO, KK, AY, MS, and KA performed data analysis. KK and KA wrote the manuscript.

FUNDING

This work was supported in part by a grant JSPS KAKENHI Grant Nos. JP18H03941 and 17K19342 and carried out under the Cooperative Research Project Program of Research Center for Biomedical Engineering.

ACKNOWLEDGMENTS

We are grateful to Ms. Keiko Ikeda for transmission electron microscopy and Dr. Masahiko Ikeuchi for a gift of anti-PsbA antibody.

SUPPLEMENTARY MATERIAL

The Supplementary Material for this article can be found online at: https://www.frontiersin.org/articles/10.3389/fpls.2020.00432/full#supplementary-material

REFERENCES

Arnon, D. I., McSwain, B. D., Tsujimoto, H. Y., and Wada, K. (1974). Photochemical activity and components of membrane preparations from blue-green algae. I. Coexistence of two photosystems in relation to chlorophyll a and removal of phycocyanin. *Biochim. Biophys. Acta* 357, 231–245. doi: 10.1016/0005-2728(74)90063-2

Awai, K., Ohta, H., and Sato, N. (2014). Oxygenic photosynthesis without galactolipids. *Proc. Natl. Acad. Sci. U.S.A.* 111, 13571–13575. doi: 10.1073/pnas.1403708111

Barthel, S., Bernát, G., Seidel, T., Rupprecht, E., Kahmann, U., and Schneider, D. (2013). Thylakoid membrane maturation and PSII activation are linked in greening *Synechocystis* sp. Plain 6803 cells. *Plant Physiol.* 163, 1037–1046. doi: 10.1104/pp.113.224428

Bligh, E. G., and Dyer, W. J. (1959). A rapid method of total lipid extraction and purification. *Can. J. Biochem. Physiol.* 37, 911–917. doi: 10.1139/o59-099

Chapman, D. J., De-Felice, J., and Barber, J. (1983). Growth temperature effects on thylakoid membrane lipid and protein content of pea chloroplasts. *Plant Physiol.* 72, 225–228. doi: 10.1104/pp.72.1.225

Collier, J. L., and Grossman, A. R. (1992). Chlorosis induced by nutrient deprivation in *Synechococcus* sp. strain Plain 7942: not all bleaching is the same. *J. Bacteriol.* 174, 4718–4726. doi: 10.1128/jb.174.14.4718-4726.1992

Deschoenmaeker, F., Facchini, R., Leroy, B., Badri, H., Zhang, C. C., and Wattiez, R. (2014). Proteomic and cellular views of *Arthrospira* sp. Plain 8005 adaptation to nitrogen depletion. *Microbiology* 160, 1224–1236. doi: 10.1099/mic.0.074641-0

Doello, S., Klotz, A., Makowka, A., Gutekunst, K., and Forchhammer, K. (2018). A specific glycogen mobilization strategy enables rapid awakening of dormant cyanobacteria from chlorosis. *Plant Physiol.* 177, 594–603. doi: 10.1104/pp.18.00297

Dorne, A. J., Joyard, J., and Douce, R. (1990). Do thylakoids really contain phosphatidylcholine? *Proc. Natl. Acad. Sci. U.S.A.* 87, 71–74. doi: 10.1073/pnas.87.1.71

Forchhammer, K., and Schwarz, R. (2019). Nitrogen chlorosis in unicellular cyanobacteria – a developmental program for surviving nitrogen deprivation. *Environ. Microbiol.* 21, 1173–1184. doi: 10.1111/1462-2920.14447

Fujii, S., Nagata, N., Masuda, T., Wada, H., and Kobayashi, K. (2019a). Galactolipids are essential for internal membrane transformation during etioplast-to-chloroplast differentiation. *Plant Cell Physiol.* 60, 1224–1238. doi: 10.1093/pcp/pcz041

Fujii, S., Wada, H., and Kobayashi, K. (2019b). Role of galactolipids in plastid differentiation before and after light exposure. *Plants* 8:357. doi: 10.3390/plants8100357

Gombos, Z., Kis, M., Páli, T., and Vigh, L. (1987). Nitrate starvation induces homeoviscous regulation of lipids in the cell envelope of the blue-green alga, *Anacystis nidulans*. *Eur. J. Biochem.* 165, 461–465. doi: 10.1111/j.1432-1033.1987.tb11461.x

Görl, M., Sauer, J., Baier, T., and Forchhammer, K. (1998). Nitrogen-starvation-induced chlorosis in *Synechococcus* PCC 7942: adaptation to long-term survival. *Microbiology* 144, 2449–2458. doi: 10.1099/00221287-144-9-2449

Grimme, L. H., and Boardman, N. K. (1972). Photochemical activities of a particle fraction P1 obtained from the green alga *Chlorella fusca*. *Biochem. Biophys. Res. Commun.* 49, 1617–1623. doi: 10.1016/0006-291X(72)90527-X

Hagio, M., Gombos, Z., Várkonyi, Z., Masamoto, K., Sato, N., Tsuzuki, M., et al. (2000). Direct evidence for requirement of phosphatidylglycerol in photosystem II of photosynthesis. *Plant Physiol.* 124, 795–804. doi: 10.1104/pp.124.2.795

Heinz, S., Rast, A., Shao, L., Gutu, A., Gügel, I. L., Heyno, E., et al. (2016). Thylakoid membrane architecture in *Synechocystis* depends on CurT, a homolog of the granal CURVATURE THYLAKOID1 proteins. *Plant Cell* 28, 2238–2260. doi: 10.1105/tpc.16.00491

Hölzl, G., Witt, S., Gaude, N., Melzer, M., Schöttler, M. A., and Dörmann, P. (2009). The role of diglycosyl lipids in photosynthesis and membrane lipid homeostasis in *Arabidopsis*. *Plant Physiol.* 150, 1147–1159. doi: 10.1104/pp.109.139758

Itoh, S., Kozuki, T., Nishida, K., Fukushima, Y., Yamakawa, H., Domonkos, I., et al. (2012). Two functional sites of phosphatidylglycerol for regulation of reaction of plastoquinone QB in photosystem II. *Biochim. Biophys. Acta* 1817, 287–297. doi: 10.1016/j.bbabio.2011.10.002

Janero, D. R., and Barrnett, R. (1981). Cellular and thylakoid-membrane glycolipids of *Chlamydomonas reinhardtii* 137+. *J. Lipid Res.* 22, 1119–1125.

Klotz, A., Georg, J., Bučinská, L., Watanabe, S., Reimann, V., Januszewski, W., et al. (2016). Awakening of a dormant cyanobacterium from nitrogen chlorosis reveals a genetically determined program. *Curr. Biol.* 26, 2862–2872. doi: 10.1016/j.cub.2016.08.054

Kobayashi, K., Endo, K., and Wada, H. (2016). Roles of lipids in photosynthesis. *Lipids Plant Algae Dev.* 86, 21–49. doi: 10.1007/978-3-319-25979-6_2

Kobayashi, K., Endo, K., and Wada, H. (2017). Specific distribution of phosphatidylglycerol to photosystem complexes in the thylakoid membrane. *Front. Plant Sci.* 8:1991. doi: 10.3389/fpls.2017.01991

Kobayashi, K., Fujii, S., Sato, M., Toyooka, K., and Wada, H. (2015). Specific role of phosphatidylglycerol and functional overlaps with other thylakoid lipids in *Arabidopsis* chloroplast biogenesis. *Plant Cell Rep.* 34, 631–642. doi: 10.1007/s00299-014-1719-z

Kobayashi, K., Narise, T., Sonoike, K., Hashimoto, H., Sato, N., Kondo, M., et al. (2013). Role of galactolipid biosynthesis in coordinated development

of photosynthetic complexes and thylakoid membranes during chloroplast biogenesis in *Arabidopsis*. *Plant J.* 73, 250–261. doi: 10.1111/tpj.12028

Kopečná, J., Pilny, J., Krynická, V., Tomčala, A., Kis, M., Gombos, Z., et al. (2015). Lack of phosphatidylglycerol inhibits chlorophyll biosynthesis at multiple sites and limits chlorophyllide reutilization in *Synechocystis* sp. *strain* Plain 6803. *Plant Physiol.* 169, 1307–1317. doi: 10.1104/pp.15.01150

Krasikov, V., Aguirre von Wobeser, E., Dekker, H. L., Huisman, J., and Matthijs, H. C. P. (2012). Time-series resolution of gradual nitrogen starvation and its impact on photosynthesis in the cyanobacterium *Synechocystis* PCC 6803. *Physiol. Plant.*145, 426–439. doi: 10.1111/j.1399-3054.2012.01585.x

Laemmli, U. K. (1970). Cleavage of structural proteins during the assembly of the head of bacteriophage T4. *Nature* 227, 680–685. doi: 10.1038/227680a0

Lea-Smith, D. J., Bombelli, P., Vasudevan, R., and Howe, C. J. (2016). Photosynthetic, respiratory and extracellular electron transport pathways in cyanobacteria. *Biochim. Biophys. Acta* 1857, 247–255. doi: 10.1016/j.bbabio.2015.10.007

Liu, L. N. (2016). Distribution and dynamics of electron transport complexes in cyanobacterial thylakoid membranes. *Biochim. Biophys. Acta* 1857, 256–265. doi: 10.1016/j.bbabio.2015.11.010

Murata, N., Sato, N., Omata, T., and Kuwabara, T. (1981). Separation and characterization of thylakoid and cell envelope of the blue-green alga (*Cyanobacterium*) *Anacystis nidulans*. *Plant Cell Physiol.* 22, 855–866. doi: 10.1093/oxfordjournals.pcp.a076231

Ogawa, T., and Sonoike, K. (2016). Effects of bleaching by nitrogen deficiency on the quantum yield of Photosystem II in *Synechocystis* sp. Plain 6803 revealed by Chl fluorescence measurements. *Plant Cell Physiol.* 57, 558–567. doi: 10.1093/pcp/pcw010

Omata, T., and Murata, N. (1983). Isolation and characterization of the cytoplasmic membranes from the blue-green alga (*Cyanobacterium*) *Anacystis nidulans*. *Plant Cell Physiol.* 24, 1101–1112. doi: 10.1093/oxfordjournals.pcp.a076614

Rast, A., Schaffer, M., Albert, S., Wan, W., Pfeffer, S., Beck, F., et al. (2019). Biogenic regions of cyanobacterial thylakoids form contact sites with the plasma membrane. *Nat. Plants* 5, 436–446. doi: 10.1038/s41477-019-0399-7

Sakurai, I., Hagio, M., Gombos, Z., Tyystjärvi, T., Paakkarinen, V., Aro, E.-M., et al. (2003). Requirement of phosphatidylglycerol for maintenance of photosynthetic machinery. *Plant Physiol.* 133, 1376–1384. doi: 10.1104/pp.103.026955

Sakurai, I., Mizusawa, N., Ohashi, S., Kobayashi, M., and Wada, H. (2007). Effects of the lack of phosphatidylglycerol on the donor side of photosystem II. *Plant Physiol.* 144, 1336–1346. doi: 10.1104/pp.107.098731

Sato, N., and Murata, N. (1988). Membrane lipids. *Methods Enzymol.* 167, 251–259. doi: 10.1016/0076-6879(88)67027-3

Spät, P., Klotz, A., Rexroth, S., Maček, B., and Forchhammer, K. (2018). Chlorosis as a developmental program in cyanobacteria: the proteomic fundament for survival and awakening. *Mol. Cell. Proteomics* 17, 1650–1669. doi: 10.1074/mcp.RA118.000699

Stanier, R. Y., Kunisawa, R., Mandel, M., and Cohen-Bazire, G. (1971). Purification and properties of unicellular blue-green algae (order Chroococcales). *Bacteriol. Rev.* 35, 171–205. doi: 10.1128/mmbr.35.2.171-205.1971

Conflict of Interest: The authors declare that the research was conducted in the absence of any commercial or financial relationships that could be construed as a potential conflict of interest.

frontiers in Plant Science

ORIGINAL RESEARCH
published: 11 August 2020
doi: 10.3389/fpls.2020.01198

PDM4, a Pentatricopeptide Repeat Protein, Affects Chloroplast Gene Expression and Chloroplast Development in *Arabidopsis thaliana*

Xinwei Wang[1,2], *Lirong Zhao*[1,2], *Yi Man*[1,2], *Xiaojuan Li*[1,2], *Li Wang*[3] *and Jianwei Xiao*[1,2]*

[1] Beijing Advanced Innovation Center for Tree Breeding by Molecular Design, Beijing Forestry University, Beijing, China, [2] College of Biological Sciences and Biotechnology, Beijing Forestry University, Beijing, China, [3] College of Horticulture and Plant Protection, Yangzhou University, Yangzhou, China

Extensive studies have been carried out on chloroplast gene expression and chloroplast development; however, the regulatory mechanism is still largely unknown. Here, we characterized Pigment-Defective Mutant4 (PDM4), a P-type PPR protein localized in chloroplast. The *pdm4* mutant showed seedling-lethal and albino phenotype under heterotrophic growth conditions. Transmission electron microscopic analysis revealed that thylakoid structure was totally disrupted in *pdm4* mutant and eventually led to the breakdown of chloroplasts. The levels of several chloroplast- and nuclear-encoded proteins are strongly reduced in *pdm4* mutant. Besides, transcript profile analysis detected that, in *pdm4* mutant, the expression of plastid-encoded RNA polymerase-dependent genes was markedly affected, and deviant chloroplast rRNA processing was also observed. In addition, we found that PDM4 functions in the splicing of group II introns and may also be involved in the assembly of the 50S ribosomal particle. Our results demonstrate that PDM4 plays an important role in chloroplast gene expression and chloroplast development in Arabidopsis.

Keywords: pigment-defective mutant4, chloroplast, pentatricopeptide repeat protein, development, gene expression

OPEN ACCESS

Edited by:
Yan Lu,
Western Michigan University, United States

Reviewed by:
Zhong-Nan Yang,
Shanghai Normal University, China
Sheng Teng,
Shanghai Institutes for Biological Sciences (CAS), China
Jeannette Pfalz,
Friedrich Schiller University Jena, Germany

***Correspondence:**
Jianwei Xiao
xiaojianwei@bjfu.edu.cn

Specialty section:
This article was submitted to Plant Physiology, a section of the journal Frontiers in Plant Science

Received: *11 January 2020*
Accepted: *23 July 2020*
Published: *11 August 2020*

Citation:
Wang X, Zhao L, Man Y, Li X, Wang L and Xiao J (2020) PDM4, a Pentatricopeptide Repeat Protein, Affects Chloroplast Gene Expression and Chloroplast Development in Arabidopsis thaliana. Front. Plant Sci. 11:1198. doi: 10.3389/fpls.2020.01198

INTRODUCTION

Chloroplasts are known for providing energy and carbon resource to the plant cell and are also indispensable for plant development and growth (Bryant et al., 2011). Derived from cyanobacterial ancestors, the chloroplasts belong to semi-autonomous organelles which possess their own genomes. Over the last billion years, the chloroplast genome has lost numerous genes in higher plants and generally remains about 120 genes which encode primary components of translation, transcription, and photosynthesis apparatus, as well as contains some critical biogenesis-related genes such as *accD*, *clpP1*, *matK*, *ycf1*, and *ycf2* (Sato et al., 1999; Leister, 2003; Ouyang et al., 2017). Although the chloroplast genome is small and with limited coding information, the transcriptional process is much more complex than that of prokaryotes which are usually organized in polycistronic transcriptional units. In particular, RNA processing from polycistronic precursors and editing are strikingly different between chloroplast and prokaryotes (Sugita and Sugiura, 1996; Sato et al., 1999).

Generally, in higher plant, two RNA polymerases with different origins participate in the transcription of plastid genes, including a plastid-encoded RNA polymerase (PEP) and nuclear-encoded RNA polymerases (Hajdukiewicz et al., 1997; Liere and Börner, 2007; NEP). During chloroplast development, the plastidic genetic system is first established within the proplastids. During this stage, the genes of PEP components and related ribosomal proteins were transcribed by NEP that is critical for the nascent construction of the plastid-genetic background. As a result, the activity of the transcriptional apparatus in the proplastid is remarkably raised. At the second stage, the well-assembled and functional PEP starts to transcribe plastid-encoded genes. Meanwhile, the photosynthetic proteins which are encoded by nuclear genes exhibit a high expression level and eventually lead to the establishment of photosynthesis systems (Mullet, 1993; Majeran et al., 2010; Tiller and Bock, 2014). PEP activity is also essential for the fully active chloroplasts formation because it promotes the expression of photosynthesis-related genes (Pfalz and Pfannschmidt, 2013). Subunits of the PEP core are present in two plastid protein preparations; one is associated with thylakoid and envelope membranes, and these are protein:DNA-complexes termed transcriptionally active chromosomes (TACs) (Krause and Krupinska, 2000; Pfalz et al., 2006; Krupinska et al., 2012). So far, the richest protein data set resulted from protein mass spectrometry analysis of isolated pTACs from Arabidopsis (*Arabidopsis thaliana*) and mustard (*Sinapis alba*), in which 35 proteins were identified (Pfalz et al., 2006). Eighteen of these proteins were denoted pTAC proteins, and three of them (pTAC2, -6, and -12) were shown to be required for plastid gene expression (Pfalz et al., 2006). Besides, PEP forms a complex with PEP-associated proteins (PAPs), and the *Arabidopsis thaliana* nuclear genome contains at least 12 PAP genes (Yu et al., 2014), and all PAPs have also been identified in the nucleoid or TAC proteomes (Pfalz et al., 2006; Majeran et al., 2012; Melonek et al., 2016).

The complexity of the chloroplast gene expression system is also highly regulated at the post-transcriptional which mainly reflects the extensive modifications exerted on transcripts during RNA processing (Chi et al., 2015). For instance, defects in endonucleolytic cleavage polycistronic transcripts would result in a blocking translation in chloroplast mRNAs (Sugiura et al., 1998; Walter et al., 2010). And critical sites of chloroplast RNAs that are essential for chloroplasts development in higher plant can be correctly spliced or edited (Bobik et al., 2017; Du et al., 2017; Zhang J. et al., 2017).

Chloroplast RNA metabolism refers to a substantial number of RNA-binding proteins (Stern et al., 2010). Due to the limited coding capacity of the chloroplast genome, the chloroplast gene expression is controlled both by plastid-encoded and nucleus-encoded proteins (Germain et al., 2013; Stoppel and Meurer, 2013; Belcher et al., 2015). As nucleus-encoded factors, it has been demonstrated that the pentatricopeptide repeat (PPR) proteins participate in chloroplast gene expression and function (Barkan and Small, 2014). Members of the PPR protein family are considerably numerous in land plants with up to 450 representatives in Arabidopsis (Lurin et al., 2004), and this family is characterized by PPR repeat with highly degenerate unit of 35 amino acids (Lurin et al., 2004). In addition, according to the variation in length and amino acid composition of PPR repeats, the PPR proteins have been used to define two categories; P-class PPR proteins are mainly composed of typical 35-amino acid sequence repeats, and the PLS-class members contain triplets of motifs by varied amino acid lengths and sometimes with an additional C-terminal domain (Lurin et al., 2004; Cheng et al., 2016).

The PPR proteins can directly bind to chloroplast RNAs and prevent targeted RNAs from RNase degradation and/or facilitate or directly participate in related processing (Small and Peeters, 2000; Pogson and Albrecht, 2011). It is widely accepted that the PLS subgroup proteins are mostly involved in RNA editing, whereas the P subgroup proteins play crucial roles in intron splicing, RNA stabilization, and translation process (Barkan and Small, 2014). For example, either PPR protein DYW2 or NUWA can be interacted with CLB19, function in editing of organelle RNA (Guillaumot et al., 2017). Seedling Lethal1 (SEL1/PDM1), a PPR protein was proved to participate in the plastid gene expression and chloroplast development at an early stage (Pyo et al., 2013). Through specifically recognizing RNA sequence of 23S–4.5S rRNA precursor, PPR protein SOT1 performs the endonucleolytic activity during the maturation of 23S and 4.5S rRNA in chloroplast (Zhou et al., 2017). SOT5/EMB2279 is involved in intron splicing of plastid *rpl2*, and PpPPR_66 acts as a processing factor to assist *ndhA* pre-mRNA splicing by bounding preferentially to the specific region (Huang et al., 2018; Ito et al., 2018). Besides, some PPR proteins are proved to be required for the accumulation/assembly of plastid ribosomes (Williams and Barkan, 2004). Synthesis of the rRNAs and proteins, with correct folding, maturation/modification, and further assembly into functional particles, are highly coordinated. The 30S subunit includes 16S rRNA and about 20 ribosomal proteins, while the 50S subunit consists of 23S, 5S, and 4.5S rRNAs and about 30 ribosomal proteins (Yamaguchi et al., 2003).

In this study, we report the *pdm4* mutant of Arabidopsis, which was generated by T-DNA insertion and screened as defective pigment and seedling-lethal phenotype. The corresponding gene, *PDM4*, encodes a putative chloroplast PPR protein. Subsequent genetic and molecular analyses suggest that PDM4 is involved in the regulation of plastid gene expression and chloroplast development.

MATERIALS AND METHODS

Plant Materials and Growth Conditions

Arabidopsis thaliana Columbia (Col-0) ecotype and the mutant *pdm4* (SALK_034168, obtained from the Arabidopsis Biological Resource Center; ecotype Columbia) were used in all experiments. The seeds were sterilized by 0.8% NaClO for 10 min, followed by 5 times rinsing with sterile double-distilled water. Then they were plated on 1/2 MS medium with 1%

sucrose and 0.8% agar (pH 6.0) at 4°C in the dark for 48 h after sterilizing. Next, they were transferred to long-day conditions (16 h light, 8 h dark) at 22°C. The T-DNA insertion was confirmed by PCR analysis and subsequent sequencing with the primers LBb1.3 (5′-ATTTTGCCGATTTCGGAAC-3′) and *pdm4*-RP. The homozygous *pdm4* mutant line was verified by PCR using specific primers *pdm4*-LP 5′-TCACTAACCAATAA CACCACC-3′ and *pdm4*-RP 5′-ATTGCTTGTGAGCC TTGGT-3′.

Total RNA Isolation and Reverse Transcription (RT)-PCR; Quantitative Real-Time PCR (qRT-PCR) Analysis

Three total RNA samples were extracted from light grown 3-week-old mutant and wild-type plants with RNeasy Mini Kit (Tiangen Biotech Company, Beijing, China). For RT-PCR analysis, first strand cDNA was synthesized by the one-step reverse-transcription system (TransGen Biotech, Beijing, China), and the operation was carried out based on previous protocol (Zhang J. et al., 2017). The qRT-PCR was performed, and the primers used in this analysis were according to Du et al. (2017). All the measurement for each sample was repeated three times.

Measurement of Chlorophyll

For measuring the chlorophyll content, leaves from 3-week-old Arabidopsis seedlings were collected. One hundred milligram of leaves was ground in liquid nitrogen into fine powder and mixed thoroughly with 250 μl 80% acetone and quantified on a UV2800 spectrophotometer (Unico Instruments Co., Ltd, USA). We calculated the chlorophyll content from the absorbance following the method of Arnon (1949). Three biological replicates, each with three repeats, were analyzed for each sample.

Optical and Transmission Electron Microscopy

To observe the development of the embryos between wild-type and the mutant plants, the seeds of heterozygous *pdm4* mutant line were removed from siliques and totally cleared in Hoyer's buffer (chloral hydrate, 50 g; gum Arabic, 3.75 g; and glycerol, 2.5 ml were dissolved in 15 ml of water) according to Meinke et al. (1994). The individual embryo in the cleared seed was examined by light microscopy (Zeiss, Axioskop, Germany) using differential interference contrast (DIC; Du et al., 2017). For transmission electron microscopy (TEM) analysis, the samples were first cut into ultra-thin pieces (LKB-8800, LKB, Broma, Sweden) and stained with alkaline lead citrate and uranyl acetate and then examined with a transmission electron microscope (JEM 1200EX, JEOL, Japan).

Northern-Blot Analysis

For northern-blot analysis, total RNA from wild-type and *pdm4* seedlings was extracted and determined by using thermo NanoDrop 2000 (Thermo, USA). Three equal content RNA samples of the wild type and *pdm4* mutant were separated on 1.3% (w/v) agarose-formaldehyde gels and subsequently blotted to a nylon membrane. Next, the membrane was hybridized with a specific probe labeled with ^{32}P. The labeled probes were obtained by using the Prime-a-Gene Labeling Kit (SGMB01-Promega-U1100, USA). The sequences of the primers were according to Du et al. (2017). All the analysis was performed at least in three independent repeats.

Subcellular Localization of Green Fluorescent Protein

In order to study the subcellular localization of PDM4, two-week-old complemented Arabidopsis seedlings (*COM*) were cut into small pieces and incubated in a solution (10 mM MES, 20 mM $CaCl_2$, 0.5 M mannitol, pH 5.8, containing 0.1 g ml^{-1} macerozyme and 0.1 g ml^{-1} cellulase) for 4 h at room temperature in the dark. Protoplasts were then isolated according to Dovzhenko et al. (2003) and assessed for fusion gene expression with a confocal microscope (TCS SP5 CLSM; Leica). The signal of green fluorescence was detected, and red fluorescence represents the auto-fluorescence of chlorophyll.

Protein Extraction and Western Blot Analyses

The total proteins were extracted from 3-week-old wild type and *pdm4* mutant with NB1 buffer (pH 8.0), including 1 mM $MgCl_2$, 5 mM DTT, 0.5 M sucrose, 50 mM Tris MES, 10 mM EDTA, and protease inhibitor cocktail. The different protein samples were separated by 15% SDS-page and then transferred onto PVDF membranes. And then, membranes were incubated with specific primary antibodies. The antibodies were used in this study according to Xiao et al. (2012). Signals were detected using enhanced chemiluminescence method (Du et al., 2017), and signal intensity of protein band was analyzed by "ImageJ" software. These experiments were repeated at least three times independently.

Chloroplast Isolation and Fractionation

Chloroplast isolation method was performed as described previously with minor modifications (Aronsson and Jarvis, 2002). Exactly, 21-day-old Arabidopsis plants were ground in extraction buffer (5 mM EGTA, 50 mM HEPES-KOH pH 8.05, 0.33 M sorbitol, 5 mM EDTA, 10 mM $NaHCO_3$, and 5 mM $MgCl_2$). After filtering through Miracloth, the sample was centrifuged for 1 min at 1,000 g. The supernatants were removed, and pellets were re-suspended and then loaded onto Percoll gradients (70 and 40% in isolated buffer respectively); then intact chloroplasts were collected and washed three times with washing buffer (3 mM $MgSO_4$, 0.33 M sorbitol, and 50 mM HEPES-KOH, pH 8.0). Chloroplasts were fractionated into the thylakoid membrane, stromal and envelope fractions as described by Du et al. (2017).

RNA Immunoprecipitation Assays

The procedures used for coimmunoprecipitation and immunoblot assays were described previously (Terzi and Simpson, 2009) using 3-week-old *35S:PDM4-GFP* complemented seedlings. Anti-GFP magnetic beads were obtained from Abcam company (ab290, http://www.abcam.com/). The sequences of primers used to

detect RNA content that coimmunoprecipitated with PDM4-GFP are listed in **Supplemental Table 1**.

RESULTS

Characterization of the *pdm4* Mutant

To identify PPR genes involved in chloroplast development, we screened a collection of T-DNA inserted mutation lines localized in *PPR* genes (Du et al., 2017; Zhang J. et al., 2017). In this study, we obtained a new mutant, designated as *pigment-defective mutant4* (*pdm4*). The position of T-DNA insertion in *pdm4* was confirmed by PCR and subsequent sequencing, and the result exhibited T-DNA inserted in 165 base pairs downstream of putative start codon (**Figure 1A**).

When cultivated on 1/2 MS medium supplemented with 1% sucrose, the *pdm4* mutant had developed purple cotyledons that were gradually bleached to white with extended growth period

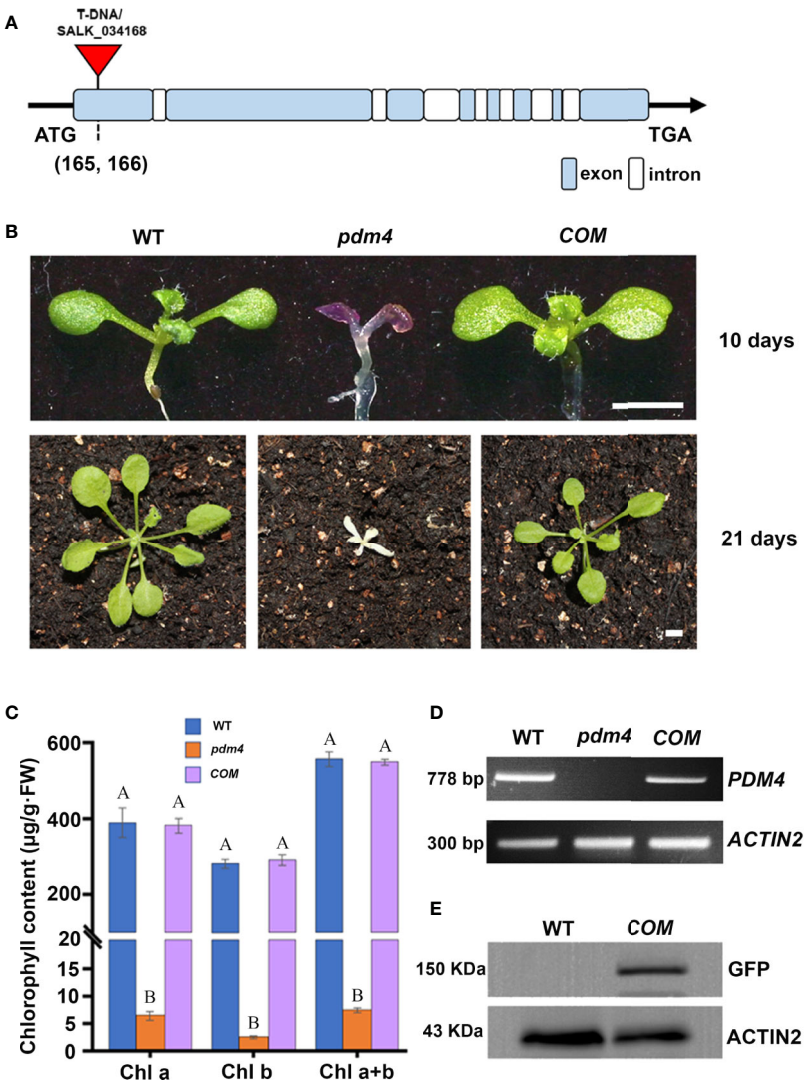

FIGURE 1 | Identification and characterization of the *pdm4* mutant. **(A)** Gene structure of the *PDM4* (AT5G27270). Exons indicated by the wathet boxes, introns by the white boxes, and the T-DNA insertion indicated by the red triangle; ATG represents the initiation codon, and TGA represents the stop codon. **(B)** Pigment-defective phenotypes and complementation of the *pdm4* mutant. The cDNA of the *PDM4* was cloned into a binary expression vector with the GFP tag and complementation of the *pdm4* mutant (*COM*). WT, wild type. 10-day-old plants were grown on sucrose-supplemented medium (up lane), and 21-day-old plants were grown in soil (down lane). Scale bar: 3 mm. **(C)** The chlorophyll content of wild-type, *pdm4* and *COM*. Chlorophyll was extracted from 14-day-old seedlings and quantified. Values given are μg/g fresh weight ± SD (n = 3). Values not connected by the same letters are significantly different (Student's t test, $p < 0.05$). The average of three replicates is shown. **(D)** Reverse transcription PCR analysis. RT-PCR was performed using specific primers for *AT5G27270* or *ACTIN2*. **(E)** Total proteins from wild-type and *COM* (15 μg) were separated by SDS-PAGE, followed by immunoblot analysis with the anti-GFP. The experiments of **(D, E)** were repeated three times independently.

(**Figure 1B**). After being transferred into the soil, the *pdm4* mutant was unable to grow and died shortly (**Figure 1B**). Homozygous *pdm4* plants are kept by segregating from a self-pollinated heterozygous plant with a ratio 3:1 in green and albino plants (data not shown). Thus, the albino phenotype is inherited as a recessive mutation. To confirm that the disruption of *PDM4* results in the lethal phenotype, we performed the functional complementation analysis. The result indicated that full-length coding region of *PDM4* gene fused a GFP tag at its C terminus successfully rescued the *pdm4* phenotypes. Among the 56 T1 transgenic lines analyzed, 16 lines were homozygous *pdm4* plants and showed a wild-type looking phenotype (**Figure 1B**).

The concentration of chlorophyll (μg/g FW) in the *pdm4* was significantly reduced compared with the wild type (**Figure 1C**). As expected, chlorophyll accumulated in *COM* plants was equivalent to the level of the wild-type plants. By reverse transcription-PCR analysis, obvious signals were obtained from *COM* and wild-type plants but not observed in homozygous *pdm4* mutant; this result demonstrated the expression of *PDM4* was completely suppressed (**Figure 1D**). Eventually, western blot result showed that PDM4-GFP proteins were located at about 150 kilodaltons (kDa) in complemented lines by using a GFP antibody, which is in accordance with the predicted protein molecular weight of GFP-tagged PDM4 (**Figure 1E**). The complementation analysis of the *pdm4* phenotype indicated that the PDM4-GFP is a functional protein, and *PDM4* gene was responsible for the phenotype of the *pdm4*.

Chloroplast Development and Accumulation of Photosynthetic Proteins in *pdm4*

Considering that most photosynthetic pigment defects may result in a retarded chloroplast development, we assessed the possibility that the *pdm4* mutation causes ultrastructural changes in the chloroplasts, and plastids from 3-week-old seedling mesophyll cells were examined by transmission electron microscopy (**Figures 2A–D**). The chloroplasts from wild type contained well-developed membrane systems featured with typical grana structure connected by the stroma lamellae, and the stroma thylakoid and grana thylakoid were easily distinguished (**Figures 2A, B**). Relative to wild-type chloroplasts, the *pdm4* plastids are smaller, deformed, and devoid of thylakoid membrane and granal stacks, and meanwhile, the membrane spacing was not clear (**Figures 2C, D**).

To obtain more information concerning the molecular lesion in *pdm4* to further explain the defects of chloroplasts development in corresponding mutant, total proteins were isolated, and equal sample volumes were loaded in denaturing polyacrylamide gel electrophoresis. Then we performed western blot analysis to detect accumulation of core subunits of photosynthetic complexes, including D1 and LHC II of PSII (encoded by *psbA* and *lhcb2*), PsaA, PsaN, and LHC I of PSI (encoded by *psaA, psaN*, and *Lhca1*), Cyt f and petD, the subunits of Cyt b_6/f, and the CF1α, CF0 II of the ATP synthase. All these proteins were markedly reduced, even barely detected in *pdm4* mutant (**Figures 2E, F**). So, due to the dramatically decreased of some representative subunits of photosynthetic complexes in *pdm4* mutant, we got a

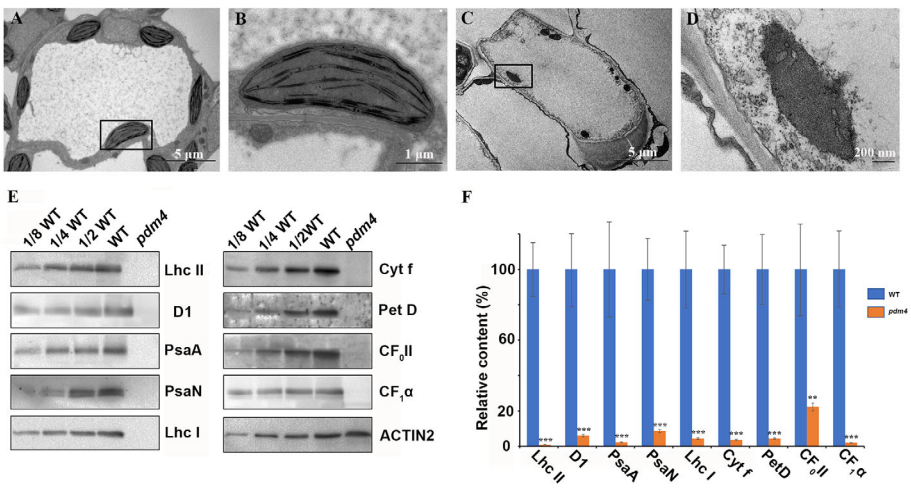

FIGURE 2 | Ultrastructure of plastids and chloroplast proteins in *pdm4*. **(A–D)** The thylakoid membrane organization in the chloroplasts of wild type **(A, B)** and *pdm4* **(C, D)**. Scale bars: 5 μm in **(A)** and **(C)**; 1 μm in **(B)**, and 500 nm in **(D)**. **(E)** Accumulation of representative subunits of photosynthetic protein complexes determined by western blot analysis with specific antibodies. Total proteins from wild-type and *pdm4* seedlings were extracted and separated by 15% SDS-PAGE. Probes used specific anti-Lhc II, anti-D1, anti-PsaA, anti-PsaN, anti-Lhc I, anti-Cyt f, anti-Pet D, anti-CF0 II, anti-CF1α, and anti-ACTIN antibodies. **(F)** Semi-quantitative analysis of chloroplast proteins. After immunoblot analysis, the average signal intensities for each protein were quantified by the ImageJ software for three independent times. The protein relative contents (per unit of total protein) were determined and compared. Error bars represent standard errors. The relative protein level of *pdm4* mutants was obtained when protein level of wild type was set to 100. Similar result to that presented in **(E)** was obtained from three independent experiments. Results from a representative experiment are shown. The asterisks indicate significant differences between WT and *pdm4* (Student's t test; **p < 0.01; ***p < 0.001).

conclusion that PDM4 is essential for the normal accumulation of thylakoid proteins.

Homozygous *pdm4* Embryos Show Delay in Embryogenesis

To reveal the defects in *pdm4* development and embryos, we examined developing seeds at various developmental stages by using the differential interference contrast (DIC) optics. Within the immature siliques of heterozygous *pdm4*, the segregation ratio of the green and white seeds was close to 3:1 (data not shown) and consistent with the segregation in albino phenotype (**Figures 3A, B**). Moreover, assessment of cleared seeds from the same heterozygous silique indicated that the wild-type and heterozygous seeds underwent normal developmental stages (**Figures 3C–G**), whereas embryo development of homozygous seeds was seriously disrupted (**Figures 3H–L**). Different developmental stages of the seeds in wild-type were well-defined and in normal condition, and no difference was visible in *pdm4* compared with wild-type embryos before or at the early globular stage (**Figure S1**). But from the late globular stage to the early heart stage, developmental deviation of mutant embryos became apparent (**Figures 3C–L**).

PDM4 Encodes a Novel P-Type PPR Protein Localized in the Chloroplast

Based on the redefined PPR motif, PDM4 is classified P-type PPR protein and possesses 16 PPR repeat domains (**Figure S2**). Sequence analysis of the *PDM4* gene revealed that it contains eight exons with a 3,114 base pair open reading frame, which encodes a polypeptide of 1,038 amino acids. By Chlorop1.1 software prediction, PDM4 possesses a putative 31 amino acid transit peptide at the N terminus. To investigate the subcellular distribution of PDM4, we extracted and observed the protoplasts from *COM* plants, and the results showed that the fusion proteins were exclusive to chloroplasts and colocalized with chlorophyll (**Figure 4A**). To further confirm the sublocalization of PDM4 within chloroplasts, intact chloroplasts from *COM* plants were isolated and further fractionated into stroma, envelop, and thylakoid membrane. **Figure 4B** shows that the GFP-tagged PDM4 protein is mainly located in the chloroplast stroma, but not in the thylakoid or envelope membrane fraction. Furthermore, qRT-PCR assay demonstrated that *PDM4* is universally transcribed throughout the various developmental stages; especially, a high expression level in the seedling and leaf and relatively low expression in the flower, stem, and root are observed (**Figure 4C**).

To identify PDM4 homologs in several species, a search was carried out using NCBI protein database and the protein sequence of PDM4 as the template. High similarity of protein sequences was selected for bioinformatics analysis. The PDM4 homologous proteins exhibited a relatively high level of similarity in *Populus trichocarpa* (Potri.T071500, 58.0%) and *Glycine max* (Glyma.08G106500, 54.8%), while they showed a low level in *Volvox carteri* (Vocar.0001s1331, 23.4%) (**Figure S3**). To further reveal the relationship between the

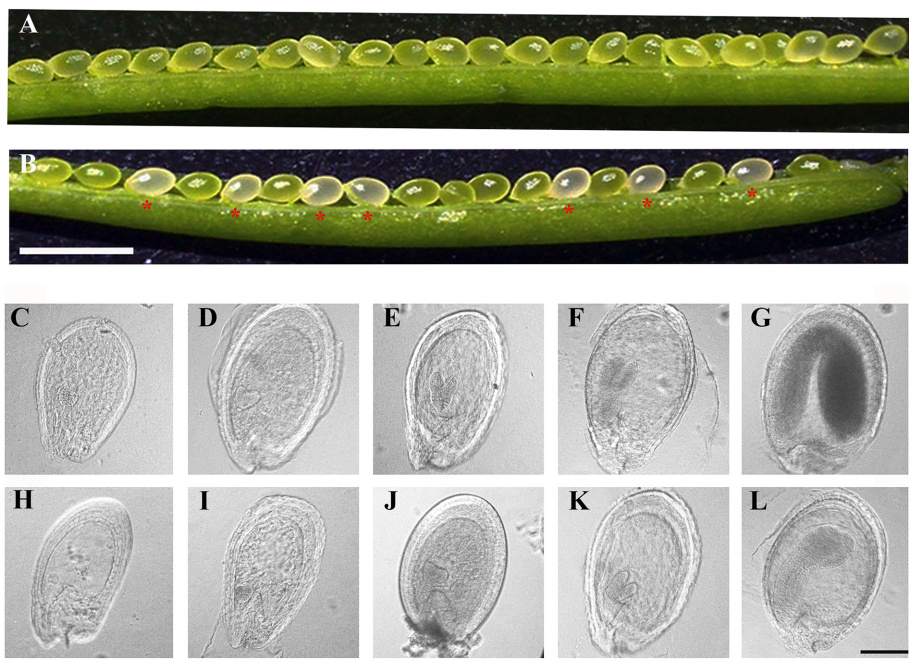

FIGURE 3 | Phenotypic analysis in siliques and embryogenesis in *pdm4* mutant. **(A)** Seeds in wild-type plants. **(B)** Seed segregation in siliques from a *pdm4*/+ heterozygous plants. **(C–L)** Cleared seeds observed under differential interference contrast (DIC). Embryo development of wild type **(C–G)** and *pdm4* **(H–L)** at globular, heart, torpedo, walking-stick, and cotyledon stages. Scale bars: **(A, B)**, 2 mm; **(C–L)**, 1 mm.

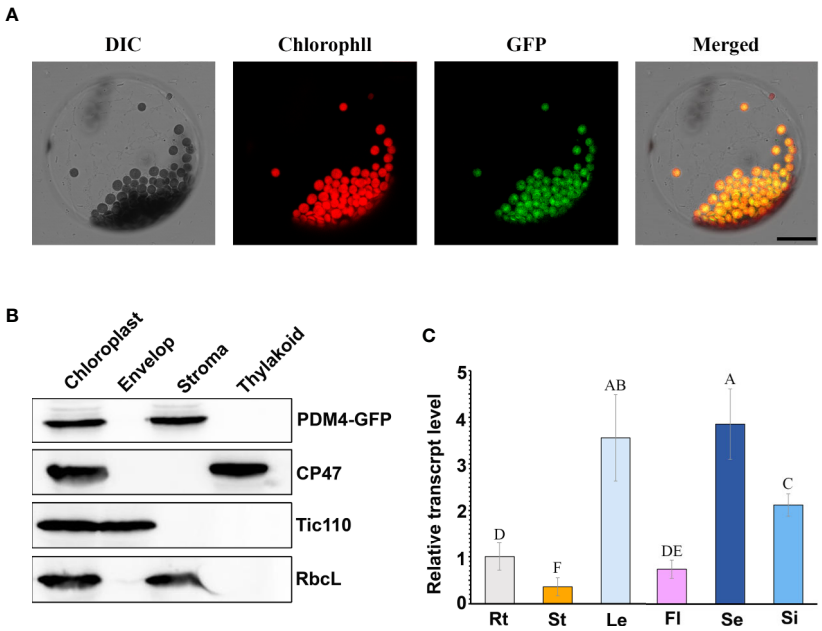

FIGURE 4 | PDM4 protein location and gene expression pattern. **(A)** Localization of the PDM4 protein within the chloroplast using the GFP assay by protoplasts of complement line. Scale bars: 25 nm. **(B)** Immunolocalization of PDM4. Intact chloroplasts were isolated from the leaves of GFP-tagged complemented Arabidopsis, and then separated into envelop, stroma, and thylakoid membrane fractions. Antisera were used against GFP, the integral thylakoid membrane protein CP47, the integral inner envelop membrane protein Tic110, and abundant stroma protein RbcL. **(C)** Quantitative real-time (qRT)-PCR analysis of the *PDM4* gene in the root (Rt), stem (St), leaf (Le), flower (Fl), seedling (Se), and silique (Si). Values not connected by the same letters are significantly different (Student's t test, $p < 0.05$). All the experiments were repeated three times independently.

PDM4 and other family member proteins in different species, we constructed a phylogenetic tree (www.phylogeny.fr) of the closest amino acid sequences from **Figure S3**, and analysis revealed that *PDM4*-like proteins are present in most chloroplastida including monocots, dicots, ferns, mosses, and algae (**Figure S4**).

The *PDM4* Mutation Affects Plastid Gene Expression

Growing mass of information supports the idea that the PPR proteins are always involved in the regulation of plastid gene expression (Barkan and Small, 2014). Depending on the different RNA polymerases required, plastid genes can be roughly divided into three categories: genes of class I are mainly synthesized by PEP, genes of class II are synthesized by both PEP and NEP, and genes of class III are synthesized by NEP. To assess the possibility that PDM4 functions in gene expression in plastid, we examined the transcript levels of three types of genes both in the *pdm4* mutant and wild-type plant by qRT-PCR analysis.

We chose the six genes as representation of PEP-dependent (class I) type, *psaA*, *psbA*, *psbB*, *petB*, *ndhA*, and *rbcL*. The results indicated that the transcription level of PEP-dependent genes in *pdm4* was dramatically decreased from about 40 to 90% (**Figure 5A**). In contrast, the transcript levels of the plastid genes, which were tested as the representatives of class III (NEP-dependent) type, including *rpoA*, *accD*, *rpoB*, *ycf2*, *rpoC1*, and *rpoC2*, were all increased by varying degrees in *pdm4* (**Figure 5B**). As for the class II genes, synthesized by both NEP and PEP, *ndhB*, *atpB*, and *ndhF* expression levels showed a reverse trend. The transcript levels of *ndhB* and *atpB* decreased by nearly 20%, while the transcripts of *ndhF* were obviously upregulated (**Figure 5C**). The contents of representative genes were also confirmed by northern-blot analysis and the result is comparable to the qRT-PCR analysis (**Figure 5D**). To further study whether the increased transcription level of *rpoB* resulted in an enhancement at protein level, we detected the RpoB protein content in the *pdm4* mutant by western blot analysis. Compared with wild type, the result showed an obviously reduced level of RpoB in the *pdm4* mutant (**Figure 5E**).

PDM4 Involved in RNA Splicing of Multiple Chloroplast Group II Introns

Dozens of P-type PPR proteins have been reported to function in RNA splicing in chloroplast (Beick et al., 2008; Barkan and Small, 2014). To determine whether PDM4 influences the splicing of the group II introns, representative splicing event was assayed in the *pdm4* mutant by performing RT-PCR analysis (**Figure 6A**). Compared with the wild-type plants, the unspliced precursors of *ndhA*, *petB*, *ycf3-int-1*, *petD*, *clpp1-int-1* accumulated to an increased level in the *pdm4* mutant (**Figure 6A**). The observation of altered intron processing was also confirmed by northern-blot analysis. The result indicated that unspliced

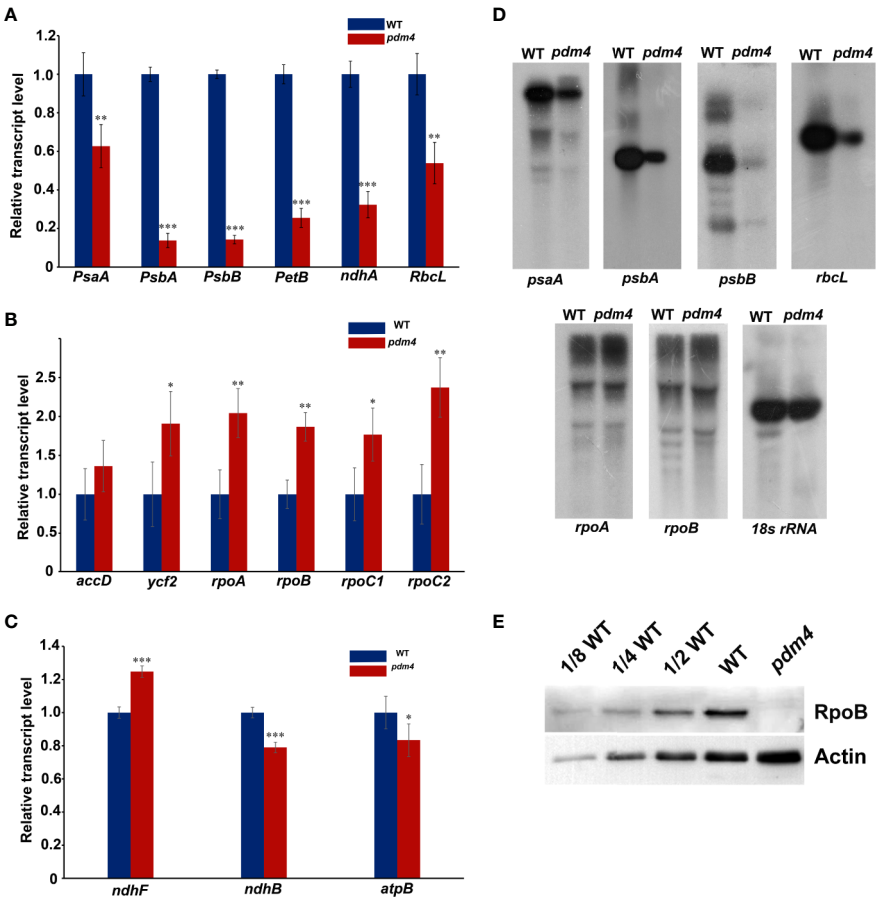

FIGURE 5 | Chloroplast gene expression in *pdm4* relative to the wild type. **(A)** The expression levels of plastid-encoded polymerase (PEP)-dependent chloroplast genes. **(B)** The expression levels of nuclear-encoded polymerase (NEP)-dependent chloroplast genes. **(C)** The expression levels of both PEP- and NEP-dependent chloroplast genes. The asterisks indicate significant differences between WT and *pdm4* (Student's t test; *p < 0.05; **p < 0.01; ***p < 0.001). **(D)** RNA gel-blot hybridization analysis of transcript levels for the different chloroplast gene classes. 5 μg of total RNA from 3-week old plants was size fractionated by agarose gel electrophoresis, transferred to a nylon membrane, and probed with ^{32}P-labeled cDNA probes for *psaA*, *psbA*, *psbB*, *rbcL*, *rpoA*, *rpoB*, and *18S rRNA*. **(E)** RpoB protein content was indicated by western blot. Total protein (50 μg or the indicated dilution of the wild-type sample) from 3-week-old seedlings was loaded per lane. Actin was used as a loading control. These experiments obtained similar results each time. Results from a representative experiment of three times are shown.

precursors of *ycf3*, *petB*, *petD*, and *ndhA* were present and accumulated in a high level in *pdm4* and absent in the wild type. By contrast, the transcripts of *rps14* showed a higher efficiency of accumulation than the wild type (**Figure 6B**). Besides, RNA immunoprecipitation, followed by a quantitative PCR assay using the GFP antibody and *COM* plants, indicated that PDM4 was specifically associated with these target sequences in the *ndhA*, *petB*, *ycf3-1*, and *petD* transcripts (**Figure 6C**). The RNA immunoprecipitation efficiency was supported by western blot analysis (**Figure S5**), and the transcripts containing 18S rRNA were used as control.

pdm4 Mutant Is Defective in Chloroplast rRNA Accumulation

The chloroplast rRNAs, as well as two tRNAs, are arranged in one operon, and transcription depends on both PEP and NEP (Tiller and Bock, 2014). When denatured rRNA samples were separated on denaturing agarose gels, it was shown that the rRNA fragmentation pattern in the wild type was obviously different from *pdm4* mutant by using the ethidium bromide staining method (**Figure 7A**). The signal intensities of the 1.5 and 1.1-kb RNA corresponding to chloroplast 16S rRNA and a breakdown product of the chloroplast 23S rRNA were dramatically reduced in the *pdm4* mutant (**Figure 7A**).

To study the impaired accumulation of chloroplast rRNAs in detail, we performed northern-blot analyses to detect the 16S, 4.5S, 5S, and 23S rRNA by using four probes with an internal region (probes a, b, c, and d, respectively, as shown in **Figure 7B**). Upregulated levels of the 3.2-kb 23S–4.5S rRNA precursor were detected in the *pdm4* mutant, whereas the levels of the 0.12-kb 5S, 0.1-kb 4.5S, 0.5-kb 23S, and 1.5-kb 16S mature rRNAs were drastically downregulated (**Figure 7C**). We also have tested

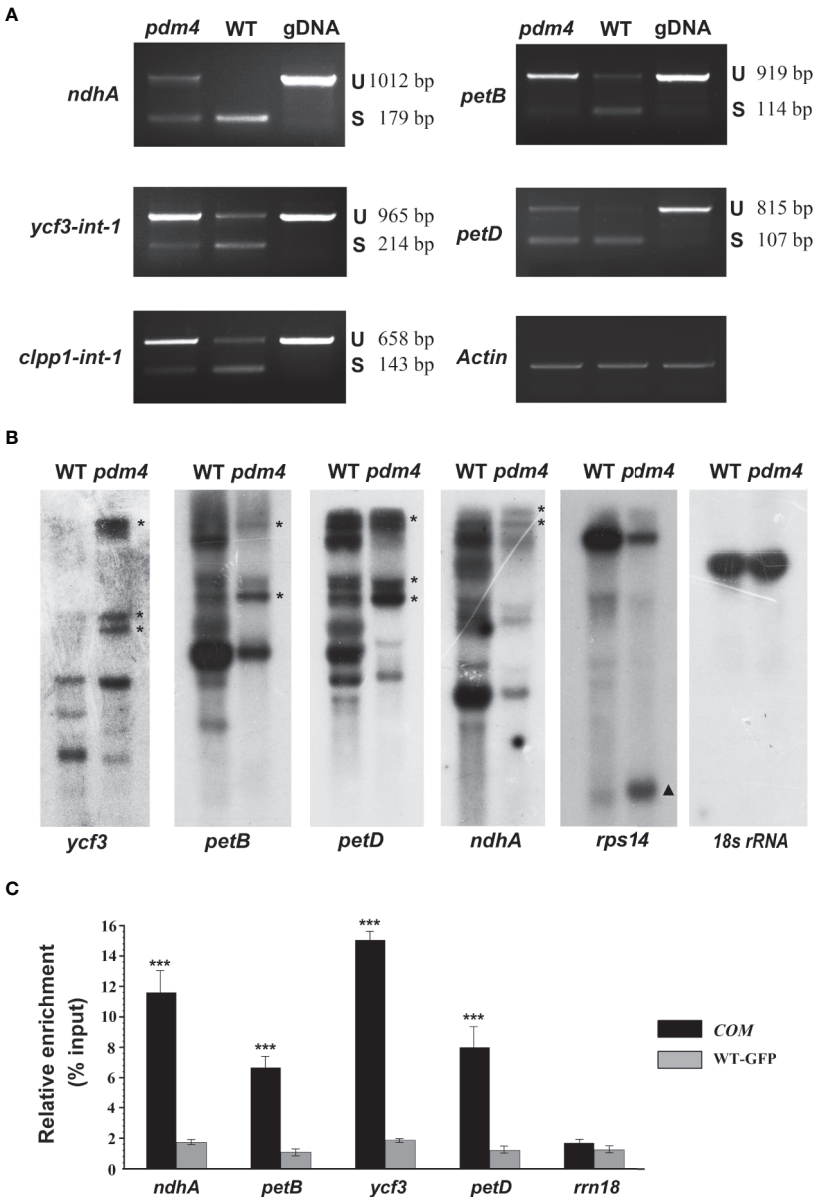

FIGURE 6 | PDM4 is involved in RNA splicing of Arabidopsis group II introns. **(A)** Inefficient splicing of group II introns of *ndhA*, *petB*, *ycf3-int-1*, *petD*, and *clpp1-int-1* in the mutant as determined by reverse-transcription (RT)-PCR. S, introns are spliced; U, introns are retained. **(B)** Northern-blot analysis for the transcript accumulation and pattern of *ycf3*, *petB*, *petD*, *ndhA*, *rps14*, and *18S rRNA*. 5 μg of total RNA from 3-week-old seedlings was analyzed by hybridization to specific probes for each gene. Gene precursor indicated by the asterisk. The results shown are representatives of three independent biological replicates. **(C)** RNA immunoprecipitation analysis followed by a quantitative PCR assay. 3-week-old 35S:PDM4-GFP complemented seedlings were used. IP+, anti-GFP immunoprecipitation; IP–, mock immunoprecipitation. The asterisks indicate significant differences between WT-GFP and *COM* (Student's t test; ***$p < 0.001$). Data are means (± SE) obtained from three replicates.

the interaction and/or association between PDM4 and its targets by RNA immunoprecipitation and qRT-PCR methods and using specific primers for transcripts containing the 23S, 5S, 4.5S, 16S rRNA, and two tRNAs, as well as the intergenic region (**Figure 7B**, probes e, f, g, h). We detected enrichment fragments of 23S, 5S, 4.5S rRNA, and the intergenic region in the anti-GFP immunoprecipitated, but not of 16S, *trnI*, *trnA*, and 18S rRNA (**Figure 7D**). Results from northern blots and RNA-Co-IPs support the conclusion that PDM4 associates with rRNA and affects rRNA processing. The RNA immunoprecipitation efficiency was also supported by western blot analysis (**Figure S5**).

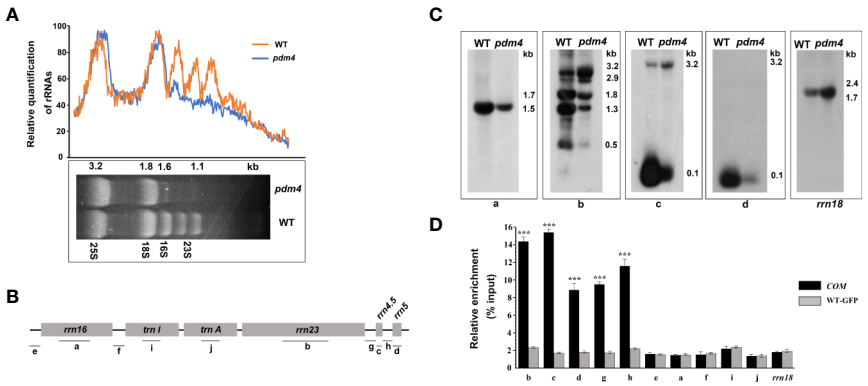

FIGURE 7 | The chloroplast rRNA processing in *pdm4* mutant. **(A)** The contents of rRNAs in wild type and *pdm4*. 5 μg of total RNA from 3-week-old wild type and *pdm4* seedlings was separated by denaturing gel. 23S* is the breakdown product of the chloroplast 23S rRNA. rRNA was quantified using "ImageJ" software. **(B)** Diagram of the chloroplast rRNA operon and the locations of the probes (a–d) used for the RNA gel-blot analysis and used for RNA immunoprecipitation analysis (a–j). **(C)** RNA gel analysis of 16S rRNA (probe a), 23S rRNA (probes b), 4.5S rRNA (probe c), and 5S rRNA (probe d). The sizes of the transcripts (in kb) are shown. The 18S rRNA is shown as a loading control. **(D)** RNA immunoprecipitation analysis followed by a quantitative PCR assay. Probes b, d, c, a, i, f, and *rrn18* are fragments from the 23S rRNA, 5S rRNA, 4.5S rRNA, 16S rRNA, *trnI*, *trnA*, and 18S rRNA, respectively and probes e, f, g, h for the intergenic region. The asterisks indicate significant differences between WT-GFP and *COM* (Student's t test; ***$p < 0.001$). Data are means (± SE) obtained from three replicates.

DISCUSSION

Contrary to the increasing information about the subfamily classification and organellar targeting of PPR proteins in plants, the cellular role and function of most PPR proteins are still so far from fully being apprehended (Lee et al., 2019). Among these PPR proteins, several mutants show pigment defective or lethal phenotypes, such as *sel1* (Pyo et al., 2013), *ecd1* (Jiang et al., 2018), *ppr4*, *emb2654* (Lee et al., 2019), and *sot5/emb2279* (Huang et al., 2018) in addition to *pdm2* and *pdm3* mutants (Du et al., 2017; Zhang J. et al., 2017) which have been reported in our lab before. These works suggest that most functional PPR proteins located in the chloroplast mainly play a critical role in accumulation of chlorophyll and are essential for plant survival. In this study, we identified and characterized a novel PPR protein PDM4; the pigment defective phenotype of the mutant and complementation analysis with the *PDM4* gene demonstrated that PDM4 is indispensable for plant survival and growth.

Chlorophyll accumulation is a prerequisite for the maintenance of functional photosynthetic reaction centers and light-harvesting complexes (Pan et al., 2013). In the *pdm4*, the albino phenotype with a decrease of chlorophyll contents was observed (**Figure 1C**), indicating the photosystem complexes might be impaired, and in accordance with this hypothesis, the result of western blot analysis confirmed this possibility (**Figure 2E**). The chloroplast ultrastructure of *pdm4* exhibited an abnormal morphology, and the structure of the thylakoid membrane was seriously disturbed, suggesting that the lethal phenotype in these plants was probably attributed to developmental defects in chloroplasts. Furthermore, proper development and biogenesis of chloroplast play an essential role in the vast majority of important biological processes, including cell proliferation, secondary metabolite synthesis, and embryogenesis (Yin et al., 2012). Compared with our previous studies in *pdm2* and *pdm3* mutants, the development of homozygous embryo was also retarded especially after globular-to-heart stage (**Figures 3H–L**), suggesting that disruption of *PDM4* is the primary cause for embryogenesis defection in the *pdm4* mutant. Several PPR mutants have similar developmental defects during the embryogenesis process, *e.g.*, *Atppr2* (Lu et al., 2011), *fac19* (Yu et al., 2012), *At_dek36* (Wang et al., 2017), *blx* (Sun et al., 2018), and *ecd1* (Jiang et al., 2018). Borisjuk et al. (2005) suggested that the probable reason for these developmenal defects is energy source transformation from the endosperm to the chloroplast in seed development because chloroplast formed transiently and transformed into storage organelles during embryo development. This view also coincided with Barkan and Small (2014). Thus, blocking embryo development in *pdm4* mutant may result from the defective chloroplast by some indirect effects.

The expression of plastid-encoded genes of photosynthesis was closely linked with the developmental state of the chloroplast (Chi et al., 2008; Zhang Z. et al., 2017). qRT-PCR and northern-blot analysis showed that the levels of PEP-dependent transcripts were dramatically reduced; on the contrary, levels of NEP-dependent transcripts were obviously increased, suggesting that NEP functions correctly or efficiently in *pdm4* (**Figures 5A–D**). Compared with upregulated transcriptional level, the protein level of RpoB is significantly decreased in *pdm4* mutant (**Figure 5E**), and we obtained a similar result in the *pdm3* mutant (Zhang J. et al., 2017). It suggests that RpoB protein biosynthesis or stability is affected in the *pdm4*, leading to a dysfunctional PEP complex, just like the case that happened in the *pdm3* (Zhang J. et al., 2017). Thus, *PDM4* is necessary for an efficient and functional PEP transcription machinery. As to the reduced PEP activity, one possible reason is that PDM4 acts as a participant of nucleoid proteins, like PAPs or pTACs, or

merely associates with them to participate in the regulation of PEP activity because *pdm4* mutant shares some similarities in molecular phenotypes with other PEP-related mutants (**Figures 5** and **6**; Zhang J. et al., 2017; He et al., 2019). As we know, pTACs always interacted with thylakoid membrane; we had not detected any signals with PDM4 in the thylakoid fragments (**Figure 4B**); this may indicate that there exists a weakly interaction between PDM4 and pTACs although none of the presented data show PEP/TAC-association or that PEP-activity is actually PDM4 dependent. Another explanation is that the stability of the transcripts may be decreased, or the rate of mRNA turnover is enhanced in those mutants. In fact, dozens of PPR proteins that affect the stability of chloroplast gene transcripts have been identified (Barkan and Small, 2014).

In higher plants, dozens of P-type PPR proteins are targeted to the chloroplasts and have been proved to be necessary in removing some distinct introns (Barkan and Small, 2014). For example, PPR5 was confirmed to promote the splicing of the group II intron within *rpl16* in Arabidopsis (Rojas et al., 2018); and in rice, AL2 collaborates a subset of chloroplast associated proteins to regulate splicing of both chloroplast group II and I introns (Liu et al., 2016). In this investigation, the disruption of *PDM4* affected the splicing of *ndhA*, *petB*, *clpP1-1*, *ycf3-1*, and *petD* transcripts, and to our surprise, *rps14* transcript accumulation was improved in this study (**Figure 6B**). This result does not fully coincide with *pdm3* in the respective transcript splicing events, *e.g.* the affected splicing sites are *ndhB*, *clpP1-1*, and *trnA*. Alternately, this probably suggests partially distinctive and redundant functions refer to PDM3 and PDM4 in the regulation of chloroplast gene expression. A recent work has shown that BFA2, a P-type PPR protein in the chloroplast, affects *atpF-atpA* transcript splicing by combining to the intergenic region of *atpF-atpA* and acts as a specific barrier to prevent *atpH/F* mRNA from exoribonuclease degradation (Zhang et al., 2019). Thus, we could not rule out the possibility that PDM4 acted as a barrier and resulted in a high efficiency in transcript accumulation of the *rps14* in *pdm4* mutant.

The result of agarose gel electrophoresis analysis validated that chloroplast rRNA was dramatically reduced in the *pdm4* mutant (**Figure 7A**). It is reported that PPR proteins are also involved in pre-rRNA processing and lead to reduced rRNA levels (Barkan and Small, 2014). To further assess this possibility, chloroplast rRNA was analyzed in detail by northern-blot analysis (**Figure 7C**). Compared with the wild type, 3.1-kb RNA representing the precursor of 23S and 4.5S rRNA was accumulated more in *pdm4* (**Figure 7C**). As a consequence of the increased precursor of rRNA in *pdm4*, we deduced that protein PDM4 was involved in the cleavage precursor of rRNA in the chloroplast, especially during the maturation of 50S rRNA. As pre-rRNA processing and ribosome assembly are intimately linked in the chloroplast, therefore, lesions in the ribosome assembly are frequently found in mutants with rRNA processing defects (Prikryl et al., 2008; Chi et al., 2011; Asakura et al., 2012). Coimmunoprecipitation assays produced evidence that PDM4 associates with rRNA and affects rRNA processing (**Figure 7D**), and we can also draw the conclusion that the PDM4 protein was specifically associated with these target sequences in the *ndhA*, *petB*, *ycf3-1*, and *petD* transcripts (**Figure 6C**). Thus, in *pdm4* mutant, the aberrant maturation and accumulation of chloroplast rRNA mutant may be due to a defect in ribosomal biogenesis/assembly. The *pmd4* mutant also showed an obvious downregulated level in the mature form of 16S rRNA, whereas an accumulation of precursor rRNA was not detected (**Figure 7C**). The decrease in mature 16S rRNA in *pdm4* appeared to be regarded as an indirect consequence of the defects in the 50S subunit biogenesis/assembly because PDM4 associated with the 30S particle was not found (**Figure 7**). This conclusion is further sustained by the identification of the RH22 in Arabidopsis (Chi et al., 2012).

PDM4 is required for PEP activity, polycistronic accumulation, and rRNA maturation. But it is hard to rule out which process is a dominant factor; because of the pleiotropic nature of knockout plants, it is particularly true when general plastid translation can be affected by the lack of ribosome processing and/or assembly, which indirectly results in dysfunctional transcription machine as the results of disrupted expression of the plastid encoded polymerase (PEP) and in turn affects RNA processing patterns and levels (Legen et al., 2002; Stoppel and Meurer, 2011). Furthermore, in *pdm4*, chloroplast development is severely damaged. We can find that PDM4 affecting the transcription level of PEP-dependent genes, RNA splicing of multiple chloroplast group II introns, and chloroplast rRNA accumulation. These processes influence and restrict each other, which together leads to the loss of chloroplast development. And based on our research, the key or the direct reason of this phenomenon is still not very clear. So, further study of PDM4 function should facilitates the general understanding the mechanism of plastid gene expression and chloroplast development.

DATA AVAILABILITY STATEMENT

All datasets generated for this study are included in the article/ **Supplementary Material**.

AUTHOR CONTRIBUTIONS

JX designed the study. XW, LZ, YM, XL, LW, and JX performed the research. XW, XL, and JX analyzed the data. JX and XW wrote the paper. All authors discussed the results and made comments on the manuscript. All authors contributed to the article and approved the submitted version.

FUNDING

This research was supported by the National Natural Science Foundation of China (grants. 31970653, 91954202 and 31670181).

ACKNOWLEDGMENTS

We thank the Arabidopsis Biological Resource Center for the *pdm4* mutant line. And we thank professor Jinxing Lin (Beijing Forestry University, Beijing 10083, China) for language editing.

SUPPLEMENTARY MATERIAL

The Supplementary Material for this article can be found online at: https://www.frontiersin.org/articles/10.3389/fpls.2020.01198/full#supplementary-material

REFERENCES

Arnon, D. I. (1949). Copper enzymes in isolated chloroplasts: polyphenoloxidase in *beta vulgaris*. *Plant Physiol.* 24, 1–15. doi: 10.1104/pp.24.1.1

Aronsson, H., and Jarvis, P. (2002). A simple method for isolating import-competent Arabidopsis chloroplasts. *FEBS Lett.* 529, 215–220. doi: 10.1016/s0014-5793(02)03342-2

Asakura, Y., Galarneau, E., Watkins, K. P., Barkan, A., and van-Wijk, K. J. (2012). Chloroplast RH3 DEAD box RNA helicases in maize and Arabidopsis function in splicing of specific group II introns and affect chloroplast ribosome biogenesis. *Plant Physiol.* 159, 961–974. doi: 10.1104/pp.112.197525

Barkan, A., and Small, I. (2014). Pentatricopeptide Repeat Proteins in Plants. *Annu. Rev. Plant Biol.* 65, 415–442. doi: 10.1146/annurev-arplant-050213-040159

Beick, S., Schmitz-Linneweber, C., Williams-Carrier, R., Jensen, B., and Barkan, A. (2008). The pentatricopeptide repeat protein PPR5 stabilizes a specific tRNA precursor in maize chloroplasts. *Mol. Cell. Biol.* 28, 5337–5347. doi: 10.1128/MCB.00563-08

Belcher, S., Williams-Carrier, R., Stiffler, N., and Barkan, A. (2015). Large-scale genetic analysis of chloroplast biogenesis in maize. *Biochim. Biophys. Acta* 1847, 1004–1016. doi: 10.1016/j.bbabio.2015.02.014

Bobik, K., McCray, T. N., Ernest, B., Fernandez, J. C., Howell, K. A., Lane, T., et al. (2017). The chloroplast RNA helicase ISE2 is required for multiple chloroplast RNA processing steps in *Arabidopsis thaliana*. *Plant J.* 91, 114–131. doi: 10.1111/tpj.13550

Borisjuk, L., Nguyen, T. H., Neuberger, T., Rutten, T., Tschiersch, H., Claus, B., et al. (2005). Gradients of lipid storage, photosynthesis and plastid differentiation in developing soybean seeds. *New Phytol.* 167, 761–776. doi: 10.1111/j.1469-8137.2005.01474.x

Bryant, N., Lloyd, J., Sweeney, C., Myouga, F., and Meinke, D. (2011). Identification of nuclear genes encoding chloroplast-localized proteins required for embryo development in Arabidopsis. *Plant Physiol.* 155, 1678–1689. doi: 10.1104/pp.110.168120

Cheng, S., Gutmann, B., Zhong, X., Ye, Y., Fisher, M. F., Bai, F., et al. (2016). Redefining the structural motifs that determine RNA binding and RNA editing by pentatricopeptide repeat proteins in land plants. *Plant J.* 85, 532–547. doi: 10.1111/tpj.13121

Chi, W., Ma, J., Zhang, D., Guo, J., Chen, F., Lu, C., et al. (2008). The pentratricopeptide repeat protein DELAYED GREENING1 is involved in the regulation of early chloroplast development and chloroplast gene expression in Arabidopsis. *Plant Physiol.* 147, 573–584. doi: 10.1104/pp.108.116194

Chi, W., He, B., Mao, J., Li, Q., Ma, J., Ji, D., et al. (2012). The function of RH22, a DEAD RNA helicase, in the biogenesis of the 50S ribosomal subunits of Arabidopsis chloroplasts. *Plant Physiol.* 158, 693–707. doi: 10.1104/pp.111.186775

Chi, W., Feng, P., Ma, J., and Zhang, L. (2015). Metabolites and chloroplast retrograde signaling. *Curr. Opin. Plant Biol.* 25, 32–38. doi: 10.1016/j.pbi.2015.04.006

Chi, Y. H., Semmes, O. J., and Jeang, K. T. (2011). A proteomic study of TAR-RNA binding protein (TRBP)-associated factors. *Cell Biosci.* 1, 9. doi: 10.1186/2045-3701-1-9

Dovzhenko, A., Bosco, C. D., Meurer, J., and Koop, H. U. (2003). Efficient regeneration from cotyledon protoplasts in *Arabidopsis thaliana*. *Protoplasma* 222 (1-2), 107–111. doi: 10.1007/s00709-003-0011-9

Du, L., Zhang, J., Qu, S., Zhao, Y., Su, B., Lv, X., et al. (2017). The pentratricopeptide repeat protein pigment-defective mutant2 is involved in the regulation of chloroplast development and chloroplast gene expression in Arabidopsis. *Plant Cell Physiol.* 58, 747–759. doi: 10.1093/pcp/pcx004

Germain, A., Hotto, A. M., Barkan, A., and Stern, D. B. (2013). RNA processing and decay in plastids. *WIREs RNA* 4, 295–316. doi: 10.1002/wrna.1161

Guillaumot, D., Lopez-Obando, M., Baudry, K., Avon, A., Rigaill, G., Falcon de Longevialle, A., et al. (2017). Two interacting PPR proteins are major Arabidopsis editing factors in plastid and mitochondria. *Proc. Natl. Acad. Sci. U. S. A.* 114, 8877–8882. doi: 10.1073/pnas.1705780114

Hajdukiewicz, P. T., Allison, L. A., and Maliga, P. (1997). The two RNA polymerases encoded by the nuclear and the plastid compartments transcribe distinct groups of genes in tobacco plastids. *EMBO J.* 16, 4041–4048. doi: 10.1093/emboj/16.13.4041

He, P., Wu, S., Jiang, Y., Zhang, L., Tang, M., Xiao, G., et al. (2019). GhYGL1d, a pentatricopeptide repeat protein, is required for chloroplast development in cotton. *BMC Plant Biol.* 19, 350–350. doi: 10.1093/emboj/16.13.4041

Huang, W., Zhu, Y., Wu, W., Li, X., Zhang, D., Yin, P., et al. (2018). The pentatricopeptide repeat protein SOT5/EMB2279 is required for plastid rpl2 and trnK intron splicing. *Plant Physiol.* 177, 684–697. doi: 10.1104/pp.18.00406

Ito, A., Sugita, C., Ichinose, M., Kato, Y., Yamamoto, H., Shikanai, T., et al. (2018). An evolutionarily conserved P-subfamily pentatricopeptide repeat protein is required to splice the plastid ndhA transcript in the moss *Physcomitrella patens* and *Arabidopsis thaliana*. *Plant J.* 94, 638–648. doi: 10.1111/tpj.13884

Jiang, T., Zhang, J., Rong, L., Feng, Y., Wang, Q., Song, Q., et al. (2018). ECD1 functions as an RNA-editing trans-factor of rps14-149 in plastids and is required for early chloroplast development in seedlings. *J. Exp. Bot.* 69, 3037–3051. doi: 10.1093/jxb/ery139

Krause, K., and Krupinska, K. (2000). Molecular and functional properties of highly purified transcriptionally active chromosomes from spinach chloroplasts. *Physiol. Plant.* 109, 188–195. doi: 10.1034/j.1399-3054.2000.100211.x

Krupinska, K., Melonek, J., and Krause, K. (2012). New insights into plastid nucleoid structure and functionality. *Planta* 237, 653–664. doi: 10.1007/s00425-012-1817-5

Lee, K., Park, S. J., Han, J. H., Jeon, Y., Pai, H.-S., and Kang, H. (2019). A chloroplast-targeted pentatricopeptide repeat protein PPR287 is crucial for chloroplast function and Arabidopsis development. *BMC Plant Biol.* 19, 244–244. doi: 10.1186/s12870-019-1857-0

Legen, J., Kemp, S., Krause, K., Profanter, B., Herrmann, R. G., and Maier, R. M. (2002). Comparative analysis of plastid transcription profiles of entire plastid chromosomes from tobacco attributed to wild-type and PEP-deficient transcription machineries. *Plant J.* 31, 171–188. doi: 10.1186/s12870-019-1857-0

Liere, K., and Börner, T. (2007). Transcription and transcriptional regulation in plastids. *Cell and Molecular Biology of Plastids* 19, 121–174. doi: 10.1007/4735_2007_0232

Leister, D. (2003). Chloroplast research in the genomic age. *Trends Genet.* 19, 47–56. doi: 10.1016/s0168-9525(02)00003-3

Liu, C., Zhu, H., Xing, Y., Tan, J., Chen, X., Zhang, J., et al. (2016). Albino Leaf 2 is involved in the splicing of chloroplast group I and II introns in rice. *J. Exp. Bot.* 67, 5339–5347. doi: 10.1093/jxb/erw296

Lu, Y., Li, C., Wang, H., Chen, H., Berg, H., and Xia, Y. (2011). AtPPR2, an Arabidopsis pentatricopeptide repeat protein, binds to plastid 23S rRNA and plays an important role in the first mitotic division during gametogenesis and in cell proliferation during embryogenesis. *Plant J.* 67, 13–25. doi: 10.1111/j.1365-313X.2011.04569.x

Lurin, C., Andrés, C., Aubourg, S., Bellaoui, M., Bitton, F., Bruyère, C., et al. (2004). Genome-wide analysis of Arabidopsis pentatricopeptide repeat proteins reveals their essential role in organelle biogenesis. *Plant Cell.* 16, 2089–2103. doi: 10.1105/tpc.104.022236

Majeran, W., Friso, G., Ponnala, L., Connolly, B., Huang, M., Reidel, E., et al. (2010). Structural and metabolic transitions of C4 leaf development and differentiation defined by microscopy and quantitative proteomics in maize. *Plant Cell.* 22, 3509–3542. doi: 10.1105/tpc.110.079764

Majeran, W., Friso, G., Asakura, Y., Qu, X., Huang, M., Ponnala, L., et al. (2012). Nucleoid-enriched proteomes in developing plastids and chloroplasts from

maize leaves; a new conceptual framework for nucleoid functions. *Plant Physiol.* 158, 156–189. doi: 10.1104/pp.111.188474

Meinke, D. W., Franzmann, L. H., Nickle, T. C., and Yeung, E. C. (1994). Leafy cotyledon mutants of Arabidopsis. *Plant Cell.* 6, 1049–1064. doi: 10.1105/tpc.6.8.1049

Melonek, J., Oetke, S., and Krupinska, K. (2016). Multifunctionality of plastid nucleoids as revealed by proteome analyses. *Biochim. Biophys. Acta* 1864, 1016–1038. doi: 10.1016/j.bbapap.2016.03.009

Mullet, J. E. (1993). Dynamic regulation of chloroplast transcription. *Plant Physiol.* 103, 309–313. doi: 10.1104/pp.103.2.309

Ouyang, M., Li, X., Zhao, S., Pu, H., Shen, J., Adam, Z., et al. (2017). The crystal structure of Deg9 reveals a novel octameric-type HtrA protease. *Nat. Plants* 12, 973–982. doi: 10.1038/s41477-017-0060-2

Pan, X., Liu, Z., Li, M., and Chang, W. (2013). Architecture and function of plant light-harvesting complexes II. *Curr. Opin. Struct. Biol.* 23, 515–525. doi: 10.1016/j.sbi.2013.04.004

Pfalz, J., and Pfannschmidt, T. (2013). Essential nucleoid proteins in early chloroplast development. *Trends Plant Sci.* 18, 186–194. doi: 10.1016/j.tplants.2012.11.003

Pfalz, J., Liere, K., Kandlbinder, A., Dietz, K. J., and Oelmüller, R. (2006). pTAC2, -6, and -12 are components of the transcriptionally active plastid chromosome that are required for plastid gene expression. *Plant Cell.* 18, 176–197. doi: 10.1105/tpc.105.036392

Pogson, B. J., and Albrecht, V. (2011). Genetic dissection of chloroplast biogenesis and development: an overview. *Plant Physiol.* 155, 1545–1551. doi: 10.1104/pp.110.170365

Prikryl, J., Watkins, K. P., Friso, G., van Wijk, K. J., and Barkan, A. (2008). A member of the Whirly family is a multifunctional RNA- and DNA-binding protein that is essential for chloroplast biogenesis. *Nucleic Acids Res.* 36, 5152–5165. doi: 10.1093/nar/gkn492

Pyo, Y. J., Kwon, K.-C., Kim, A., and Cho, M. H. (2013). Seedling Lethal1, a pentatricopeptide repeat protein lacking an E/E+ or DYW domain in Arabidopsis, is involved in plastid gene expression and early chloroplast development. *Plant Physiol.* 163, 1844–1858. doi: 10.1104/pp.113.227199

Rojas, M., Ruwe, H., Miranda, R. G., Zoschke, R., Hase, N., Schmitz-Linneweber, C., et al. (2018). Unexpected functional versatility of the pentatricopeptide repeat proteins PGR3, PPR5 and PPR10. *Nucleic Acids Res.* 46, 10448–10459. doi: 10.1093/nar/gky737

Sato, S., Nakamura, Y., Kaneko, T., Asamizu, E., and Tabata, S. (1999). Complete structure of the chloroplast genome of *Arabidopsis thaliana*. *DNA Res.* 6, 283–290. doi: 10.1093/dnares/6.5.283

Small, I. D., and Peeters, N. (2000). The PPR motif - a TPR-related motif prevalent in plant organellar proteins. *Trends Biochem. Sci.* 25, 45–47. doi: 10.1016/s0968-0004(99)01520-0

Stern, D. B., Goldschmidt-Clermont, M., and Hanson, M. R. (2010). Chloroplast RNA metabolism. *Annu. Rev. Plant Biol.* 61, 125–155. doi: 10.1146/annurev-arplant-042809-112242

Stoppel, R., and Meurer, J. (2011). The cutting crew - ribonucleases are key players in the control of plastid gene expression. *J. Exp. Bot.* 63, 1663–1673. doi: 10.1093/jxb/err401

Stoppel, R., and Meurer, J. (2013). Complex RNA metabolism in the chloroplast: an update on the psbB operon. *Planta* 237, 441–449. doi: 10.1007/s00425-012-1782-z

Sugita, M., and Sugiura, M. (1996). Regulation of gene expression in chloroplasts of higher plants. *Plant Mol. Biol.* 32, 315–326. doi: 10.1007/bf00039388

Sugiura, M., Hirose, T., and Sugita, M. (1998). Evolution and mechanism of translation in chloroplasts. *Annu. Rev. Genet.* 32, 437–459. doi: 10.1146/annurev.genet.32.1.437

Sun, Y., Huang, J., Zhong, S., Gu, H., He, S., and Qu, L. (2018). Novel DYW-type pentatricopeptide repeat (PPR) protein BLX controls mitochondrial RNA editing and splicing essential for early seed development of Arabidopsis. *J. Genet. Genomics* 45, 155–168. doi: 10.1016/j.jgg.2018.01.006

Terzi, L. C., and Simpson, G. G. (2009). Arabidopsis RNA immunoprecipitation. *Plant J.* 59, 163–168. doi: 10.1111/j.1365-313X.2009.03859.x

Tiller, N., and Bock, R. (2014). The translational apparatus of plastids and its role in plant development. *Mol. Plant* 7, 1105–1120. doi: 10.1093/mp/ssu022

Walter, M., Piepenburg, K., Schöttler, M. A., Petersen, K., Kahlau, S., Tiller, N., et al. (2010). Knockout of the plastid RNase E leads to defective RNA processing and chloroplast ribosome deficiency. *Plant J.* 64, 851–863. doi: 10.1111/j.1365-313X.2010.04377.x

Wang, G., Zhong, M., Shuai, B., Song, J., Zhang, J., Han, L., et al. (2017). E+ subgroup PPR protein defective kernel 36 is required for multiple mitochondrial transcripts editing and seed development in maize and Arabidopsis. *New Phytol.* 214, 1563–1578. doi: 10.1111/nph.14507

Williams, P. M., and Barkan, A. (2004). A chloroplast-localized PPR protein required for plastid ribosome accumulation. *Plant J.* 36, 675–686. doi: 10.1046/j.1365-313x.2003.01915.x

Yamaguchi, K., Beligni, M. V., Prieto, S., Haynes, P. A., McDonald, W. H., Yates, J. R., et al. (2003). Proteomic characterization of the *Chlamydomonas reinhardtii* chloroplast ribosome. Identification of proteins unique to the 70S ribosome. *J. Biol. Chem.* 278, 33774–33785. doi: 10.1074/jbc.M301934200

Xiao, J., Li, J., Ouyang, M., Yun, T., He, B., Ji, D., et al. (2012). DAC is involved in the accumulation of the cytochrome b6/f complex in Arabidopsis thaliana. *Plant Physiol.* 160, 1911–1922. doi: 10.1104/pp.112.204891

Yin, T., Pan, G., Liu, H., Wu, J., Li, Y., Zhao, Z., et al. (2012). The chloroplast ribosomal protein L21 gene is essential for plastid development and embryogenesis in Arabidopsis. *Planta* 235, 907–921. doi: 10.1007/s00425-011-1547-0

Yu, D., Jiang, L., Gong, H., and Liu, C.-M. (2012). EMBRYONIC FACTOR 19 encodes a pentatricopeptide repeat protein that is essential for the initiation of zygotic embryogenesis in Arabidopsis. *J. Integr. Plant Biol.* 54, 55–64. doi: 10.1111/j.1744-7909.2011.01089.x

Yu, Q. B., Huang, C., and Yang, Z. N. (2014). Nuclear-encoded factors associated with the chloroplast transcription machinery of higher plants. *Front. Plant Sci.* 5, 316. doi: 10.3389/fpls.2014.00316

Zhang, J., Xiao, J., Li, Y., Su, B., Xu, H., Shan, X., et al. (2017). PDM3, a pentatricopeptide repeat-containing protein, affects chloroplast development. *J. Exp. Bot.* 68, 5615–5627. doi: 10.1093/jxb/erx360

Zhang, Z., Cui, X., Wang, Y., Wu, J., Gu, X., and Lu, T. (2017). The RNA editing factor WSP1 is essential for chloroplast development in rice. *Mol. Plant* 10, 86–98. doi: 10.1016/j.molp.2016.08.009

Zhang, L., Zhou, W., Che, L., Rochaix, J.-D., Lu, C., Li, W., et al. (2019). PPR protein BFA2 is essential for the accumulation of the atpH/F transcript in chloroplasts. *Front. Plant Sci.* 10, 446. doi: 10.3389/fpls.2019.00446

Zhou, W., Lu, Q., Li, Q., Wang, L., Ding, S., Zhang, A., et al. (2017). PPR-SMR protein SOT1 has RNA endonuclease activity. *Proc. Natl. Acad. Sci. U.S.A.* 114, E1554–E1563. doi: 10.1073/pnas.1612460114

Conflict of Interest: The authors declare that the research was conducted in the absence of any commercial or financial relationships that could be construed as a potential conflict of interest.

Advantages of publishing in Frontiers

OPEN ACCESS
Articles are free to read for greatest visibility and readership

FAST PUBLICATION
Around 90 days from submission to decision

HIGH QUALITY PEER-REVIEW
Rigorous, collaborative, and constructive peer-review

TRANSPARENT PEER-REVIEW
Editors and reviewers acknowledged by name on published articles

Frontiers
Avenue du Tribunal-Fédéral 34
1005 Lausanne | Switzerland

Visit us: www.frontiersin.org
Contact us: frontiersin.org/about/contact

REPRODUCIBILITY OF RESEARCH
Support open data and methods to enhance research reproducibility

DIGITAL PUBLISHING
Articles designed for optimal readership across devices

FOLLOW US
@frontiersin

IMPACT METRICS
Advanced article metrics track visibility across digital media

EXTENSIVE PROMOTION
Marketing and promotion of impactful research

LOOP RESEARCH NETWORK
Our network increases your article's readership